SCHOLARLY PUBLICATIONS

A CURRENT AWARENESS BULLETIN
OF RESEARCH OUTPUT

@DTU

(67th Edition)

JULY, 2018

BY: CENTRAL LIBRARY

DELHI TECHNOLOGICAL UNIVERSITY
(FORMERLY *DELHI COLLEGE OF ENGINEERING)*
GOVT. OF N.C.T. OF DELHI
SHAHBAD DAULATPUR, MAIN BAWANA ROAD
DELHI 110042

PREFACE

This is the **Sixty Seventh** Issue of Current Awareness Bulletin started by Delhi Technological University, Central Library. The aim of the bulletin is to compile, preserve and disseminate information published by the faculty, students and alumni for mutual benefits. The bulletin also aims to propagate the intellectual contribution of Delhi Technological University (DTU) as a whole to the academia.

The bulletin contains information resources available in the internet in the form of articles, reports, presentations published in international journals, websites, etc. by the faculty and students of DTU. The publications of faculty and student which are not covered in this bulletin may be because of the reason that the full text either was not accessible or could not be searched by the search engine used by the library for this purpose.

The learned faculty and students are requested to provide their uncovered publications to the library either through email or in CD, etc. to make the bulletin more comprehensive.

This issue contains the information published during **July, 2018**. The arrangement of the contents is alphabetical. The full text of the article which is either subscribed by the university or available in the web is provided in this bulletin.

Central Library

CONTENTS

1. A study on Sewage Treatment and Disposal in Delhi, ***6.Shreya Gupta***, ***3.SK Singh*** and Vishal Gandhi, Environmental, DTU

2. Acceptably consistent incomplete interval-valued intuitionistic multiplicative preference relations, ***6.Mamata Sahu***, ***3.Anjana Gupta*** and Aparna Mehra, Applied Mathematics, DTU

3. Adoption of B2B E-Commerce in India: A Theoretical Framework, Sanjay Chaudhary and ***3.P.K. Suri***, DSM, DTU

4. Analysis of Three Types of Solar Systems: PV, Flat Plate Thermal, and Hybrid PV-T Using TRNSYS Model, ***7.Piyush Rawat*** and ***3.Dr J. P. Kesari***, Mechanical, DTU

5. Analyzing Environmental Kuznets Curve and Pollution Haven Hypothesis in India in the Context of Domestic and Global Policy Change, ***3.K. V. Bhanu Murthy*** and ***6.Sakshi Gambhir,*** DSM, DTU

6. Asymmetric U-shaped printed monopole antenna embedded with T-shaped strip for bluetooth, WLAN/WiMAX applications, Rakesh Nath Tiwari, ***7.1.Prabhakar Singh*** and Binod Kumar Kanaujia, Electronics and Communication, DTU

7. Biometric re-authentication: an approach towards achieving transparency in user authentication, Neha and ***6.1.Kakali Chatterjee***, Computer Science, DTU

8. COMMERCIAL AND TECHNOLOGICAL FEASIBILITY STUDY OF USING SOLAR E-RICKSHAW FOR SEMI-URBAN AREAS, ***8.Tarun Saxena***, ***8.Manish Kumar*** and ***3.Dr. Kesari, J. P.***, Mechanical, DTU

9. Content Driven Enrichment of Formal Text using Concept Definitions and Applications, Abhinav Jain, Nitin Gupta, Shashank Mujumdar, Sameep Mehta and ***6.Rishi Madhok,*** DTU

10. CP-ABE for Selective Access with Scalable Revocation: A Case Study for Mobile-based Healthfolder, ***Divyashikha Sethia***, Huzur Saran, and ***3.Daya Gupta***, Computer Science and Engg, DTU

11. Design of Horse Shoe Patch antenna for wireless Applications, ***3.N. Jayanti***, Electronics and Communication, DTU

12. Design of Solar Photovoltaic Based Water Pumping for Automatic Irrigation System, ***6.Mohit Kumar***, ***6.Namita Vats***, ***6.Anshul Chaudhary***, ***6.Abhishek Kumar Dev*** and ***3.Dr. J.P.Kesari***, DTU

13. Dual- and Triple-Band Polarization Insensitive Ultrathin Conformal Metamaterial Absorbers With Wide Angular Stability, ***7.1.Amit Kumar Singh***, Mahesh P. Abegaonkar and Shiban K. Koul, Electronics, DTU

14. Effect of Goal Orientation on Job Performance : Moderating Effect of Situational Strength at Work, Shivganesh Bhargava and ***3.Harsh Pradhan***, Management, DTU

15. Electron Acceleration by a Relativistic Electron Plasma Wave in Inverse-Free-Electron Laser Mechanism, ***6.Monika Yadav***, ***3.Suresh C. Sharma*** , and Devki Nandan Gupta, Physics, DTU

16. EMPIRICAL BASIS FOR MEASUREMENT OF IDIOSYNCRATIC VOLATILITY IN THE INDIAN STOCK MARKET, ***3.K. V. Bhanu Murthy***, Sartaj Hussain AND DR. Amit Kumar, Humanities, DTU

17. Energy- and exergy-based performance evaluation of solar powered combined cycle (recompression supercritical carbon dioxide cycle/organic Rankine cycle), ***6.Harwinder Singh*** and ***3.R.S. Mishra***, Mech, Produ, & Indust & Automobile, DTU

18. Experimental comparative study of chrome steel pin with and without chrome plated cast iron disc in situ fully flooded interface lubrication, ***3.Roop Lal*** and ***3.R. C. Singh***, Mechanical, DTU

19. Fabrication of 3D Self-Assembled Nonmulberry Antheraea Mylitta (tasar) Fibroin Nonwoven Mats for Wound Dressing Applications, ***6.Chandra Mohan Srivastava*** and ***3.Roli Purwar***, Applied Chemistry, DTU

20. Ferromagnetic Resonance Tunability by Microwave Frequency in Bilayer Fe97Si3 /Pt Thin Film, Ahmad S, Shah J , ***3.Chaujar R*** , Puri NK , Negi PS and Kotnala RK, Applied Physics, DTU

21. Hydraulic Analysis and Modelling of Small Hydro Power: A Case Study of a Plant at Gogripur, Karnal, ***7.Satish Kumar Kadian***, ***3.Dr. J.P. Kesari*** and ***3.Dr. R.S. Mishra***, Mechanical, DTU

22. Improving the Tractive Performance with Four-Wheel Drive (4WD) System, ***6.Neeraj Budhraja*** and ***3.Amit Pal***, Mechanical, DTU

23. Influence of geotextiles in enhancing shear strength of Yamuna sand, ***6.Ankur Mudgal***, ***3.Raju Sarkar*** and ***3.Amit Kumar Shrivastava***, Civil, DTU

24. Influent of Overall Architectural Arrangement on Structural Elements Design, ***6.Gatbel Buony*** and ***3.Dr. A. K. Gupta***, Civil, DTU

25. Investigations on the plasma enabled growth of vertical graphene sheets on CNT surface, ***6.Neha Gupta*** and ***3.Suresh C. Sharma***, Applied Physics, DTU

26. Material Selection for a Fuel Tank and its FE Simulation in deep drawing, ***3.Vijay Gautam*** and ***6.Subhajit Konar***, Mechanical, DTU

27. Microbiomics in the Molecular Era: A Bird's Eye View into the Future of Personalized Medicine, Ritcha Saxena, ***6.Ritwik Saxena*** and ***6.Ananya Raj***, Biomedical, DTU

28. Molecular characterization, modeling, and docking analysis of late phytic acid biosynthesis pathway gene, inositol polyphosphate 6-/3-/5-kinase, a potential candidate for developing low phytate crops, ***6.Mansi Punjabi***, ***3.Navneeta Bharadvaja***, Archana Sachdev and Veda Krishnan, Biotechnology, DTU

29. New transitivity property of intuitionistic multiplicative preference relation and its application in missing value estimation, ***6.Mamata Sahu*** and ***3.Anjana Gupta***, Mathematics, DTU

30. PRESENT SCENARIO AND SUGGESTION FOR WATERSHED MANAGEMENT PROGRAMME: A REVIEW, ***3.Dr. Munendra Kumar*** and ***6.Ruchika Dabas***, Civil DTU

31. Reverse supply chain issues in Indian electronics industry: a case study, ***3.Saurabh Agrawal***, Rajesh K. Singh & ***3.Qasim Murtaza***, Mechanical, Production & Industrial Engineering, DTU

32. Risks in Renewable Energy Markets in Emerging Economies, KANIKA CHAWLA, MANU AGGARWAL, ANJALI VISWAMOHANAN, ***8.1.ARJUN DUTT*** AND NEERAJ KULDEEP, Electronics and Communication, DTU

33. Thickness Computation for Byrd Glacier, East Antarctica, ***6.Anubha Agrawal*** and ***3.Anubha Mandal***, Environemtnal, DTU

34. UWB and miniaturized meandered stripline fed metamaterial loaded antenna for satellite applications, P.Dawar***, 3.N.S. Raghava*** and ***3.A. De***, Electronics and Communication, DTU

1. *Chancellor*

2. *Pro Vice Chancellor*	***2.1.*** *Ex Pro Vice Chancellor*
3. *Faculty*	***3.1.*** *Ex Faculty*
4. *Teaching-cum-Research Fellow*	***4.1.****Asst. Librarian*
5. *Alumni*	
6. *Research Scholar*	***6.1.*** *Ex Research Scholar*
7. *PG Scholar*	***7.1.*** *Ex PG Scholar*
8. *Undergraduate Student*	***8.1.*** *Ex Undergraduate Student*

Volume 6 Issue 2(2018) 88-91 ISSN 2347 - 3258
International Journal of Advance Research and Innovation

A study on Sewage Treatment and Disposal in Delhi

Shreya Gupta[1], SK Singh[1,*], Vishal Gandhi[2]
[1]Department of Environmental Engineering, Delhi Technological University, Delhi, India
[2]Central Pollution Control Board, Delhi, India

Article Info
Article history:
Received 10 May 2018
Received in revised form 25 May 2018
Accepted 1 June 2018
Available online 15 June 2018

Keywords
Delhi, Disposal, Sewage, STPs, Treatment.

Abstract
Delhi, which is the capital of India and also the fastest growing metropolitan city, does not have adequate sewage treatment and disposal infrastructure. In most of the cases wastewater is let out untreated and it either seeps into the ground as a potential pollutant of groundwater or is discharged into the natural drainage system causing pollution in downstream areas. Wastewater needs to be conveyed to sewage treatment plants for treatment and treated sewage must meet the aesthetic standards of ambient environment for receiving water bodies. This paper gives an overview on sewage treatment plants (STPs) in Delhi, focusing majorly on the Okhla wastewater plants. The total treatment capacity of STPs in Delhi, was mapped against the total sewage generation and hence the gap between the two was found. This information will be very useful for further allocation of STPs and also for safeguarding the health of people and Environment

1. Introduction

In the past circumstances, sewage from a city or a state was less polluted but rather more today. The development in population, urbanization and the enhanced ways of life have, in any case, expanded the quality and amount of city sewage as of late. Thus proper treatment and management of sewage becomes an essential process for ensuring healthy and good quality of life of living beings. Presently sewage, before being discarded either in waterway streams or ashore, has to be properly treated, to make it safe. Sewage treatment basically incorporates expulsion of small-scale life forms, toxins or contaminants from wastewater. This is done using various technologies like in Delhi, 6 different types of technologies are used in the 35 sewage treatment plants (STPs).

Despite being one of the first Indian cities to come up with a City Development Plan way back in 1962, Delhi has been ientified as the top-priority city for the work to be done to combat the magnitude of pollution in the river's 22km stretch through the city. Therefore, to improve the present situation, this paper offers solutions to various problems of sewage treatment and disposal in Delhi.

2. Sewage Generation in Delhi

In Delhi, out of the total population of 16.75 million in the year 2011, about 16.34 million live in urban areas. The percentage of urban population to the total population of the country, which in the year 1991 was 89.9 percent, stands at 97.5 percent in the year 2011 (Table 1).

Table 1: Urban and Rural population of Delhi

Population	Delhi		
	1991	2001	2011
Rural	949,019	944,727	419,319
Urban	8,471,625	12,905,780	16,333,916
Total	9,420,644	13,850,507	16,753,235

Due to such drastic growth in urban population of Delhi the quality and strength of sewage has also increased with time.

It was found that currently, 3909 million liter per day (MLD) of sewage is being generated in Delhi. However, available sewage treatment capacity is only 2940.66 million liter per day (MLD). Further only 74.9% of this available capacity is actually treated i.e. 2202.56 million liter per day. So a huge gap is present between the total sewage generated in Delhi and the sewage that is actually treated i.e. 1706.44 million liter per day (MLD).

3. Treatment of Sewage in Delhi

Sewage treatment is the way of expelling contaminants from wastewater, essentially from domestic areas sewage. Physical, synthetic and natural procedures are utilized to expel contaminants and create treated wastewater that is more secure for the earth. A by-product of sewage treatment is generally a semi-strong waste or slurry, called sewage sludge. The sludge needs to experience assist treatment before being appropriate for disposal on land or water.

Delhi Jal Board is in charge of treatment and transfer of waste water through a proficient system of around 7000 Km of Sewage lines crosswise over Delhi.

There are 35 Sewage treatment plants in Delhi, out of which 31 were found to be operational and 4 were non-operational. Table 2 shows the break-up of STPs in Delhi.

Table 2: Break-up of STPs in Delhi

Sl No.	Status	No. Of STPs	Installed Capacity (MLD)	Actual Treatment (MLD)
1.	Operational	31	2799.82	2202.56
2.	Non-operational	4	140.84	0
3.	Total	35	2940.66	2202.56

3.1 Treatment Technologies Used For Sewage Treatment

The break-up of different treatment technologies used in the different sewage treatment plants in Delhi is shown in table 3.

Table 3: Technologies used in Delhi STPs

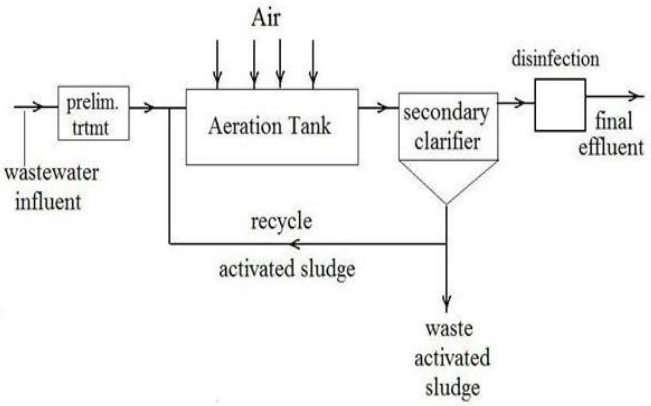

S.No.	Technology	No. of STPs
1.	Activated sludge process (ASP)	26

***Corresponding Author,**
E-mail-address: sksingh@dce.ac.in
Phone No--+91- 9891599903

All rights reserved: http://www.ijari.org

2.	Biofilters (BIO-FAR)	3
3.	Extended Aeration (EA)	2
4.	Moving Bed Biofilm Reactor (MBBR)	2
5.	Oxidation Pond (OP)	1
6.	Interchange Sequencing Batch Reactor (ISBR)	1

Fig. 1: Activated Sludge Process (Flow diagram)
Source: https://www.researchgate.net/figure/237841340_Fig-2-1-Activated-Sludge-Process-Flow-diagram

3.1.1 Activated Sludge Process (ASP)

Activated-sludge technique, a sewage-treatment process in which sludge, the amassed, microbe's rich deposits of settling tanks and basins, is seeded into the approaching wastewater and the blend agitated for a few hours (4-8 hours) within the sight of an adequate air supply. Suspended solids and numerous organic solids are adsorbed by the sludge, while organic matter is oxidized by the microorganisms. The measures of air and sludge utilized can be differed to control the level of treatment got. The sludge is then isolated out in a settling tank.

Activated sludge plant involves:

1. Wastewater aeration in the presence of a microbial suspension,
2. Solid-liquid separation following aeration,
3. Discharge of clarified effluent,
4. Wasting of excess biomass, and
5. Return of remaining biomass to the aeration tank.

3.1.2 Extended Aeration (EA)

The conventional activated sludge plant has been modified to eliminate the primary sedimentation tank, and sludge digestion tank, in a process called Extended Aeration, which aims at providing an aeration tank with a longer aeration time.It is more economical for upto 1.5 lakh population, than a conventional activated sludge plant.

Figure 2: Extended Aeration (Flow diagram)
Source: http://www.brighthub.com/environment/science-environmental/articles/66157.aspx

3.1.3 Moving Bed Biofilm Reactor (MBBR)

It's a mix of activated sludge process (suspended growth) and bio filter processes (attached growth). Moving Bed Biofilm Reactor (MBBR) process utilizes the entire tank volume for biomass development. It utilizes basic drifting media, which are transporters of attached growth of biofilms. Biofilm carrier movement is caused by the disturbance of air bubbles. This minimal treatment framework is viable in the expulsion of BOD as well as nitrogen and phosphorus while encouraging successful solids separation.

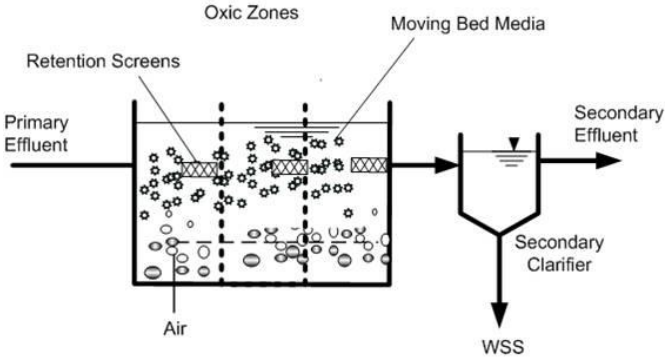

Fig.3: A schematic of the Moving Bed Biofilm Reactor (MBBR)
Source: http://www.aesarabia.com/moving-bed-bioreactor-mbbr/

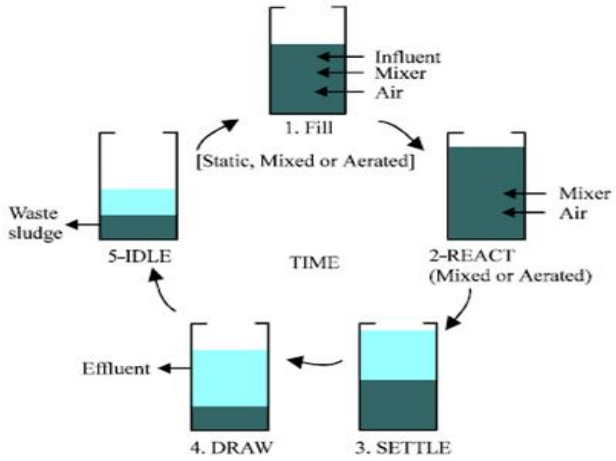

Fig.4: 5 Stages of Sequential Batch Reactor (SBR)
Source: http://www.seamak.com/service_6.html

3.1.4 Sequential Batch Reactor (SBR)

The sequencing batch reactor (SBR) process is a progressive suspended growth (activated sludge) process in which each major progress occur in a common tank in sequential order. The aggregate five phases happen in a single reactor by which way it diminishes the impression. SBRs can be designed and operated to enhance removal of nitrogen, phosphorus, and ammonia, despite clearing TSS and BOD. The five stages of SBR are:

• FILL: Wastewater fills the tank, mixing with biomass that settles in the midst of the past cycle.
• REACT: Air is added to the tank to enable biological growth and felicitate waste diminishment.
• SETTLE: Mixing and Aeration quit in the midst of this stage to empower solids to settle.
• DRAW: Clarified profluent is discharged.
• IDLE: Sludge can be removed in the midst of this stage.

3.1.5 Vermifiltration Technology

Vermifiltration was found as one of the new, creative and sustainable innovation. It comprises of a natural reactor containing media that filters organic material from sewage. It depends on the symbiotic connection amongst earthworms and microorganisms. Vermifilters provide an aerobic environment and wet substrate that encourages small scale living beings development as a biofilm. Micro-organisms perform biochemical degradation of organic matter present in wastewater, while earthworms expel the unsafe pathogens in wastewater by eating them up. This technology involves all the three primary, secondary and tertiary forms of treatment.

In all vermifiltration removes nearly 90% of BOD, 80% of COD and pathogens. It also reduces ammonium content.

Advantages of this technology and why it is better than other conventional technologies are:-

1) It has high treatment effeciency given the low space requirement.
2) Odourless and cost effecient technology
3) Energy is not required for aeration, so these filters can be considered 'Passive Treatment' systems.
4) Resulting vermifiltered water is clean and disinfected enough to be reused for irrigation and in parks and gardens.

The main challenge that should be tended to before vermi-filtration can be received on a substantial scale is its reliance on earthworms which ultimately depends on temperature, pH
level and moisture. Additionally, detachment of earthworms by hand from the filter bed is a tedious procedure.

4.Disposal of Sewage Through Natural and Manmade drains in Delhi

4.1 Natural Drain

Delhi has been separated into six seepage zones (I) Northern Zone, (ii) Western Zone, (iii) Central North West and South East Zone, (iv)

Central South and South East Zone, (v) East Zone and (vi) South Zone.

Table 4: The catchment region of the common depletes in the city.

S No	Catchments	Location	Length of main drains (km)	Drainage channels	Discharge (comecs)
1.	Alipur	North	140	Supplienatry Bhiwana Escape -No6 drain new Drain	141 33
2	Kanjhawala	west	120	Mungespur	52
3	Najafgarh	Central-North, West and South West	105	Najafgarh Palam Bhupania-Chudania (from Haryana)	283 86 40
4	Khushak Barapulla	Central-South and South - East		Khushak and Barapulla drainsn(' nallah')	120
5	Trans-Yamuna	East	45	Shahdara outfall-Gazipur Trunk drain No-1	158 86
6	Mehrauli	South	5		

4.2 Manmade Drains

The aggregate length of channels is 1700 km spread over 12 municipal zones. There are around 1300 channels with 339 km in Civil Lines Area and 5 km in Paharganj Sadar Area.

Table 5: Length of drains in different zone

S. No.	Zone	Number of drains	Total length of drains (km)
1	Central	41	47
2	South	127	102
3	Sadar-Paharganj	10	4.5
4	Karolbagh	47	23
5	City Zone	10	8.6
6	Civil Lines	77	339
7	Shahadara South	174	134
8	Shahadara North	197	135
9	Narela	84	83
10	Rohini	142	180
11	West	185	410
12	Najafgarh	202	228
	Total	**1296**	**1694.1**

Source: Nav Bharat Times, New Delhi, 31st July, 2006

There are two general ways of disposing of the sewage effluents:

1) Dilution i.e. disposal in water; and
2) Effluent Irrigation or disposal on land

Disposal by dilution strategy is more typical in Delhi. The greater part of the sewage release in Delhi is in the waterway Yamuna. 21 nullahs release around 850 MGD of sewage into the Yamuna consistently, of which 67 percent contamination is caused by the Najafgarh deplete alone.

The Yamuna stream, frequently called Delhi's lifesaver, is panting forever. The 22-km extend along the national capital has virtually no oceanic life - on account of more than 20 drains that pour untreated sewage and other waste into the stream.

After the mid-1990s, the Delhi government has put resources into making a foundation for stream tidy up. What's more, there has been arranging and subsidizing through the Yamuna Action Plan, or YAP. In 2005, the Rs 380-crore YAP-II was endorsed for Delhi. In 2006-07, the DJB acquainted its interceptor design with lay more than 60 km of sewers along Najafgarh, supplementary and Shahdara channels. This gigantic equipment program, in any case, did not give any idea to capturing the contamination. As indicated by a report of the Central Pollution Control Board, the current level of DO in the waterway is just around 1 mg for each litre, while it ought to be between 4 to 5 mg/l to manage life.

5. Status of Sewage Treatment Plants (STPs) in Delhi

35 STPs of Delhi were studied, it was found 31 out of them were operational and 4 (Kondli III, Yamuna Vihar II, Ghittorni and Timarpur) of them were found to be non-operational.

After studying 35 STPs of Delhi, 6 of them (Okhla) were visited and studied in detail. One of the Delhi's major wastewater plant with 30 MGD treatment capacity, is located in Okhla. This was built under the Yamuna Action Plan-II. It not only treats sewage, but also produces electricity from sludge using biogas system. It is fully-automated and SCADA-controlled. Estimated cost of this plant is Rs 149.5 crore. It uses Activated Sludge Process as it's treatment technology.

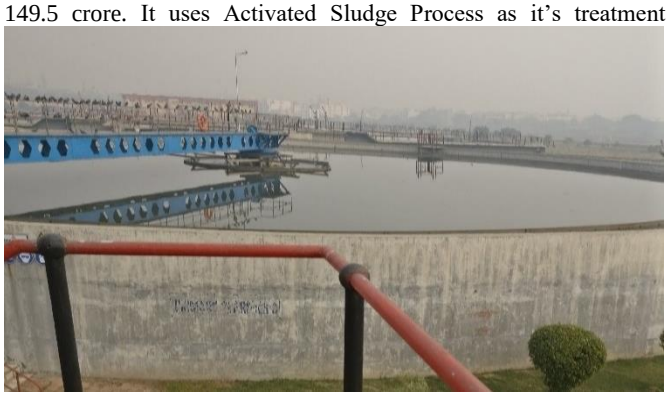

Fig. 5: Primary Clarifier of Okhla Plant

Fig. 6: Aeration Tank of Okhla Plant using ASP

Fig.7: Secondary Clarifier of Okhla Plant

All STPs in Delhi were studied with respect to their location, treatment capacity, technology used and reuse of treated water. A huge gap between the total sewage generated in Delhi and the sewage that is actually treated was found i.e. 1706.4 million liter per day (MLD).The problem is not just that there is inadequate treatment capacity in Delhi, but proper management of the existing STPs is also required. So bridging the gap is not the only solution, but proper operation and management of treatment plants is required.

Numerous new treatment advancements are ascending in various districts. After comparing different treatment technologies, Vermifiltration was found as one of the new, creative and sustainable innovation. It comprises of a natural reactor containing media that filters organic material from sewage. It depends on the symbiotic connection amongst earthworms and microorganisms. Vermifilters provide an aerobic environment and wet substrate that encourages small scale living beings development as a biofilm. Micro-organisms perform biochemical degradation of organic matter present in wastewater, while earthworms expel the unsafe pathogens in wastewater by eating them up.

6. Conclusions

In the present study survey was done in Delhi area for sewage treatment and disposables.Following conclusions are drawn from the study:

1. In Delhi there are a total of 35 STPs (31 – Operational and 4 – Non Operational).
2. Around 3909 million liter per day (MLD) of sewage is being generated in Delhi. However, available sewage treatment capacity is only 2940.66 million liter per day.
3. A huge gap between the total sewage generated in Delhi and the sewage that is actually treated was found i.e. 1706.4 million liter per day (MLD).
4. STPs in Delhi are based on ASP, BIO-FAR, EA, MBBR, OP, ISBR and Vermifiltration technologies.
5. Vermifiltration was found as one of the new, creative and sustainable innovation for treatment of sewage.
6. STPs based on Vermifiltration technology involves all the three primary, secondary and tertiary forms of treatment.

Acknowledgment

Authors are thankful to CPCB for providing help to carry out the study.

References

[1] Eawag (Swiss Federal Institute of Aquatic Science and Technology) Dorothee Spuhler (seecon international gmbh), Activated Sludge, https://www.sswm.info/category/implementation-tools/wastewater-treatment/hardware/semi-centralised-wastewater-treatments-3

[2] CPCB, Performance Evaluation of Sewage Treatment Plants in Central Zone. http://cpcb.nic.in/displaypdf.php?id=em9iaG9wYWwvU1RQX0NlbnRyYWxfWm9uZV8yMDE1LnBkZg==

[3] CPCB. Performance Evaluation of STPs under NRCD Under http://cpcb.nic.in/openpdffile.php?id=UmVwb3J0RmlsZXMvMjlfMTQ1ODExMDk5Ml9OZXdJdGVtXzE5NV9TVFBfUkVQT1JULnBkZg==, 2013

[4] CPCB, Status of STPs http://cpcb.nic.in/status-of-stps/2017

[5] HECS (2016), Sewage treatment plant technologies http://www.hecs.in/Turnkey%20Solutions/Sewage%20Treatment%20Plant/stp-technology

[6] A Kaushal, SK Singh. Adsorption Phenomenon and Its Application in Removal of Lead from Waste Water: A Review, International Journal of Hydrology, 1 (2), 2017, 1-11.

[7]P Rustogi, SK Singh. Revival and rejuvenation strategy of water bodies in a metropolitan city: a case study of najafgarh lake, Delhi, india. International Journal of Advanced Research 5 (2), 2017, 189-195

[8]D Gupta, SK Singh. Energy Use And Greenhouse Gas Emissions From Waste water Treatment Plants. International Journal of Environmental Engineering- inderscience, 7(1), 2015, 1-10,

[9]SK.Singh, A Raghu. Application of Membrane Bioreactor Technology for Wastewater Treatment and reuse: Case study of MBR Plant in Luxury Hotel in Delhi, International Journal for Innovative Research in Science & Technology (IJIRST), 1(12), 2015

[10]SS Singh, SK.Singh. Evaluating Water Quality of River Yamuna in Delhi by Regression Analysis International journal of Engineering and Management Research 5(3), 2015, 218-221

[11] AM Aenab, SK Singh. Critical Assessment of River water Quality and Wastewater Treatment Plant (WWTP), IOSR Journal Of Environmental Science, Toxicology And Food Technology (IOSR-JESTFT), 8(2)Ver. IV, 2014, 44-48

[12]J Inamdar, SK Singh. Performance analysis of Activated Sludge Process for waste water treatment and its comparison with Fixed Film Bioreactor, Journal of Environmental Science and Engineering.

[13]SK Singh,Y Srikanth. Role of microrganisms in waste water treatment, Jour. of Chemical Weekly, 4,1992.

Nomenclature

MGD	million gallon per day
mg/l	milligram per litre
MLD	million litres per day
STP	sewage treatment plant

Soft Computing
https://doi.org/10.1007/s00500-018-3358-8

FOCUS

Acceptably consistent incomplete interval-valued intuitionistic multiplicative preference relations

Mamata Sahu[1] · **Anjana Gupta**[1] · **Aparna Mehra**[2]

© Springer-Verlag GmbH Germany, part of Springer Nature 2018

Abstract
We study the consistency property, and especially the acceptably consistent property, for incomplete interval-valued intuitionistic multiplicative preference relations. We propose a technique which first estimates the initial values for all missing entries in an incomplete interval-valued intuitionistic multiplicative preference relation and then improves them by a local optimization method. Two examples are presented in order to illustrate applications of the proposed method in group decision-making problems.

Keywords Multiplicative preference relation · Interval-valued intuitionistic fuzzy number · Acceptably consistent preference relation · Multi-criteria group decision-making problems

1 Introduction

Multi-criteria group decision-making (MCGDM) problems aim to rank a finite number of alternatives based on specific criteria relevant to the characteristics of alternatives in context. The issues require deliberations from experts/decision makers and stakeholders to compare these alternatives on the pre-identified criteria. Different techniques for aggregating the elicited information thus received dates back to the classical works of Roy (1991) (ELECTRE), Saaty (1977, 1980) (AHP), Brans and Vincke (1985) (PROMETHEE), Hwang and Yoon (1981) (TOPSIS), to name a few. One can refer to the good texts (Figueira et al. 2005; Triantaphyllou 2000) for a detailed description of these methods along with numerous real-life case studies. The process of comparing different alternatives naturally embeds the preference of an alternative over the other alternatives by an expert, and hence preference relations are an integral part of such problems. Because of varying evaluation scales across the problems, the preference relations have been studied in more than one way, for instance, see (Alonso et al. 2010; Gong et al. 2011; Jiang et al. 2015; Kou et al. 2009; Liu et al. 2012; Xu 2004a, b, 2007a, b), and many more.

A preference relation on a finite set of alternatives $X = \{x_1, \ldots, x_n\}$ is represented by a matrix $R = [r_{ij}]_{n\times n}$ whose entries depict a certain form of preference information. A preference relation is classified primarily into two types: an additive preference relation, more commonly known as a fuzzy preference relation (FPR) (Fan et al. 2006; Orlovsky 1978; Ureña et al. 2015), where an expert provides the preference information using the $0-1$ scale, and a multiplicative preference relation (MPR) (Saaty 1977) in which the $(1/9)-9$ ratio scale is used to measure the intensity of the pairwise comparison of alternatives. Chiclana et al. (2001) proved that MPR and FPR are isomorphic.

On occasions, an expert is not habituated with some aspects of a criterion or an alternative and hence is not able to discriminate the preference degree of an option over the other. This situation leads Xu (2004b) to define an interval-valued fuzzy preference relation (IV-FPR) in which the preference degrees are described using intervals in [0, 1]. Xu (2004b) also provided a compatibility index to measure group consensus. Meng et al. (2017) pointed out shortcomings in the

Communicated by A. Genovese, G. Bruno.

✉ Anjana Gupta
anjanagupta@dce.ac.in

Mamata Sahu
munmun.sahu@gmail.com

Aparna Mehra
apmehra@maths.iitd.ac.in

[1] Department of Applied Mathematics, Delhi Technological University, Delhi 110042, India

[2] Department of Mathematics, Indian Institute of Technology Delhi, Hauz Khas, Delhi 110016, India

Published online: 03 July 2018

existing notions of multiplicative consistency for IV-FPR and formulated a new consistency notion for an IV-FPR.

Saaty and Vargas (1987) defined an interval-valued multiplicative preference relation (IV-MPR) allowing an expert to use the interval-values in $(1/9)-9$ scale to record their preferences. Liu (2009) introduced the notion of consistency for an IV-MPR and presented a formula of possibility degree approaching to rank interval weights for decision making. A linear programming method was proposed by Wang et al. (2005) to derive consistent interval weights from consistent IV-MPR. Yager and Xu (2006) developed a continuous ordered weighted geometric operator and presented its application to decision making with IV-MPR. Recently, Meng et al. (2017) noticed the limitations in the previously existing consistency concepts for IV-MPR and introduced a new consistency concept for IV-MPR with several desirable properties.

In the process of elicitation, an expert may not be completely confident about the preference degree, and it may so transpire that the negation of the preference degree is not the customary complement of the preference degree. In such cases, motivated by the idea of an intuitionistic fuzzy set (IFS) (Atanassov 2012), an expert prefers to express the imprecise cognition in the sense of positive (preference), negative (non-preference), and hesitant (indeterminacy) degrees leading to an intuitionistic preference relation (IPR). Szmidt and Kacprzyk (2002) and later Xu (2007b) studied intuitionistic fuzzy preference relations (I-FPR). Since an interval-valued fuzzy number is equivalent to an intuitionistic fuzzy number, an IV-FPR is isomorphic to an I-FPR.

Lio and Xu (2014) formulated a fractional programming problem to calculate priority weights of I-FPR using multiplicative consistency. Xu et al. (2016) introduced a new consistency index and used it to define an acceptable consistency for an I-FPR. They followed a goal-programming approach to simultaneously improve upon the consensus among several experts and consistency in their I-FPRs which are not acceptably consistent and consensus.

Recently, Wan et al. (2018) defined consistency and acceptable consistency of an interval-valued intuitionistic fuzzy preference relation (IVI-FPR) by separating it into two I-FPRs. A new three-phase method is proposed for GDM problems with IVI-FPRs by eliciting the full importance degrees of experts, extracting the most optimistic and pessimistic consistent I-FPRs from an IVI-FPR, and minimizing the deviations and the hesitancy degrees via linear goal-programming model. In another paper, Wan et al. (2017) designed a novel likelihood comparison algorithm to rank interval-valued intuitionistic fuzzy values. They also defined additive consistency of an IVI-FPR according to the additive consistency of I-FPR. They proposed a linear programming model by maximizing the group consensus to derive the weights of experts. Subsequently, a collective IVI-FPR is applied to calculate the priority weights. Using the likelihood comparison algorithm, the order of alternatives is generated by ranking their priority weights. Before these papers, Wan et al. (2016) put forward a new iterative algorithm to repair consistency of an IVI-FPR with unacceptable consistency. They established an optimization model by minimizing the deviations between each IVI-FPR and a collective one. A TOPSIS-based approach is designed to rank interval-valued Atanassov intuitionistic fuzzy (IVAIF) priority weights in MCGDM problems.

On the similar lines, an intuitionistic multiplicative number on an unbalanced scale of $(1/9)-9$ gives rise to an intuitionistic multiplicative preference relation (I-MPR) proposed by Xia et al. (2013). Each entry $\tilde{r}_{ij}$ in the matrix $\tilde{R}$ representing I-MPR is a two-tuple the first component in which is used for depicting the certainty degree of preference of an alternative x_i over an alternative x_j, and the second component is used to indicate the certainty degree of not preferring x_i to x_j. The surplus, one minus the sum of the first and the second components is an uncertainty degree (or an indeterminacy degree or hesitancy degree) of an expert in distinguishing between two extremes.

Xu (2013) developed a method to derive the priority weights of alternatives from an I-MPR. Jiang et al. (2013) defined compatibility measure for I-MPR and developed two models for group decision-making (GDM) problems. Some intuitionistic multiplicative aggregation operators were designed and applied to the GDM problems by Xia and Xu (2013).

In any of the framework mentioned above, although the scale and the domain of the preference relations may differ, yet an expert has to populate $n(n-1)/2$ judgments for presenting a complete preference relation matrix of order n. It is indeed an enormous task especially when n is reasonably large. Rezaei (2015) proposed the best-worst multi-criteria decision-making method which reduces the number of pairwise comparisons of n alternatives to $2n-3$. The technique requires identifying a priori the best among all and the worst among all criteria.

1.1 Incomplete preference relations and a research gap addressed in the present paper

The above-cited works assume that an expert is always able to provide information on each entry in a preference relation matrix. It may not be the case forever. An expert may not have expertise on a particular criterion or considers two alternatives incomparable on satisfied criterion(a). An extreme example is when an expert does not provide any information about an alternative on a particular criterion. This situation is called ignorance in the literature. As a result, an expert declines to make a comparison between two choices leading to an incomplete preference relation, that is,

a preference relation matrix with missing entries. The critical issue to address is how to apply the MCGDM methods in incomplete preference relations? The majority of the studies in the literature suggested carrying out a completion process before the aggregation of information in an MCGDM problem.

Though we shall be concentrating and studying a class of MPR (called interval-valued intuitionistic multiplicative preference relations), for the sake of convenience and completeness, we briefly present the literature on incomplete FPR and its various variants.

Xu (2004a) first studied an incomplete FPR. Fedrizzi and Giove (2007) proposed a method for calculating the missing values of an incomplete FPR. Alonso et al. (2008) defined four type of incomplete preference relations: incomplete FPR, incomplete MPR, incomplete interval-valued preference relations, incomplete linguistic preference relations based on the 2-tuple linguistic model. They used an iterative procedure to estimate the missing values in any incomplete relation using only the available preference data from experts. Alonso et al. (2010) presented a web consensus support system to deal with MCGDM problems with different types of incomplete preference relations. Chen et al. (2014) computed the missing preference values in an incomplete FPR based on additive consistency. They then constructed the modified consistency matrices which satisfy the additive consistency and order consistency simultaneously. Meng et al. (2017) formulated goal-programming models to determine missing values in an incomplete IV-FPR that have the highest consistent level concerning known values.

On the other hand, in the area of incomplete MPR, Harker (1987b) devised different methods for dropping the complexity of the eliciting process with incomplete MPR. Nishizawa (1997) developed an algorithm based on a directed graph for evaluating the elements in circles of various lengths in an intransitive incomplete MPR.

The process of checking consistency makes sure that the preferences of experts have no self-contradiction. The notion of consistency is the most important tool used to estimate the missing values in an incomplete preference relation (Liao et al. 2014). Xu and Cai (2009) introduced additive consistent, multiplicative consistent, and acceptably consistent incomplete preference relations. Xu (2012) extended an incomplete MPR into a complete MPR using multiplicative transitivity property and utilized a simple iterative procedure to improve consistency. Liu et al. (2012) initiated the notion of incomplete IV-MPR and presented an algorithm to obtain a priority vector from it based on the consistency property of IV-MPR. Meng and Tan (2017) defined a new notion of consistency for IV-MPR and applied it to formulate a 0–1 mixed goal-programming model to determine the missing values in an incomplete IV-MPR.

Jiang et al. (2015) introduced the concept of incomplete I-MPR and considered its application to MCGDM problems. They also talked about consistent and acceptably consistent incomplete I-MPRs. Two approaches were proposed to complement all missing elements of an incomplete I-MPR which involved the 'estimating step' and the 'adjusting step.'

To the best of our literature survey, there does not exist any study in the literature guiding how to populate the missing entries in an interval-valued intuitionistic multiplicative preference relation (IVI-MPR). This research gap incentivizes us to fixate on this topic in the present study.

1.2 Contributions of the present work

The present paper aims to analyze the class of IVI-MPR and incomplete IVI-MPR preference relations. The proposed work demonstrates an approach to determine the missing elements in an incomplete IVI-MPR. The procedure comprising of the estimating step (based on the elementary connecting paths of length two) and the adjusting step (requiring to solve an optimization problem iteratively) is formulated to determine all missing elements in an incomplete IVI-MPR.

1.3 Organization of the paper

The remainder of the paper unfolds as follows. Section 2 reviews the concepts of MPR, I-MPR, IVI-MPR, acceptable consistent IVI-MPR and incomplete IVI-MPR. In Sect. 3, a two-step procedure is devised to compute the missing entries of IVI-MPR. The algorithm uses the geometric mean to calculate the initial estimates of all missing entries in the first step called 'estimating step.' After that, an optimization model is presented to improve these initial estimates in the second step called the 'adjusting step.' Section 4 presents an application of incomplete IVI-MPR to MCGDM problems together with illustrative examples. Section 5 makes a comparative analysis of the proposed methodology with the two existing works relevant to the context. The paper concludes in Sect. 6. To comprehend the text, two Appendices, briefly describing operators on IFS and interval-valued IFS and a deviation model for computing the missing entries in IVI-MPR, are provided toward the end.

Since we shall be studying the multiplicative preference relations with information in $(1/9)-9$ ratio scale,[1] from now onward, we shall be concentrating on MPRs only.

[1] In Saaty (1977), the MPRs assessed on the discrete $(1/9)-9$ scale has values only in the set $\{1/9, 1/8, 1/7, \ldots, 1/2, 1, 2, \ldots, 7, 8, 9\}$.

Table 1 Random index

n	1	2	3	4	5	6	7	8	9	10
RI_n	0	0	0.52	0.89	1.11	1.25	1.35	1.40	1.45	1.49

2 Interval-valued intuitionistic multiplicative preference relation

Let $X = \{x_1, \ldots, x_n\}$ be a discrete set of alternatives in a decision-making problem which a decision maker has to compare in pairs. Set $N = \{1, \ldots, n\}$.

Definition 1 (Saaty 1977) A multiplicative preference relation (MPR) over X is defined by $R = [r_{ij}]_{n\times n}$ where r_{ij} is the preference value to which an alternative x_i is preferred to an alternative x_j satisfying

$$1/9 \le r_{ij} \le 9, \quad r_{ij} r_{ji} = 1\,, \; r_{ii} = 1, \; \forall\, i,\; j \in N.$$

Definition 2 (Saaty 1977) An MPR $R = [r_{ij}]_{n\times n}$ is said to be consistent if it satisfies the transitivity property, $r_{ij} = r_{ik} r_{kj}\,, \; \forall\, i,\; j,\; k \in N$.

For a consistent MPR, there exists a positive vector $w = (w_1, \ldots, w_n)^t$ such that $r_{ij} = \dfrac{w_i}{w_j}$, where w_i denotes the priority weight of $x_i,\; i \in N$, and $\sum_{i=1}^{n} w_i = 1$.

For an inconsistent MPR R, Saaty (1977) defined the consistency index CI and the consistency ratio CR to measure the level of inconsistency

$$\text{CI} = \frac{\lambda_{\max} - n}{n-1}\,, \quad \text{CR} = \frac{\text{CI}}{\text{RI}_n}\,,$$

where $\lambda_{\max}$ is the largest eigenvalue of the matrix $[r_{ij}]$ and RI_n is the random index (depending on the order n of a preference relation matrix) generated as an average CI of a large number of randomly generated MPRs of order n (see, Saaty 1977), and quoted in Table 1.

Definition 3 An MPR R is said to be acceptably consistent if $\text{CR} \le 0.1$, else R is announced not acceptably consistent (or simply inconsistent), and returned to an expert to have a re-look at the preferences evaluations.

Xia et al. (2013) extended MPR to develop a new preference relation in an intuitionistic framework.

Definition 4 (Xia et al. 2013) An intuitionistic multiplicative preference relation (I-MPR) is $\tilde{R} = [\tilde{r}_{ij}(x_i, x_j)]_{n\times n}$, where $\tilde{r}_{ij}(x_i, x_j) = (\mu(x_i, x_j), \nu(x_i, x_j))$, $i, j \in N$, is an intuitionistic multiplicative number (IMN), and $\mu(x_i, x_j)$ indicates certainty degree to which x_i is preferred to x_j and $\nu(x_i, x_j)$ is the certainty degree to which x_i is not preferred to x_j, and they satisfy the following characteristics:

$$\begin{aligned}
&1/9 \le \mu(x_i, x_j)\,, \quad \nu(x_i, x_j) \le 9\,,\\
&\mu(x_i, x_j) = \nu(x_j, x_i)\,, \quad \nu(x_i, x_j) = \mu(x_j, x_i)\,,\\
&\mu(x_i, x_i) = \nu(x_i, x_i) = 1,\\
&0 < \mu(x_i, x_j)\, \nu(x_i, x_j) \le 1, \; \forall\, i, j \in N.
\end{aligned}$$

If $\mu_{ij}(x_i, x_j)\, \nu_{ij}(x_i, x_j) = 1, \; \forall\; i, j \in N$, then the I-MPR $\tilde{R}$ is equivalent to a MPR.

For convenience and without ambiguity, we shall be denoting $\tilde{r}_{ij}(x_i, x_j) = (\mu(x_i, x_j), \nu(x_i, x_j))$ by $\tilde{r}_{ij} = (\mu_{ij}, \nu_{ij})$.

Xu (2013) defined the notion of consistency for I-MPR $\tilde{R} = [\tilde{r}_{ij}]_{n\times n} = [(\mu_{ij},\; \nu_{ij})]_{n\times n}$ using multiplicative transitivity.

Definition 5 An I-MPR $\widetilde{R}$ is called multiplicative transitive if

$$\mu_{ij} = \mu_{ik}\, \mu_{kj}\,, \nu_{ij} = \nu_{ik}\, \nu_{kj}\,, \forall\, i \le k \le j, \quad i, k, j \in N. \tag{1}$$

Note that, in an I-MPR, the multiplicative transitivity property is restricted to indices (that is, $i \le k \le j$) while the similar property in MPR (Definition 2) is described to hold for all indices $i,\; j,\; k \in N$.

Jiang et al. (2014) introduced the concept of interval-valued intuitionistic multiplicative set (IVI-MS) as follows.

$$\tilde{D} = \{\langle x, \tilde{\mu}_D(x), \tilde{\nu}_D(x)\rangle \mid x \in X\},$$

where $\tilde{\mu}(x) \subseteq [1/9, 9]$ and $\tilde{\nu}(x) \subseteq [1/9, 9]$ are intervals satisfying $0 < \sup_{x\in X} \tilde{\mu}(x)\, \sup_{x\in X} \tilde{\nu}(x) \le 1$. The pair $(\tilde{\mu}_D(x), \tilde{\nu}_D(x))$ is called interval-valued intuitionistic multiplicative number (IVI-MN).

Based on the result of Jiang et al. (2014), interval-valued intuitionistic multiplicative preference relation (IVI-MPR) is introduced where the preference degree and the non-preference degree of x_i over x_j are now interval-valued. Let us denote $\widetilde{r}_{ij}(x_i, x_j) = ([\underline{\mu}_{ij}(x_i, x_j), \overline{\mu}_{ij}(x_i, x_j)], [\underline{\nu}_{ij}(x_i, x_j), \overline{\nu}_{ij}(x_i, x_j)])$ by $\widetilde{r}_{ij} = ([\underline{\mu}_{ij}, \overline{\mu}_{ij}],\; [\underline{\nu}_{ij}, \overline{\nu}_{ij}])$.

Definition 6 *(IVI-MPR)* An IVI-MPR is defined as $\widetilde{R} = [\widetilde{r}_{ij}]_{n\times n}$, where $\widetilde{r}_{ij} = ([\underline{\mu}_{ij}, \overline{\mu}_{ij}]\;\; [\underline{\nu}_{ij}, \overline{\nu}_{ij}])$, $i, j \in N$, and $[\underline{\mu}_{ij},\; \overline{\mu}_{ij}]$ indicates the interval of certainty degree to which x_i is preferred to x_j, while $[\underline{\nu}_{ij},\; \overline{\nu}_{ij}]$ is the interval of certainty degree to which x_i is not preferred to x_j, and they satisfy the following characteristics:

$$\begin{aligned}
&1/9 \le \underline{\mu}_{ij} \le \overline{\mu}_{ij} \le 9, \quad 1/9 \le \underline{\nu}_{ij} \le \overline{\nu}_{ij} \le 9\,,\\
&0 \le \overline{\mu}_{ij}\, \overline{\nu}_{ij} \le 1,\\
&[\underline{\mu}_{ij}\,,\; \overline{\mu}_{ij}] = [\underline{\nu}_{ji}\,,\; \overline{\nu}_{ji}]\,,\\
&[\underline{\nu}_{ij}\,,\; \overline{\nu}_{ij}] = [\underline{\mu}_{ji}\,,\; \overline{\mu}_{ji}]\,,\\
&[\underline{\mu}_{ii}\,,\; \overline{\mu}_{ii}] = [\underline{\nu}_{ii}\,,\; \overline{\nu}_{ii}] = [1, 1]\,, \quad \forall\, i, j \in N.
\end{aligned}$$

If we define consistency for IVI-MPR by simply extending the relation in (1) as follows:

$$\begin{aligned}&([\underline{\mu}_{ij}, \overline{\mu}_{ij}],\ [\underline{\nu}_{ij}, \overline{\nu}_{ij}])\\&= ([\underline{\mu}_{ik}, \overline{\mu}_{ik}][\underline{\mu}_{kj}, \overline{\mu}_{kj}],\ [\underline{\nu}_{ik}, \overline{\nu}_{ik}][\underline{\nu}_{kj}, \overline{\nu}_{kj}]),\\&\quad i \le k \le j\ ,\ i,\ j,\ k \in N\ ,\end{aligned} \tag{2}$$

where, $\underline{\mu}_{ij} = \min\{\underline{\mu}_{ik}\underline{\mu}_{kj},\ \underline{\mu}_{ik}\overline{\mu}_{kj},\ \overline{\mu}_{ik}\underline{\mu}_{kj},\ \overline{\mu}_{ik}\overline{\mu}_{kj}\}, \overline{\mu}_{ij} = \max\{\underline{\mu}_{ik}\underline{\mu}_{kj},\ \underline{\mu}_{ik}\overline{\mu}_{kj},\ \overline{\mu}_{ik}\underline{\mu}_{kj},\ \overline{\mu}_{ik}\overline{\mu}_{kj}\}$, $\underline{\nu}_{ij} = \min\{\underline{\nu}_{ik}\underline{\nu}_{kj},\ \underline{\nu}_{ik}\overline{\nu}_{kj},\ \overline{\nu}_{ik}\underline{\nu}_{kj},\ \overline{\nu}_{ik}\overline{\nu}_{kj}\}, \overline{\nu}_{ij} = \max\{\underline{\nu}_{ik}\underline{\nu}_{kj},\ \underline{\nu}_{ik}\overline{\nu}_{kj},\ \overline{\nu}_{ik}\underline{\nu}_{kj},\ \overline{\nu}_{ik}\overline{\nu}_{kj}\}$, then an IVI-MPR $\widetilde{R}$ may not be consistent according to (2).

For example, consider an IVI-MPR described by

$$\widetilde{R} = \begin{bmatrix} ([1,1],[1,1]) & ([\frac{1}{6},\frac{1}{5}],[3,4]) & ([\frac{1}{3},\frac{1}{3}],[3,3]) \\ ([3,4],[\frac{1}{6},\frac{1}{5}]) & ([1,1],[1,1]) & ([\frac{1}{4},\frac{1}{3}],[\frac{1}{5},\frac{3}{2}]) \\ ([3,3],[\frac{1}{3},\frac{1}{3}]) & ([\frac{1}{5},\frac{3}{2}],[\frac{1}{4},\frac{1}{3}]) & ([1,1],[1,1]) \end{bmatrix} \tag{3}$$

We have

$$\begin{aligned}\widetilde{r}_{12}\,\widetilde{r}_{23} &= ([\underline{\mu}_{12}, \overline{\mu}_{12}][\underline{\mu}_{23}, \overline{\mu}_{23}],\ [\underline{\nu}_{12}, \overline{\nu}_{12}][\underline{\nu}_{23}, \overline{\nu}_{23}])\\&= ([0.04167, 0.067],\ [0.6, 6]) \neq \widetilde{r}_{13}\ ,\end{aligned}$$

hence, the above $\widetilde{R}$ is not consistent according to (2).

To overcome the limitation, imposed by the restriction on indices in the transitivity property, we discuss a more general consistent property of an IVI-MPR by splitting an IVI-MPR into matrices.

An interval-valued intuitionistic multiplicative number (IVI-MN) $\widetilde{r}_{ij} = ([\underline{\mu}_{ij}, \overline{\mu}_{ij}],\ [\underline{\nu}_{ij}, \overline{\nu}_{ij}])$ contains two parts, $[\underline{\mu}_{ij}, \overline{\mu}_{ij}]$ is the preferred information and $[\underline{\nu}_{ij}, \overline{\nu}_{ij}]$ is the non-preferred information. In this sense, an IVI-MPR $\widetilde{R} = [\widetilde{r}_{ij}]_{n\times n}$ can be split into two matrices, $A = [a_{ij}]_{n\times n}$ and $B = [b_{ij}]_{n\times n}$ expressing the preferred information and the non-preferred information in $\widetilde{R}$, respectively. The concrete forms are listed as follows.

$$a_{ij} = \begin{cases} [\underline{\mu}_{ij}, \overline{\mu}_{ij}] & i < j \\ [1,1] & i = j \\ [\dfrac{1}{\overline{\nu}_{ij}}, \dfrac{1}{\underline{\nu}_{ij}}] & i > j \end{cases} \text{ and } b_{ij} = \begin{cases} [\underline{\nu}_{ij}, \overline{\nu}_{ij}] & i < j \\ [1,1] & i = j \\ [\dfrac{1}{\overline{\mu}_{ij}}, \dfrac{1}{\underline{\mu}_{ij}}] & i > j \end{cases} \tag{4}$$

For instance, going back to example in (3) of IVI-MPR $\widetilde{R}$, we have

$$A = \begin{bmatrix} [1,1] & [\frac{1}{6},\frac{1}{5}] & [\frac{1}{3},\frac{1}{3}] \\ [5,6] & [1,1] & [\frac{1}{4},\frac{1}{3}] \\ [3,3] & [3,4] & [1,1] \end{bmatrix},$$

$$B = \begin{bmatrix} [1,1] & [3,4] & [3,3] \\ [\frac{1}{4},\frac{1}{3}] & [1,1] & [\frac{1}{5},\frac{3}{2}] \\ [\frac{1}{3},\frac{1}{3}] & [\frac{2}{3},5] & [1,1] \end{bmatrix}.$$

Definition 7 (Liu 2009) An interval-valued multiplicative reciprocal matrix $S = [\tilde{s}_{ij}]_{n\times n} = ([s_{ij}^-, s_{ij}^+])_{n\times n}$, where

$$S = \begin{bmatrix} [1,1] & [s_{12}^-, s_{12}^+] & \cdots & [s_{1n}^-, s_{1n}^+] \\ [s_{21}^-, s_{21}^+] & [1,1] & \cdots & [s_{2n}^-, s_{2n}^+] \\ \vdots & \vdots & \cdots & \vdots \\ [s_{n1}^-, s_{n2}^+] & [s_{n2}^-, s_{n2}^+] & \cdots & [1,1] \end{bmatrix},$$

with $0 \le s_{ij}^- \le s_{ij}^+,\ \ s_{ij}^- s_{ji}^+ = 1,\ \ s_{ij}^+ s_{ji}^- = 1$, is said to be consistent if the two multiplicative reciprocal matrices, $S^{(1)} = [s_{ij}^{(1)}]_{n\times n}$ and $S^{(2)} = [s_{ij}^{(2)}]_{n\times n}$, obtained by splitting S as follows, are consistent, where

$$s_{ij}^{(1)} = \begin{cases} s_{ij}^+ & i < j \\ 1 & i = j \\ s_{ij}^- & i > j \end{cases} \text{ and } s_{ij}^{(2)} = \begin{cases} s_{ij}^- & i < j \\ 1 & i = j \\ s_{ij}^+ & i > j\ . \end{cases} \tag{5}$$

Here, by consistency of matrices $S^{(1)}$ and $S^{(2)}$, we mean that they both satisfy the transitivity property $s_{ij}^{(1)} = s_{ik}^{(1)} s_{kj}^{(1)}$ and $s_{ij}^{(2)} = s_{ik}^{(2)} s_{kj}^{(2)},\ \forall\, i, j, k \in N$.

Motivated by Definition 7, we propose to further split the matrix A into $C^{(q)},\ q = 1, 2$, and matrix B into $C^{(q)},\ q = 3, 4$, in spirit of (5). The elements in $C^{(q)}$ satisfy the relation $c_{ij}^{(q)}\, c_{ji}^{(q)} = 1,\ \forall\, i, j \in N$, and $q = 1, 2, 3, 4$. Thus, $[c_{ij}^{(q)}]_{n\times n},\ q = 1, 2, 3, 4$, are four MPRs obtained from an IVI-MPR $\widetilde{R}$.

Definition 8 An IVI-MPR $\widetilde{R} = [\widetilde{r}_{ij}]_{n\times n} = ([\underline{\mu}_{ij}, \overline{\mu}_{ij}],\ [\underline{\nu}_{ij}, \overline{\nu}_{ij}])_{n\times n}$, is said to be consistent if the four MPRs $C^{(q)},\ q = 1, 2, 3, 4$, obtained using (4) and (5), are consistent, that means

$$c_{ij}^{(q)} = c_{ik}^{(q)}\, c_{kj}^{(q)},\quad \forall\, i, j, k \in N,\ q = 1, 2, 3, 4. \tag{6}$$

Definition 9 An IVI-MPR $\widetilde{R} = [\widetilde{r}_{ij}]_{n\times n} = ([\underline{\mu}_{ij}, \overline{\mu}_{ij}],\ [\underline{\nu}_{ij}, \overline{\nu}_{ij}])_{n\times n}$ is called acceptably consistent if the four MPRs $C^{(q)},\ q = 1, 2, 3, 4$, obtained using (4) and (5), are acceptably consistent; otherwise $\widetilde{R}$ is called not acceptably consistent or inconsistent.

Consider an IVI-MPR given by

$$\tilde{R} = \begin{bmatrix} ([1,1],[1,1]) & ([3,4],[\frac{1}{5},\frac{1}{4}]) & ([2,3],[\frac{1}{9},\frac{1}{8}]) \\ ([\frac{1}{5},\frac{1}{4}],[3,4]) & ([1,1],[1,1]) & ([\frac{2}{3},\frac{3}{2}],[\frac{1}{4},\frac{1}{2}]) \\ ([\frac{1}{9},\frac{1}{8}],[2,3]) & ([\frac{1}{4},\frac{1}{2}],[\frac{2}{3},\frac{3}{2}]) & ([1,1],[1,1]) \end{bmatrix}.$$

This IVI-MPR is split into the following four MPRs

$$C^{(1)} = \begin{bmatrix} 1 & 4 & 3 \\ \frac{1}{4} & 1 & \frac{3}{2} \\ \frac{1}{3} & \frac{2}{3} & 1 \end{bmatrix}, \quad C^{(2)} = \begin{bmatrix} 1 & 3 & 2 \\ \frac{1}{3} & 1 & \frac{2}{3} \\ \frac{1}{2} & \frac{3}{2} & 1 \end{bmatrix}$$

$$C^{(3)} = \begin{bmatrix} 1 & \frac{1}{4} & \frac{1}{8} \\ 4 & 1 & \frac{1}{2} \\ 8 & 2 & 1 \end{bmatrix}, \quad C^{(4)} = \begin{bmatrix} 1 & \frac{1}{5} & \frac{1}{9} \\ 5 & 1 & \frac{1}{4} \\ 9 & 4 & 1 \end{bmatrix}.$$

Observe $C^{(1)}$ and $C^{(4)}$ are not consistent, whereas $C^{(2)}$ and $C^{(3)}$ are consistent (in spirit of Definition 2). Moreover, CR < 0.1 for all four matrices. Hence $\tilde{R}$ is not consistent but acceptably consistent.

Now, if we replace $\underline{v}_{12} = \frac{1}{5}$ by $\underline{v}_{12} = \frac{1}{7}$ in $\tilde{R}$, then the CR of the MPR $C^{(4)}$ is 0.1392; and then $\tilde{R}$ is not acceptably consistent.

We next propose to extend the above situation to incomplete IVI-MPR where some elements are missing in the preference relation matrix.

Definition 10 An IVI-MPR $\widetilde{R} = [\widetilde{r}_{ij}]_{n\times n} = ([\underline{\mu}_{ij}, \overline{\mu}_{ij}], [\underline{v}_{ij}, \overline{v}_{ij}])_{n\times n}$ is called an incomplete IVI-MPR if some elements in it are missing, and all available elements satisfy the characteristics of IVI-MPR stated in Definition 6.

Definition 11 An incomplete IVI-MPR $\widetilde{R} = [\widetilde{r}_{ij}]_{n\times n} = ([\underline{\mu}_{ij}, \overline{\mu}_{ij}], [\underline{v}_{ij}, \overline{v}_{ij}])_{n\times n}$ is called consistent if all known elements of the associated four MPRs $C^{(q)}$, $q = 1, 2, 3, 4$, satisfy condition in (6).

Definition 12 An incomplete IVI-MPR $\widetilde{R} = [\widetilde{r}_{ij}]_{n\times n} = ([\underline{\mu}_{ij}, \overline{\mu}_{ij}], [\underline{v}_{ij}, \overline{v}_{ij}])_{n\times n}$ is called acceptably consistent if the associated four MPRs $C^{(q)}$, $q = 1, 2, 3, 4$, are acceptably consistent; otherwise, $\widetilde{R}$ is called not acceptably consistent or inconsistent.

3 Complementing the incomplete IVI-MPR

In this section, taking inspiration from the work of Jiang et al. (2015), we propose a two-step procedure to calculate all missing entries in an IVI-MPR. The idea is first to estimate their values using the simple connecting path approach and subsequently improve upon them using an optimization problem. In the latter step, an optimization problem is constructed so to achieve transitivity and hence acceptably consistent resultant complete IVI-MPR. The objective function of the optimization problem is designed to minimize the overall absolute error occurring in the transitivity equation of the logarithmic values of the (missing) entries in an IVI-MPR. The detailed description of the procedure is laid down in the following sections.

3.1 Estimating step

We first review the work of Harker (1987a, b) who designed a geometric mean method based on connecting paths to complement the missing elements in an incomplete MPR.

The general construction of a connecting path of length $\ell + 1$, denoted by $cp_{(\ell+1)}$, has the following form: $cp_{(\ell+1)}$: $*_{ij} = p_{i\,k_1} p_{k_1\,k_2} \cdots p_{k_\ell\,j}$, where $*_{ij}$ denotes the missing element to be estimated and the elements on the right-hand side are known entities in the path connecting i with j, where $i, j, k_1, \ldots, k_\ell \in N$, $0 \le \ell \le n-2$. The connecting path of length two is an elementary connecting path $cp_{(2)} : *_{ij} = p_{i\,k_1} p_{k_1\,j}$ for $k_1 \in N$, and $k_1 \neq i, j$. Harker (1987a, b) argued that the value of the missing element $*_{ij}$ is the geometric mean of all elementary connecting paths related to it with no vertex repeats more than once in the path. Consequently, $*_{ij} = \left(\prod_{r=1}^{n_\ell} cp_{(r)}\right)^{1/n_\ell}$, where n_ℓ is the number of all possible connecting fully known paths (that is, no missing entries along the path) from i to j. A major limitation of this method is that the number of connecting paths of different lengths between i and j may be extremely large and computationally intractable for many real problems. For instance, Deschrijver and Kerre (2003) presented an example of a matrix of size 10 only with the number of connecting paths exceeding 109,000. Jiang et al. (2015) improved this method for incomplete I-MPR. We are inspired by this work and extend their method to the incomplete IVI-MPR.

We shall be using the following notations.

Let Ω be the set of all known elements in IVI-MPR $\widetilde{R} = [\widetilde{r}_{ij}]_{n\times n}$; $\Gamma = \{(i, j) \in N \times N \,|\, \widetilde{r}_{ij} \text{ is missing}\}$; the associated four MPRs be $C^{(q)} = [c_{ij}^{(q)}]_{n\times n}$, $q = 1, 2, 3, 4$; $\Omega^{(q)}$ be the set of all known elements in $C^{(q)}$, $q = 1, 2, 3, 4$; $\Gamma^{(q)} = \{(i, j) \in N \times N \,|\, c_{ij}^{(q)} \text{ is missing}\}$, $q = 1, 2, 3, 4$. Then, $\Omega = \bigcup_{q=1}^{4} \Omega^{(q)}$ and $\Gamma = \bigcup_{q=1}^{4} \Gamma^{(q)}$.

The missing value $\widetilde{*}_{ij} = ([c_{ij}^{(*2)}, c_{ij}^{(*1)}], [c_{ij}^{(*4)}, c_{ij}^{(*3)}])$ can be estimated by

$$c_{ij}^{(*q)} = \left(\prod_{k_1 \in MC_{ij}^{(q)}} \left(c_{ik_1}^{(q)} c_{k_1 j}^{(q)} \right) \right)^{\frac{1}{mc_{ij}^{(q)}}}, \quad q = 1, 2, 3, 4, \qquad (7)$$

where $MC_{ij}^{(q)} = \{k_1 \,|\, c_{ik_1}^{(q)}, c_{k_1 j}^{(q)} \in \Omega^{(q)}\}$, and $mc_{ij}^{(q)}$ is the cardinality of the set $MC_{ij}^{(q)}$, $q = 1, 2, 3, 4$.

If the length of the path $cp_{(\ell+1)}$ increases, then the value of $c_{ij}^{(*q)} \equiv \widetilde{*}_{ij}$ decreases. It means that the value of $*_{ij}$ is largely determined by the paths of smaller lengths. The elementary connecting paths of length 2 are indeed the smallest one and hence significant contributors to estimating the value of $\widetilde{*}_{ij}$. This idea is used in formulating (7). We shall be denoting the initial values, obtained from (7), by $\widetilde{*}_{ij}^{((0))}$, $i, j \in N$.

3.2 Adjusting step: optimization model

If $\widetilde{R}$ is an incomplete IVI-MPR, then at least one of the associated four MPRs $C^{(q)}$ is an incomplete MPR. In other words, an incomplete IVI-MPR $\widetilde{R}$ can be complemented by complementing $C^{(q)}$. This task is proposed to be accomplished by solving an optimization problem.

If $\widetilde{R}$ is consistent then by Definition 8, (6) holds, and hence we have,

$$\log c_{ij}^{(q)} = \log c_{ik}^{(q)} + \log c_{kj}^{(q)}, \quad i,\ j,\ k \in N,\ i \neq j \neq k,\ q = 1, 2, 3, 4. \tag{8}$$

Using this, we propose to solve the following scalar-optimization problem (P) (next page) which aims at minimizing the total absolute error in (8). The formulation of (P) is in the spirit to ensure that the optimal values lie in the interval range of IVI-MPR. Also, the optimal values of the missing entries will bring the complete IVI-MPR more closer (if not exactly) to acceptably consistent.

Starting from the initial values $c_{ij}^{(*q)((0))}$ for $c_{ij}^{(*q)}$, $(i, j) \in \Gamma^{(q)}$, $q = 1, 2, 3, 4$, model (P) is iteratively solved to generate all unknown elements in the incomplete MPRs $C^{(q)}$, $q = 1, 2, 3, 4$. Consequently the complete IVI-MPR $\widetilde{R}$ can be obtained.

The following two examples illustrate the above methodology for finding the missing elements in an IVI-MPR.

$$\widetilde{R} = \begin{bmatrix} ([1,1],[1,1]) & ([1/6,1/5],[*,*]) & ([*,1/3],[3,3]) \\ ([*,*],[1/6,1/5]) & ([1,1],[1,1]) & ([1/4,*],[1/5,3/2]) \\ ([3,3],[*,1/3]) & ([1/5,3/2],[1/4,*]) & ([1,1],[1,1]) \end{bmatrix}$$

where $*$ denotes the missing element. Using (4) and (5), the associated four MPRs are as follows:

$$C^{(1)} = \begin{bmatrix} 1 & 1/5 & 1/3 \\ 5 & 1 & c_{23}^{(*1)} \\ 3 & 1/c_{23}^{(*1)} & 1 \end{bmatrix}, \quad C^{(2)} = \begin{bmatrix} 1 & 1/6 & c_{13}^{(*2)} \\ 6 & 1 & 1/4 \\ 1/c_{13}^{(*2)} & 4 & 1 \end{bmatrix},$$

$$C^{(3)} = \begin{bmatrix} 1 & c_{12}^{(*3)} & 3 \\ 1/c_{12}^{(*3)} & 1 & 3/2 \\ 1/3 & 2/3 & 1 \end{bmatrix}, \quad C^{(4)} = \begin{bmatrix} 1 & c_{12}^{(*4)} & 3 \\ 1/c_{12}^{(*4)} & 1 & 1/5 \\ 1/3 & 5 & 1 \end{bmatrix}.$$

The initial values of the missing elements are calculated using (7) as follows:

$$c_{23}^{(*1)((0))} = c_{21}^{(1)} c_{13}^{(1)} = 1.67,\ c_{13}^{(*2)((0))} = c_{12}^{(2)} c_{23}^{(2)} = 0.041,$$
$$c_{12}^{(*3)((0))} = c_{13}^{(3)} c_{32}^{(3)} = 2,\ c_{12}^{(*4)((0))} = c_{13}^{(4)} c_{32}^{(4)} = 15.$$

Sometimes the initial values do not lie in the range of IVI-MPRs, like the values $c_{13}^{(*2)((0))}$ and $c_{12}^{(*4)((0))}$ in above example. To adjust these initial values, we solve problem (P) using LINGO software, and after 34 iterations we obtain

$$c_{23}^{(*1)} = 0.667, \quad c_{13}^{(*2)} = 0.111, \quad c_{12}^{(*3)} = 5, \quad c_{12}^{(*4)} = 5.$$

Therefore, the complete IVI-MPR is

$$\widetilde{R} = \begin{bmatrix} ([1,1],[1,1]) & ([1/6,1/5],[5,5]) & ([0.111,1/3],[3,3]) \\ ([5,5],[1/6,1/5]) & ([1,1],[1,1]) & ([1/4,0.667],[1/5,3/2]) \\ ([3,3],[0.111,1/3]) & ([1/5,3/2],[1/4,0.667]) & ([1,1],[1,1]) \end{bmatrix}.$$

Example 1 Consider a simple case involving an incomplete IVI-MPR with at most one missing entry in $C^{(q)}$, $q = 1, 2, 3, 4$.

Since the CR for $C^{(q)}$, $q = 2, 4$, are greater than 0.1, the complete IVI-MPR $\widetilde{R}$ is not acceptably consistent.

$$(P) \quad \min \sum_{q=1}^{4} \sum_{(i,j)\in\Gamma^{(q)}} \sum_{k\in\Omega^{(q)}} \varepsilon_{ijk}^{c^{(q)}}$$

subject to

$$\begin{aligned} \varepsilon_{ijk}^{c^{(q)}} - |\log c_{ij}^{(q)} - (\log c_{ik}^{(q)} + \log c_{kj}^{(q)})| &= 0 && q = 1, 2, 3, 4, \\ c_{ij}^{(q)} &\geq (1/9) && q = 1, 2 \\ c_{ij}^{(q)} &\leq 9 && q = 3, 4 \\ c_{ij}^{(q)}\, c_{ij}^{(q+2)} &\leq 1 && q = 1, 2,\ i,\ j,\ k \in N,\ i \neq j \neq k \\ c_{ij}^{(q+1)} &\leq c_{ij}^{(q)} && q = 1, 3,\ i < j,\ i,\ j \in N \\ c_{ij}^{(q+1)} &\geq c_{ij}^{(q)} && q = 1, 3,\ i > j,\ i,\ j \in N. \end{aligned}$$

Example 2 Consider an incomplete IVI-MPR with more than one missing element in the associated MPRs.

$$\widetilde{R} = \begin{bmatrix} ([1,1],[1,1]) & ([*,*],[*,*]) & ([0.2,0.4],[0.3,0.5]) & ([0.2,0.4],[0.4,*]) \\ ([*,*],[*,*]) & ([1,1],[1,1]) & ([0.2,0.3],[*,0.7]) & ([*,0.4],[0.4,0.6]) \\ ([0.3,0.5],[0.2,0.4]) & ([*,0.7],[0.2,0.3]) & ([1,1],[1,1]) & ([0.2,0.2],[0.5,0.7]) \\ ([0.4,*],[0.2,0.4]) & ([0.4,0.6],[*,0.4]) & ([0.5,0.7],[0.2,0.2]) & ([1,1],[1,1]) \end{bmatrix}.$$

The associated four MPRs are as follows:

$$C^{(1)} = \begin{bmatrix} 1 & c_{12}^{(*1)} & 0.4 & 0.4 \\ 1/c_{12}^{(*1)} & 1 & 0.3 & 0.4 \\ 1/0.4 & 1/0.3 & 1 & 0.2 \\ 1/0.4 & 1/0.4 & 1/0.2 & 1 \end{bmatrix},$$

$$C^{(2)} = \begin{bmatrix} 1 & c_{12}^{(*2)} & 0.2 & 0.2 \\ 1/c_{12}^{(*2)} & 1 & 0.2 & c_{24}^{(*2)} \\ 1/0.2 & 1/0.2 & 1 & 0.2 \\ 1/0.2 & 1/c_{24}^{(*2)} & 1/0.2 & 1 \end{bmatrix},$$

$$C^{(3)} = \begin{bmatrix} 1 & c_{12}^{(*3)} & 0.5 & c_{14}^{(*3)} \\ 1/c_{12}^{(*3)} & 1 & 0.7 & 0.6 \\ 1/0.5 & 1/0.7 & 1 & 0.7 \\ 1/c_{14}^{(*3)} & 1/0.6 & 1/0.7 & 1 \end{bmatrix},$$

$$C^{(4)} = \begin{bmatrix} 1 & c_{12}^{(*4)} & 0.3 & 0.4 \\ 1/c_{12}^{(*4)} & 1 & c_{23}^{(*4)} & 0.4 \\ 1/0.3 & 1/c_{23}^{(*4)} & 1 & 0.5 \\ 1/0.4 & 1/0.4 & 1/0.5 & 1 \end{bmatrix}.$$

The following initial values of missing elements are calculated using (7)

$$\begin{aligned} c_{12}^{(*1)((0))} &= [(c_{13}^{(1)} c_{32}^{(1)})\,(c_{14}^{(1)} c_{42}^{(1)})]^{1/2} = 1.1547, \\ c_{12}^{(*2)((0))} &= c_{13}^{(2)} c_{32}^{(2)} = 1, \\ c_{24}^{(*2)((0))} &= c_{23}^{(2)} c_{34}^{(2)} = 0.04, \\ c_{12}^{(*3)((0))} &= c_{13}^{(3)} c_{32}^{(3)} = 0.7143\,, \\ c_{14}^{(*3)((0))} &= c_{13}^{(3)} c_{34}^{(3)} = 0.35, \\ c_{12}^{(*4)((0))} &= c_{14}^{(4)} c_{42}^{(4)} = 1\,, \\ c_{23}^{(*4)((0))} &= c_{24}^{(4)} c_{43}^{(4)} = 0.8. \end{aligned}$$

In this case $c_{24}^{(*2)((0))} = 0.04$ does not satisfies the condition of IVI-MPRs. To adjust the initial value solving problem (P) in LINGO, after 42 iteration yield, $c_{12}^{(*1)} = 1$, $c_{12}^{(*2)} = 1$, $c_{24}^{(*2)} = 0.111$, $c_{12}^{(*3)} = 0.714$, $c_{14}^{(*3)} = 0.4$, $c_{12}^{(*4)} = 0.714$, $c_{23}^{(*4)} = 0.7$.

It is observed that $C^{(q)}$, $q = 2, 3, 4$, are acceptably consistent while CR of $C^{(1)} = 0.155 > 0.1$; hence it is not acceptably consistent.

4 Acceptably consistent multi-criteria group decision making

For a more informed recommendation, it is essential to have a collective opinion of experts and participating stakeholders. Though GDM mostly increases the complexity of decision making yet, it is unavoidable in many strategic decisions. In this section, we aim to extend the results of the earlier section to GDM.

Consider m decision makers/experts and their weight vector $w = (w_1, \ldots, w_m)^t$, with $w_i \geq 0$, and $\sum_{i=1}^{m} w_i = 1$. Set, $M = \{1, \ldots, m\}$. Suppose each decision maker e_g ($g \in M$) provides a preference relation matrix in the form of IVI-MPR $\widetilde{R}_g = [\widetilde{r}_{ij,g}]_{n\times n} = ([\underline{\mu}_{ij,g}, \overline{\mu}_{ij,g}],\ [\underline{\nu}_{ij,g}, \overline{\nu}_{ij,g}])$.

Before proceeding ahead, we must verify whether each preference matrix $\widetilde{R}_g$ is consistent. This can be accomplished by invoking the following result from Elsner et al. (1988) (see, Theorem 1) on acceptably consistent aggregation of MPRs.

Proposition 1 *Let m experts provide $n \times n$ acceptably consistent MPRs, $T_1 = [t_{ij}^{(1)}], \ldots, T_m = [t_{ij}^{(m)}]$. Let the importance (or weight) of the g-th expert be γ_g, $\gamma_g \in (0,1)$, $g = 1, \ldots, m$, $\sum_{g=1}^{m} \gamma_g = 1$. Then, the weighted geometric mean aggregated MPR, $\overline{T} = [\overline{t_{ij}}]_{n\times n} = T_1^{\gamma_1} T_2^{\gamma_2} \cdots T_m^{\gamma_m}$, where $\overline{t_{ij}} = \prod_{g=1}^{m} \left(t_{ij}^{(g)}\right)^{\gamma_g}$, $\forall\ (i,j) \in N \times N$, is an acceptably consistent MPR.*

Proof Since T_g, $g = 1, \ldots, m$, are acceptably consistent MPRs, by Definition 3, we have

$$\lambda_{T_g,\max} < 0.1(n-1)\,\mathrm{RI}_n + n, \quad g = 1, \ldots, m\,,$$

where $\lambda_{T_g,\max}$ denotes the maximum eigenvalue of the MPR matrix T_g. The above along with $\sum_{g=1}^{m} \gamma_g = 1$, yields

$$\prod_{g=1}^{m}(\lambda_{T_g,\max})^{\gamma_g} < 0.1(n-1)\,\mathrm{RI}_n + n. \tag{9}$$

Invoking the following result from Elsner et al. (1988),

$$\rho(\overline{T}) = \rho(T_1^{\gamma_1}\,T_2^{\gamma_2}\cdots T_m^{\gamma_m}) \le \rho(T_1)^{\gamma_1}\rho(T_2)^{\gamma_2}\cdots\rho(T_m)^{\gamma_m},$$

where $\rho(T_g)$ is the spectral radius of the MPR matrix T_g, along with (9), we get,

$$\lambda_{\overline{T},\max} < 0.1\,(n-1)\,\mathrm{RI}_n + n,$$

yielding acceptably consistent MPR $\overline{T}$. □

Remark 1 It may so happen that each MPR is not acceptably consistent, but the weighted geometric mean aggregated MPR is acceptably consistent.

Let m decision makers provide $n \times n$ MPRs out of which k MPRs are acceptably consistent and remaining $m-k$ are not acceptably consistent. Suppose $T_1, \ldots, T_k$ are acceptably consistent while $T_{k+1}, \ldots, T_m$ are not acceptably consistent. By above Proposition, for any scalars $\gamma_1, \ldots, \gamma_k$, all in (0, 1) with their sum being 1, the weighted geometric mean aggregated MPR $\overline{T} = T_1^{\gamma_1}T_2^{\gamma_2}\cdots T_k^{\gamma_k}$ is acceptably consistent.

Petra and Lidija (2012) provided the following sufficient condition for the weighted geometric mean aggregated MPR, constituted from the MPRs $\overline{T}$, $T_{k+1}, \ldots, T_m$, to be acceptably consistent, and that is,

$$(\lambda_{\overline{T},\max})^{\delta}(\lambda_{T_{k+1},\max})^{\delta_1}\cdots(\lambda_{T_m,\max})^{\delta_{m-k}} < (n-1)\beta\,\mathrm{RI}_n + n\,,$$

where $\lambda_{T,\max}$ is the maximum eigenvalue of the MPR matrix T, and $\delta, \delta_1, \ldots, \delta_{m-k}$, are scalars all in (0, 1), with $\delta + \sum_{g=1}^{m-k}\delta_g = 1$. Also, β is the threshold of acceptably consistent[2] aggregated matrix.

Hence, we can identify scalars δ, $\delta_1, \ldots, \delta_{m-k}$ in (0, 1) with their sum being 1, in such a way that the weighted geometric mean aggregated MPR of the given m MPRs is acceptably consistent although some of the individual MPRs are not acceptably consistent.

Consider the following 4×4 MPRs

$$T_1 = \begin{pmatrix} 1 & 1 & 2 & 6 \\ 1 & 1 & 2 & 3 \\ 1/2 & 1/2 & 1 & 5 \\ 1/6 & 1/3 & 1/5 & 1 \end{pmatrix}, \quad T_2 = \begin{pmatrix} 1 & 2 & 3 & 4 \\ 1/2 & 1 & 3 & 2 \\ 1/3 & 1/3 & 1 & 2 \\ 1/4 & 1/2 & 1/2 & 1 \end{pmatrix},$$

$$T_3 = \begin{pmatrix} 1 & 3 & 5 & 6 \\ 1/3 & 1 & 6 & 9 \\ 1/5 & 1/6 & 1 & 7 \\ 1/6 & 1/9 & 1/7 & 1 \end{pmatrix}, \quad T_4 = \begin{pmatrix} 1 & 4 & 3 & 6 \\ 1/4 & 1 & 7 & 8 \\ 1/3 & 1/7 & 1 & 6 \\ 1/6 & 1/8 & 1/6 & 1 \end{pmatrix},$$

$$T_5 = \begin{pmatrix} 1 & 2 & 2 & 3 \\ 1/2 & 1 & 1 & 3 \\ 1/2 & 1 & 1 & 2 \\ 1/3 & 1/3 & 1/2 & 1 \end{pmatrix}$$

The maximum eigenvalues are, respectively, 4.14, 4.1179, 4.6169, 4.7867, 4.0458. Then, three MPRs T_1, T_2 and T_5 are acceptably consistent (with $n = 4$ and $\beta = 0.08$) while the remaining two MPRs T_3 and T_4 are not so. Now, aggregating the acceptably consistent MPRs with $\alpha_1 = \alpha_2 = \alpha_3 = \frac{1}{3}$. The aggregated matrix $\overline{T}$ is as follows:

$$\overline{T} = \begin{pmatrix} 1 & 1.5874 & 2.2894 & 4.1601 \\ & 1 & 1.8171 & 2.6207 \\ & & 1 & 2.7144 \\ & & & 1 \end{pmatrix}$$

The MPR $\overline{T}$ has maximum eigenvalue $\lambda_{\overline{T},\max} = 4.0386$, and hence it is acceptably consistent. Next, we choose scalars δ, δ_1, δ_2 so to satisfy the following conditions:

$$\begin{aligned} (4.0386)^{\delta}(4.6169)^{\delta_1}(4.7867)^{\delta_2} &< (n-1)\,\beta\,\mathrm{RI}_4 \\ &= 4.2136 \\ \delta + \delta_1 + \delta_2 &= 1 \\ \delta,\ \delta_1,\ \delta_2 &\ge 0. \end{aligned}$$

This system has infinitely many solutions. One such solution is $\delta = 0.73$, $\delta_1 = 0.13$, $\delta_2 = 0.14$.

Remark 2 For $w_g \ge 0$, $g \in M$, $\sum_{g=1}^{m} w_g = 1$, it follows from Petra and Lidija (2012) that a sufficient condition for the weighted geometric mean aggregated MPR (matrix) $C_{\mathrm{agg}}^{(q)} = \left(C_{\widetilde{R}_1}^{(q)}\right)^{w_1}\cdots\left(C_{\widetilde{R}_m}^{(q)}\right)^{w_m}$, to be acceptably consistent is that

$$\prod_{g=1}^{m}\left(\lambda_{C_{\widetilde{R}_g}^{(q)},\max}\right)^{w_g} < (n-1)\beta\,\mathrm{RI}_n + n\,, \tag{10}$$

where $\lambda_{C_{\widetilde{R}_g}^{(q)},\max}$ is the maximum eigenvalue of the MPR matrix $C_{\widetilde{R}_g}^{(q)}$, and β is the threshold of acceptably consistent aggregated matrix.

Returning back to our main discussion, we propose an algorithm which identifies acceptably consistent IVI-MPR in a MCGDM scenario.

Algorithm 1 *1. Elicit g, $g \in M$, incomplete IVI-MPR $\widetilde{R}_t = [\widetilde{r}_{ij,g}]_{n\times n} = ([\underline{\mu}_{ij,g}, \overline{\mu}_{ij,g}],\ [\underline{\nu}_{ij,g}, \overline{\nu}_{ij,g}])$, for all $i, j \in N$, and represent the missing elements by $*$.*

[2] Saaty (2001) showed that $\beta = 0.05$ and $\beta = 0.08$ are quite reasonable for $n = 3$ and $n = 4$, respectively, for acceptably consistent aggregated matrix computed by geometric mean. Note, $\beta = 0.1$ in Definition 3.

2. *Using* (4) *and* (5)*, construct the incomplete MPRs* $C_g^{(*q)}$, $q = 1, 2, 3, 4,\ g \in M$.
3. *Calculate the initial values of the missing elements in* $C_g^{(*q)}$, $q = 1, 2, 3, 4,\ g \in M$, *using* (7).
4. Using the local optimization model (P), adjust the initial values and obtain the complete MPRs $C_g^{(q)}$, $q = 1, 2, 3, 4,\ g \in M$.
5. Check the consistency of $C_g^{(q)}$, $q = 1, 2, 3, 4,\ g \in M$. If the consistency ratio of $C_g^{(q)} < \beta,\ \forall\, q = 1, 2, 3, 4,\ g \in M$, then use geometric mean[3] to aggregate the decision matrices are corresponding to these MPRs.
   Else, compute the weighted geometric mean matrix and test whether it is acceptably consistent using (10).

The following example illustrates the algorithm.

Example 3 Suppose three experts e_g, $g = 1, 2, 3$, with the weight vector $w = (1/3, 1/3, 1/3)^t$, provide their individual judgement on four alternatives in terms of incomplete IVI-MPRs given by $\widetilde{R}_g$, $g = 1, 2, 3$, where the missing elements are marked distinctly.

$$\widetilde{R}_1 = \begin{bmatrix} ([1,1],[1,1]) & ([*,*],[*,*]) & ([0.4,0.6],[0.2,0.4]) & ([0.2,0.3],[0.5,0.6]) \\ ([*,*],[*,*]) & ([1,1],[1,1]) & ([0.6,0.7],[*,0.3]) & ([0.4,0.7],[0.2,0.2]) \\ ([0.2,0.4],[0.4,0.6]) & ([*,0.3],[0.6,0.7]) & ([1,1],[1,1]) & ([0.5,*],[0.2,0.3]) \\ ([0.5,0.6],[0.2,0.3]) & ([0.2,0.2],[0.4,0.7]) & ([0.2,0.3],[0.5,*]) & ([1,1],[1,1]) \end{bmatrix}$$

$$\widetilde{R}_2 = \begin{bmatrix} ([1,1],[1,1]) & ([0.3,0.6],[0.3,0.4]) & ([*,*],[*,*]) & ([0.3,0.4],[0.2,0.2]) \\ ([0.3,0.4],[0.3,0.6]) & ([1,1],[1,1]) & ([0.5,0.5],[*,*]) & ([0.2,0.5],[0.3,0.4]) \\ ([*,*],[*,*]) & ([*,*],[0.5,0.5]) & ([1,1],[1,1]) & ([*,*],[0.2,0.5]) \\ ([1,2],[0.3,0.4]) & ([0.3,0.4],[0.2,0.5]) & ([0.2,0.5],[*,*]) & ([1,1],[1,1]) \end{bmatrix}$$

$$\widetilde{R}_3 = \begin{bmatrix} ([1,1],[1,1]) & ([0.5,0.6],[0.3,0.4]) & ([0.3,*],[0.2,0.3]) & ([*,0.4],[0.2,0.5]) \\ ([0.3,0.4],[0.5,0.6]) & ([1,1],[1,1]) & ([0.6,0.7],[0.2,0.2]) & ([*,*],[*,*]) \\ ([0.2,0.3],[0.3,*]) & ([0.2,0.2],[0.6,0.7]) & ([1,1],[1,1]) & ([0.3,0.5],[0.2,0.4]) \\ ([0.2,0.5],[*,0.4]) & ([*,*],[*,*]) & ([0.2,0.4],[0.3,0.5]) & ([1,1],[1,1]) \end{bmatrix}.$$

For the first expert preference relation matrix $\widetilde{R}_1$, the four incomplete MPRs are obtained using (4) and (5) as follows:

$$C_{\widetilde{R}_1}^{(1)} = \begin{bmatrix} 1 & c_{12}^{(*1)} & 0.6 & 0.3 \\ 1/c_{12}^{(*1)} & 1 & 0.7 & 0.7 \\ 1/0.6 & 1/0.7 & 1 & c_{34}^{(*1)} \\ 1/0.3 & 1/0.7 & 1/c_{34}^{(*1)} & 1 \end{bmatrix},$$

$$C_{\widetilde{R}_1}^{(2)} = \begin{bmatrix} 1 & c_{12}^{(*2)} & 0.4 & 0.2 \\ 1/c_{12}^{(*2)} & 1 & 0.6 & 0.4 \\ 1/0.4 & 1/0.6 & 1 & 0.5 \\ 1/0.2 & 1/0.4 & 1/0.5 & 1 \end{bmatrix},$$

$$C_{\widetilde{R}_1}^{(3)} = \begin{bmatrix} 1 & c_{12}^{(*3)} & 0.4 & 0.6 \\ 1/c_{12}^{(*3)} & 1 & 0.3 & 0.2 \\ 1/0.4 & 1/0.3 & 1 & 0.3 \\ 1/0.6 & 1/0.2 & 1/0.3 & 1 \end{bmatrix},$$

$$C_{\widetilde{R}_1}^{(4)} = \begin{bmatrix} 1 & c_{12}^{(*4)} & 0.2 & 0.5 \\ 1/c_{12}^{(*4)} & 1 & c_{23}^{(*4)} & 0.2 \\ 1/0.2 & 1/c_{23}^{(*4)} & 1 & 0.2 \\ 1/0.5 & 1/0.2 & 1/0.2 & 1 \end{bmatrix}.$$

The initial values are described as follows:

$$\begin{aligned} c_{12}^{(*1)((0))} &= ((c_{13}^{(1)} c_{32}^{(1)})(c_{14}^{(1)} c_{42}^{(1)}))^{1/2} = 0.6060, \\ c_{34}^{(*1)((0))} &= ((c_{31}^{(1)} c_{14}^{(1)})(c_{32}^{(1)} c_{24}^{(1)}))^{1/2} = 0.7071, \\ c_{12}^{(*2)((0))} &= ((c_{13}^{(2)} c_{32}^{(2)})(c_{14}^{(2)} c_{42}^{(2)}))^{1/2} = 0.577, \\ c_{12}^{(*3)((0))} &= ((c_{13}^{(3)} c_{32}^{(3)})(c_{14}^{(3)} c_{42}^{(3)}))^{1/2} = 2, \\ c_{12}^{(*4)((0))} &= c_{14}^{(4)} c_{42}^{(4)} = 2.5, \quad c_{23}^{(*4)((0))} = c_{24}^{(4)} c_{43}^{(4)} = 1. \end{aligned}$$

Solving problem (P), using these initial values, we obtain,

$$\begin{aligned} &c_{12}^{(1)} = 0.5,\ c_{12}^{(2)} = 0.5,\ c_{12}^{(3)} = 2,\ c_{12}^{(4)} = 2, \\ &c_{23}^{(4)} = 0.3,\ c_{34}^{(1)} = 1. \end{aligned}$$

[3] Aczél and Saaty (1983) proved that to synthesize the group judgments, the geometric mean must be used in order to preserve the reciprocal property, that is, $r_{ij} r_{ji} = 1,\ \forall\, i, j \in N$, must hold in the resultant aggregated matrix. Note that the weighted geometric mean preserves reciprocality on aggregation resulting in an aggregated MPR, while the same gets distorted if instead arithmetic mean is used for aggregating two or more MPRs.

Table 2 Consistency of the weighted geometric mean aggregated preference relation matrix

Aggregated matrix	$(w_1, w_2, w_3)^t$	$\prod_{t=1}^{3}\left(\lambda_{C_{\widetilde{R}_t}^{(q)}}, \max\right)^{w_t}$	Is (10) satisfied?	$\lambda_{\max}$	Is $C_{\text{agg}}^{(q)}$, $q = 1, 2, 3, 4$, acceptably consistent?
$C_{\text{agg}}^{(1)}$	$(\frac{1}{3}, \frac{1}{3}, \frac{1}{3})^t$	4.037	Yes	4.1033	Yes
	$(\frac{9}{20}, \frac{1}{10}, \frac{9}{20})^t$	4.0473	Yes	4.0918	Yes
	$(\frac{1}{5}, \frac{3}{5}, \frac{1}{5})^t$	5.7133	No	4.0888	Yes
	$(\frac{1}{20}, \frac{9}{10}, \frac{1}{20})^t$	4.0145	Yes	4.0366	Yes
	$(\frac{1}{100}, \frac{98}{100}, \frac{1}{100})^t$	4.0112	Yes	4.0160	Yes
$C_{\text{agg}}^{(2)}$	$(\frac{1}{3}, \frac{1}{3}, \frac{1}{3})^t$	4.1156	Yes	4.0475	Yes
	$(\frac{9}{20}, \frac{1}{10}, \frac{9}{20})^t$	4.0400	Yes	4.1232	Yes
	$(\frac{1}{5}, \frac{3}{5}, \frac{1}{5})^t$	4.2039	Yes	4.2650	Yes
	$(\frac{1}{20}, \frac{9}{10}, \frac{1}{20})^t$	4.3054	No	4.3242	No
	$(\frac{1}{100}, \frac{98}{100}, \frac{1}{100})^t$	4.3329	No	4.3369	No
$C_{\text{agg}}^{(3)}$	$(\frac{1}{3}, \frac{1}{3}, \frac{1}{3})^t$	4.3418	No	4.1302	Yes
	$(\frac{9}{20}, \frac{1}{10}, \frac{9}{20})^t$	4.4533	No	4.2868	No
	$(\frac{1}{5}, \frac{3}{5}, \frac{1}{5})^t$	4.2177	No	4.0333	Yes
	$(\frac{1}{20}, \frac{9}{10}, \frac{1}{20})^t$	4.0824	Yes	4.0203	Yes
	$(\frac{1}{100}, \frac{98}{100}, \frac{1}{100})^t$	4.0471	Yes	4.0338	Yes
$C_{\text{agg}}^{(4)}$	$(\frac{1}{3}, \frac{1}{3}, \frac{1}{3})^t$	4.5057	No	4.3099	No
	$(\frac{9}{20}, \frac{1}{10}, \frac{9}{20})^t$	4.6591	No	4.9598	No
	$(\frac{1}{5}, \frac{3}{5}, \frac{1}{5})^t$	4.3365	No	4.6849	No
	$(\frac{1}{20}, \frac{9}{10}, \frac{1}{20})^t$	4.1538	Yes	4.1048	Yes
	$(\frac{1}{100}, \frac{98}{100}, \frac{1}{100})^t$	4.1064	Yes	4.1350	Yes

Similarly, we work out the missing elements values for the MPRs of the other two experts. For an expert e_2, we obtain,

$$c_{13}^{(1)} = 0.3,\ c_{34}^{(1)} = 1,\ c_{13}^{(2)} = 0.15,\ c_{34}^{(2)} = 0.4,$$
$$c_{13}^{(3)} = 0.4,\ c_{23}^{(3)} = 1.5,\ c_{13}^{(4)} = 0.4,\ c_{23}^{(4)} = 1.5,$$

while for an expert e_3, we have,

$$c_{13}^{(1)} = 0.8,\ c_{24}^{(1)} = 0.67,\ c_{14}^{(2)} = 0.111,\ c_{24}^{(2)} = 0.18,$$
$$c_{24}^{(3)} = 1.25,\ c_{24}^{(4)} = 0.66.$$

It is noted that among the twelve MPRs, $C_{\widetilde{R}_1}^{(q)}$, $q = 1, 2, 3$, $C_{\widetilde{R}_2}^{(q)}$, $q = 1, 3, 4$, and $C_{\widetilde{R}_3}^{(q)}$, $q = 1, 2$, are acceptably consistent, while $C_{\widetilde{R}_1}^{(4)}$, $C_{\widetilde{R}_2}^{(2)}$, $C_{\widetilde{R}_3}^{(3)}$, and $C_{\widetilde{R}_3}^{(4)}$, are not acceptably consistent.

For $w_1 = w_2 = w_3 = 1/3$, construct the weighted geometric mean judgement matrix of the three matrices $C_{\widetilde{R}_1}^{(1)}$, $C_{\widetilde{R}_2}^{(1)}$, and $C_{\widetilde{R}_3}^{(1)}$,

$$C_{\text{agg}}^{(1)} = \begin{pmatrix} 1 & 0.567 & 0.567 & 0.367 \\ 1.778 & 1 & 0.633 & 0.623 \\ 2.083 & 1.619 & 1 & 0.833 \\ 2.778 & 1.640 & 1.333 & 1 \end{pmatrix}.$$

Then, $\lambda_{C_{\text{agg}}^{(1)},\,\max} = 4.103$ which is less than $(n-1)\beta\text{RI}_n + n = 4.2136$, for $n = 4$, $\beta = 0.08$. Hence, $C_{\text{agg}}^{(1)}$ is acceptably consistent.

In Table 2, we summarize the acceptably consistent behavior of the weighted geometric mean matrices for different weights of three experts. For notational convenience the maximum eigenvalue of the weighted geometric mean comparison matrices $C_{\text{agg}}^{(q)}$, $q = 1, 2, 3, 4$, is denoted by $\lambda_{\max}$ in Table 2.

From Table 2, we find that though the individual preference matrices are not acceptably consistent yet their geometric mean aggregated preference matrix turns out to be acceptably consistent for some specific choices of weight vectors w indicating the significance of importance attached to the experts. Also, from Table 2, note that (10) is only a sufficient condition for the aggregated matrix (and hence of MPR) to be acceptably consistent as, for some specific weight vector w, we do have (10) failing to hold yet the weighted geometric mean $C_{\text{agg}}^{(q)}$ is acceptably consistent.

Table 3 Missing entries x and y values and the CR values of the original MPR A (in columns 2–4) and the MPR A with two changes (in columns 5–7)

Optimization model	x	y	CR	x	y	CR
Meng and Chen (2015) model (OP)	0.579	0.483	0.0097	1.0583	2.6458	0.4169
Our proposed (P) model	0.579	0.483	0.0097	1.0583	2.6458	0.4169

5 A comparative analysis with existing methods

Research studies on FPR, I-FPR, and IVI-FPR exist in the literature. For instance, one may refer to Xu and Cai (2009), Chen et al. (2014), Meng et al. (2017). In the present paper, we primarily focused on IVI-MPR rather than IVI-FPR. To the best of our understanding, there does not exist any study in the literature guiding how to populate the missing entries in an IVI-MPR.

In this section, we compare our proposed method with those of Meng and Chen (2015) for MPR and Jiang et al. (2015) for I-MPR and show that our method generalizes their works.

1. Meng and Chen (2015) proposed the notion of the multiplicative geometric consistent index (MGCI) to measure the multiplicative consistency of an MPR. The consistency of an MPR is considered to be unacceptable if the MGCI of an MPR is less than the average value tabulated in Table 1 in their paper. The authors continued their study to include the case of incomplete MPR. They formulated a multi-objective programming model to estimate the missing values. Using the goal-programming approach and a suitable transformation, the proposed model was converted into an equivalent linear program. The missing values in an MPR were then obtained using the inverse transformation at the optimal solution of the linear program.
   Observe that if we set $q = 1$, $C^{(q)} = C^{(q+\theta)}$, $\theta = 1, 2, 3$, in model (P) of Sect. 3.2, and use only the first three constraints of model (P), then the deviation model (OP) of Meng and Chen (2015) follows as a special case of (P). Our proposed approach thus encompasses the case of incomplete MPR. However, for the wholeness of discussion, we additionally provide the linear goal-programming deviation model for IVI-MPR in Appendix 2.
   The method proposed by us in the current work and the one suggested by Meng and Chen (2015) are based fundamentally on the principle of transitivity for MPR. However, unlike the approach by Meng and Chen (2015) for MPR, which requires solving a goal-programming model, our proposed method for IVI-MPR is a two-stage iterative scheme involving initial estimation of missing values and after that improving upon them by solving optimization model (P). Though it may so happen that the stage one itself is sufficient to produce optimal values of the missing entries making the second stage redundant. Consider the following incomplete MPR

$$A = \begin{bmatrix} 1 & 0.6 & \text{x} & 0.4 \\ 1/0.6 & 1 & 0.7 & \text{y} \\ 1/\text{x} & 1/0.7 & 1 & 0.5 \\ 1/0.4 & 1/\text{y} & 1/0.5 & 1 \end{bmatrix}$$

   The results on solving the proposed model (P) and the (OP) model of Meng and Chen (2015) are same. Moreover, in this matrix, if 0.6 and 0.4 are changed to 0.2 and 4, respectively, then also the two approaches yield same results; see, Table 3.
2. In Sect. 3, if $C^{(1)} = C^{(2)}$ and $C^{(3)} = C^{(4)}$, then the IVI-MPR gets converted into I-MPR studied by Jiang et al. (2015). In fact, our proposed methodology is very much inspired by the work of Jiang et al. (2015).
   We can conclude that our methodology is an alternative procedure to compute missing entries. The proposed method is indeed not inferior to the one existing for incomplete MPR in the literature despite IVI-MPR being a generalization of MPR and its other variants.

6 Concluding remarks

The contribution of the paper is twofold. Firstly, we introduce the notion of acceptably consistent for IVI-MPR, and secondly, we propose a two-step method to populate the missing entries in an incomplete IVI-MPR. The first step of the recommended two-step approach identifies the initial values of all missing entries in an incomplete IVI-MPR, and the subsequent second step improves the initial values by solving a linear programming problem. Although certain research papers are available in the literature on MPRs in the intuitionistic framework, yet the proposed integration of IVI-MNs in MPR, especially in the incomplete preference relations, can be considered as a novel contribution of this paper.

The primary limitation of the proposed procedure for finding the missing entries lies in its estimating step where we have assumed that, for a missing entry $\widetilde{*}_{ij}$, we can always find an elementary connecting path in the given preference relation matrix such that all other entries along this path are completely known. This assumption may not hold. Another concern in the present study is that the weights or different

levels of expertise of experts are assumed to be precisely known. A suitable choice of a weight vector ensures acceptably consistent group aggregated preference relation matrix. However, we have not explored a mechanism to guide on the selection of weight vector for experts to enable them to converge to an acceptably consistent aggregated preference matrix. The only sufficient condition available to guide on this choice of weight vector is the inequality in (10). Besides the weights of experts, for aggregation, the weights/importance of the evaluation criteria can be devised using their importance ratings from experts.

These gray patches in the present study can be quickly filled in near future research taking inspiration from the approaches of very recent works of Wan, Xu, Wang, and their co-researchers (2016–2017). One can also investigate Choquet integral approach for aggregating information in preference relation matrices than the presently used traditional geometric mean operator. Moreover, one can attempt to define group consensus in IVI framework and design a procedure to accomplish the same.

Acknowledgements The authors are thankful to the esteemed referees for their valuable comments which help to improve the presentation of the paper substantially. The authors acknowledge the editor-in-chief for being considerate and supportive.

Compliance with ethical standards

Conflict of interest All three authors declare that they have no conflict of interest regarding the publication of this manuscript.

Appendix-1

We briefly include the operators of interval-valued intuitionistic fuzzy sets and numbers for the completeness of the ground-work theory. All notions and operators are described in Atanassov and Gargov (1989) and Xu and Cai (2012), while some of the interesting applications of I-MPRs and IVI-MPR are also included in (Xu et al. 2012).

Definition 13 Let X be a universal set. An intuitionistic fuzzy set (IFS) drawn from X is defined as $\tilde{A} = \{\langle x, \mu_{\tilde{A}}(x), \nu_{\tilde{A}}(x)\rangle \mid x \in X\}$, where $\mu_{\tilde{A}},\ \nu_{\tilde{A}} : X \to [0,1]$ define, respectively, the degree of membership and the degree of non-membership of an element $x \in X$ to the set $\tilde{A} \subseteq X$ such that $\mu_{\tilde{A}}(x) + \nu_{\tilde{A}}(x) \leq 1, \forall\, x \in X$.

An intuitionistic fuzzy number (IFN) is defined by $\alpha = (\mu_\alpha, \nu_\alpha)$, where $\mu_\alpha,\ \nu_\alpha \in [0,1],\ \mu_\alpha + \nu_\alpha \leq 1$.

Definition 14 Let X be a universal set. An IVIFS drawn from X is $\tilde{A} = \{\langle x,\ \tilde{\mu}_{\tilde{A}}(x),\ \tilde{\nu}_{\tilde{A}}(x)\rangle \mid x \in X\}$, where $\tilde{\mu}_{\tilde{A}},\ \tilde{\nu}_{\tilde{A}} : X \to 2^{[0,1]}$ are, respectively, the interval-valued membership and the interval-valued non-membership degrees of an element $x \in X$ to the set $\tilde{A}$, such that, $\sup_{x\in X} \tilde{\mu}_{\tilde{A}}(x) + \sup_{x\in X} \tilde{\nu}_{\tilde{A}}(x) \leq 1$.

Clearly if, $\inf_{x\in X} \tilde{\mu}_{\tilde{A}}(x) = \sup_{x\in X} \tilde{\mu}_{\tilde{A}}(x)$ and $\inf_{x\in X} \tilde{\nu}_{\tilde{A}}(x) = \sup_{x\in X} \tilde{\nu}_{\tilde{A}}(x)$, then the IVIFS $\tilde{A}$ reduces to the intuitionistic fuzzy set (IFS).

Definition 15 Let $\tilde{A} = \{\langle x, \tilde{\mu}_{\tilde{A}}(x), \tilde{\nu}_{\tilde{A}}(x)\rangle \mid x \in X\},\ \tilde{A}_1 = \{\langle x, \tilde{\mu}_{\tilde{A}_1}(x), \tilde{\nu}_{\tilde{A}_1}(x)\rangle \mid x \in X\}$ and $\tilde{A}_2 = \{\langle x, \tilde{\mu}_{\tilde{A}_2}(x), \tilde{\nu}_{\tilde{A}_2}(x)\rangle \mid x \in X\}$ be IVIFSs, and $\lambda > 0$.

1. $\tilde{A}^{\mathfrak{c}} = \{\langle x,\ \tilde{\nu}_{\tilde{A}}(x),\ \tilde{\mu}_{\tilde{A}}(x)\rangle \mid x \in X\}$;

2. $\tilde{A}_1 \cap \tilde{A}_2 = \{\langle x,\ \Big[\min\{\inf \tilde{\mu}_{\tilde{A}_1}(x), \inf \tilde{\mu}_{\tilde{A}_2}(x)\},$
$\min\{\sup \tilde{\mu}_{\tilde{A}_1}(x), \sup \tilde{\mu}_{\tilde{A}_2}(x)\}\Big],$
$\Big[\max\{\inf \tilde{\nu}_{\tilde{A}_1}(x), \inf \tilde{\nu}_{\tilde{A}_2}(x)\},$
$\max\{\sup \tilde{\nu}_{\tilde{A}_1}(x), \sup \tilde{\nu}_{\tilde{A}_2}(x)\}]\rangle \mid x \in X\}$;

3. $\tilde{A}_1 \cup \tilde{A}_2 = \{\langle x,\ \Big[\max\{\inf \tilde{\mu}_{\tilde{A}_1}(x), \inf \tilde{\mu}_{\tilde{A}_2}(x)\},$
$\max\{\sup \tilde{\mu}_{\tilde{A}_1}(x), \sup \tilde{\mu}_{\tilde{A}_2}(x)\}\Big],$
$\Big[\min\{\inf \tilde{\nu}_{\tilde{A}_1}(x), \inf \tilde{\nu}_{\tilde{A}_2}(x)\},$
$\min\{\sup \tilde{\nu}_{\tilde{A}_1}(x), \sup \tilde{\nu}_{\tilde{A}_2}(x)\}\Big]\rangle \mid x \in X\}$;

4. $\tilde{A}_1 + \tilde{A}_2 = \{\langle x,\ \Big[\inf \tilde{\mu}_{\tilde{A}_1}(x) + \inf \tilde{\mu}_{\tilde{A}_2}(x) - \inf \tilde{\mu}_{\tilde{A}_1}(x)\ \inf \tilde{\mu}_{\tilde{A}_2}(x),$
$\sup \tilde{\mu}_{\tilde{A}_1}(x) + \sup \tilde{\mu}_{\tilde{A}_2}(x) - \sup \tilde{\mu}_{\tilde{A}_1}(x)\ \sup \tilde{\mu}_{\tilde{A}_2}(x)\Big],$
$\Big[\inf \tilde{\nu}_{\tilde{A}_1}(x)\ \inf \tilde{\nu}_{\tilde{A}_2}(x),\ \sup \tilde{\nu}_{\tilde{A}_1}(x)\ \sup \tilde{\nu}_{\tilde{A}_2}(x)\Big]\rangle \mid x \in X\}$;

5. $\tilde{A}_1\,\tilde{A}_2 = \{\langle x,\ \Big[\inf \tilde{\mu}_{\tilde{A}_1}(x)\ \inf \tilde{\mu}_{\tilde{A}_2}(x),\ \sup \tilde{\mu}_{\tilde{A}_1}(x)\ \sup \tilde{\mu}_{\tilde{A}_2}(x)\Big],$
$\Big[\inf \tilde{\nu}_{\tilde{A}_1}(x) + \inf \tilde{\nu}_{\tilde{A}_2}(x) - \inf \tilde{\nu}_{\tilde{A}_1}(x)\ \inf \tilde{\nu}_{\tilde{A}_2}(x),$
$\sup \tilde{\nu}_{\tilde{A}_1}(x) + \sup \tilde{\nu}_{\tilde{A}_2}(x) - \sup \tilde{\nu}_{\tilde{A}_1}(x)\ \sup \tilde{\nu}_{\tilde{A}_2}(x)\Big]\rangle \mid x \in X\}$;

6. $\lambda\tilde{A} = \{\langle x,\ \big[1 - (1 - \inf \tilde{\mu}_{\tilde{A}}(x))^{\lambda},\ 1 - (1 - \sup \tilde{\mu}_{\tilde{A}}(x))^{\lambda}\big],$
$\big[(\inf \tilde{\nu}_{\tilde{A}}(x))^{\lambda},\ (\sup \tilde{\nu}_{\tilde{A}}(x))^{\lambda}\big]\rangle \mid x \in X\}$;

7. $\tilde{A}^{\lambda} = \{\langle x,\ \Big[(\inf \tilde{\mu}_{\tilde{A}}(x))^{\lambda},\ (\sup \tilde{\mu}_{\tilde{A}}(x))^{\lambda}\Big],$
$\Big[1 - (1 - \inf \tilde{\nu}_{\tilde{A}}(x))^{\lambda},\ 1 - (1 - \sup \tilde{\nu}_{\tilde{A}}(x))^{\lambda}\Big]\rangle | x \in X\}$.

The basic component of an IVIFS is an ordered pair, characterized by an interval-valued membership degree and an interval-valued non-membership degree of x in $\tilde{A}$. This ordered pair is called an interval-valued intuitionistic fuzzy number (IVIFN).

An IVIFN is generally simplified as $([a,b],\ [c,d])$, where $[a,b] \subseteq [0,1]$, $[c,d] \subseteq [0,1]$, $b + d \leq 1$.

Obviously, when $a = b$ and $c = d$, then IVIFN reduces to an intuitionistic fuzzy number (IFN).

Definition 16 Let $\tilde{\alpha} = ([a, b], [c, d])$, $\tilde{\alpha_1} = ([a_1, b_1], [c_1, d_1])$ and $\tilde{\alpha_2} = ([a_2, b_2], [c_2, d_2])$ be IVIFNs, and $\lambda > 0$. Then

1. $\tilde{\alpha}^{\mathfrak{c}} = ([c, d], [a, b])$
2. $\tilde{\alpha_1} \wedge \tilde{\alpha_2} = ([\min\{a_1, a_2\}, \min\{b_1, b_2\}], [\max\{c_1, c_2\}, \max\{d_1, d_2\}])$;
3. $\tilde{\alpha_1} \vee \tilde{\alpha_2} = ([\max\{a_1, a_2\}, \max\{b_1, b_2\}], [\min\{c_1, c_2\}, \min\{d_1, d_2\}])$;
4. $\tilde{\alpha_1} \oplus \tilde{\alpha_2} = ([a_1 + a_2 - a_1a_2, b_1 + c_2 - b_1b_2], [c_1c_2, d_1d_2])$;
5. $\tilde{\alpha_1} \otimes \tilde{\alpha_2} = ([a_1a_2, b_1b_2], [c_1 + c_2 - c_1c_2, d_1 + d_2 - d_1d_2])$;
6. $\lambda\tilde{\alpha} = (\left[1 - (1 - a)^{\lambda}, 1 - (1 - b)^{\lambda}\right], \left[c^{\lambda}, d^{\lambda}\right])$;
7. $\tilde{\alpha}^{\lambda} = (\left[a^{\lambda}, b^{\lambda}\right], \left[1 - (1 - c)^{\lambda}, 1 - (1 - d)^{\lambda}\right])$.

Appendix-2

Meng and Chen (2015) developed a deviation model for an MPR. In the same spirit, we formulate an equivalent deviation model for the model (P) proposed in Sect. 3.

$$\min \quad D = \sum_{q=1}^{4} \sum_{i,j=1, i<j,\ k\in\Omega(q)}^{n} (d_{ij,\,k}^{(q)+} + d_{ij,\,k}^{(q)-})$$

subject to

$$\delta_{ij}\left(\log a_{ij}^{(q)} - (\log a_{ik}^{(q)} + \log a_{kj}^{(q)})\right) - d_{ij,\,k}^{(q)+} + d_{ij,\,k}^{(q)-} = 0, \quad i < j,\ \forall\, i,\ j \in N,\ k \in \Omega(q),\ q = 1, 2, 3, 4$$
$$1/9 \le a_{ij}^{(q)}, q = 1, 2, \quad a_{ij}^{(q)} \in \Gamma(q)$$
$$a_{ij}^{(q)} \le 9,\ q = 3, 4, \quad a_{ij}^{(q)} \in \Gamma(q)$$
$$a_{ij}^{(q)} a_{ij}^{(q+2)} \le 1, \quad q = 1, 2,\ i,\ j,\ k \in N,\ \ i \ne j \ne k$$
$$a_{ij}^{(q+1)} \le a_{ij}^{(q)}, \quad q = 1, 3,\ i < j, \quad i, j \in N$$
$$a_{ij}^{(q+1)} \ge a_{ij}^{(q)}, \quad q = 1, 3,\ i > j, \quad i, j \in N$$
$$d_{ij,\,k}^{(q)+},\ \ d_{ij,\,k}^{(q)-} \ge 0, \quad i,\ j = 1, \ldots, n,\ i < j,$$

where $d_{ij,\,k}^{(q)+} = \left(\log a_{ij}^{(q)} - (\log a_{ik}^{(q)} + \log a_{kj}^{(q)})\right) \vee 0,\ k \in \Omega(q)$, and $d_{ij,\,k}^{(q)-} = \left((\log a_{ik}^{(q)} + \log a_{kj}^{(q)}) - \log a_{ij}^{(q)}\right) \vee 0,\ k \in \Omega(q)$, and

$$\delta_{ij} = \begin{cases} 1 & k \in \Omega(q) \\ 0 & \text{otherwise} \end{cases}$$

It is observed that both model (P) and the above deviation model are equivalent and yield the same optimal outputs. Moreover, the model formulated by Meng and Chen (2015) is a particular case of the above model and hence of model (P).

References

Aczél J, Saaty TL (1983) Procedures for synthesizing ratio judgments. J Math-Mat Psychol 27:93–102

Alonso S, Chiclana F, Herrera F, Herrera-viedma E, Alcala-Fernadez J, Porcel C (2008) A consistency based procedure to estimate missing pairwise preference values. Int J Intell Syst 23:155–175

Alonso S, Herrera-Viedma E, Chiclana F, Herrera F (2010) A web based consensus support system for group decision making problems and incomplete preferences. Inf Sci 180:4477–4495

Atanassov, K. (2012). On intuitionistic fuzzy sets theory. Springer, Berlin

Atanassov K, Gargov G (1989) Interval valued intuitionistic fuzzy sets. Fuzzy Sets Syst 31:343–349

Brans JP, Vincke P (1985) A preference ranking organization method. Manag Sci 31:647–656

Chen SM, Lin TE, Lee LW (2014) Group decision making using incomplete fuzzy preference relations based on the additive consistency and the order consistency. Inf Sci 259:1–15

Chiclana F, Herrera F, Herrera Viedma E (2001) Integrating multiplicative preference relations in a multipurpose decision-making model based on fuzzy preference relations. Fuzzy Sets Syst 122:277–291

Deschrijver G, Kerre EE (2003) On the composition of intuitionistic fuzzy relations. Fuzzy Sets Syst 136:333–361

Elsner L, Johnson CR, Dias Da Silva JA (1988) The Perron root of a weighted geometric mean of nonnegative matrices. Linear and Multilinear Algebra 24:1–13

Fan ZP, Ma J, Jiang YP, Sun YH, Ma L (2006) A goal programming approach to group decision making based on multiplicative preference relation and fuzzy preference relations. Eur J Oper Res 174:311–321

Fedrizzi M, Giove S (2007) Incomplete pair wise comparison and consistency optimization. Eur J Oper Res 183:303–313

Figueira J, Greco S, Ehrgott M (eds) (2005) Multiple criteria decision analysis: state of the art surveys. International series in operations research and management science. Springer, New York, p 78

Gong ZW, Li LS, Forrest J, Zhao Y (2011) The optimal priority models of the intuitionis tic fuzzy preference relation and their application in selecting industries with higher meteorological sensitivity. Expert Syst Appl 38:4394–4402

Harker PT (1987a) Alternative modes of questioning in the analytic hierarchy process. Math Modell 9:353–360

Harker PT (1987b) Incomplete pairwise comparisons in the analytic hierarchy process. Math Modell 9:837–848

Hwang CL, Yoon K (1981) Multiple attribute decision making: methods and applications. Springer, New York

Jiang Y, Xu ZS, Xu JP (2014) Interval-valued intuitionistic multiplicative sets. Int J Uncertain, Fuzziness Knowl-Based Syst 22(3):385–406

Jiang Y, Xu ZS, Yu XH (2013) Compatibility measures and consensus models for group decision making with intuitionistic multiplicative preference relations. Appl Soft Comput 13:2075–2086

Jiang Y, Xu ZS, Yu XH (2015) Group decision making based on incomplete intuitinistic multiplicative preference relations. Inf Sci 295:33–52

Kou G, Peng Y, Chen Z, Shi Y (2009) Multiple criteria mathematical programming for multi-class classification and application in network intrusion detection. Inf Sci 179:371–381

Liao HC, Xu ZS, Xia MM (2014) Multiplicative consistency of interval-valued intuitionistic fuzzy preference relation. J Intell Fuzzy Syst 27:2969–2985

Lio H, Xu Z (2014) Priorities of intuitionistic fuzzy preference relation based on multiplicative consistency. IEEE Trans Fuzzy Syst 22:1669–1689

Liu F (2009) Acceptable consistency analysis of interval reciprocal comparison matrices. Fuzzy Sets Syst 160:2686–2700

Liu F, Zhang WG, Wang ZX (2012) A goal programming model for incomplete interval multiplicative preference relations and its application in group decision-making. Eur J Oper Res 218:747–754

Meng F, Chen X (2015) An approach to incomplete multiplicative preference relations and its application in group decision making. Inf Sci 309:119–137

Meng F, Tan C (2017) A new consistency concept for interval multiplicative preference relations. Appl Soft Comput 52:262–276

Meng F, Tan C, Chen X (2017) Multiplicative consistency analysis for interval fuzzy preference relations: a comparative study. Omega 68:17–38

Nishizawa K (1997) A method to find elements of cycles in an incomplete directed graph and its applications-binary AHP and petri nets. Comput Math Appl 33:33–46

Orlovsky SA (1978) Decision-making with a fuzzy preference relation. Fuzzy Sets Syst 1:155–167

Petra G, Lidija ZS (2012) Acceptably consistency of aggregated comparison matrices in analytic hierarchy process. Eur J Oper Res 223:417–420

Rezaei J (2015) Best-worst multi-criteria decision-making method. Omega 53:49–57

Roy B (1991) The outranking approach and the foundations of ELECTRE methods. Theor Decis 31:49–73

Saaty TL (1977) A scaling method for priorities in hierarchical structures. J Math Psychol 15:234–281

Saaty TL (1980) The analytic hierarchy process. McGraw-Hill, New York

Saaty TL (2001) Fundamentals of decision making and priority theory with the analytic hierarchy process. RWS Publications, Pittsburgh

Saaty TL, Vargas LG (1987) Uncertainty and rank order in the analytic hierarchy process. Eur J Oper Res 32:107–117

Szmidt E, Kacprzyk J (2002) Using intuitinistic fuzzy sets in group decision making. Control Cybernet 31:1037–1053

Triantaphyllou E (2000) Multi-criteria decision making methods: a comparative study, applied optimization series 44. Springer, NewYork

Ureña R, Chiclana F, Morente-Molinera JA, Herrera-Viedma E (2015) Managing incomplete preference relations in decision making: a review and future trends. Inf Sci 302:14–32

Wan S, Wang F, Dong J (2017) Additive consistent interval-valued Atanassov intuitionistic fuzzy preference relation and likelihood comparison algorithm based group decision making. Eur J Oper Res 263:571–582

Wan S, Wang F, Dong J (2018) A threephase method for group decision making with interval-valued intuitionistic fuzzy preference relations. IEEE Trans Fuzzy Syst 26(2):998–1010

Wan S, Xu GL, Dong J (2016) A novel method for group decision making with interval-valued Atanassov intuitionistic fuzzy preference relations. Inf Sci 372:53–71

Wang YM, Yang JB, Xu DL (2005) A twostage logarithmic goal programming method for generating weights from interval comparison matrices. Fuzzy Sets Syst 152:475–498

Xia MM, Xu ZS (2013) Group decision making based on intuitionistic multiplicative aggregation operators. Appl Math Model 37:5120–5133

Xia MM, Xu ZS, Liao HC (2013) Preference relations based on intuitionistic multiplicative information. IEEE Trans Fuzzy Syst 21:113–133

Xu ZS (2004a) Goal programming models for obtaining the priority vector of incomplete fuzzy preference relation. Int J Approx Reason 36:261–270

Xu ZS (2004b) On compatibility of interval fuzzy preference relations. Fuzzy Optim Decis Making 3:217–225

Xu ZS (2007a) A survey of preference relations. Int J Gen Syst 36:179–203

Xu ZS (2007b) Intuitionistic preference relations and their application in group decision making. Inf Sci 177:2363–2379

Xu ZS (2012) A consensus reaching process under incomplete multiplicative preference relations. Int J Gen Syst 41:333–351

Xu ZS (2013) Priority weight intervals derived from intuitionistic multiplicative preference. IEEE Trans Fuzzy Syst 21:642–654

Xu ZS, Cai XQ (2009) Incomplete interval-valued intuitionistic preference relations. Int J Gen Syst 38:871–886

Xu ZS, Cai XQ (2012) Intuitionistic fuzzy information aggregation: theory and applications. Science Press, Berlin

Xu GL, Wan S, Wang F, Dong J, Zeng YF (2016) Mathematical programming methods for consistency and consensus in group decision making with intuitionistic fuzzy preference relations. Knowl-Based Syst 98:30–43

Yager RR, Xu ZS (2006) The continuous ordered weighted geometric operator and its application to decision making. Fuzzy Sets Syst 157:1393–1402

Publisher's Note Springer Nature remains neutral with regard to jurisdictional claims in published maps and institutional affiliations.

BULMIM Journal of Management & Research (July-December 2018) 3(2): 55–63
DOI: 10.5958/2455-3298.2018.00008.9

Adoption of B2B E-Commerce in India: A Theoretical Framework

Sanjay Chaudhary[1]* and P.K. Suri[2]

[1]Associate Professor, PGDM, Delhi School of Business, AU Block, Outer Ring Road, Pitampura, Delhi, India

[2]Professor, Management, Delhi School of Management, Delhi Technological University, Shahbad Daulatpur, Main Bawana Road, Delhi, India

(*Corresponding author) email id: *one.sanjay@gmail.com, [2]pks.suri@gmail.com

www.IndianJournals.com
Members Copy, Not for Commercial Sale
Downloaded From IP - 14.139.251.107 on dated 26-Jul-2018

Abstract

Purpose: The authors propose the conceptual B2B e-commerce adoption framework. The framework clearly defines the linkages among the determinant adoption factors and enhance our understanding of online individual and organisational behaviour in India.

Methodology: The factors in adoption framework are identified using literature review. Results of The opinion survey questionnaire responses are analysed using descriptive statistical analysis to explain the relative importance of factors. The factors are further subjected to confirmatory factor analysis.

Findings: In general, the user opinion shows that the B2B e-commerce adoption will increase, if the system helps in the work performance improvement, transaction costs are low, and trustworthiness is attached to the system. In addition, if the required infrastructure with support is in place and users are encouraged to use the new system, then the actual usage of B2B e-commerce will increase in India.

Research Implications: This research has attempted to extend the applicability of the unified theory of acceptance and use of technology (UTAUT) framework in the B2B e-commerce area by two additional factors (trust and cost). It also helps answer some of the queries for B2B e-marketplace providers.

Keywords: Adoption framework, B2B e-commerce adoption, B2B e-commerce in India, Modified UTAUT, Technology adoption

INTRODUCTION

The market is experiencing a huge rise in the e-commerce industry. The e-commerce is changing the traditional transaction methods and causes big changes (Karami, 2014). Within e-commerce, the business to business (B2B) e-commerce refers to Internet enablement of it. In the Indian context, the B2B e-commerce industry, currently at $300 billion, is expected to grow to $700 billion by 2020 (Regina M., 2016).

It has been generally accepted that the adoption of e-commerce is a significant indicator of economic growth in developing countries. But till date, many enterprises in India still have not used e-commerce (Vaithianathan, 2010). The low B2B e-commerce adoption situation is not specific to India, it is true for many developed and developing countries, resulting in the broadening digital divide (Zhu and Thatcher, 2010).

Now, the challenge is to ensure that the opportunities and benefits of e-commerce reached all types of economies including India via high adoption. The B2B e-commerce adoption is described as a business engagement and goods/service – money exchange via the Internet. Even though few success stories are usually highlighted, it is of importance to study the general factors that influence the adoption of B2B e-commerce by businesses in developing countries (Upadhyaya and Mohanan, 2009).

In developing countries like India, the better understanding of factors determining adoption of B2B e-commerce platforms shall help companies and policymakers, in terms of devising a suitable strategy and may lead to a structured approach to their management. Doing it early in the lifecycle, most probably, will result in e-market success and desired benefits reaching participants. The better understanding of factors to be managed by platform operators may ensure requisite liquidity necessary for the very survival of B2B e-marketplace.

OBJECTIVE OF THE RESEARCH

The primary purpose of this research study is to theoretically propose the adoption framework for the B2B e-commerce in India.

The relationship, between constructs in the adoption framework is explored based on the statistical analysis of the user opinion survey. The explanation enhances our understanding of online individual and organisational behaviour.

SIGNIFICANCE OF THE RESEARCH

An extensive empirical research has been undertaken for business-to-consumer and consumer-to-consumer platforms (Bailey, 1998; Brynjolfsson and Smith, 2000) in the developed countries. The B2B e-commerce is a relatively new activity with an insignificant research in the developing countries. Thus, this research focuses on a fast-growing, developing country, India, thus filling the geographic focus as well as a knowledge gap in the theoretical framework for B2B e-commerce adoption.

The existing research in the B2B e-commerce adoption has still to establish a strong theoretical foundation. This has been reflected in less than an overwhelming success in publishing on the subject (Pousttchi *et al.*, 2015). While at the same time, B2B e-commerce is at the epicentre of reader interest. The authors take the challenge to understand one of the important phenomena, known as B2B e-commerce.

To reap the benefits of e-commerce, Indian firms must understand its potential, its components, their own businesses and the businesses of trading partners (Gunasekarana *et al.*, 2002). Going with the recent trend of growth in a theme of supply chain management, marketing and selling (Chen and Holsapple, 2013), the adoption framework proposed in this research work, help answer some of the important queries for B2B e-marketplace providers. What factors can increase the adoption? How are the non-adopters encouraged to adopt? What are the intended benefits for participants, and how to make the B2B e-commerce marketplace successful?

PROPOSED RESEARCH METHODOLOGY

To figure out research design, a systematic literature review is carried out, taking into account the guidelines explained in two leading articles on the topic (Biolchini, 2005; Kitchenham, 2007).

Based on the literature review of research journal articles, conference papers and relevant news articles, the possible adoption factors affecting B2B e-commerce adoption are identified and a modified framework is proposed.

The Likert scale-based multiple questions covering respondent opinions on the factors/variables were framed post-discussion with experts. The Likert scale has options of 1 to 7, where 1 means 'Extreme Negative' and 7 means 'Extremely Positive' influence on e-commerce adoption. For optimum results, the author uses both an online and offline approaches to distribute and collect the questionnaires.

For reliability of measures, the calculated Cronbach's alpha test value is more than 0.70, thus acceptable (Nunnally, 1978; Hair *et al.*, 2006).

In terms of research method, survey method within quantitative approaches is the dominant method with 74.3% researcher using it (Chen and Holsapple, 2013). Therefore, the author also has selected the survey method to validate the framework in an Indian context.

For this research, convenience sampling is used to collect 31 responses from working executives and business owners in India. The survey questionnaire results are entered into SPSS for descriptive statistical analysis. The construct are subjected to confirmatory factor analysis using Smart PLS.

LITERATURE REVIEW

Empirically, the key factors of B2B marketplace usage are low cost, high-transaction efficiency, better rights transfer, which is at the right price, the right time, right quality and the right quantity of the verified source (Smart and Harrison, 2003; Shirzad and Bell, 2013). Also, the three key adoption factors found in the literature are, 'firm characteristics' (demands from inside the company), 'competitiveness of the business environment' (stress from the outside) and 'promotion/ support from top management' (Yu, 2007).

From a participant (supplier and buyer) point of view, to join the B2B e-marketplace, they shall be knowledgeable about the benefits. The main benefit quoted is enabling a company to ascertain its position in a marketplace and to expand the barriers to entry, thus giving it a competitive stance in regard to other companies (Botha *et al.*, 2004).

The empirical studies on the e-commerce found that the interplay of technology, culture and socio-economic factors affect the diffusion of B2B e-commerce. Besides technology,

www.IndianJournals.com
Members Copy, Not for Commercial Sale
Downloaded From IP - 14.139.251.107 on dated 26-Jul-2018

cultural and socio-economic factors are pivotal in bridging the gap between Internet usage and e-commerce diffusion (Yap *et al.*, 2006).

In a particular market, aid from the government, supportive policies, effective legal environment and encouraging socio-cultural environment act as the facilitators of e-commerce. As e-commerce becomes popular, these facilitators are still relevant, though effective legal environments become less of a facilitator (Zhu and Thatcher, 2010).

The B2B e-commerce industry in India is facing obstacles, evident from growth lag compared with the developed countries (Franco and Regi, 2016). A review of the literature reveals that in past little attention has been given to the participant's willingness to adopt an e-marketplace. Therefore, to propose an adoption framework, the current research study investigates the empirical and theoretical research to identify the factors that affect participants' willingness to adopt B2B e-commerce.

THEORIES ON B2B E-COMMERCE ADOPTION

The author, found around 10 technology adoption theories in the literature, directly or indirectly explaining e-commerce adoption (Hong and Zhu, 2006). Most of these theories (Table 1) have their origin in systems, psychology and sociology.

There are other not too prominent theories, but they do provide some explanations of the subject. For example, resource-based view (Wernerfelt, 1984) and expectation-confirmation theory (Oliver, 1980).

The author did a search of online research database 'PRO-QUEST' on 25 April 2017, with the search item 'Theory name' and 'Author name' and number of hits/search results are as follows: IDT: 4,808 hits, TOE: 321 hits, TRA: 2,982 hits, TPB: 5,266 hits, TAM: 12,827 hits and UTAUT: 1,000 hits.

The UTAUT has got numerous citations in the short time since 2011. The model is also confirmed in a cross-cultural study also applicable across countries (Oshlyansky *et al.*, 2007).

www.IndianJournals.com
Members Copy, Not for Commercial Sale
Downloaded From IP - 14.139.251.107 on dated 26-Jul-2018

Table 1: Popular technology adoption theories used to explain B2B e-commerce adoption

Theory	Author	No. of Search Hits (on "ProQuest")	Explanation
Innovation Diffusion Theory (DOI)	Rogers (1967)	4808	The individual receiver's perceptions of the five attributes of innovations (relative advantage, compatibility, complexity, trial ability and observability) predict an innovation's rate of adoption. In addition, other variables affecting innovation rate of adoption include; the type of innovation-decision, the nature of communication channels, the nature of the social system, and the extent of change agents' efforts in diffusing the innovation
TOE Framework	Tornatzky and Fleischer (1990)	321	It identifies three types of factors that affect technology innovation adoption: the technological context (e.g., availability, characteristics), organizational context (e.g., size, complexity of managerial structures, communication processes, availability of slack resources), and environmental context (e.g., industry characteristics and market structure, IT infrastructure, government regulation).
Theory of Reasoned Action (TRA)	Fishbein and Ajzen (1975)	2982	The beliefs influence attitudes, which, in turn, leads to the intention to use and finally to the actual performance of the behaviour. The stronger the intention, the more likely it will lead to the actual behaviour. Its main constructs are Attitude, Subjective Norm, Behavioural Intention & behaviour.
Theory of Planned Behaviour (TPB)	Ajzen (1985)	5266	TPB is an expansion of TRA, in which the construct behaviour is expanded to perceived behavioural control (Perceived ease difficulty of performing the behaviour and reflects past experience as well as anticipated impediments and obstacles).
The Technology Acceptance Model (TAM)	Davis *et al.* (1989)	12827	The TAM is to predict the consumer's acceptance of technology. Its main constructs are Behavioural Intention, Attitude, Perceived Usefulness and Perceived Ease of Use.
Unified Theory of Acceptance and Use of Technology (UTAUT)	Venkatesh *et al.* (2003)	1000	The theory has three direct determinants of intention to use (performance expectancy, effort expectancy, and social influence) and two direct determinants of usage behaviour (intention and facilitating conditions).

The UTAUT is as a better choice based on the variance analysis done by several researchers. The competing frameworks explained between 17% and 53% of the variance in the usage intentions, compared with UTAUT, that explains about 70% of the variance (adjusted R^2) in usage intention (Venkatesh *et al.*, 2003). The UTAUT is suitable at both organisational and individual levels.

It is used to explain acceptance and use of a technology (Baron *et al.*, 2006; Venkatesh and Zhang, 2010; Chen and Chang, 2011) in many research studies. Few of these include; a study of cognition of 243 users in northern Finland towards mobile services (Koivumäki *et al.*, 2008), a study of workplace superiors and colleagues on intention to use technology in 152 German enterprises (Eckhardt *et al.*, 2009), the adoption of social media by 409 United States non-profit organisations (Curtis *et al.*, 2010). The theory is also used to explain mobile technologies (Park *et al.*, 2007), mobile learning (Wang *et al.*, 2009), mobile shopping services (Yang, 2010), mobile banking (Yu, 2012), mobile stock trading (Tai and Ku, 2013) and location-based services (Zhou, 2012). Several studies found new constructs and extended UTAUT, for example two new constructs added in a study (attitude toward using technology, leadership) on the physicians' adoption of robotic-assisted surgery (Ben Messaoud *et al.*, 2011) and two new constructs (perceived playfulness, self-management) in the study of the acceptance of mobile learning in Taiwan (Wang *et al.*, 2009). For e-commerce, a positive relationship is found for three variables [usefulness, ease and social influence (SI)] to the intention to adopt m-banking (Deb and David, 2014). In negative opinion, the presence of a high number of independent variables is highlighted by critics (Bagozzi, 2007).

PROPOSED FRAMEWORK

Based on the literature review of B2B e-commerce adoption theories detailed above, an extension of UTAUT, the seven factors appeared to be significant direct determinants of intention or adoption in one or more of the individual models. These suitable factors form the proposed theoretical framework (Figure 1) addressing the B2B e-commerce adoption.

As per the framework, it is likely that performance expectancy (PE), effort expectancy and SI have a positive effect on behavioural intention (BI) to adopt B2B e-commerce platform. And, BI, facilitating conditions (FC) and cost have a positive effect on B2B e-commerce adoption.

The following text lists the constructs as per original UTAUT:

In UTAUT framework, the PE is defined as the extent to which an individual believes that using the system will help improve job performance (Venkatesh *et al.*, 2003). Effort expectancy (EE) is defined as the extent of ease connected with the use of the system (Venkatesh *et al.*, 2003). SI is defined as the extent of perception that influencers want him or her to use the new system (Venkatesh *et al.*, 2003). FC is defined as the

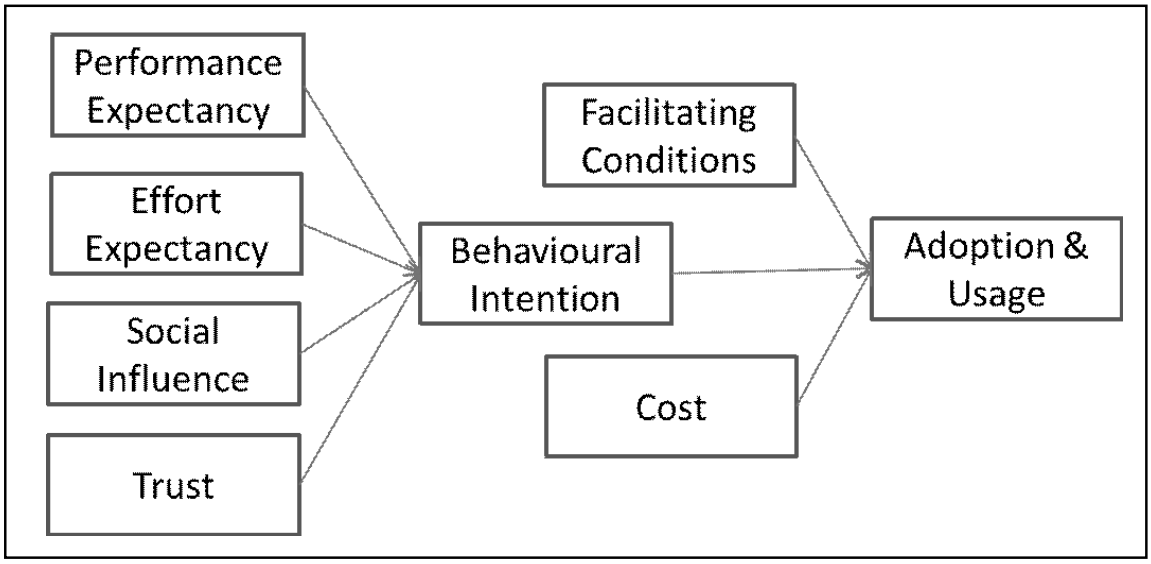

Figure 1: Graphical view of proposed research model
Note: The labels are used to describe the basic nature of the factors.

www.IndianJournals.com
Members Copy, Not for Commercial Sale
Downloaded From IP - 14.139.251.107 on dated 26-Jul-2018

extent of belief that the infrastructure is in place to support the use of the system (Venkatesh *et al.*, 2003).

The additional constructs added to the framework as following:

Trust (T) comprises the trusted confidence in the trustee's actions (Lee *et al.*, 2006). It is also a looking forward to that the trustee's promise can be relied on and that the trustee will act in benevolence. Trust is of utmost importance in e-commerce as we have limited or partial information about other trading-party (Hawes *et al.*, 1989; Ridings *et al.*, 2002). It reduces the information asymmetry between the parties. It is also the main harbinger of user participation and sustainable communities' formation (Casalo *et al.*, 2011). An Indian study discloses that trust has an indirect positive effect on the BI to adopt the Internet banking (Kesarwani and Bisht, 2012).

Cost (C) is another major factor. In India, a study in Andhra Pradesh state found that 'economic', has the positive influence on shoppers purchase decision through e-commerce (Kumar and Rao, 2015). In this context, it is suggested that the lower Internet service costs or low e-commerce cost, can encourage businesses to adopt e-commerce (Zhu *et al.*, 2006; Solaymani *et al.*, 2012). Evidence suggests that transaction costs in e-marketplace should be lower than those of traditional markets (Garcicano and Kaplan, 2001) so as to increase liquidity and chances for success (Clasen and Mueller, 2006). For this research, the author has considered the 'transaction cost'.

The BI is the degree to which an individual has made a conscious plan to perform or not perform a future behaviour.

For context variable, it is empirically found that they influenced some of the adoption factors of B2B e-commerce (Sila, 2013). Due to time and sample size constraints, the authors have not analysed the three context variables, namely firm type, firm size and firm's reputation.

FINDINGS

In Table 2, the statistical analysis of the user opinion survey response shows that all the items (variables, forming the construct) loading barring one is above 0.8, indicating that more than half of the variance is captured by the constructs. The internal consistency reliability of each construct is tested via Cronbach's alpha and the composite reliability. The score for both (barring cost) is above 0.70, that is an acceptable value of internal consistency for exploratory research (Backlay *et al.*, 1995).

The percentage of the variance captured by a construct is given by the average variance extracted (AVE), demonstrating the convergent validity. As per Table 3, all AVE values pertaining to each construct are higher than the suggested threshold value of 0.50. Also shown in Table 3, is that constructs are distinct from the others as the square root of its AVE is greater than its correlation with other latent constructs (Backlay *et al.*, 1995) as a proof of discriminant validity.

www.IndianJournals.com
Members Copy, Not for Commercial Sale
Downloaded From IP - 14.139.251.107 on dated 26-Jul-2018

Table 2: Survey items, factor loadings and reliability estimates

Construct	Items	Loadings	Cronbach's Alpha	Composite Reliability
Effort expectancy (EE)	EE1	0.944	0.824	0.917
	EE2	0.897		
Facilitating conditions (FC)	FC1	0.929	0.791	0.904
	FC2	0.888		
Performance expectancy (PE)	PE1	0.940	0.847	0.929
	PE2	0.922		
Social influence (SI)	SI1	0.971	0.926	0.964
	SI2	0.959		
Intent (I)	I	1.000	1.000	1.000
Trust (T)	T1	0.802	0.762	0.880
	T2	0.964		
Cost (C)	C1	0.926	0.461	0.768
	C2	0.637		

Table 3: Convergent and discriminant validity

	Average Variance Extracted (AVE)	Cost	Effort Expectancy	Facilitating Conditions	Intent	Performance Expectancy	Social Influence	Trust	Use
Cost	0.632	0.795							
Effort expectancy	0.847	0.205	0.921						
Facilitating conditions	0.826	0.059	0.400	0.909					
Intent	1.000	0.141	0.082	0.486	1.000				
Performance expectancy	0.867	0.387	0.477	0.134	0.410	0.931			
Social influence	0.931	0.420	0.314	0.090	0.259	0.572	0.965		
Trust	0.787	-0.379	-0.435	-0.196	-0.095	-0.730	-0.479	0.887	
Use	1.000	-0.003	-0.019	0.517	0.721	0.323	0.089	-0.062	1.000

Table 4: Descriptive statistical analysis

Descriptive Statistics (*N* = 31, Minimum =1, Maximum = 7)						
Construct	**Mean**	**Observed Variables**	**Mean**	**Std. Deviation**	**Skewness**	**Kurtosis**
Performance expectancy	4.58	Useful in job/business	4.58	1.649	-0.844	0.257
		Increase in productivity	4.58	1.501	-0.989	0.623
Effort expectancy	4.97	System: interaction is clear and understandable	4.84	1.344	-0.479	1.036
		System: easy to use	5.1	1.399	-0.73	0.943
Social influence	4.12	Influenced by important people	4	1.713	-0.255	-0.523
		Senior management is helpful	4.23	1.783	-0.025	-0.671
Facilitating conditions	4.86	Has necessary knowledge/resources	4.9	1.326	-0.087	-1.269
		Assistance available	4.81	1.515	-0.695	0.124
Trust	4.31	Information is valid and accurate	4.23	1.647	-0.243	-0.663
		Buyer/seller will fulfil promise	4.39	1.52	-0.47	0.048
Cost	4.63	Transaction cost	4.84	1.551	-0.744	-0.038
		Produce cost	4.42	1.587	-0.377	-0.324

www.IndianJournals.com
Members Copy, Not for Commercial Sale
Downloaded From IP - 14.139.251.107 on dated 26-Jul-2018

The descriptive statistical analysis results are shown in Table 4. The standard error associated with all the variables being negligible, the observed sample mean values can be interpreted in general. The observed mean value of the construct (and variables) shows relatively more or less significance of that constructs over others.

CONCLUSION

This study proposes a comprehensive framework to explain the factors affecting B2B e-commerce adoption in India.

The data analysis of a user opinion survey, indicate that the constructs 'Performance Expectancy', 'Social Influence' and 'Trust' are all determinants of BI to use B2B e-commerce. In addition, 'behavioural intention', 'facilitating conditions' and 'cost' are determinants of actual usage of B2B e-commerce.

The EE is a relatively most important factor with 'Ease of Use' and 'Clear and Understandable' system interaction, making more and more users to intend or actually adopt the B2B e-commerce systems; thus, service providers and organisations shall concentrate on awareness, training and education of users. The FC are also relatively major factors highlighting the need for making available assistance, technical support as well as resources (technical, infrastructure and organisational) required for B2B e-commerce system use. The author found that beyond the select department and users lacks in resource support, thus require an extra-budgetary provision and management attention.

The cost of a transaction on B2B e-commerce is lower and this point has to be promoted and advertised to small and medium enterprises so as tip them from intent to actual usage of the system, thus getting the requisite benefits. The PE (usefulness, improvement in productivity) also influences the intent to adopt. The non-adopters can be made aware of the benefits via advertisements.

The SI and trust are factors, but relatively not as important for the B2B e-commerce system implementation decision is normally done at the top level (who anyway support B2B e-commerce) and most of the platforms in the country are implemented by well-funded large organisations/industry consortium with or without government support. In view of significant SI, the influencers (who can affect their peer group) shall be given special attention and promotional offers.

This research has successfully extended the applicability of the UTAUT in the B2B e-commerce adoption context by incorporating 'trust' and 'cost'.

www.IndianJournals.com
Members Copy, Not for Commercial Sale
Downloaded From IP - 14.139.251.107 on dated 26-Jul-2018

LIMITATION OF THE RESEARCH

The fellow researchers can further build on the research via framework validation using structural equation modelling on a larger dataset of responses collected across India. The logical relationship between constructs can be explained using the total interpretive structural modelling (TISM) methodology. The framework can be further tested on different industries, respondent demography, geography or organisational characteristic perspective. The B2B e-commerce adoption framework/model fit may be improved with larger survey dataset and a better mix of respondents.

The study is cross-sectional as it measured perceptions and intentions at a single point in time. However, perceptions may change over time with experience (Venkatesh and Davis, 2000; O'Neill, 2003); thus, a longitudinal study may add some more insights on causality and interrelationships. The effect of mediating variables (firm size, firm type and firm reputation) is not analysed in the present study, but it is further explored in the future study.

REFERENCES

Ajzen I, 1985. "From intentions to actions: A theory of planned behaviour", Kuhl J and Beckmann J, *Action Control: From Cognition to Behaviour*, Springer-Verlag, Berlin; Heidelberg; New York, pp. 11–39.

Backlay D, Higgins C and Thompson R, 1995. "The partial least square approach to causal modelling: Personal computer adoption and use as an illustration", *Technology Studies*, Vol. 2, No. 2, pp. 285–309.

Bagozzi RP, 2007. "The legacy of the technology acceptance model and a proposal for a paradigm shift", *Journal of the Association for Information Systems*, Vol. 8, No.4, pp. 244–254.

Bailey J, 1998. "Internet price discrimination: Self-regulation, public policy, and global electronic commerce", *Presented at twenty sixth annual telecommunications policy research conference*, Technology Management and Policy, MIT, Cambridge, MA.

Baron S, Patterson A and Harris K, 2006. "Beyond technology acceptance: Understanding consumer practice", *International Journal of Service Industry Management*, Vol. 17, No. 2, pp. 111–135.

BenMessaoud C, Kharrazi H and MacDorman KF, 2011. "Facilitators and barriers to adopting robotic-assisted surgery: Contextualizing the unified theory of acceptance and use of technology", *PLoSOne*, Vol. 6, No. 1.

Biolchini J, Mian PG, Natalie AC and Travassos, 2005. "Systematic review in software engineering", System engineering and computer science department. COPPE/UFRJ. Technical Report ES 679/05, Rio De Janerio, Brazil.

Botha J, Bothma C and Geldenhuys P, 2004. *Managing E-Commerce*, Juta and Co, Lansdowne.

Brynjolfsson E and Smith M, 2000. "Frictionless commerce–a comparison of internet and conventional retailers", *Management Science*, Vol. 46, No.4, pp. 563–585.

Casalo L, Flavian Cand Guinaliu M, 2011. "The generation of trust in the online services and product distribution: The case of Spanish electronic commerce", *Journal of Electronic Commerce Research*, Vol. 12, No. 3, pp. 199–213.

Chen KY and Chang ML, 2011. "User acceptance of NFC mobile phone service: An investigation based on the UTAUT model", *The Service Industries Journal*.

Chen L and Holsapple CW, 2013. "E-business adoption research: State of the art", *Journal of Electronic Commerce Research*, Vol. 14, No. 3, pp. 261–287.

Clasen M and Mueller RAE, 2006. "Success factors of agribusiness digital marketplaces", *Electronic Markets*, Vol. 16, No.4, pp. 349–360.

Curtis L, Edwards C, Fraser KL, Gudelsky S, Holmquist J, Thornton K and Sweetser KD, 2010. "Adoption of social media for public relations by non-profit organizations", *Public Relations Review*, Vol. 3, No. 1, pp. 90–92

Davis FD, 1989. "Perceived usefulness, perceived ease of use and user acceptance of information technology", *MIS Quarterly*, Vol. 13, No.3, pp. 319–340.

Deb M and David EL, 2014. "An empirical examination of customers' adoption of m-banking in India", *Marketing Intelligence and Planning*, Vol. 32, No.4, pp. 475–494.

Eckhardt A, Laumer S and Weitzel T, 2009. "Who influences whom? Analyzing workplace referents' social influence on IT adoption and non-adoption", *Journal of Information Technology*, Vol. 24, No. 1, pp. 11–24.

Fishbein M and Ajzen I, 1975. *Belief, Attitude, Intention and Behaviour: An Introduction to Theory and Research*, Addison-Wesley, Reading, MA.

Franco CE and Bulomine RS, 2016. "Advantages and challenges of e-commerce customers and businesses: In Indian perspective",

International Journal of Research – Granthaalayah, Vol. 4, No. 3, pp. 7–13.

Garcicano L and Kaplan SN, 2001. "The effect of business to business e-commerce on transaction costs", *Journal of Industrial Economics*, Vol. 49, pp. 463–485.

Gunasekarana A, Marrib HB, McGaughey RE and Nebhwani MD, 2002. "E-commerce and its impact on operations management", *International Journal of Production Economics*, Vol. 75, pp. 185–197.

Hair JF, Anderson RE, Tatham RL and Black WC, 2006. *Multivariate Data Analysis*,5th ed., Dorling Kindersley (India), Patparganj, Delhi.

Hawes J, Mast K and Swan J, 1989. "Trust earning perceptions of sellers and buyers", *Journal of Personal Selling and Sales Management*, Vol. 9, pp. 1–8.

Hong W and Zhu K, 2006. "Migrating to internet-based e-commerce: Factors affecting e-commerce adoption and migration at the firm level", *Information and Management*, Vol. 43, No.2, pp. 204–221.

Karami A, 2014. "The effects of electronic commerce on development of business activities in developing countries", *International Journal of e-Education, e-Business, e-Management and e-Learning*, Vol. 4, No. 3, pp. 166–171.

Kesharwani A and Bisht SS, 2012. "The impact of trust and perceived risk on internet banking adoption in India", *International Journal of Bank Marketing*, Vol. 30, No. 4, pp. 303–322.

Kitchenham B and Charters S, 2007. "*Guidelines for Performing Systematic Literature Reviews in Software Engineering"*, Technical Report, EBSE 2007-001, 2.

Koivumäki T, Ristola A and Kesti M, 2008. "The perceptions towards mobile services: An empirical analysis of the role of use facilitators", *Personal and Ubiquitous Computing*, Vol. 12, No. 1, pp. 67–75.

Kumar DU and Rao KV, 2015. "Structural equation modelling of factors that influence the shopper's purchase decision through e-commerce", *Indian Journal of Management Science*, Vol. 5, No. 2, pp. 27.

Lee HY, Ahn H and Han I, 2006. "Analysis of trust in the e-commerce adoption", *Proceedings of the 39th Hawaii international conference on system sciences*, Big Island, HI.

Nunnally JC, 1978. *Psychometric Theory*, 2nd ed., McGraw-Hill, New York, NY.

O'Neill M, 2003. "The influence of time on student perceptions of service quality: The need for longitudinal measures', *Journal of Educational Administration*, Vol. 41, No. 3, pp. 310–325.

Oliver RL, 1980. "A cognitive model for the antecedents and consequences of satisfaction", *Journal of Marketing Research*, Vol. 17, pp. 460–469.

Oshlyansky L, Cairns P and Thimbleby H, 2007. "Validating the unified theory of acceptance and use of technology (UTAUT) tool cross culturally", *Proceedings of the 21st British HCI Group annual conference on people and computers*, British Computer Society, pp. 83–86.

Park JK, Yang SJ and Lehto X, 2007. "Adoption of mobile technologies for Chinese consumers", *Journal of Electronic Commerce Research*, Vol. 8, No. 3, pp. 196–206.

Pousttchi K, Tilson D, Lyytinen K and Hufenbach Y, 2015. "Introduction to the special issue on mobile commerce: Mobile commerce research yesterday, today, tomorrow-what remains to be done?", *International Journal of Electronic Commerce*, Vol. 19, No. 4, pp. 1–20.

Regina M, 2016. "Mobile only wydr targets one stop B2B marketplace", Business World Magazine, N/A. Retrieved from http://bwdisrupt.businessworld.in/article/Mobile-Only-Wydr-Targets-One-Stop-B2B-Marketplace-/30-08-2016-105006/

Ridings C, Gefen D and Arinze B, 2002. "Some antecedents and effects of trust in virtual communities", *Journal of Strategic Information Systems*, Vol. 11, pp. 271–295.

Shirzad SR and Bell D, 2013. "A systematic literature review of flexible e-procurement marketplace", *Journal of Theoretical and Applied Electronic Commerce Research*, Vol. 8, No. 2, pp. 49–70.

Sila I, 2013. "Factors affecting the adoption of B2B e-commerce technologies", *Electronic Commerce Research*, Vol. 13, pp. 199–236.

Smart A and Harrison A, 2003. "Online reverse auctions and their role in buyer-supplier relationships", *Journal of Purchasing and Supply Management*, Vol. 9, No. 5–6, pp. 257–268.

Solaymani S, Sohaili K and Esmaeil AY, 2012. "Adoption and use of e-commerce in SMEs: A case study', *Electronic Commerce Research*, Vol. 12, pp. 249–263.

Tai YM and Ku YC, 2013. "Will stock investors use mobile stock trading? A benefit-risk assessment based on a modified UTAUT model", *Journal of Electronic Commerce Research*, Vol. 14, No. 1, pp. 67–86.

Tornatzky L and Fleischer M, 1990. *The Process of Technology Innovation*, Lexington Books, Lexington, MA.

Upadhyaya P and Mohanan P, 2009. *Electronic Marketplace Adoption: A Case Study of Manufacturing SME*, The ICFAI University Press, pp. 30–42.

Vaithianathan S, 2010. "A review of e-commerce literature on India and research agenda for the future", *Electronic Commerce Research*, Vol. 10, pp. 83–97.

Venkatesh V and Davis FD, 2000. "A theoretical extension of the technology acceptance model: Four longitudinal field studies", *Management Science*, Vol. 46, No. 2, pp. 186–204.

Venkatesh V and Zhang X, 2010. "Unified theory of acceptance and use of technology: U.S. vs. China", *Journal of Global Information Technology Management*, Vol. 13, No. 1, pp. 5–27.

Venkatesh V, Morris MG, Davis GB and Davis FD, 2003. "User acceptance of information technology: Toward a unified view", *MIS Quarterly*, Vol. 27, No. 3, pp. 425–478.

Wang YS, Wu MC and Wang HY, 2009. "Investigating the determinants and age and gender differences in the acceptance of mobile learning", *British Journal of Educational Technology*, Vol. 40, No. 1, pp. 92–118.

Wernerfelt B, 1984. "A resource-based view of the firm", *Strategic Management Journal*, Vol. 5, pp. 171–180.

Yang K, 2010. "Determinants of US consumer mobile shopping services adoption: Implications for designing mobile shopping services", *Journal of Consumer Marketing*, Vol. 27, No. 3, pp. 262–270.

Yap A, Das J, Burbridge J and Cort K, 2006. "A composite-model for e-commerce diffusion: Integrating cultural and socioeconomic dimensions to the dynamics of diffusion", *Journal of Global Information Management*, Vol. 14, No. 3, pp. 17–34.

www.IndianJournals.com
Members Copy, Not for Commercial Sale
Downloaded From IP - 14.139.251.107 on dated 26-Jul-2018

Yu CS, 2012. "Factors affecting individuals to adopt mobile banking: Empirical evidence from the UTAUT model", *Journal of Electronic Commerce Research*, Vol. 13, No. 2, pp. 104–121.

Yu CS, 2007. "What drives enterprises to trading via B2B e-marketplaces?", *Journal of Electronic Commerce Research*, Vol. 8, No. 1, pp. 84–102.

Zhou T, 2012. "Examining location-based services usage from the perspectives of UTAUT and privacy risk", *Journal of Electronic Commerce Research*, Vol. 13, No. 2, pp. 135–144.

Zhu K, Dong S, Xu SX and Kraemer KL, 2006. "Innovation diffusion in global contexts: Determinants of post-adoption digital transformation of European companies", *European Journal of Information Systems*, Vol. 15, No. 6, pp. 601–616.

Zhu L and Thatcher SMB, 2010. "Information ecology: A new institutional economics perspective on global e-commerce adoption", *Journal of Electronic Commerce Research*, Vol. 11, No. 1, pp. 53–74.

www.IndianJournals.com
Members Copy, Not for Commercial Sale
Downloaded From IP - 14.139.251.107 on dated 26-Jul-2018

ISSN: 2350-0328

International Journal of AdvancedResearch in Science, Engineering and Technology

Vol. 5, Issue 6 , June 2018

Analysis of Three Types of Solar Systems: PV, Flat Plate Thermal, and Hybrid PV-T Using TRNSYS Model

Piyush Rawat, Dr J. P. Kesari

M.Tech, Department of Mechanical Engineering, Delhi Technological University, Delhi
Associate Professor, Department of Mechanical Engineering, Delhi Technological University, Delhi

ABSTRACT: The upcoming years for India are not only important for the development of the country but also creating opportunities and awareness within the society. Most of our industrial processes and buildings need energy including both heat and electricity, and both of them can be provided using hybrid solar photovoltaic/thermal system. Solar thermal and photovoltaic systems absorb energy from solar radiation, but due to limited availability of area, installing separate system is expensive and land consuming. Hence a combined system for improved utilisation of solar radiation is suitable, less expensive and consumes less area for installation. In this paper, simulation models of the solar thermal collector, photovoltaic system and photovoltaic thermal system are presented.

I. INTRODUCTION

The most important development of solar technology is a photovoltaic: a solar energy utilising system that uses semi-conductors for direct conversion of solar radiation into electricity. Photovoltaic (PV) systems are made up of a large number of cells, generally made of crystalline silicon. They are connected in series or parallel to form a metal frame which is known as a module. The module is further connected in series and parallel combination as per the requirement. When solar radiation falls on the module, a small current of electricity is produced.

Flat plate thermal collector harnesses the energy provided by the sun for heating the water. The hot water produced by the solar heating system is stored and can be used to supplement domestic hot water requirement, larger stores of water (like swimming pools), under-floor heating, and for space heating/cooling.

Photovoltaic thermal hybrid solar collector (PV-T) converts the solar radiation into thermal and electrical energy. This system consists of solar cells which are directly pasted over a thermal collector. The hybrid system produces electricity and process heat from sun's radiation. It is highly recommended for industries which demand high process heat and electricity.

These three systems are base of solar energy; hence a comparative study is to be done between the systems for choosing the most reliable system for a particular situation. Using TRNSYS simulation tool, these systems are modelled and executed and the results are compared.

II. MATHEMATICAL MODELLING

A. Photovoltaic (PV) System

A photovoltaic component (Type94) is used for simulating the electrical performance, storage, utility grid, the area required etc. for aPV module. The I-V characteristics of a single module are predicted by an empirical equivalent circuit model (Type94) using mathematical equations governing it. The slope of the IV curve at short-circuit conditions is assumed to be zero. The four-parameter equivalent circuit was developed by Townsend in 1989 [1] and further detailing was done by Duffie and Beckam in 1991 [2]. The model was further added in TRNSYS by Eckstein [1990].

The "four parameters" in the model are $I_{L,ref}$, $I_{o,ref}$, γ, andR_s.

ISSN: 2350-0328
International Journal of AdvancedResearch in Science, Engineering and Technology
Vol. 5, Issue 6 , June 2018

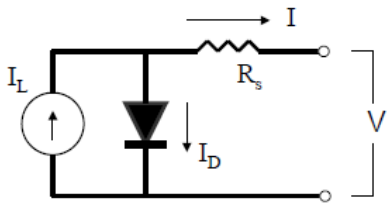

Figure 2.1: Four Parameter Model

where, $I_{L,ref}$= module photocurrent at reference condition, I_o = Diode reverse saturation current, γ= empirical PV curve-fitting parameter, R_s = Module series resistance

B.Performance under operating conditions

The IV characteristics of a PV change with both insolation and temperature. For every time step, the PV model employs environmental condition like insolation and temperature, and the four constants $I_{L,ref}$, $I_{o,ref}$, γ, and R_s. The equation of circuit shown in fig. 2.1 is as follows,

$$I = I_L - I_o\left[\exp\left(\frac{q}{\gamma k T_c}(V + IR_s)\right) - 1\right] \quad (2.1.1)$$

where,
q = Electron charge constant
k = Boltzmann constant 1.38 x 10^{-23} ($kg.m^2.s^{-2}.K^{-1}$)
T_c= Module temperature (K)
I_L = Photo-current and depends linearly on incident radiation.

C. Calculating $I_{L,ref}$, $I_{o,ref}$, γ, and R_s

To calculate $I_{L,ref}$, $I_{o,ref}$, γ, andR_s, certain parameters are required Type94 component. The first step is to substitute the current and voltage into eq. (2.1.1) at the open-circuit, short circuit and maximum power conditions and neglecting the negative term for simplifying the algebra because I_o is very small, generally of order 10^{-6} A.Hence after rearrangement,

$$I_{L,ref} \approx I_{sc,ref} \quad (2.1.2)$$

$$\gamma = \frac{q\left(V_{mp,ref} - V_{oc,ref} + I_{mp,ref}R_s\right)}{kT_{c,ref}\ ln\left(1 - \frac{I_{mp,ref}}{I_{sc,ref}}\right)} \quad (2.1.3)$$

$$I_{o,ref} = \frac{I_{sc,ref}}{exp\left(qV_{oc,ref} \Big/ \gamma k T_{c,ref}\right)} \quad (2.1.4)$$

$$\frac{\partial V_{oc}}{\partial T_c} = \mu_{voc} = \frac{\gamma k}{q}\left(ln\left(\frac{I_{sc,ref}}{I_{o,ref}}\right) + \frac{T_c \mu_{isc}}{I_{sc,ref}} - \left(3 + \frac{q\varepsilon}{AkT_{c,ref}}\right)\right) \quad (2.1.5)$$

where, $A = \gamma / N_s$

$V_{oc,ref}$= Open circuit voltage at reference condition (K)
$V_{mp,ref}$ = Voltage at maximum power point along IV curve, reference condition
$I_{sc,ref}$ = Short circuit current at reference condition
$I_{mp,ref}$ = Current at maximum power point along IV curve, reference condition
$I_{o,ref}$ = Diode saturation current at reference condition
μ_{voc} = temperature coefficient of open-circuit voltage (V/K)
μ_{voc}= temperature coefficient of short-circuit current (A/K)
N_s = Number of individual cells

ISSN: 2350-0328

International Journal of AdvancedResearch in Science, Engineering and Technology

Vol. 5, Issue 6 , June 2018

One additional equation is required in order to calculate the last unknown parameterR_s. To derive the fourth equation, analytic derivative of voltage with respect to temperature for open-circuit condition is taken (2.1.5). Circuit characteristics are calculated by these 4 equations using iterative method.

D. Solar Thermal Collector System

Evaluation of flat plate solar collector performance was done by H. C. Hottel and A. Willier in 1958 at University of Arizona[3]. The collector efficiency of a flat-plate solar collector is defined as the ratio of useful heat gain to the solar radiation incident on the collector. At any instant mathematically,

$$\eta = \frac{q_u}{AI} \quad (2.2.1)$$

where,

q_u = Useful Heat Gain (rate of heat transferred to the working fluid (kJ/hour)

A = Area of Absorbing Plate (m^2)

I = Instantaneous Radiation Energy (kJ/m^2.hour)

Energy balance for absorbing plate, $q_u = AS - q_L$ (2.2.2)

$$q_L = U_L A(T_{mp} - T_a) \quad (2.2.3)$$

$$q_u = AS - U_L A(T_{mp} - T_a) \quad (2.2.4)$$

where,

S = Incident Solar Flux absorbed by the collector plate

q_L = Rate at which Energy is lost

T_{mp}= mean plate temperature of absorber plate

T_a = ambient temperature

A modified equation is also employed, if T_{mp} is replaced with temperature of fluid flowing in the pipe also called local fluid temperature (T_f).

$$q_u = F'[AS - U_L A(T_f - T_a)] \quad (2.2.5)$$

where, F' is the collector efficiency factor and it is defined as the ratio of actual useful heat collection rate to the useful heat collection rate, if mean plate temperature is at local fluid temperature. Since, it is difficult to find local fluid temperature or mean plate temperature. Hence equation was further modified on the basis on inlet fluid temperature,

$$q_u = F_R A[S - U_L(T_{in} - T_a)] \quad (2.2.6)$$

Where F_R is called the collector heat-removal factor. It is the ratio of actual useful heat collection rate to the useful heat collection rate, if mean plate temperature is at inlet fluid temperature.

$$F_R = \frac{\dot{m}C_p}{U_L A}\left[1 - exp\left(-\frac{F' U_L A}{\dot{m}C_p}\right)\right] \quad (2.2.7)$$

This equation (2.2.7) is also known as Hottel – Whillier – Bliss Equation.

E. Photovoltaic Thermal (PV-T) System

L.W. Florschuetz [1979] extended the work of Hottel-Whillier model and performed the analysis of combined photovoltaic/thermal (PV/T) flat plate collectors [4]. The temperature gradients in the absorber, transverse to the direction of flow field were treated independently of those parallel to the flow direction. Also, the temperature gradient across the absorber thickness was neglected and the cell efficiency was represented as a linearly decreasing function of cell temperature.

The modified overall loss heat transfer coefficient ($\bar{U}_L$)

$$\bar{U}_L = U_L - (S/\alpha).\eta_r.\beta_r = U_L - \tau.H_T.\eta_r.\beta_r \quad (2.3.1)$$

$$\bar{S} = S(1 - \eta_a/\alpha) \quad (2.3.2)$$

where,

U_L = overall loss heat transfer coefficient for flat plate collector (W/m^2.K)

S = solar radiation per unit area absorbed at absorber surface and $\bar{S}$ modified value

α = effective absorptance of collector absorber

η= cell array efficiency (η_r refers to value evaluated at reference temperature)

β_r = temperature coefficient of solar cell efficiency (1/K)

τ = transmittance of collector cover system

H_T = solar radiation per unit area incident on collector (W/m^2)

ISSN: 2350-0328
International Journal of AdvancedResearch in Science, Engineering and Technology
Vol. 5, Issue 6 , June 2018

k = thermal conductivity (W/m.K)
t = thickness of absorber (mm)

Collector efficiency factor and collector heat removal factor were also modified by Florschuetz which were originally given by Hottel and Whiller.

Modified collector efficiency factor $(\bar{F}') = \frac{1}{1/F_{WD} + \bar{U}_L/U_f}$ (2.3.3)

where $F_{WD} = \left(1 - \frac{D}{W}\right)F + \frac{D}{W}$ (2.3.4)

with $F = \frac{\tanh[m(W-D)/2]}{m(W-D)/2}$ and $m = \bar{U}_L/kt$ (2.3.5)

Finally modified useful energy $(\bar{Q}_u) = A_c.\overline{F}_R\ .\ [\bar{S} - \bar{U}_L\ (T_{f,i} - T_a)$ (2.3.6)

where, the modified collector heat removal factor, $\overline{F}_R$ is given by,

$\overline{F}_R = \frac{G.C_p}{\overline{U}_L}[1 - exp(-\overline{U}_L.\overline{F'}/GC_p)]$ (2.3.7)

Using energy balance electrical output $(Q_e) = S.A_c - \bar{Q}_u - Q_L$ (2.3.8)

Therefore, $Q_e = \frac{A_c.\eta_a.S}{\alpha}\{1 - \frac{\eta_r.\beta_r}{\eta_a}[\bar{F}_R(T_{f,i} - T_a) + \frac{\bar{S}}{\bar{U}_L}(1 - \bar{F}_R)]\}$ (2.3.9)

where,

F_R = Collector heat removal factor ($\overline{F}_R$ is modified collector heat removal factor for cell/plate collector)
G = collector fluid mass flow rate per unit collector area (kg/sec.m^2)
C_p = specific heat of collector fluid (kJ/kg.K)
t = thickness of plate (mm)
A_c =collector area (m^2)
T_a = Ambient temperature (K)
$T_{f,i}$ = Inlet fluid temperature (K)

His results showed that $\overline{F}_R$ and $\bar{F}'$differ from $F_R$and F' respectively because of the modified value of U_L. No more than about 1% of $\overline{F}_R$ and $\bar{F}'$differ from F_R and F' respectively for any thermal design. Hence it was concluded that for practical purposes $F_R$and F' can be used instead of $\overline{F}_R$ and $\bar{F}'$ respectively.

III. SIMULATION MODEL

Project models made on TRNSYS are set up by connecting various components together and outputs are graphically displayed on a different window. Each component described by TRNSYS is mathematically modelled with proper units.

A. Load profile

Time dependent forcing function is used for creating a load profile. An average value of the function is multiplied with a common magnitude which produces a load profile for a given time step. A time step of 0.25 hour is considered. A load profile for a load of 6 kWh or 21,600 kJ is created using the time dependent forcing function, i.e. the area under the load profile is 21,600. The electrical load or the demand per day is assumed constant throughout the year. Figure 3.1shows the load profile of 6kWh per day.

ISSN: 2350-0328
International Journal of AdvancedResearch in Science, Engineering and Technology
Vol. 5, Issue 6 , June 2018

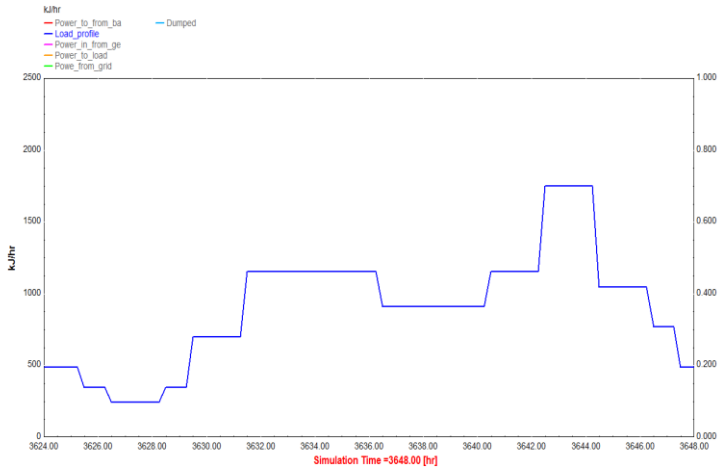

Figure 3.1: Load profile per day.

B. Photovoltaic (PV) model

For modelling PV system, module's details are taken from Vikram Solar panel, model number: ELDORA 300P. Details of the module are given in table 3.1. Standard test conditions for the module are 1000 W/m^2 of solar insolation, AM 1.5 and 25^{o}C cell temperature. The incident angle on the title surface is 45^o.

Table 3.1: Vikram Solar ELDORA 300P specifications

Sno.		
1	Rated Peak Power (P_{mpp})	300W
2	Open Circuit Voltage (V_{oc})	45.1V
3	Short Circuit Current (I_{sc})	8.74A
4	Rated Voltage (V_{mpp})	37.28V
5	Rated Current (I_{mpp})	8.05A
6	Fill Factor (FF)	76.31%
7	Efficiency	15.63%
8	Module Temperature at NOCT	45^{o}C
9	Dimensions	1955x982x36 mm
10	Temperature coefficient at I_{sc}	0.052
11	Temperature coefficient at V_{oc}	-0.310
12	Number of cell wired in series	72
13	Insolation at NOCT	800 W/m^2

Connections are made in such a way that power generated by the PV array is provided to the electrical load first. If the demand of load is fully filled, then power produced by the PV array is transferred to the battery for storage. Also, power from the battery will be withdrawn if the required power is not provided to the load. During low power generation, the grid is connected to supply the power. Specification for inverter/regulator and battery are shown in table 3.2.

Table 3.2: Inverter/regulator and Battery PARAMETERS

Sno.		
1	Regulator efficiency	0.78
2	Inverter Efficiency	0.96
3	High limit on fractional state of charge (FSOC)	0.95
4	Low limit on FSOC	0.1
5	Charge to discharge limit on FSOC	0

ISSN: 2350-0328

International Journal of AdvancedResearch in Science, Engineering and Technology

Vol. 5, Issue 6 , June 2018

6	Cell energy capacity	300Wh
8	Cell in series and parallel	12, 1 resp.
9	Charging Efficiency	0.9

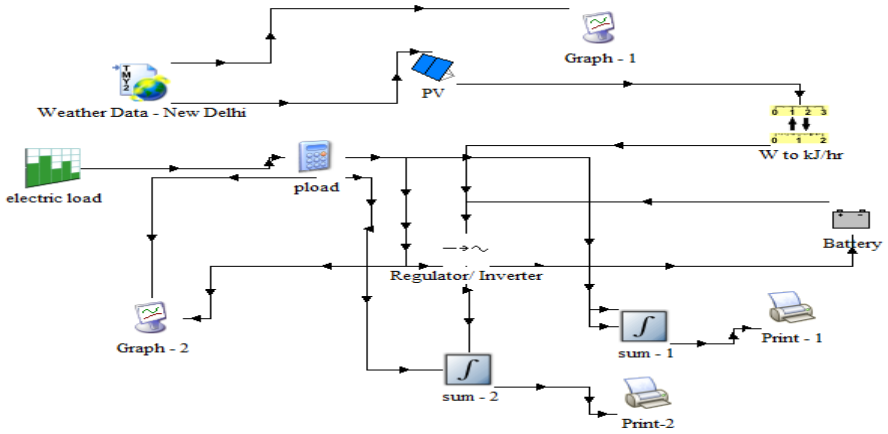

Figure 3.3: PV model.

C. Photovoltaic Thermal (PV/T) model

For modelling PV/T system, work of Florschuetz for the flat plate collector operating at peak power is employed. PV cells are directly pasted over the collector and it is assumed that the cell temperature is equal to collector temperature. PARAMETER details for PV-Thermal collector Type50 are shown in table 3.3.

Table 3.3: PV-Thermal collector (type50) PARAMETER details.

Sno.		
1	Collector Area	10m^2
2	Collector Efficiency Factor	0.7
3	Fluid thermal Capacity	4.19 kJ/kg.K
4	Collector plate absorptance	0.7
5	Number of glass cover	1
6	Collector plate emittance	0.9
7	Loss coefficient	20 kJ/hr.m^2.K
8	Collector Slope	45^o
9	Extinction Coefficient Thickness Product	0.03
10	Temperature Coefficient of PV cell efficiency	-0.0041 1/K
11	Temperature at cell reference efficiency	25^{0}C
12	Packing factor	1
13	Cell Efficiency	15.63%

Water is pump below the PV-T collector from 8 hour to 18 hour with a mass flow rate of 50kg/hour. Other parameters like collector plate absorbtance, emittance, and the loss coefficient are taken from the work done by Ram Kumar Agarwal and H. P. Garg [1994] [6] Packing factor is the ratio of PV cell area to absorber area with a default value of 1. A similar approach is also considered for the electrical part of the PV-T system, i.e. regulator/inverter compares the electrical load and the power produced by the PV array as explained in section 3.2. Parameters for regulator/inverter and battery are given in table 3.2.

ISSN: 2350-0328
International Journal of AdvancedResearch in Science, Engineering and Technology
Vol. 5, Issue 6 , June 2018

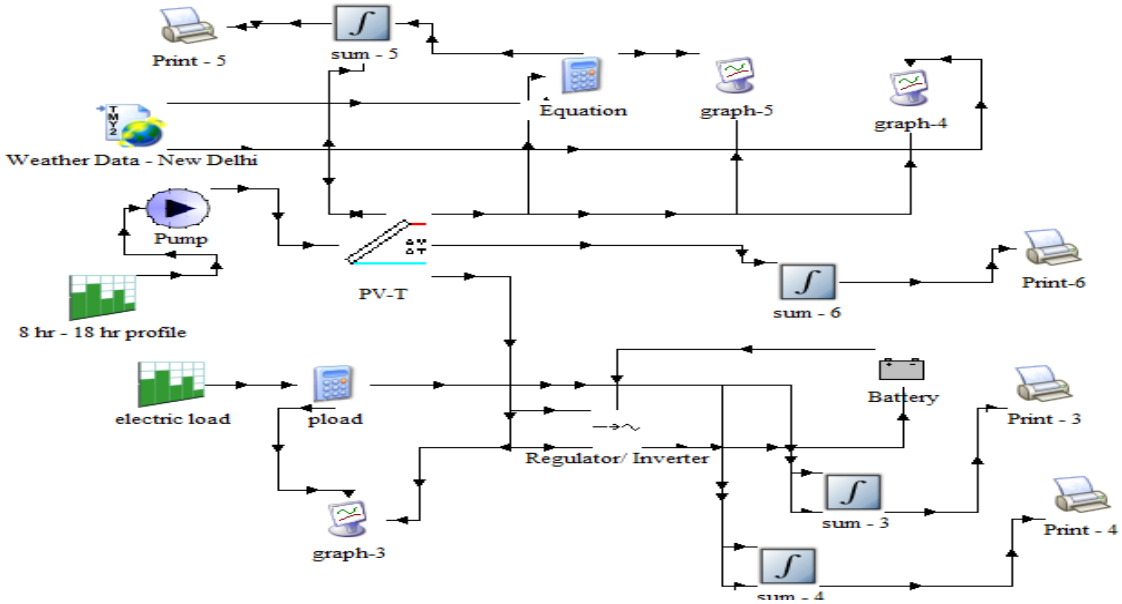

Figure 3.4: PV-T model

D. Flat plate solar thermal collector model

For modelling solar thermal collector, work done by H. C. Hottel and A. Willier in 1958 at University of Arizona for evaluating the performance of flat plate collector is employed. TRNSYS describes the work done by H. C. Hottel and A. Willier using a Type73 component.

Table 4.5: PARAMETER details for thermal collector.

Sno.	Parameter	
1	Number in series	1
2	Collector Area	$10m^2$
3	Fluid Specific heat	4.190 kJ/kg.k
4	Collector fin efficiency	0.7
5	Bottom, Edge loss coefficient	20 kJ/hr.m2.K
6	Absorber plate emittance	0.9
7	Absorptance of absorber plate	0.9
8	Number of covers	1
9	Extinction coeff. thickness product	0.03

ISSN: 2350-0328
International Journal of AdvancedResearch in Science, Engineering and Technology
Vol. 5, Issue 6 , June 2018

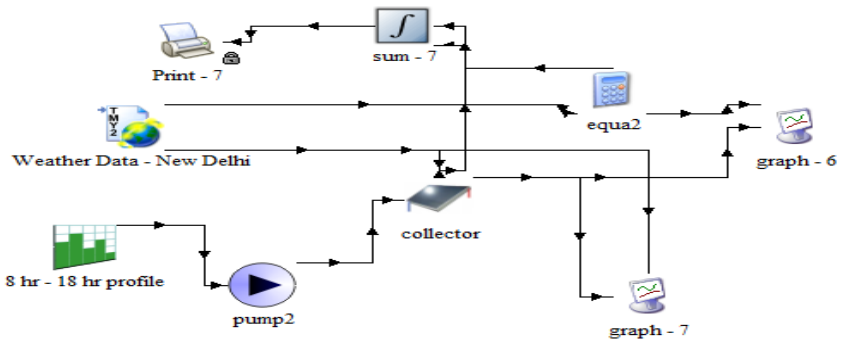

Figure 4.13: Flat plate solar thermal collector model.

IV. SIMULATION AND RESULTS

A. PV model

Table 4.1: Total energy provided to load from PV and grid annually for PV model.

	Time (hour)	Total Radiation (MJ)	Electrical Output (kJ)	Load (MJ)	Energy to Load (PV) (MJ)	Energy from Grid (MJ)
Total	8760	7591.95	1199.72	790.77	721.55	69.21

For an annual electric load of 790.77 MJ, 721.55 MJ of energy is supplied by PV array and the rest 69.21 MJ of energy is supplied from grid. Annually the efficiency of PV model is around 15.80%.

B. PV-T model

Table 4.2: Total energy provided to load from PV and grid annually for PV-T model.

	Time (hour)	Total Radiation (MJ)	Electrical Output (MJ)	Load (MJ)	Energy to Load (PV) (MJ)	Energy from Grid (MJ)
Total	8760	7591.95	1103.26	790.77	692.033	98.74

Table 4.3: Total energy obtained annually for PV-T model.

	Time (hour)	TotalRadiation for 10 m^2 area (MJ)	Total Energy gained (electrical + thermal) (MJ)	Electrical Energy obtained (MJ)	Thermal Energy obtained (MJ)
Total	8760	7591.95	3147.30	1103.27	2044.03

The total radiation falling on PV-T model of area 10 m^2 annually is 7591.95 MJ out of which 1103.27 MJ of energy is converted to electricity and 2044.03 MJ of energy is utilised as thermal energy. Electrical efficiency is 14.53% and thermal efficiency is around 26.92%. The total efficiency of PV-T model is the sum of respective efficiency, (i.e. electrical plus thermal efficiencies) = 41.45% annually.

C. Flat Plate Solar Thermal collector model

Table 4.4: Total Radiation and useful energy gained annually.

Time (hours)	Total Radiation (MJ)	Useful energy gained (MJ)
8760	7591.95	2543.7904

The useful energy obtained for a flat plate solar thermal collector is 2543.79 MJ with an efficiency of 33.50%.

ISSN: 2350-0328

International Journal of AdvancedResearch in Science, Engineering and Technology

Vol. 5, Issue 6 , June 2018

V. CONCLUSION

From table 5.1 it is clear that in their respective fields the efficiencies of PV and flat plate solar thermal models are more than PV-T model but overall efficiency of the PV-T model is more than other two models. Also the electrical efficiency of PV-T model is 91.96% to the electrical efficiency of PV model and thermal efficiency is around 80.35% to thermal efficiency of solar thermal collector model annually.

Most of our industrial processes and buildings need energy including both heat and electricity, and both of them can be provided using hybrid solar photovoltaic/thermal system. Solar thermal and photovoltaic systems absorb energy from solar radiation but due to limited availability of area, installing separate system is expensive and land consuming. Hence the combined system for improved utilisation of solar radiation is suitable, less expensive and consumes less area for installation.

Table 5.1: Efficiency comparison between PV-T, PV, and flat plate collector model.

		Photovoltaic (PV) Model	Photovoltaic Thermal (PV-T) Model	Flat Plate Thermal Collector
Annually	Electrical Efficiency	15.8%	14.53%	--
	Thermal Efficiency	--	26.92%	33.50%
	% of energy to electric load from PV array	91.24%	87.5%	--
	% of energy to electric load from Grid	8.76%	12.5%	--

REFERENCES

[1] Townsend, T.U., 1989. MS thesis, A Method for Predicting the Long-Term Performance of Directly-Coupled Photovoltaic Systems.University of Wisconsin, Madison.

[2] Duffie JA, Beckman WA. 1991. Solar engineering of Thermal Processes. Second edition. John Wiley and Sons Inc., New York.

[3] Hottel HC, Willier A. 1958. Evaluation of flat-plate solar collector performance. Transactions of the Conference on the Use of Solar Energy, vol. 2, University of Arizona Press, Tucson, Arizona

[4] L.W. Florschuetz, Extension of the Hottel-Whillier model to the analysis of combined photovoltaic/thermal flat plate collectors, Solar Energy, Volume 22, Issue 4, 1979, Pages 361-366, ISSN 0038-092X, https://doi.org/10.1016/0038-092X(79)90190-7.

[5] TrondBergene, Ole Martin Løvvik, Model calculations on a flat-plate solar heat collector with integrated solar cells, Solar Energy, Volume 55, Issue 6, 1995, Pages 453-462, ISSN 0038-092X, https://doi.org/10.1016/0038-092X(95)00072-Y.

[6] Ram Kumar Agarwal, H.P. Garg, Study of a photovoltaic-thermal system—Thermosyphonic solar water heater combined with solar cells, Energy Conversion and Management, Volume 35, Issue 7, 1994, Pages 605-620, ISSN 0196-8904, https://doi.org/10.1016/0196-8904(94)90044-2

[7] Akio Suzuki and Susumu Kitamura, Combined photovoltaic and thermal hybrid collector, J. Appt. Phys. 19, 79-83 (1980).

[8] Martin Wolf, Performance analyses of combined heating and photovoltaic power systems for residences, Energy Conversion, Volume 16, Issues 1–2, 1976, Pages 79-90, ISSN 0013-7480, https://doi.org/10.1016/0013-7480(76)90018-8.

[9] Adel A. Hegazy, Comparative study of the performances of four photovoltaic/thermal solar air collectors, Energy Conversion and Management, Volume 41, Issue 8, 2000, Pages 861-881, ISSN 0196-8904, https://doi.org/10.1016/S0196-8904(99)00136-3.

[10] B.J Huang, T.H Lin, W.C Hung, F.S Sun, Performance evaluation of solar photovoltaic/thermal systems, Solar Energy, Volume 70, Issue 5, 2001, Pages 443-448, ISSN 0038-092X, https://doi.org/10.1016/S0038-092X(00)00153-5.

[11] Soteris A. Kalogirou, Use of TRNSYS for modelling and simulation of a hybrid pv–thermal solar system for Cyprus, Renewable Energy, Volume 23, Issue 2, 2001, Pages 247-260, ISSN 0960-1481, https://doi.org/10.1016/S0960-1481(00)00176-2.

[12] Y. Tripanagnostopoulos, Th. Nousia, M. Souliotis, P. Yianoulis,Hybrid photovoltaic/thermal solar systems,SolarEnergy,Volume 72, Issue 3,2002,Pages 217-234,ISSN 0038-092X,https://doi.org/10.1016/S0038-092X(01)00096-2.

[13] HisashiSaitoh, Yasuhiro Hamada, Hideki Kubota, Makoto Nakamura, Kiyoshi Ochifuji, Shintaro Yokoyama, KatsunoriNagano,Field experiments and analyses on a hybrid solar collector,Applied Thermal Engineering,Volume 23, Issue 16,2003,Pages 2089-2105,ISSN 1359-4311,https://doi.org/10.1016/S1359-4311(03)00166-2.

[14] Fu Huide, Zhao Xuxin, Ma Lei, Zhang Tao, Wu Qixing, Sun Hongyuan, A comparative study on three types of solar utilization technologies for buildings: Photovoltaic, solar thermal and hybrid photovoltaic/thermal systems, Energy Conversion and Management, Volume 140, 2017, Pages 1-13, ISSN 0196-8904, https://doi.org/10.1016/j.enconman.2017.02.059.

[15] University of Wisconsin--Madison. Solar Energy Laboratory. TRNSYS (version 16.00.0037), a Transient Simulation Program. Madison, Wis. :The Laboratory, 1975.

[16] Klein, S.A. & Beckman, W.A.. (2007). TRNSYS 16: A transient system simulation program: mathematical reference. TRNSYS. 5. 389-396.

UNIVERSITY
OF WOLLONGONG
AUSTRALIA

Australasian Accounting, Business and Finance Journal

Volume 12
Issue 2 *The Impact of Regulations and Technology on Business Environment in India*

Article 9

Analyzing Environmental Kuznets Curve and Pollution Haven Hypothesis in India in the Context of Domestic and Global Policy Change

K. V. Bhanu Murthy
East Delhi Campus, Delhi Technological University, India.

Sakshi Gambhir
Delhi School of Economics, India.

Follow this and additional works at: http://ro.uow.edu.au/aabfj
Copyright ©2018 Australasian Accounting Business and Finance Journal and Authors.

Recommended Citation
Murthy, K. V. Bhanu and Gambhir, Sakshi, Analyzing Environmental Kuznets Curve and Pollution Haven Hypothesis in India in the Context of Domestic and Global Policy Change, *Australasian Accounting, Business and Finance Journal*, 12(2), 2018, 134-156. doi:10.14453/aabfj.v12i2.9

Research Online is the open access institutional repository for the University of Wollongong. For further information contact the UOW Library: research-pubs@uow.edu.au

Analyzing Environmental Kuznets Curve and Pollution Haven Hypothesis in India in the Context of Domestic and Global Policy Change

Abstract
While the notion of Environmental Kuznets Curve (EKC), which relates economic development to pollution, is well established, there is controversy about its shape, incidence and determinants. Moreover, there is an avowed relationship between economic development and international trade. This leads to the conceptualization of the trade-environment triangle between type of economic development, environment and trade and investment. Therefore, the study of EKC is incomplete without accounting for the pollution haven hypothesis (PHH). The original EKC literature restricts itself to a quadratic form whereas the new literature establishes that a cubic form is more appropriate. Also, the traditional EKC literature with few exceptions (Murthy and Bhasin, 2016) is stand-alone and does not incorporate PHH. Against this backdrop, we evolve a framework, which is based on both the critical evaluation of extant studies and an extension of these studies to the Indian context. We model EKC using alternative model specifications to bridge the gap between conventional and modern EKC literature. We further synthesize a model that combines the effect of EKC as well as PHH in the Indian context.

We substantiate a cubic form of EKC for India for the time period 1991 to 2014. With aggregate CO_2 emissions as the dependent variable, the linear (2.34E-06), quadratic (-1.2E-18) and cubic (2.64E-31) terms are all significant with the right signs, which confirms an N-shaped EKC for India. We also validate PHH for India in our model integrating EKC and PHH. Even with per capita emissions as the dependent variable, existence of an N-shaped EKC is established. In this case however, evidence on the cubic term is rather weak (p-value = 0.1250), which points towards the difference in the socio-psychological factors that influence the revival of the upturn in the case of India. Also, FDI has a smaller influence in per capita terms, but its coefficient is more significant, which means that we cannot ignore this phenomenon yet numerically its impact is much smaller. Our findings are in accordance with the new literature, which is the basis of the trade, environment and economic development triangle.

Keywords
Environment and Development, Environment and Trade, Environment and Growth, Environmental Kuznets Curve, Pollution Haven Hypothesis.

This article is available in Australasian Accounting, Business and Finance Journal: http://ro.uow.edu.au/aabfj/vol12/iss2/9

Analyzing Environmental Kuznets Curve and Pollution Haven Hypothesis in India in the Context of Domestic and Global Policy Change

K.V. Bhanu Murthy[1] and Sakshi Gambhir[2]

Abstract

While the notion of Environmental Kuznets Curve (EKC), which relates economic development to pollution, is well established, there is controversy about its shape, incidence and determinants. Moreover, there is an avowed relationship between economic development and international trade. This leads to the conceptualization of the trade-environment triangle between type of economic development, environment and trade and investment. Therefore, the study of EKC is incomplete without accounting for the pollution haven hypothesis (PHH). The original EKC literature restricts itself to a quadratic form whereas the new literature establishes that a cubic form is more appropriate. Also, the traditional EKC literature with few exceptions (Murthy and Bhasin, 2016) is stand-alone and does not incorporate PHH. Against this backdrop, we evolve a framework, which is based on both the critical evaluation of extant studies and an extension of these studies to the Indian context. We model EKC using alternative model specifications to bridge the gap between conventional and modern EKC literature. We further synthesize a model that combines the effect of EKC as well as PHH in the Indian context.

We substantiate a cubic form of EKC for India for the time period 1991 to 2014. With aggregate CO_2 emissions as the dependent variable, the linear (2.34E-06), quadratic (-1.2E-18) and cubic (2.64E-31) terms are all significant with the right signs, which confirms an N-shaped EKC for India. We also validate PHH for India in our model integrating EKC and PHH. Even with per capita emissions as the dependent variable, existence of an N-shaped EKC is established. In this case however, evidence on the cubic term is rather weak (p-value = 0.1250), which points towards the difference in the socio-psychological factors that influence the revival of the upturn in the case of India. Also, FDI has a smaller influence in per capita terms, but its coefficient is more significant, which means that we cannot ignore this phenomenon yet numerically its impact is much smaller. Our findings are in accordance with the new literature, which is the basis of the trade, environment and economic development triangle.

[1] *East Delhi Campus, Delhi Technological University, India*
[2] *Delhi School of Economics, India*

In terms of EKC the policy implication is that gains of green technologies are being wiped out by over-consumption of environmentally unfriendly goods. In terms of PHH the policy recommendation is clear that indiscriminate introduction and encouragement of FDI that raises the level of pollution is not welcome in India.

JEL Classification: F18, F64, O44, Q56.

Keywords: Environment and Development, Environment and Trade, Environment and Growth, Environmental Kuznets Curve, Pollution Haven Hypothesis.

1. INTRODUCTION

There have been vast changes in global policy since the emergence of WTO. Efforts have been made to narrow down the divergence between developed and developing countries and create a level playing field, through removal of tariff and non-tariff barriers and establishment of certain agreements, mainly TRIPS and TRIMs. Although the initial impetus came globally during the late eighties, in India it happened in 1991. During this period, the Indian economy was deregulated wherein various controls such as industrial licensing, exchange rates and interest rates were deregulated. There is a clear association between opening up, liberalization, deregulation, growth in trade and the international business environment brought about by the alignment of domestic policy with international policy.

There is an intertwining of technology, investment, industrialization, growth and pollution within India, due to a complex set of global and domestic policies adopted after liberalization and globalization. On the one hand, liberalization and domestic policy has encouraged industrialization and growth but on the other hand it has encouraged polluting industries and higher emissions leading to the emergence of the Environmental Kuznets Curve (EKC), which demonstrates that CO2 emissions increase with growth in per capita income (PCI) and fall when a sufficient threshold of PCI is achieved. Global policies initiated through WTO and other frameworks have resulted in Foreign Direct Investment inflows to India. This gives rise to the added dimension of environmental degradation, that is, Pollution Haven Hypothesis (PHH) in India.

Motivation

This entire gamut of factors has led to complex relationships between the three dimensions: economic development, trade and environment. Traditionally, the debate on economic development has been centered on the trade and development aspects. After the 1980s, particularly since the era of liberalization and globalization, the debate shifted to free trade, which transcended to reality only with the emergence of WTO. In recent times, however, the realization has dawned upon the world at large that the overarching issue is the environment leading to the emergence of a three-dimensional relationship between trade, environment and economic development. Figure 1 below illustrates the relationship between trade, economic development and the environment envisaged in the form of a global trade-environment triangle.

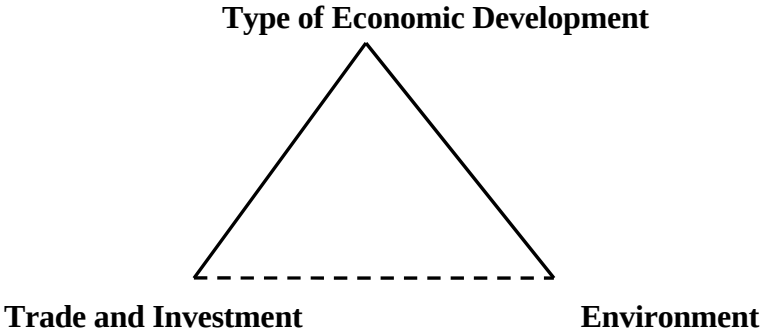

Figure 1. Trade-Environment Triangle (Murthy and Gambhir, 2017)

On one hand, we have the relationship between type of development and trade and investment; and on the other hand, we have the relationship between environment and type of economic development. With the help of these two broad relationships, we can examine the linkages between trade and environment. The kind of economic development that has resulted from liberalization and globalization, more particularly, is characterized by a high volume of trade (export + import), a high degree of urbanization and energy intensive industrialization (Jha and Murthy, 2006, p.12). Such a type of economic development has led to growth of multinationals and hence, foreign direct investment outflows. The multinationals tend to corner foreign trade, energy resources as well as urban resources. They, therefore lead to a peculiar model of growth, which in turn affects environment on the one hand and GDP growth on the other hand. In the past two or more decades, these dominance patterns have come to stay, thereby reinforcing the trade-environment triangle.

Furthermore, two of these broad relationships, one between environment and economic development; and the other between environment and trade and investment, could be comprehended in terms of two broad constructs. The former could be studied with the help of EKC while the latter could be studied with the help of PHH. In this work, we are specifically examining carbon dioxide (CO_2) emissions, which are a major indicator of environmental degradation; Gross Domestic Product (GDP), a proxy of economic development along with Foreign Direct Investment (FDI), which is a major determinant of international factors that affect the environment. These variables enable us to analyze the phenomena of EKC and PHH in the Indian context and model these two constructs with different model specifications while synthesizing a model that combines the effect of the two, for a robust analysis.

India's development strategy has shifted from import substituting industrialization to export oriented industrialization after the major domestic policy change towards liberalization. The policy of liberalization in India was largely an exercise in domestic decontrol but it also involved partial dismantling of trade barriers. This has led to the emergence of Home Country Multinationals to target developing countries like India to establish manufacturing hubs as export platform through assembly of semi-knock down (SKD) and completely knock down (CKD) kits. This involved international relocation of production or the introduction of FDI inflows in to India which was an otherwise closed economy. A vital dimension to the emergence of such global phenomena has been the increasing stringency in pollution control regimes in developed countries. They have been on the look out to exploit the relatively laxer policy environment in emerging market economies like India and continue to gain from employing greener technologies in their own countries while pushing polluting technologies

to the developing countries. This happens as a result of global and domestic policy change and further complicates the matter, leading to PHH. We can therefore relate emergence of EKC with domestic policy change and PHH with global policy change.

Hence, the main motivation is to try and answer the questions:

1. Does EKC exist in the Indian context?
2. Does PHH exist in the Indian context?
3. Do these two phenomena exist as a joint hypothesis in the Indian context?

It is in the light of this, the following work is set.

Our ***broad objectives*** are:

- ✓ To test for the different forms of EKC in the Indian context.
- ✓ To test for the impact of PHH in the Indian context.
- ✓ To synthesize a model to test for the joint hypothesis of EKC and PHH in the Indian context.

Against this backdrop, we formulated the following **primary hypotheses**:

- There is no evidence to validate EKC in the Indian context.
- There is no evidence of re-linking hypothesis in the Indian context.
- There is no evidence to validate PHH in the Indian context.
- The joint hypothesis of EKC and PHH does not exist in the Indian context.

The rest of the study is organized as follows. Section 2 lays down the conceptual framework for EKC and PHH highlighting some crucial dimensions of the trade-environment relationship. Section 3 provides a brief review of the extant literature on EKC and PHH. Section 4 discusses the data sources and the methodology employed. Section 5 presents the analysis and results. Section 6 concludes.

2. CONCEPTUAL FRAMEWORK

The pattern of FDI growth is driven by trade being substituted by FDI; adoption of energy intensive technologies whose ownership lies with multinationals; and urbanization which results in industry rather than primary activity that is largely controlled by multinationals. Thus, the type of economic development (characterized by a high volume of trade, a high degree of urbanization and energy intensive industrialization) determines the pattern of growth and development of FDI on the one hand, and the emergence of pollution patterns, especially in the developing economies on the other hand. This means that multinationals' growth takes place in the home country, that is, the developed country and they are able to corner the fruits of the type of economic development in terms of trade and industrialization. In turn, they impose a pattern of environmental degradation and pollution in the entire global economy. This is also enabled by global policies. One of the implications of the level playing field, envisaged and promoted through WTO, is that FDI is allowed to enter anywhere that it pleases. This permits the perpetuation of certain global patterns in FDI as well as the nature of industry that is being spread through FDI. Here, it is necessary to disabuse ourselves of the notion that multinationals have advanced technologies and hence are likely to be more energy efficient and less polluting. Labor-intensive technologies are by themselves less polluting. Secondly, the type of industry which is being relocated from the home country to the host –

developing country is by design those polluting industries which are not sustainable in the home country (Murthy and Gambhir, 2017).

Literature has been treating the relationship between economic development and pollution levels through EKC in a rather uncomplicated manner, while viewing FDI as international relocation of production and not just a neutral capital flow, whereas there is a clear bias in the nature of capital flows.

Environmental Kuznets Curve (EKC)

According to the EKC hypothesis, environmental damage increases in the early stages of economic development, but diminishes once nations reach higher levels of income, suggesting that the relationship between income (economic development) and environmental degradation takes the shape of an inverted U (Figure 2). This happens because developed countries have the necessary technologies for pollution abatement and also the necessary capital for implementing such technologies.

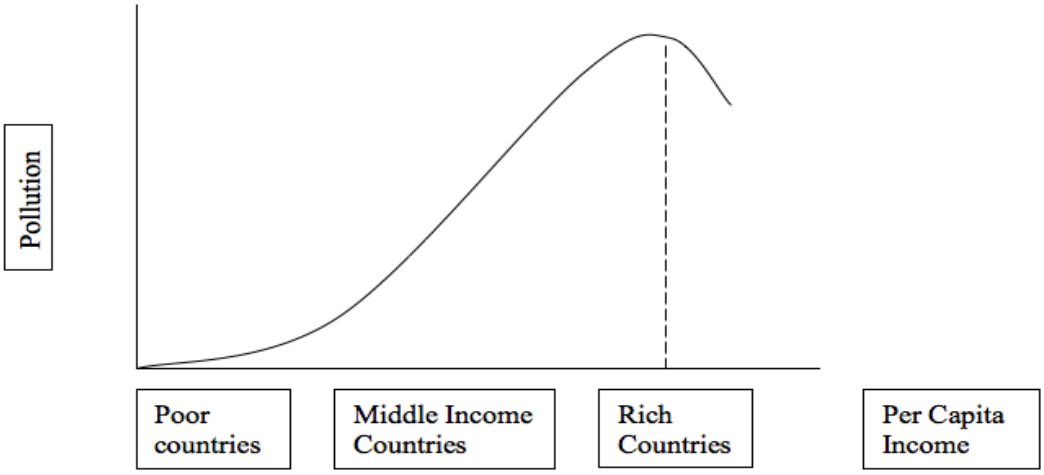

Figure 2. A hypothetical global EKC (Murthy and Bhasin, 2016)

The turning point in Figure 2 represents that level of income beyond which environmental degradation gets delinked from the process of economic growth. This is called the threshold level.

The De-linking and Re-linking Hypothesis

Some explanation for the EKC downturn is the explanation that comes from literature emanating from the developed countries themselves. It is argued that technology and capital, both of which developed countries have in abundance, are the main reason for establishing the de-linking hypothesis. De-linking refers to decoupling of environmental impacts from economic growth. The argument is that developed countries have the capital because they are capital intensive and that capital can buy green technologies. This leads to de-linking in the sense, when the developed countries go beyond a threshold, they can afford to harness such technologies, which are expensive but effective in reducing environmental degradation. Meanwhile, developing countries neither possess the technology nor do they have the necessary resources to implement these technologies. Further, developing overpopulated economies have two invariably negative features that are likely to aggravate the environmental problem, namely poverty and overpopulation. It is, therefore argued that developed countries alone have the potential to delink pollution from growth. Nevertheless, even if the de-linking hypothesis holds true, one

could still doubt if the observed improvements in environmental quality would sustain in the long run. If such improvements could not be extrapolated into the future, delinking would only be a temporary phenomenon. This implies that there might come an income level, where there would be technological and economic upper bounds to improvements in environmental efficiencies. At this stage, environmental degradation and economic growth would be relinked again. This is referred to as the re-linking hypothesis (de Bruyn and Opschoor, 1997).

Pollution Haven Hypothesis (PHH)

It basically states that the emission reductions achieved in developed nations are partly the result of shifting "dirty" production to developing nations with lax environmental standards. When income and environmental degradation rise substantially, more severe environmental regulations would be imposed in an economy, inducing relocation of pollution intensive industries to developing countries with weaker environmental legislations. This would result in a 'race to the bottom' whereby developing nations lower their environmental and social standards in order to gain a competitive advantage (Bu et al., 2013). The outcome would be greater environmental damage in the developing nations.

The unfolding of globalization and inception of WTO led to the creation of a level playing field by narrowing down the divergence between developed and developing countries. This rendered some degree of commonness to nations, by virtue of which developed countries could consider the possibility of international relocation of production. At the same time, developed countries continued to experience mounting pressures to reduce their emissions levels due to stringent environmental regimes. These countries thus saw the level playing field as an opportunity to relocate production elsewhere and depress their emissions (Murthy and Bhasin, 2016). But it is important to note here that there are additional determinants to a country's comparative advantage such as population density, size, absorptive capacity etc. Thus, to be able to make inferences about the patterns of trade, one would have to weigh the influences derived from the environmental policy against other determinants of trade.

Moreover, EKC, necessarily points out that the delinking hypothesis would be effective if and only if, further growth is delinked from pollution and since the home countries had failed to do so, it led to the relinking hypothesis (Jha and Murthy, 2003). So, as a strategy to deviate the relinking hypothesis, the developed economies resorted to transfer of polluting industries (pollution haven hypothesis) (Murthy and Bhasin, 2016). This completes the triangle between the type of economic development, FDI flows and pollution patterns.

3. LITERATURE REVIEW

The literature devoted to examining the three-dimensional relationship of economic development, trade and environment, is rather limited (Jha and Murthy, 2004; Murthy and Bhasin, 2016). There are many studies, which focus on examining the phenomena of EKC and PHH individually but fail to combine the effect of the two, in the realm of the trade-environment triangle at the global level. Shafik and Bandyopadhyay, 1992; Holtz-Eakin and Selden, 1995; Jha and Murthy, 2003; Babu and Datta, 2013; Zhao et al., 2013, examine the relationship between economic growth and environmental quality (EKC) using specific environmental indicators. While the conventional EKC studies validate a quadratic EKC, the modern EKC literature establishes that a cubic form of EKC seems more appropriate. Meanwhile, Taylor, 2005; Erdogan, 2013; Poelhekke and Ploeg, 2012; Kim and Adilov, 2011; Bu et al., 2013, explicate the theory behind PHH and its implications for the debate surrounding

international trade flows and environmental regulations. Of the myriad literature devoted to examining EKC and PHH individually, the endeavors to synthesize a model combining the effect of two, specifically in the Indian context have been further limited (Pao and Tsai, 2011; Jayanthakumaran et al., 2012; Kanjilal and Ghosh, 2013). We, therefore attempt to examine this joint phenomenon through a framework, which is based on the following critical evaluation of extant literature and an extension of these studies to the Indian context.

The early EKC estimates showed that some important indicators of environmental quality such as the levels of sulfur dioxide and particulates in the air actually improved as incomes and levels of consumption went up. Since then, this theory has been tested and validated for certain countries using specific indicators of environmental degradation. But, there have been some key concerns:

- The inverted-U shape of EKC is taken for granted and empirically examined for countries by relating individual degraders with individual indicators of economic development. But, linking individual pollutants to the level of per capita income (as done in most cases) could produce misleading conclusions. Also, a country's per capita income maybe only an imperfect indicator of its development (Jha and Murthy, 2003).
- There are several econometric concerns. To begin with, the earliest studies were simple quadratic functions of the levels of income, which seemed rather inappropriate. Some studies used a cubic EKC in levels and found an N-shaped pattern. The standard EKC regression model assumed same income elasticity across all countries at a given level of income. Most studies used panel data attempting to estimate both the fixed and random-effects models, but only fixed effects could be estimated consistently. This implied that results based on a particular sample of data could not be extrapolated to other samples (Stern, 2004).
- Most empirical EKC studies have attempted to estimate the level of average income that would correspond to the threshold level of the typical EKC pattern, with the implicit assumption that world income is normally distributed. However, world income distribution is highly skewed with much larger number of people below world mean income than above it. Therefore, it is the median rather than mean income that is the relevant variable (Stern et al., 1996).
- The early-EKC literature implicitly assumed a uni-directional causality running from income to environmental degradation, thereby ignoring the rebound effects of energy efficiency (Kaika and Zervas, 2013).
- Also, validity of the EKC pattern has been contingent on the type of pollutant considered. The inverted-U shape has been supported mostly when the pollutants in question were associated with low and local short-term abatement costs such as sulfur dioxide, particulates, etc. No apparent patterns could be found for pollutants with long-term effects such as CO_2 emissions. (Kaika and Zervas, 2013).
- EKC studies have not given consideration to the consumption side of the economy. Hence, if the needs of domestic consumption were satisfied by imports, then this effect would not be taken into account in an EKC analysis focusing only on domestic production (Rothman, 1998; Cole, 2004; Jha and Murthy, 2004).

In the light of the aforesaid concerns, the validity of EKC as a universal phenomenon has remained questionable. Empirical analysis has revealed that it may apply to select pollutants and to certain countries assuming different forms (inverted-U, U shaped, N-shaped or monotonic).

Moreover, though the premise of PHH seems intuitive; evidence substantiating the same has been at best mixed. It continues to remain highly contentious in debates surrounding trade, foreign investment and environment.

The uncertainty surrounding its validity rests on some of these arguments.

- Capital abundant developed countries with investible resources and technology could attract polluting industries from developing economies to adhere to stricter environmental standards so there could be a possible reverse transfer of FDI from the developing countries to the developed world. However, this phenomenon of a so-called reverse transfer seems largely theoretical.
- Though industries seem likely to relocate from developed countries to the developing world, the environmental philosophy pursued by a firm also has some role to play. (Poelhekke and Ploeg, 2012). The multinationals with higher social responsibility were less likely to be attracted by a weak environmental regulation regime (Bu et al., 2013). Also, there has been evidence suggesting that foreign firms could export greener technologies to developing economies and be even less polluting than the domestic firms, referred to as the 'pollution halo' hypothesis (Kim and Adilov, 2011).
- A firm's investment location decision rests on many factors such as market potential, labor costs, capital abundance, political stability, infrastructure, cultural compatibility etc. Pollution abatement costs are not found to be a major influence in FDI decisions. In this sense, the pollution haven effect is present but PHH is not empirically supported (Erdogan, 2013).
- Against the 'race to the bottom' argument, it is reasoned that pressures to lower environmental standards are contingent on country-specific factors such as the extent of political lobbying, consumer sensitivity, level of government corruption etc. Thus, endogenous determination of environmental standards with respect to FDI could alter the results obtained under the exogeneity assumption (Erdogan, 2013).

In the light of these arguments, validation of PHH as a global phenomenon has been rather difficult. It has been justified for some pollutants and certain industries, but widespread evidence has been hard to find (Kim and Adilov, 2011; Bu et al., 2013; Al-mulali and Tang, 2013).

4. DATA AND METHODOLOGY

4.1. Data

Data for the study were sourced from the World Development Indicators, World Bank.

Time series data were collected for our two sets of variables; the dependent variable, namely aggregate CO_2 emissions (kt) in model A and CO_2 emissions per capita (metric tons) in model B along with the independent variables, namely, GDP (current US$) and FDI, net inflows (BOP, current US$) in model A, and GDP per capita (current US$) and FDI, net inflows (BOP, current US$) in model B, for the time period 1991 to 2014.

4.2. Methodology

Conventionally, EKC is measured either through aggregate CO_2 emissions or per capita CO_2 emissions (Murthy and Bhasin, 2016). The expected functional form is one where the underlying pattern of emissions is quadratic. The original literature restricts itself to such a form. This is on account of the delinking hypothesis. Such a relationship has been tested by various authors (Grossman and Krueger, 1993; Shafik and Bandyopadhyay, 1992; Cole et al., 1997, etc.). Sometimes the specifications in these works are couched in terms of per capita emissions (Shafik,

1994; Holtz-Eakin and Selden, 1995, etc.). However, some of the studies question the quadratic form, by arguing that the so-called delinking is followed by a phase of relinking (Jha and Murthy, 2003). This gives rise to an N-shaped EKC due to the relinking hypothesis. What literature does not state with some exceptions (Jha and Murthy, 2006), is that this relinking is not due to technology and investment but it is due to consumption, which increases disproportionately due to socio-psychological factors. Consequently, the new literature challenges the quadratic form of the EKC and clearly establishes that the EKC shows up as an N-shaped curve represented by a cubic form of the equation, explained through three phases. In the first phase, poorer countries, which have a lower level of consumption, lead to pollution because they cannot afford cleaner technologies. In the second phase, the middle-income level, the investment in cleaner technologies manifests in the form of a dip in the emissions. In the third phase, which is achieved at relatively higher levels of income, the benefit from cleaner technologies is outweighed by the degradation caused due to excessive consumption (Gambhir, 2017). Another dimension to the measurement issues is that the traditional literature on EKC with few exceptions (Murthy and Bhasin, 2016) is stand-alone and does not incorporate the pollution haven hypothesis.

Against this backdrop, our focus has been on evolving a framework (Table 1), which enables modeling of EKC through alternative model specifications and synthesizing a model that combines the effect of EKC and PHH in the Indian context.

Table 1. Framework for analyzing EKC-PHH in the Indian context

Dep. Var. / Model No.	**Aggregate Carbon dioxide emissions (CO_2) (in kilotons) (A)**	**Per Capita Carbon dioxide emissions (CO_2PC) (in metric tons) (B)**
1	Quadratic EKC	Quadratic EKCPC
2	Cubic EKC	Cubic EKCPC
3	Cubic EKC with FDI	Cubic EKCPC with FDI

In line with the above stated framework, we formulated the following estimating equations.

A. With aggregate carbon dioxide emissions (CO_2) (in kilotons) as the dependent variable

A.1. Quadratic EKC

Functional form: $CO_{2t} = f(GDP_t, GDP_t^2)$

Estimating equation

$$CO_{2t} = \alpha_1 + \beta_1 GDP_t + \beta_2 (GDP^2)_t + e_{t1} \quad \ldots(1)$$

where

α_1 = intercept (initial level of aggregate CO_2 emissions)

β_1 and β_2 = indicators for testing the existence of a quadratic EKC with aggregate CO_2 emissions and GDP. The expected sign of β_1 is positive while that of β_2 is negative. If these coefficients turn out to be significant with these expected signs,

it would confirm the existence of an inverted-U shaped relationship between aggregate CO_2 emissions and GDP for India over the time period 1991 to 2014

A.2. Cubic EKC

Functional form: $CO_{2t} = f(GDP_t, GDP_t^2, GDP_t^3)$

Estimating equation

$$CO_{2t} = \alpha_2 + \beta_3 GDP_t + \beta_4 (GDP^2)_t + \beta_5 (GDP^3)_t + e_{t2} \quad \ldots(2)$$

where

α_2 = intercept (initial level of aggregate CO_2 emissions)

β_3, β_4 and β_5 = indicators for testing the existence of a cubic EKC with aggregate CO_2 emissions and GDP. The expected sign of β_3 and β_5 is positive while that of β_4 is negative. If these coefficients turn out to be significant with these expected signs, it would confirm the existence of an N-shaped shaped relationship between aggregate CO_2 emissions and GDP for India over the time period 1991 to 2014

A.3. Cubic EKC with FDI

Functional form: $CO_{2t} = f(GDP_t, GDP_t^2, GDP_t^3, FDI_t)$

Estimating equation

$$CO_{2t} = \alpha_3 + \beta_6 GDP_t + \beta_7 (GDP^2)_t + \beta_8 (GDP^3)_t + \beta_9 FDI_t + e_{t3} \quad \ldots(3)$$

where

α_3 = intercept (initial level of aggregate CO_2 emissions)

β_6, β_7 and β_8 = indicators for testing the existence of a cubic form of the relationship between aggregate CO_2 emissions and GDP, that is, a cubic EKC. The expected sign of β_6 and β_8 is positive while that of β_7 is negative. If these coefficients turn out to be significant with these expected signs, it would confirm the existence of an N-shaped shaped relationship between aggregate CO_2 emissions and GDP for India over the time period 1991 to 2014

B_9 = indicator for testing the validity of pollution haven hypothesis. The expected sign of this coefficient is positive. If it were significant with the expected sign, it would be a confirmation of the pollution haven hypothesis for India during the period 1991 to 2014

B. With per capita carbon dioxide emissions (CO_2PC) (in metric tons) as the dependent variable

B.1. Quadratic EKCPC

Functional form: $CO_2PC_t = f(GDPC_t, GDPC_t^2)$

Estimating equation

$$CO_2PC_t = \alpha_4 + \beta_{10} GDPC_t + \beta_{11} (GDPC^2)_t + e_{t4} \quad \ldots(4)$$

where

α_4 = intercept (initial level of per capita CO_2 emissions)

β_{10} and β_{11} = indicators for testing the existence of a quadratic EKCPC with per capita CO_2 emissions (CO_2PC_t) and per capita GDP ($GDPC_t$). The expected sign of β_{10} is positive while that of β_{11} is negative. If these coefficients turn out to be significant with these expected signs, it would confirm the existence of an inverted-U shaped relationship between per capita CO_2 emissions and per capita GDP for India over the time period 1991 to 2014

B.2. Cubic EKCPC

Functional form: $CO_2PC_t = f(GDPC_t, GDPC_t^2, GDPC_t^3)$

Estimating equation

$$CO_2PC_t = \alpha_5 + \beta_{12} GDPC_t + \beta_{13} (GDPC^2)_t + \beta_{14} (GDPC^3)_t + e_{t5} \quad \ldots(5)$$

where

α_5 = intercept (initial level of per capita CO_2 emissions)

β_{12}, β_{13} and β_{14} = indicators for testing the existence of a cubic EKCPC with per capita CO_2 emissions and per capita GDP. The expected sign of β_{12} and β_{14} is positive while that of β_{13} is negative. If these coefficients turn out to be significant with these expected signs, it would confirm the existence of an N-shaped shaped relationship between per capita CO_2 emissions and per capita GDP for India over the time period 1991 to 2014

B.3. Cubic EKCPC with FDI

Functional form: $CO_2PC_t = f(GDPC_t, GDPC_t^2, GDPC_t^3, FDI_t)$

Estimating equation

$$CO_2PC_t = \alpha_6 + \beta_{15} GDPC_t + \beta_{16} (GDPC^2)_t + \beta_{17} (GDPC^3)_t + \beta_{18} FDI_t + e_{t6} \quad \ldots(6)$$

where

α_6 = intercept (initial level of per capita CO_2 emissions)

β_{15}, β_{16} and β_{17} = indicators for testing the existence of a cubic form of the relationship between per capita CO_2 emissions and per capita GDP, that is, a cubic EKCPC. The expected sign of β_{15} and β_{17} is positive while that of β_{16} is negative. If these coefficients turn out to be significant with these expected signs, it would confirm the existence of an N-shaped shaped relationship between per capita CO_2 emissions and per capita GDP for India over the time period 1991 to 2014

B_{18} = indicator for testing the validity of pollution haven hypothesis. The expected sign of this coefficient is positive. If it were significant with the expected sign, it would be a confirmation of the pollution haven hypothesis for India during the period 1991 to 2014

In this context, we formulated the following **secondary hypotheses**:

1) $H_0: \beta_1 = 0$
   $H_1: \beta_1 > 0$
2) $H_0: \beta_2 = 0$
   $H_1: \beta_2 < 0$

} where β_1 and β_2 are indicators for testing the existence of a quadratic EKC relationship for aggregate CO_2 emissions during 1991 to 2014

3) $H_0: \beta_3 = 0$
   $H_1: \beta_3 > 0$
4) $H_0: \beta_4 = 0$
   $H_1: \beta_4 < 0$
5) $H_0: \beta_5 = 0$
   $H_1: \beta_5 > 0$

} where β_3, β_4 and β_5 are indicators for testing the existence of a cubic EKC relationship for aggregate CO_2 emissions during 1991 to 2014

6) $H_0: \beta_6 = 0$
$H_1: \beta_6 > 0$
7) $H_0: \beta_7 = 0$
$H_1: \beta_7 < 0$
8) $H_0: \beta_8 = 0$
$H_1: \beta_8 > 0$

where β_6, β_7 and β_8 are indicators for testing the existence of a cubic EKC relationship for aggregate CO_2 emissions during 1991 to 2014

9) $H_0: \beta_9 = 0$

$H_1: \beta_9 > 0$

where β_9 is an indicator for testing the validity of PHH (with aggregate CO_2 emissions as the dependent variable) for India during 1991 to 2014

10) $H_0: \beta_{10} = 0$
$H_1: \beta_{10} > 0$
11) $H_0: \beta_{11} = 0$
$H_1: \beta_{11} < 0$

where β_{10} and β_{11} are indicators for testing the existence of a quadratic EKC for per capita CO_2 emissions during 1991 to 2014

12) $H_0: \beta_{12} = 0$
$H_1: \beta_{12} > 0$
13) $H_0: \beta_{13} = 0$
$H_1: \beta_{13} < 0$
14) $H_0: \beta_{14} = 0$
$H_1: \beta_{14} > 0$

where β_{12}, β_{13} and β_{14} are indicators for testing the existence of a cubic EKC relationship for per capita CO_2 emissions during 1991 to 2014

15) $H_0: \beta_{15} = 0$
$H_1: \beta_{15} > 0$
16) $H_0: \beta_{16} = 0$
$H_1: \beta_{16} < 0$
17) $H_0: \beta_{17} = 0$
$H_1: \beta_{17} > 0$

where β_{15}, β_{16} and β_{17} are indicators for testing the existence of a cubic EKC relationship for per capita CO_2 emissions during 1991 to 2014

18) $H_0: \beta_{18} = 0$
$H_1: \beta_{18} > 0$

where β_{18} is an indicator for testing the validity of PHH (with per capita CO_2 emissions as the dependent variable) for India during 1991 to 2014

5. ANALYSIS AND RESULTS

The results obtained for each model specification are presented below:

A. With aggregate carbon dioxide emissions (CO_2) (in kilotons) as the dependent variable

A.1. Quadratic EKC

Table 2. Summary output for Quadratic EKC

Regression statistics

Multiple R	0.98842
R Square	0.97699
Adjusted R Square	0.97479
Standard Error	72497.13893
Observations	24

	Coefficients	**Standard Error**	**t Stat**	**P-value**
Intercept	447761.9	56894.29	7.87006	1.0697E-07
GDP	1.51E-06	1.39E-07	10.87174	4.3968E-10
GDP^2	-3.5E-19	6.23E-20	-5.65448	1.3012E-05

The R-square is 0.976, which indicates that our regression line is a good fit of the data.

Estimated equation

$$CO_{2t} = 447761.9 + 1.51E\text{-}06\,GDP_t - 3.5E\text{-}19\,(GDP^2)_t + e_{t1} \quad \ldots(7)$$

(p-value) (1.0697E-07) (4.3968E-10) (1.3012E-05)

The estimated equation shows that the initial level of CO_2 emissions is 447761.9 kilotons. The t-statistic (7.870068) and the p-value (1.0697E-07) show that the intercept is highly significant. The coefficient of GDP (1.51E-06) is rather small; however the t-statistic (10.87174) and the p-value (4.3968E-10) show that it is highly significant. The quadratic GDP variable also has an extremely small coefficient (3.5E-19) but it is highly significant on account of the t-statistic (-5.65448) and p-value (1.3012E-05). The important thing to note is that there is the typical alternation of signs. The linear term has a positive sign while the quadratic term has a negative sign. This is indicative of a bell-shaped curve where initially aggregate CO_2 emissions rise with respect to GDP and later fall with respect to $(GDP)^2$. Therefore, we reject our null hypothesis for β_1 and β_2.

Further, from Figure 3 below, it can be inferred that although aggregate CO_2 emissions do not show a smooth quadratic pattern, in the year 2012 there is a small dip in the level of emissions. Subsequently, since the emissions rise once again, this is an indication of the presence of a cubic form.

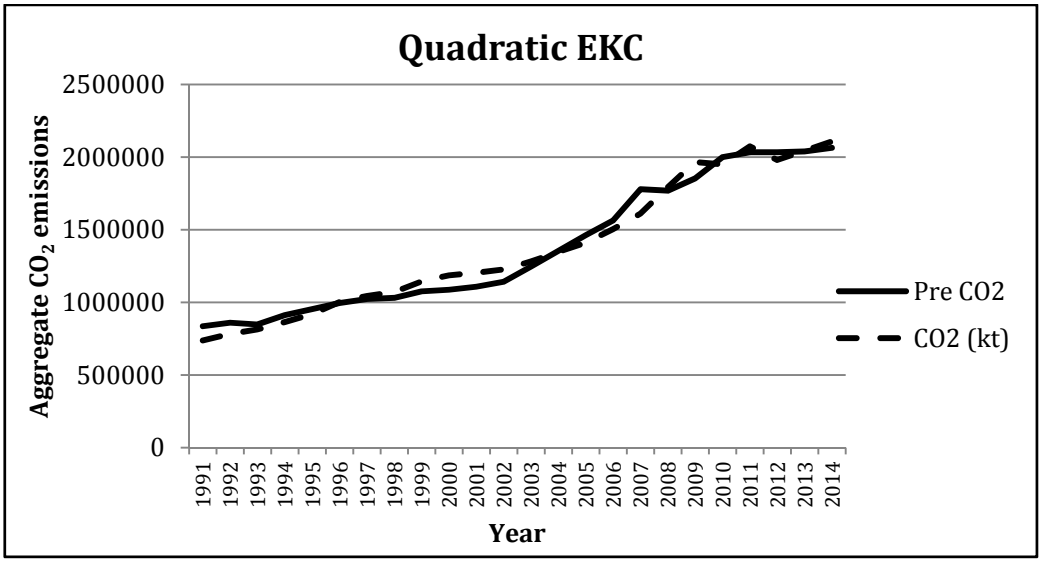

Figure 3. Quadratic EKC

A.2. Cubic EKC

Table 3. Summary output for Cubic EKC

Regression statistics

Multiple R	0.99045
R Square	0.98100
Adjusted R Square	0.97815
Standard Error	67500.27777
Observations	24

	Coefficients	***Standard Error***	***t Stat***	***P-value***
Intercept	241680.3	113401.7	2.13118	0.04566
GDP	2.34E-06	4.25E-07	5.51241	2.14E-05
GDP^2	-1.2E-18	4.32E-19	-2.85157	0.00986
GDP^3	2.64E-31	1.28E-31	2.05529	0.05314

The cubic equation has a slightly higher coefficient of determination (0.981) as compared to the quadratic equation (0.976). This shows that the cubic equation is a better fit.

Estimated equation

$CO_{2t} = 241680.3 + 2.34E\text{-}06\, GDP_t - 1.2E\text{-}18\, (GDP^2)_t + 2.64E\text{-}31\, (GDP^3)_t + e_{t2}$ ..(8)

(p-value) (0.0456) (2.14E-05) (0.0098) (0.0531)

The intercept term is also smaller (241680.3) which shows that the cubic equation accounts for more of the explained variation. This also indicates that the cubic form of relationship between aggregate CO_2 emissions and GDP is more appropriate as compared to a quadratic form of relationship between the two variables. In other words, the influence of the cubic term was perhaps being merged in the intercept of the quadratic equation as an omitted variable. Moreover, although the coefficient of GDP in the cubic equation is very small (2.34E-06), it is highly significant as indicated by the p-value (2.14E-05). But when we compare the quadratic

and the cubic form of equation, the linear term's coefficient in the quadratic equation (1.51E-06) is two-thirds of the linear term's coefficient in the cubic equation (2.34E-06).
Further, both the quadratic terms are extremely small, yet they are significant in both the equations. However, the coefficient of the quadratic term in the cubic equation (-1.2E-18) is about three times the coefficient of the quadratic term in the quadratic equation (-3.5E-19). The implication is that the quadratic term in the cubic equation makes emissions fall faster because it bears a negative sign. In addition to this, the cubic term also has a small (2.64E-31) but significant (0.0531) influence that forces the emissions to rise again.
On the whole, we reject our null hypothesis for β_3, β_4 and β_5. This renders evidence for an N-shaped EKC for India during 1991-2014.

Moreover, from Figure 4 below, it can be inferred that the apparent pattern of a cubic EKC is not very different from the quadratic EKC. However, a closer look shows that the predicted CO_2 is closely hugging the actual in the cubic form. It also confirms that 2011 is the peak before which there is a dip in 2012, similar to the quadratic form. On the whole, this confirms the N-shaped EKC as purported in recent literature.

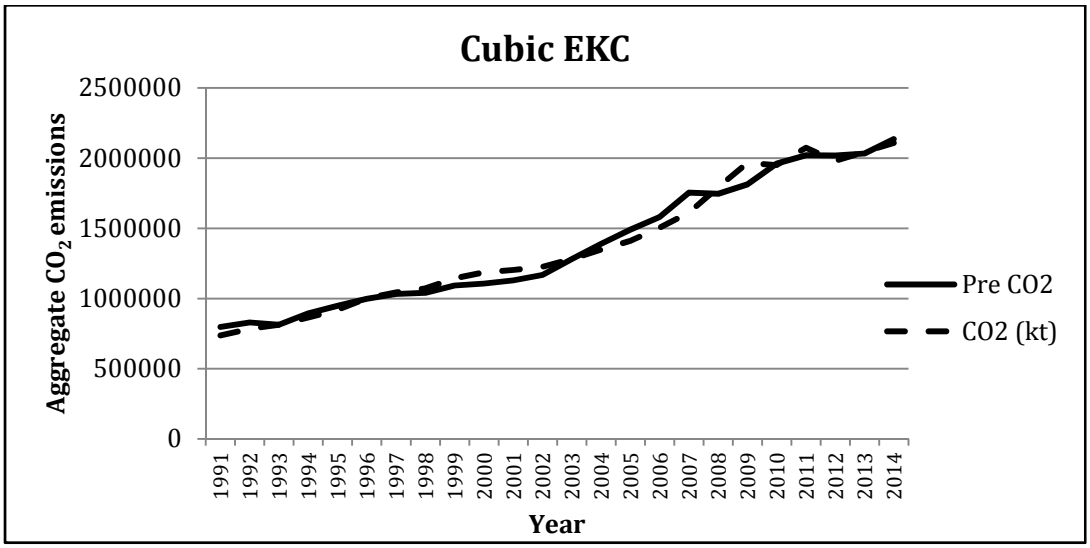

Figure 4. Cubic EKC

A.3. Cubic EKC with FDI

Table 4. Summary output for Cubic EKC with FDI

Regression statistics	
Multiple R	0.99194
R Square	0.98395
Adjusted R Square	0.98057
Standard Error	63657.02
Observations	24

	Coefficients	Standard Error	t Stat	P-value
Intercept	240942.2	106945.7	2.25294	0.03627
GDP	2.41E-06	4.03E-07	5.99413	9.09E-06
GDP^2	-1.5E-18	4.32E-19	-3.47178	0.00255
GDP^3	3.63E-31	1.32E-31	2.74558	0.01285
FDI	4.87E-06	2.61E-06	1.86758	0.07732

The R-square is very high (0.983), which again indicates that the fit is very good.

Estimated equation

$$CO_{2t} = 240942.2 + 2.41E\text{-}06\,GDP_t - 1.5E\text{-}18\,(GDP^2)_t + 3.63E\text{-}31\,(GDP^3)_t + 4.87E\text{-}06\,FDI_t + e_{t3} \quad ..(9)$$

(p-value) (0.0362) (9.09E-06) (0.0025) (0.0128) (0.0773)

The intercept (240942.2) is significant because the p-value is 0.0362. Once again it is noticed that the intercept in this equation (240942.2) almost halves in comparison to the intercept in the quadratic EKC equation (447761.9). The implication is that the cubic GDP and the FDI variable add to the explanatory power and take away from the unaccounted or omitted variables. Although FDI has a very small coefficient (4.87E-06), it is significant at 10% level (0.0773). Hence, we reject our null hypothesis for β_9 and validate the PHH for India during 1991-2014. The other coefficients, that is, the linear (2.41E-06), quadratic (-1.5E-18) and cubic (3.63E-31) terms are all small but highly significant (9.09E-06, 0.0025 and 0.0128 respectively). Also each of these terms bears the right sign, that is, the linear and the cubic terms are positive while the quadratic term is negative. Hence, we reject our null hypothesis for β_6, β_7 and β_8 and validate a cubic EKC for India.

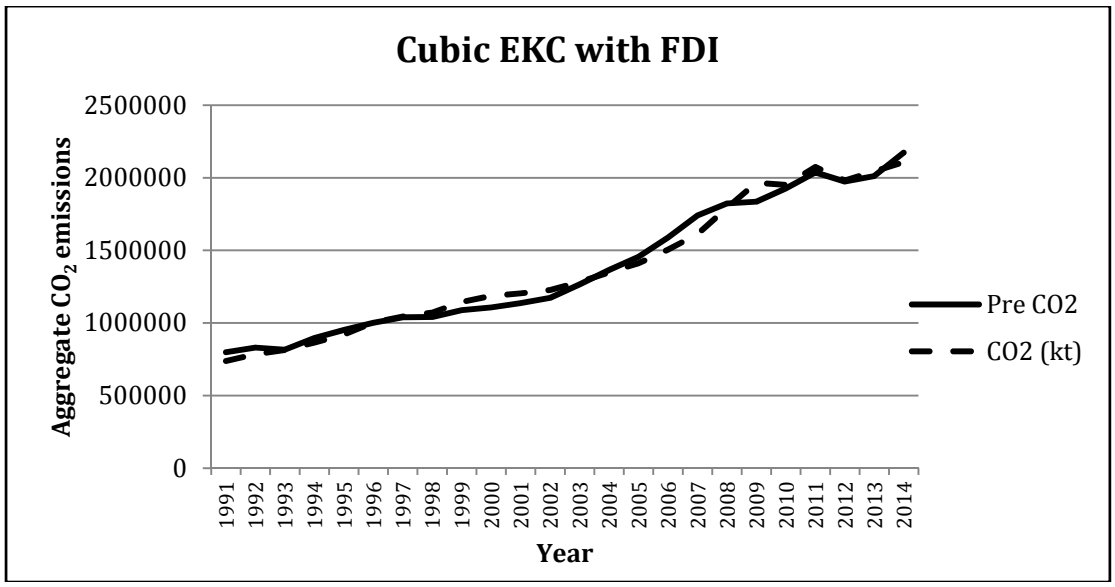

Figure 5. Cubic EKC with FDI

As has been observed in the earlier formulations, in Figure 5 also the downturn occurs after 2011. In addition, the two curves, actual CO_2 and predicted CO_2, do display a fair amount of cohesion.

B. With per capita carbon dioxide emissions (CO_2PC) (in metric tons) as the dependent variable

B.1. Quadratic EKCPC

Table 5. Summary output for Quadratic EKCPC

Regression statistics

Multiple R	0.98255
R Square	0.96542
Adjusted R Square	0.96212
Standard Error	0.05467
Observations	24

	Coefficients	Standard Error	t Stat	P-value
Intercept	0.54828	0.05963	9.19433	8.25783E-09
GDPC	0.00127	0.00016	7.66319	1.62971E-07
$GDPC^2$	-3.6E-07	9.03E-08	-3.99877	0.00065

The R-square is 0.965, which indicates that the regression line is a good fit.

Estimated equation

$$CO_2PC_t = 0.548287 + 0.001271\,GDPC_t - 3.6E\text{-}07\,(GDPC^2)_t + e_{t4} \quad \ldots(10)$$

(p-value) (8.25783E-09) (1.62971E-07) (0.0006)

Now, we consider the quadratic equation with per capita CO_2 emissions as the dependent variable. Once again, we first consider the intercept whose value is 0.54828 metric tons, which is statistically significant (8.25783E-09). This indicates the initial level of per capita emissions. It also implies that two-thirds of the initial emissions (0.83043 in 1991) form the intercept (0.54828), while the intercept as a proportion of the final per capita emissions (1.67872 in 2014) is 0.32660. The situation has reversed because initially two-thirds were being contributed by the intercept, whereas now, the same is contributing only one-third. Thus, overtime there have been other determinants, which have aggravated the per capita emissions.

The other factor in this case is clearly identified as GDP. Over the 24-year period (1991 to 2014), GDP has acted as a proxy for economic development. Thus, the quadratic per capita emissions pattern is maintained wherein both the linear per capita GDP term (0.0012) and the quadratic per capita GDP term (-3.6E-07) are statistically significant (1.62971E-07 and 0.0006 respectively). These terms also bear the correct signs such that the linear term is positive while the quadratic term is negative. Consequently, we reject our null hypotheses for β_{10} and β_{11}.

Figure 6 below, shows that the patterns observable in the per capita emissions are quite similar to what were observed for aggregate emissions. The timing of the downturn is also parallel to what was observed for aggregate emissions. The turning point is the same and the impact is also temporary. The small dip that happens around 2012 gets converted into a rising trend very soon. Hence, both the aggregate emissions as well as per capita emissions point towards the need for implementing a cubic equation.

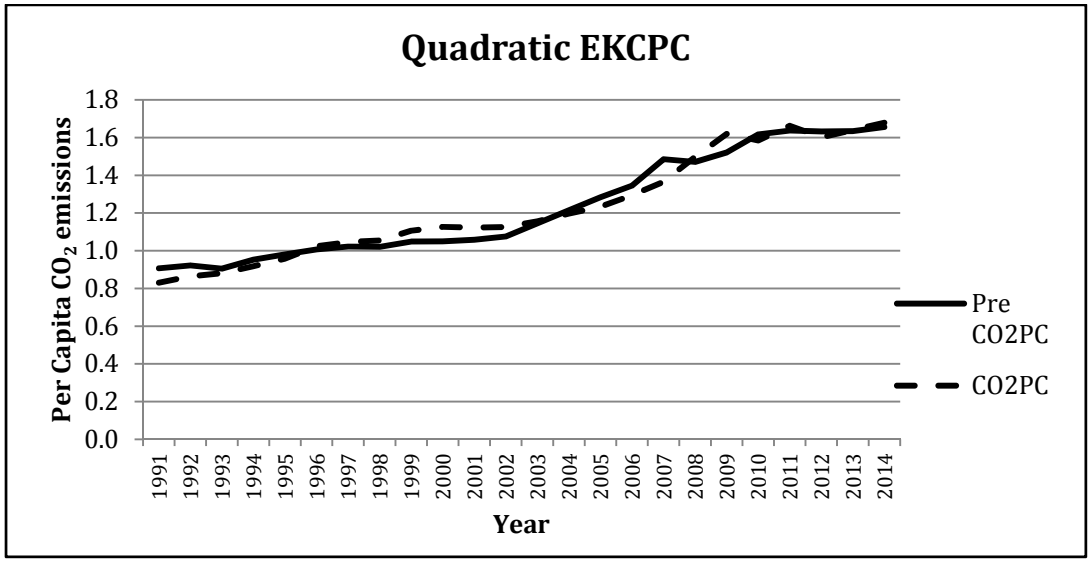

Figure 6. Quadratic EKCPC

B.2. Cubic EKCPC

Table 6. Summary output for Cubic EKCPC

Regression statistics	
Multiple R	0.98455
R Square	0.96935
Adjusted R Square	0.96475
Standard Error	0.05274
Observations	24

	Coefficients	Standard Error	t Stat	P-value
Intercept	0.32681	0.14980	2.18163	0.04124
GDPC	0.00223	0.00062	3.58067	0.00187
$GDPC^2$	-1.56E-06	7.5354E-07	-2.06959	0.05165
$GDPC^3$	4.3688E-10	2.7285E-10	1.60117	0.12501

The R-square is 0.969, which indicates that the regression is a good fit.

Estimated equation

$$CO_2PC_t = 0.32681 + 0.00223\,GDPC_t - 1.56E\text{-}06\,(GDPC^2)_t + 4.3688E\text{-}10(GDPC^3)_t + e_{t5} \quad \ldots(11)$$

(p-value) (0.0412) (0.0018) (0.0516) (0.1250)

A similar cubic equation is constructed for per capita emissions as was constructed for the aggregate emissions. Here, the intercept is smaller (0.32681) than that of the quadratic EKC per capita (0.54828). It reflects the same phenomenon of the cubic term being absorbed in the intercept in the quadratic equation. Moreover, the linear terms in both the equations are not very further apart (0.00127 in Quadratic EKCPC and 0.00223 in Cubic EKCPC). However, the coefficient of the quadratic term in the cubic equation (-1.56E-06) is around 2.5 times the coefficient of the quadratic term in the quadratic equation (-3.6E-07). This also shows that the cubic function is a better fit because it explains the variation better. Finally, the cubic term

(4.3688E-10) in this case bears the right sign (positive) but the p-value is 0.1250, which means that the evidence on relinking hypothesis in per capita terms is weak. Nevertheless, we reject our null hypothesis for β_{12}, β_{13} and β_{14}. However, weak evidence on the cubic term points towards the difference in the socio-psychological factors that influence the revival of the upturn in the case of India. In other words, India might not necessarily behave like the developed countries at later stages of development, unlike the implicit EKC assumption of common developmental patterns of nations.

Moreover, since the cubic term is not so significant, the predicted CO_2 per capita does not perfectly match the actual CO_2 per capita in Figure 7 below. The point of downturn however, is the same as for the equations previously discussed.

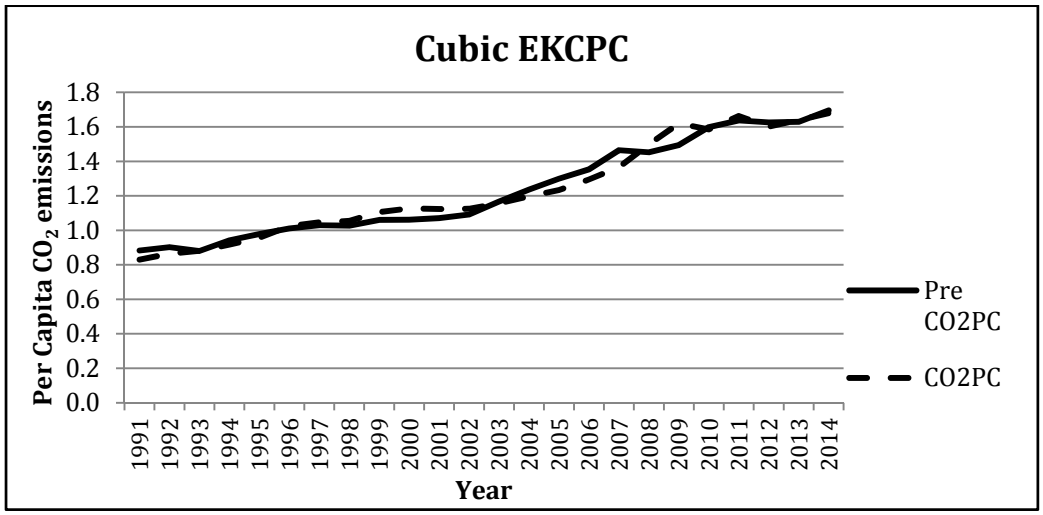

Figure 7. Cubic EKCPC

B.3. Cubic EKCPC with FDI

Table 7. Summary output for Cubic EKCPC with FDI

Regression statistics

Multiple R	0.98796
R Square	0.97608
Adjusted R Square	0.97104
Standard Error	0.04780
Observations	24

	Coefficients	**Standard Error**	**t Stat**	**P-value**
Intercept	0.28907	0.13674	2.11392	0.04797
GDPC	0.00253	0.00058	4.36096	0.00033
$GDPC^2$	-2.2E-06	7.41E-07	-3.00031	0.00735
$GDPC^3$	7.17E-10	2.75E-10	2.60325	0.01746
FDI	4.65E-12	2.01E-12	2.31272	0.03210

The R-square is 0.976, which indicates the goodness of fit of the regression line.

Estimated equation

$CO_2PC_t = 0.28907 + 0.00253\ GDPC_t - 2.2E\text{-}06(GDPC^2)_t + 7.17E\text{-}10(GDPC^3)_t + 4.65E\text{-}12\ FDI_t + e_{t6}$ …(12)

(p-value) (0.0479) (0.0003) (0.0073) (0.0174) (0.0321)

We now estimate a cubic form of equation on the basis of per capita emissions and per capita GDP. Once again, all the coefficients are significant at 5% level and bear the right signs such that the linear and cubic GDP terms are positive while the quadratic GDP term is negative. The intercept is 0.28907 with a p-value of 0.0479. The linear, quadratic and cubic GDP terms are 0.00253, -2.2E-06 and 7.17E-10 respectively with 0.0003, 0.0073 and 0.0174 as their respective p-values. We therefore, reject our null hypothesis for β_{15}, β_{16} and β_{17}. This confirms an N-shaped EKC in terms of per capita emissions. Also, the FDI coefficient is 4.65E-12 with a p-value of 0.0321, which makes us reject our null hypothesis for β_{18}. Hence in this case, both the relinking hypothesis and the pollution haven hypothesis show more robust results.

As between the two equations, the cubic term in the per capita form is 7.17E-10 whereas the cubic term in the aggregate form is 3.63E-31. Secondly, the FDI term has a p-value of 0.0773 in the aggregate form whereas in the per capita form the p-value is below 5% (0.0321). In per capita terms, it would be obvious that FDI is likely to have a smaller influence, which can be gauged from the respective coefficients, 4.87E-06 in aggregate terms and 4.65E-12 in per capita terms. This means that the pollution haven hypothesis (PHH) is not really working at the individual level. But, since FDI is more significant in per capita terms, it implies that we cannot ignore this phenomenon in spite of its impact being smaller numerically.

Also, according to Figure 8 below, the two curves, predicted CO_2 per capita and actual CO_2 per capita, lie very close to each other. Therefore, the inclusion of FDI in the per capita equation has really benefitted in terms of the goodness of fit.

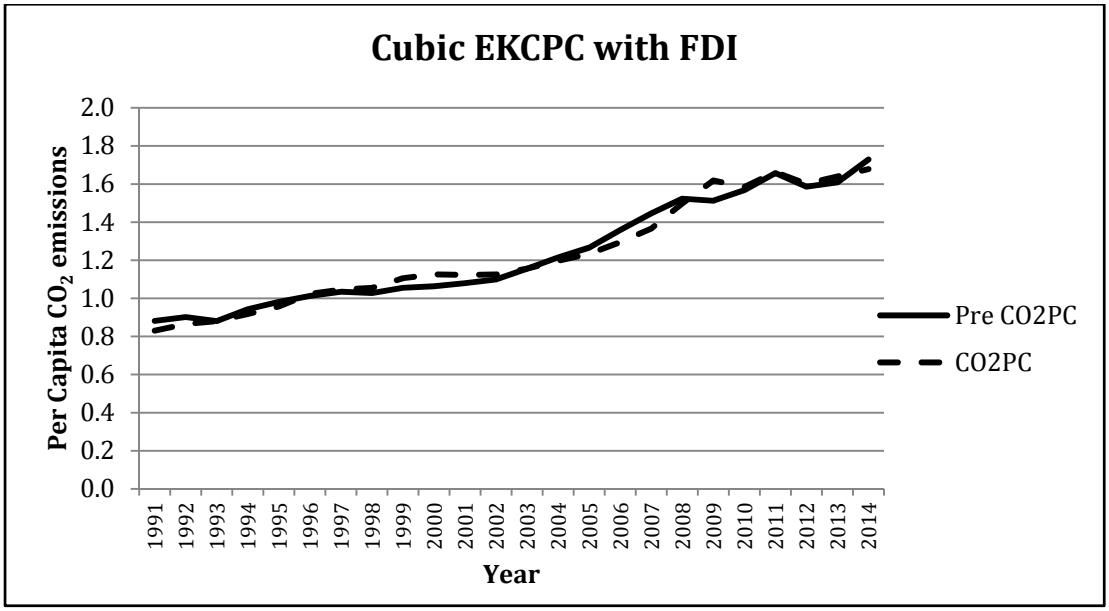

Figure 8. Cubic EKCPC with FDI

6. CONCLUSION AND POLICY RECOMMENDATIONS

The original EKC literature restricts itself to a quadratic form of the relationship between GDP and CO_2 emissions, in aggregate or per capita terms. This is on account of the delinking hypothesis. The new literature challenges this quadratic form of EKC where it is clearly established that the EKC shows up as an N-shaped curve. We have modeled the relationship between GDP and CO_2 emissions (aggregate and per capita) with alternative model specifications to bridge the gap between conventional and modern EKC studies. Our analysis of the alternative model specifications (with aggregate CO_2 emissions as the dependent variable) substantiates a cubic form of EKC in the Indian context. The linear (2.34E-06), quadratic (-1.2E-18) and cubic (2.64E-31) terms are all significant with the right signs, which confirms an N-shaped EKC as has been purported in the recent literature. Moreover, when we add the FDI variable to the model of cubic EKC, we find that FDI has a small but positive and significant coefficient (at 10 % level). Hence, we validate PHH for India in our model integrating EKC and PHH.

Even with per capita emissions as the dependent variable, the N-shaped EKC is established. But, in this case, evidence on the cubic term is rather weak (p-value = 0.1250), which points towards the difference in the socio-psychological factors that influence the revival of the upturn in the case of India. Also, FDI has a smaller influence in per capita terms, which could be gauged from the respective coefficients, in aggregate and per capita equations. This implies that PHH is not really working at the individual level. However, FDI is more significant in per capita terms, which means that we cannot ignore this phenomenon yet numerically its impact is much smaller.

On the whole, our study substantiates that a cubic form of relationship between aggregate CO_2 emissions and GDP is more appropriate as compared to a quadratic form of relationship between the two variables. In other words, India exhibits an N-shaped EKC pattern during 1991 to 2014, which implies that at relatively higher levels of income, the benefit from cleaner technologies is outweighed by the degradation caused due to excessive consumption. We also validate PHH in the Indian context through our model synthesizing EKC and PHH, both in aggregate and per capita terms. Hence, we reject both our primary hypotheses that there is not enough evidence to validate EKC in the Indian context and that there is not enough evidence to validate PHH in the Indian context. Also the non-existence of a joint EKC-PHH hypothesis in India is rejected. These findings are in accordance with the new literature, which is the basis of the trade, environment and economic development triangle.

The policy recommendation, therefore, is that both policy makers and literature needs to recognize that in the Indian context the re-linking hypothesis exists. The policy implication is that gains of green technologies are being wiped out by over-consumption of environmentally unfriendly goods. India may be falling into the trap that developed economies already experienced (the *N*-shaped EKC). In terms of PHH the policy recommendation is clear that indiscriminate introduction and encouragement of FDI that raises the level of pollution is not welcome in India. She needs to evolve screening procedures and active research to identify such foreign investment that does not dump polluting technologies in India. Moreover, over consumption needs to be curbed. Especially, conspicuous consumption of environmentally unfriendly goods and bad practices need to be checked.

References

Al-mulali, U & Tang, C.F. 2013, 'Investigating the validity of pollution haven hypothesis in the gulf cooperation council (GCC) countries'. *Energy Policy*, vol. 60, pp. 813-819. https://doi.org/10.1016/j.enpol.2013.05.055

Babu, S.S. & Datta, S.K. 2013, 'The relevance of environmental Kuznets curve (EKC) in a framework of broad-based environmental degradation and modified measure of growth – a pooled data analysis'. *International Journal of Sustainable Development and World Ecology*, vol. 20, no. 4, pp. 309-316. https://doi.org/10.1080/13504509.2013.795505

Bu, M. et al. 2013, 'Corporate social responsibility and the pollution haven hypothesis: evidence from multinationals' investment decision in China'. *Asia-Pacific Journal of Accounting and Economics*, vol. 20, no.1, pp. 85-99. https://doi.org/10.1080/16081625.2013.759175

Cole, M.A. 2004, 'Trade, the pollution haven hypothesis and the environmental Kuznets curve: examining the linkages'. *Ecological Economics*, vol. 48, no. 1, pp. 71–81. https://doi.org/10.1016/j.ecolecon.2003.09.007

Cole, M.A. et al. 1997, 'The Environmental Kuznets Curve: An empirical analysis'. *Environment and Development Economics*, vol. 2, no. 4, pp. 401-416. https://doi.org/10.1017/S1355770X97000211

de Bruyn, S.M. & Opschoor, J.B. 1997, 'Developments in the throughput-income relationship: theoretical and empirical observations'. *Ecological Economics,* vol. 20, no. 3, pp. 255-268. https://doi.org/10.1016/S0921-8009(96)00086-9

Erdogan, A.M. 2013, 'Foreign Direct Investment and Environmental Regulations: A Survey'. *Journal of Economic Surveys*, vol. 00, no. 0, pp. 1-13.

Gambhir, S. 2017, 'Environmental Kuznets Curve: An Empirical Analysis in the Indian Context'. *Pragati: Journal of Indian Economy (forthcoming).*

Grossman, G.M. & Krueger, A.B. 1993, 'Environmental impacts of the North American Free Trade Agreement'. *In P.M. Garber (ed.) The Mexico-US Free Trade Agreement, Cambridge, MA, MIT Press*, pp. 13-56. https://doi.org/10.3386/w4597

Holtz-Eakin, D. & Selden, T.M. 1995, 'Stoking the fires? CO_2 emissions and economic growth'. *Journal of Public Economics*, vol. 57, no. 1, pp. 85-101. https://doi.org/10.1016/0047-2727(94)01449-X

Jayanthakumaran, K. et al. 2012, 'CO_2 emissions, energy consumption, trade and income: A comparative analysis of China and India'. *Energy Policy*, vol. 42, pp. 450-460. https://doi.org/10.1016/j.enpol.2011.12.010

Jha, R. & Bhanu Murthy, K.V. 2003, 'An Inverse Global Environmental Kuznets Curve'. *Journal of Comparative Economics*, vol. 31, no. 2, pp. 352-368. https://doi.org/10.1016/S0147-5967(03)00042-8

Jha, R. & Bhanu Murthy, K.V. 2004, 'A Consumption Based Human Development Index and the Global Environmental Kuznets Curve'. *RSPAS, ANU Trade and Development Economics Working Paper*, pp. 1-36.

Jha, R. & Bhanu Murthy, K.V. 2006, 'Environmental Sustainability: A Consumption Approach'. *Routledge, London*, pp. 12.

Kaika, D. & Zervas, E. 2013, 'The Environmental Kuznets Curve (EKC) theory. Part B: Critical issues'. *Energy Policy*, vol. 62, pp. 1403-1411. https://doi.org/10.1016/j.enpol.2013.07.130

Kanjilal, K. & Ghosh, S. 2013, 'Environmental Kuznets curve for India: Evidence from tests for cointegration with unknown structural breaks'. *Energy Policy*, vol. 56, pp. 509-515. https://doi.org/10.1016/j.enpol.2013.01.015

Kim, M.H. & Adilov, N. 2011, 'The lesser of two evils: an empirical investigation of foreign direct investment-pollution tradeoff'. *Applied Economics*, vol. 44, no. 20, pp. 2597-2606. https://doi.org/10.1080/00036846.2011.566187

Murthy, K.V.B. & Bhasin, N. 2016, 'Environmental Kuznets Curve: CO_2 Emissions, Pollution Havens and Type of Economic Development'. *Ch. X, in Ed. John R McIntyre et al. Emerging Dynamics of Sustainability in Multinational Enterprises, Edward Elgar, Cheltenham,* pp. 209-231. https://doi.org/10.4337/9781784718534.00020

Murthy, K.V.B. & Gambhir S. 2017, 'International trade and foreign direct investment: empirical testing of the trade-environment triangle'. *Transnational Corporations Review*, vol. 9, no. 2, pp. 122-134. https://doi.org/10.1080/19186444.2017.1326718

Pao, H.T. & Tsai, C.M. 2011, 'Multivariate Granger causality between CO2 emissions, energy consumption, FDI (foreign direct investment) and GDP (gross domestic product): Evidence from a panel of BRIC (Brazil, Russian Federation, India, and China) countries'. *Energy*, vol. 36, no. 1, pp. 685-693. https://doi.org/10.1016/j.energy.2010.09.041

Poelhekke, S. & Ploeg, R. 2012, 'Green havens and pollution havens'. *CESifo Working Paper: Resource and Environment Economics, No. 3841.*

Rothman, D.S. 1998, 'Environmental Kuznets curves—real progress or passing the buck? A case for consumption-based approaches'. *Ecological Economics*, vol. 25, no. 2, pp. 177–194. https://doi.org/10.1016/S0921-8009(97)00179-1

Shafik, N. 1994, 'Economic Development and Environmental Quality: An Econometric Analysis'. *Oxford Economic Papers*, vol. 46, no. 5, pp. 757-773. https://doi.org/10.1093/oep/46.Supplement_1.757

Shafik, N. & Bandyopadhyay, S. 1992, 'Economic Growth and Environmental Quality: Time Series and Cross-country Evidence'. *World Bank Policy Research Working Paper No. 904, Washington, DC.*

Stern D.I. 2004, 'The Rise and Fall of the Environmental Kuznets Curve'. *World Development*, vol. 32, no. 8, pp. 1419-1439. https://doi.org/10.1016/j.worlddev.2004.03.004

Stern, D.I. et al. 1996, 'Economic growth and environmental degradation: The environmental Kuznets curve and sustainable development'. *World Development*, vol. 24, no. 7, pp. 1151–1160. https://doi.org/10.1016/0305-750X(96)00032-0

Taylor, M.S. 2005, 'Unbundling the Pollution Haven hypothesis'. *The B.E. Journal of Economic Analysis and Policy*, vol. 3, no. 2, pp.1-28. https://doi.org/10.2202/1538-0637.1408

Zhao, F. et al. 2013, 'Improving the environmental Kuznets curve for evaluating the relationships between carbon dioxide emissions and economic development'. *Journal of Food, Agriculture and Environment*, vol. 11, no. 2, pp. 1193-1199.

Wireless Networks
https://doi.org/10.1007/s11276-018-1781-5

Asymmetric U-shaped printed monopole antenna embedded with T-shaped strip for bluetooth, WLAN/WiMAX applications

Rakesh Nath Tiwari[1] · Prabhakar Singh[2,3] · Binod Kumar Kanaujia[4]

© Springer Science+Business Media, LLC, part of Springer Nature 2018

Abstract
In the present paper, a microstrip line fed compact monopole printed antenna is designed for Bluetooth, WLAN and WiMAX applications. The designed antenna has a compact size of dimensions 34 × 20 × 1.6 mm^3. The proposed antenna comprises asymmetric U-shaped radiator embedded with a T-shaped strip in the middle of the patch. Stair shaped defected ground plane with rectangular slit is used for the bandwidth enhancement. The antenna design achieves the maximum impedance bandwidth of 107.35% (2.27–7.53 GHz). Radiation efficiency is higher than 70.0% throughout the entire operating band. The simulated and measured realised antenna gains are in good agreement and vary in the range of 2.14–4.83 and 2.20–4.91 dBi respectively. Radiation patterns are almost omnidirectional in H-plane and bidirectional pattern in E-plane. The antenna characteristics are calculated using CST Microwave Studio and the results are compared with the measured results.

Keywords Asymmetric U-shaped patch · Wideband antenna · Stair shaped defected ground · Microstrip line · Planar monopole antenna

1 Introduction

In modern communication industry, monopole antennas are in great demand for wireless personal area as a network, body area network for medical applications, RFID technology etc. [1, 2]. Thus, in the process of improvements, many efforts are still going on such as to minimize the overall size, compactness of antenna and enhancement of impedance bandwidth. Therefore, several monopole antennas are designed by modifying the radiating patch and creating defects in the ground plane [3–7]. Moreover, monopole antennas are easily designed to achieve dual/multiband operation for wireless local area network/worldwide interoperability for microwave area (WLAN/WiMAX) applications [8–10]. In [11], a microstrip line fed printed wide slot antenna with a rotated slot is presented and achieves an enhanced bandwidth of 2.2 GHz. However, the overall size of the antenna is quite large. In [12], printed wide-slot antenna with a fractal shaped slot is reported to increase the bandwidth. A complex diversity monopole antenna comprising two crescent shaped with modified ground plane achieves impedance matching with reduced mutual coupling [13]. A compact microstrip line-fed printed wide-slot antenna is proposed in [14] which enhances the bandwidth and improves the radiation pattern using the parasitic patch. The dielectric loaded shorted loop monopole printed dual band antenna works at 2.45/5 GHz for WLAN and at 2.1 GHz for WCDMA band [15]. M-shaped patch with modified ground

✉ Rakesh Nath Tiwari
srakeshnath@gmail.com

Prabhakar Singh
prabhakarsingh3@gmail.com

Binod Kumar Kanaujia
bkkanaujia@yahoo.co.in

[1] Department of Electronics and Communication Engineering, Uttarakhand Technical University, Dehradun, Uttarakhand 248007, India

[2] Department of Physics, Galgotias University, Greater Noida, Uttar Pradesh 201310, India

[3] Department of Applied Sciences, Galgotias College of Engineering and Technology, Greater Noida, Uttar Pradesh 201306, India

[4] School of Computational and Integrative Sciences, Jawaharlal Nehru University, New Delhi 110067, India

Published online: 28 June 2018

plane and curved slot loaded monopole antennas report enhanced bandwidth [16, 17]. Fork shaped dual band planar monopole antenna is presented in [18] covering WLAN and WiMAX range. One of the latest approaches to enhance the impedance bandwidth of the antenna is the modification in the ground plane itself or embedding the different shapes of slot in the ground plane. Thus, the various defected ground plane structures (DGS) such as E-shaped, M-shaped, fractal shaped slot loaded, T-shaped, slit loaded etc. are employed to miniaturize the antenna. Such structure achieves compact ground plane and multi-band/UWB operations. However, almost all these antennas are either bearing large size or complex in design. Here, in this paper the state of art is introduced using the stepped ground plane technique to achieve the UWB response.

Thus, a compact and planar design of asymmetric U-shaped printed monopole antenna embedded with T-shaped strip with a defected ground plane is proposed. The overall dimensions of the proposed antenna including ground plane are 34 (L_s) × 20 (W_s) × 1.6 (H) mm^3 on a low cost FR4 material and fed by 50 Ω microstrip line. The novel design of U-shaped radiating patch acts as a matching stub with a T-shaped strip connected at the end of the microstrip line. This structure produces multiple resonances and improves the antenna bandwidth. This antenna successfully covers the frequency band for Bluetooth (2.4 GHz), WLAN (2.4, 5.1–5.8 GHz), WiMAX (2.3–5.7 GHz) and ISM (2.4/5.2/5.8 GHz) band applications. The proposed antenna is simulated with CST Microwave Studio and results are compared with the measured results.

2 Antenna configuration and its specifications

The modern communication systems are getting smaller and compact day by day. Therefore, to cover the wireless spectrum such as Bluetooth, WLAN/WiMAX etc., a single antenna is required which must be compact and small along with very large bandwidth. In this view, a simple, light weight and compact UWB antenna is investigated to fulfill these requirements. Figure 1 shows the evolution of the proposed monopole planar antenna. The patch dimensions of the conventional monopole antenna are taken as Lp × Wp (19 × 18 mm^2) and shown in Fig. 1(a). A rectangular portion of dimensions 15 × 16 mm^2 is removed from the patch resulting into a symmetrical U-shaped monopole antenna (Fig. 1b). Further, the left arm of symmetrical U-shaped monopole antenna is reduced and a centre strip is used to realise Fig. 1(c). Finally, a horizontal strip of dimensions L_4 × W_4 is place at the top of the centre strip which makes the asymmetric U-shaped antenna embedded with T-shaped centre strip (Fig. 1d) for wideband applications. Figure 2 shows the top, bottom, front and side view geometry of the proposed planar antenna.

Removing the ground plane conductor (dimensions L_g × W_s) of constant dimensions (L × W) from the two ends modify the ground plane into stair shape. Further, a rectangular slot is used in the ground plane to improve the impedance of the antenna. Relative position of the radiator and the ground plane is taken as g = 4.5 mm. The details of the antenna design are presented in Table 1. The return loss values for different antenna structures are depicted in Fig. 3. Antenna I operates in dual band mode with lower and higher impedance bandwidth of 2.37–3.54 and 3.99–6.73 GHz respectively. In case of antenna II, the higher resonance frequency is shifted towards higher side while the lower resonance frequency remains same as in case of antenna I. However, the matching condition is deteriorated because of the removal of the conductor from the patch which certainly changes the impedance of the antenna. The operating bands for antenna II are 2.26–3.05 GHz (lower band) and 4.97–6.37 GHz (higher band) respectively. Moreover, when the centre strip is used in antenna (antenna III) again dual response is observed but with improved operating bands i.e. 2.43–3.63 GHz (lower band) and 4.37–7.13 GHz (upper band) respectively. Further, to achieve wideband characteristics, a horizontal strip of dimensions (L_4 × W_4) is placed at the top of the central strip. Consequently, in proposed antenna IV, a wide bandwidth of 4.89 GHz (2.26–7.15 GHz) is obtained.

3 Parametric study of the proposed antenna

Various design parameters are studied to investigate their effect on the impedance bandwidth of the antenna. The variation of asymmetric U-arm strip and T-strip of the radiator affect the antenna resonance and its bandwidth. The variation of number of step slots (N) created in the ground plane is also studied. Finally the variation of slit in the ground plane is investigated to optimise the impedance bandwidth.

3.1 Effect of the radiating patch

3.1.1 Current distribution

The simulated surface current distribution of the proposed antenna at different resonance frequencies at 2.40, 2.68, 3.24 and 5.77 GHz are shown in Fig. 4. From Fig. 4(a), it is observed that the first resonance at 2.40 GHz is contributed by both T-strip (L_3) and right asymmetric U-arm strip (L_5) of the radiator and the second resonance (2.68 GHz) is created due to L_5 and microstrip line

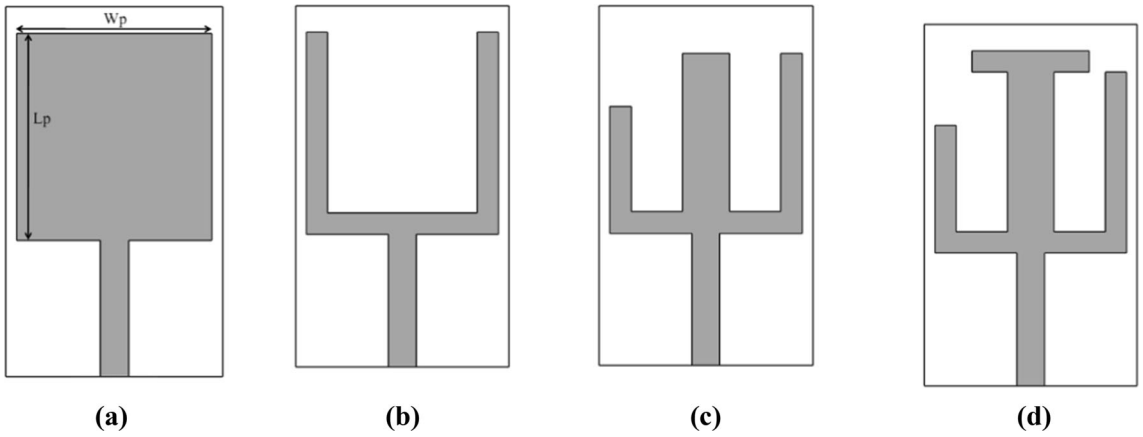

Fig. 1 Evolution of the proposed antenna. **a** antenna I **b** antenna II **c** antenna III **d** antenna IV (proposed)

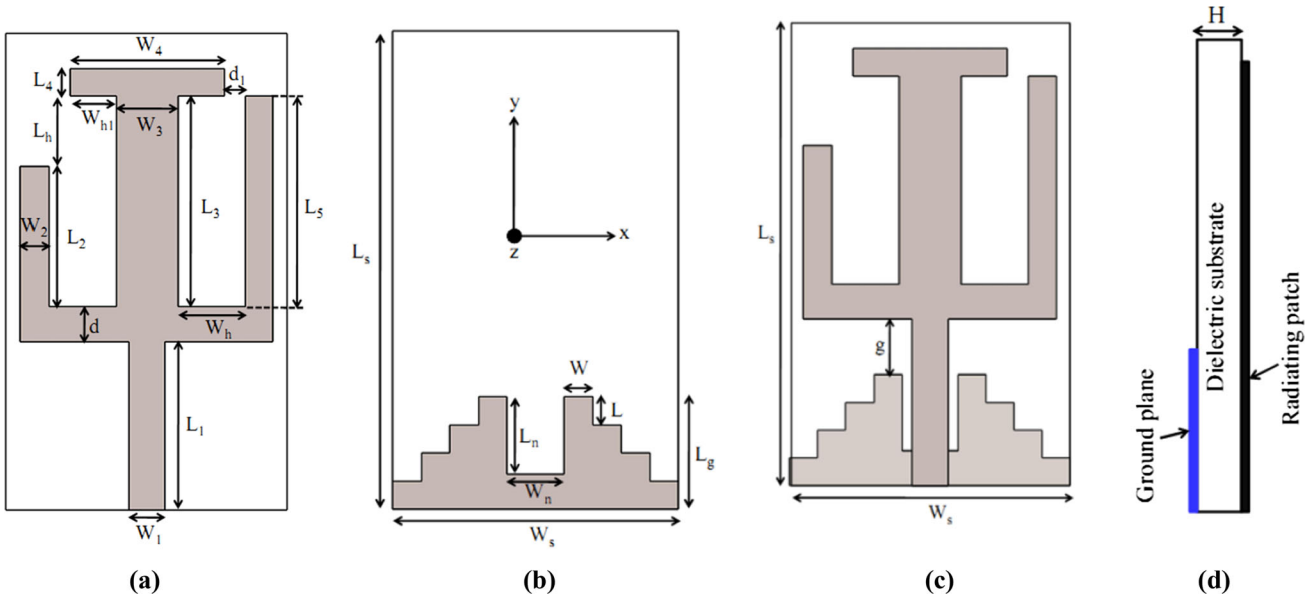

Fig. 2 Geometry of the proposed antenna. **a** Top view **b** bottom view **c** front view **d** side view

Table 1 Design parameters of the proposed antenna

Parameters	Unit (mm)	Parameters	Unit (mm)
$L_s \times W_s$	34 × 20	Lp × Wp	19 × 18
$L_1 \times W_1$	12.5 × 2.2	$L_2 \times W_2$	10 × 2
$L_3 \times W_3$	15 × 4.4	$L_4 \times W_4$	2 × 11
L_5	15	d	2
H	1.6	$L_n \times W_n$	6 × 4
$L_g \times W_s$	8 × 20	g	4.5
L × W	2 × 2	W_h	4.8
W_{h1}	3.3	L_h	5
d_1	1.5		

(Fig. 4b). The current density concentrated at the left arm (L_2) and microstrip line reveals that the third resonance (3.24 GHz) is totally contributed by L_2 and microstrip line (Fig. 4c). From Fig. 4(d) it is clear that the fourth resonance mode (5.77 GHz) is produced solely by the microstrip line because current density is maximum on the strip line at this frequency.

3.1.2 First resonance

A theoretical analysis is presented to calculate the various resonance mode created due to the effect of the arms of the asymmetric U-shaped radiator, T-strip and microstrip line.

The resonance frequency of the radiating patch is calculated using the formula [19].

$$f_r = \frac{c}{2L_r\sqrt{\varepsilon_e}} \quad (1)$$

in which,

$$\varepsilon_e = \frac{\varepsilon_r + 1}{2} + \frac{\varepsilon_r - 1}{2}\left(1 + \frac{12\mathrm{H}}{\mathrm{Wp}}\right)^{-1/2}$$

here, L_r is the resonant length, ε_r is the relative permittivity of the substrate, Wp is the width of the patch and H is thickness of the substrate.

The first resonance is attributed due to T-strip and L_5 (Fig. 4a). At the first resonance, the effective length L_{r1} is calculated as:

$$L_{r1} = L_3 + (L_5 - d_1) + (W_h - W_2) + W_{h1} + (L_4 - d) \quad (2)$$

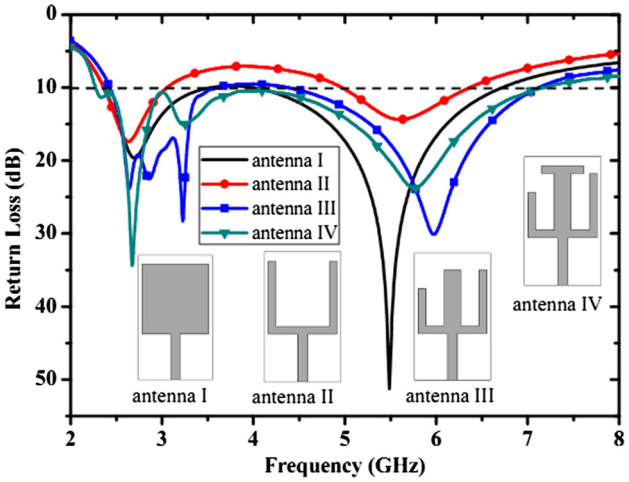

Fig. 3 Return loss variation of different antennas

Theoretically predicted resonance frequency is calculated using Eqs. (1) and (2). The CST simulated results plotted in Fig. 5 are compared with the predicted results and presented in Table 2. The designed resonance

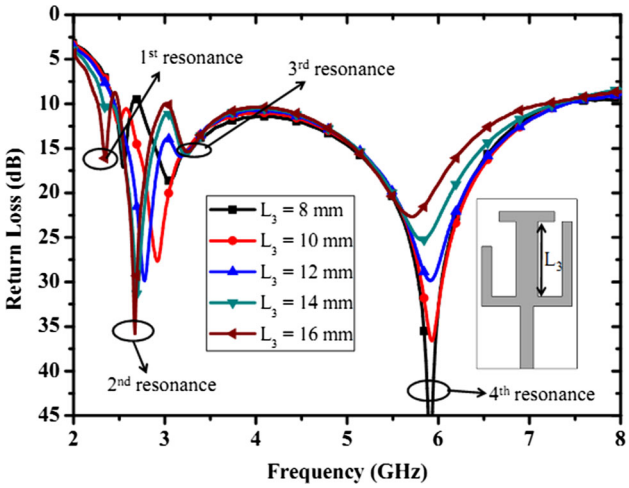

Fig. 5 Return loss variation of the proposed antenna for different values of L_3

Table 2 Comparison for the second resonance frequency

L_3 (mm)	L_{r1} (mm)	Resonance frequency (GHz)		% difference
		f_{r1} (Theory)	f_{r1} (Simulated)	
8	27.6	2.76	2.55	8.24
10	29.6	2.57	2.49	3.21
12	31.6	2.41	2.45	1.63
14	33.6	2.27	2.37	4.23
16	35.6	2.14	2.34	8.55

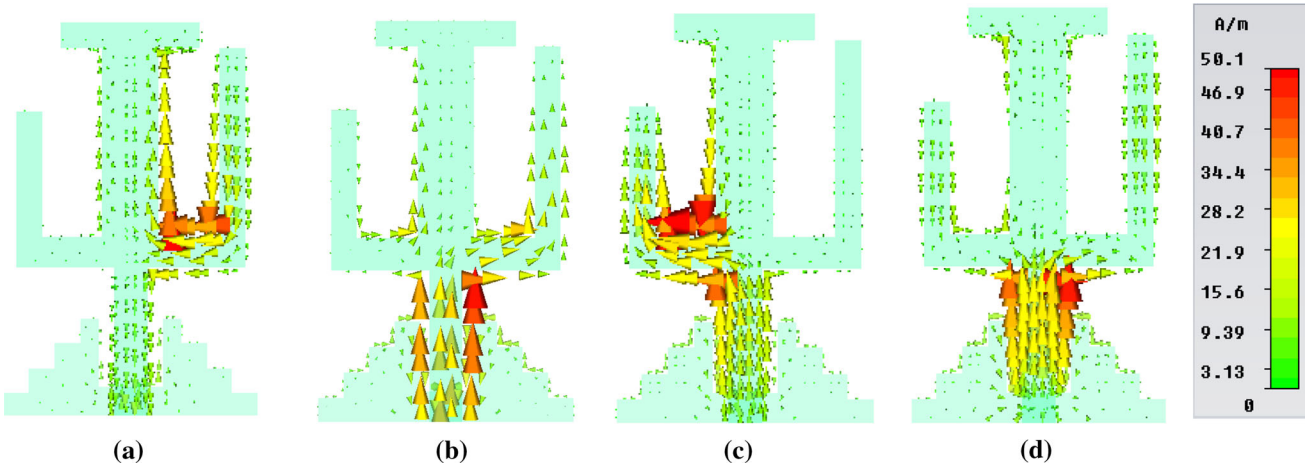

Fig. 4 Surface current distribution at various sample frequencies of the proposed antenna. **a** f = 2.40 GHz **b** f = 2.68 GHz **c** f = 3.24 GHz **d** f = 5.77 GHz

frequencies show quite good agreement with the simulated data.

3.1.3 Second resonance

The second resonance is excited by the microstrip line and L_5 and it is evident from Fig. 4(b). In this case the resonant length is calculated as:

$$L_{r2} = L_5 + L_1 + d \quad (3)$$

The resonance frequencies are calculated for different values of L_5 as shown in Fig. 6 and a comparison with simulated results is given in Table 3.

3.1.4 Third resonance

The third resonance is observed due to the current concentration on the feed line and L_2 which is verified by Fig. 4(c). The corresponding resonant length for this frequency can be calculated as:

$$L_{r3} = L_2 + L_1 + d + W_h - L_h \quad (4)$$

The resonance frequency calculated for different values of L_2 is validated with the simulated results as shown in Fig. 7 and presented in Table 4. Good agreement between theory and simulation results validates the proposed designed formula for the resonance frequency.

3.1.5 Fourth resonance

From Fig. 4(d) it is clear that the fourth resonance is excited due to the strong current density on the feed line. Hence only the feed line length will give the fourth resonance and it can be calculated using the resonant length

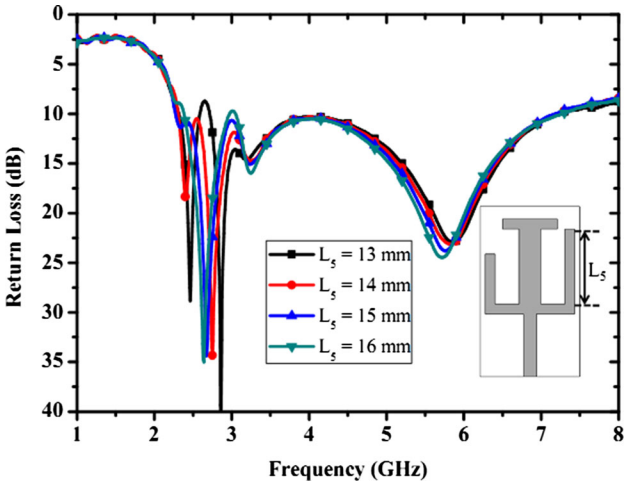

Fig. 6 Return loss variation of the proposed antenna for different values of L_5

Table 3 Comparison for the third resonance frequency

L_5 (mm)	L_{r2} (mm)	Resonance frequency (GHz)		% difference
		f_{r2} (Theory)	f_{r2} (Simulated)	
13	27.5	2.76	2.86	3.50
14	28.5	2.67	2.75	2.91
15	29.5	2.58	2.67	3.37
16	30.5	2.50	2.64	5.30

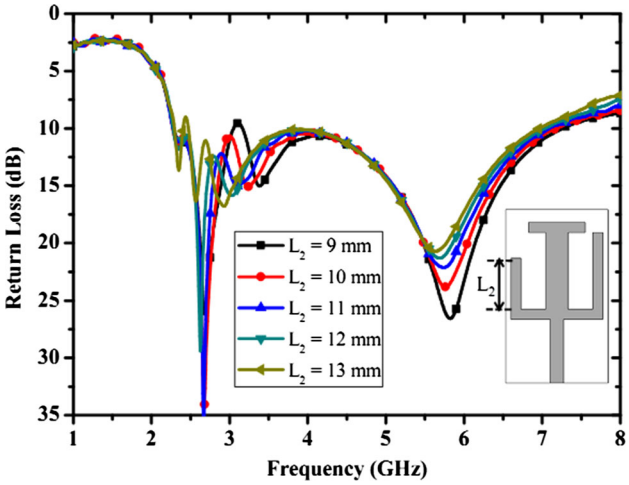

Fig. 7 Return loss variation of the proposed antenna for different values of L_2

Table 4 Comparison for the fourth resonance frequency

L_2 (mm)	L_{r3} (mm)	Resonance frequency (GHz)		% difference
		f_{r3} (Theory)	f_{r3} (Simulated)	
9	23.3	3.27	3.38	3.25
10	24.3	3.13	3.23	3.10
11	25.3	3.01	3.10	2.90
12	26.3	2.90	3.03	4.29
13	27.3	2.79	2.93	4.78

$L_{r4} = L_1$ in Eq. (1). The predicted resonance frequency is 6.09 GHz while the simulated one is 5.77 GHz with 5.54% difference which is in good agreement.

It is noted that, while varying an antenna parameter to study the impedance bandwidth and resonance frequencies, the rest of antenna dimensions are fixed and given in Table 1. The variation of return loss for different values of L_3 is shown in Fig. 5. From the figure it can be observed that the first and second resonances (2.4 and 2.68 GHz) are controlled by L_3. The maximum bandwidth 4.97 GHz

(2.33–7.30 GHz) is obtained for L_3 = 14 mm. Therefore, L_3 can be optimized for Bluetooth/WLAN applications.

The variation of return loss for different values of L_5 is plotted in Fig. 6. From the figure, it is clear that the first resonance frequency (2.4 GHz) is controlled by varying the value of L_5. This is due to the fact that the effective length of the radiating patch is increased and hence the lowest resonance frequency is affected. Thus, L_5 is again an optimisation tool to achieve the Bluetooth/WLAN band. In this case the maximum bandwidth achieved is 4.91 GHz (2.27–7.18 GHz).

Figure 7 shows that the third resonance (3.24 GHz) is controlled by L_2 and it is shifted towards the lower side as the value of L_2 increases. This shift can be explained by getting the effective resonance length L_{r3} using the value of L_2 and Eq. (4) and then calculating the corresponding resonance frequencies. The maximum bandwidth is found to be 4.91 GHz (2.27–7.18 GHz) for L_2 = 10 mm.

In Fig. 8, both the values of L_2 and L_5 are varied for the optimisation and to achieve maximum impedance bandwidth. The optimized values of L_2 and L_5 are 12 mm and 17 mm respectively at which the highest bandwidth of 4.90 GHz (2.34–7.24 GHz) is obtained.

3.2 The effect of gap between ground plane and radiating patch

The relative gap (g) between the ground plane and the radiating patch affects the impedance bandwidth and it acts as an impedance matching network. The return loss of the proposed antenna at different gap 'g' is shown in Fig. 9. At the optimized value of g = 4.0 mm, the maximum bandwidth of 4.90 GHz (2.28–7.18 GHz) is achieved. It is also noted that above and below g = 4.0 mm, antenna exhibits dual characteristics.

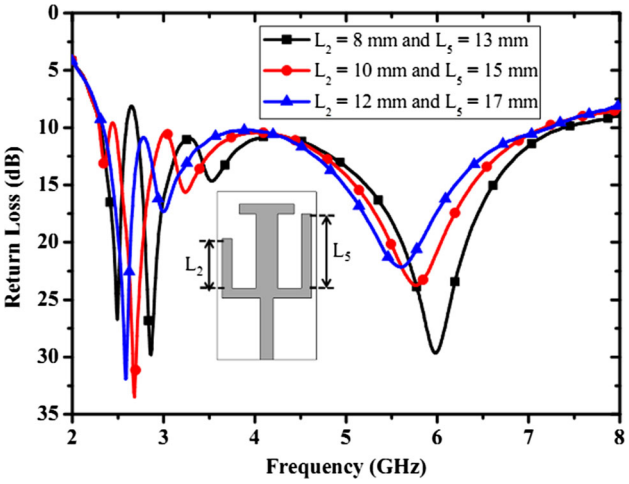

Fig. 8 Return loss variation of the proposed antenna for different values of L_2 and L_5

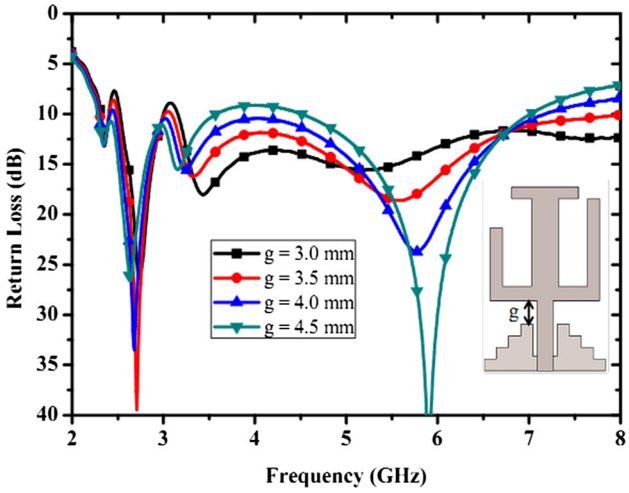

Fig. 9 Return loss variation of the proposed antenna for different values of g

3.3 The effect of ground plane structure

The dimensions of ground plane are very important parameter to optimise the impedance of the antenna which ultimately improves the antenna bandwidth. The variation of number of step slots (N) in the ground plane is studied to observe the difference between the proposed ground plane structure and the conventional partial ground plane with a notch. In Fig. 10, the return loss is plotted for different values of N incorporated in the ground plane. It shows that the bandwidth significantly depends on the values of N. It

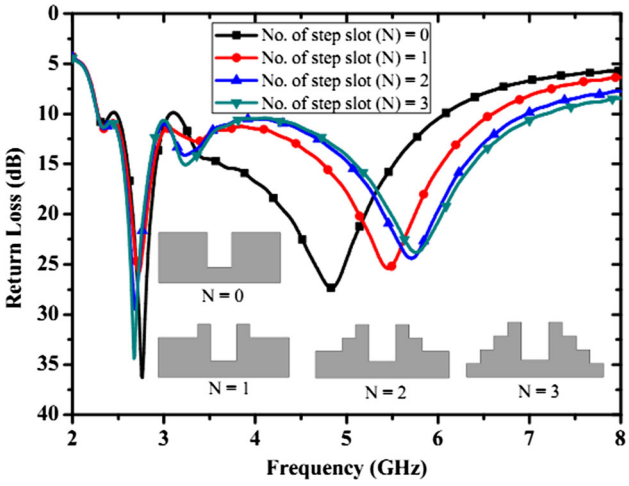

Fig. 10 Return loss variation of the proposed antenna for different number of step slots (N)

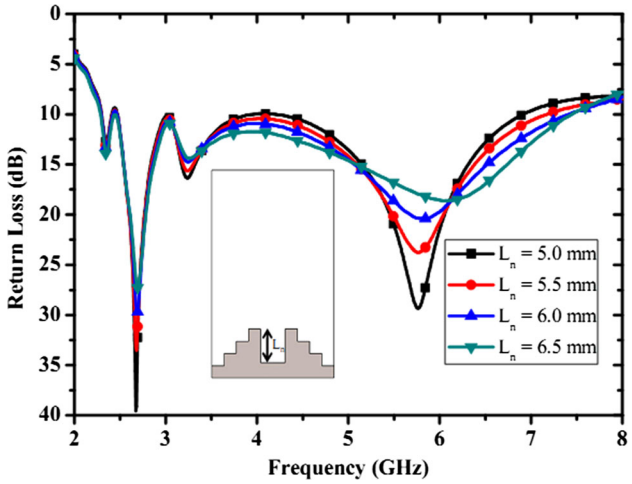

Fig. 11 Return loss variation of the proposed antenna for different values of L_n

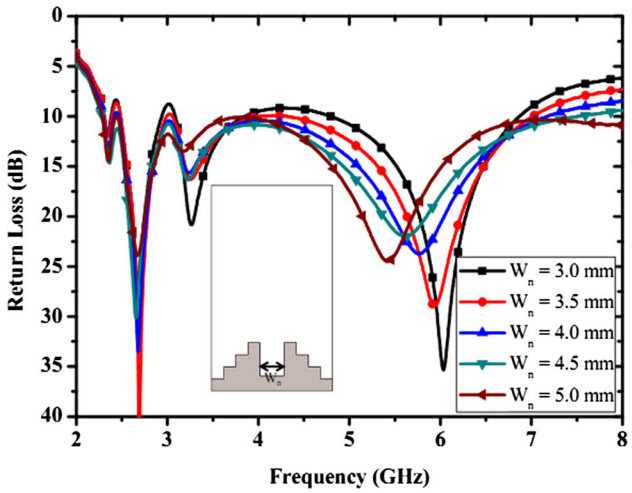

Fig. 12 Return loss variation of the proposed antenna for different values of W_n

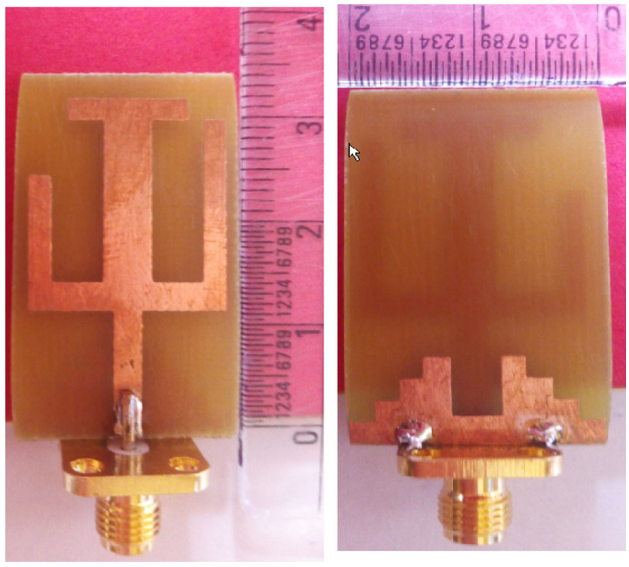

Fig. 13 Fabricated prototype antenna

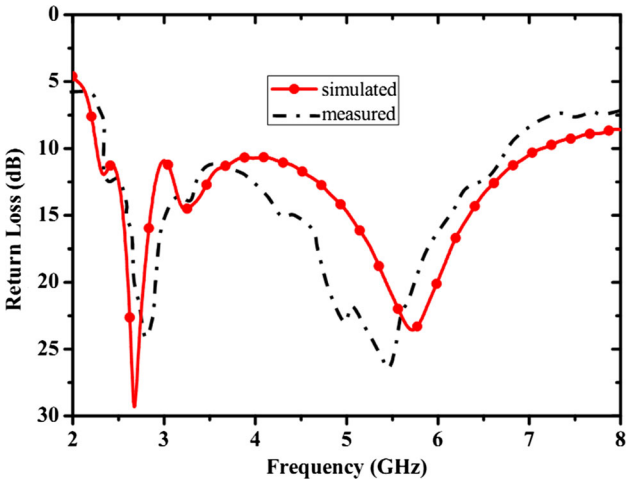

Fig. 14 Simulated and measured return loss of the proposed antenna

is interesting to note that the lower end of the operating band is constant at 2.27 GHz but the upper end of the band decreases abruptly as N goes to zero. The maximum bandwidth of 4.92 GHz (2.27–7.19 GHz) is observed at N = 3. The effect of the notch in the ground plane is also studied for the optimisation of the result. The variation of return loss for different values of L_n (Fig. 11) shows that the bandwidth of the antenna improves up to 5.16 GHz (2.29–7.45 GHz) as L_n increases. It is also observed that Bluetooth/WLAN band is unaffected by varying the notch length. Figure 12 shows the variation of return loss with different values of W_n. From the figure, it is clear that the fourth resonance is shifted towards lower side with increasing values of W_n. This is due to the variation in the coupling strength between the ground plane and microstrip line. At the optimum value of W_n = 4.5 mm, the maximum bandwidth of 5.26 GHz (2.27–7.53 GHz) is achieved.

4 Antenna fabrication and measured results

The top and bottom view of the fabricated prototype antenna is shown in Fig. 13. The antenna is fabricated on a FR4 substrate having dielectric constant 4.4 and loss tangent 0.02 with overall dimensions of 34 × 20 × 1.6 mm^3.

Table 5 Antenna comparison with earlier reported results

References	Dimensions (mm^3)	Frequency band (GHz)	Bandwidth ratio	Reduction in volumetric size (in %)
[11]	70 × 70 × 1.6	2.2 (3.4–5.6)	1.6:1	86.1
[12]	35 × 35 × 1.5	2.46 (2.71–5.17)	1.9:1	40.8
[13]	90 × 40 × 0.79	1.8 (2.4–4.2)	1.8:1	60.2
[14]	37 × 37 × 1.6	3.13 (2.23–5.36)	2.4:1	50.3
[15]	58 × 62 × 2.0	0.62 (1.9–2.52) and 1.2 (5.0–6.2)	1.3:1 and 1.2:1	84.9
[16]	26 × 26 × 1.6	5.76 (2.94–8.7)	3.0:1	− 0.6
[17]	50 × 55 × 1.5	4.8 (2.0–6.8)	3.4:1	73.6
[18]	24 × 35 × 1.6	0.41 (2.26–2.67) and 3.78 (3.0–6.78)	1.2:1 and 2.3:1	19.0
Proposed antenna	20 × 34 × 1.6	5.26 (2.27–7.53)	3.3:1	–

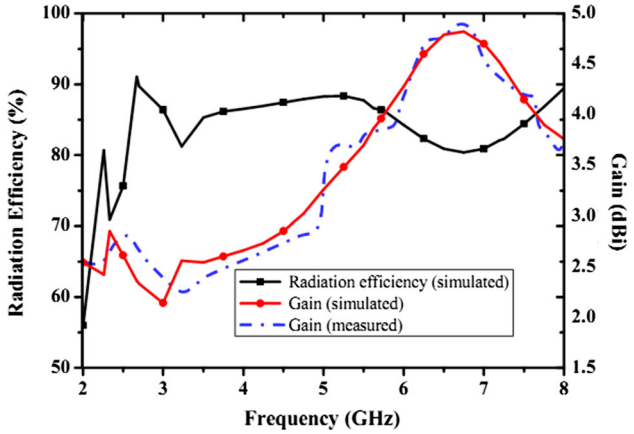

Fig. 15 Measured and simulated gain and radiation efficiency

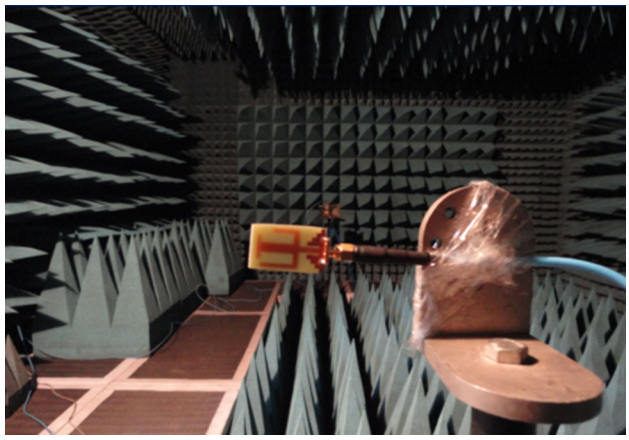

Fig. 16 Radiation pattern measurement setup

The return loss of the proposed antenna is measured using Agilent N5230A vector network analyser and compared with the simulated results (Fig. 14). The measured and simulated antenna bandwidths are 4.47 GHz (2.28–6.75 GHz) and 4.92 GHz (2.27–7.19 GHz) respectively which are in good agreements. The proposed antenna can be used for Bluetooth (2.4 GHz), WLAN (2.4, 5.1–5.8 GHz), WiMAX (2.3–5.7 GHz) and ISM bands (2.4/5.2/5.8 GHz) applications. A comparison is given in Table 5 which comprises the earlier reported results with proposed antenna structure in terms of overall antenna dimensions, frequency bands, bandwidth ratio and volumetric size reduction [11–18]. From the table it can be clearly observed that the proposed antenna is simple, compact, wideband and small in overall dimensions as compared to most of the reported structures.

The radiation efficiency and gain of the antenna are plotted in Fig. 15. From the figure it is clear that the simulated radiation efficiency is always above 70.0% throughout the entire operating band. The realised antenna gains are in good agreement and vary between 2.14–4.83 dBi (simulated) and 2.20–4.91 dBi (measured).

The far field radiation patterns are measured in a microwave shielded Anechoic chamber of dimensions 7.0 × 5.0 × 3.0 m^3 (length × width × height) as shown in Fig. 16. The test antenna is placed at a distance 3.2 m from the horn antenna. The simulated and measured co and cross polarization patterns are plotted in Fig. 17 for frequencies 2.4, 4.0 and 5.5 GHz respectively. Co-polar plot at $\varphi = 0^0$ (H-plane) is almost omnidirectional for entire operating band with low cross polarization level. At $\varphi = 90^0$ (E-plane), the co-polarization is showing bidirectional pattern at two sampling frequencies 2.4 and 4.0 GHz while at 5.5 GHz E-plane pattern is showing quasi omnidirectional pattern due to high mode generation. The cross polar pattern in E-plane is lower than the co-polar pattern for all the frequencies. The simulated and measured radiation patterns are in good agreement.

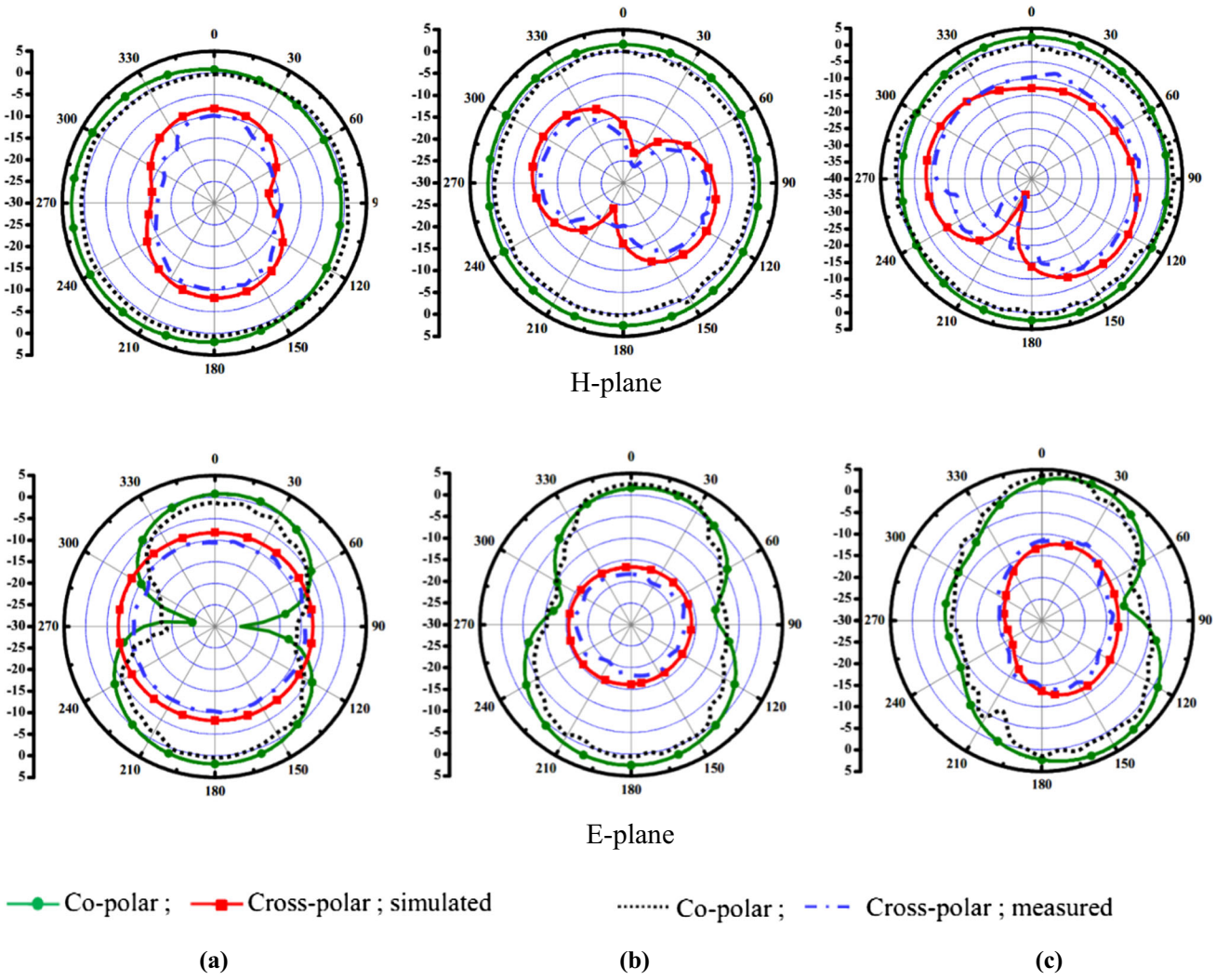

Fig. 17 Simulated and measured radiation patterns at 2.4 GHz, 4.0 GHz and 5.5 GHz. **a** f = 2.4 GHz **b** f = 4.0 GHz **c** f = 5.5 GHz

5 Conclusion

In this paper, a compact, wideband monopole antenna is designed, fabricated and measured. Parametric study of patch and ground plane shows that the impedance bandwidth and various resonance frequencies can be tuned by optimising the values of L_2, L_3, L_5 and N. The maximum bandwidth of 107.35% (2.27–7.53 GHz) is obtained by optimizing the dimensions of the radiating patch and ground plane. Various resonance frequencies are formulated theoretically which are agreeing well with the simulated resonance frequencies. H-plane patterns calculated at different frequencies are stable and omnidirectional while E-plane patterns are showing bidirectional radiation. Thus the proposed antenna characteristics are quite suitable for the Bluetooth, WLAN/WiMAX applications.

References

1. Li. H. B. & Kohno, R. (2007). Introduction of SG-BAN in IEEE 802.15 with related discussion. In *Proceedings of 2007 IEEE international conference on ultra-wideband*, Singapore (pp. 134–139).
2. Kohno, R., Hamaguchi K., Li, H. B., & Takizawa, K. (2008). R&D and standardization of body area network (BAN) for

medical healthcare. In *Proceedings of 2008 IEEE international conference on ultra-wideband* (Vol. 3, pp. 5–8).
3. Shrivastava, M. K., Gautam, A. K., & Kanaujia, B. K. (2014). An M-shaped monopole-like slot UWB antenna. *Microwave and Optical Technology Letters, 56*(1), 127–131.
4. Abbaspour, M., & Hassani, H. R. (2008). Wideband star-shaped microstrip patch antenna. *Progress Electromagnetics Research Letters, 1,* 61–68.
5. Yu, Z. W., Wang, G. M., Liang, J. G., & Gao, X. J. (2010). A semicircular band-notch ultra-wideband printed antenna based on CSRR. *Microwave and Optical Technology Letters, 52*(10), 2387–2390.
6. Jaglan, N., Gupta, S. D., Kanaujia, B. K., & Srivastava, S. (2016). Band notched UWB circular monopole antenna with inductance enhanced modified mushroom EBG structures. *Wireless Networks*. https://doi.org/10.1007/s11276-016-1343-7.
7. Rani, S. A., & Aziz, M. Z. A. (2014). An elliptically planar UWB monopole antenna with step slots defective ground structure. *Microwave and Optical Technology Letters, 56*(9), 2084–2088.
8. Kumar, L., Gautam, A. K., Kanaujia, B. K., & Rambabu, K. (2016). Design of compact F-shaped slot triple band antenna for WLAN/WiMAX applications. *IEEE Transactions on Antennas and Propagation, 64*(3), 1101–1105.
9. Pei, J., Wang, A. G., Gao, S., & Leng, W. (2011). Miniaturized triple-band antenna with a defected ground plane for WLAN/WiMAX applications. *IEEE Antennas and Wireless Propagation Letters, 10,* 298–301.
10. Kunwar, A., Gautam, A. K., & Kanaujia, B. K. (2017). Inverted L-slot triple-band antenna with defected ground structure for WLAN and WiMAX applications. *International Journal of Microwave and Wireless Technologies, 9*(1), 191–196.
11. Jan, J. Y., & Su, J. W. (2005). Bandwidth enhancement of a printed wide-slot antenna with a rotated slot. *IEEE Transactions on Antennas and Propagation, 53*(6), 2111–2114.
12. Chen, W. L., Wang, G. M., & Zhang, C. X. (2009). Bandwidth enhancement of a microstrip-line-fed printed wide-slot antenna with a fractal-shaped slot. *IEEE Transactions on Antennas and Propagation, 57*(7), 2176–2179.
13. See, C. H., Abd-Alhameed, R. A., Abidin, Z. Z., McEwan, N. J., & Excell, P. S. (2012). Wideband printed MIMO/diversity monopole antenna for WiFi/WiMAX applications. *IEEE Transactions on Antennas and Propagation, 60*(4), 2028–2035.
14. Sung, A. Y. (2012). Bandwidth enhancement of a microstrip line-fed printed wide-slot antenna with a parasitic center patch. *IEEE Transactions on Antennas and Propagation, 60*(4), 1712–1716.
15. Yildirim, B., Başaran, E., & Türetken, B. (2013). Dielectric-loaded compact WLAN/WCDMA antenna with shorted loop and monopole elements. *IEEE Antennas and Wireless Propagation Letters, 12,* 288–291.
16. Mondal, K., & Sarkar, P. P. (2015). M-shaped broadband microstrip patch antenna with modified ground plane. *Microwave and Optical Technology Letters, 57*(6), 1308–1312.
17. Baudha, S., & Vishwakarma, D. K. (2016). Bandwidth enhancement of a planar monopole microstrip patch antenna. *International Journal of Microwave and Wireless Technologies, 8*(2), 237–242.
18. Kunwar, A., & Gautam, A. K. (2017). Fork-shaped planar antenna for Bluetooth, WLAN, and WiMAX applications. *International Journal of Microwave and Wireless Technologies, 9*(4), 859–864.
19. Balanis, C. A. (2005). *Antenna theory analysis and design* (3rd ed.). Hoboken: Wiley.

Rakesh Nath Tiwari received his B.Sc. and M.Sc. (Electronics) degree from University of Allahabad and Deen Dayal Upadhyaya Gorakhpur University, Gorakhpur, India in 2002 and 2004 respectively. He received M.Tech. degree in Optical and Wireless Communication Technology from Jaypee University of Information Technology, Waknaghat, Solan, India in 2008. He has published more than 21 papers in peer reviewed International/National journals and conferences. Currently, he is a Ph.D. scholar in Electronics and Communication Engineering from Uttarakhand Technical University, Dehradun, India. His research interests include design and modeling of slot patch antennas, UWB antennas, microwave/millimeter wave integrated circuits and devices.

Prabhakar Singh was born in village Semra, Chandauli (U.P), India in 1984. He received his B.Sc. and M.Sc. degree from V. B. S. Purvanchal University in 2004 and 2006, respectively. He received his Ph.D. degree from J. K. Institute of Applied Physics, Department of Electronics and Communication, University of Allahabad, India in 2010. He taught B.Tech. and M.Tech. students at Delhi Technological University, Delhi, India for 1 year from 2009 to 2010. He worked as assistant professor at Bahra University, Shimla Hills, Himanchal Pradesh, India from 2010 to 2011. Presently he is working at Galgotias University, Greater Noida, India. He has published more than 50 research papers in peer reviewed International/National journals and conference proceedings. He is reviewer of many International and National journals. He is presently working on broadband microstrip antennas, size miniaturization techniques in patch antennas, UWB and photonic band gap antennas.

Binod Kumar Kanaujia is working as Professor in School of Computational and Integrative Sciences, Jawaharlal Nehru University, New Delhi since August, 2016. Before joining Jawaharlal Nehru University, he had been in the Department of Electronics and Communication Engineering in Ambedkar Institute of Advanced Communication Technologies and Research (formerly, Ambedkar Institute of Technology), Delhi as a Professor since Feb. 2011and Associate Professor (2008–2011). Earlier, Dr. Kanaujia held the positions of Lecturer (1996–2005), Reader (2005–2008) and Head of Department in Department of Electronics and Communication Engineering, M.J.P. Rohilkhand University, Bareilly, India. Prior to his career in academics, Dr. Kanaujia had worked as Executive Engineer

in the R&D division of M/s UPTRON India Ltd. Dr. Kanaujia had completed his B.Tech. in Electronics Engineering from KNIT Sultanpur, India in 1994. He did his M.Tech. and Ph.D. in 1998 and 2004; respectively from Department of Electronics Engineering, Indian Institute of Technology Banaras Hindu University, Varanasi, India. He has been awarded Junior Research Fellowship by UGC Delhi in the year 2001–2002 for his outstanding work in the electronics field. He has a keen research interest in design and modelling of microstrip antenna, dielectric resonator antenna, left-handed metamaterial microstrip antenna, shorted microstrip antenna, ultra wideband antennas, reconfigurable and circular polarized antennas for wireless communication. He has been credited to publish more than 220 research papers with more than 1000 citations with h-index of 17 in several peer-reviewed journals and conferences. He had supervised 50 M.Tech. and 15 Ph.D. research scholars in the field of microwave engineering. He is a reviewer for several journals of international repute i.e. IET Microwaves, Antennas & Propagation, IEEE Antennas and Wireless Propagation Letters, Wireless Personal Communications, Journal of Electromagnetic Wave and Application, Indian Journal of Radio and Space Physics, IETE Technical Review, International Journal of Electronics, International Journal of Engineering Science, IEEE Transactions on Antennas and Propagation, AEU-International Journal of Electronics and Communication, International Journal of Microwave and Wireless Technologies, etc. Dr. Kanaujia had successfully executed 05 research projects sponsored by several agencies of Government of India i.e. DRDO, DST, AICTE and ISRO. He is also a member of several academic and professional bodies i.e. IEEE, Institution of Engineers (India), Indian Society for Technical Education and The Institute of Electronics and Telecommunication Engineers of India.

Multimedia Tools and Applications
https://doi.org/10.1007/s11042-018-6448-9

Biometric re-authentication: an approach towards achieving transparency in user authentication

Neha[1] · **Kakali Chatterjee**[1]

Received: 29 October 2017 / Revised: 14 July 2018 / Accepted: 20 July 2018 /
Published online: 28 July 2018
© Springer Science+Business Media, LLC, part of Springer Nature 2018

Abstract
Providing fixed re-authentication attempts to the user in case of password mismatch is a very old concept. But as password based authentication mechanisms are prone to many security attacks, user's biometric properties along with passwords are highly in use for user authentication these days. It will be more secure and convenient if re-authentication influenced by the biometric behavior of the user is applied in the authentication system. It is a challenging task to identify a genuine user using behavioral biometric due to its low repeatability and wide variation. So, to increase the efficiency and robustness of the authentication system in case of score mismatch, the clustering of user's behavior and assigning different re-authentication attempt to different cluster is needed. In this paper, we have proposed a transparent fixed text, keystroke based user authentication framework, which will enhance the security of traditional password based authentication mechanism. A new classification algorithm and dynamic attempt allocation algorithm have been proposed which will make the authentication system smart enough to provide the genuine user a fare authentication attempt.

Keywords Authentication · Keystroke dynamics · Behavioral biometrics · Security

1 Introduction

A lot of devices and applications these days requires a good user authentication scheme to validate the user's identity, requesting their services. A few examples of these application includes: computer systems, digital lockers, cell phones, ATMs, laptops etc. Depending upon the level of security needed, different authentication techniques are being adopted in these applications. Mostly, user Id & password along with some other security features like

✉ Neha
neha.cse14@nitp.ac.in

Kakali Chatterjee
kakali@nitp.ac.in

[1] Department of Computer Science and Engineering, National Institute of Technology, Patna, India

OTP on phone based entry point user authentication techniques are used. Many papers have been proposed in these directions [11, 18, 24, 31, 38, 45]. The security of the password based technique totally depends upon the uniqueness and the toughness of the password. But it is very difficult for a user to remember different passwords for multiple applications they are using. So, for user's convenience, in case of initial password miss-match, they have been provided, a few more chances to authenticate themselves. Here in this paper, we are referring to this technique as ***Re-Authentication***. To avoid *Brute Force Attack* often the user is given a fixed number of re-authentication attempts. And in many cases genuine users have been denied access for a few hours after four to five wrong attempts. Now, for a genuine user it is a very troublesome situation. Here the attempt number has been fixed considering security factors in mind. Hence, there is a contradiction between user ***convenience and security***. For any authentication mechanism to be implemented, an equilibrium must be maintained between the level of security achieved and the extent of convenience provided to the end users. So, there is a strong need of smart decision for number of re-authentication attempt provided to a user.

Targeting above two issues (security & convenience), biometric authentication along with password based authentication is a good alternative for these applications. In biometric authentication, users are recognized on the basis of biometric characteristics of themselves, which can be broadly categorized as physiological and behavioral. Physiological characteristics are based upon the measure of physical characteristic of the human body that can provide his identity. Many work has been done in the direction of user authentication through physiological characteristics like: fingerprint scanning [17, 28], retina scan [27], facial recognition [26, 40, 42–44], hand geometry recognition [22, 23, 34], vain pattern recognition [19] etc. According to Prabhakar et al. [30] physiological biometrics have high repeatability and consistent authentication performance, which satisfies the security requirements. But in the above proposed scenario, user convenience and acceptability is quite much important. So, in such cases, behavioral biometrics are more acceptable than physiological. Behavioral biometrics refers to the characteristics or actions in the behavior of the person, unique enough to authenticate a person. Many work has been done in behavioral biometrics, like:keystroke dynamics [2, 5, 6, 8–10, 13–16, 21, 25, 29, 32, 33, 36, 37, 39, 41, 46], signature recognition [4], voice identification [4], mouse dynamics [1, 35, 47] etc.

Behavioral biometric provides simple password based authentication an extra layer of security. These techniques are also quite convenient for the users to accept as these are transparently implemented without direct user intervention. In this paper we are using keystroke dynamics of a user as a behavioral biometric for user authentication. Many works have been done in the area of keystroke dynamics based user authentication. Gaines et. al [39] in 1980, experimented with it and proposed its use for user authentication. Statistically independent of properties were tested using T-test under the consideration that the mean of the digraph times were same and variance were different at both the sessions. In 2000, Morose et al. [29] proposed a keystroke dynamics based biometrics for authentication. In this paper he presented a classification technique based on template matching and Bayesian likely hood models. Yu and Cho, [46] in 2003 proposed "Novelty Detection Approach for Keystroke Dynamics Identity Verification" using 4-Layer Auto Associative Multilayer Perceptron. Latter in 2004 Liew et al. [25] experimented with the efficiency of SVM for keystroke dynamic verification. He found it quite better in terms of computation time and performance than the neural network. But the major limitation of this work is that it is necessary to have at least 50 user typing patterns to create the user template. Hocquet et al. [15] in 2005, proposed "Fusion of Methods for Keystroke Dynamics Authentication". The inclusion of pause

and cues during typing was proposed by Cho et al. [6] in 2006. It will make password hacking and cracking more difficult. To increase the keystroke dynamic performance Hocquet et al. [16] in 2007, proposed the inclusion of two user dependent parameters: security threshold and fusion weights of different classifiers to the users profile. They concluded that the use of optimal personal parameters improves the performance a lot. For this they divided the authentication process in two parts. In the first part the user is associated with a cluster and in the second part, the clustered parameter is used for authentication step. Azevedo et al. [2] in 2007, proposed "An Approach of Feature Selection for Keystroke Dynamics System Based on PSO and Feature Weighting". In this paper they analyzed optimization algorithm for feature selection. Its concluded here that PSO out performed GA considering parameters like: feature reduction rate, processing time and classification error. In 2008 Rybnik et al. [33] proposed a keystroke dynamics based user identification technique. They used dwell time and flight time for user authentication. Their work also specifies the various keystroke features that can be extracted and used for authentication but, it fails to provide sufficient measures for a better outcome. Hempstalk et al. [13] in 2008, proposed "One-Class Classification by Combining Density and Class Probability Estimation". A comparison of one class classification using SVM is also performed here. Davoudi & Kabir [8] in 2009, proposed "A New Distance Measure for Free Text Keystroke Authentication Uses Histogram Based Identity Estimator". In 2009 [32] Revett and Kenneth in his paper, discussed typing evolution of the user. In this work the update of database with user's current typing pattern will be performed, if he is authenticated as a valid user. This will improve the performance as keystroke dynamics are subject to evolve through the lifetime. But in case of impersonation, where impostor is authenticated as genuine user, its fake template will get added to the database. Shimshon et al. [36] in 2010, proposed "Clustering Di-graph for Continuously Verifying Users According to their Typing Patterns". This technique joins similar pair of consecutive keystroke. Singh & Arya [37] 2011, proposed "Key Classification : A New Approach in Free Text Keystroke Authentication System". Latter many papers discussed various classification techniques for performance improvement, but all needed large registration data set. So, eliminating this deficiency of verification system, Giot et al. [10] in 2011, proposed a new method based on SVM learning, which needs a few users sample for enrollment and template creation. But it takes larger template creation time. In 2015, Visumathi et al. [41] proposed a new keystroke authentication system using biometric information of users available at runtime. Chandrasekar et al. [5] in 2016, proposed an authentication system based on keystroke dynamics using stochastic diffusion algorithm. Here the stochastic diffusion search is used for feature subset selection. Ho & Kang, [14] 2018, proposed "One Class Naive Bayes with Duration Feature Ranking for Accurate User Authentication Using Keystroke Dynamics". In this paper a new feature, the typing speed information of the user is being used for authentication. For this they introduced speed inspection in typing skills (SITS) algorithm. The one class naive bayes algorithm has been used here for calculation of attributes likely hood in keystroke dynamics. Kolakowska [21] 2018, proposed "Usefulness of Keystroke Dynamics Features in User Authentication and Emotion Recognition" . In this study the author concludes that a universal feature set for a defined task can not be predicted in advance.

Analyzing all these works, it is observed that using a single fixed threshold for covering a wide range of users keystroke behavior will result more rejection to the genuine user. Thus, there is a need to cluster(unsupervised technique), each user's varying data range into different groups. Each cluster should be given different threshold value. And in case of login data which is not lying in any of the cluster range, re-authentication attempts depending upon the closeness of login phase data to the different cluster data should be provided to

them. For this reason we have proposed a novel attempt calculator theorem which will increase the user authentication performance and there convenience.

Our Contribution in this paper is as follows:

1. A novel behavioral biometric based user authentication framework has been proposed. It uses machine learning techniques for achieving good user authentication performance.
2. A concept of behavioral re-authentication is implemented using the dataset clustering concept. Different cluster is provided a different number of re-authentication attempts using attempt calculator. The uniqueness of this re-authentication technique is that it uses behavior dependent attempt calculator theorem for determining the number of attempts.
3. An analysis of efficient feature set for fixed text, keystroke dynamics user authentication has been done here. The analysis shows the performance variation accordingly.
4. We have proposed here a new classification algorithm to achieve transparency in user authentication through fixed text keystroke dynamics. This classification algorithm is a modified version of existing J48 algorithm, which suits the proposed scenario.

2 Background

The basic process of Keystroke Dynamics authentication consists of: *Keystroke Dynamics enrollment, Identification and Verification* as shown in the Fig. 1.

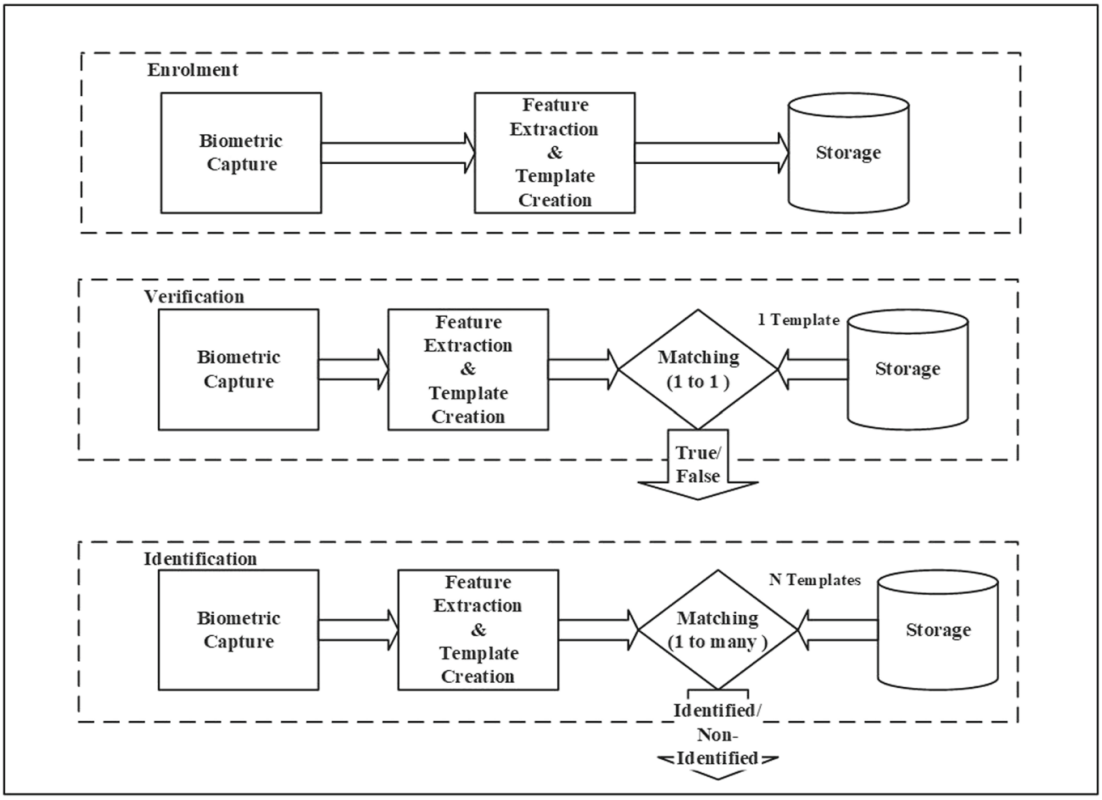

Fig. 1 Biometric Enrollment, Identification & Verification for User Authentication

2.1 Enrollment

The keystroke enrollment process consists of *keystroke dynamics capture, feature extraction & template creation* . In keystroke dynamics no extra hardware is needed for biometric capture. It is done transparently while the user is entering their login credentials like: user ID and password. The performance of a keystroke dynamic system depends upon, what features are being selected for authentication. It captures typed rhythm while using the keyboard. It means, pressing and releasing of keys.

2.1.1 Features

The keystroke features in the fixed text authentication system can be broadly classified as *homogeneous vectors, heterogeneous vectors* and *aggregate vectors* [3].

1. **Homogeneous Feature Vector:** A keystroke feature vector is homogeneous if only it has key hold latencies or key interval latencies as its features. A homogeneous vector is the simplest of all keystroke vectors and is indecomposable. In this if the password is of n digits, then there will be n key press duration (KP) and n-1 key latencies(KL). So, the homogeneous feature set can be: $(KP_1, KP_2, KP_3..., KP_n)$ or $(KL_1, KL_2, KL_3, ...KL_{n-1})$. Where, the n key press durations will be formally calculated as:
$$KP_i = KU_i - KD_i \tag{1}$$
And the n-1 key latencies for n digit password can be formally calculated as:
$$KL_i = KD_i - KU_{i-1} \tag{2}$$
2. **Heterogeneous Feature Vector:** A keystroke feature vector is heterogeneous if it has both key hold and key interval latencies as features. So, if n is the length of the password then, there will be n number of key press durations (KP) and n-1 times key interval latencies (KL). For n digit password a total of 2n-1 features will be there. $(KP_1, KP_2, KP_3..., KP_n, KL_1, KL_2, KL_3,$
$....KL_{n-1})$. Where, the n key press durations will be formally calculated as:
$$KP_i = KU_i - KD_i \tag{3}$$
And the n-1 key latencies for n digit password can be formally calculated as:
$$KL_i = KD_i - KU_{i-1} \tag{4}$$
3. **Aggregate Feature vector:** If the features are derived by aggregating key hold and key interval latencies together, then these are called aggregate feature vectors. In this category, let n be the password length. Then for typing the password there is pressing of key, i.e KD(Key Down) time and the releasing of the key i.e, KU(Key Up) time. Now for n letter password, we have the feature set as:(DT, FT). DT is the sum of press duration of all the n letters of the password. FT is the sum of interval duration in between pressing of two characters of the n digit password.
$$DT = \sum_{i=1}^{n} KU_i - KD_i \tag{5}$$
$$FT = \sum_{i=1}^{n} KD_{i+1} - KU_i \tag{6}$$

2.1.2 Clustering

Clustering is a task of grouping the set of objects in such a manner that the objects clustered in a group are more similar to each other than the other.
In our framework we need to categorize each user training set data into three categories having a different range of centroids. And the system will provide different categories for different numbers of re-authentication attempts in case of failure to login. So, for this we will use K-Mean clustering algorithm.

K-Means Algorithm [12] It is a exclusive clustering algorithm. It classify a given dataset into certain number of clusters fixed a prior. After clustering the dataset the template is saved in the database.

Algorithm 1 K-Means algorithm

1: **procedure** INPUT:(K: Number of clusters, D: A dataset of N points)
2: OUTPUT: A set of K clusters.
3: **BEGIN**
4: Take K initial cluster points in the given dataset D of N points.
5: **for** Each point P in D **do**
6: Find the nearest center and assign P to the corresponding cluster, minimizing the objective function:

$$J = \sum_{j=1}^{K} \sum_{i=1}^{K} \left\| {x_i}^j - c_j \right\|^2 \tag{7}$$

Where,$|{x_i}^j - c_j|^2$ is a chosen distance measure between a data point ${x_i}^j$ and the cluster center c_j.
7: **end for**
8: Update clusters by calculating new centers using mean of the members.
9: Until stop iterating criteria satisfied.
10: **end procedure**

2.2 Identification

In this phase the system identifies a user based upon his presented identity features in the login phase, by matching it with all other users identity features (one to many matching) saved in the system [20]. Let's suppose the input feature vector be V_Q, now we need to find the suitable identity I_K, $where K \epsilon \{1, 2, .., N\}$ are the identities of N number of users saved in the system. Formally, it is represented as in (7).

$$V_Q \varepsilon \begin{cases} I_K, if\ max_K S(V_Q, V_I) \geq t, K = 1, 2, ..., N \\ Unidentified, otherwise \end{cases} \tag{7}$$

2.3 Verification

In this phase the system validates the person's claimed identity by comparing its login phase data with the registered data (one to one matching) [20]. Let us suppose the login feature

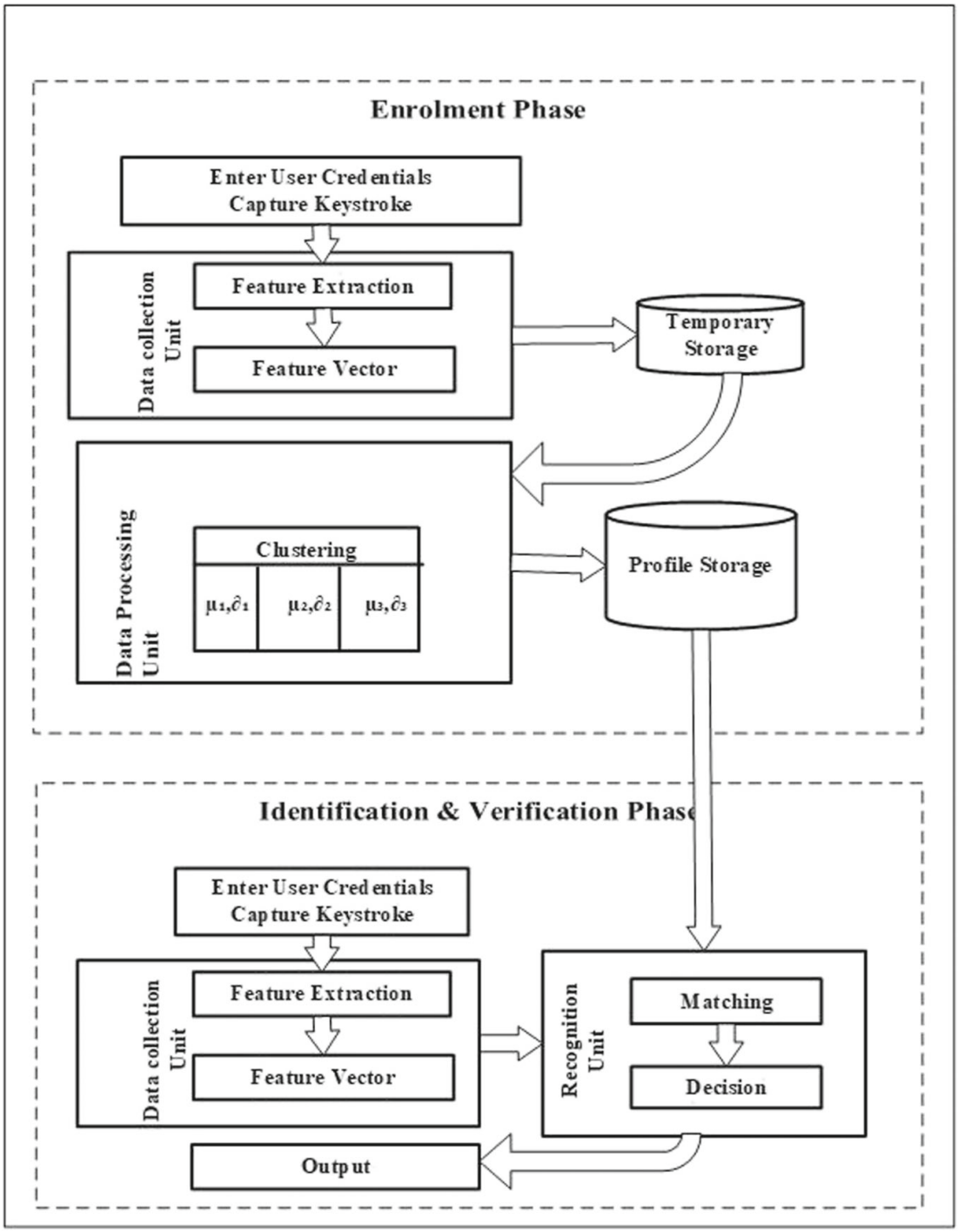

Fig. 2 Authentication Framework

vector for the claimed identity I is V_Q. Now if (I, V_Q) is matched with the corresponding identities registered feature vectors V_I. If the matching score calculated using function $d()$ is under the given threshold 't' then the user belongs to genuine user class C_1 otherwise non-genuine class C_2. Formally the process is represented as in (8),

$$(I, V_Q)\varepsilon \begin{cases} C_1, if d(V_Q, V_I) \geq t \\ C_2, otherwise \end{cases} \tag{8}$$

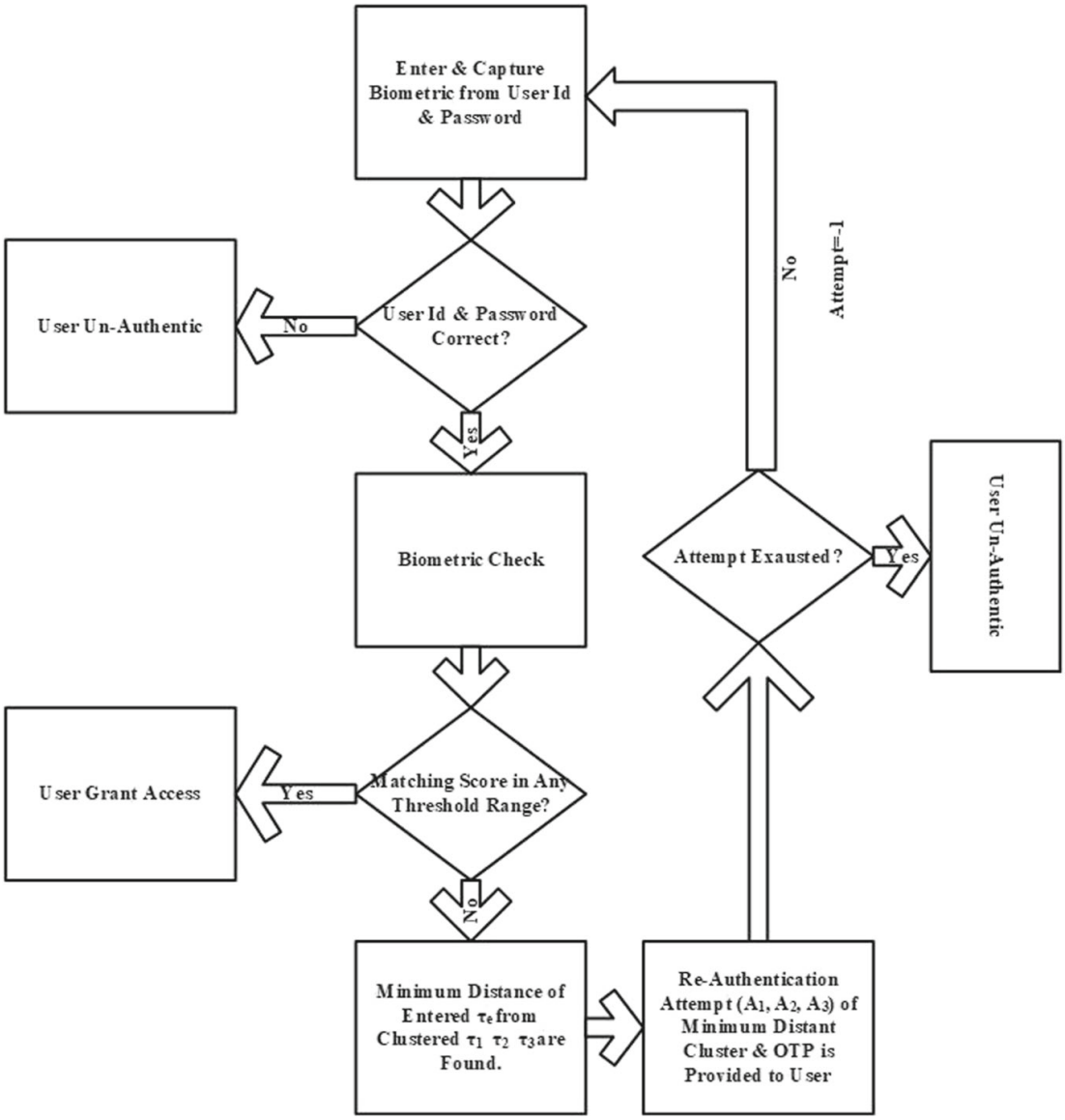

Fig. 3 Authentication Flow chart

Euclidean Distance [7] Let us consider two sets of vector, the training sets vector $X_1, X_2....X_n$ and the corresponding test vector $Y_1, Y_2....Y_n$. Then the Euclidean distance between these sets of vectors can be defined as:

$$E = \sqrt{\sum_{i=1}^{n}(X_i - Y_i)^2} \tag{9}$$

3 Proposed work

In this section the proposed user authentication framework and the re-authentication logic has been discussed.

The proposed authentication framework is divided into two phases: *Enrollment Phase* and *Identification & Verification Phase* . The authentication framework in shown in Fig. 2. A flow chart explaining the work flow of the proposed frame work has been shown in Fig. 3.

Table 1 Feature details of current database

S.No	Feature type	Features	Formula
1	Homogeneous	KP1, KP2, KP3, KP4	KPi=KUi-KDi
2	Hetrogeneous	KP1, KP2, KP3, KP4,	KPi=KUi-KDi
		KL1, KL2, KL3	KLi=KDi-KUi-1
3	Aggregate	DT	$DT = \sum_{i=1}^{n} KU_i - KD_i$
		FT	$FT = \sum_{i=1}^{n} KD_{i+1} - KU_i$

1. **Enrollment Phase:** Initially the user who wants to use the system will register them self to the system through the registration interface. For registration, user has to enter their user name, password, phone number and some text in the text box. The password has to be entered 10 times in a day and there will be 10 such sessions on different days. These are done to capture users maximum possible keystroke behavior. These data will be temporarily saved in a database. These data will be then clustered and stored as template in profile storage as ***current database***. Table 1 shows feature description of analyzed features for current database. Next there is another database the ***backup database***, which will store users typing features for typing all characters from A to Z, 0 to 9 and Z to A ten times in one day and repeating it in ten different sessions. This database is only used in case of password change phase. In case it is known to the user that the password is compromised, then for the new password the feature values will be initially taken from the backup database and are updated with time. A functionality flow diagram has been shown in Fig. 3.
2. **Verification Phase:** In this phase the user when want to use the application, will try to login, by entering his user id and password at the start of the session. Then authentication will be processed. To authenticate a user through proposed framework, four possibilities arise as shown in Table 2.

Table 2 Authentication sequence of password and biometric

S.No	Password	Biometrics	Result
1	Correct	Correct	Accept
2	Correct	Wrong ($Score > \tau$)	Reject
3	Correct	τ_1 τ_2 τ_3 If Score lies in any of threshold Range	Accept
4	Correct	τ_1 τ_2 τ_3 Score does not lie in any threshold range. Distance from τ calculated	Re-authentication attempt provided according to τ range
5	Wrong	No verification	Reject

At the first stage his user name is matched, if it is correct? The password is checked. There are two cases here, either password is correct or wrong. Now referring the 1st case the password is correct, then the biometric matching of the password is done using the proposed classification Algorithm 2.

Algorithm 2 Modified J48 classification algorithm (MJ48)

procedure INPUT:(The data set D with n attributes.)
    OUTPUT: User Authentic or Un-authentic
    BEGIN
    if entered User ID, Password == Stored User ID, Password && Attempt No.==0 **then**
        for All attributes $A \epsilon D$ **do**
            Calculate Information Gain by formula

$$Entropy : E(S) = \sum_{i=1}^{n} -P(C_i) * \log P(C_i) \tag{11}$$

$$Gain : G(S, A) = E(S) - \sum_{i=1}^{m} P(A_i) E(S_{A_i}) \tag{12}$$

        end for
        A_{best}= Highest information gain attribute.
        if $A_{best}(Test)$ Lies between $[A_{best}(Fullcentroid)]Min - Max$ **then**
            User Grant Access.
        else
            Find and Calculate minimum distance of
            $A_{best}(Test)$ form $A_{best}(centroid1)$, $A_{best}(centroid2)$, $A_{best}(centroid3)$.
            if $MinDis == E[A_{best}(Test), A_{best}(centroid1)] \cap MinDis < [A_{best}(centroid1)]_{Min-Max}$ **then**
                Re-Authentication Attempt= A_1

            else
                if $MinDis == E[A_{best}(Test), A_{best}(centroid2)] \cap MinDis < [A_{best}(centroid2)]_{Min-Max}$ **then**
                    Re-Authentication Attempt= A_2

                else
                    if $MinDis == E[A_{best}(Test), A_{best}(centroid3)] \cap MinDis < [A_{best}(centroid3)]_{Min-Max}$ **then**
                        Re-Authentication Attempt= A_3

                    else
                        Block User for time T.

                    end if
                end if
            end if
        end if
    end if
end procedure

According to the proposed algorithm, first the maximum information gain attribute is determined from registered data, and if that attributes login value lies in the range of centroid min-max registered value, the user access is granted. Here the min-max centroid value of the registered data is calculated using Theorem 1.

Theorem 1 (Min-Max Calculator) *Let* $A_1, A_2, A_3 ...., A_n$ *be the keystroke dynamics attributes each having x entries. These are being divided into K clusters,* $C_1, C_2, ...C_K$ *where,* $K < x$. *If* $M_{1_m}, M_{2_m} ...., M_{n_m}$ *be the calculated main centroid of each attribute set values and* $[M_{1_{C_1}}, M_{1_{C_2}} ...., M_{1_{C_K}}]$, $[M_{2_{C_1}}, M_{2_{C_2}} ...., M_{2_{C_K}}]$, ..., $[M_{n_{C_1}}, M_{n_{C_2}} ...., M_{n_{C_K}}]$ *be the each attributes different clusters centroid values. The acceptable threshold range for the login attributes in different cases with given M value will be between* M_{Min} *to* M_{Max}. *These are formally defined as:*

$$M_{Min} = M - (M * .01) \tag{10}$$

$$M_{Max} = M + (M * .01) \tag{11}$$

The 2nd case mentioned in Table 2 is generally followed these days. Improving this, our proposal works from 3rd case onwards. It says that in case if password is correct, then it checks the biometrics. Whether the entered login phase biometrics lie in the registered biometric selected attribute main centroid's M_{min} to M_{max} range or not? If yes, then the user is accepted. Else, case 4: if the password is correct, but the biometric value does not come in this range, then rather than rejecting the user he will be given re-authentication attempts. For this it is checked that the login biometric value is closest to which cluster's registered value. It means the highest information gain attribute's login value's distance is calculated from each cluster centroid using Euclidean Distance (9) given in Section 2.3. Hence, the minimum distant cluster is found. Now it is checked whether this calculated minimum distance is less than the selected cluster's centroid Min-Max range or not? If it satisfies both these conditions, the user will be provided re-authentication attempts and a one time password (OTP) is sent to the user's registered phone number. Each registered cluster has been given fixed attempt number defined using the Theorem 2.

Theorem 2 (Attempt Calculator) *Let* $A_1, A_2, A_3 ...., A_n$ *be the attribute of keystroke dynamics dataset, each having x entries. These are being divided into K clusters,* $C_1, C_2, ...C_K$ *where* $K < x$. *Now* $G_1, G_2 ...., G_n$ *be the calculated Information Gains of each of these attributes. Let* A_i *where,* $1 \leq i \leq n$ *be the maximum information gain attribute. If* $[M_{i_{c1}}, M_{i_{c2}}, ..., M_{i_{ck}}]$ *be the the maximum information gain attributes centroid value in respective clusters, and* M_{i_m} *be the main centroid of the respective attribute, then attempt number alloted to each cluster is given by:*

$$AttemptNo = \begin{cases} 6, & \textbf{\textit{if}}\ (M_{i_{c1}} isleastdistant from M_{i_m}) \\ 4, & \textbf{\textit{if}}\ (M_{i_{c2}} is 2ndindistance from M_{i_m}) \\ 2, & \textbf{\textit{if}}\ (M_{i_{c3}} ismostdistant from M_{i_m}) \end{cases} \tag{12}$$

Algorithm 3 Re-authentication attempt algorithm

```
procedure INPUT:(Attempt No.)
    OUTPUT: User Authentic or Un-authentic
    BEGIN
    if Attempt No>0 then
        if entered User ID, Password == Stored User ID, Password then
            A_best = Highest information gain attribute.
            if A_best(Test) Lies between [A_best(Fullcentroid)]Min−Max then
                User Grant Access.
            else
                Attempt No.–
            end if
        else
            Attempt No.–
        end if
    else
        User Un-Authentic
    end if
end procedure
```

After that the minimum distance cluster's allotted re-authentication attempt is provided to the user. The re-authentication process will be done using the proposed Algorithm 3. Lastly in case 5, if the password is wrong, the user is rejected without any biometric verification.

4 Implementation results

In this section we will discuss about the implementation details of the proposed framework.

We implemented the proposed authentication framework for computer system security. First of all we created the user's dataset. Here we have created three types of data sets. One having heterogeneous feature set, second having homogeneous feature set and the third having aggregate feature set. All the data set has been created and tested on the system with 64 bit windows operating system, with 26 GB RAM, Intel(R) Core(TM)i5-7200U CPU 2.50GHz 2.17GHz processor. In each data set we registered 25 users in 10 different sessions on different days. In each session, each users 10 consecutive entries are captured. So, a total of 100 data entries per user is there.

4.1 Data set creation

First of all we tried to find out which type of keystroke feature vector will be more discriminative for user authentication. For this purpose we created three datasets consisting of homogeneous, heterogeneous and aggregate feature vectors, and then performed user recognition based on these datasets.

In the Table 3 the users keystroke data capture using a heterogeneous feature set are being shown. Here the KP 1, KP 2, KP 3, KP 4 are being calculated for two users for their respective password of same length using (3), and the feature KL 1, KL 2, KL 3 are being calculated using (4).

Table 3 Data set snap showing 2 users heterogeneous features value in millisecond

Users	1	1	1	2	2	2
KP 1 (millisec)	177	177	182	75	73	86
KP 2 (millisec)	93	89	92	89	88	85
KP 3 (millisec)	81	87	90	116	111	109
KP 4 (millisec)	96	88	88	65	69	70
KL 1 (millisec)	203	203	251	493	475	414
KL 2 (millisec)	191	195	178	138	187	212
KL 3 (millisec)	150	150	130	139	129	126

In the Table 4 keystroke dataset snap showing a two users two entries for homogeneous features value (millisecond). Here the features KP 1, KP 2, KP 3, KP 4 are being calculated using (1).

The Table 5 shows a snap of uses keystroke dataset created using aggregate features. The features DT and FT used in the table are calculated using the (5) and (6) respectively.

After data set creation, we performed a comparative analysis over these datasets to observe whether these feature sets variation affect the classification results or not. All the performance analysis is done using Weka software Version 3-8-1. The obtained results has been shown in Table 6.

4.2 Template creation

For further implementation of our framework, we proceeded with the heterogeneous feature dataset. To identify a particular user's behavior variation, to treat them accordingly, we clustered each user registered dataset into three parts using K-Mean algorithm. Here, the K value is taken as three. The K value can be increased as per the possible variation in the data set, but as we have not captured a user keystroke behavior for long and for experimental convenience it is taken as three. A snap of user 'a' clustered dataset and the cluster centroids have been shown in Figs. 4 and 5 respectively.

Similarly, other users registered datasets are also clustered and saved as template.

4.3 Identification & verification

To analyze the user identification performance of the proposed algorithm with respect to the other existing algorithm the Table 7 shows the results. Here we found that in the given scenario identification accuracy of the modified J48 is slightly better than the other existing algorithms.

Table 4 Data set snap showing 2 users homogeneous features value in millisecond

Users	KP 1 (millisec)	KP 2 (millisec)	KP 3 (millisec)	KP 4 (millisec)
1	177	93	81	96
1	177	89	87	88
2	75	89	116	65
2	73	88	111	69

Table 5 Data set snap showing 2 users aggregate features value in millisecond

Users	1	1	1	2	2	2
DT (millisec)	187	176	179	409	431	400
FT (millisec)	568	551	553	694	671	690

After template creation, the user verification will be done. When the user tries to login, by entering their credentials like user Id, password etc, the login template were created from the entered text in the login phase. Let us denote the login template as $[KP_{(t1)}, KP_{(t2)}, KP_{(t3)}, KP_{(t4)}, KL_{(t1)}, KL_{(t2)}, KL_{(t3)}]$, where $KP_{(t1)}, KP_{(t2)}, KP_{(t3)}, KP_{(t4)}$ denotes test phase first, second, third, forth text key press time respectively and $KL_{(t1)}, KL_{(t2)}, KL_{(t3)}$ denotes test phase first, second, third key latency time respectively. Now these test phase data have to be matched to the users registered template using proposed classification Algorithm 2. In the above discussed setup when we performed the comparative classification analysis of our created dataset using algorithms: SVM, J48 and proposed MJ48 algorithm, our proposed classification algorithm shows a better performance with FAR of 0.1 and FRR of 0.2. The classification results are shown in Table 8.

Table 6 Accuracy of different feature types using different algorithms with variation in character length of password(L)

Feature type	Features	Algorithm		Accuracy (%) (Character length)		
				L=4	L=6	L=8
Heterogeneous	KP_i, KL_i	BayesNet		80.02	87.5	95.67
		K-Mean	K=1	80.38	84.5	85.00
			K=3	82.05	87.5	95.76
			K=5	84.21	87.5	95.78
Agregate	DT, FT	BayesNet		52.33	54.65	54.89
		K-Mean	K=1	55.16	56.43	66.34
			K=3	55.11	55.73	48.22
			K=5	55.25	51.66	52.03
Homogeneous	KP_i	BayesNet		66.6	68.45	69.12
		K-Mean	K=1	68.24	72.32	72.43
			K=3	68.3	72.12	74.66
			K=5	70.7	75.32	78.34
	KL_i	BayesNet		66.23	67.43	67.99
		K-Mean	K=1	66.54	70.61	70.02
			K=3	66.34	72.22	72.32
			K=5	66.9	74.74	74.72

```
@attribute Instance_number numeric
@attribute user {a}
@attribute KP1 numeric
@attribute KP2 numeric
@attribute KP3 numeric
@attribute KP4 numeric
@attribute KL1 numeric
@attribute KL2 numeric
@attribute KL3 numeric
@attribute Cluster {cluster0,cluster1,cluster2}

@data
1,a,84,232,190,178,264,339,422,cluster0
2,a,85,223,182,138,240,312,410,cluster0
3,a,88,251,178,130,200,321,487,cluster0
4,a,99,242,186,146,303,364,481,cluster0
5,a,77,198,152,181,246,310,444,cluster1
6,a,91,195,129,146,287,301,429,cluster1
7,a,91,200,115,145,267,297,404,cluster1
8,a,92,193,149,157,341,350,439,cluster1
9,a,98,214,120,139,257,331,441,cluster1
10,a,74,191,209,202,229,298,374,cluster2
11,a,82,212,170,159,205,288,377,cluster2
12,a,88,203,195,150,224,277,334,cluster2
13,a,92,190,162,150,235,298,381,cluster2
14,a,94,199,142,183,155,340,434,cluster2
15,a,96,203,191,150,225,371,371,cluster2
```

Fig. 4 A Snap of User 'a' Clustered Dataset

```
Final cluster centroids:
                          Cluster#
Attribute    Full Data          0          1          2
                (15.0)      (4.0)      (5.0)      (6.0)
=============================================================
user                  a          a          a          a
KP1            88.7333         89       89.8    87.6667
KP2           209.7333        237        200   199.6667
KP3           164.6667        184        133   178.1667
KP4           156.9333        148      153.6   165.6667
KL1             245.2     251.75      279.6   212.1667
KL2             319.8        334      317.8        312
KL3             415.2        450      431.4      378.5
```

Fig. 5 A Snap of User 'a' Data Cluster Centroids

Table 7 Identification results with proposed algorithm, SVM and J48

S.No	Classifiers	Identification(%) (10-fold CV)
1	SVM	85.69
2	J48	96.22
3	MJ48	96.68

Table 8 Classification result with proposed algorithm, SVM and J48

S.No	Classifiers	Accuracy	Precision	Specificity	Prevalence	FAR	FRR
1	SVM	0.63	0.32	0.7	0.2	0.2	0.6
2	**J48**	0.73	0.6	0.8	0.3	0.2	0.4
3	**MJ48**	0.82	0.7	0.9	0.3	0.1	0.2

5 Analysis and comparison

5.1 Dataset analysis

For analyzing the comparative performance of various feature types presented above we performed the user recognition through heterogeneous, aggregate and homogeneous feature vector dataset having various features. The various features taken here are: heterogeneous feature vector we have taken KP_i and KL_i referring equation 3 and 4, the aggregate feature vector $DT\&FT$ are taken referring (5) and (6) and the homogeneous feature vector with two features KP_i and KL_i separately referring (1) and (2) respectively. We have used three different machine learning algorithms (viz: Bayes Net, K-Mean and J48) for user recognition. The effect of user recognition on varying the length of password $'L'$ has also been observed. By observing the accuracy performance, a few points has been observed. The accuracy performance of heterogeneous features KP_i and KL_i is highest among the other feature sets, the homogeneous features being the second and aggregate being the least. With character length L=4, heterogeneous features using k-mean algorithm (K=5) have highest accuracy percentage of 84.21%. With character length L=8, the heterogeneous feature using k-mean classifier achieved highest accuracy of 95.78%. It has also been observed that, in heterogeneous features with the increase in length of characters, the Bayes Net classifier showed an increase in accuracy performance till L=10 to 12, then decreases. But using K-Mean classifier, with different values of k, the accuracy performance increases with increase in character length. A plot of accuracy percentage of heterogeneous feature vector using different classification algorithm with varying character length has been shown in Fig. 6. This analysis justifies our calmed contribution 3, in this paper.

5.2 Algorithm analysis

Our proposed framework's performance can be analyzed on two aspects: security and user convenience. To evaluate the performance on these parameters two cases arise.

- Case 1:What security and convenience is provided to the genuine user using the system,
- Case 2:How security and convenience parameter varies when an impostor is using the system.

For evaluating the above cases we have made a real time Java based interface. We have made an assumption that; for each re-authentication attempt the :

$$Re-authenticationSessiontime = OTPValidityPeriod \tag{13}$$

This assumption has been made to ensure that in one re-authentication attempt only one OTP can be received by the authenticator with a validity period of 3 minutes.
For testing case 1, genuine user ('a') login phase value are matched against there registered dataset using MJ48(modified J48) algorithm.

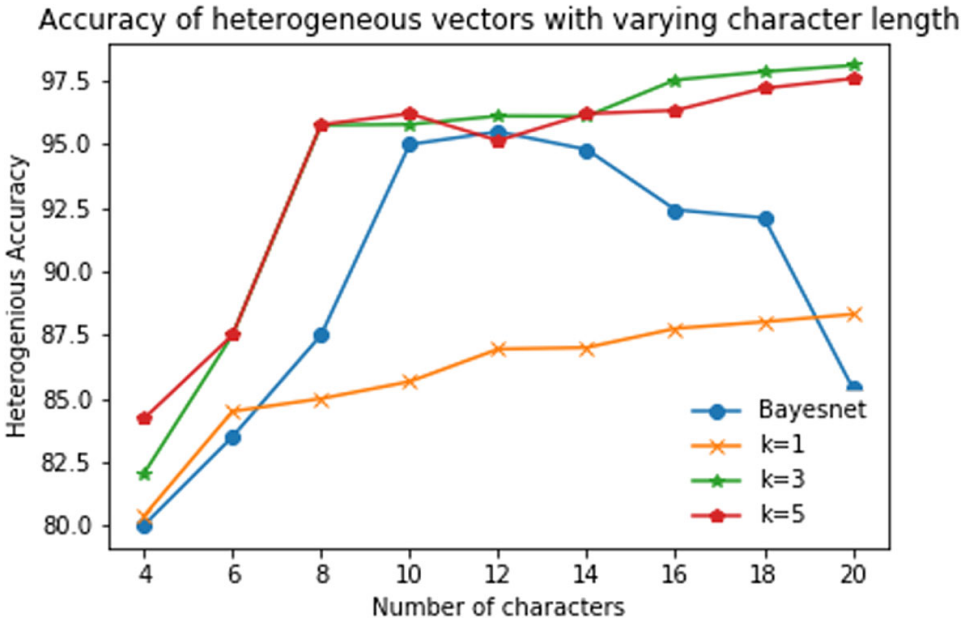

Fig. 6 Variation of accuracy percentage of heterogeneous feature vector with varying character length

According to the algorithm, first feature vectors with the highest information gain attribute is determined. Here with user 'a' registered feature vector, $[KP_{(t1)}, KP_{(t2)}, KP_{(t3)}, KP_{(t4)}, KL_{(t1)}, KL_{(t2)}, KL_{(t3)}]$, we found $KP_{(t2)}$ to be the highest information gain attribute with the value 1.56 in the first iteration. So, the $KP_{(t2)}$ login value will be matched with the corresponding registered value. Now according to the proposed algorithm, while matching the various possibilities that can arise are mentioned in Table 9.

So, as in Table 9 case 1, first the login KP2 value was matched with the KP2 Full data centroid as shown in Fig. 5. If it lies in the threshold range, the user is authenticated. But if not the minimum distance cluster centroid is found. If it satisfies that threshold range, the corresponding re-authentication attempt is provided, otherwise user rejected. With each re-authentication attempt an OTP is sent to the registered user phone no., which is valid for 3 minutes. We simulated our interface for login by genuine user 40 times, in which 60% cases it satisfied the case 1 of Table 9, where as 15%, 20% and 5% in clusters 1, 2 and 3 respectively. But while lying in case 2 of Table 9, it means when they entered into the re-authentication phase through cluster 1, they received the OTP but in 5% cases the user is rejected because of lying out of threshold range. While lying in re-authentication phase through cluster 2, in 9 % cases, while getting the OTP correctly user is rejected due to out of threshold range. Where as while lying in re-authentication phase through cluster 3, in 10 % cases after successfully receiving the OTP user is rejected due to out of threshold range. All these cases resulted in an FRR of 0.2 as mentioned in Table 8.

Then we tried to validate the case 2 of this section, it means variation in performance when an impostor tries to impersonate as a genuine user. For an impostor to be able to login successfully two things are needed: the password and in case of re-authentication the OTP. For simulating this, we provided the impostor with the password, and then tried to login. We did this 40 times. In this we found 48 % cases impostor is rejected, due to not lying in any threshold range. We found 10% impostors KP2 login feature value lie in full centroid min-max range. The 48% impostor got re-authentication through different clusters. But as in re-authentication phase an OTP is sent to the genuine user, which need to be entered within validity period for authentication. So in all these cases 60% of times we did not provided the OTP to the impostors, hence they got rejected. But rest 40 % times we provided them

Table 9 Security test cases of algorithm

	Classification	Algorithm	Re-Authentication attempt no. & OTP	Genuine user(%)	Impostor (%)	Accept/Reject % (OTP exhausted/Not in threshold range in any attempt)	
						Genuine user	Impostor
Case :1	Lies in KP2 main centroide range	MJ48	–	60	10	–	–
Case :2	Cluster 1 range	MJ48	6	15	16	OTP not exhausted ever but rejected 5% times due to threshold miss match	OTP exhausted 60% cases. Rejected 10% cases due to threshold miss match.
	Cluster 2 range	MJ48	4	20	10	OTP not exhausted ever but rejected 9% times due to threshold miss match	OTP exhausted 60% cases. Rejected 7% cases due to threshold miss match.
	Cluster 3 range	MJ48	2	5	22	OTP not exhausted ever but rejected 10% times due to threshold miss match	OTP exhausted 60% cases. Rejected 12% times due to threshold miss match.

Table 10 Comparison with recent works

Research work	No. of users	Biometric feature	Technique	Result
Yu.E 2003 [46]	21	Keystroke Dynamics	ANN	FAR:0, FRR:0.84
Hocquet 2005 [15]	13	Keystroke Dynamics	Statistical, Degree of disorder & Time Discretization	FAR:14, FRR:1.69
Azevedo 2007 [2]	24	Keystroke Dynamics	SVM	FAR:0.76, FRR:0.81
Hempstalk 2008 [13]	19	Keystroke Dynamics	One-class Gaussian	FAR:11.3, FRR:20.4
Davoudi & Kabir 2009 [8]	21	Keystroke Dynamics	Statistical	FAR:9, FRR:5
Shimshon 2010 [36]	10	Keystroke Dynamics	Random Forest Decision Tree	FAR:0.41, FRR:0.63
Singh 2011 [37]	20	Keystroke Dynamics	Statistical	FAR:2, FRR:4
Our Work	25	Keystroke Dynamics	Clustering based authentication	FAR:0.1, FRR:0.2

the OTP also. So out of 48% in case 2, 16 % impostor got re-authentication through cluster 1 range. But in that case also 10% impostor's got rejected due to threshold miss match. In the cluster 2 range 10% impostors got re-authentication, but in 7% cases got rejected due to threshold miss match. Where as 22% impostors while lying in the cluster 3 range, 12% cases got rejected due to threshold miss match. All this resulted into an FAR of 0.1 as mentioned in Table 8.

After all these analysis, we concluded that in the presented scenario, our proposed algorithm provides the genuine user a slight decrease in the rejection rate, and increase in user convenience by providing them a chance to re-authenticate themselves. Whereas in the same scenario the impostors instead of getting the re-authentication attempt are unable to get authenticated compared to the genuine user. This justifies our contribution 2 and 4 in this paper.

The comparison of the proposed work with a few recent works is shown in Table 10.

6 Conclusion

In this paper, we have proposed a novel behavioral biometric user authentication framework, which used a behavior dependent re-authentication concept based on attempt number calculator theorem. The proposed concept will try to give the genuine user a fair chance to authenticate themselves. We also did an investigation on the feature set to be used for keystroke dynamics to achieve greater authentication accuracy.

Publisher's Note Springer Nature remains neutral with regard to jurisdictional claims in published maps and institutional affiliations.

References

1. Ahmed A, Traore I (2007) A new biometric technology based on mouse dynamics. IEEE Trans Dependable Secure Comput 4:165e79
2. Azevedo GLFBG, Cavalcanti GDC, Edson CB, Filho C (2007) An approach to feature selection for keystroke dynamics systems based on PSO and feature weighting. In: Evolutionary Computation, 2007. CEC IEEE Congress on, pp 3577-3584. IEEE
3. Balagani KS, Phoha VIRV, Ray A, Phoha S (2011) On the discriminability of keystroke feature vectors used in fixed text keystroke authentication. Pattern Recogn Lett 32(7):1070–1080
4. Bhattacharyya D, Ranjan R, Alisherov F, Choi M (2009) Biometric authentic: a review. Int J Serv Sci Technol 2:13e28
5. Chandrasekar V, Suresh Kumar S, Maheswari T (2016) Authentication based on keystroke dynamics using stochastic diffusion algorithm. Stoch Anal Appl 34(1):155–164
6. Cho S, Hwang S (2006) Artificial rhythms and cues for keystroke dynamics based authentication. In: International conference on biometrics. Springer, Berlin, pp 626–632
7. Danielsson P-E (1980) Euclidean distance mapping. Comput Graphics Image Process 14(3):227–248
8. Davoudi H, Kabir E (2009) A new distance measure for free text keystroke authentication. In: Computer Conference CSICC 2009. 14th International CSI, pp. 570–575. IEEE
9. Garcia JD (1986) Personal identification apparatus. U.S. Patent 4,621,334 issued November 4
10. Giot R, El-Abed M, Hemery B, Rosenberger C (2011) Unconstrained keystroke dynamics authentication with shared secret. Comput Secur 30(6):427–445
11. Gong L, Pan J, Liu B, Zhao S (2013) A novel one-time password mutual authentication scheme on sharing renewed finite random sub-passwords. J Comput Syst Sci 79(1):122–130
12. Hartigan JA, Wong MA (1979) Algorithm AS 136: A k-means clustering algorithm. J R Stat Soc Ser C Appl Stat 28(1):100–108
13. Hempstalk K, Frank E, Witten IH (2008) One-class classification by combining density and class probability estimation. In: Joint european conference on machine learning and knowledge discovery in databases. Springer, Berlin, pp 505–519

14. Ho J, Kang D-K (2018) One-class nave Bayes with duration feature ranking for accurate user authentication using keystroke dynamics. Appl Intell 48(6):1547–1564
15. Hocquet S, Ramel J-Y, Cardot H (2005) Fusion of methods for keystroke dynamic authentication. In: IEEE workshop on automatic identification advanced technologies 4th, pp 224-229. IEEE
16. Hocquet S, Ramel J-Y, Cardot H (2007) User classification for keystroke dynamics authentication. Advances in biometrics, pp 531–539
17. Hong L, Jain AK (1998) Integrating faces and fingerprints for personal identification. IEEE Trans Pattern Anal Mach Intell 20(12):1295–1307
18. Huang Y, Huang Z, Zhao H, Lai X (2013) A new one-time password method. IERI Procedia 4:32–37
19. Im S, Park H, Kim Y, Han S, Kim S, Kang C, Chung C (2001) A biometric identification system by extracting hand vein patterns, journal of the korean physical society. Korean Publ 38(3):268–272
20. Jain AK, Ross A, Prabhakar S (2004) An introduction to biometric recognition. IEEE Trans Circuits Syst Video Technol 14(1):4–20
21. Koakowska A (2018) Usefulness of keystroke dynamics features in user authentication and emotion recognition. In: Human-Computer Systems Interaction. Springer, Cham, pp 42–52
22. Kukula E, Elliott S (2001) Implementation of Hand Geometry at Purdue University's Recreational Center: An Analysis of User Perspectives and System Performance. In: Proc. of 35th annual international carnahan conference on security technology, UK, pp 83–88
23. Kumar A, Wong DC, Shen HC, Jain AK (2003) Personal Verification using Palmprint and Hand Geometry Biometric. In: Proc. of 4th international conference on audio- and video-based biometric person authentication, Guildford, UK, pp 668–678
24. Lee N-Y, Chiu Y-C (2005) Improved remote authentication scheme with smart card. Computer Standards and Interfaces 27(2):177–180
25. Liew K-M, Shen H, See S, Cai W, Fan P, Horiguchi S (eds) (2004) Parallel and distributed computing: Applications and technologies: 5th international conference, PDCAT 2004, vol 3320. Springer, Singapore. Proceedings
26. Marcolin F, Vezzetti E (2017) Novel descriptors for geometrical 3D face analysis. Multimed Tools Appl 76(12):13805–13834
27. Mariño C, Penedo MG, Penas M, Carreira MJ, Gonzalez F (2006) Personal authentication using digital retinal images. Pattern Anal Applic 9(1):21
28. Matsumoto T, Hoshino H, Yamada K, Hasino S (2002) Impact of artificial gummy fingers on fingerprint systems. In Proc SPIE 4677:275–289
29. Monrose F, Rubin AD (2000) Keystroke dynamics as a biometric for authentication. Futur Gener Comput Syst 16(4):351–359
30. Prabhakar S, Pankanti S, Jain AK (2003) Biometric recognition: Security and privacy concerns. IEEE Secur Priv 99(2):33–42
31. Prakash M, Viju P, Infant A, Shobana J (2010) Eliminating vulnerable attacks using one time password and passtext analytical study of blended schema. Universal J Comput Sci Eng Technol 1(2):133–140
32. Revett K (2009) A bioinformatics based approach to user authentication via keystroke dynamics. Int J Control Autom Syst 7(1):7–15
33. Rybnik M, Tabedzki M, Saeed K (2008) A keystroke dynamics based system for user identification. In: Computer information systems and industrial management applications CISIM'08. 7th, pp 225–230. IEEE
34. Sanchez-Reillo R, Sanchez-Avila C, Gonzales-Marcos A (2000) Biometric identification through hand geometry measurements. IEEE Trans Pattern Anal Mach Intell 22(10):1168–1171
35. Shen C, Guan X, Cai J (2010) A hypo-optimum feature selection strategy for mouse dynamics in continuous identity authentication and monitoring, pp 349e53 [IEEE International Conference on Information Theory and Information Security]
36. Shimshon T, Moskovitch R, Rokach L, Elovici Y (2010) Clustering di-graphs for continuously verifying users according to their typing patterns. In: Electrical and Electronics Engineers in Israel (IEEEI) IEEE 26th Convention of, pp. 000445-000449. IEEE
37. Singh S, Arya KV (2011) Key classification: a new approach in free text keystroke authentication system. In: 2011 3rd pacific-asia conference on circuits, communications and system (PACCS), pp 1–5. IEEE
38. Song R (2010) Advanced smart card based password authentication protocol. Computer Standards and Interfaces 32(5):321–325
39. Stockton GR, Lisowski W, Press JS, Shapiro N (1980) Authentication by keystroke timing: Stockton Some preliminary results. No. RAND-R-2526-NSF RAND CORP SANTA MONICA CA
40. Vezzetti E, Marcolin F, Tornincasa S, Ulrich L, Dagnes N (2017) 3D geometry-based automatic landmark localization in presence of facial occlusions . Multimed Tools Appl 77:1–29
41. Visumathi J, Jayarin JP (2015) "C". J Appl Secur Res 10(3):375–384

42. Wan M, Lai Z, Yang G, Yang Z, Zhang F, Zheng H (2017) Local graph embedding based on maximum margin criterion via fuzzy set. Fuzzy Set Syst 318:120–131
43. Wan M, Li M, Yang G, Gai S, Jin Z (2014) Feature extraction using two-dimensional maximum embedding difference. Inform Sci 274:55–69
44. Wan M, Yang G, Gai S, Yang Z (2017) Two-dimensional discriminant locality preserving projections (2DDLPP) and its application to feature extraction via fuzzy set. Multimed Tools Appl 76(1):355–371
45. Xu J, Zhu W-T, Feng D-G (2009) An improved smart card based password Authentication scheme with provable security. Computer Standards and Interfaces 31(4):723–728
46. Yu E, Cho S (2003) Novelty detection approach for keystroke dynamics identity verification. In: International conference on intelligent data engineering and automated learning, pp 1016–1023. Springer, Berlin
47. Zheng N, Paloski A, Wang H (2011) An efficient user verification system via mouse movements, pp 1e12 [ACM Conference on Computer and Communications Security]

Neha is a Ph.D scholar at National Institute of Technology Patna, in computer science department. She has completed her M.Tech from National Institute of Technology Durgapur, India. She has some published research papers in CCIS (Springer) and International Journals. Presently, she is working in the field of Information Security.

Kakali Chatterjee is Assistant Professor in Computer Science and Engineering Department of National Institute of Technology Patna, India. She has completed her Ph.D from Delhi University (formerly Delhi College of Engineering). She has done M.Tech from Centre for Development of Advanced Computing, a R&D and Academic centre of Govt. of India. She has many published research papers in LNCS (Springer) and reputed International Journals. She is working in the field of Information Security and Cryptography.

ResearchGate

See discussions, stats, and author profiles for this publication at: https://www.researchgate.net/publication/326571403

COMMERCIAL AND TECHNOLOGICAL FEASIBILITY STUDY OF USING SOLAR E-RICKSHAW FOR SEMI-URBAN AREAS

Article *in* International Journal of Development Research · December 2017

CITATIONS
0

3 authors, including:

Manish Kumar
Havells
1 PUBLICATION **0** CITATIONS

SEE PROFILE

Some of the authors of this publication are also working on these related projects:

COMMERCIAL AND TECHNOLOGICAL FEASIBILITY STUDY OF USING SOLAR E-RICKSHAW FOR SEMI-URBAN AREAS View project

Characterization of Friction Stir Processed Aluminium Alloy Matrix using Artificial Neural Network View project

All content following this page was uploaded by Manish Kumar on 24 July 2018.

The user has requested enhancement of the downloaded file.

ISSN: 2230-9926

Available online at http://www.journalijdr.com

IJDR

International Journal of Development Research
Vol. 07, Issue, 12, pp.17432-17439, December, 2017

ORIGINAL RESEARCH ARTICLE OPEN ACCESS

COMMERCIAL AND TECHNOLOGICAL FEASIBILITY STUDY OF USING SOLAR E-RICKSHAW FOR SEMI-URBAN AREAS

[1,*]Tarun Saxena, [1]Manish Kumar and [2]Dr. Kesari, J. P.

[1]Department of Mechanical Enginnering, Delhi Technological University, Bawana Road, Delhi-110042
[2]Associate Professor, Department of Mechanical Enginnering, Delhi Technological University, Bawana Road, Delhi-110042

ARTICLE INFO

Article History:
Received 09th September, 2017
Received in revised form
06th October, 2017
Accepted 15th November, 2017
Published online 29th December, 2017

Key Words:
Efficiency,
e-Rickshaw,
Optimisation,
Life cycle cost,
Payback, Renewable energy,
Solar PV,
Zero-mile Connectivity.

ABSTRACT

This research paper basically deals with improvement in the mode of transportation. Due to the extinction of non-renewable energy, we are focusing on making current transportation fuel free. The energy generation as well as utilization, both should be from renewable. Our objective in presenting this research paper is to improve and upgrade e-Rickshaw, which are currently in use, with solar PVs in semi-urban areas of India.

Copyright ©2017, Tarun Saxena et al. *This is an open access article distributed under the Creative Commons Attribution License, which permits unrestricted use, distribution, and reproduction in any medium, provided the original work is properly cited.*

Citation: Tarun Saxena, Manish Kumar and Dr. Kesari, J.P. 2017. "Commercial and Technological Feasibility Study of using Solar e-Rickshaw for Semi-urban areas", *International Journal of Development Research*, 7, (12), 17432-17439.

INTRODUCTION

NDIA, as well as the whole world, are dwelling with problems of traffic congestion & emission and it is going to worse in coming years. The automobile industry is going through tremendous pressure of producing better and more environmentally sound vehicles. The government of India is seeking a way to increase public transport services which are eco-friendly as well as economy efficient (backed up by the renewable source of energy). In urban cities like Delhi, there exists public transport like Metro (Mass Transit System) which are somehow reducing traffic congestion problems but it lacks in first & last-mile connectivity. Today, Electric Vehicles (EVs) like e-Rickshaw serve as a Special Purpose Vehicle (SPVs), being used for first and last-mile connectivity as a means of public transport in many urban and semi-urban areas like Delhi and NCR. At present, India is highly dependent on non-renewable resources for its energy requirements.

Corresponding author: **Tarun Saxena,**
*Department of Mechanical Enginnering, Delhi Technological University, Bawana Road, Delhi-110042.

Thus, the EVs would not entirely benefit until and unless they use a renewable source of energy to power the battery bank. It is very clear that relying on a non-renewable source of energy like crude oil is not only hampering our health and environment but also causing a huge dent in our economy. National Electrical Mobility Plan (NEMMP) 2020 has set target of deploying 5 to 7 million EVs in India by 2020 of which it is targeted to have 4,00,000 Passenger Battery Electric Vehicles (BEVs) which will avoid 120 million barrels of oil & 4 million tons of CO_2 and hence lowering vehicular emission by 1.3% by 2020. NITI Aayog in collaboration with Colorado-based Rocky Mountain Institute report on Transformative Mobility Solutions says India can save as much as $60 billion in energy costs by 2030 and one gigatons of CO_2 emissions from 2017 to 2030 if it adopts more electric and shared vehicle. On basis of India's new green car policy, Govt. may consider doling out both fiscal & non-fiscal incentives and subsidies to push sales of EVs while discouraging the use of petrol and diesel-run vehicles. Tsinghua University, China studies says that the photovoltaic powered electric vehicle model has pollutant reduction

potentials of 99.8%, 99.7% and 100% for CO_2, SO_2, and nitrogen oxides, respectively, compared with a traditional gasoline-fueled car. Keeping in mind, Sustainability, Govt. policies & initiatives and research works, Solar e-Rickshaw (Emission free & Powered by renewable energy) is proposed in our paper for first and last-mile connectivity in semi-urban areas and will provide employment opportunities for lower middle-class people. Solar e-Rickshaw can be described as the application of solar PVs/energy to power & run wheels of e-Rickshaw. It has low maintenance, low running cost, is eco-friendly and non-polluting product and can be used for public mobility solutions in semi-urban areas. E-Rickshaws are ideal for electrification powered by solar PVs due to its low speeds and a relatively small distance covered in a day. Therefore, we are set out to make solar e-Rickshaw the example of environment consciousness & sustainable product in semi-urban areas of India with use of e-Rickshaw powered by Solar PVs. Although solar e-Rickshaw is costly to afford, Government fiscal & non-fiscal incentives and subsidies and daily earnings from solar e-Rickshaw can payback with a payback period of one to two years. This paper contains brief knowledge of technical, economic & social aspects of solar e-Rickshaw in semi-urban areas.

Literature Review

As time is passing by, society is observing a depletion in conventional sources of energy at a faster rate. To avoid the loss due to depletion, the main focus of study and researchers has now shifted to alternative energy like solar energy. A handsome amount of work has already been done, in this field, till now. Semi-urban and rural areas are going to be the major victims of this, as fossil fuels are depleting and its' prices are constantly increasing. Due to this, the price of electricity supplied to them is considerably higher when compared with alternative source electricity production. So there is an urgent need for a system which can provide them with electricity at cheaper rates. So, the government has decided to provide subsidized solar PV system. A photovoltaic (PV) module is a packaged, connected assembly of typically 6×10 photovoltaic solar cells. Photovoltaic modules constitute the photovoltaic array of a photovoltaic system that generates and supplies solar electricity in commercial and residential applications. Each module is rated by its DC output power under standard test conditions (STC), and typically ranges from 100 to 365 watts. The solar panel works on photo electric effect. They use light energy (photons) from the sun to generate electricity through the photovoltaic effect.

Various automobile companies are working on vehicles that can run on clean energy. One such example is The Solar Electric Vehicle Company running in the United States of America. This plant is producing 14 passenger enclosed shuttle and 23 passengers solar electric vehicle which can replace the traditional bus system in polluted cities such as Beijing and Delhi. Many other companies are also doing the study in this field such as Tesla. Photovoltaic (PV) cells contained in solar panels convert the sun's energy directly into electric energy. This electric energy is then transmitted as power for vehicle propulsion. Not only land vehicles are using solar to travel but nowadays airplanes are also powered using solar energy. Solar Impulse is first such plane which is powered by solar energy.
Various colleges and universities are also studying this field to improve people's lives and reduce people dependency on traditional fuels. In one of the papers, published by Delhi Technological University, mobile solar photovoltaics system is very useful in providing electricity. They have designed a system to meet the agricultural and household needs of a farmer by moving solar photovoltaic system. This kind of system is being designed in various college. An example for this is a solar powered vehicle designed by Industrial Design Center of IIT Mumbai.

Description of e-Rickshaw

E-Rickshaws have been becoming a mode of transport in semi-urban areas for first & last-mile connectivity to bus stands, metro stations, etc. since 2010 as an alternative to petrol/diesel/CNG auto-rickshaws & pulled rickshaws because of their low running cost and less human effort compared to pulled rickshaws. These are 3-wheelers pulled by an electric motor ranging from 650-1400 Watts for a route of less than 5 km.

Manufacturing, Design, Construction & Working Principle

Manufacturing of e-Rickshaws are done on customisation of drivers in an unorganized sector and final cost ranges from Rs. 1,00,000 to 1,50,000. These are mostly manufactured in China & India and only a few other countries. E-Rickshaws are built on M.S. (Mild Steel) Chassis which consists of 3-wheel with a differential at rear wheels. Body design varies from passenger segment to load carriers. These are designed to carry a weight ranging from 400Kg to 500Kg according to their type of operation. The working of e-Rickshaw is based on DC motor, battery & suspension system different from conventional auto-rickshaws. It uses a Brush Less DC motor ranging from 650-1400 Watts with a differential mechanism at rear wheels. The electrical system used in Indian cities is 48V. Some variants made in fiber are also in use due to their strength and durability, resulting in low maintenance. It consists of the controller unit.The battery used is mostly Lead acid/Li-ion battery with a life of 6-12 months. Deep discharge/cycle batteries designed for EVs are mostly used.

Major Parts and Components

Electric Motor: Brush Less Direct Current (BLDC) type 650-1400W & 48V (Input) motor is used. It is controlled via an electronic controller.

Electronic Motor Controller: The controller includes a manual or automatic switch turning the motor on/off, selecting forward or reverse motion, selecting and regulating speed, regulating or limiting torque and protecting against overloads. It is connected to battery pack and controller feeds the input to the motor, lamp, AC/DC converter and Speedometer/ Indicator.

Battery: Set of four 12V deep cycle lead acid/Li-ion batteries are used since the required voltage is 48V. These batteries are connected in series to the controller unit.

Differential: Chinese manufactured differential is used in e-Rickshaws which is connected to the electric motor and rear wheels.

Front Shock Absorbers: Helical Spring with dampener with hydraulic telescopic shock absorbers are used.

Rear Suspension: Leaf spring carriage spring with rear shocker

Brakes: Drum brakes, actuated internally, expanding shoe type are used. Brakes are mounted on the chassis (Pedal-brakes), so on pressing the pedal, the brakes will engage stopping the rear wheels.

Speedometer/Indicator: Speedometer generally used have analog dials. The one the left side indicates vehicle speed and one on the right side indicate battery charge level. It is connected to the controller unit.

Steering: Handle bar type steering is used.

Miscellaneous Spare parts: Centre locking, Alloy wheel, Rear light, Front glass, Front Indicator, Head light, Ignition switch, Charger, Converter, left-right switch, Tyre, Wirings, Throttle set etc.

Block Diagram

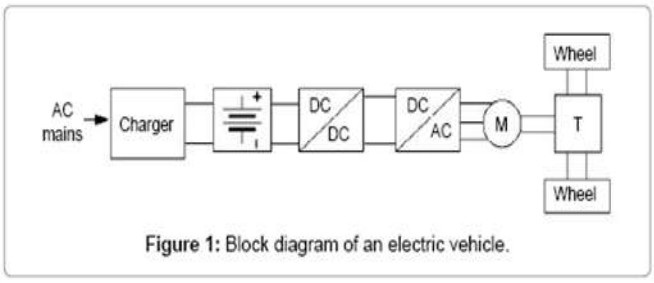

Figure 1: Block diagram of an electric vehicle.

Technical Specifications

S.No.	PARAMETER	SPECIFICATION
1.	Dimensions (l*b*h)	2870mm*1000mm*1760mm
2.	Seating Capacity	4+1+(40 Kg Luggage)
3.	Tyre Size	90*90*12, 3.75*12
4.	Battery Type	Exide/JPM/TRONTEK/Altimo
5.	Electricity Consumption/Charge	5-6 units
6.	Charging Time	8-10 hours
7.	Range per charge	*90 Km & above
8.	Battery dimensions (l*b*h)	400mm*180mm*205mm
9.	Differential length	970mm
10.	Motor Max Power	1140W & 48V
11.	Motor Type	BLDC
12.	Max. Speed	25 Km/hr
13.	Controller	24 Tubes 50A
14.	Charger	10-15 A
15.	Front Powerful Shocker	Helical Spring with dampener with hydraulic telescopic, shock absorber
16.	Rear Suspension	Leaf Spring Carriage Spring with Rear Shocker
17.	Brakes	Drum brakes actuated + Expanding Shoe Type, Combined
18.	Brake Shoe Thickness	50mm
19.	Drum Width	145mm
20.	Steering	Handle Bar Type
21.	System Voltage	12 V
22.	Performance	Excellent
23.	Rim	Alloy wheel/steel rim
24.	Rear Track	960mm
25.	Ground Clearance	135mm

Since the manufacturing of e-Rickshaw is done in an unorganized sector so there is no standardization of its parts. However, technical specifications of e-Rickshaw listed below are from Speego Vehicles Company Pvt. Ltd. (An ISO 9001:2015 Certified Company) in Delhi:

Courtesy: Speego Vehicles Company Pvt. Ltd. (An ISO 9001:2015 Certified Company)

Energy Requirement and Efficiency

Charging time for e-Rickshaw to its full is about 8-10 hours and Electricity consumption per charge is about 5-6 units or KWh. With the full charge, it covers a range of 90 Km and more i.e. Rs. 2-3 per Km and fare is Rs. 10 per passenger for 2Km in cities like Delhi. Detailed Earnings & Savings of e-Rickshaw drivers are described later in this paper. On comparing e-Rickshaw with other fuelled vehicle in semi-urban areas, it is found that e-Rickshaw stands at position one in mileage and cost. Hence, e-Rickshaw is currently the most efficient transport. We can imagine if electricity in e-Rickshaw is powered by Solar PVs which our paper presents then it will be a grace to society especially semi-urban areas.

Comparison of e-Rickshaw with other fueled vehicle

S.no.	Fuel type	Mileage (avg.)	Cost (avg.)	Rank
1.	CNG	21Km/Kg	Rs. 38/Kg	3
2.	LPG	21Km/Kg	Rs. 40/Kg	4
3.	Diesel	17Kmpl	Rs. 55/litre	5
4.	Petrol	15Kmpl	Rs. 65/litre	6
5.	Electricity(e-Rickshaw)	18Km/KWh	Rs. 10/KWh	2
6.	Solar e-Rickshaw	18Km/KWh	Rs. 1.30/KWh	1

Present Scenario of e-Rickshaw in semi-urban areas

In million plus population cities like Amritsar, Kanpur, and Delhi, e-rickshaw plays a major role as feeder services to public transport in metro cities, public transport in small & medium towns and mode of transport for tourists. All age group people travel by e-Rickshaw mostly for their work trip. Urban Mobility India Conference & Expo 2015 says 90% e-rickshaws on average carry more than 50 passengers per day. In areas like Kanpur, most of the e-rickshaws carry more than 80 passengers per day due to overloading and used as a public transport. In cities like Amritsar, 90% are occasional users (tourists) and in Kanpur & Delhi, there is 70:30 daily and occasional users respectively. In Delhi, 70% of e-Rickshaws are owned while other 30% are rented on average Rs. 300 per day.

Present e-Rickshaw Services

Laws: The Motor Vehicles (Amendment) Act, 2015

Regulatory bodies: RTO (Registration), Municipality (Infrastructure) & Traffic Police (Enforcement)

Route: Fixed by drivers (In Delhi, 236 roads are banned by authority). Travel distance less than 5 Km.

Fare Structure: Flat fare for fixed routes (Rs. 5, 10, 20). About Rs. 50 for personalized services.

Infrastructure Facilities: No charging points. No Stands for Halts & Go. No parking areas.

Permit Issue: Only Delhi Govt. has a permit fee of Rs. 1,510 valid for five years and recognized 33 models & 20 dealers for

sale. No other cities have defined the structure yet. Cities like Amritsar charges similar permit fees as that of auto rickshaw.

Earnings & Savings per Month from e-Rickshaw

Average revenue earned by owned e-Rickshaws drivers is Rs. 15,000 per month whereas average revenue earned by rented drivers is Rs. 9,000 per month. High Operation & Maintenance (O&M) cost of Rs. 3,000 per month for owners as compared to rented vehicles. An average of additional Rs. 300 per month is spent by all drivers including expenses for charging, bribes to traffic police & parking in few areas. The income earned by the e-Rickshaw drivers in all cases is more than the minimum wage level, 2015 (Rs. 4,800 per month) specified by Govt. of India.

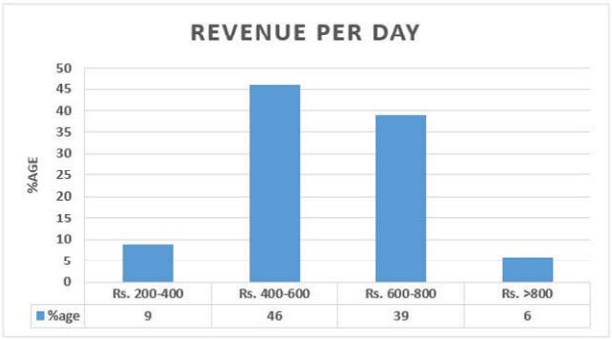

Reasons for using e-Rickshaw

User's Perspective: Users mostly prefer e-Rickshaw due to easy availability & accessibility and experience high level of comfort. Low fare, time savings, and travel in a small group are some other factors.

Other than this, first & last mile connectivity to bus stands, metro stations, etc. facilitates users to use e-Rickshaw. Most of the users felt e-Rickshaws provide good service and must be operational in urban & semi-urban areas. More than 30% of users wanted e-Rickshaw to be more safe and free from overloading.

Driver's Perspective: More than 50% of drivers are illiterate and e-Rickshaw is a good source of employment for them. It reduced pulling effort which was required in hand or cycle-rickshaw and hence effortless to drive. Fuel cost i.e. charging cost is very less as compared to other transport and running on small routes Frequent availability of passengers.

Engineer's Perspective: It is sustainable, eco-friendly and economical transport in semi-urban areas. Based on the comparison of the different fuelled vehicle, e-Rickshaw ranks position 1 in mileage and cost.

Government's Perspective: India's new green car policy, Govt. may consider doling out both fiscal & non-fiscal incentives and subsidies to push sales of EVs while discouraging the use of petrol and diesel-run vehicles. This action will increase modal share of e-Rickshaw in public transport.

Industry's Perspective: India is set to become the 3rd largest automotive market by 2020 and currently has one of the lowest vehicle penetration in the world making it a viable market for Electric Vehicle Manufacturers (EVMs). EV industry is at a nascent stage in India, comprising less than 1% of total vehicle sales, however, it has the potential to grow significantly in the coming years. EV sales are expected to grow at high double digit growth rates annually till 2020 due to Govt. green car policies and relaxation/subsidies on EVs.

Drawbacks of Present Scenario

- Absence of Policy/Regulatory framework for e-Rickshaw for permit issue, route rationalization, fare fixation
- No Infrastructure facility: Stands facilities, Halt & Go Stands, parking areas for the night, Availability of charging points 250m from junctions.
- Lack of specified schedules, performance/standards and Fixing & Revising fares.

Earnings per month

Description	Earning per day (rs.)	Rent per day (rs.)	Total earning per month (rs.)
Income in case of owned e-rickshaws on less-profitable routes	200-400	-	6,000-12,000
Income in case of owned e-rickshaws on average profitable routes	400-600	-	12,000-18,000
Income in case of owned e-rickshaws on profitable routes like bus stands, metro station, railway stations, market areas	600-800	-	18,000-24,000
Income in case of rented e-rickshaws on average profitable routes	400-600	300	3,000-9,000
Income in case of rented e-rickshaws on profitable routes like bus stands, metro station, railway stations, market areas	600-800	300	9,000-15,000

Savings per month

Description	Avg. Earnings per month (rs.)	Avg. O&m cost per month (rs.)	Avg. Other expenses per month (rs.)	Total savings per month (rs.)
Income in case of owned e-rickshaws on less-profitable routes	9,000	3,000	300	5,700
Income in case of owned e-rickshaws on average profitable routes	15,000	3,000	300	11,700
Income in case of owned e-rickshaws on profitable routes like bus stands, metro station, railway stations, market areas	21,000	3,000	300	17,700
Income in case of rented e-rickshaws on average profitable routes	6,000	500	300	5,200
Income in case of rented e-rickshaws on profitable routes like bus stands, metro station, railway stations, market areas	12,000	500	300	11,200

- Lack of Institution governing e-rickshaws.
- Lack of financing: Cities like Kanpur, Amritsar lacks loan facilities for e-Rickshaws.

MATERIALS AND METHODS

In designing of this solar e-rickshaw, basically, the work has been done on providing the power supply for charging to the e-rickshaw by attachment of solar panels over its roof.

The basic things that were kept under observations were choosing panels and equipment in such a way that they won't increase the size of the roof, it should be economical and should be light in weight. It is basically light weight because it is a passenger vehicle and the maximum load is attained from it only, so other parts should be light in weight. The basic design of E-rickshaw will be same but alterations have been done in setting and adjusting the solar panels over the roof and adjusting its wiring and circuits accordingly.

After proper research and analysis, the result suggested that the design should be carried forward with three solar panels adjusted over the roof of the solar rickshaw. They are placed in such a manner that all the axis of panels (passing horizontally) will be kept at x-axis and the roof axis (passing horizontally) will be kept at the y-axis. This is done in this manner so that three panels can be adjusted properly to it. They all will be placed adjacent to each other. Panels are mounted on the roof properly and an option for rotating them manually at and a particular angle is also provided. It is rotated manually to avoid the issues like the weight of the motor and the power supply need for the motor to work. Their mounting is explained properly in the fabrication part. All the other components like solar charge converter, fuses and battery will be kept inside the compartment, which is placed below the passenger seat. The decision for choosing 250 watts three panels instead of 300 watts, is that the weight of the 250-watt panels is coming less and this is solving the excessive weight problem. The price of 300-watt panels is more and by neglecting it, we can economize our product. The problem for the accommodation of these panels is also solved by using 250-watt panels, as their length size is less than the 300 watts one. So, all the conditions asked are fulfilled by choosing this one. The power produced by these panels will completely charge the battery in 8hrs. So once a fully charged battery is used in starting the first run then there will be no need of charging the battery again by external output.
The advantage of using this system in semi-urban areas will be that it will easily charge the system while vehicle will be standing ideal. For this, a switch will be provided at the steering of the vehicle, when it is ideal mode the battery will be getting charged and when in working mode, batteries will be discharging. So by this method at the end of the day, the battery of this rickshaw will be completely charged and next day they can easily make their conveyance properly.

Fabrication

During the fabrication of this system, the points to be considered are: the attachment of solar panels is done in such a manner that they don't fall or break during mobility of vehicle, second thing to be considered is that the panels can be rotated manually by the driver according to the sun rays while vehicle is standing ideal, all the other components should be placed so that they do not create any irritation to the passengers and the drivers. The comfortability of both the rider and the passengers is kept at high priority. Firstly, the attachment of solar panel is done on the roof. Prime roofing is done with Aqua proof profile sheet. Then two metal bars (act as chassis of the roof) are welded on the roof corners, where the panels are actually mounted upon. On these rods, the panel's attachments are screwed and then on these attachments panels are fixed using bolts. The attachments are mounted in such a manner that the panel after placement face towards the south, as it is the best position.

After this, the wires from the panels, are drawn to setup, under the passenger seat, inside an insulated casing. These wires connect panels to MPPT charge controller. This controller then connected with a relay in between pass to battery charge controller. This battery charge controller is then connected to the battery. There is a relay placed between battery and motor drive (basically dc to ac inverter). Then this drive is connected to BLDC motor. Both these relays are controlled by an MCB switch, which is placed at steering of driver, when this MCB switch is on then charging of battery will take place (at that time the relay connected between battery and drive will cut off the connection) and when this MCB switched off then discharging of battery will take place (at that time the relay connected between MPPT charge controller and Battery charge controller will cut off the connection) i.e. power will be drawn by motors.

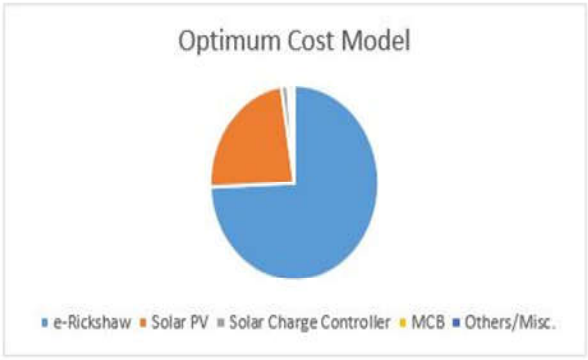

All the other circuit will remain the same as basic e-rickshaw design. And no further attachments need to be done because keeping the design simple will improve its efficiency and don't affect its load carrying capability.

Cost estimation of Solar e-Rickshaw

The cost of Solar e-Rickshaw is estimated using different tools & techniques such as Expert judgement, Analogous estimating, Three-point estimates (Best case, optimum case, worst case), spreadsheets and statistical tools.

Expert Judgement: Project mentor Dr. J P Kesari and expert from Zun Roof Solar, Vikram Solar have been consulted while preparing the cost estimation.

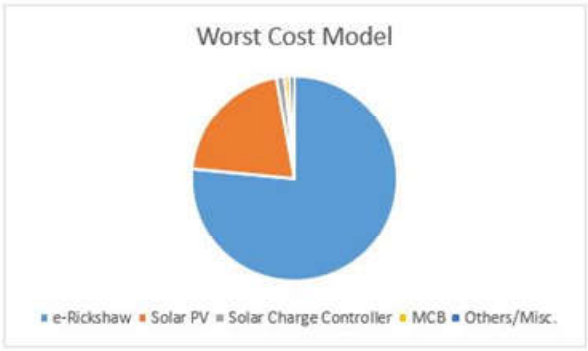

Analogous Estimating: Analogy has been used in the cost estimation from previous project and data.

Three-point Estimates: For 3-point estimates (Best, Optimum, and Worst), separate estimates are made for cost and brand. The proposed model requires an e-rickshaw, 3 units 250W Solar PV, Solar charge controller (MPPT type), MCBs and wires.

Table for cost estimation

S.No.	Equipment/ Component	Quantity	Cost (in INR)			Brand (with Specifications)		
			Best	Optimum	Worst	Best	Optimum	Worst
1.	e-Rickshaw	1	1,60,000	1,20,000	1,00,000	Mayuri	Sarthi	Baba
2.	Solar Panels	3*250W	48,000	37,500	27,000	Vikram Solar	Su-kam	Solar Power
3.	Solar charge Controller	1 (MPPT type)	2200	2000	1700	Su-kam	-	-
4.	MCBs	-	-	-	-	-	-	-
5.	Wires	-	-	-	-	-	-	-
Total			2,10,200+	1,59,500+	1,28,700+	-	-	-

Pie Chart Comparison

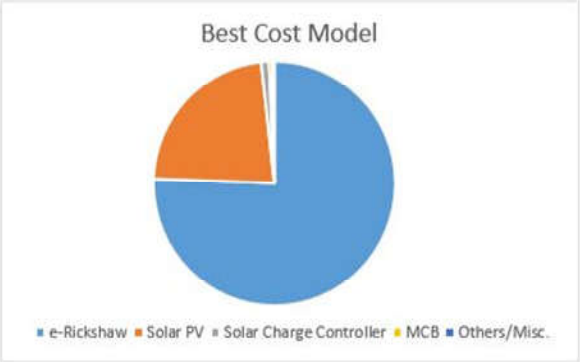

Cost Comparison-Retailer, Wholesaler & Manufacturer

For the comparison of the cost of components required for Solar e-Rickshaw, various retailers, wholesalers & manufacturers were contacted. Based on the discussion, a bar graph has been plotted between cost from retailer, wholesaler & manufacturer for different components.

Solar PV 250W: Based on discussion with 10 Retailers, 5 wholesalers & 5 manufacturers, the comparison shows Retailer price Rs. 12,500 | Wholesaler price Rs. 12,000 | Manufacturer Rs. 11,500.

Solar Charge Controller: 5 of each retailer, wholesaler & manufacturer were contacted. Taking multiplier 0.1 on bar-graph, the cost comes out to be Retailer price Rs. 2000 Wholesaler price Rs. 1900 | Manufacturer Rs. 1850.

e-Rickshaw: 5 of each retailer, wholesaler & manufacturer were contacted. Taking base price Rs. 1, 00,000, cost comes out to be Retailer price Rs. 1, 25,000 | Wholesaler price Rs. 1, 20,000 | Manufacturer Rs. 1, 20,000.

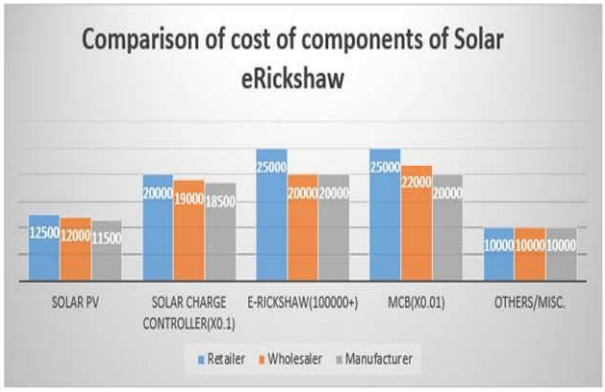

MCBs- To be found

Others- If required

Payback Period

Consideration

With Solar Panels (All in Rupees)

Cost of E Rickshaw = 1, 00,000/-
Cost of Solar Panels = 27,000/-
MPPT = 1,700/-
Others = 1,500/-
Attachments = 1,500/-
Total Cost = 1, 31,700/-

Without Panels (All in Rupees)
Cost of E Rickshaw = 1, 00,000/-
Others = 1,500/-

Calculations

Cost of Electricity for Charging (per day) = Rs.10 * 5 unit = Rs.50

Cost of Electricity for Charging (per year) = Rs. 50* 365 = Rs.18, 250

Payback period = 28,700/18,250 = 1.6 Years

Cost of Production of Electricity

Cost of Solar PV = Rs.27, 000/-
Cost of Mounting attachments = Rs.1, 500/-
MPPT = Rs.1, 700/-
Miscellaneous and others = Rs.1, 500/-
Total Cost of the proposed system = Rs.31, 700/-
Daily usage of e-Rickshaw (in kWh) = 5
Monthly usage of e-Rickshaw (in kWh) = 5*30 = 150
Yearly usage of e-Rickshaw (in kWh) = 5*365 = 1825
Average Sun hours for Delhi = 7 hours

A system of 0.75 kW Solar PVs will produce 80% of rated power i.e. 0.80*0.75=0.6 DC kWh

So, this system will cover around 68% to 70% of monthly usage of e-Rickshaw i.e. system will produce 0.7*5= **3.5 kWh**

Financial benefits

While considering life of Solar PV as 20 years

Years	Per Year (In kWh)	Total (In kWh)	Rated Capacity
1-5	3.5*365=1277.5	1277.5*=6387.5	100%
6-10	0.92*3.5*365=1175.3	1175.3=7555.5	92%
11-15	0.85*3.5*365=1085.875	1085.875=5429.375	85%
15-20	0.75*3.5*365=958.125	958.125=4790.625	75%

Total kWh (For 20 years) = 24, 163 Units
Total cost of production per unit = 31,700/24,163 = Rs.1.31
= Rs. 1.30

With all above considerations, the cost of electricity generated for e-Rickshaw while considering a time span for 20 years will be Rupees 1.30 per unit or kWh.

Environmental benefits

This system will able to eliminate 11290 Ibs or 5121.05 Kgs of CO_2 per year and is equivalent to planting 16 trees every year.

Conclusion

By the research and study done by us on making e-Rickshaw powered by solar energy revealed that Solar e-Rickshaw is a feasible mode of transport for first and last mile connectivity in semi-urban areas. As e-Rickshaws are already in use for covering short distances, so we decided to make it more efficient and eco-friendly. This is more environmentally friendly and is much better alternative fuel vehicle. Our economic feasibility states that the optimum cost of a single unit of Solar e-Rickshaw found is Rs. 1, 31,700 and Calculation reveals that the payback period of this system is around 1.3 years & the cost of production of a single unit of electricity for a span of 20 years comes out to be Rs. 1.3(One Rupee & Thirty Paise). Also, the average revenue earned by owned drivers is Rs. 15,000 and average revenue earned by rented drivers is Rs. 9,000. The overall study reveals that in all cases income earned by drivers is more than minimum wage level, 2015 (Rs. 4,800) specified by Govt. of India. Solar e-Rickshaw is found to be technically feasible than many vehicles on the road as it is noise free, cheaper and most efficient of all another type. These rickshaws are a replacement for other fuelled vehicle. A parking shed with a roof made up of Solar PVs and charging units (Plug-in Electric vehicle) will be grace for the owners of Solar e-Rickshaw and enhance technical feasibility. Solar e-Rickshaw is also socially feasible as it ensures the employment of drivers and low cost & noise-free rides also motivate users to use these rickshaws for their short distances.

Way forward and future works

Since our study was based on sustainable transport system for masses in tropical countries with growing economies like India due to a surge in the no. of vehicles across major cities. These cities seldom have an efficient mass transit system, forcing people to operate private vehicles. This problem is compounded by the social stigma, where people view operating a private vehicle as a sign of prosperity, while public transport is viewed as being used by the lower echelons of the society.

In coming future, we look forward to

- Design Solar Halt & Go Stand for these rickshaws like Bus stand which will use Off grid & On grid Solar Charging Station.
- Feasibility study of Mass Transit system equipped with Solar energy which will state how more efficient and clean system can be.
- Design Solar Charging Station like conventional fuel stations

Moreover, we expect from government to

- Promote fiscal & non-fiscal incentives and subsidies to push sales of renewable energy powered vehicle and discourage conventional fuelled vehicle.
- Roll out public transport based on renewable energy.
- Awareness of sustainable program among citizens to encourage people to use public transport and provide first & last mile connectivity.

In next one to two decades, we can imagine whole India run on renewable energy and we look forward that India will be a role model country for countries with growing economies in Renewable Energy based Transport.

REFERENCES

8th Global Summit Vibrant Gujarat 2017. Manufacturing of Electric vehicles: Two wheelers/Three wheelers/ Passengers Cars. Government of Gujarat

8th Urban Mobility India Conference & Expo 2015. Improving and upgrading electric rickshaws in Indian cities. Institute of Urban Transport India

ADB Open Innovation Forum, Manila 2015. Electric Vehicles in India: Policies, Opportunities, and Current Scenario. National Institute of Urban Affairs

Available Online: http://www.internationaltransportforum.org/Updates/index.html

Dr. J.P. Kesari and Rajat Sharma 2015. Design and Development of Solar Electric Vehicles at Delhi Technological University. IJISET - International Journal of Innovative Science, Engineering & Technology, Vol. 2 Issue 3, March 2015. http://ijiset.com/articlesv2/articlesv2s3.html ISSN 2348 – 7968

KPMG India 2010. Indian Automotive Industry

KPMG International 2013. Tax and incentives for Renewable energy

NASA. Surface Meteorology and Solar energy. Available Online: https://eosweb.larc.nasa.gov/sse/

Sehgal Lakshey, Prasath Arun R.and Rehalia Arvind, 2015. Proposal of Integral Mounted Solar Charging and External Solar Charging Station for an Electric Rickshaw in Delhi. American Journal of Renewable and Sustainable Energy Vol. 1, No. 3, pp.86-89

Singh Manoj et al (NITI Aayog), Marshall Abramczyk et al (RMI) 2017. India Leaps Ahead: Transformative Mobility Solutions for all. NITI Aayog, India-Rocky Mountain Institute, America. Available Online: http://niti.gov.in/writereaddata/files/document_publication/RMI_India_Report_web.pdf https://www.rmi.org/insights/reports/transformative_mobility_solutions_india

Tang, J. et al 2014. Economic analysis of photovoltaic electricity supply for an electric vehicle fleet in Shenzhen, China. International Journal of Sustainable Transportation 8, 202-204

Tarun Saxena, J P Kesari and Sudhir Y Kumar 2017. Solar Energy is the Path For India's Rural Prosperity: A Mobile Solar PV Application, Proceedings of International

Conference on Renewable Energy and Smart Grids Technology, ISBN 978-93-86432-07-0, Feb 24-25, 2017, Mody University, Laxmangarh, Rajasthan.

Technical Specification e-Rickshaw. Speego Vehicles Company Pvt. Ltd. (An ISO 9001:2015 Certified Company)

World Bank Study on Sustainable Transportation. Available Online: http://www.web.worldbank.com

Ye Bin, et al 2015. Feasibility study of a Solar-powered Electric Vehicle Charging Station Model. MDPI Energies 8, 13265-13283

****

View publication stats

Available online at www.ijapie.org

INTERNATIONAL JOURNAL OF ADVANCED PRODUCTION AND INDUSTRIAL ENGINEERING

IJAPIE-2018-01-124, Vol 3 (1), 14-16

IJAPIE
Connecting Science & Technology with Management.
A Journal for all Products & Processes.

Design of Horse Shoe Patch antenna for wireless Applications

N. Jayanti
(*Department of Electronics and Communication Engineering, Delhi Technological University, Delhi, India)*
njayanthi@dce.ac.in

Abstract : This paper illustrates design and analysis of a horse shoe patch antenna and compares the results of antenna for Duroid (ε_r = 2.2), Rogers RO4350 (ε_r = 3.66) and FR-4 (ε_r = 4.3) as substrate material and other comparison is between proposed antenna with and without an upper layer of substrate (duroid). Substrate thickness taken for this antenna is 1.57mm and for substrate layer above patch, thickness is 0.2mm. Comparison of these different structures has been done on the basis of return loss, VSWR, efficiency and far-field. In these structures a horse shoe shaped patch is placed above substrate. The proposed antenna has been designed and simulated using CST microwave studio 2014. The proposed antenna design can be used for WLAN, WiMAX and IMT applications.

Keywords: Horse shoe patch, antenna, wireless, CST microwave studio.

I. INTRODUCTION

Many applications such as communication to spacecrafts, aircrafts require a small antenna having reasonable gain that is easy to mount on them. Microstrip patch antenna being a low-profile radiator is ideal option for that purpose. It can easily provide 5-6dB gain. Using array of patch antenna, we can increase the gain as required. Other advantages of patch antenna include easier fabrication, low cost and conformability. But it also has disadvantages such as narrow bandwidth, spurious feed radiation, surface waves, large size for higher frequency applications. Bandwidth can be increased using impedance matching, stacking and EBG structures. For its practical application there are many trade-offs

II. DESIGN PROCEDURE

In the proposed design a Horse-shoe shaped patch is printed above FR-4 substrate. The thickness for ground plane and patch is 0.02mm. structure of ground plane is shown in figure.

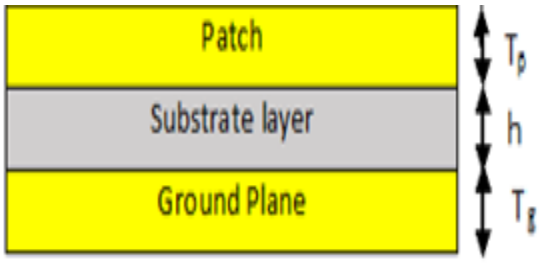

(a)

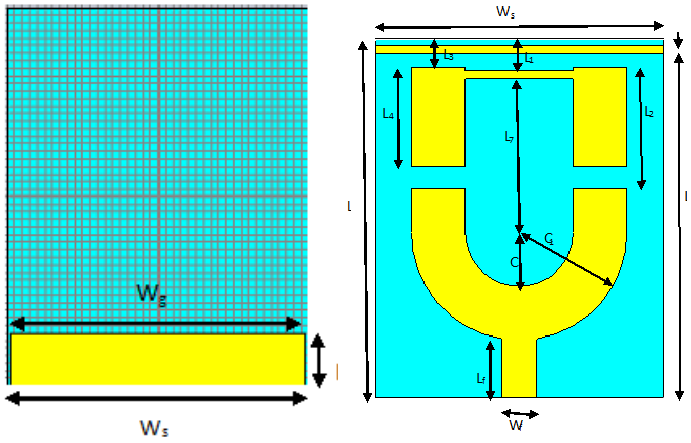

(b) (c)

Fig.1.The Horse Shoe Antenna (a) Cross sectional view, (b) Top view, and (c) Bottom view.

III. HORSE SHOE PATCH ANTENNA WITH FR-4, ROGERS RO4350 AND DUROID AS SUBSTRATE

For this comparison the substrate between patch and ground is changed among FR-4, Rogers RO4350 and Duroid. The performance is compared in terms of return loss, efficiency, VSWR and far field. The results are simulated using CST microwave studio 2014.

For FR-4 the parameters taken for the design are (in mm) –

C = 7.5	L_1 = 4.5
C_1 = 15	L_2 = 16.8
L = 50	L_3 = 4

$W_s = 40$ $L_4 = 13.8$
$L_g = 7$ $L_5 = 48$
$W_g = 39$ $L_6 = 1$
$L_f = 8$ $L_7 = 21.8$
$W_f = 3.035$ $h = 1.57$
$T_p = T_g = 0.02$ $T_s = 0.2$

For different substrates W_f is taken such that microstrip line impedance is 50Ω.

(a) **Return loss**

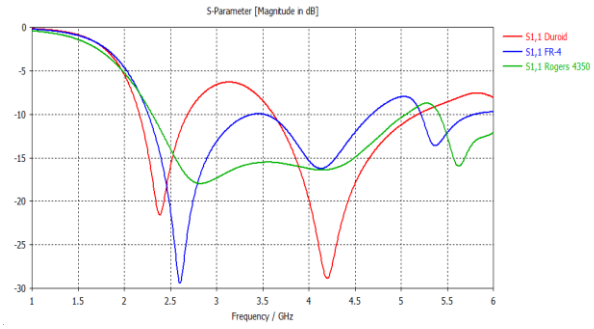

Fig.2. Return loss comparison for Duroid, FR-4 and Rogers 4350 as substrate

(b) **Efficiency**

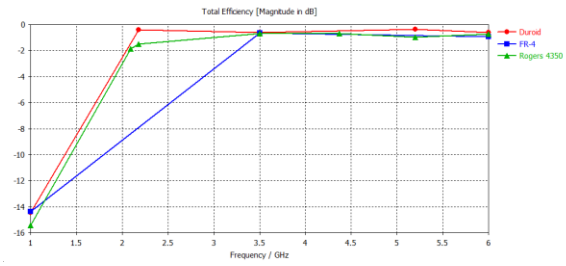

Fig.3. Efficiency comparison for Duroid, FR-4 and Rogers 4350 as substrate

(c) **VSWR**

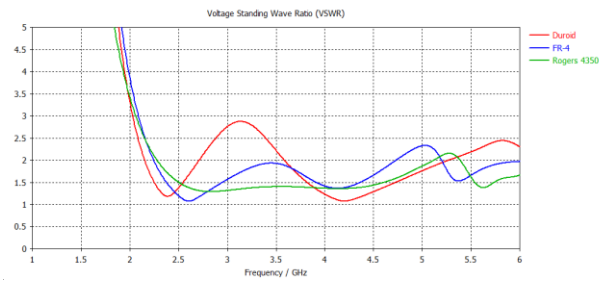

Fig.4. VSWR comparison for Duroid, FR-4 and Rogers 4350 as substrate

(d) **Far-Field**

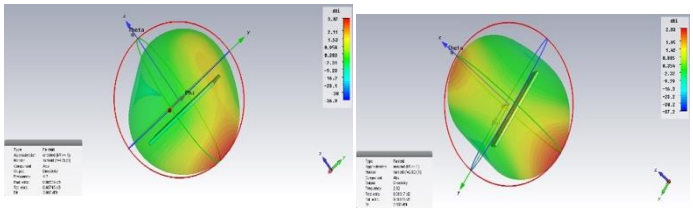

(a) (b)

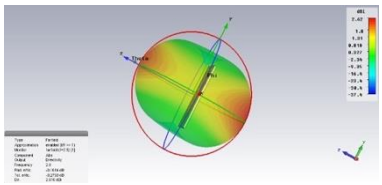

(c)

Fig.5. Far field (a) for Duroid substrate at 4.15GHz, (b) for Rogers 4350 substrate at 2.82GHz, (c) for FR-4 substrate at 2.6GHz

IV. HORSE SHOE PATCH ANTENNA WITH AND WITHOUT DUROID AS SUBSTRATE LAYER ABOVE PATCH

For this comparison as the substrate between patch and ground once FR-4 is used. For first case a layer of Duroid of thickness 0.2mm is placed above patch and in the second case this layer is removed and there is only air above patch. The performance of both structures is compared in terms of return loss, efficiency, VSWR and far field. The results are simulated using CST microwave studio 2014.

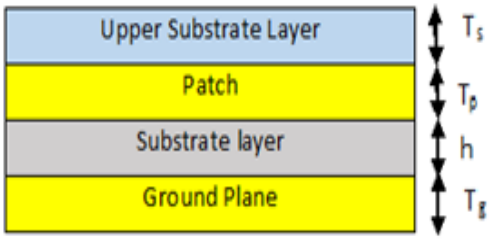

Fig.6. Cross sectional view of patch antenna with upper substrate

a) **Return Loss**

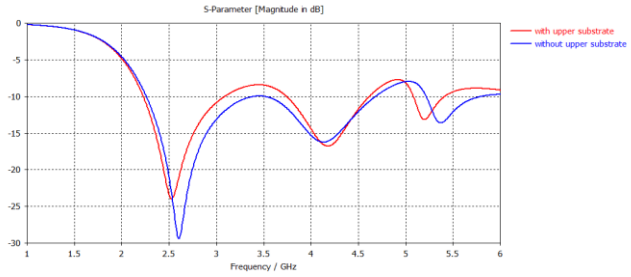

Fig.7. Return loss comparison for patch antenna with and without upper substrate

b) **Efficiency**

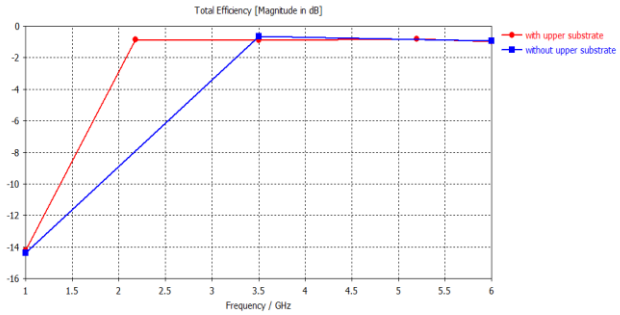

Fig.8. Efficiency comparison for patch antenna with and without upper substrate

c) **VSWR**

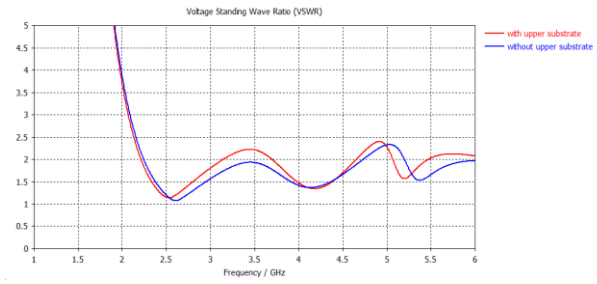

Fig.9. VSWR comparison for patch antenna with and without upper substrate

d) **Far-field**

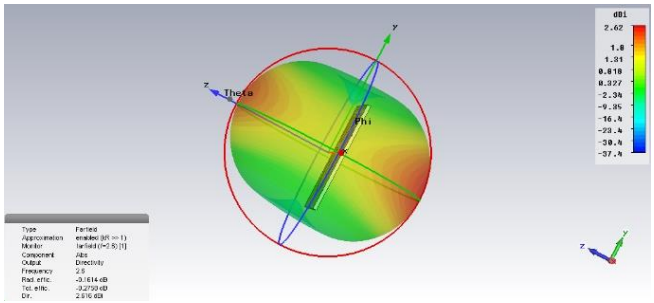

(a)

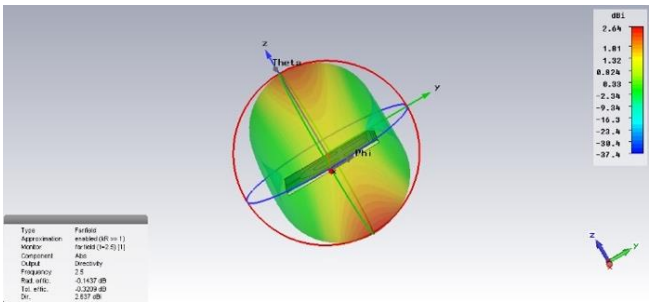

(b)

Fig.10. Far field for patch antenna (a) without upper substrate at 2.6GHz, (b) with upper substrate at 2.5GHz

V. CONCLUSION

Horse shoe patch antenna with different substrates and with an upper substrate layer is compared successfully**.** The proposed antenna designs can be used for WLAN, WiMAX and IMT applications

REFERENCES

[1] D. M. Pozar and D. H. Schaubert, Microstrip Antennas: The Analysis and Design of Microstrip Antennas and Arrays, IEEE Press, 1995.

[2] C. A. Balanis, “Antenna Theory, Analysis and Design,” John Wiley & Sons, New York, 1997.

[3] H. Pues and A Van de Capelle, “Accurate transmission-line model for the rectangular microstrip antenna,” Proc. IEE, vol. 131, pt. H, no. 6, pp. 334-340, Dec. 1984.

[4] W. F. Richards, Y. T. Lo, and D. D. Harrison, “An improved theory of microstrip antennas with applications,” IEEE Trans. Antennas and Propagation, vol. AP-29, pp, 38-46, Jan. 1981.

[5] W. F. Richards, Y. T. Lo, and D. D. Harrison, “An improved theory of microstrip antennas with applications,” IEEE Trans. Antennas and Propagation, vol. AP-29, pp, 38-46, Jan. 1981.

[6] W. F. Richards, Y. T. Lo, and D. D. Harrison, “An improved theory of microstrip antennas with applications,” IEEE Trans. Antennas and Propagation, vol. AP-29, pp, 38-46, Jan. 1981.

ISSN: 2350-0328
International Journal of AdvancedResearch in Science, Engineering and Technology
Vol. 5, Issue 6 , June 2018

Design of Solar Photovoltaic Based Water Pumping for Automatic Irrigation System

Mohit Kumar, Namita Vats, Anshul Chaudhary, Abhishek Kumar Dev , Dr. J.P.Kesari

Delhi Technological University,Bawana Road, Delhi-110042

ABSTRACT -This article investigates the feasibility of solar powered irrigation process in India where photovoltaic technology could be used to gather solar energy for running a submersible pump and supply water for crop cultivation Photovoltaic solar energy has been gaining market share over the years due to lower prices and to a significant incentive from the government. It is a clean, static and promising energy
source, and such technology has been applied to various applications. This paper presents a prototype of an automated irrigation system for later installation on the field. After the prototype development, we analysed the use of a previously built photovoltaic microgeneration, in order to insert the electricity generated in the automated irrigation system. The photovoltaic microgeneration has an installed capacity of 2.76 kWp and a battery bank with 24 V. The integration of photovoltaic solar energy in the automated irrigation system represented a good application for family farming, minimizing water waste, besides representing the use of a renewable energy source.

KEYWORDS: Automated irrigation, Solar photovoltaic, Micro generation, Renewableenergy

I.INTRODUCTION

A. Energy scenario in India as on March 31,2018[1]

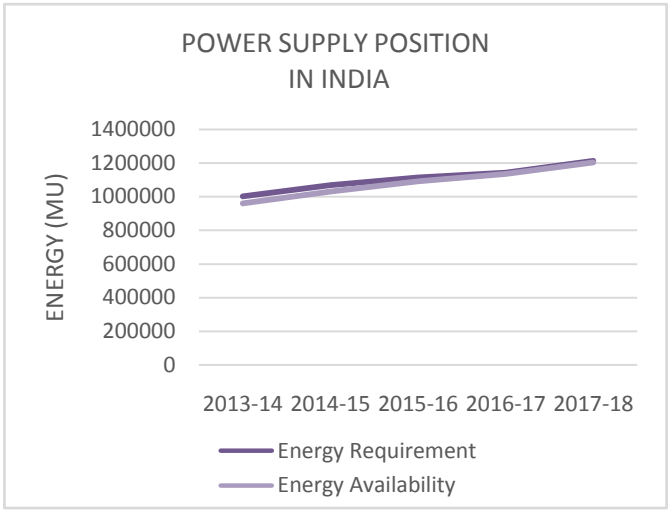

Power supply position in India

Electrical phenomenon generation is an economical approach for exploitation solar power. The energy issue is a global concern, given the recurrent crises in the electricity sector. Over the past decade, the energy sectors of many countries endured intense changes with stimulus to the decentralization of power generation, giving the distribution network a central role in this new model. Energy generation plays a key role in human life, along with means of transportation, telecommunications, water and sanitation. However, both the generation and use of energy should be handled in a harmonious way and appropriate to the environment, so that natural resources can be used rationally and sustainably. Agricultural field always needs and depends on the water level of the soil. But continuous extraction of water from soil

ISSN: 2350-0328

International Journal of Advanced Research in Science, Engineering and Technology

Vol. 5, Issue 6 , June 2018

reduces the moisture level of soil to avoid this problem planned irrigation system should be followed. For this purpose, an irrigation system is introduced in this paper. The proposed system derives power from sunlight through photo-voltaic cells. Hence, the system cannot depend on the electricity. In this proposed model by using sunlight energy, power the irrigation pump, the irrigation of field in cultivation of crops can be achieved in a more simpler and environment friendly manner. The system proposed for irrigation takes into account the solar energy, direct form of energy from the sun, and PV cells to convert energy from one form to another to finally supply water to the fields.

Photovoltaic cell is a system converts light energy into electricity. Photovoltaic cell is otherwise known as "solar cells". The PV cells which takes sunlight and convert it into electricity this is kept as a small grid. Solar electric panels more commonly referred to as photovoltaic, or PV, panels, it converts sunlight into electricity. The electricity is used to run appliances and electrical devices or stored in batteries to be used later. There are many plants which required minimum level of moisture. If the required level of water is not provided, then the plant will die and results in low production. By irrigate the crop according to the moisture level they need, is provided by the soil moisture sensor.

Even though photovoltaic systems applied in distributed generation are less used than other generation technologies, they are gaining ground globally due to incentive programs and regulations, obtaining strong growth in the market. This type of energy generation from the sun presents itself as one of the most rational forms of electricity generation. Once static and silent, it is a promising technologyfor electricity generation.

Residents of rural areas sometimes have no access to electricity because of distance from the distribution power grid. In this case, they can choose to install photovoltaic panels with an integrated battery system which, during the night, can also make use of electricity. In turn, residents who already have access to electricity in their homes could install photovoltaic panels in order to save money spent on electricity. Those who do not have a place available for installation of photovoltaic panels can install them on the roof of their homes.

B.**Solar Photovoltaic applications in water pumping**

The majority of India's poor (some 770 million people or about 70 percent) are found in rural areas. And third, India's food security depends on producing cereal crops, as well as increasing its production of fruits, vegetables and milk to meet the demands of a growing population with rising incomes. To do so, a productive, competitive, diversified and sustainable agricultural sector will need to emerge at an accelerated pace. agriculture sector challenges will be important to India's overall development and the improved welfare of its rural poor. Raising productivity per unit of land will need to be the main engine of agricultural growth as virtually all cultivable land is farmed. Water resources are also limited and water for irrigation must contend with increasing industrial and urban needs. Promoting new technologies and reforming agricultural research and extension: Major reform and strengthening of India's agricultural research and extension systems is one of the most important needs for agricultural growth. Incentives to pump less water such as levying electricity charges or community monitoring of use have not yet succeeded beyond sporadic initiatives. Other key priorities include: (i) modernizing Irrigation and Drainage Departments to integrate the participation of farmers and other agencies in managing irrigation water; (ii) improving cost recovery; (iii) rationalizing public expenditures, with priority to completing schemes with the highest returns; and (iv) allocating sufficient resources for operations and maintenance for the sustainability of investments. Therefore, to tackle the issues faced by the rural farmers in India and increase the pace of agriculture in India to match with that of world, we need to use technology as a tool to achieve the desired results. This papers aims at introducing technology as a way to improve the irrigation system in rural areas through the use of solar energy. With decreasing solar modules prices (70% in the last 4 years), solar pumps are fast becoming a viable financial solution for irrigation. Some factors restrict the use of this technology, such as the high cost of photovoltaic modules, the growing worldwide manufacturing of photovoltaic modules and it's no operation during the night. However, future generations will benefit from the use of clean and sustainable energy sources in order to contribute to the preservation of the environment, speeding up implementation of photovoltaic energy in the market. This study aims at introducing a solar energy powered irrigation system for agriculture use in rural areas and the implementation of technology in irrigation systems.

ISSN: 2350-0328

International Journal of Advanced Research in Science, Engineering and Technology

Vol. 5, Issue 6 , June 2018

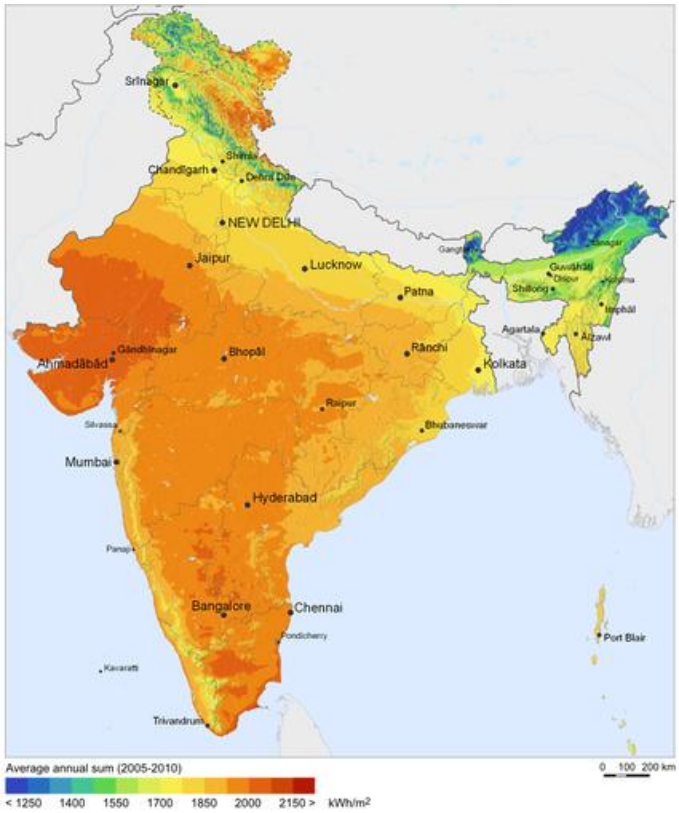

The above map shows the average solar radiation in India

II.REVIEW OF LITERATURE

The World Bank in its report on Solar Power Barrier in India mentions the current energy scenario in the country and various barriers hindering the development of this renewable energy in India. The report focuses on the availability of solar radiation data and technological equipment required. Mahendra Lalwani and Mool Singh in Conventional and Renewable Energy Scenario of India display the distribution of different energy sectors across the country and their usage in the present scenario. Dr. J.P Kesri, Mohit Gupta, Aadish Jain and A.K,Ojha in Review of Concentrated Solar Thermal Technologies(2015) explain the various type of solar concentrators used, their usage on capturing the solar radiation to operate solar powered equipments. The paper focuses on the urgent need to adopt renewable energy resources as alternative in the current stage of fossils and oil. Jia Uddin, S.M Taslin Reza (2012) mention the proposed model of Solar Irrigation system. The paper supports the statement that variable rate automated controlling approach improves the overall irrigation system reducing the total cost and increase the production of crop yield. The irrigation model displayed uses PV cells to operate and offers a better alternative. Satyendra Tripathi and Lakshmi N (2013) in Solar Powered intelligent irrigation system focus on the need to modernize the irrigation system of India and propose an irrigation model, a low cost and reliable model, for farmers which can be operated easily through solar radiation and moisture content of the field.

III.THEORETICAL CONSIDERATION AND COMPONENTS OF SOLAR PHOTOVOLTIC SYSTEM

A. Photovoltaic Energy and its components

In recent years, there was an increase in the use of alternative energy sources to complement the global energy matrix. However, such sources of global renewable energy generation have impacts and constraints, imposing some limitations.

ISSN: 2350-0328

International Journal of Advanced Research in Science, Engineering and Technology

Vol. 5, Issue 6 , June 2018

These limits are important for the planning and design of sustainable energy policies, demanding specialized studies for obtaining good performances in the installation of systems, in order to avoid serious consequences. Renewable energy sources are classified as hydro, thermal solar, photovoltaic solar, wind, ocean, geothermal and biomass. These sources use natural resources such as wind, water, solar radiation and heat as the operating principle for its generation. Hence, the applications of renewable energy sources are quite diverse and have been sought by several users.

The basic photovoltaic unit is called a solar cell, which together in groups form the photovoltaic panels, interconnected elements that compose the electric generator of a photovoltaic installation. The panels convert radiation into electrical energy by the photovoltaic effect. Such a phenomenon can be done because the panel is composed of semiconductor materials with specific properties.
Its production of electricity is the photovoltaic effect based on direct or indirect conversion of sunlight. The direct sunlight is extremely important for the generation of photovoltaic energy once the indirect approach does not produce an ideal performance to the system. Therefore, the panels should be able to capture the maximum amount of solar radiation during the day.

Since the conversion of solar energy to electrical energy is accomplished by converting the radiation into electrical energy, the higher the incidence of solar rays on the panel, the greater will be the power generated by the photovoltaic system. There are some methods used for increasing energy production, such as solar trackers, which provide a performance better than those with fixed angle due to the amount of direct radiation on the panels.In power generation, some concepts are fundamental, such as solar radiation that is transmitted to our planet through space as electromagnetic radiation. The incidence of this radiation on the photovoltaic modules cause the photovoltaic effect, which is the operating basis of solar photovoltaic systems. From this transformation of solar radiation into electrical energy, a potential difference arises, which is an electrical voltage.

Solar radiation suffers the influence of atmospheric air, clouds and pollution before reaching the ground. Hence, it is necessary that the photovoltaic panels are properly installed for capturing as much solar energy as possible. The classification regarding the connection to the power grid is of three types: isolated generators (off-grid), network-connected generators (Grid-tie) and hybrid generators. The off-grid generators are those with no connection to the electrical distribution network. These systems are usually installed in places not served by power distribution companies, thus requiring the use of a battery bank to store the generated energy and to provide it during the period of no solar radiation. They are mainly composed of photovoltaic panels, charge controller, batteries and inverters, as shown.

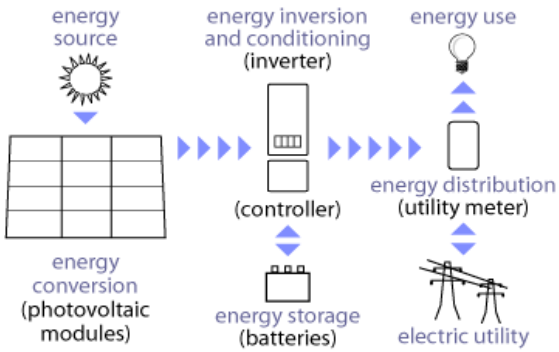

The Grid-tie generators are effectively connected to the public power grid. Once they are directly injected into the power grid, there is no need for battery bank. They are basically composed of the photovoltaic panel and the inverter, besides the components of control, protection and monitoring of the energy generation. The photovoltaic park of Sarnia, in Canada, is an example of a large centralized photovoltaic plant with an installed capacity of 80 MWp. Hybrid generators are isolated systems operating together with other generators such as wind, gas, diesel, coal, nuclear, etc., as shown in Figure 3. In some cases, this union may be more beneficial than a photovoltaic system operating independently, since it promotes a reduction of the installed power of solar panels, thereby reducing the total costs

ISSN: 2350-0328

International Journal of Advanced Research in Science, Engineering and Technology

Vol. 5, Issue 6 , June 2018

B. Automated Irrigation System

The agricultural industry is interested in improving its production process in order to reduce spending on labour, energy, water waste in irrigation, excessive use of pesticides, fertilizers, among others, andreductions in these costs will increase profit. One of the solutions is applying automation in the farm, through an interdisciplinary work of distinct areas, which can bring positive results Some automated systems are controlled by Programmable Logic Controller (PLC), a technically viable alternative able to control and monitor processes such as the irrigation system, amount of energy used, pesticide use etc. Other automated systems may be controlled by microcontrollers, such as ArduinoR, which use Atmega family's chip in their microcontrollers

Automated systems provide a great improvement in production processes. Besides reducing human-based problems, it will also reduce problems related to inadequate operation and/or to waste of any raw material. However, designing fully autonomous systems may sometimes not be a viable alternative due to complexity and to socioeconomic conditions.The automation of irrigation is a very important step both for those who work directly with this process and for humanity in general, thereby minimizing water waste. New irrigation strategies have been constantly created, especially in regions where such resources are scarce, thus forcing the installation of modern irrigated crops

systems. The installation of real-time sensors provides the linking of information about spatial and time development of biotic and abiotic stress, such as instructions of the irrigation system allowing producers to maximize the efficiency of the proper use of water, to generate sustainability and to decrease negative effects on the environment.

IV. AUTOMATIC IRRIGATION SYSTEM AND ITS COMPONENTS

With the alarming rate of depletion of fossil fuels, it is more ethical to shift on Renewable Energy Sources like Solar energy and wind energy.The vehicle designed for AIS(Automated Irrigation System) completely runs on Solar Energy making it more efficient to run and environment friendly.Automatic Irrigation system shows the steps required to convert solar energy into irrigate crops in the fields through technology.

Solar Panel: A solar panel is a set of solar photovoltaic modules electrically connected and mounted on a supporting structure. A photovoltaic module is a packaged, connected assembly of solar cells. The solar panel can be used as a component of a larger photovoltaic system to generate and supply electricity in commercial and residential applications.

Charge Controller : A solar charge controller manages the power going into the battery bank from the solar array. It ensures that the deep cycle batteries are not overcharged during the day, and that the power doesn't run backwards to the solar panels overnight and drain the batteries. Some charge controllers are available with additional capabilities, like lighting and load control, but managing the power is its primary job.

ISSN: 2350-0328

International Journal of Advanced Research in Science, Engineering and Technology

Vol. 5, Issue 6 , June 2018

Rechargeable Batteries: the rechargeable batteries enable to covert electric energy into the storable chemical energy and realize the recyclable conversion/storage between electric energy and chemical energy. the exploitation of solar energy in rechargeable batteries could not only achieve the large-scale application of solar energy, but also assist the conventional rechargeable batteries in saving the input electric energy.

Inverters: electrical energy from photovoltaic solar panels to drive AC motor water pumps. electrical energy from photovoltaic solar panels to drive AC motor water pumps.

Pump: A typical solar water pumping system is known by the sum total of solar array size that is required to run the attached pump. Each solar array has a number of solar modules connected in parallel or series. Every solar PV panel generates current by converting solar radiation to electrical energy. The electrical energy from the entire array is controlled, tuned and directed by the inbuilt controller in DC pumps or through the Variable Frequency Driver(VFD) and enables the connected pump (may be submersible or surface) to draw water and feed the delivery pipelines. The water thus drawn from ponds, rivers, bore wells or other sources by a solar water pump is pumped to supply water as required. It can be stored in tanks from where it is later channelled to fields or the supply from the pump may be coupled with drip irrigation systems to provide optimised water to fields directly.

A. Proposed model of Automated Irrigation System

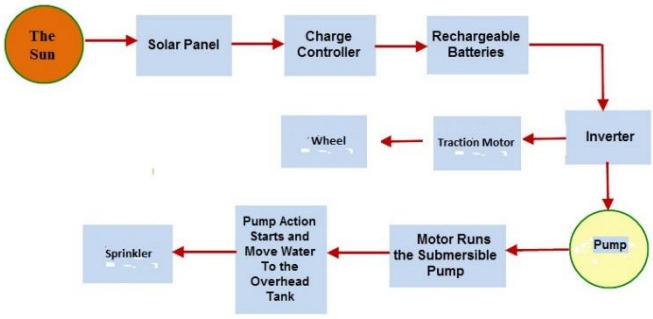

The below proposed system shows the practical usage of the irrigation system designed.
The wheels attached at the bottom of the system rotate as the system starts operating and let the water in into the machine. As the water is pulled into the machines through wheels, it passes through the pump, the battery and the inverter. Traction motor refers to a type of electric motor. Attraction motor is used to make rotation torque on a machine. It is usually changed into a straight line motion. Motors on solar positioning equipment orient panels to follow the sun daily and seasonally. Motors on solar trackers must withstand extreme temperatures, twice that of a normal industrial setting, they also must have protection against water and dust. This can be achieved with sealing. The solar energy derived from the sun. although varying at different time of the day, is focused on the solar panels attached at the roof of the system.

ISSN: 2350-0328

International Journal of Advanced Research in Science, Engineering and Technology

Vol. 5, Issue 6 , June 2018

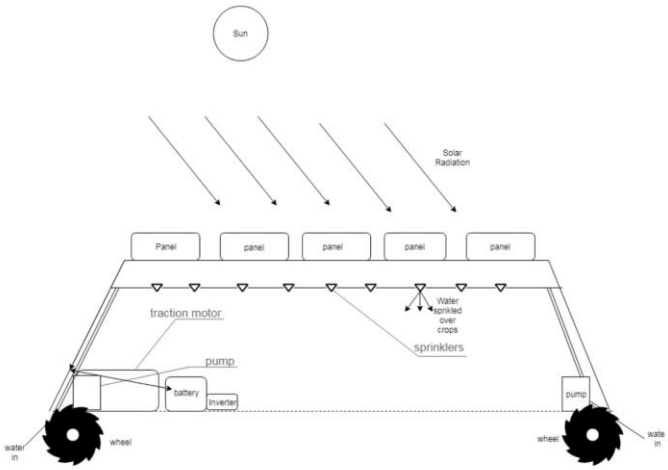

B. DESIGN OF SOLAR PV WATER PUMPING SYSTEM

A solar water pumping system is designed with solar photovoltaic panels and locally available electric pumps. All components in the system design have been procured locally except solar panels. A DCDC Buck converter is used to integrate with the solar water pumping system to operate it efficiently. The microcontroller based solar tracking system has incorporated in order to attain maximum solar power for electricity generation and thereby increasing the system efficiency.

B.1 Solarwaterpumpingsystem:

The solar-powered pumping system can be used anywhere but it is appropriate for rural areas of India which is facing energy crisis like other developing countries of the world. However due to geographical position, India has ample sunshine through the year which makes it ideal location for utilization of solar energy. Small farms, villages, and animal herds in developing countries require hydraulic output power of less than a kilowatt. Many of these potential users are too far from an electrical grid to economically tap that source of power, and engine-driven pumping tends to be prohibitively expensive as well as unreliable due to the high cost of purchased fuel and insufficient maintenance and repair capabilities. Though the installation cost of solar powered pumping system is more than that of gas, diesel, or propane-powered generator based pumping system but it requires far less maintenance cost. However, by comparing installation costs (including labour), fuel costs and maintenance costs over 10 years with other conventional fuel based pumping system, the solar PV water pumping system can be a suitable alternate option. This system has the added advantage of storing water for use when the sun is not shining, eliminating the need for batteries, simplicity and reducing overall system costs. Solar water pumps are designed to use the direct current (DC) provided by a PV array, although some newer versions use a variable frequency AC motor and a three-phase AC pump controller that enables them to be powered directly by the solar modules. Since solar cell is expensive and its electricity production is of intermittent nature therefore solar pumps need to be as efficient as possible i.e. they need to maximize the gallons of water pumped per watt of electricity used.
The long-term cost analysis makes the solar PV pumping system comparable to most other remote watering options in the rural areas. The lifetime of solar water pump is usually 20 years, which ultimately is lower than the life span period cost compared to the conventional pumps. By using solar PV pumps, load on the grid system can be reduced and the subsidy on the diesel can be lowered.

B.2 Components used for the designed system:

1. Solar Panel
2. Chopper
3. Battery

ISSN: 2350-0328

International Journal of Advanced Research in Science, Engineering and Technology

Vol. 5, Issue 6 , June 2018

4. D C Motor
5. Connector

In Components are sized accordingly and then connected directly with the panels to examine the converter design. There are different sizes of PV modules commercially available. For the proposed system, solar panels are used. The specifications of the solar panels are provided below:

Rated Current: 7amps
Rated Voltage: 24volts
Short Circuit (SC) Current: 8.07amp
Open Circuit (OC) Voltage: 42volt
Cell Temperature: 25°c

Six 250Wp solar panels have been used to provide DC power supply for the water pumping system. Such 6 solar panels supply 1500Wp power during the normal condition. The solar panels are connected in two arrays, the first, second arrays and 6 panels. All six panels are connected in parallel to provide power supply to the pumping system.

B.3 solar panel **(Stand-Alone System):**

- 1500W
- Inverter set
- Charge regulators
- FF~70%
- Efficiency =15-20%
- Tolerance =-3 to +15
- V max =34v
- Vo c =42v
- Imax =7A
- Is c =7.05A
- UPS back up
- Battery of 1800 Ah

Calculation for the number of batteries that we use in our project

Generally the sun gives 1000W/sq.mt

A solar panel is 15% efficient, So we get 150 WattPanel size=10*10[1sq.m=10.7sq.ft]10sq.m=107sq.ft=>10sq.m=10.344

We use 6 panels each of 250 watts (250*6=1500 watts)
The size of the motor that we use is 1hp (750watts) (Watts) 750*5=3750 w-hr
Usually battery is specified in amp-hr
The specification of the battery that we use is 180Ah

- We require 3750/.8=4687.5 whr
- .8 is efficiency of motor
- We use 12vbattery so4687.5/12=390.62Ah
- Battery energy stored 390.62/180*.6=3.66(Since battery is 60% efficient)
- We require 4 batteries to supply power to load for 4-5 hrs.
- Module costs typically represents only 40-60% of total PV system cost and the rest is accounted by inverter, PV array support, electrical cabling and installation
- Most PV solar technologies rely on semiconductor-grade crystalline silicon
- The high initial cost of the equipment they require discourages their largescale commercialization
- Initial cost of system
- 1 watt = Rs. 95.50

ISSN: 2350-0328

International Journal of Advanced Research in Science, Engineering and Technology

Vol. 5, Issue 6 , June 2018

- Total system wattage 1500
- 1500 x 95.50= Rs. 143250
- 1.5 kw means 1.5 unit
- According to government rules 1 unit cost for commercial purpose is Rs. 13
- In one day this system works for 6+2 hrs means 8 hrs
- 8 x 1.5=12 units
- 12 x 13 = Rs. 156 daily
- Total 300 days we will get sunshine because we ar in tropical zone
- 300 x 156 = Rs. 46800
- Now 143250/46800 = 3.2 years
- Reliability of solar is 15 - 20 years
- Hence after 4 years we will get profit
- Thus this recommends use of solar
- If Rs. 5.50 for unit thus payback period is 7 years
- 13 years of profit
- If Rs. 3.50 for unit payback period is 9.6 years
- 10 years profit

V. CASE STUDIES

A. CASE STUDY 1

Building a 5 MW solar PV plant in Rajasthan, India, under Phase 1 of the Jawaharlal Nehru National Solar Mission (NSM) presented a number of challenges for Mahindra EPC (MEPC), a wholly-owned subsidiary of the Mahindra Group, as this was their first experience with utility-scale solar. The plant needed to live up to the expectations of the Mahindra Group, one of the most respected corporations in India, known for "getting it right the first time". The developer wanted to be the first to achieve non-recourse funding, meaning lenders would demand rock-solid guarantees of the plant's long-term performance. And it was crucial to meet the commissioning deadline to avoid high penalties imposed by the government under the NSM. Wanting to take no risks, Mahindra EPC partnered with SunPower for their bankable technology, proven experience and collaborative approach, choosing SunPower's single-axis Trackers as the most efficient, reliable and cost-effective way to maximise power generation. SunPower assured the MEPC team that, despite their lack of familiarity with trackers, the SunPower single-axis Tracker was easy to install, and that the SunPower team would be available to help every step of the way, from site preparation to commissioning. Thanks to SunPower's support and to its own highly committed and energetic team, MEPC managed to commission the 5 MW plant ahead of schedule, in a record time of just 110 days.

Project Overview Location: Phalodi, Rajasthan, India
Completed: January 2012
System Size: 5 MW
System type: SunPowerTM SerengetiTM modules mounted on SunPowerTM Trackers
Project Partners EPC Contractor: Mahindra EPC Services Pvt. Limited
Project developer: Mahindra Solar One PVT. Limited, a joint venture between the Mahindra Group (26%) and Kiran Energy (74%)
Benefits
• 5 MW plant commissioned in just 110 days
• First PV plant connected to the grid under Phase 1 of India's NSM scheme
• First power plant in India to obtain non-recourse financing
• Solar electricity generated powers 60,000 rural homes

ISSN: 2350-0328

International Journal of Advanced Research in Science, Engineering and Technology

Vol. 5, Issue 6 , June 2018

B. CASE STUDY 2

World's Largest Solar Steam Cooking System at Tirumala, Andhra Pradesh The world's largest solar steam cooking system has been installed by the Tirumala Tirupathi Devasthanam (TTD) at Tirumala in Andhra Pradesh. The system has a capacity to prepare food for 15,000 people/day and employs automatic tracking solar dish concentrators, which convert water into high pressure steam. The steam thus generated is being used for cooking purposes in the kitchen of TTD. It has been hooked up with the existing boiler working on diesel so as to make the system reliable under all climatic conditions. The system has been designed to generate over 4000 kgs of steam/day at 180 degrees centigrade and 10 kg/sqcm which is sufficient to cook two meals for around 15,000 persons. It is modular in nature and consists of 106 automatic tracked parabolic concentrators arranged in series and parallel combination, each of 9.2 sq meter reflector area. Each unit of concentrators is connected to a central steam pipeline going to the kitchen. The system is made of indigenous components and the reflectors are of acrylic mirrors having reflectivity over 75%. Its installation was completed during September 2002 and was inaugurated on 11th October 2002. The system is expected to save around 1,18,000 litres of diesel per year, valued at Rs. 2.3 million. The total cost of the system is about Rs. 110 million, which includes back up boiler, utensils and annual maintenance contract for five years. The system has been installed by M/s Gadhia Solar Energy Systems, Valsad under a demonstration scheme of MNES with 50% financial support. Balance of the cost has been borne by the TTD trust. A total of 6 such systems have been installed in the country. This technology could be very useful at places where rice is the staple food and cooking is done on a very large scale.

VI.ECONOMIC ANALYSIS

The Indian renewable energy sector is the second most attractive renewable energy market in the world as per the Renewable Energy Attractiveness Index 2017. India's installed renewable power generation capacity (including hydropower) increased from 42.4 gigawatts (GW) in FY07 to 107.81 GW in FY18 (as of February 2018), which is 32.26 per cent of the total installed capacity. Power generation from renewable energy sources in India reached 85.65 billion units in FY18 (up to January 2018). India has the fourth largest installed capacity of wind power and the third largest installed capacity of concentrated solar power (CSP). India added record 11.0 GW of combined wind and solar capacity in 2016-17. Hydro power forms the largest source of energy constituting over 43 per cent of the total renewable power generation installed capacity. India witnessed highest ever solar power capacity addition of 5,525.98 MW and 467.11
MW of wind power capacity addition in 2017-18 (up to November 2017). 15,000 biogas plants were installed during the same time period. Off-grid power equivalent to 168.87 MW was added in the country during January – November 2017.
The Ministry of New and Renewable Energy, Government of India, has formulated an action plan to achieve a total capacity of 60 GW from hydro power and 175 GW from other RES by March, 2022, which includes 100 GW of Solar power, 60 GW from wind power, 10 GW from biomass power and 5 GW from small hydro power. This has been proving to be the major thrust for the sector in India as the market players have sufficient incentives to move to clean source. Under Union Budget 2018-19, Rs 3,762 crore (US$ 581.09 million) has been allocated for grid-interactive renewable energy schemes and projects.
As India looks to meet its energy demand on its own, which is expected to reach 15,820 TWh by 2040, renewable energy is set to play an important role. By 2030, renewable sources are expected to help meet 40 per cent of India's power needs. The non-conventional energy sector has received a total FDI equity inflow of US$ 6.26 billion during April 2000 to December 2017.

The features that affect the economic viability may be summarized as,
1) cost of the system
2) depreciation
3) interest on capital
4) cost of energy and the scenario, i.e, the variation of the cost of energy during the life time of the system
5) subsidies or incentives.
The total solar energy available is enormous. Total human energy needs by the turn of the century are estimated at ~43 TW (Terra Watts). The total energy available from the sun is estimated to be between 85,000 and 120,000 TWs. Solar energy is clean, safe and easy to install. The energy captured is immediately available. Maintenance of equipment is

ISSN: 2350-0328

International Journal of Advanced Research in Science, Engineering and Technology

Vol. 5, Issue 6 , June 2018

low and the life expectancy of equipment is measured in decades, not years. Equipment is modular, so repair and replacement do not require a complete changeout.

A. Employment

The first point is that there are a huge number of people employed in renewable energy jobs globally. There are almost 10 million of them around the world. Slightly over 3 million are employed in solar power. Large hydropower employs about 1.5 million people, and 1.2 million are in wind power employment. Advanced energy — which includes solar, wind, energy efficiency, energy storage and EVs — contributed $1.4 trillion to the global economy in 2016. Another benefit is that wind turbines can be installed in rural areas at existing farms to provide much-needed income to local people. Here's another fascinating example: "The report looked at the 23 largest wind farms in Illinois, finding that they will add almost $6 billion to local economies over their lifetimes and have resulted in the creation of more than 19,000 jobs during the construction periods. The projects will also support 814 in the state. The Union of Concerned Scientists made a great point in one its recent articles on renewable energy: "Compared with fossil fuel technologies, which are typically mechanized and capital-intensive, the renewable energy industry is more labour intensive. Solar panels need humans to install them; wind farms need technicians for maintenance. This means that, on average, more jobs are created for each unit of electricity generated from renewable sources than from fossil fuels." That is true even when wind and solar power are *cheaper* for the customer.There are two main reasons why renewable energy technologies offer an economic advantage: (1) they are labour intensive, so they generally create more jobs per dollar invested than conventional electricity generation technologies, and (2) they use primarily indigenous resources, so most of the energy dollars can be kept at home. So, renewable energy can generate better jobs and more of them.

B. Economic simulation

Renewable energy contributes more economically than only jobs and pollution reduction. Doubling the share of renewables in the global energy mix by 2030 would increase global GDP by up to 1.1% or USD 1.3 trillion. The report shows that such a transition increases global GDP in 2030 between 0.6% and 1.1%, or between around USD 700 billion and USD 1.3 trillion compared to business as usual. Another key, and very striking, benefit is how renewable energy investment can impact trade. "For fossil fuel importers, the switch to a greater share of renewables has potentially favourable trade implications. Reducing fuel imports can improve trade balance and improve GDP. According to an analysis conducted by the Union of Concerned Scientists, implementing a national 25% by 2025 renewable electric standard would result in the following benefits: $263.4 billion in new capital investment for RE technologies, $13.5 billion in new landowner income from biomass production and/or wind land lease payments, and $11.5 billion in new property tax revenue for local communities In the development scenario, the quantitative analysis implies that the added value brought about by wind and solar PV power industry, directly and directly, is about 5.0 times in 2030 more than that in 2015," a study of renewable energy economic benefits in China estimated. "During 2016–2030, about 8674 billion RMB (1300 billion dollars) and 6949 billion RMB (1042 billion dollars) added value could be generated respectively by wind power industry and solar PV power industry, accounting for about 0.58% and 0.47% of GDP.

C. Government initiatives

Some initiatives by the Government of India to boost the Indian renewable energy sector are as follows:
In December 2017, a new policy was released for testing, standardisation and certification of products used in the renewable energy sector to address quality issues and develop standards as per international practices.

- Around 4.96 million household size biogas plants were installed in the country under the National Biogas and Manure Management Programme (NBMMP) by 2016-17 end.
- The Government of India has announced plans to implement a US$ 238 million National Mission on advanced ultra-supercritical technologies for cleaner coal utilisation.
- The Ministry of New and Renewable Energy (MNRE) has decided to provide custom and excise duty benefits to the solar rooftop sector, which in turn will lower the cost of setting up as well as generate power, thus boosting growth.

ISSN: 2350-0328

International Journal of Advanced Research in Science, Engineering and Technology

Vol. 5, Issue 6 , June 2018

- The Indian Railways is taking increased efforts through sustained energy efficient measures and maximum use of clean fuel to cut down emission level by 33 per cent by 2030.
- The Union Cabinet has approved raising of bonds worth Rs 2,360 crore (US$ 366.2 million) by the Indian Renewable Energy Development Agency (IREDA), which will be used in various renewable energy projects in FY 2017-18.
- The Union Cabinet has approved construction of 10 units of indigenous Pressurized Heavy Water Reactors (PHWR), with a nuclear capacity of 700 MW each, which is expected to bring substantial economies of scale and maximise cost and time efficiencies, and thereby boost India's nuclear industry.

ACKNOWLEDGEMENT

The authors wish to thank Dr. J.P Kesri, Department of Mechanical Engineering, Delhi Technological University for their extremely helpful guidance in carrying out the review paper and providing them with the appropriate data required.

REFERENCES

[1] João M. G. Figueiredo1 , José M. G. Sá da Costa2, "Intelligent Sun-Tracking System for Efficiency Maximization of Photovoltaic Energy Production".
[2] Tarujyoti Buragohain, "Impact of Solar Energy in Rural Development in India", International Journal of Environmental Science and Development, Vol. 3, No. 4, August 2012
[3] Soteris A. Kalogirou, "SOLAR ENERGY, POWER GENERATION AND DESALINATION SYSTEMS", Cyprus University of Technology, Limassol, Cyprus
[4] Chetan Singh Solanki, Solar Photovoltaics Fundamentals, Technologies and Applications, 2nd ed. New Delhi, India: PHI Learning Private Limited, 2011.
[6] http://www.cea.nic.in/index.html
[7] J.P. Reges, A.R. de Alexandria, L.C. dos S. Mazza, E.J.Braga," Inserting Photovoltaic Solar Energy to an Automated Irrigation System".

This article has been accepted for inclusion in a future issue of this journal. Content is final as presented, with the exception of pagination.

Dual- and Triple-Band Polarization Insensitive Ultrathin Conformal Metamaterial Absorbers With Wide Angular Stability

Amit Kumar Singh, *Student Member, IEEE*, Mahesh P. Abegaonkar, *Senior Member, IEEE*, and Shiban K. Koul, *Fellow, IEEE*

***Abstract*—This paper describes a dual-band electromagnetic (EM) absorber for *C*- and *X*-band applications. The proposed structure consists of two circular ring resonators that are modified to make the absorber compact. The proposed absorber is demonstrated to be conformal, insensitive to polarization and angle of oblique incidence of incoming EM wave. To the authors' knowledge, it is the thinnest absorber reported with a thickness of $\lambda_0/142.65$ at lowest frequency of absorption. The absorption bands with absorption peaks of about 97% and 99% are observed at center frequencies of 4.19 and 9.75 GHz, respectively. The absorption frequency bandwidth (more than 90% of peak absorption) at these frequencies is 665 and 860 MHz, respectively. The double-band absorber can be extended to work at three frequencies by simply adding another ring between the two modified circular rings of dual-band absorber. The modified structure has absorption bandwidth of 610, 670, and 570 MHz with absorption peaks of 97.50%, 96.50%, and 98.85% at resonant center frequencies 4.19, 6.64, and 9.95 GHz, respectively. The temperature profile of the proposed absorber is measured by using lock-in infrared thermography and a temperature increase of 1.5 °C is observed at all the absorbing frequencies with transmitted RF power of 10 dBm. The experimental results agree well with the simulation results, and the proposed structure is insensitive for the transverse magnetic/transverse electric field polarization of incident waves and also the angle of incidence. It provides wide angular stability up to 45°. Along with a flat surface, the proposed absorbers are tested on a curved surface to exhibit its conformal nature.**

***Index Terms*—Absorber, conformal, double-band absorber, metamaterial, polarization insensitive, triple-band absorber, ultrathin, wide-angle incidence.**

I. Introduction

MICROWAVE absorbers are the materials that absorb the electromagnetic (EM) energy [1]. Absorbers are used in a wide range of applications to eliminate unwanted radiations in defense applications, EM interference/EM compatibility (EMI/EMC) reduction, radar applications, anechoic chamber, and medical applications. Conventional microwave absorbers have several limitations in practical applications. The advancement in the designing of microwave absorbers using metamaterial is the solution to those limitations. EM metamaterials have a strong potential to control EM responses of many microwave materials and devices by tailoring EM properties of material, such as permittivity and permeability, by designing proper unit cells. Research focusing on metamaterials has generated devices such as super lens and invisibility cloaks.

Landy *et al.* [1] in 2008 proposed a single-band perfect metamaterial absorber. Subsequently, various single-band, double-band, and multiband metamaterial absorbers were reported [2]–[6]. Wideband metamaterial absorbers by using multiple layer approach and resistive and capacitive loaded structures are proposed in [7]–[10]. A wearable ultrathin metamaterial absorber is presented in [11]. A microwave absorber for energy harvesting is presented in [12]. A metamaterial absorber loaded with resistor is reported in [13] for wideband absorption. Polarization insensitive wideband metamaterial absorbers are reported in [14] and [15]. Ultrathin- and multiple-band absorbers are presented in [16] and [17]. A conformal metamaterial absorber for curved surface as well as flat surface application is presented in [18] and [19]. A polarization insensitive metamaterial absorber by using compact unit cell with triple-band operation is presented in [20]. Several frequency selective surface applications are proposed in [21]–[23]. As can be seen from the literature surveyed, it is difficult to get all the characteristics, such as ultrathin, polarization insensitive, conformal, multiband, and wide angular stability, in a single structure.

In this paper, the design of a multiband, conformal, ultrathin, polarization insensitive metamaterial absorber is proposed. The proposed metamaterial unit cell structure consists of a compact modified double circular ring resonator (MDCRR) backed with metal ground as a unit cell. The proposed MDCRR unit cell is found to have dual-band characteristics. The MDCRR unit cell is modified to obtain triple-band absorption characteristic called modified triple circular ring resonator (MTCRR). A 16×16 array of prototype absorber is fabricated and tested in an anechoic chamber on a flat surface as well as on a curved surface. The measured and simulated results of both absorbers are found to be in good agreement.

The proposed double- and triple-band absorbers are compared with several reported similar type absorbers in Table I.

Manuscript received March 20, 2018; revised April 18, 2018; accepted May 17, 2018. *(Corresponding author: Amit Kumar Singh.)*

The authors are with the Centre for Applied Research in Electronics, Indian Institute of Technology Delhi, New Delhi 110016, India (e-mail: amitkumarcareiitd@gmail.com; mpjosh@care.iitd.ac.in; s.k.koul@ieee.org).

Color versions of one or more of the figures in this paper are available online at http://ieeexplore.ieee.org.

Digital Object Identifier 10.1109/TEMC.2018.2839881

0018-9375 © 2018 IEEE. Personal use is permitted, but republication/redistribution requires IEEE permission.
See http://www.ieee.org/publications_standards/publications/rights/index.html for more information.

This article has been accepted for inclusion in a future issue of this journal. Content is final as presented, with the exception of pagination.

TABLE I
COMPARISON OF THE OTHER REPORTED ABSORBERS WITH PROPOSED ULTRATHIN CONFORMAL DUAL- AND TRIPLE-BAND ABSORBERS

Ref.	Substrate Thickness (λ_0)	Unit Cell Size (λ_0)	Operating Bands (GHz)	Conformal
14	-	-	9.4, 11.7	No
18	$\lambda_0/138$	$0.216\lambda_0$	7.22, 14.55	Yes
19	$\lambda_0/126$	$0.253\lambda_0$	9.5, 15	Yes
Proposed double band absorber	$\boldsymbol{\lambda_0/142.65}$	$\boldsymbol{0.167\lambda_0}$	**4.19, 9.75**	**Yes**
16	$\lambda_0/92.24$	$0.12\lambda_0$	3.2, 9.45, 10.90	No
17	$\lambda_0/77$	$0.206\lambda_0$	4.11, 7.91, 10.13, 11.51	No
20	$\lambda_0/91$	$0.11\lambda_0$	4.19, 9.34, 11.48	No
Proposed triple band absorber	$\boldsymbol{\lambda_0/142.65}$	$\boldsymbol{0.167\lambda_0}$	**4.19, 6.64, 9.95**	**Yes**

The designed absorbers are found to be ultrathin, compact, and conformal with more number of absorption bands. The same proposed absorber can be easily extended to higher number of band applications.

The paper is organized as follows. Section II presents the proposed designing of MDCRR unit cell and its modified version called MTCRR unit cell and their absorption mechanism. Section III presents measurement results. This paper is concluded in Section IV.

II. DESIGNING OF A METAMATERIAL UNIT CELL AND THE ABSORPTION MECHANISM

In this section, the designing method of the proposed novel MDCRR metamaterial unit cell and its modified form MTCRR metamaterial unit cell with their absorption mechanism is discussed. The designing of the proposed absorber is a three-step process starting with designing of the circular ring resonator (CRR) unit cell followed by the capacitive loading of CRR unit cell, using metallic slots to achieve compactness and designing of an array of modified CRR. Initially, two metallic rings on a grounded substrate are designed. The circumferences of the rings are approximately equal to guide the wavelength at the frequencies of 4.75 and 14.45 GHz, respectively. To support larger wavelength to propagate or absorb and to achieve compactness, the closed metallic rings can be loaded with additional capacitors. The loading capacitor is designed by modifying the ring with periodic slots as seen in Fig. 1(a). A compactness of 11.80% and 32.50% are achieved with resonating frequencies at 4.19 and 9.75 GHz, respectively. The capacitance of slot depends on the slot dimension and the number of slot. The number and dimensions of slots are optimized by using CST microwave studio to get desired frequency band. The decrease in the number of slots causes decrease in effective capacitance of metallic ring and, hence, increases the resonant frequencies and vice versa, as shown in Fig. 2(a). The increase in area of slot (length and width) results into decrease in the resonant frequency due to the increase in effective capacitance and vice versa, as shown in Fig. 2(b) and (c). The 50% change in slot

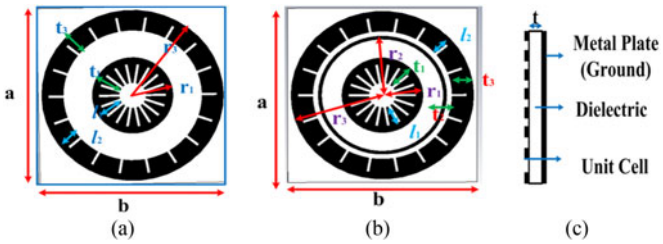

Fig. 1. (a) MDCRR unit cell. (b) MTCRR unit cell. Dimensions are $a = 14.0$, $b = 14.0$, $r_1 = 3.0$, $r_2 = 4.75$, $r_3 = 6.75$, $l_1 = 1.51$, $l_2 = 1.10$, $t = 0.50$, $t_1 = 2.0$, $t_2 = 0.25$, and $t_3 = 1.6$. (All dimensions are in millimeter.) (c) Proposed metamaterial absorber side view.

width will cause a change of 5.9%, 1.5%, and 1.9% in first, second, and third resonant frequency, respectively. The 20% change in slot length will cause a change of 4.75%, 1.2%, and 3.5% in first, second, and third resonant frequency, respectively. Hence, the proposed absorber can be considered as fabrication tolerant. The closed metallic rings will produce self-inductance due to the EM incidence. The magnetic flux incident on metallic ring generates rotating currents, which induce their own magnetic flux. The slots provide additional capacitance, resulting in *LC* resonant circuit. The proposed MDCRR unit cell is complementary to double annular slot ring resonator [24]. Next, the MDCRR unit cell is modified to achieve triple-band resonance condition by introducing a metallic ring, as shown in Fig. 1(b). This ring produces self-inductance and mutual capacitance due to other structures. The new modified MDCRR unit cell is called MTCRR. The geometrical details of MDCRR and MTCRR unit cells are shown in Fig. 1, where black color represents metal. The unit cell is printed on one side with another side of substrate as continuous metal ground on GML 1000 substrate with permittivity of 3.2 and thickness of 0.502 mm, as shown in Fig. 1(c).

The equivalent circuit of proposed metal backed MDCRR and MTCRR unit cell is given in Fig. 3(a) and (b), respectively. In the equivalent circuit, "Z_d" is impedance offered by the dielectric of thickness "$t_d = 0.50$ mm". The dielectric impedance "Z_d" can be given by

$$Z_d = \frac{Z_0}{\sqrt{\varepsilon}_r} \tan(\beta t_d) \tag{1}$$

where Z_0 is the characteristic impedance, β is the propagation constant, and t_d is the substrate thickness. In the equivalent circuit, "Z_{uc}" is the impedance due to proposed unit cell design. "L_1" is the effective inductance due to inner modified CRR (MCRR) and "C_1" is the effective capacitance due to slots on the inner MCRR. "L_2" is the effective inductance due to middle MCRR and "C_2" is the effective capacitance due to outer MCRR and middle MCRR of the MTCRR unit cell. "L_3" is the effective inductance due to outer MCRR and "C_3" is the effective capacitance due to slots on the outer MCRR and gaps between the adjacent unit cells, as shown in Fig. 3. The values of effective inductances and capacitances are calculated by using fundamental equations as reported in [25] and [26].

This article has been accepted for inclusion in a future issue of this journal. Content is final as presented, with the exception of pagination.

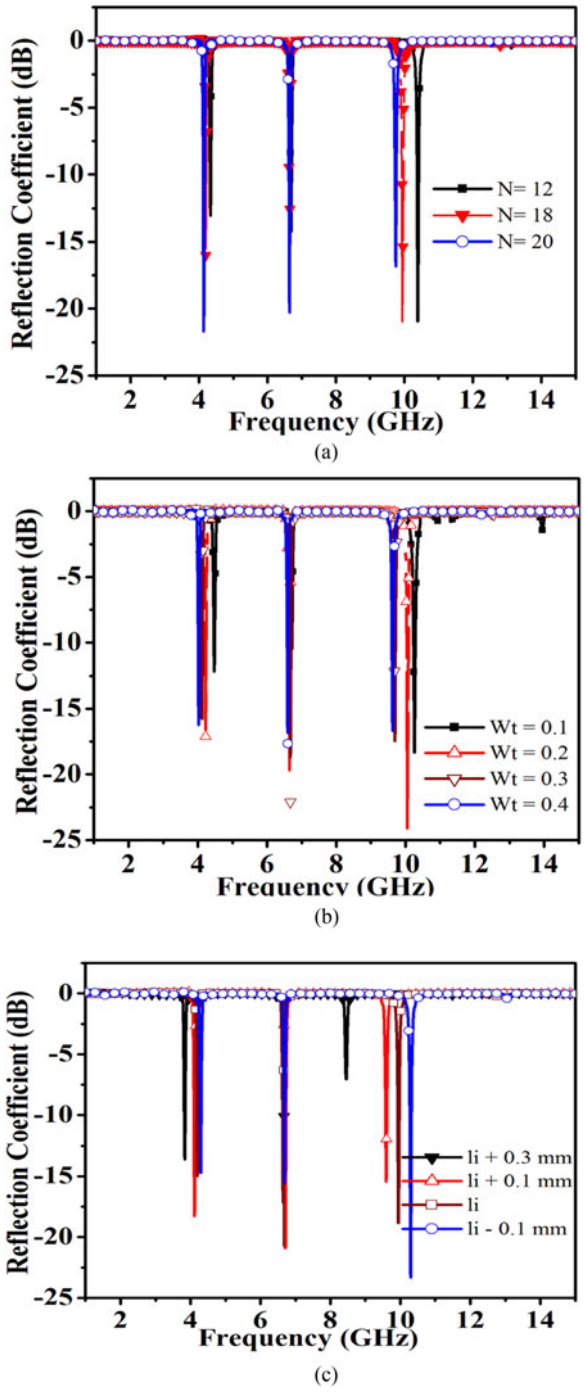

Fig. 2. (a) Number of slot "*N*" variations, (b) slot width "Wt" variations and (c) slot length "*Li*" variations, where $i = 1, 2$ for the MTCRR unit cell.

The total input impedance from Fig. 3 can be given by

$$Z_{\text{in}} = Z_{\text{uc}} \;||\; Z_d \tag{2}$$

$Z_{\text{in}} = (j\omega L_1 + \frac{1}{j\omega C_1})||(j\omega L_3 + \frac{1}{j\omega C_3})||\frac{Z_0}{\sqrt{\varepsilon}_r}\tan(\beta t_d)$ for MDCRR

$Z_{\text{in}} = (j\omega L_1 + \frac{1}{j\omega C_1})||(j\omega L_2 + \frac{1}{j\omega C_2})$ $||(j\omega L_3 + \frac{1}{j\omega C_3})||\frac{Z_0}{\sqrt{\varepsilon}_r}\tan(\beta t_d)$ for MTCRR.

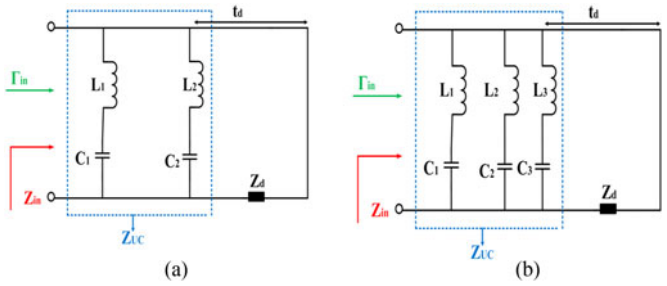

Fig. 3. Equivalent circuit model of the proposed unit cells. (a) MDCRR unit cell. (b) MTCRR unit cell.

The input reflection coefficient "Γ_{in}" can be given by

$$\Gamma_{\text{in}} = \frac{Z_{\text{in}} - Z_0}{Z_{\text{in}} + Z_0}. \tag{3}$$

When equivalent parallel circuit resonates, the overall reactance of "Z_{uc}" and "Z_d" becomes equal in magnitude but opposite in phase, this results into a pure real value of "Z_{in}". When the pure real "Z_{in}" matches with free space impedance "Z_0", the input reflection "Γ_{in}" becomes minimum. This minimum reflection results in maximum absorption. The frequency dependent absorption is defined in the following:

$$A(\omega) = 1 - T(\omega) - R(\omega). \tag{4}$$

Here, $T(\omega) = |S_{21}(\omega)|^2$ is the transmission coefficient and $R(\omega) = |S_{11}(\omega)|^2$ is the reflection coefficient.

Since the MDCRR and MTCRR unit cells are metal backed, so $T(\omega) = 0$, and $A(\omega)$ will be given by

$$A(\omega) = 1 - R(\omega). \tag{5}$$

If $T(\omega_0) = R(\omega_0) = 0$, at some resonant frequency ω_0, then this will lead to maximum absorption. The circuit parameters are calculated by using fundamental relationships, as shown in [25] and [26]. The self-inductance of a strip of length l and width t_i $(i = 1, 2, 3)$ can be given by (6). The effective inductance of ring circumference can be calculated by (7) and effective capacitance of a small strip can be calculated by (8). The calculated circuit parameters are $L_1 = 46.22$ nH, $L_2 = 0.358$ nH, $L_3 = 93.50$ nH, $C_1 = 4.97$ fF, $C_2 = 2.30$ pF, and $C_3 = 3.62$ fF

$$L_i = 2 \times 10^{-4} l \left[\ln\left(\frac{l}{\text{t}_\text{i} + t}\right) + 1.193 + 0.2235\frac{\text{t}_\text{i} + t}{l}\right] \tag{6}$$

$$L = \mu_0 \mu_{\text{eff}} \frac{r_i}{2\pi} \ln\left(\frac{1}{\sin\frac{\pi\omega}{2r_i}}\right). \tag{7}$$

Consider $d = 2\pi r_i/N$, where $N =$ number of strips.

$$C = \varepsilon_0 \varepsilon_{\text{eff}} \frac{2l_i}{\pi} \ln\left(\frac{1}{\sin\frac{\pi d}{2l_i}}\right). \tag{8}$$

The proposed MDCRR and MTCRR unit cells are simulated under the periodic boundary condition under normal incidence of EM waves in the CST microwave studio software. The EM simulated reflection coefficient by using CST microwave studio

This article has been accepted for inclusion in a future issue of this journal. Content is final as presented, with the exception of pagination.

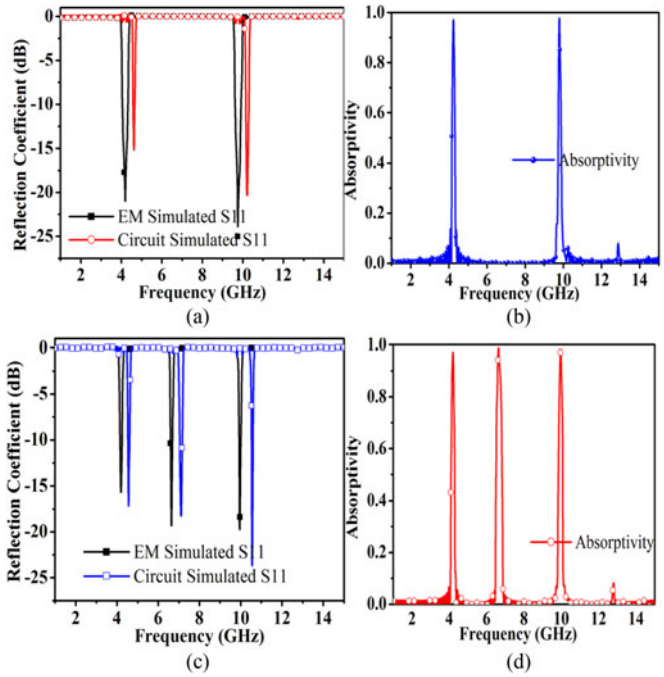

Fig. 4. (a) Circuit and EM simulated reflection coefficient of the MDCRR unit cell. (b) Absorptivity of the MDCRR unit cell. (c) Circuit and EM simulated reflection coefficient of the MTCRR unit cell. (d) Absorptivity of the MTCRR unit cell.

software and the circuit simulated reflection coefficient by using ADS software (using circuit parameters given above) with simulated absorption are plotted in Fig. 4(a) and (b) for the MDCRR unit cell and Fig. 4(c) and (d) for the MTCRR unit cell, respectively. A dual-band resonance is observed in the case of MDCRR unit cell with resonating frequencies at 4.19 and 9.75 GHz with reflection coefficient of −19.16 and −24.93 dB and absorption of 97.21% and 98.85%, respectively. The triple-band resonance is observed with the MTCRR unit cell at 4.19, 6.64, and 9.94 GHz with reflection coefficient of −15.87, −17.50, and −20.25 dB and absorption of 97.50%, 96.50%, and 98.85%, respectively. Adding middle MCRR causes decrease in effective capacitance due to coupling resulting into increase in higher frequency only. The parasitic due to mutual coupling of MCRRs (between outer and middle MCRRs for MTCRR unit cell) and mutual coupling of metallic slots on the MCRR are not considered in equivalent circuit parameter calculation. Due to this, a circuit simulated reflection coefficient is slightly deviated from EM simulated reflection.

To get an insight into generated resonance band E-field distribution, H-field distribution, and surface current distribution on the unit cells are observed and studied. As the MTCRR unit cell is a modified form of MDCRR unit cell, so surface current and field distributions on both unit cells will remain similar at corresponding resonating frequencies except the modified region. Hence, surface current and field distribution is analyzed on the MTCRR unit cell. Similar field distributions can be obtained on the MDCRR unit cell also. Figs. 5–7 depict the E-field distribution, the H-field distribution, and the surface current distribution, respectively. It is seen that the fields as well as surface

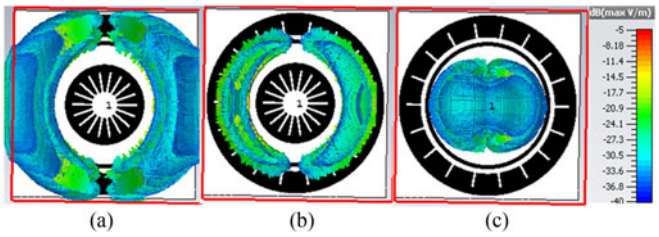

Fig. 5. Electric field distribution. (a) At 4.19 GHz. (b) At 6.64 GHz. (c) At 9.94 GHz.

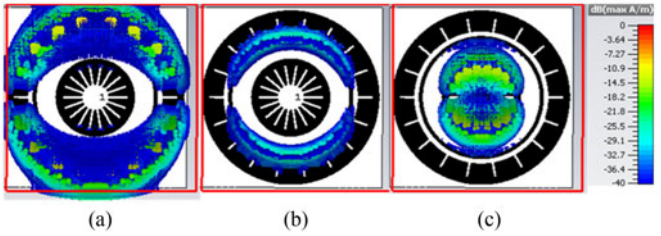

Fig. 6. Magnetic field distribution. (a) At 4.19 GHz. (b) At 6.64 GHz. (c) At 9.94 GHz.

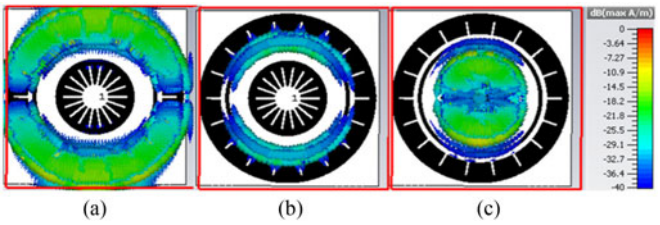

Fig. 7. Surface current distribution. (a) At 4.19 GHz. (b) At 6.64 GHz. (c) At 9.94 GHz.

currents are concentrated on the outer MCRR at 4.19 GHz, on the middle MCRR at 6.64 GHz, and on the inner MCRR at 9.95 GHz.

The direction of flow of surface current on unit cell and ground plane are found to be antiparallel, resulting in circulating current loop formations and, hence, strong magnetic resonance. Due to E-field distribution, concentrations on unit cell electric resonance occur. The common E- and H-resonance regions cause maximum EM absorption [15]–[17].

The field and current distribution plots suggest that the resonance band at 4.19 GHz is generated due to outer MCRR, the resonance band at 6.64 GHz is generated due to middle MCRR, and the resonance at 9.95 GHz is generated due to inner MCRR. To verify the above-mentioned results, the parametric variation of radius of outer MCRR, middle MCRR, and inner MCRR of the MTCRR unit cell is done and plotted in Figs. 8–10, respectively. The parametric variations suggest that all the three absorption bands can be controlled independently.

III. Experimental Results

The prototypes of conformal double-band and triple-band absorbers are fabricated and tested in an anechoic chamber. A

This article has been accepted for inclusion in a future issue of this journal. Content is final as presented, with the exception of pagination.

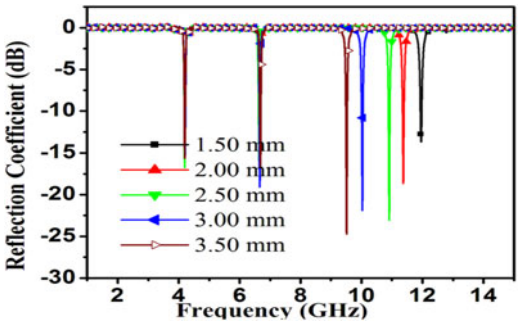

Fig. 8. Reflection coefficient versus frequency plot at different r_1 for the MTCRR unit cell.

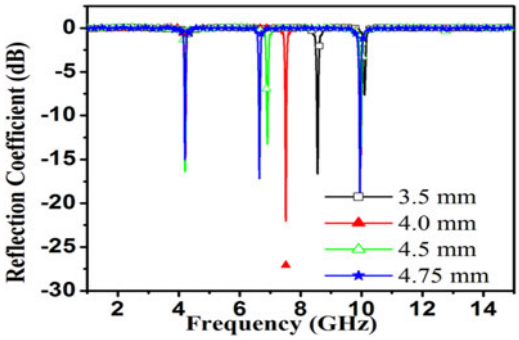

Fig. 9. Reflection coefficient versus frequency plot at different r_2 for the MTCRR unit cell.

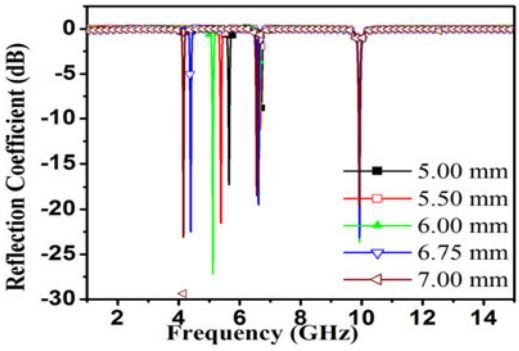

Fig. 10. Reflection coefficient versus frequency plot at different r_3 for the MTCRR unit cell.

16×16 array of the proposed MDCRR and MTCRR unit cells is fabricated on GML 1000 substrate with thickness of 0.50 mm and permittivity of 3.2. The fabricated prototypes of dual-band and triple-band absorbers with flat and curved surface are shown in Figs. 11 and 12, respectively. The fabricated absorber is a periodic arrangement of proposed MDCRR and MTCRR unit cells.

To measure the performance of the proposed absorber, a portable vector network analyzer (Anritsu MS2028C) and two wideband horn antennas as transmitter and receiver are used. The used horn antennas are separated by pyramidal foam absorber to reduce EM coupling at low frequency. The sample under test (SUT) is placed in far field of antenna to realize

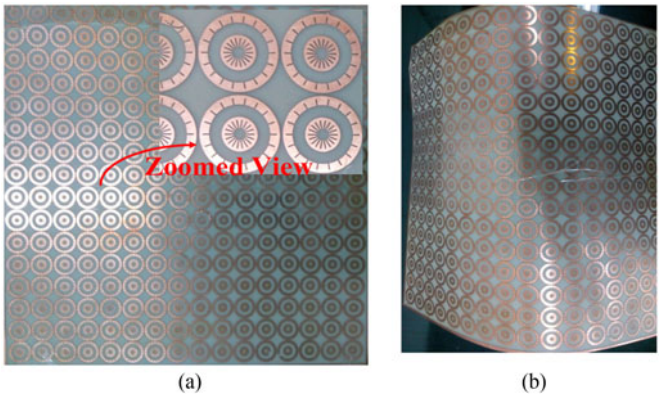

Fig. 11. Fabricated double-band flat and curved surfaces of the proposed absorber. (a) Flat surface of the proposed absorber. (b) Curved surface of the proposed absorber.

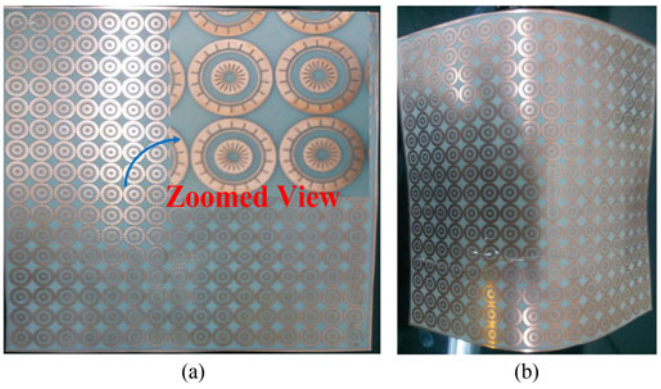

Fig. 12. Fabricated triple-band flat and curved surface of the proposed absorber. (a) Flat surface of the proposed absorber. (b) Curved surface of the proposed absorber.

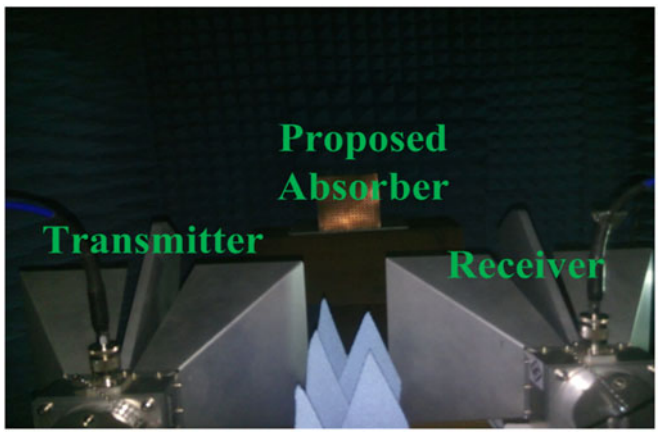

Fig. 13. Measurement setup for absorber measurement.

normal incidence on SUT. The setup is placed into an anechoic chamber. The used measurement setup is shown in Fig. 13.

The background noise of anechoic chamber is measured by recording reflection coefficient by vector network analyzer in the absence of any sample. The measured noise level is below

This article has been accepted for inclusion in a future issue of this journal. Content is final as presented, with the exception of pagination.

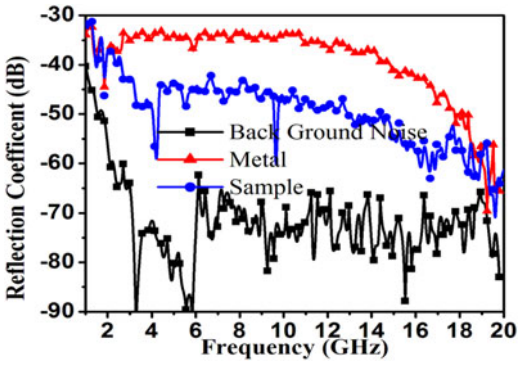

Fig. 14. Measured background noise and reflection coefficient due to metal plate and fabricated double-band prototype absorber.

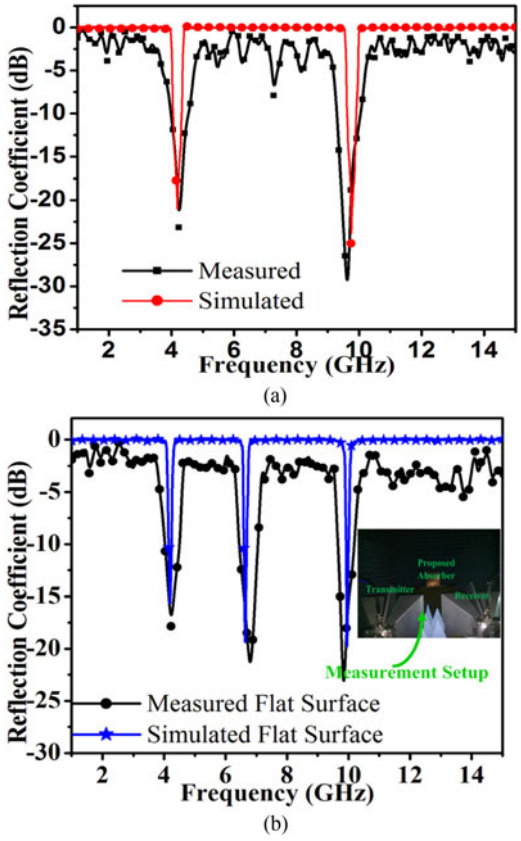

Fig. 15. Simulated and measured reflection coefficient of the proposed absorbers. (a) Double-band absorber. (b) Triple-band absorber.

−65 dB for entire desired frequency range, as shown in Fig. 14. The reflection coefficient of a metal plate of same dimension as the absorber is measured first. The metal plate is replaced with fabricated flat dual-band prototype absorber surface and reflection coefficient is measured. The obtained results are plotted in Fig. 14. The actual reflection coefficient of fabricated dual-band absorber is the difference between reflection coefficients of metal plate and fabricated prototype absorber.

The measured and simulated results of double-band and triple-band metamaterial absorbers are plotted in Figs. 15(a) and (b), respectively, and a good agreement is seen in both the

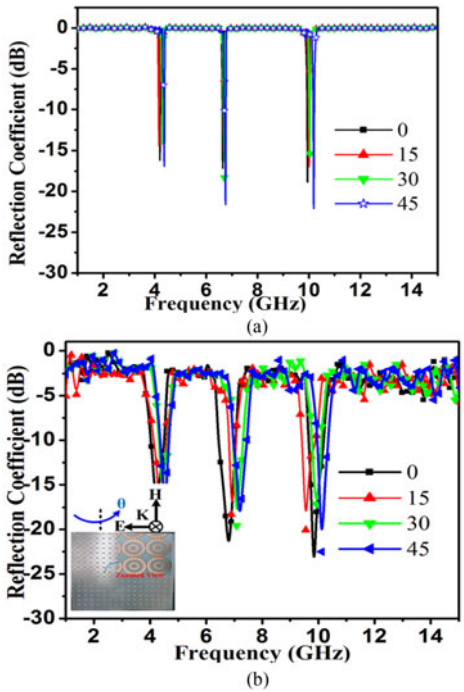

Fig. 16. Reflection coefficient due to various TM polarized angle of incidence of EM wave. (a) Simulated. (b) Measured.

cases. The measured −10 dB impedance bandwidth of double-band metamaterial absorber is 0.67 and 0.86 GHz at center frequencies of 4.19 and 9.75 GHz with more than 90% absorption. For the triple-band metamaterial absorber, the bandwidths with absorption more than 90% are 0.61 GHz around 4.19 GHz, 0.67 GHz around 6.64 GHz, and 0.57 GHz around 9.95 GHz.

The reflection from the absorber for transverse magnetic (TM) and transverse electric field (TE) polarization when angle between the transmitting and receiving antennas is changed is studied (this is equivalent to changing the angle of incidence in an azimuth plane). The simulated and measured reflection coefficients of triple-band absorber for TM polarized wave and TE polarized waves with varying angle between the transmitter and receiver is shown in Figs. 16 and 17, respectively. It is seen that the measured and simulated results are in good agreement. From the figures, it can be inferred that the proposed absorber has a wide angular stability up to 45°.

The proposed triple-band absorber structure is studied for various oblique angle of incidence in elevation plane. The simulated and measured results are compared in Fig. 18(a) and (b). Both are in good agreement. After 45° incident angle, the measured reflection coefficient is improper in nature and do not have any significant resonant deep due to TE and TM polarized EM wave incidence at the absorption frequencies, due to which, the proposed absorber's applicability is not suitable in the desired absorption frequency band after 45° incident angle. The measured reflection coefficient due to 60° angle of incidence of TM polarized EM wave is plotted in Fig. 19. Similar reflection coefficient is observed due to 60° angle of incidence of TE polarized EM wave.

This article has been accepted for inclusion in a future issue of this journal. Content is final as presented, with the exception of pagination.

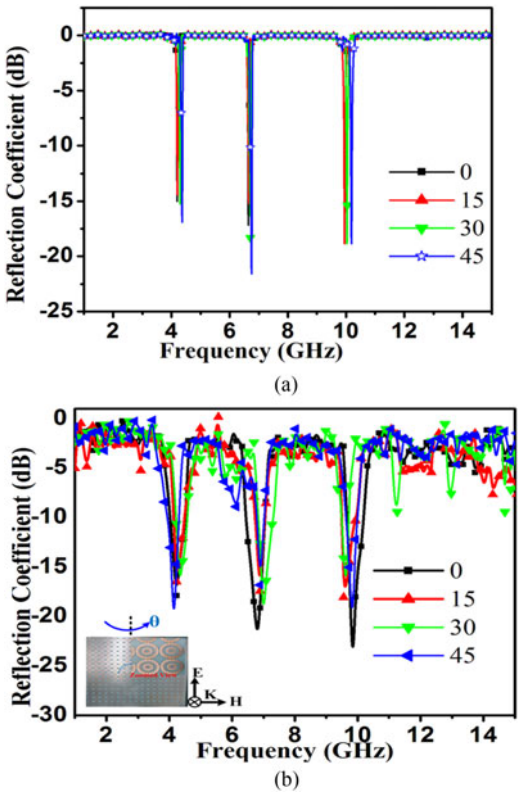

Fig. 17. Reflection coefficient due to various TE polarized angle of incidence of EM wave. (a) Simulated. (b) Measured.

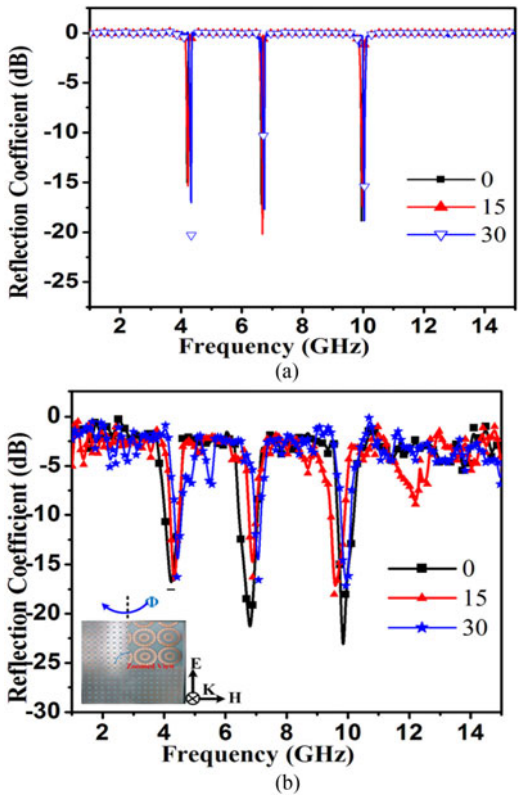

Fig. 18. Reflection coefficient due to various oblique angle of incidence of EM wave. (a) Simulated. (b) Measured.

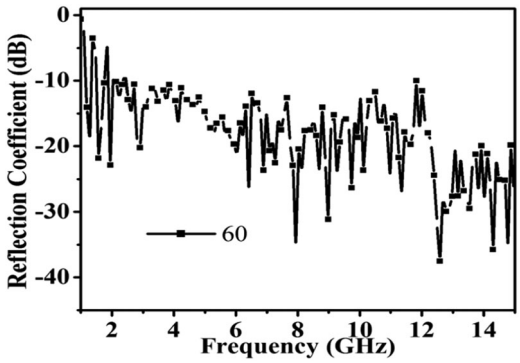

Fig. 19. Reflection coefficient due to TM polarized EM wave at 60° angle of incidence.

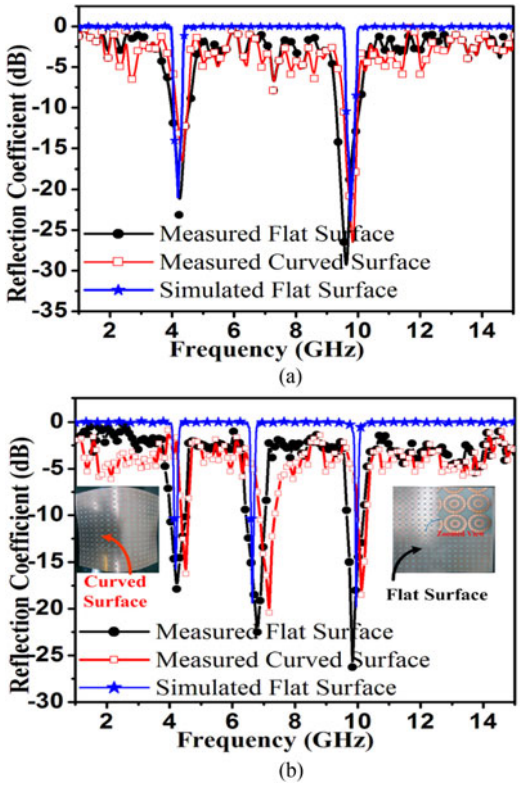

Fig. 20. Measured reflection coefficient of the proposed fabricated prototype absorber with flat surface and curved surface compared with simulated flat absorber. (a) Double-band metamaterial absorber. (b) Triple-band metamaterial absorber.

Hence, the proposed absorber is insensitive to polarization and angle of incidence of the EM waves. The polarization insensitivity is attributed to fourfold symmetry of the MTCRR unit cell. Similar results are obtained for the MDCRR absorber.

To verify the conformal characteristics of proposed absorber, absorber is pasted on a curved surface and reflection coefficient is recorded under normal incidence. Same process is repeated by pasting metal sheet on the same curved surface. The actual reflection coefficient of curved surface absorber is the difference between both these reflection coefficients. The fabricated absorber is pasted on a curved surface with curvature angle of

This article has been accepted for inclusion in a future issue of this journal. Content is final as presented, with the exception of pagination.

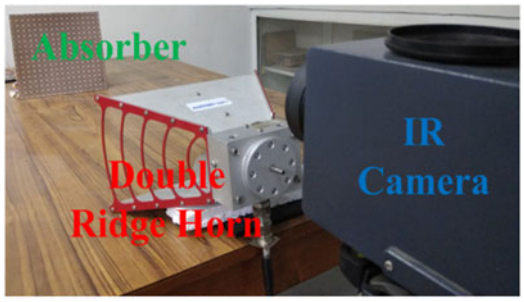

Fig. 21. Measurement setup for temperature profile measurement.

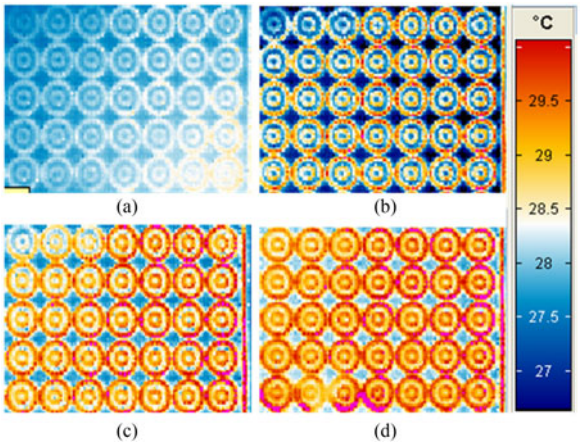

Fig. 22. Measured temperature profile of the proposed fabricated prototype triple-band absorber by using lock-in IR thermography. Microwave source radiating at (a) 7.50 GHz, (b) 4.19 GHz, (c) 6.64 GHz, and (d) 9.95 GHz.

about 120° with curvature radius of 80 mm. The reflection coefficients of proposed absorber for flat surface and curved surface are compared with simulated flat surface in Fig. 20(a) and (b) for proposed double-band and triple-band conformal absorbers, respectively. The compared results are in good agreement. Hence, the proposed double- and triple-band absorber surfaces are conformal.

To achieve more number of band operations, the additional MCRRs can be added as per the requirement of resonant frequency band. If the required resonant frequency band is smaller than first resonant frequency (4.19 GHz), then a simple ring having radius larger than the outer MCRR (in this paper) can be added. Its reverse can be done for achieving higher resonant frequency band as compared with first resonant frequency 4.19 GHz. This simple ring can further be modified by capacitive loading slots to achieve compactness.

It is expected that when the absorber absorbs the EM wave, the result should be increase in its temperature on absorber surface. To confirm the absorption properties of the proposed structure, its temperature profile is measured by using lock-in infrared (IR) thermography as reported in [27]. The prototype triple-band absorber is excited by a wideband double ridge horn antenna acting as a microwave source, and a temperature profile is plotted by thermal images of absorber screen as recorded by an IR camera. The RF power is set to 10 dBm. The measurement setup is shown in Fig. 21. The measured temperature profile is plotted in Fig. 22. The temperature profile of fabricated prototype absorber is measured at nonabsorbing frequency of 7.5 GHz first [see Fig. 22(a)]. A rise of about 1.5 °C in the temperature of prototype absorber surface is recorded at the absorbing frequencies 4.19, 6.64, and 9.95 GHz, as shown in Fig. 22(b)–(d), respectively. It is also observed that the rise in temperature is on the unit cell metallic surface. Hence, the wave is absorbed by a unit cell structure.

IV. Conclusion

A novel approach for designing a multiband conformal ultrathin polarization insensitive metamaterial absorber is successfully demonstrated. Starting with a dual-band metamaterial absorber, it is demonstrated that the technique can be extended to multiband absorption. The proposed absorber is polarization insensitive with wideangular stability up to 45° in azimuth and 30° in the elevation plane. The absorption peaks of 97.50%, 96.50%, and 98.85% at 4.19, 6.64, and 9.95 GHz, respectively, are obtained. The absorption bandwidths at these frequencies are 0.61, 0.67, and 0.57 GHz, respectively, with more than 90% absorption. The thickness of proposed absorber surface is $\lambda_0/142.65$, where λ_0 is the free space wavelength at first center frequency of absorption of 4.19 GHz, making the absorber ultrathin. The conformal behavior of proposed absorber makes it suitable for a lot of practical applications. The proposed absorber is demonstrated to be insensitive to TE and TM polarized EM waves. The absorption of EM waves by the structure is confirmed experimentally through lock-in IR thermography. A temperature increase of 1.5 °C is observed when a microwave source is radiating at the absorbing frequencies as compared with the nonabsorbing frequency. A good agreement between simulation and measured results is seen. The proposed absorber can be used for stealth technology in defense applications, radar applications, and EMI/EMC reduction. The same prototype absorber can be easily extended to multiband applications by introducing additional MCRRs.

References

[1] N. I. Landy, S. S. Sajuyigbe, J. J. Mock, D. R. Smith, and W. J. Padilla, "A perfect metamaterial absorber," *Phys. Rev. Lett.*, vol. 100, pp. 207–402, 2008.

[2] B. Ma *et al.*, "Novel three-band microwave metamaterial absorber," *J. Elect. Wave Appl.*, vol. 28, pp. 113–119, 2014.

[3] S. Bhattacharyya, S. Ghosh and K. V. Srivastava, "Equivalent circuit modeling of an ultra-thin dual-band microwave metamaterial absorber," in *Proc. Asia-Pac. Microw. Conf.*, Sendai, Japan, 2014, pp. 1244–1246.

[4] N. Wang *et al.*, "Novel quadruple-band microwave metamaterial absorber," *IEEE Photon. J.*, vol. 7, no. 1, pp. 1–6, Feb. 2015.

[5] C. Sabah, F. Dincer, M. Karaaslan, E. Unal, and O. Akgol, "Polarization-insensitive FSS-based perfect metamaterial absorbers for GHz and THz frequencies," *Radio Sci.*, vol. 49, no. 4, pp. 306–314, Apr. 2014.

[6] B. X. Wang, X. Zhai, G. Z. Wang, W. Q. Huang, and L. L. Wang, "Design of a four-band and polarization-insensitive terahertz metamaterial absorber," *IEEE Photon. J.*, vol. 7, no. 1, pp. 1–8, Feb. 2015.

[7] S. Bhattacharyya, S. Ghosh, D. Chaurasiya and K. V. Srivastava, "Wide-angle broadband microwave metamaterial absorber with octave bandwidth," *IET Microw., Antennas, Propag.*, vol. 9, no. 11, pp. 1160–1166, Aug. 20, 2015.

[8] N. T. Q. Hoa, P. H. Lam, and P. D. Tung, "Wide-angle and polarization-independent broadband microwave metamaterial absorber," *Microw. Opt. Technol. Lett.*, vol. 59, no. 5, pp. 1157–1161, May 2017.

This article has been accepted for inclusion in a future issue of this journal. Content is final as presented, with the exception of pagination.

[9] Y. Fan *et al.*, "An active wideband and wide-angle electromagnetic absorber at microwave frequencies," *IEEE Antennas Wireless Propag. Lett.*, vol. 15, pp. 1913–1916, 2016.
[10] S. Deepak and C. C. Tripathi, "Broadband ultrathin low-profile metamaterial microwave absorber," *Appl. Phys. A*, vol. 122, no. 4, pp. 1–7, 2016.
[11] J. Tak and J. Choi, "A wearable metamaterial microwave absorber," *IEEE Antennas Wireless Propag. Lett.*, vol. 16, pp. 784–787, 2017.
[12] Y. Z. Cheng *et al.*, "A compact and polarization-insensitive perfect metamaterial absorber for electromagnetic energy harvesting application," in *Proc. Prog. Electromagn. Res. Symp.*, Shanghai, 2016, pp. 1910–1914.
[13] X. Q. Lin, P. Mei, P. C. Zhang, Z. Z. D. Chen, and Y. Fan, "Development of a resistor-loaded ultrawideband absorber with antenna reciprocity," *IEEE Trans. Antennas Propag.*, vol. 64, no. 11, pp. 4910–4913, Nov. 2016.
[14] X. Liu, C. Lan, B. Li, Q. Zhao, and J. Zhou, "Dual band metamaterial perfect absorber based on artificial dielectric 'molecules'," *Sci. Rep.*, vol. 6, pp. 1–6, 2016.
[15] M. Yoo, H. K. Kim, and S. Lim, "Angular- and polarization-insensitive metamaterial absorber using subwavelength unit cell in multilayer technology," *IEEE Antennas Wireless Propag. Lett.*, vol. 15, pp. 414–417, 2016.
[16] H. Zhai, C. Zhan, Z. Li, and C. Liang, "A triple-band ultrathin metamaterial absorber with wide-angle and polarization stability," *IEEE Antennas Wireless Propag. Lett.*, vol. 14, pp. 241–244, 2015.
[17] D. Chaurasiya, S. Ghosh, S. Bhattacharyya, A. Bhattacharya, and K. V. Srivastava, "Compact multi-band polarisation-insensitive metamaterial absorber," *IET Microw., Antennas, Propag.*, vol. 10, no. 1, pp. 94–101, Jan. 9, 2016.
[18] N. Hakla, S. Ghosh, K. V. Srivastava, and A. Shukla, "A dual-band conformal metamaterial absorber for curved surface," in *Proc. URSI Int. Symp. Electromagn. Theory*, Espoo, 2016, pp. 771–774.
[19] S. K. Sharma *et al.*, "Ultra-thin dual-band polarization-insensitive conformal metamaterial absorber," *Microw. Opt. Technol. Lett.*, vol. 59, no. 2, pp. 348–353, Feb. 2017.
[20] N. Mishra, D. Choudhary, R. Chowdhury, K. Kumari, and R. Chaudhary, "An investigation on compact ultra-thin triple band polarization independent metamaterial absorber for microwave frequency applications," *IEEE Access*, vol. 5, pp. 4370–4376 , 2017.
[21] C. Buccella, V. De Santis, and M. Feliziani, "Prediction of temperature increase in human eyes due to RF sources," *IEEE Trans. Electromagn. Compat.*, vol. 49, no. 4, pp. 825–833, Nov. 2007
[22] C. N. Chiu, Y. C. Chang, H. C. Hsieh, and C. H. Chen, "Suppression of spurious emissions from a spiral inductor through the use of a frequency-selective surface," *IEEE Trans. Electromagn. Compat.*, vol. 52, no. 1, pp. 56–63, Feb. 2010.
[23] S. Ghosh and K. V. Srivastava, "Broadband polarization-insensitive tunable frequency selective surface for wideband shielding," *IEEE Trans. Electromagn. Compat.,* vol. 60, no. 1, pp. 166–172, Feb. 2018.
[24] A. K. Singh, M. P. Abegaonkar, and S. K. Koul, "High gain and high aperture efficiency cavity resonator antenna using metamaterial superstrate," *IEEE Antennas Wireless Propag. Lett.*, vol. 16, pp. 2388–2391, 2017.
[25] A. Ebrahimi *et al.*, "Second-order terahertz bandpass frequency selective surface with miniaturized elements," *IEEE Trans. THz Sci. Technol.*, vol. 5, no. 5, pp. 761–769, Sep. 2015.
[26] L. Kurra, M. P. Abegaonkar, and S. K. Koul, "Equivalent circuit model of resonant EBG band stop filter," *IETE J. Res.,* vol. 62, no. 1, pp. 17–26, Jan. 2016.
[27] K. Muzaffar, S. Tuli, and S. Koul, "Determination of polarization of microwave signals by lock-in infrared thermography," *IETE J. Res.*, vol. 62, pp. 81–90, Oct. 2015.

Amit Kumar Singh (S'12) received the master's degree in microwave and optical communication from Delhi Technological University, New Delhi, India, in 2013. Since 2014, he has been working toward the Ph.D. degree at the Centre for Applied Research in Electronics, Indian Institute of Technology Delhi, New Delhi, India.

He was a Student Research Assistant and Teaching Assistant with the Indian Institute of Technology Delhi, India, under the Fellowship of Ministry of Human Resource, Government of India. He was an Assistant Professor with Galgotias University, Greater Noida, India, from 2013 to 2014. His current research interests include microwave metamaterial, high gain antenna design, metasurface lens design, microwave absorber design, and miniaturization of patch antenna.

Mahesh P. Abegaonkar (M'08–SM'13) received the Ph.D. degree in physics (microwaves) from the University of Pune, Pune, India, in 2002.

He was a Postdoctoral Researcher and an Assistant Professor with Kyungpook National University, Daegu, South Korea, during 2002–2005. He is currently an Associate Professor with the Centre for Applied Research in Electronics, Indian Institute of Technology, Delhi. He is currently the Secretary and Treasurer of IEEE MTT-S Chapter under Delhi Section. His current research interests include microwave and millimeter wave antennas, Electromagnetic Band Gap (EBG) and Defected Ground Structures (DGS), microwave metamaterial, and reconfigurable microstrip circuits.

Shiban K. Koul (S'81–M'83–SM'91–F'10) received the B.E. degree in electrical engineering from the Regional Engineering College, Srinagar, India, in 1977, and the M.Tech. and Ph.D. degrees in microwave engineering from the Indian Institute of Technology Delhi, New Delhi, India, in 1979 and 1983, respectively.

He is currently a Chairman of M/S Astra Microwave Pvt. Ltd., Hyderabad, India, where he is involved in the development of RF and microwave systems in India. He is currently a Dr. R. P. Shenoy, Astra Microwave Chair Professor with the Centre for Applied Research in Electronics, Indian Institute of Technology Delhi, and the Deputy Director (strategy & planning, international affairs and research) with the Indian Institute of Technology Jammu, Jammu, India. He has authored or coauthored 350 research papers and 8 state-of-the-art books, and 3 book chapters. He has successfully completed 34 major sponsored projects, 52 consultancy projects, and 48 technology development projects, and holds 9 patents and 6 copyrights. His current research interests include RF MEMS, nonlinear device modeling, microwave and millimeter-wave active and passive circuit design, and reconfigurable microwave circuits including antennas.

Prof. Koul is a Fellow of the Indian National Academy of Engineering, India, and Institution of Electronics and Telecommunication Engineers (IETE), India. He was the recipient of Gold Medal from the Institution of Electrical and Electronics Engineers Calcutta in 1977, the Indian National Science Academy Young Scientist Award in 1986, the International Union of Radio Science Young Scientist Award in 1987, the Top Invention Award in 1991 of the National Research Development Council for his contributions to the indigenous development of ferrite phase shifter technology, the VASVIK Award in 1994 for the development of *Ka*-band components and phase shifters, the Ram Lal Wadhwa Gold Medal in 1995 from the Institution of Electronics and Communication Engineers, the Academic Excellence Award in 1998 from the Indian Government for his pioneering contributions to phase-control modules for the Rajendra Radar, Shri Om Prakash Bhasin Award in 2009 in the field of electronics and information technology, the Teaching Excellence Award in 2012 from Indian Institute of Technology Delhi, the award for Special Recognition of Contributions made to the Growth of Smart Materials Technology in 2012 by the Institute of Smart Materials and Systems, ISSS, Bangalore, the VASVIK Award in 2012 for contributions to the area of information, communication and technology, the M. N. Saha Memorial Award in 2013 for the best application oriented paper from the IETE, and the Distinguished Educator Award in 2014 from the IEEE MTT-S Society. He served as a Distinguished IEEE Microwave Theory and Techniques Lecturer for 2012–2014 and a Distinguished Microwave Lecturer Emeritus for 2015. He has been an elected AdCom member of the IEEE MTT-S society since 2010.

Journal of Management Research
Vol. 18, No. 2, April-June 2018, pp. 90-101

Effect of Goal Orientation on Job Performance

Moderating Effect of Situational Strength at Work

Shivganesh Bhargava and Harsh Pradhan

Abstract

The purpose of the study is to examine the effects of types of goal orientation (performance and mastery) on two types of job performance (task and adaptive). These effects are expected to be affected by situational factors, conceptualized using situational strength at work. The construct of situational strength at work (SSW) has four facets, consequence, clarity, constraints and consistency. This paper is based upon and contributes to achievement goal theory also known as goal orientation theory. A survey of 868 managers from different organizations in India was undertaken. The results suggested that mastery goal orientation had significant effect on both types of job performance while performance goal orientation had no effect. The relationship of performance orientation and task performance becomes significant at high consequences. Constraints and mastery orientation interact to effect adaptive performance. Paper discusses the contribution of the findings to the literature and their applications.

Keywords: Job Performance, Goal Orientation, Situational Strength

www.IndianJournals.com
Members Copy, Not for Commercial Sale
Downloaded From IP - 14.139.251.107 on dated 29-Jul-2018

INTRODUCTION

To facilitate achievement of organizational goals, enhancement of individual job performance is important. Researchers have found many individual factors like motivation, ability, knowledge and personality effect performance (Boselie, Dietz, & Boon, 2005; Kanfer & Kantrowitz, 2002; Vroom, 1964). One of the predictors that has been studied extensively is goal orientation, which explains why do employees respond differently to different kinds of challenges (VandeWalle, Brown, & Cron, 1999). Achievement goal theory (AGT) suggests that job performance is dependent on goal orientation (van Yperen & Janssen, 2002). Goal orientation (GO) influences affective, behavioral and cognitive reactions of individuals (VandeWalle, 1997). There have been attempts to understand the effect of types of orientation on performance, but research in this area is still equivocal (Sackett, Lievens, Van Iddekinge, & Kuncel, 2017; VandeWalle, Cron, & Slocum Jr, 2001). Therefore, there is a need to further study the effect of goal orientation on performance in work setting.

Hurtz & Donovan (2000) have argued that there is need to look beyond the influence of individual factors on job performance. While examining the individual-performance relationship, the moderating effect of environmental and organizational factors have also been studied (Beaty Jr., Cleveland, & Murphy, 2001; Mischel, 1999). Thus while examining goal orientation-performance relationship, in this study the moderating effect of environmental factors have also been incorporated.

Shivganesh Bhargava
SJMSOM, IIT Bombay, Powai
Mumbai - 400076
Harsh Pradhan
USME, Delhi Technological University
Vivek Vihar-II, Delhi - 110095

Job Performance

Rotundo (2002) conceptualized "job performance as those actions and behaviors that are under the control of the individual and contribute to the

goals of the organization". Job performance is a latent construct of multiple dimensions (Sonnentag, Volmer, & Spychala, 2008). These dimensions are in turn made up of indicators that can be measured. Campbell & Wiemik (2015) in their review identified four dimensions of job performance [a] task performance [b] contextual performance [c] counterproductive work behavior [d] adaptive performance. From the ambidexterity literature (Birkinshaw & Gupta, 2013) we found that a firm has to strike balance between exploitation and exploration. Applying similar concept at the individual level, we can assume an individual has to strike balance especially between task and adaptive performance. Task performance includes role-prescribed behaviors, core tasks and behaviors that maintain technical core (Campbell, 1990; Motowidlo, Borman, & Schmit, 1997). Adaptive performance refers to behaviors which reflect a response to changes in task requirement as well as in their work environment. The changes can occur at task, team or organizational level (Griffin, Neal, & Parker, 2007). Adaptive performance reflects behaviors with competency acquisition and task performance reflects behaviors with competency expression (Shoss, Witt, & Vera, 2012). Allworth & Hesketh (1999) have found adaptive and task performance items to be loaded on different factors, they also have different predictors. Job performance in this study incorporates both adaptive and task performance.

Goal Orientation

In this study, goal orientation is conceptualized in line with VandeWalle(1997) as *'disposition toward developing or demonstrating ability in achievement situations'* (pp. 95). This disposition determines how and when the ability, will transfer into performance-oriented behavior. Achievement goal theory also advises that employees goal orientation affects achievement of performance goals (Janssen & van Yperen, 2004). Goal orientations can be broadly classified into mastery and performance goal orientation (Lee, Hui, Tinsley, & Niu, 2006).

Mastery orientation is also known as learning orientation, it involves acquiring new skills and mastering upcoming tasks. It stems from the *'belief that ability is malleable and can be developed with effort and practice '* (growth mindset) (Porter, 2005, pp. 811). A person with mastery goal orientation approaches tasks as opportunities to enhance skills or to learn something new. The focus is on improving past performance through experimentation and learning from past mistakes. Mastery orientation (GOMO) promotes knowledge development through experimentation and risk-taking. Failure is considered a part of the developmental and learning process. It includes an ongoing examination of how to define and solve problems (Lee et al., 2006).

Performance orientation (GOPO) involves outperforming other individuals at the job. This approach stems from the *'belief that attributes are fixed, concrete and internal entities'* (fixed mindset) (Porter, 2005, pp. 811). People with this mindset want to outperform others (in mastery mindset people compete with themselves) (Dietz, van Knippenberg, Hirst, & Restubog, 2015). A person with a performance goal orientation approaches tasks as opportunities to demonstrate already acquired competence. The focus is to do well on current tasks in order to gain positive judgments or avoid negative judgment. It leads people to focus on demonstrating high levels of ability. Failure of any kind is regarded as a sign of low ability or incompetence. The desire to demonstrate high-performance levels, creates the desire to be efficient or to reduce errors.

Button, Mathieu, & Zajac (1996) provided empirical evidence that these two goal orientations are separate constructs. It is possible for an individual to have both goal orientations simultaneously. An interesting issue is whether these goal orientations may interact if an individual holds both orientations simultaneously. However Patrick, Ryan, & Pintrich (1999) found no evidence of an interaction between these two goal orientations, but rather each goal type exerts a separate main effect on individuals. Thus, consistent with Patrick et al.(1999), in this research individuals are expected to have both mastery and performance goal orientation.

www.IndianJournals.com
Members Copy, Not for Commercial Sale
Downloaded From IP - 14.139.251.107 on dated 29-Jul-2018

Goal Orientation and Performance

Although research on job performance has been conducted for more than five decades, there has been scant research when it needs to be studied from achievement goal theory perspective (Janssen & van Yperen, 2004). Achievement goal theory has been majorly studied in education settings (Porath & Bateman, 2006). This study attempts to study job performance from the achievement goal setting perspective.

VandeWalle, Cron, & Slocum Jr (2001) reported that relationship between goal orientation and performance to be equivocal. Bell & Kozlowski (2002) found performance orientation to be negatively related with performance contradicting (Porath & Bateman, 2006). Lee et al., (2006) found no association between performance orientation and in-role/task performance.

Consistent with Lee et al. (2006) we consider that individual may have both orientations (although one may be dominant or activated at any point in time) and that each orientation may have an independent main effect on performance. Complex tasks may require a mastery goal orientation, whereas simple tasks may be accomplished better when motivated by a performance goal orientation. Both , motivation to improve one's performance (mastery goal orientation) and motivation to perform well relative to others (performance goal orientation) should enhance an employee's job performance (Lee et al., 2006). This study will examine whether both goal orientation types are needed to enhance employee's job performance

Hypothesis 1: Goal orientation (a. mastery b. performance) will be positively related to task performance

Hypothesis 2: Goal orientation (a. mastery b. performance) will be positively related to adaptive performance

Situational Strength at Work

Though both, situation and individual factors affect performance. There has been more focus on personality performance relationship as compared to situation performance relationship (Judge & Ilies, 2002). The reason for this is that '*there is a good deal of confusion concerning how situations should be conceptualized*' (Meyer, Dalal, & Hermida, 2010, pp. 21). Hogan (2009) also agreed that though there exists a specific and valid definition of personality, but such is not the case with the definition of the situation. There have been various attempts to conceptualize structure and nature of the situation, many have highlighted the importance of situational strength to conceptualize the same (Mischel, 1977). Situational strength is defined as '*implicit or explicit cues, provided by entities external to the individual, regarding the desirability of various forms of behavior*' (Meyer et al., 2014, pp. 2). There have been various vague attempts to articulate the construct of situational strength in work context (Judge & Zapata, 2015). Meyer et al., (2014) brought some operational clarity by introducing situational strength at work scale (SSW) (Judge & Zapata 2015, pp. 1150) to conceptualize the situational strength at work context. Hence to conceptualize the work context, we adopted the construct of situational strength at work (SSW). SSW is a multiple facet structure (clarity, consistency, constraints and consequences) which were operationalized by Meyer et al. (2010) to measure situational strength at work. Its measurement was validated by Meyer et al. (2014). They also demonstrated that SSW moderates the effect of personality on organizational citizenship behavior. Definitions of the facets can be found in the appendix. The scale is very new and is yet to be tested in non-western context.

Goal Orientation, Performance, and Situation

VandeWalle et al. (2001) suggested goal orientation should be tested in context instead of a global measurement. People may vary their goal orientation depending on the context. One may be heavily learning oriented in academic fields but not in general. In a given context-specific goal orientations are expected to have stronger relationships with performance. This lack

www.IndianJournals.com
Members Copy, Not for Commercial Sale
Downloaded From IP - 14.139.251.107 on dated 29-Jul-2018

of context explains lack of association of goal orientation with performances in many studies. Hence there is need to study the combined effect of goal orientation and SSW on performance. It is expected that main effect of goal orientation on job performance will be moderated by SSW.

Hypothesis 3: The performance orientation will be more positively associated with task performance when SSW (a. clarity b. consistency c. constraints and d. consequences) is high than when SSW is low.

Hypothesis 4: The mastery orientation will be more positively associated with task performance when SSW (a. clarity b. consistency c. constraints and d. consequences) is high than when SSW is low.

Hypothesis 5: The performance orientation will be more positively associated with adaptive performance relationship when SSW (a. clarity b. consistency c. constraints and d. consequences) is high than when SSW is low.

Hypothesis 6: The mastery orientation will be more positively associated with adaptive performance when SSW (a. clarity b. consistency c. constraints and d. consequences) is high than when SSW is low.

METHODOLOGY

Sample

The questionnaire was prepared in English as it is the second official language of India. The survey was only distributed to executives or managers in various firms. For the pilot study (to check reliabilities of measures) fifty-four responses were collected. For the main study, a total of one thousand and thirty-three responses were received through different mode of data collection. One hundred fifty-eight responses were deleted as they were either incomplete or unengaged (zero variance), or were not from executives. Seven responses were removed from the sample as outliers on the basis of Mahalanobis distance criteria. For the final analysis, we had eight hundred sixty-eight responses. The sample had 84.2% males, the median and mean age was 31 and 33.54 years. 57.1% of the respondents had educational qualification of post-graduation or above. The respondents majorly were from three different sectors manufacturing (31.3%), finance (31.5%), and infrastructure (17.1%).

Measures

There are many measures of job performance, indicating there is confusion about the nomenclature. *"The lack of an agreed-upon nomenclature is striking, and it gives the impression that attempts to explicate the latent structure of performance are quite in disorder"* (Campbell & Wiemik, 2015, pp. 48). Moreover, many measures do not provide a complete range of behaviors, which can account for job performance especially in this age of dynamism (Griffin et al., 2007). Hence, there was need to explore the relevant measures of job performance in context of study. To achieve this we combined (as practiced by Jiwen Song, Tsui, & Law (2007)) items (Table 1) to form a relevant measure of task and adaptive performance in Indian context.

As an alternative to self-reported and supervisor ratings on job performance, Schoorman & Mayer (2007) suggested researchers should ask respondents for their supervisor's assessment of their performance rather than for their own assessment. Hence we asked the question to the employee**;** how would your supervisor have rated you on the following (Table 1) on five points from low (1) to high (5). The factor analysis for combined items of task and adaptive performance gave two factors.

Both goal orientations (performance orientation (GOPO) (α = 0.791) & mastery orientation (GOMO) (α = 0.858)) and SSW were measured using (van Yperen & Janssen, 2002) and (Meyer et al., 2014) respectively. All the measures were on five-point Likert scale. We averaged all the items to generate scores for a construct. The reliabilities, median, standard deviation and correlation between all constructs have been reported in Table 2.

www.IndianJournals.com
Members Copy, Not for Commercial Sale
Downloaded From IP - 14.139.251.107 on dated 29-Jul-2018

Table 1: Factors of Performance

Items	AP	TP
Adaptive Performance		
She/He comes up with ideas to improve core tasks	0.711	
She/He applies innovative ideas	0.822	
She/He develops skills to adapt to changes in core tasks	0.317	
Task Performance		
She/He participates in meetings.		0.465
She/He has knowledge required to get the job done		0.508
She/He expresses him/herself and understands others in writing		0.690
She/He gathers and transmits information appropriately in oral form		0.664
She/He maintains smooth and effective working relationship		0.585
She/He produces quality work, even under time pressures		0.543

Extraction Method: Principal Axis Factoring
Rotation Method: Oblimin with Kaiser Normalization
a. Rotation converged in 7 iterations

The correlations are in italics, S.D = Standard Deviation, Cron α = Cronbach Alpha, Con.= Constraint, Cons. = Consequences, Clar. = Clarity, Consi. = Consistency,AP = Adaptive Performance TP = Task Performance, GOPO = Performance Orientation, GOMO = Mastery Orientation

RESULTS

We used SPSS 18.0 to regress GOPO and GOMO, on task and adaptive performance, to find their main effect on performance. We had a controlled for gender, age and education. Results can be seen in Table 3. Performance orientation has no effect on either of performances. On the other hand, mastery orientation has an effect on both types of performances. This supports hypotheses 1a and 2a.

To test moderation, we used hierarchical moderated regression analysis. All the four facets of SSW (clarity, consistency, consequences and constraints) are tested as moderators. Following Baron & Kenny (1986) in the first step, we regressed all control variables, in second step

Table 2: Descriptive Statistics, Reliability and Correlation

	Mean	S.D	Cron α	Con.	Cons.	Clar.	Consi.	AP	TP	GOPO	GOMO
Con.	2.868	0.820	0.872	*1*							
Cons.	3.336	0.656	0.789	*0.283***	*1*						
Clare.	3.566	0.773	0.887	*-0.120***	*0.191***	*1*					
Consi.	3.467	0.707	0.836	*-0.105***	*0.182***	*0.724***	*1*				
AP	4.011	0.670	0.767	*-0.173***	*0.075**	*0.273***	*0.244***	*1*			
TP	4.075	0.559	0.769	*-0.177***	*0.031*	*0.235***	*0.219***	*0.581***	*1*		
GOPO	3.335	0.662	0.791	*0.180***	*0.223***	*0.152***	*0.146***	*0.102***	*0.094***	*1*	
GOMO	4.182	0.507	0.858	*-0.112***	*0.112***	*0.278***	*0.253***	*0.278***	*0.311***	*0.180***	*1*

Table 3: Main Effect (after controlling for control variables)

Dep Variable	Ind Variable	Estimate	S.E.	C.R.	P value
AP	GOPO	0.052	0.034	1.578	0.122
AP	GOMO	0.271	0.044	8.105	**0.000**
TP	GOPO	0.048	0.028	1.459	0.145
TP	GOMO	0.297	0.036	8.983	**0.000**

AP = Adaptive Performance TP = Task Performance, GOPO = Performance Orientation, GOMO = Mastery Orientation

www.IndianJournals.com
Members Copy, Not for Commercial Sale
Downloaded From IP - 14.139.251.107 on dated 29-Jul-2018

all main effects and in last step the interaction effect. The main effects were mean centered as suggested by Cohen, Cohen, West, & Aiken (2003). The results of hierarchical moderated regression analysis are presented in Table 4. As can be seen from Table 4 we observed significant interaction between (i) GOPO and CQ ($\beta = 0.085$, $p < 0.05$) on TP (ii) GOMO and CO ($\beta = 0.073$, $p < 0.05$) on AP, hence hypothesis 3d and 6c are supported.

Interaction plots for the significant interactions are presented in *Figure* 1 (GOPO*CQ) and *Figure* 2 (GOMO*CO). In the figures Y, X, M, L,0 and H denotes dependent variable, independent variable, moderator, low level (mean-SD), mean and high level (mean + SD) respectively. Using Johnson-Neyman technique for finding the areas of significance we found that effect of performance orientation on task performance becomes significant at ($ZCQ_{standard} > -0.2470$), below this value performance orientation does not significantly affect task performance.

DISCUSSION

The study aimed at assessing the effect of goal orientation on job performance, and moderating effect of situational strength at work therein. We

Table 4: Moderation Effect

		Task Performance			Adaptive Performance		
		β	R^2	ΔR^2	β	R^2	ΔR^2
Step 2	GOPO	0.072**	0.069	0.60	0.065**	0.079	0.077
	CL	0.226***			0.264***		
Step 3	GOPO*CL	0.031	0.070	0.001	0.020	0.080	0.001
Step 2	GOPO	0.076**	0.063	0.054	0.071**	0.066	.064
	CY	0.209***			0.232***		
Step 3	GOPO*CY	0.040	0.064	0.001	-0.009	0.066	0
Step 2	GOPO	0.141***	0.056	0.045	0.140***	0.051	.049
	CO	-0.195***			-0.198***		
Step 3	GOPO*CO	0.044	0.058	0.002	0.005	0.051	0
Step 2	GOPO	0.103***	0.020	0.011	0.094***	0.016	0.014
	CQ	0.019			0.052		
Step 3	GOPO*CQ	0.085**	0.027	0.007	0.018	0.016	0
Step 2	GOMO	0.259***	0.125	0.116	0.222***	0.120	0.118
	CL	0.162***			0.210***		
Step 3	GOMO*CL	0.044	0.127	0.002	0.020	0.120	0
Step 2	GOMO	0.266***	0.123	0.114	0.234***	0.112	0.110
	CY	0.152***			0.182***		
Step 3	GOMO*CY	0.022	0.123	0	-0.003	0.112	0
Step 2	GOMO	0.291***	0.120	0.111	0.226***	0.102	0.100
	CO	-0.140***			-0.147***		
Step 3	GOMO*CO	0.032	0.121	0.001	0.073**	0.107	0.005
Step 2	GOMO	0.305***	0.101	0.092	0.277***	0.082	0.080
	CQ	0.001			0.037		
Step 3	GOMO*CQ	0.032	0.102	0.001	0.026	0.083	0.001

www.IndianJournals.com
Members Copy, Not for Commercial Sale
Downloaded From IP - 14.139.251.107 on dated 29-Jul-2018

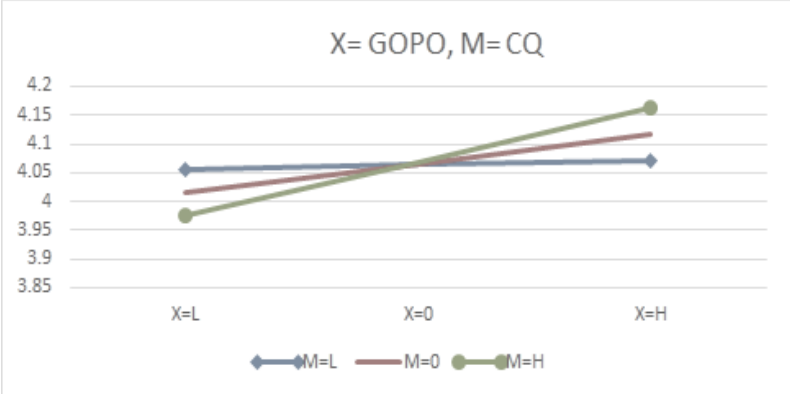

Fig. 1: Interaction give below Performance Orientation and Consequences to Effect Task Performance

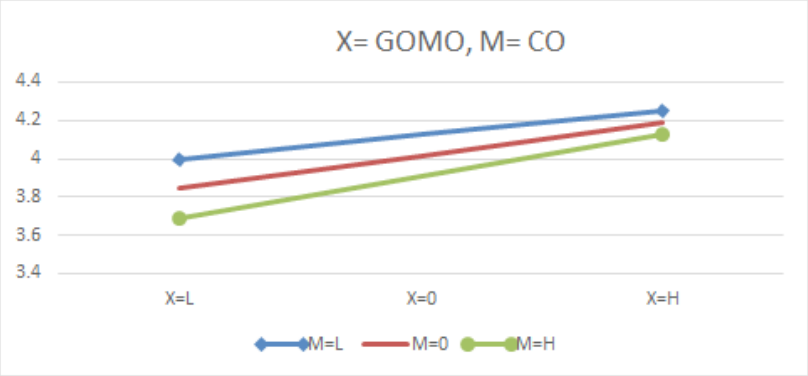

Fig. 2: Interaction between Mastery Orientation and Constraint to Effect Adaptive Performance

found that mastery orientation impacts both adaptive and task performance at managerial/ executive level. In today's dynamic world, it is very difficult to define specifics tasks for the managerial job, a manager has to keep learning, should be ready to experiment and exhibit his mastery orientation.

While studying moderation only two pairs out of sixteen pairs have reported significant moderation. From Table 4 we can see [a] performance orientation - consequence [b] mastery orientation – constraints, showed significant ($p < 0.05$) moderation effect on task performance and adaptive performance respectively.

We can say that the effect of performance orientation on task performance increases as the consequences of the task increases. In other words, the effort to perform, put in by performance oriented person is not much affected by autonomy or constraints at job, but is affected by consequences of the task. The result may be attributed to fact that performance orientation is *"desire to prove one's competence and to gain favorable judgments about it"* (VandeWalle, 1997, pp. 999).

Performance goal orientation would motivate employees to perform well to perform task requirements (Janssen & van Yperen, 2004). An employee with such orientation perceives task requirements as competitive standard to outperform others. Hypothesis 1b posits that performance orientation is positively related to task performance. This hypothesis was not supported.

www.IndianJournals.com
Members Copy, Not for Commercial Sale
Downloaded From IP - 14.139.251.107 on dated 29-Jul-2018

This finding is consistent with (Lee et al., 2006). However, there are studies like (VandeWalle et al., 2001), contradicting our finding. It has been found that even though one may have high GOPO, still he will not be able to perform until he has required knowledge, skill and ability (KSA) for the job (Seijts & Latham, 2005). When an employee has required KSA, a high GOPO employee would be able to give high task performance. As mentioned by Locke & Latham (2002) in a well-defined work environment a performance goal increases task performance. A well-defined work environment consists of clear processes to achieve the task and the employee has been trained to have required KSA to implement the processes. Moreover, if the task to be performed has high consequence, then it is expected that GOPO employee will increase his effort to achieve the task. This postulate has been captured in hypothesis 3d, which has been supported. As far as performance orientation is concerned with external evaluation and appraisals, we expected people with high-performance approach orientation to have better work performance in high-rewarding climates (Izadikhah, Jackson, & Ireland, 2012).

Similarly, mastery orientation is defined as "*entail striving to develop one's skills and abilities, advance one's learning, understand material, or complete or master a task*" (VandeWalle, 1997, pp. 999). Adaptive performance is the ability of an individual to alter behavior in response to new task, environment or situation. As the learning oriented person promotes his knowledge development, it is expected that GOMO will positively affect adaptive performance. Bell & Kozlowski (2008) found GOMO operates through increased task-relevant knowledge to affect adaptive performance. Coget (2010) found sales performance to be better for LGO employee. LGO is associated with a variety of adaptive behaviors like a high level of self-efficacy, setting high goals and persisting in adversity (Payne et al., 2007). In a review, Jundt, Shoss & Huang (2014) established LGO as a predictor of adaptive performance. In line with the literature, we find support for hypothesis 2a, where LGO is positively related to adaptive performance.

The effort put in by a mastery-oriented person, is not much affected by autonomy or consequences at the job but is affected by constraints. A mastery orientation person will put more efforts to counter the obstacles (Payne, Youngcourt, & Beaubien, 2007). Employee view such oppositions as challenges and increase their efforts. Hence hypothesis 6c is supported, the effect of mastery orientation on adaptive performance would be more in high constraints job. However, if employee has high mastery orientation, constraints will not affect performance much.

Managerial Implications

This study testifies the combined effect of situational factors and goal orientation on job performance. Selection criteria for managers should give more preference to mastery orientation than performance orientation. This stems from the result that performance orientation does not affect performance.

An organization should look to hire people according to the situations that are prevalent in the company. If there are lots of constraints (internal or external) in the organization, then high mastery oriented person should be hired. In case of management attaches set of incentives for any managerial task, then high performance oriented person should be preferred for that task (though for managerial jobs, mastery orientation is also required). If person with low-performance orientation is hired, then increase in incentives will decrease his/her performance.

Theoretical Implications

According to the framework of theoretical contribution by Colquitt & Zapata-Phelan (2007), this study qualifies as an expander, which actually refines and tests the theory by hypothetico-empirical methods. Expanders explore the moderators that identify the boundary conditions of theory.

This study makes contribution to achievement goal theory [AGT] by refining the goal orientation - job

www.IndianJournals.com
Members Copy, Not for Commercial Sale
Downloaded From IP - 14.139.251.107 on dated 29-Jul-2018

performance relationship. The basic contention of AGT is depending on its subjective purposes achievement goals influence task achievement via variations in self-regulation (Covington, 2000). We here present some contribution of application of AGT while studying performance.

Locke & Latham (2006) identified feedback, importance of goal and task complexity as moderator of goal orientation and performance relationship. However, in this study importance of goal (referred as consequences in this study) is moderator of GOPO-performance and not for GOMO-performance relationship. Similarly, task complexity (inferred as constraints) is moderator of only GOMO-performance and not for GOPO-performance relationship. Moreover, at higher level of GOMO the effect of constraints on performance is reduced.

The study has been conducted in different context, as most of the studies have been conducted in western countries. Even the existing studies in work context have been majorly for blue collar jobs. The present study contributes to AGT by providing a non-western perspective, by using a sample of white-collar Indian employees.

In literature goal orientations have been associated with performance in various contexts and results have been mixed. Debicki, Kellermanns, & Barnett (2016) found no association between GOMO and academic performance, and positive association between GOPO and academic performance, contrary to the finding of Richardson & Remedios (2014). Brett & VandeWalle (1999) found only GOMO to be related to training performance. Bell & Kozlowski (2002) found performance orientation to be negatively related with performance contradicting (Porath & Bateman, 2006). Lee et al. (2006) found no association between performance orientation and in-role/task performance.

In relationship with goal orientation, till now performance has been studied majorly as a unidimensional (with some exception (Janssen & van Yperen, 2004)) construct. In this study, we have studied two dimensions of performance and have identified moderators for their relationship with two types of goal orientation.

Finally, from literature, one can infer that in an organization setting, the relationship of GOMO and performance is well established. However the GOPO performance relationship is equivocal (VandeWalle et al., 2001). In this study also we find that GOPO performance relationship is not significant ($p<0.05$), however, it becomes significant ($p <0.05$) when consequences (as defined in appendix) of job are high.

Direction for Future Research

The findings in this study are subject to a number of caution needs to be exercised while interpreting the results. First, the cross-sectional design of the present study does not allow us to determine the direction of causality among the variables. In future, longitudinal studies are suggested for assessment of causality.

Our results may partly be influenced by common method variance as all data were collected through self-report. Although most studies in the field rely predominantly on self-reports. Future research should replicate the findings of this study, ideally, on outcomes measured through methods other than self-report. This study has used a generic measure of job performance. If there are enough number of respondents, a specific measure of job performance can be used, to have greater internal consistency of findings. As the data collected was only from organizations in western India, the generalizability of results cannot be assured.

Another interesting domain would be to test effects of individual, organization and other contextual variables on various relationships. To further understand the effect of GOPO on performance further research should bifurcate GOPO into performance approach and performance avoidance goal orientation. Previous researchers found different effects of these two type of orientations on performance (Van Yperen, Blaga, & Postmes, 2015)

www.IndianJournals.com
Members Copy, Not for Commercial Sale
Downloaded From IP - 14.139.251.107 on dated 29-Jul-2018

CONCLUSION

Previous studies testing goal orientation performance orientation have been majorly in an academic setting (Porath & Bateman, 2006). The current study is in an organizational setting and extends goal setting theory by identifying the boundaries of performance orientation-performance relationship, which has been equivocal till now. The study identifies the condition under which performance goal orientation-job performance relationship changes from insignificant to significant, keeping other variables unchanged. The relationship between mastery orientation and performance has been found significant, supporting the contemporary literature on goal setting. To our knowledge, the findings of an interaction between two pairs [a] performance orientation- consequence on task performance [b] mastery orientation – constraints on adaptive performance are unique. This moderation highlights the effect of the situation on goal orientation-performance relationship. This is one of the rare studies where the simultaneous effect of goal orientation on both types of performance has been seen and respective strength of relationship have been reported.

REFERENCES

Allworth, E., & Hesketh, B. (1999). Construct-oriented biodata :Capturing change-related and contextually relevant future performance. *International Journal of Selection and Assessment*, *7*(2), 97–111. doi:10.1111/1468-2389.00110

Baron, R. M., & Kenny, D. A. (1986). The moderator-mediator variable distinction in social psychological research: Conceptual, strategic, and statistical considerations. *Journal of Personality and Social Psychology*, *51*(6), 1173–1182. doi:10.1037/0022-3514.51.6.1173

Beaty Jr., J. C., Cleveland, J. N., & Murphy, K. R. (2001). The relation between personality and contextual performance in "strong" versus "weak" situations. *Human Performance*, *14*(2), 125–148. doi:10.1207/S15327043HUP1402

Bell, B. S., & Kozlowski, S. W. J. (2002). Goal orientation and ability: Interactive effects on self-efficacy, performance, and knowledge. *Journal of Applied Psychology*, *87*(3), 497–505.

Birkinshaw, J., & Gupta, K. (2013). Clarifying the distinctive contribution of ambidexterity to the field of organization studies. *Academy of Management Perspectives*, *27*(4), 287–298.

Boselie, P., Dietz, G., & Boon, C. (2005). Commonalities and contradictions in research on human resource management and performance. *Human Resource Management Journal*, *15*(3), 67–94. doi:10.1111/j.1748-8583.2005.tb00154.x

Brett, J. F., & VandeWalle, D. (1999). Goal orientation and goal content as predictors of performance in a training program. *Journal of Applied Psychology*, *84*(6), p.863.

Button, S., Mathieu, J., & Zajac, D. (1996). Goal orientation in organizational research: A conceptual and empirical foundation. *Organizational Behavior and Human Decision Processes*, *67*(1), 26–48.

Campbell, J. P. (1990). Modeling the performance prediction problem in industrial and organizational psychology. In M. Dunnette & L. M. Hough (Eds.), *Handbook of Industrial and Organizational Psychology* (Second, 687 – 732). Palo Alto: Consulting Psychologist Press.

Campbell, J. P., & Wiernik, B. M. (2015). The modeling and assessment of work performance. *Annual Review of Organizational Psychology and Organizational Behavior*, *2*(1), 48. doi:10.1146/annurev-orgpsych-032414-111427

Coget, J. (2010). Performance orientation or learning orientation: Which helps salespeople better adapt to organizational change? *Academy of Management Perspectives*, *24*(3), 106–108.

Cohen, J., Cohen, P., West, S. G., & Aiken, L. S. (2003). *Applied Multiple Regression Correlation Analysis For The Behavioral Sciences*. (D. Riegert & J. Planer, Eds.) (Third). London: Lawrence Erlbaum Associates.

Colquitt, J. A., & Zapata-Phelan, C. P. (2007). Trends in theory building and theory testing: A five-decade study of the Academy of Management Journal. *Academy of Management Journal*, *50*(6), 1281–1303.

Covington, M. V. (2000). Goal theory, motivation, and school achievement: An integrative review. *Annual Review of Psychology*, *51*, 171–200. doi:10.1146/annurev.psych.51.1.171

www.IndianJournals.com
Members Copy, Not for Commercial Sale
Downloaded From IP - 14.139.251.107 on dated 29-Jul-2018

Debicki, B., Kellermanns, F., & Barnett, T. (2016). Beyond the big five: The mediating role of goal orientation in the relationship between core self-evaluations and academic performance. *The International Journal of Management Education*, *14*(3), 273–285.

Dietz, B., van Knippenberg, D., Hirst, G., & Restubog, S. L. D. (2015). Outperforming whom? A multilevel study of performance-prove goal orientation, performance, and the moderating role of shared team identification. *Journal of Applied Psychology*, *100*(6), 1811–1824. doi:10.1037/a0038888

Griffin, M. A., Neal, A., & Parker, S. (2007). A new model of work role performance: Positive behavior in uncertain and interdependent contexts. *Academy of Management Journal*, *50*(2), 327–347. doi:10.5465/amj.2007.24634438

Hogan, R. (2009). Much ado about nothing: The person-situation debate. *Journal of Research in Personality*, *43*(2), p.249. doi:10.1016/j.jrp.2009.01.022

Hurtz, G. M., & Donovan, J. J. (2000). Personality and job performance: The big five revisited. *Journal of Applied Psychology*, *85*(6), 869–879. doi:10.1037/0021-9010.85.6.869

Izadikhah, Z., Jackson, C., & Ireland, M. J. (2012). Effect of context on performance approach orientation. *American Journal of Psychology*, *125*(2), 193–207. doi:10.5406/amerjpsyc.125.2.0193

Janssen, O., & van Yperen, N. W. (2004). Employees' goal orientations, the quality of leader-member exchange, and the outcomes of job performance and job satisfaction. *Academy of Management Journal*, *47*(3), 368–384.

Judge, T. A., & Ilies, R. (2002). Relationship of personality to performance motivation: A meta-analytic review. *Journal of Applied Psychology*, *87*(4), 797–807. doi:10.1037/0021-9010.87.4.797

Judge, T. A., & Zapata, C. P. (2015). The person-situation debate revisited: Effect of situation strength and trait activation on the validity of the big five personality traits in predicting job performance. *Academy of Management Journal*, *58*(4), 1149–1179. doi:10.5465/amj.2010.0837

Jundt, D. K., Shoss, M. K., & Huang, J. L. (2014). Individual adaptive performance in organizations: A review. *Journal of Organizational Behavior*, *36*(S1), S53–S71. doi:10.1002/job.1955

Kanfer, R., & Kantrowitz, T. M. (2002). Ability and Non-ability predictors of job performance. In S. Sonnentag (Ed.), *Psychological Management Of Individual Performance Management* (27–50). John Wiley & Sons Inc.

Lee, C., Hui, C., Tinsley, C., & Niu, X. (2006). Goal orientations and performance: Role of temporal norms. *Journal of International Business*, *37*(4), 484–498.

Locke, E. A., & Latham, G. P. (2006). New directions in goal-setting theory. *Current Directions in Psychological Science*, *15*(5), 265–268.

Meyer, R. D., Dalal, R. S., & Hermida, R. (2010). A review and synthesis of situational strength in the organizational sciences. *Journal of Management*, *36*(1), 121–140. doi:10.1177/0149206309349309

Meyer, R. D., Dalal, R. S., José, I. J., Hermida, R., Chen, T. R., Vega, R. P., … Khare, V. P. (2014). Measuring job-related situational strength and assessing its interactive effects with personality on voluntary work behavior. *Journal of Management*, *40*(4), 1010–1041. doi:10.1177/0149206311425613

Mischel, W. (1977). The interaction of person and situation. In D. Magnusson & N. S. Endler (Eds.), *Personality at the crossroads: Current issues in interactional psychology* (pp. 333–352). Hillsdale, NJ: Laurence Earlbaum Associates.

Mischel, W. (1999). Implications of person–situation interaction: Getting over the field's borderline personality disorder. *European Journal of Personality*, *13*(5), 455–461.

Motowidlo, S. J., Borman, W. C., & Schmit, M. J. (1997). A theory of individual differences in task and contextual performance. *Human Performance*, *10*(2), 71–83. doi:10.1207/s15327043hup1002_1

Patrick, H., Ryan, A., & Pintrich, P. (1999). The differential impact of extrinsic and mastery goal orientations on males' and females' self-regulated learning. *Learning and Individual Differences*, *11*(2), 153–171.

Payne, S. C., Youngcourt, S. S., & Beaubien, J. M. (2007). A meta-analytic examination of the goal orientation nomological net. *Journal of Applied Psychology*, *92*(1), p.128.

Porath, C. L., & Bateman, T. S. (2006). Self-regulation: From goal orientation to job performance. *Journal of Applied Psychology*, *91*(1), 185–192. doi:10.1037/0021-9010.91.1.185

www.IndianJournals.com
Members Copy, Not for Commercial Sale
Downloaded From IP - 14.139.251.107 on dated 29-Jul-2018

Porter, C. O. L. H. (2005). Goal orientation: Effects on backing up behavior, performance, efficacy, and commitment in teams. *Journal of Applied Psychology*, *90*(4), 811–818.

Richardson, J. T. E., & Remedios, R. (2014). Achievement goals, approaches to studying and academic attainment. In D. Gijbels, V. Donche, J. T. E. Richardson, & J. D. Vermunt (Eds.), *Learning patterns in Higher Education: Dimensions and Research Perspectives* (pp. 125–140).

Rotundo, M. (2002). *Defining and Measuring Individual Level Job Performance: A Review and Integration (Thesis)*. University of Toronto.

Sackett, P. R., Lievens, F., Van Iddekinge, C. H., & Kuncel, N. R. (2017). Individual differences and their measurement: A review of 100 years of research. *Journal of Applied Psychology*, *102*(3), p.254.

Schoorman, F. D., & Mayer, R. C. (2007). The value of common perspectives in self-reported appraisals: You get what you ask for. *Organizational Research Methods*, *11*(1), 148–159. doi:10.1177/1094428107307168

Seijts, G. H., & Latham, G. P. (2005). Learning versus performance goals : When should each be used ? *Acadmey of Management Executive*, *19*(1), 124–131.

Shoss, M. K., Witt, L. A., & Vera, D. (2012). When does adaptive performance lead to higher task performance? *Journal of Organizational Behavior*, *33*(7), 910–924. doi:10.1002/job.780

Song, L. J., Tsui, A. S., & Law, K. S. (2007). A review and synthesis of situational strength in the organizational sciences. *Journal of Management*, *35*(1), 56–93. doi:10.1177/0149206308321544

Sonnentag, S., Volmer, J., & Spychala, A. (2008). Job Performance. In J. Barling & C. L. Cooper (Eds.), *Sage Handbook of Organizational Behavior:Micro Perspectives* (pp. 427–447). New Delhi, India: SAGE Publications.

Van Yperen, N. W., Blaga, M., & Postmes, T. (2015). A meta-analysis of self-reported achievement goals and nonself-report performance across three achievement domains. *Human Performance*, *April*, 165–182. doi:10.1371/journal.pone.0093594

van Yperen, N. W., & Janssen, O. (2002). Fatigued and dissatisfied or fatigued but satisfied? Goal orientations and responses to high job demands. *Academy of Management Journal*, *45*(6), 1161–1171. doi:10.2307/3069431

VandeWalle, D. (1997). Development and validation of a work domain goal orientation instrument. *Educational and Psychological Measurement*, *57*(6), 995–1015.

VandeWalle, D., Brown, S., & Cron, W. (1999). The influence of goal orientation and self-regulation tactics on sales performance: A longitudinal field test. *Journal of Applied Psychology*, *84*(2), p.249.

VandeWalle, D., Cron, W. L., & Slocum Jr, J. W. (2001). The role of goal orientation following performance feedback. *Journal of Applied Psychology*, *86*(4), 629–640.

Vroom, V. H. (1964). *Work and Motivation*. New York: Wiley.

www.IndianJournals.com
Members Copy, Not for Commercial Sale
Downloaded From IP - 14.139.251.107 on dated 29-Jul-2018

APPENDIX

Definition of SSW facets (taken from (Judge & Zapata, 2015, 1150))

- Clarity: *Extent to which one's job responsibilities are readily available and easy to understand*
- Constraints: *Extent to which an employee's freedom to make decisions or take action on the job is limited by outside forces.*
- Consistency: *Degree to which one's job responsibilities are compatible with one other*
- Consequences: *The extent to which an employee's decisions or actions have significant implications for relevant stake holder*

This article has been accepted for inclusion in a future issue of this journal. Content is final as presented, with the exception of pagination.

Electron Acceleration by a Relativistic Electron Plasma Wave in Inverse-Free-Electron Laser Mechanism

Monika Yadav, Suresh C. Sharma, and Devki Nandan Gupta

***Abstract*— It has been revealed that a relativistic plasma wave, having an extremely large electric field, may be utilized for the acceleration of plasma particles. The large accelerating field gradient driven by a plasma wave is the basic motivation behind the acceleration mechanism. Such a plasma wave can be excited by a single laser in the form of wakefield in laser–plasma interactions. In this paper, we study the enhancement of electron acceleration by plasma wave in the presence of a wiggler magnetic field. Electrons trapped in the plasma wave are accelerated due to the additional resonance provided effectively by the wiggler field, which contributes in large energy gain of electrons during acceleration. The resonant enhancement of electron acceleration by the wiggler magnetic field has been validated by single particle simulations. The dependence of energy gain on plasma wave amplitude, initial electron energy, wiggler magnetic field strength has been investigated. Using the model, the involvement and importance of inverse free-electron laser mechanism in electron acceleration by the plasma wave was analyzed. A scaling law for electron energy optimization was proposed for future electron accelerator development.**

***Index Terms*— Inverse-free-electron laser (IFEL), laser wakefield accelerator (LWFL), plasma wave.**

I. Introduction

THE generation of high-intensity laser pulses ($\geq$10 TW) has led to the development of laser-driven electron acceleration and electromagnetic radiation generation in plasmas and free-electron laser (FEL) [1]–[5]. Large amplitude plasma wave has been considered a potential mode for accelerating charged particles. It was first proposed in 1979 by Tajima and Dawson that the plasma wakefield can be excited due to the ponderomotive force generated by high-intensity laser and plasma interactions [6]. Relativistic electrons [7] from plasma background (or injected from outside) can get trapped [8] in the wakefield and accelerated to very high energies (on the order of gigaelectronvolt) [9]. These large amplitude plasma waves can be generated through different accelerator schemes [10]–[13] such as the plasma beat-wave accelerator (PBWA), the laser wakefield accelerator (LWFA), the self-modulated LWFA and the plasma wakefield accelerator. LWFA scheme utilizes a single laser pulse to generate the plasma wakefield. In PBWA, two laser pulses with frequency difference comparable to the plasma wave frequency are used to excite a large amplitude plasma wave.

Everett *et al.* [14] observed the electron energy gain of 28 MeV when 2-MeV electrons are injected in to the plasma wave, where the plasma wave is excited by beating of two laser beams in hydrogen plasma. Modena *et al.* [15] observed the electron energy gain of 44 MeV at wave-breaking and a sudden increase in number of accelerated plasma electrons also. In this scheme, the electron gain is limited by wave particle dephasing, which can be addressed using surfatron concept. Leemans *et al.* [16] have experimentally demonstrated the high-quality electron bunches of energy of 1 GeV using a plasma channel guided laser. It has also been observed theoretically that the electron gain can be increased by imposing a transverse [17] and oblique [18] magnetic field to the plasma wave. This prevents the electron to outrun the wave and thus the electron remains in phase with it. A model has also been developed for azimuthal magnetic field to study the electron acceleration by plasma wave in its presence [19], [20]. Gahn *et al.* [21] experimentally measured multi millielectronvolt electrons in high-density gas jet using 1.2-TW power, 200-fs laser pulses and verified it by 3-D PIC simulation. Kaur and Gupta [22] studied the increment in electron acceleration by plasma wave in an ion channel in presence of guiding azimuthal magnetic field.

Inverse-FEL (IFEL), as a vacuum acceleration process, was first proposed by Palmer [23] in 1972. IFEL acceleration experiments were performed at brookhaven national laboratory using CO_2 laser in 1990s [24]. In an IFEL, the electron beam and the laser both co-propagate through a magnetic array called wiggler. Here, energy is transferred from laser beam to electrons, contrary to FEL. For the maximum transfer of energy from laser to electrons, the IFEL resonance condition [25] is given by $\lambda_l \approx (1 + b_w^2)\lambda_w/2\gamma^2$, where λ_l is the laser wavelength, λ_w is the wiggler wavelength, b_w is the wiggler field amplitude, and γ is the Lorentz factor. Mirzanejhad *et al.* [26] examined the electron bunch acceleration using circularly polarized laser pulse in helical wiggler. Hartemann *et al.* [27] have demonstrated the increment in the IFEL interaction bandwidth and the energy gain by using

Manuscript received March 20, 2018; revised May 7, 2018; accepted May 27, 2018. This work was supported by the University Grant Commission, Delhi, Government of India for JRF fellowship to Monika Yadav. The review of this paper was arranged by Senior Editor C. A. Ekdahl. *(Corresponding author: Devki Nandan Gupta.)*

M. Yadav and S. C. Sharma are with the Department of Applied Physics, Delhi Technological University, Delhi 110086, India (e-mail: suresh321sharma@gmail.com).

D. N. Gupta is with the Department of Physics and Astrophysics, University of Delhi, New Delhi 110007, India (e-mail: dngupta@physics.du.ac.in).

Color versions of one or more of the figures in this paper are available online at http://ieeexplore.ieee.org.

Digital Object Identifier 10.1109/TPS.2018.2843362

0093-3813 © 2018 IEEE. Personal use is permitted, but republication/redistribution requires IEEE permission.
See http://www.ieee.org/publications_standards/publications/rights/index.html for more information.

This article has been accepted for inclusion in a future issue of this journal. Content is final as presented, with the exception of pagination.

ultrashort and super intense laser pulse. Good focusing and high-quality electron beams in IFEL makes it suitable for advanced light sources, next linear collider, and biomedical applications. One of the major drawbacks of this acceleration process is the electron wave dephasing. Diffraction of laser pulse over the IFEL length is also a limiting factor. With the increase in the electron energy gain, FEL resonance condition no longer holds. One of the ways to prevent this discrepancy is to taper the wiggler period [28] or using chirped laser pulse. Kumar and Yoon [29] investigated the combined effect of chirped laser pulse and tapered wiggler on the electron acceleration and hence explained dependence of electron energy on these parameters. Electron capture and high accelerating gradient of monoenergetic electron beam using IFEL was first shown by Duris *et al.* [30] in 2014. In this case, energy gain >20 MeV was demonstrated using laser pulse of intensity $\sim 10^{13}$ W/cm^2 and a tapered undulator of length 0.5 m.

In this paper, we, first time, use the IFEL mechanism to study the electron acceleration using a relativistic plasma wave. Here, in order to overcome the above-mentioned drawbacks of laser in IFEL, the plasma wave has been used to accelerate the electrons. A transverse velocity component is provided by the wiggler field, which further enhances the longitudinal momentum to accelerate the electrons considerably. The transverse motion of electrons is stabilized using the focusing property of wiggler field. The FEL arrangement prevents the accelerated electrons to escape and thus, helps to extract electrons when required.

This paper has been divided into four sections. In Section II, the electron dynamics has been discussed analytically using energy and momentum equations. Single particle MATLAB code has been utilized to validate the theoretical model. The dependence of various plasma wave and wiggler parameters on electron acceleration has been examined in Section III. Scaling laws have also been given for optimization of electron energy to obtain efficient electron acceleration. Plasma wave intensity, wiggler magnetic field, wiggler period, and tapering parameter have been optimized to overcome the dephasing limits and to attain substantial electron acceleration. We draw the conclusion in Section IV.

II. Mathematic Formulation

In an underdense plasma when an intense enough laser pulse is propagated, the electrons are expelled from the high intensity region creating a density depression on the axis of the laser. It leads to the nonuniform plasma frequency across the laser cross section. Thus, considering a nonlinear profile [13], [31] of plasma wave propagating in the z-direction as

$$\mathbf{E}_p = \mathbf{A} e^{-x^2/r_p^2} \left(\hat{z} \cos\eta + \hat{x} e^{-x^2/r_p^2} \frac{2x}{k r_p^2} \sin\eta \right) \tag{1}$$

where r_p is the radius of the wakefield, $\eta = (\omega t - kz + \delta)$ is the phase of the plasma wave, δ is the initial phase, and the potential ϕ of the wave can be calculated using $\mathbf{E} = -\nabla\phi$. Here, E_p can be written as $\mathbf{E}_p = \mathbf{E}_x\hat{x} + \mathbf{E}_z\hat{z}$ for our convenience.

We also assume a planar tapered wiggler magnetic field given by

$$\mathbf{B}_w = \hat{x} B_{0w} \sin[k_w z/(1+\alpha z)] \tag{2}$$

where B_{0w} represents the wiggler magnetic field, k_w is the wiggler wavenumber, α is the tapering parameter along the z-axis, and the wiggler magnetic field is polarized in the x-direction. The value of wiggler wavenumber k_w is optimized using the resonance condition. This condition shows a unique relation between wiggler wavelength (Λ_w), laser wavelength (Λ_l), wiggler magnetic field amplitude (B_{0w}), and electron energy gain (γmc^2). Hence, the deviation from the resonance condition limits the electron energy gain.

In the presence of plasma wave and the wiggler magnetic field, the governing energy and momentum equations are given by

$$\frac{d\mathbf{p}}{dt} = -e(\mathbf{E}_p + \mathbf{v} \times \mathbf{B}) \tag{3}$$

$$(mc^2)\frac{d\gamma}{dt} = -e(\mathbf{E}_p \cdot \mathbf{v}) \tag{4}$$

respectively, where $\mathbf{p} = \gamma m\mathbf{v}$ is the electron momentum, γmc^2 is the electron energy, and $\gamma^2 = 1 + (p_x^2 + p_y^2 + p_z^2/m^2c^2)$ stands for the relativistic gamma factor. Substituting the plasma wave and the wiggler fields from (1) and (2) in energy and momentum equations and writing them in components, we get

$$\gamma \frac{dv_x}{dt} = \left(v_x^2 - 1\right)a_x + v_x v_z a_z \tag{5}$$

$$\gamma \frac{dv_y}{dt} = -v_z b_w + v_x v_y a_x + v_y v_z a_z \tag{6}$$

$$\gamma \frac{dv_z}{dt} = \left(v_z^2 - 1\right)a_z + v_x v_z a_x + v_y b_w \tag{7}$$

$$\frac{d\gamma}{dt} = -v_x a_x - v_z a_z. \tag{8}$$

Equations (5)–(8) are normalized using dimensionless physical quantities as: $t \to \omega t$, $x \to kx$, $z \to kz$, $v_x \to v_x/c$, $v_z \to v_z/c$, $k_w \to ck_w/\omega_p$, $\alpha \to \alpha/k$, $a_x = eE_x/m\omega c$, $a_z = eE_z/m\omega c$, $a_p = eE_p/m\omega c$, $b_w = eB_w/m\omega$, where $-e$ and m are electron charge and mass, respectively. Equations (5)–(8) are ordinary coupled differential equations describing relativistic electron dynamics. These equations have been solved numerically using a relativistic single-particle code.

III. Numerical Results and Discussion

We numerically solve the relativistic equations of motion and the energy equation using the fourth order Runge–Kutta method in MATLAB with adaptive step size. The dimensionless parameters have been used for the calculations. Electron acceleration and energy gain have been estimated for distinct plasma and wiggler parameters. These parameters are optimized to get the maximum acceleration. We consider a plasma wave with the normalized amplitude of $a_p = 0.3$ and the wavelength of 3.3 μm. The optimized value of normalized plasma wave spot size is 40. The wiggler parameters have been optimized as: the normalized wiggler magnetic field strength is $b_w = 0.06$ (corresponds to the tapered wiggler

This article has been accepted for inclusion in a future issue of this journal. Content is final as presented, with the exception of pagination.

field of 2 KG), the wiggler period is $\Lambda_w = 3.07$ cm, and the tapering parameter is $\alpha = 9 \times 10^{-3}$. The electron is assumed to be originated at $(x_0, y_0, z_0) = (0, 0, 0.2)$ with the initial velocity components $(v_{x0}, v_{y0}, v_{z0}) = (0, 0, 0.92c)$. The electron trajectories and the variation of electron energy gain with different numerical parameters have been investigated and discussed in this section. In our study, we observed that the plasma wave gives an initial kick to the electrons by transferring the energy. The tapered wiggler magnetic field sustains the energy gain resonantly due to its longer wavelength.

IFEL concept has already been proposed and investigated as an efficient source of electron beam. Laser pulse has been utilized to accelerate electrons in IFEL mechanism till now. To maintain the IFEL resonance condition over the interaction region, effect of tapering of magnetic wiggler and chirping of laser pulse has also been studied. And it has been observed that these parameters are quite effective in enhancing the electron energy gain. The maximum electron energy gain (without taking chirping parameter in to account) recorded is approximately 200 MeV [29]. Because, confining the high-intensity laser beam over the acceleration region is a major challenge. Diffraction also limits the acceleration length. To overcome these issues, we here propose to study the electron acceleration by the plasma wave instead of the laser pulse in the presence of magnetic wiggler. The electron Larmor frequency for the used wiggler magnetic field is very less compare to the pump frequency. Thus, the dispersion relation of the plasma wave may not be affected for this strength of the magnetic field. The smaller magnetic field justifies avoiding the modification in plasma wave dispersion relation. Enhancement in electron energy has been confirmed from the results (∼400 MeV) to validate our proposed idea for feasible numerical parameters.

The plasma wave is one of the major source for electron energy gain. Thus, the plasma wave amplitude plays a crucial role in this mechanism. Fig. 1(a) shows the electron energy during acceleration for different plasma wave amplitudes ($a_p = 0.25$, 0.3, and 0.4). For these estimations, the initial electron energy $\gamma_0 mc^2 = 2.5$ MeV is considered for the corresponding initial electron velocity $v_{z0} = 0.92c$. It could easily be understood by momentum equations that the electrons trapped in high-intensity plasma waves experience a stronger longitudinal force (in the direction of propagation of the plasma wave). Thus, in a result, the electrons are accelerated to higher energies due to the dominant ponderomotive effects. Higher electron energy gain is predicted for large amplitude plasma wave in this mechanism. However, the electron acceleration would be limited due to the wave-breaking related nonlinearity.

The optimum ratio of wiggler to plasma wavelength (Λ_w/Λ_p) also plays a significant role in electron energy gain. In Fig. 1(b), the electron energy gains for different ratios of wiggler to plasma wavelength ($\Lambda_w/\Lambda_p = 1/9320$, 1/7320, and 1/5320) have been estimated. Other optimized wiggler parameters are kept same as shown in Fig. 1(a). It can be noted that the electron energy increases with the wiggler wavelength. This is due to the fact of interaction length enhancement for larger wiggler wavelength to sustain the resonant oscillations

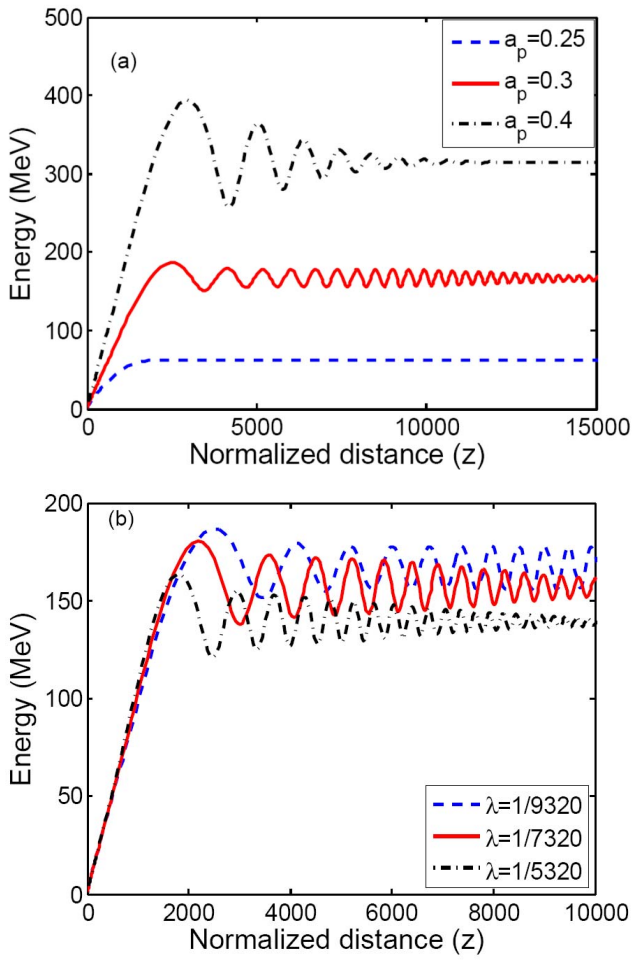

Fig. 1. (a) Electron energy (γmc^2 in MeV) as a function of normalized distance (z) for $a_p = 0.25$ (blue curve), $a_p = 0.3$ (red curve), $a_p = 0.4$ (green curve) and (b) corresponding electron energy (γmc^2 in MeV) for electrons originated at position of $z_0 = 0.2$ for different values of $\lambda = \Lambda_w/\Lambda_p = 1/9320$ (blue curve), 1/7320 (red curve), and 1/5320 (green curve) for wiggler magnetic field strength of $b_w = 0.06$. Other parameters are, $\alpha = 9 \times 10^{-3}$, $a_p = 0.3$, $\delta = 0$, $v_{z0} = 0.9c$, and $\gamma_0 mc^2 = 2.5$.

for longer time. This means that the electron can stay in the interaction region longer for the larger wiggler wavelength. Eventually, the electrons energy may be increased.

Electrons trapped in the accelerating phase of the plasma wave can be accelerated to high energies. Here, the tapered planar wiggler magnetic field plays a crucial role in enhancement of electron energy gain during acceleration via IFEL mechanism. Fig. 2(a) represents the variation of electron energy gain with the propagation distance (z) for different wiggler field strength ($b_w = 0$, 0.02, and 0.06), keeping $a_p = 0.3$, $\Lambda_w/\Lambda_p = 1/9320$, and $v_{z0} = 0.92c$. The electron energy gain increases with the wiggler magnetic field strength. However, the electron enegy gain can be maximized for a particular value of the normalized wiggler magnetic field of $b_w = 0.06$. Thus, this strength is the optimized wiggler magnetic field for which the electron energy gain is maximum and will be used in these estimations. The physics behind this can be understood as follows: the wiggler magnetic field

This article has been accepted for inclusion in a future issue of this journal. Content is final as presented, with the exception of pagination.

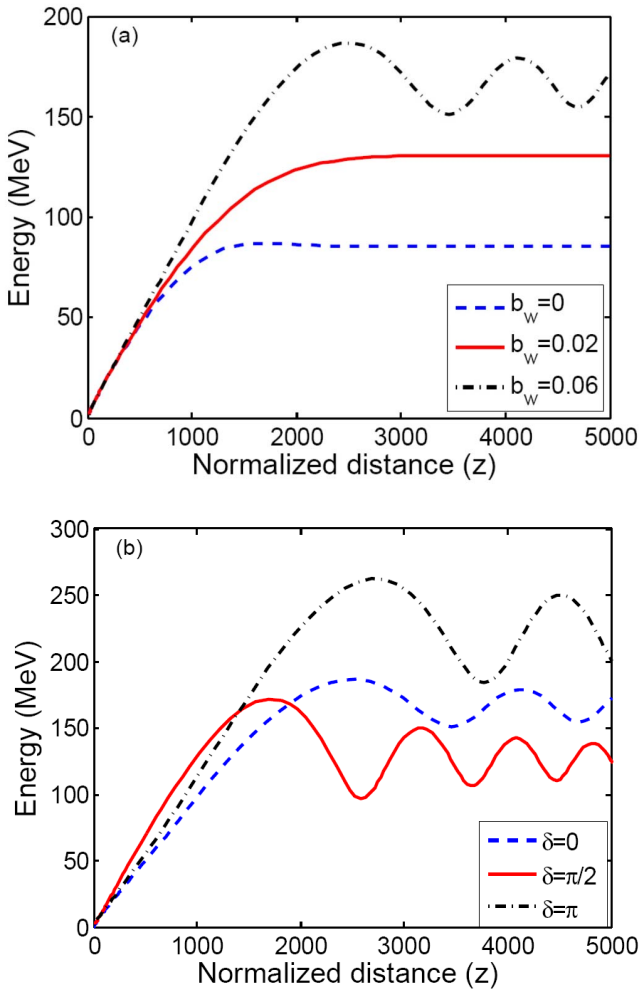

Fig. 2. (a) Electron energy (γmc^2) as a function of normalized distance (z) for different values of wiggler magnetic field $b_w = 0$(blue curve), $b_w = 0.02$ (red curve), and $b_w = 0.06$ (green curve). (b) Electron energy (γmc^2) as a function of normalized distance (z) for electrons originated at $z_0 = 0.2$ for different initial phases of the plasma wave $\delta = 0$ (blue curve), $\delta = \pi/2$ (red curve), and $\delta = \pi$ (green curve). Other parameters are, $\alpha = 9 \times 10^{-3}$, $a_p = 0.3$, $\delta = 0$, $v_{z0} = 0.9c$, and $\gamma_0 mc^2 = 2.5$, keeping $a_p = 0.3$, $\lambda = \Lambda_w/\Lambda_p = 1/9320$, and initial velocity of electron $v_{z0} = 0.9c$.

provides an additional transverse component of velocity to the electrons in the direction perpendicular to the propagation of plasma wave. The Lorentz force contributes to the net increase in longitudinal momentum. Hence, the net energy gain of the electrons trapped by the plasma wave is enhanced. It can also be seen from the results shown in Fig. 2(a) that the large wiggler magnetic field leads to energy oscillations to retain the electron energy. Our findings show that the electron energy gain is about twofold for an optimized strength of the magnetic field. For example, the electron energy gain is about 100 MeV in the absence of the magnetic field (where, the plasma wave is the only factor contributing in electron energy gain). The magnetic field bends the electrons to stay in the acceleration region, hence, the electron gains higher energy for an optimum magnetic field (i.e., 200 MeV for $b_w = 0.06$) due the cyclotron resnance. However, the electron energy gain may be reduced for higher magnetic field due to mismatch in resonance during the acceleration. Thus, a set of optimized parameters is necessary to achieve the energetic electrons in this mechanism.

The electron energy gain is sensitive with the initial phase by which it enters in the acceleration region. We estimate the contribution of initial phase (δ) of the electrons (with respect to the plasma wave) to the energy gain. It has already been known that an electron can only be accelerated if it is trapped in the accelerating phase of plasma wave. Hence, it is a necessity to inject the test electrons in the accelerating phase of the plasma wave. In Fig. 2(b), the electron energy gain for different initial phases ($\delta = 0, \pi/2, \pi$) have been plotted. It shows that the energy gain is maximum for the electrons those have the initial phase of $\delta = \pi$. This indicates that the electron in any other initial phase enters in decelerating phase of the plasma wave. Hence, such electrons do not gain much energy and are deaccelerated. This means an optimum value of initial phase of electron is required for maximum energy gain.

Electron energy can be enhanced if the preaccelerated electrons are injected in the acceleration region. We have also confirmed this from our calculations. The effect of initial electron energy on plasma wave acceleration has been depicted in Fig. 3. It shows the variation of electron energy with the propagation distance for different initial electron energies (corresponding to different initial electron velocities $v_{z0} = 0.88, 0.9, 0.92$). It is concluded that the electron energy increases with the initial electron kinetic energy due to the strengthening of the relativistic effect. The electrons with higher initial kinetic energy are more collimated, thus they interact with the plasma wave more efficiently to gain the energy via cyclotron resonance in IFEL mechanism. The electrons with velocity close to the speed of light in vacuum c remain in phase with the accelerating phase of the plasma wave. Thus, the efficient acceleration may be occurred for the electrons injected with higher kinetic energies. The emission angle (θ) of electrons can be calculated using

$$\tan\theta(\gamma) = \frac{\sqrt{2(\gamma/\gamma_0 - 1)/(1+\beta_0)}}{\gamma - \gamma_0(1-\beta_0)}$$

where $\beta_0 = v_0/c$ and $\gamma_0 = (1-\beta_0^2)^{1/2}$. The scattering angle for electron initial velocities ($v_{z0} = 0.92$, 0.9 and $0.88c$) are approximately 0.04, 0.05, and 0.06 radian, respectively. This indicates that the electron preaccelerated with greater initial velocity is scattered less [Fig. 3(b)] and trajects toward the interaction region to gain energy during acceleration. Our results shows that the electrons having large initial kinetic energy may be accelerated to higher energy.

The tapering parameter of wiggler is one of the key parameters to sustain the electron acceleration to enhance the electron energy gain. It is an arbitrary constant which indicates the tapering in the magnetic field. Fig. 4 shows the variation of electron energy for distinct values of normalized tapering parameter $\alpha = 5 \times 10^{-4}$ (blue curve), 5×10^{-3} (red curve), 9×10^{-3} (green curve). It can be noted from Fig. 4 that the electron energy is enhanced with tapering of the wiggler (i.e., for larger tapering parameter, the electron energy is improved). The larger tapering parameter enhances

This article has been accepted for inclusion in a future issue of this journal. Content is final as presented, with the exception of pagination.

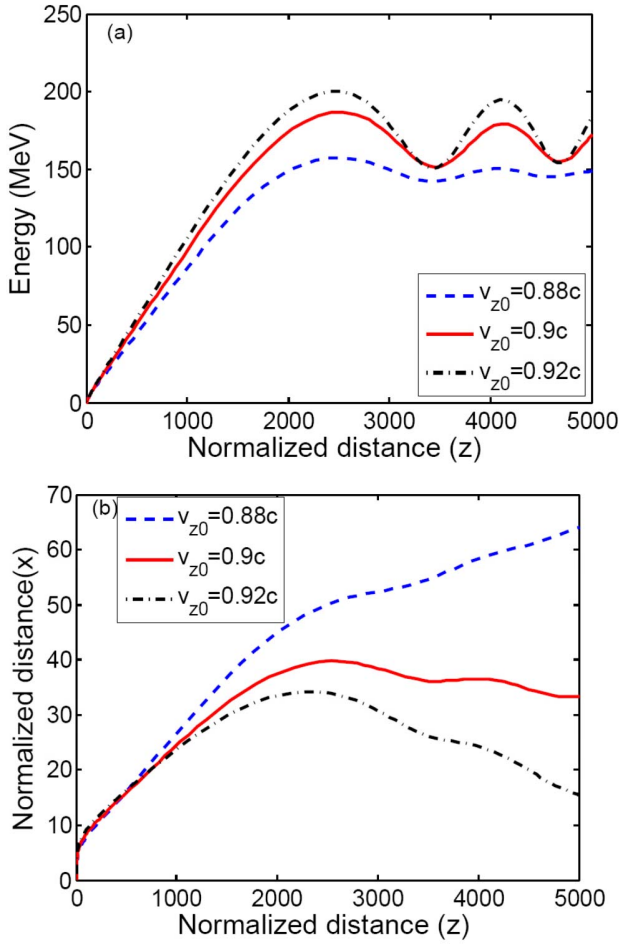

Fig. 3. (a) Electron energy (γmc^2) as a function of normalized distance (z) for electrons originated at $z_0 = 0.2$ with normalized magnetic wiggler field $b_w = 0.06$ for different initial velocities $v_{z0} = 0.88c$ (blue curve), $v_{z0} = 0.9c$ (red curve), and $v_{z0} = 0.92c$ (green curve). (b) Corresponding electron trajectories in xz plane for the same parameters used in Fig. 3(a).

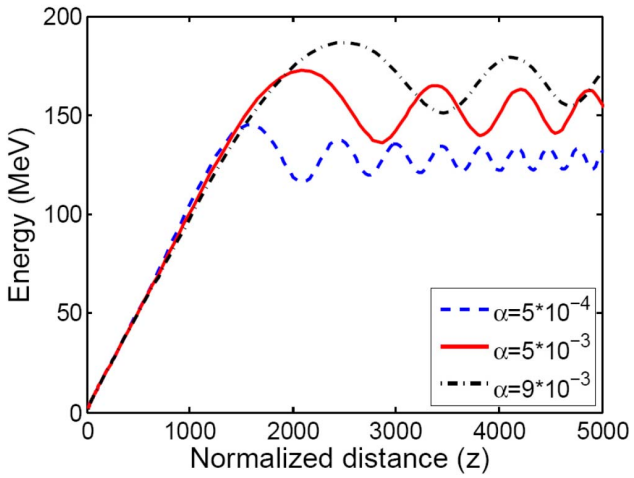

Fig. 4. Electron energy (γmc^2) as a function of normalized distance (z) for different values of tapering parameter (α) in the presence of a wiggler magnetic field of 2 KG. Other parameters are $\alpha = 9 \times 10^{-3}$, $a_p = 0.3$, $\delta = 0$, $v_{z0} = 0.9c$, and $\gamma_0 mc^2 = 2.5$.

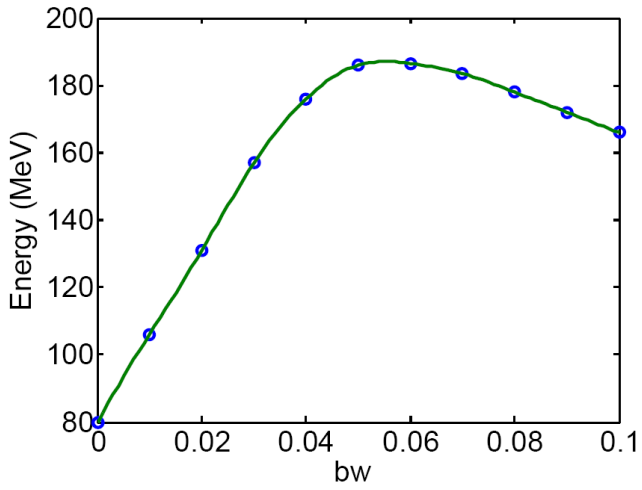

Fig. 5. Electron energy (γmc^2) with the wiggler magnetic field strength (b_w) for plasma wave amplitude $a_p = 0.3$. Other parameters are $\alpha = 9 \times 10^{-3}$, $a_p = 0.3$, $\delta = 0$, $v_{z0} = 0.9c$, and $\gamma_0 mc^2 = 2.5$.

the acceleration gradient. Thus, the electron can be trapped in the accelerating phase to gain higher energy. In other words, the larger tapering parameter can compensate the electron dephasing by increasing the interaction bandwidth. The magnetic wiggler sustains the energy gain by maintaining the resonance due to longer wiggler wavelength (Λ_w). In this paper, scaling laws have been developed for electron energy gain (γmc^2) with the tapered normalized wiggler magnetic field (b_w) by keeping the ratio of wiggler to plasma wavelength $\Lambda_w/\Lambda_p = 1/9320$. In the absence of wiggler magnetic field ($b_w = 0$), the observed energy gain of electron is 80 MeV. Our results shows that the electron energy can be enhanced more than twofold using suitable plasma parameters in the presence of wiggler magnetic field. Moreover, this energy gain can be fivefold if a large amplitude plasma wave is introduced for acceleration (i.e., $a_p = 0.4$). The results shown here suggest the use of the plasma wave in IFEL mechanism for significant electron energy gain.

The strength of wiggler magnetic field is also crucial in this mechanism. The scaling law for electron energy gain with the wiggler magnetic field can also be understood from this paper. The electron energy gain increases with the magnetic field and starts to decrease after attaining the peak energy. The results of Fig. 5 shows that the electron energy gain increases with the wiggler magnetic field strength ($b_w = 0.0 - 0.06$). Beyond a certain strength of wiggler magnetic field, the energy gain of electron starts to decrease due to resonance mismatch. The maximum energy attained by the electron is about 200 MeV for the wiggler magnetic field of $b_w = 0.06$. The peak arises at the specific value of magnetic field strength because the most of energy of the plasma wave transfers to the electrons via cyclotron resonance for that magnetic field. Moreover, after achieving a particular accelerating gradient, IFEL interaction region detunes and gets saturated. Hence, this optimized wiggler magnetic field has been considered to study the dependence of electron energy gain on other parameters.

This article has been accepted for inclusion in a future issue of this journal. Content is final as presented, with the exception of pagination.

IV. Conclusion

Electrons injected at 2.5 MeV have been accelerated to 200 MeV by the plasma wave over an interaction length of approximately 2.5 mm for an optimized wiggler magnetic field of 2 KG. This corresponds to the optimized wiggler magnetic field and electrons and plasma wave parameters. Higher electron energy can be predicted for large amplitude plasma wave in this mechanism.

The maximum electron energy is obtained due to the cyclotron resonance for an optimum wiggler magnetic field. The energy gain of electrons is measured for an optimum magnetic field strength and plasma wave amplitude. We have estimated the electron energy gain by optimizing the plasma wave amplitude, the wiggler magnetic field, and the initial momentum of electrons while keeping the initial position fixed. There is a considerable increase in electron energy gain for higher plasma wave amplitude. The magnetic field focuses and stabilizes the motion of the electrons to keep them in the accelerating zone. Thus, the electron gains improved energy level during acceleration by the plasma wave. The electrons having initial velocity close to the velocity of light in vacuum can interact resonantly with the plasma wave and the wiggler magnetic field leading to significantly enhanced energy gain during acceleration. The dependence of electron energy gain with the initial phase of plasma wave was also estimated. The electron gains a maximum energy for an optimum initial phase of the plasma wave. The electron energy gain can also be increased if they are preaccelerated. Optimization of the magnetic field along with the electron and plasma parameters is necessary for appropriate electron energy gain in this mechanism. This idea may replace the laser pulse in IFEL mechanism to accelerate the electrons to high-energy level. One may overcome the laser related critical issues by using the plasma wave in IFEL. This paper may be crucial to produce an energetic electron beam in IFEL mechanism, which may further be used in X-FEL for compact electromagnetic radiation source generation.

References

[1] V. Malka, J. Faure, Y. A. Gauduel, E. Lefebvre, A. Rousse, and K. Ta Phuoc, "Principles and applications of compact laser–plasma accelerators," *Nature Phys.*, vol. 4, pp. 447–453, Jun. 2008.

[2] T. Tajima and J. M. Dawson, "Laser electron accelerator," *Phys. Rev. Lett.*, vol. 43, pp. 267–270, Jul. 1979.

[3] K. Nakajima *et al.*, "Observation of ultrahigh gradient electron acceleration by a self-modulated intense short laser pulse," *Phys. Rev. Lett.*, vol. 74, no. 22, pp. 4428–4431, 1995.

[4] J. Panwar and S. C. Sharma, "Modeling the emission of high power terahertz radiation using Langmuir wave as a wiggler," *Phys. Plasmas*, vol. 24, no. 8, p. 083101, 2017.

[5] S. C. Sharma, J. Panwar, and R. Sharma, "Modeling of terahertz radiation emission from a free-electron laser," *Contrib. Plasma Phys.*, vol. 57, no. 4, pp. 167–175, 2017.

[6] P. Gibbon, *Short Pulse Laser Interactions with Matter: An Introduction*, London, U.K.: Imperial College Press, 2005.

[7] D. Umstadter, "Relativistic laser–plasma interactions," *J. Phys. D, Appl. Phys.*, vol. 36, no. 8, pp. R151–R165, 2003.

[8] A. Pukhov and J. Meyer-ter-Vehn, "Laser wake field acceleration: The highly non-linear broken-wave regime," *Appl. Phys. B, Lasers Opt.*, vol. 74, nos. 4–5, pp. 355–361, 2002.

[9] C. Joshi, W. B. Mori, T. Katsouleas, J. M. Dawson, J. M. Kindel, and D. W. Forslund, "Ultrahigh gradient particle acceleration by intense laser-driven plasma density waves," *Nature*, vol. 311, pp. 525–529, Oct. 1984.

[10] C. E. Clayton *et al.*, "Ultrahigh-gradient acceleration of injected electrons by laser-excited relativistic electron plasma waves," *Phys. Rev. Lett.*, vol. 70, no. 1, pp. 37–40, 1993.

[11] C. S. Liu and V. K. Tripathi, *Interaction of Electromagnetic Waves with Electron Beams and Plasmas*. Singapore: World Scientific, 2005.

[12] W. Leemans and E. Esarey, "Laser-driven plasma-wave electron accelerators," *Phys. Today*, vol. 62, no. 3, pp. 44–49, 2009.

[13] P. Sprangle, E. Esarey, and J. Krall, "Laser driven electron acceleration in vacuum, gases, and plasmas," *Phys. Plasmas*, vol. 3, no. 5, pp. 2183–2190, 1996.

[14] M. Everett, A. Lal, D. Gordon, C. E. Clayton, K. A. Marsh, and C. Joshi, "Trapped electron acceleration by a laser-driven relativistic plasma wave," *Nature*, vol. 368, pp. 527–529, Apr. 1994.

[15] A. Modena *et al.*, "Electron acceleration from the breaking of relativistic plasma waves," *Nature*, vol. 377, pp. 606–608, Oct. 2002.

[16] W. P. Leemans *et al.*, "GeV electron beams from a centimetre-scale accelerator," *Nature*, vol. 2, pp. 696–699, Sep. 2006.

[17] T. Katsouleas and J. M. Dawson, "Unlimited electron acceleration in laser-driven plasma waves," *Phys. Rev. Lett.*, vol. 51, no. 5, pp. 392–395, 1983.

[18] H. Mehdian, A. Kargarian, and A. Hasanbeigi, "Numerical study of electron acceleration by plasma wave in an ion channel under obliquely applied magnetic field," *Optik*, vol. 126, no. 21, pp. 3299–3302, Nov. 2015.

[19] K. P. Singh, V. L. Gupta, L. Bhasin, and V. K. Tripathi, "Electron acceleration by a plasma wave in a sheared magnetic field," *Phys. Plasmas*, vol. 10, no. 5, pp. 1493–1499, 2003.

[20] D. N. Gupta, M. Kaur, K. Gopal, and H. Suk, "Space-charge field assisted electron acceleration by plasma wave in magnetic plasma channel," *IEEE Trans. Plasma Sci.*, vol. 44, no. 11, pp. 2867–2873, Nov. 2016.

[21] C. Gahn *et al.*, "Multi-MeV electron beam generation by direct laser acceleration in high-density plasma channels," *Phys. Rev. Lett.*, vol. 83, no. 23, pp. 4772–4775, 1999.

[22] M. Kaur and D. N. Gupta, "Electron acceleration by a radially polarized laser pulse in an ion channel," *IEEE Trans. Plasma Sci.*, vol. 45, no. 10, pp. 2841–2847, Oct. 2017.

[23] R. B. Palmer, "Interaction of relativistic particles and free electromagnetic waves in the presence of a static helical magnet," *J. Appl. Phys.*, vol. 43, no. 7, pp. 3014–3022, 1992.

[24] A. V. Steenbergen and J. C. Gallardo, "Inverse free electron laser accelerator development," in *Proc. PAC*, Vancouver, BC, Canada, May 1997, pp. 616–620.

[25] E. D. Courant, C. Pellegrini, and W. Zakowicz, "High-energy inverse free-electron-laser accelerator," *Phys. Rev. A, Gen. Phys.*, vol. 32, no. 5, pp. 2813–2823, 1985.

[26] S. Mirzanejhad, F. Sohbatzadeh, M. Asri, and E. S. Toosi, "Electron bunch acceleration in an inverse free-electron laser with a helical magnetic wiggler and axial guide field," *Phys. Plasmas*, vol. 13, no. 12, p. 123105, 2006.

[27] F. V. Hartemann *et al.*, "The chirped-pulse inverse free-electron laser: A high-gradient vacuum laser accelerator," *Phys. Plasmas*, vol. 6, no. 3, pp. 4104–4110, 1999.

[28] K. P. Singh and V. K. Tripathi, "Laser induced electron acceleration in a tapered magnetic wiggler," *Phys. Plasmas*, vol. 11, no. 2, pp. 743–746, 2004.

[29] S. Kumar and M. Yoon, "Electron acceleration by a chirped circularly polarized laser pulse in vacuum in the presence of a planar magnetic wiggler," *Phys. Scripta*, vol. 77, no. 2, p. 025404, 2008.

[30] J. Duris *et al.*, "High-quality electron beams from a helical inverse free-electron laser accelerators," *Nature Commun.*, vol. 5, Sep. 2014, Art. no. 4928.

[31] N. E. Andreev, L. M. Gorbunov, and S. V. Kuznetsov, "Energy spectra of electrons in plasma accelerators," *IEEE Trans. Plasma Sci.*, vol. 24, no. 2, pp. 448–452, Apr. 1996.

Monika Yadav was born in Delhi, India. She received the master's degree from the University of Delhi, New Delhi. India, in 2012, and is currently pursuing the Ph.D. degree with the Delhi Technological University, Delhi, in collaboration with the University of Delhi.

She is currently involved in theory and simulation of laser-plasma interaction and its applications for particle acceleration and electromagnetic radiation generation.

This article has been accepted for inclusion in a future issue of this journal. Content is final as presented, with the exception of pagination.

Suresh C. Sharma received the M.Sc., M.Phil., and Ph.D. degrees from Agra University, Agra, India, in 1986, 1989, and 1994, respectively.

From 1990 to 1996, he was a Senior Research Assistant with the Department of Physics, IIT Delhi, New Delhi, India. He was awarded the Young Scientist project as a principal Investigator by the Department of Science and Technology (DST), Government of India for a two-year duration from 1997 to 1999 and worked with the Department of Physics and Astrophysics, University of Delhi, New Delhi. He was a Monbusho Post-Doctoral Fellow under Japanese Government Fellowship, Department of Physics, Ehime University, Matsuyama, Japan, in 1997. He has been a JSPS (Invitation) Post-Doctoral Fellow and a Visiting Researcher with the Centre for Atomic and Molecular Technology, Osaka University, Japan, from 2004 to 2005. He has guided numerous Ph.D., M.Tech and B.Tech students. Since 2012, he has been a Professor and the Head with the Department of Applied Physics, Delhi Technological University, Delhi. He has authored over 136 research papers in Journals of International repute and Proceedings of International Conferences. His current research interests include plasma physics/plasma applications, nanotechnology, high-power microwave devices, dusty plasma/strongly coupled dusty plasma, and terahertz radiation emission/short pulse lasers and plasma medicines.

Prof. Sharma is a member of the American Physical Society, the Association of Asia Pacific Physical Societies-Division of Plasma Physics, the Life Member of Plasma Science Society of India DST, Life Member-Indian Science Congress Association, and Life Member-Indian Society for Technical Education, New Delhi.

Devki Nandan Gupta was born in Alwar, India. He received the Ph.D. degree from the University of Rajasthan (research work was carried out at Indian Institute of Technology, Delhi), Jaipur, India, in 2004.

In 2010, he joined with the Department of Physics and Astrophysics, University of Delhi, New Delhi, India, as a Faculty. His current research interests include laser–plasma interaction for applications in electromagnetic radiation generation and particle accelerations.

EMPIRICAL BASIS FOR MEASUREMENT OF IDIOSYNCRATIC VOLATILITY IN THE INDIAN STOCK MARKET

Prof. K. V. Bhanu Murthy, Professor, Delhi Technological University, Delhi.

Sartaj Hussain*, PhD Scholar, Department of Commerce, Delhi School of Economics, University of Delhi.

Dr. Amit Kumar Singh, Associate Professor, Department of Commerce, Delhi School of Economics, University of Delhi

Correspondence concerning this article should be addressed to Sartaj Hussain, PhD Scholar, Department of Commerce, Delhi School of Economics, University of Delhi.

Contact: sartaj.hussain@gmail.com

Empirical Basis for Measurement of Idiosyncratic Volatility in the Indian Stock Market

Abstract

The pioneering Capital Asset Pricing Model (CAPM) argues that only systematic risk should be priced, while as idiosyncratic risk being diversifiable need not be compensated. Since investors face constraints to diversify idiosyncratic risk fully, such risk is borne by them in general, and therefore, should command a premium. However, the present study attempts to model the behaviour of stock prices and returns by incorporating the effect of global financial crisis through a semi-log growth model with a crisis dummy, in the Indian stock market. We argue that time is a "catch all variable" that explains exogenous variation in stock price and returns due to systematic risk factors and crisis as an external systemic influence that effects all stocks uniformly. We use a crisis adjusted unit root test for testing stationarity property of log index prices because if crisis is not incorporated while modelling idiosyncratic volatility, the resultant measure of the estimated random error would bias the estimate of idiosyncratic risk. The study uses a dummy regression which is believed to be a parsimonious estimation of excess returns as explained by the systematic risk factors, the residuals of this model forms the basis of measurement of a preliminary estimate of idiosyncratic volatility. Finally, we conduct a trend analysis of idiosyncratic volatility which reveals a statistically significant downward trend.

Key words: diversification, crisis, idiosyncratic volatility.

INTRODUCTION

A financial market is (informationaly) efficient when market prices reflect all available information about value. Two principal concepts in the above statement require a particular attention. It mentions about *'all available information'* and *'reflect all available information'*. First, all available information refers to information about past prices, public information, like news and private information, like inside information. Hence, there are levels or degree about available information that effect the current prices in the market. Second, prices reflect all available information" is indicative of the fact that financial transactions at market prices, using the available information, are zero NPV activities Malkiel (2005) argues that equity prices adjust to new information without delay and, as a result, no arbitrage opportunities exist that would allow investors to achieve above-average returns without accepting above-average risk. This hypothesis is associated with the view that stock market price movements approximate those of a random walk. Information flows randomly, so do market prices behave, making them unpredictable apart from its long-run uptrend. Burton G. Malkiel, in his book: '*A Random Walk Down Wall Street'* illustrates the concept of market efficiency by mentioning that if it were a blindfolded chimpanzee throwing darts at the stock pages, it could select a portfolio that would do as well as the experts would do. To wrap up, there is a common belief that markets are efficient and as such, nobody can beat the market.

In essence, the idea of efficient market hypothesis and random walk go hand in hand. If markets do not follow a random walk, then they could be possibly predicted. Such predictions could lead to abnormal profits without assuming commensurate risk. Over past, since its development, Efficient Market Hypothesis has been highly questioned by the theorists who argue if markets were efficient, there would have been no anomalies, like weekend or particular month of the year effect etc. In fact, there seem to be several instances like periods of large scale irrationality during technology-internet bubble of 1990's spreading to 2000, market crash and follow on recession of 2007 US crisis etc., where market prices seem to have failed to reflect available information. There is also a body of theorist who argue that stock returns are at least predictable partly from past returns or with the help of a firm's fundamentals like dividend yields or price earnings ratios. Malkiel (2005) contrary to these arguments of market anomalies argues that if market prices often failed to reflect rational estimates of the prospects of companies, and if markets consistently overreacted (or under-reacted) to underlying conditions, then professional investors, who are richly incentivized to outperform passive

investors, should be able to produce excess returns. Hence, according to the author, the strongest evidence suggesting that markets are generally quite efficient is that professional investors do not beat the market, i.e., they are not able to outdistance a passive index fund that simply buys and holds the market portfolio.

The question of whether markets are efficient or not on one side, another controversy among academicians has been about inability of agents to diversify. Huberman (2001) argues that investors may have more tendency to invest in familiar stocks and often ignore the principles of portfolio diversification. Should the total risk of a stock be considered for pricing or is it only systematic risk. The fact that unsystematic or idiosyncratic risk can't be eradicated completely, hence, being significant, idiosyncratic risk should be given cognizance in risk-return trade of stock market assets. Goyal and Santa Clara (2001) argue that investors generally hold undiversified asset portfolios and pricing of risk under such conditions gains importance particularly when the component of idiosyncratic risk in the total stock risk is significantly larger than the systematic risk. The contemporary asset pricing models should be flexible to accommodate idiosyncratic risk so that its importance for an investor could be found out. All this assumes significance, given the fact that diversification which is argued to overcome idiosyncratic risk is fraught with issues concerning how many and what type of assets does it require to achieve diversification. Finally, when diversification looks not possible, question that should asset returns include compensation for diversifiable risk or not needs to be resolved.

With all this discussion, some of important questions that emerge about idiosyncratic volatility in the Indian stock market can be enumerated as follows:

1. How do stock prices and returns behave?
2. Is there any role of crisis in explaining the pattern of stock price (of the Index)?
3. How should we measure a preliminary estimate of idiosyncratic volatility?
4. Should any time trend present in the idiosyncratic volatility matter?
5. What are the properties of the preliminary estimate of idiosyncratic volatility?

OBJECTIVES

With the given research questions, we base the objectives of the study as:

1. To examine time series properties of log index monthly closing prices and returns.

2. To investigate about the presence of any trend in the log index monthly closing prices and returns.
3. To analyse the differences in minimum and trend of log index monthly closing prices and returns across various economic phases including crisis.
4. To model idiosyncratic volatility of index monthly returns by incorporating effect of systematic factors and financial crisis.
5. To investigate about the presence of any trend in the idiosyncratic volatility of index returns.
6. To investigate about the properties of the preliminary estimate of idiosyncratic volatility of index returns

CONCEPTUAL FRAMEWORK

The measurement of idiosyncratic volatility hinges upon an ideal asset pricing model and the fact that asset pricing models in finance rest on Efficient Market Hypothesis (EMH). The asset pricing models like CAPM under EMH mainly account for systematic risk or volatility without emphasis on inclusion of idiosyncratic volatility. These models believe that idiosyncratic risk is diversifiable and hence, should not command any price or premium to the investor. Hence, estimation of idiosyncratic volatility largely depends upon the efficiency of the asset pricing model. If an asset pricing model is correctly specifying risk-return trade-off of financial assets, then ideally idiosyncratic risk can be ignored. However, testing of any asset pricing model confronts a joint hypotheses problem. "We can't test whether the market does what it is supposed to do unless we specify what it is supposed to do." [Fama (1970)]. If an empirical test of the asset pricing model fails, we do not know whether the market is inefficient or whether it is the model that is not the correct specification of market equilibrium. Roll (1977) argued that in practice it is impossible to have a true proxy of the market portfolio, so that an asset pricing model like CAPM can be empirically tested. To form a true proxy of market portfolio which should characterise a fully diversified portfolio, all type of assets from every market, like commodities, real estate, currencies etc. should be included in it.

Under Efficient Markets framework, the modern portfolio theory in fiancé given by Markowitz and the standard asset pricing models of Sharpe 1964 and Lintner 1965, introduced the notion of decomposing total risk into systematic or un-diversifiable risk and idiosyncratic or diversifiable risk. Using CAPM framework, these studies argue that idiosyncratic risk should not play any role in price formation as long as representative agents hold the market portfolio because a market portfolio replicates a well-diversified portfolio free from any firm-specific or

idiosyncratic risk. Marcelo et al. (2012) argue that relation between idiosyncratic risk and expected returns depends on the extent to which investors hold diversified portfolios and that diversification is related to investors characteristics (including income and risk tolerance) and market characteristics (including information and transaction costs). Malkiel and Xu (2006) have mentioned in their study a number of possible reasons about why holding a well-diversified portfolio may not be practically possible. First, institutional investors will often deliberately structure their portfolios to accept considerable idiosyncratic risk in an attempt to obtain extraordinary returns. Second, individual investors are unable to hold well-diversified portfolios due to problems of incomplete information, and institutional constraints such as, taxes, liquidity needs, imperfect divisibility of securities, restrictions on short sales, and so on. Third, most of the investments are usually done through brokerage houses who try to exploit unique characteristics of individual stocks, thus normally hold only a handful of stocks. Fourth, many companies provide stock options to their employees in order to give them financial incentive that are often linked to their retirement plans. These employees thus face constraints to liquidate or hedge their positions, and hence tend to hold highly unbalanced portfolios. Finally, a large number of mutual funds and pension funds do not hold mean-variance efficient portfolios because these active portfolio managers obtain large management fees based on their claim of being able to find undervalued stocks to offer investors the opportunity to earn risk adjusted returns more than the market averages. Given Roll's critique of inability to have an ideal market proxy that could represent a diversified portfolio and Malkiel's argument of inability of achieving complete diversification, we argue that idiosyncratic volatility should also be included in the asset pricing models for characterising true risk-return relationship.

Now, we introduce structure of the paper. Our main purpose is to examine the behavioural properties of stock prices and returns and finally attempt to model idiosyncratic volatility. Towards achieving this goal, the study has been designed as, the first segment will discuss concept of Efficient Market Hypothesis (EMH) and asset pricing models, diversification argument and role of idiosyncratic volatility. In the second segment, literature review and formulation of hypothesis has been addressed to. The third segment will discuss in detail nature of data and methodology adopted and the fourth segment will undertake empirical testing of hypothesis and analysis and interpretation of results. Finally, the segment five will summarise the main findings of the study and in the end segment six will give the reference of the literature surveyed.

REVIEW OF LITERATURE

We examine empirical literature on the two main aspects of idiosyncratic volatility that we believe are essential given the context of present study. These include behaviour of idiosyncratic volatility through time and the effect of crisis on modelling of trend in idiosyncratic volatility. There are mixed results about the trending behaviour of idiosyncratic volatility characterised by sample and regional differences. Changes in idiosyncratic volatility over time generally have implications for diversification. A rise (fall) in idiosyncratic volatility over time leads to increase (decrease) in the number of assets need to achieve a well-diversified asset portfolio. Nartea et al. (2013) argue that an increasing idiosyncratic volatility over time coupled with stable market volatility implies that the correlation among stocks is decreasing, which would normally mean an increase in the benefits from diversification. It is important for investors who cannot fully diversify their investments, to recognize these episodes as they could severely impact investment performance. Researchers have investigated various reasons for changes in trending behaviour of idiosyncratic volatility. A few have attributed surge in idiosyncratic volatility due to increase in new risky firms in the market, while few others have attributed it to the change in average size of firms listed in the market.

Campbell et al. (2001) found evidence of increased idiosyncratic volatility relative to market volatility in the US market during 1962–1997. A surge in the idiosyncratic volatility is indicative of increase in cost of diversifying, as more number of stocks are needed to achieve a certain level of diversification. Hence, investors who are not able to adjust to such trends in idiosyncratic volatility cannot fully diversify and consequently, experience a deteriorating investment performance. Kearney and Poti (2008) observe a rise in idiosyncratic volatility in European equity market during the period 1974-2004, however, unlike US, market risk is found trended upwards and correlations are not trended down. These results imply that cost of diversification has gone up with the rise in average idiosyncratic risk and it would now require increasingly more stocks to capture the benefit of diversification in the European markets than before. Bali, Cakici and Levy (2008) introduce a direct and model-independent measure of aggregate idiosyncratic risk, which does not require estimation of market betas or correlations. These researchers argue that their model-independent measure is a better version than one used by Campbell et al. (2001) for estimating idiosyncratic volatility. Using the new model, researchers observe an upward trend in average idiosyncratic volatility. The level and trend differences are more noticeable for the NASDAQ stocks, but rather weak for the NYSE/AMEX

and NYSE sample. The researchers found much stronger upward trend in idiosyncratic volatility for smaller, lower-priced, and younger firms.

Brown and Kapadia (2007) argue that upward trend in the idiosyncratic volatility in US market as substantiated by some researchers like Campbell, et al. (2001) is due to new listing of riskier companies into the stock market. This increasing trend in the publicly listing of new firms has led to significant change in the overall composition of publicly traded firms which in turn has caused idiosyncratic volatility to surge upwards. Brandt, et al. (2010) in contrast to prior evidence of a positive trend in idiosyncratic volatility in US during 1962-1997 given by Campbell, et al. (2001) show that idiosyncratic volatility dropped to below pre-1990s levels by 2003, reversing any evidence of a time trend in the 1962-1997 time period. They further argue that high and rising idiosyncratic volatility patterns were particularly acute in firms with low share prices which were also a favourite trading spot of retail investors. The authors conclude that spike in idiosyncratic risk through the internet boom of 1990s was more an episodic phenomenon than a time trend which was driven by irrational "noise" traders as was observable from a positive correlation between volatility and trading of retail investors.

Fink, et al. (2010) examined determinants of rise in the idiosyncratic volatility during the internet boom of 1990's and substantiate argument of Brown and Kapadia (2007) by suggesting that spike in the idiosyncratic risk during the late 1990's could be explained by interaction of two main factors, a dramatic increase in the number of new listings, and a simultaneous decline in the age of the firm at initial public offering (IPO). The authors found that from 1960 to 1990's, age of the typical firm issuing public equity in US had fallen from almost 40 years to less than 5 years. Contrasting Brandt et al. (2010) that trend in the idiosyncratic volatility was mainly due to irrational noise trading, the authors argue that idiosyncratic risk is driven by the age characteristics of listed firms and increased proportion of young firms in the market explained a large fraction of the trend in idiosyncratic risk during the internet boom of the late 1990s. Further, the authors analyse time trend in idiosyncratic volatility and found regime switching episodic trends characterised by either shifts in the average value or slope of the value weighted idiosyncratic volatility of firms in the US market. The authors use a simple regime switching model incorporating for effects due to market crash following the great depression, oil price shocks of early 1970's and internet bubble of late 1990's, results of which support rise in the idiosyncratic volatility during all these crises.

Sousa and Serra (2008) examine idiosyncratic volatility in case of Portuguese stock market and found that there was no statistically significant rise in firm specific volatility during 1991-2005, however, ratio of firm-specific risk to total risk slightly underwent a decrease. Unlike Brown and Kapadia (2007), Fink et al. (2010), who argue that rise in idiosyncratic volatility was due to listing of new and riskier firms, the researchers argue absence of a trend in the idiosyncratic volatility was driven by the increasing proportion of large firms with low idiosyncratic volatility that made their listing into the market. However, collectively they believe that that changes in idiosyncratic volatility are related to changes in the composition of the market. Angelidis (2010) argues that idiosyncratic volatility in case of emerging markets does not exhibit either an upward or a downward trend and as such investors do not have to increase, on average, the number of stocks they hold to keep the active risk constant. Further, emerging markets being less efficient, it is observed that proportion of total volatility attributed to asset-specific risk is lower in these markets than their counterpart developed markets. The researcher also found that both idiosyncratic risk and market risk together predict market returns as there is negative (positive) relation between idiosyncratic (market) risk and subsequent stock returns. Nartea et al. (2013) report absence of any long-term trend in idiosyncratic volatility in the Chinese market. The behaviour of idiosyncratic volatility in the Chinese market is instead episodic, that is best characterized by an autoregressive process with regime shifts that coincide with structural market reforms. Liu, et al. (2017) in a study on French stock market observe that idiosyncratic and market volatility do not exhibit long-term trends, instead their patterns are consistent with regime switching behaviour. Using bi-variate Fama-MacBeth regressions, these researchers found a strong significant negative idiosyncratic volatility effect in the French stock market.

The above literature on the behaviour of idiosyncratic volatility points towards the fact that there still exists a lack of resolution about trending behaviour of idiosyncratic volatility and the underlying causes of such property. While as in the more matured markets of developed economies, studies show evidence of upward trend in idiosyncratic volatility, however, the less matured markets of emerging economies are featured by absence of any significant trend in idiosyncratic volatility. The second segment of our review includes studies that incorporate effect of crisis on modelling of trend in idiosyncratic volatility. Some studies after having incorporated for shifts in intercept and changes in slope due to structural changes show that a series that may be apparently random walk could be rather a trend stationary process. Among others, Chaudhuri and Wu (2003) conducted a study on monthly prices series of seventeen

emerging market stock indexes during the period 1985 -1997 and found that in case of fourteen countries, the stock markets revealed significant structural breaks, which appear either in the intercept, in the time trend, or in both. After accounting for the effect of different break points due to outbreak of crisis or structural changes, it was found that price series of ten out of seventeen indexes followed a mean-reverting process. The researchers finally argued that if a break point is taken into account, stock prices may reasonably be modelled as a trend-stationary process, rather as a random walk process. Gerlach, et al. (2015) examined the relationship between idiosyncratic risk and returns of REIT's incorporating effect of 2007 financial crisis into their methodology. For analysing the effect of crisis, the study split sample data into pre-crisis, during crisis and post crisis segments. The study found strong correlation between leverage and the idiosyncratic risk. Without controlling for leverage, it is found that a significant, negative relationship can be established between idiosyncratic risk and returns. However, after controlling for leverage, researchers observe that market did not price idiosyncratic risk into REITs either before or during the crisis once the impact of leverage is controlled for. Under such conditions, evidence of a positive, significant relationship is found only during after the crisis period.

Earlier, Perron (1989) had demonstrated that failure to take into account the breaking points may significantly reduce the power of traditional tests and mistakenly produce evidence in support of the random walk hypothesis. The author argues that events like great crash of 1929 and oil price crisis of 1973 were not a realization of the underlying data-generating mechanism of the various series but an exogenous influence. While the former shock led to the change in the mean level of most aggregate variables, the later was responsible for change in the slope of the trend for most of them. Hence, most macroeconomic variables are trend-stationary when two single changes, one for intercept of the trend function after 1929 and another in the slope of the trend function after 1973 are properly incorporated in a unit root test. Hamao, et al. (2002) observe an unusual reduction in idiosyncratic volatility accompanied by rising overall market volatility across firms after the Japanese stock market crash. During this time, however, there was a sharp increase in Japanese equity co-movement which resembled that of U.S. equities during the Great Depression, both of which show a prolonged large co-movement in equity prices. Bekaert, et al. (2009) found that there is no upward trend in idiosyncratic volatility anywhere in the developed world, however, idiosyncratic volatility is well described by a stationary mean-reverting process with occasional shifts to a higher-mean, higher-variance regime. In times of crisis, all risk variables increase disproportionally, it becomes hard to capture regime

switching characteristics of idiosyncratic volatility with the help of linear models and hence require more scrutiny. The researchers also observed idiosyncratic volatility is highly correlated across countries, and this correlation has increased over time.

From these studies, it emerges that incorporation of the effect of crisis or regime shifts due policy changes leads to a better analysis of properties of idiosyncratic volatility. An inherently trend stationary time series of idiosyncratic volatility may be misconstrued as a pure random walk process, if effect of crisis or policy shift is not taken into account while modelling trend in idiosyncratic volatility. Finally, we look a few studies that focus on the issues concerning modelling of idiosyncratic volatility. Garcia et al. (2014) propose a model free cross-sectional variance (CSV) measure of idiosyncratic volatility that doesn't need to obtain residuals from a particular model like CAPM or Fama and French factor model to compute idiosyncratic volatility and has a distinct advantage of being readily computable at any frequency, with no need to estimate other parameters. This CSV measure of idiosyncratic volatility is better able to predict the cross section of expected returns due to exposure to aggregate idiosyncratic volatility risk of portfolios based on size and book-to-market ratios. Chen and Petkova (2012) argue that puzzling negative relation between idiosyncratic volatility and future returns observed by Ang, et al. (2006, 2009) could be due to the problem of omitted risk factor by asset pricing model used for estimating idiosyncratic volatility. If a risk factor is missing from the model, idiosyncratic volatility may appear to be priced simply because it proxies for a risk exposure with respect to the missing factor. The authors argue average stock variance as missing factor in the Fama and French three factor model and after introducing it in a cross sectional set up, price of risk for average variance is found to be negative. Marcelo et al. (2012) introduce idiosyncratic risk into the asset pricing process as a friction and as a source of another kind of systematic risk un-captured by beta coefficient. The researchers analysed idiosyncratic volatility in the Spanish stock market for the period 1987-2007 observing that firm-specific volatility represents the largest share of total volatility and idiosyncratic volatility has a significant and positive relation to future stock market returns.

In order to achieve objectives of this study, we have come up the following set of hypotheses based on the above review of literature:

HYPOTHESES

$H_{0(1)}$: Log of SENSEX monthly closing prices are normally distributed.

$H_{1(1)}$: Log of SENSEX monthly closing prices are not normally distributed.

$H_{0(1a)}$: Log of SENSEX monthly closing prices in the pre-crisis period are normally distributed.
$H_{1(1a)}$: Log of SENSEX monthly closing prices in the pre-crisis period are not normally distributed.
$H_{0(1b)}$: Log of SENSEX monthly closing prices in the crisis period are normally distributed.
$H_{1(1b)}$: Log of SENSEX monthly closing prices in the crisis period are not normally distributed.
$H_{0(1c)}$: Log of SENSEX monthly closing prices in the post crisis period are normally distributed.
$H_{1(1c)}$: Log of SENSEX monthly closing prices in the post crisis period are not normally distributed.

$H_{0(2)}$: Log of SENSEX monthly closing prices have a unit root.
$H_{1(2)}$: Log of SENSEX monthly closing prices doesn't have a unit root.

$H_{0(2a)}$: Log of SENSEX monthly closing prices in the pre-crisis period have a unit root.
$H_{1(2a)}$: Log of SENSEX monthly closing prices in the pre-crisis period doesn't have a unit root.
$H_{0(2b)}$: Log of SENSEX monthly closing prices in the crisis period have a unit root.
$H_{1(2b)}$: Log of SENSEX monthly closing prices in the crisis period doesn't have a unit root.
$H_{0(2c)}$: Log of SENSEX monthly closing prices in the post crisis period have a unit root.
$H_{1(1c)}$: Log of SENSEX monthly closing prices in the post crisis period doesn't have a unit root.

$H_{0(3)}$: Log of SENSEX monthly closing prices does not exhibit any significant trend.
$H_{1(3A)}$: Log of SENSEX monthly closing prices exhibits a significant upward trend.
$H_{1(3B)}$: Log of SENSEX monthly closing prices exhibits a significant downward trend.

$H_{0(3a)}$: Log of SENSEX monthly closing prices does not exhibit any significant trend in the pre-crisis period.
$H_{1(3aA)}$: Log of SENSEX monthly closing prices exhibits a significant upward trend in the pre-crisis period.
$H_{1(3aB)}$: Log of SENSEX monthly closing prices exhibits a significant downward trend in the pre-crisis period.
$H_{0(3b)}$: Log of SENSEX monthly closing prices does not exhibit any significant trend in the crisis period.
$H_{1(3bA)}$: Log of SENSEX monthly closing prices exhibits a significant upward trend in the crisis period.

$H_{1(3bB)}$: Log of SENSEX monthly closing prices exhibits a significant downward trend in the crisis period.
$H_{0(3c)}$: Log of SENSEX monthly closing prices does not exhibit any significant trend in the post-crisis period.
$H_{1(3cA)}$: Log of SENSEX monthly closing prices exhibits a significant upward trend in the post-crisis period.
$H_{1(3cB)}$: Log of SENSEX monthly closing prices exhibits a significant downward trend in the post-crisis period.

$H_{0(4a)}$: There is no significant difference in average log SENSEX monthly closing prices as well as trend across pre-crisis and crisis period.
$H_{1(4a)}$: There is a significant difference in average log SENSEX monthly closing prices as well as trend across pre-crisis and crisis period.

$H_{0(4b)}$: There is no significant difference in average log SENSEX monthly closing prices as well as trend across post-crisis and crisis period.
$H_{1(4b)}$: There is a significant difference in average log SENSEX monthly closing prices as well as trend across post-crisis and crisis period.

$H_{0(5)}$: De-trended log of SENSEX monthly closing prices have a unit root.
$H_{1(5)}$: De-trended log of SENSEX monthly closing prices doesn't have a unit root.

$H_{0(6)}$: Monthly SENSEX logarithmic returns are normally distributed.
$H_{1(6)}$: Monthly SENSEX logarithmic returns are not normally distributed.

$H_{0(7)}$: Monthly excess SENSEX logarithmic returns are normally distributed.
$H_{1(7)}$: Monthly excess SENSEX logarithmic returns are not normally distributed.

$H_{0(8)}$: Monthly SENSEX logarithmic returns have a unit root.
$H_{1(8)}$: Monthly SENSEX logarithmic returns doesn't have a unit root.

$H_{0(9)}$: Monthly excess SENSEX logarithmic returns have a unit root.
$H_{1(9)}$: Monthly excess SENSEX logarithmic returns doesn't have a unit root.

$H_{0(10)}$: Monthly excess SENSEX logarithmic returns does not exhibit any significant trend.
$H_{1(10A)}$: Monthly excess SENSEX logarithmic returns exhibits a significant upward trend.

$H_{1(10B)}$: Monthly excess SENSEX logarithmic returns exhibits a significant downward trend.

$H_{0(11a)}$: There is no significant difference in average monthly excess SENSEX logarithmic returns as well as trend across pre-crisis and crisis period.
$H_{1(11a)}$: There is a significant difference in average monthly excess SENSEX logarithmic returns as well as trend across pre-crisis and crisis period.

$H_{0(11b)}$: There is no significant difference in average monthly excess SENSEX logarithmic returns as well as trend across post-crisis and crisis period.
$H_{1(11b)}$: There is a significant difference in average monthly excess SENSEX logarithmic returns as well as trend across post-crisis and crisis period.

$H_{0(12)}$: Monthly idiosyncratic volatility of SENSEX returns does not exhibit any significant trend.
$H_{1(12A)}$: Monthly idiosyncratic volatility of SENSEX returns exhibits a significant upward trend.
$H_{1(12B)}$: Monthly idiosyncratic volatility of SENSEX returns exhibits a significant downward trend.

1. DATA & METHODOLOGY

Data

The basic aim of our study is to make a preliminary assessment of idiosyncratic volatility of returns in the Indian stock market. For this purpose, we have used monthly closing price series of Bombay Stock Exchange (BSE) main index, SENSEX, comprising of 171 observations from January 2003 to March 2017. We prefer to sample on the basis of monthly frequency because such a length of time helps to capture more information about a given variable, for example, price or returns in our case. The distributions of daily and monthly stock returns are generally symmetric about their means, but the tails are fatter (i.e., there are more outliers) than would be expected with normal distributions. We argue that SENSEX as a benchmark and investible index comprising of a collection of thirty largest, most liquid and financially sound companies across key sectors of Indian economy represents a well-diversified value weighted (float adjusted) portfolio which could be used as a suitable proxy for systematic risk. The volatility that is not explained by the Index would reasonably represent a preliminary measure of

idiosyncratic volatility in the given context. We break our sample into three period to enable inclusion of crisis effect in our analysis. These three periods are set as:

January 2003 to December 2007 - Pre-crisis period.

January 2008 to February 2009 - Crisis period.

March 2009 to March 2017 - Post-crisis period.

Methodology

This study has been designed so as to divide the analysis into two distinct part:

I. The first part intends to measure the impact of crisis on the stock index, so as to arrive at a preliminary measure of idiosyncratic volatility.
II. The second part of our study analyses logarithmic index returns corrected for crisis effects. Further it studies the properties of the residuals which forms the basis for idiosyncratic volatility in the context of crisis.

Our methodology has been laid out in the following steps:

i) As a first step, we transform raw monthly closing prices into logarithmic form and also logarithmic difference (return) form. Strong (1992) suggests that empirically logarithmic returns are more likely to be normally distributed and so conform to the assumptions of the standard statistical techniques. Panait and Constantinescu (2012) argue that monthly index logarithmic returns in comparison to daily logarithmic returns tend to have a normal distribution. We begin with the idea of stock returns. Stock market returns follow continuous compounding and as such are generally measured on natural logarithmic scale. We have calculated stock returns as the log difference of successive prices which can expressed as:

$$\ln r_t = \log(p_t) - \log(p_{t-1}) \text{ or else; } \ln r_t = \log(\frac{p_t}{p_{t-1}}) \quad (1)$$

ii) Before applying any econometric model to prices/returns, we need to check their time series for unit root properties. Absence of unit root in a time series (stationarity) is an essential condition for OLS, failing which it may lead to spurious regression. To check stationarity of the series, we have used Augmented Dickey Fuller (ADF) test.

iii) Since the standard unit root test like ADF test in our case doesn't account for the variation in prices due to crisis, we introduce a model with a set of intercept and slope dummies to account for the effect of various economic phases surrounding crisis. Our argument is that

the conventional ADF test doesn't account for the variation in trends across different economic phases and tests the unit root properties of a particular time series with a single undifferentiated time trend while ignoring the possible shifts in the trend within the entire series, both in terms of shift in the drift (intercept) and change in the trend (slope). Our methodology of testing for non-stationarity is a modified version of the ordinary ADF test wherein we don't test the stationarity of a series with a single time trend but also introduce separate intercept and slope dummies to account for variation in prices due to the effect of various economic phases around crisis.

iv) Next, we analyse trend in the logarithmic return series and study if crisis has any role in explaining behaviour of the trend. We use a parsimonious model with time and dummy variables to capture idiosyncratic volatility of returns of the broader market index SENSEX. Essentially, logarithmic returns (of the SENSEX) are regressed on time. We argue that time is a 'catch-all' variable which captures the exogenous factors and further, we add crisis as another dimension to explain the systematic part of risk. This would ultimately help in measuring the idiosyncratic volatility. Idiosyncratic volatility is not directly observable. Thus, the residual of such an equation would form the basis of idiosyncratic volatility. Therefore, square of the residual from the dummy regression model is used as a proxy for idiosyncratic volatility.

v) After having the estimate of idiosyncratic volatility, we use a simple linear trend model to investigate presence of any trend. Besides this, we compare our idiosyncratic volatility estimate with the market volatility of index returns. We work out market volatility as a difference between total volatility (measured as square of monthly returns) and estimate of idiosyncratic volatility.

vi) To make a comparison between simple linear trend and dummy variable model, we calculate the efficiency ratio, which is a measure of actual over predicted observations. The average efficiency ratio allows to compare the predictive efficiency of the models used in the analysis. If the efficiency ratio is close to 1, it implies that the underlying model is a more accurate model. Now we present an overview of the various tool and techniques used for analysis in our study.

Descriptive statistics

Descriptive statistics provides information regarding the statistical characteristics of the data sample. These characteristics include, mean, median, range, standard deviation, skewness, kurtosis and normality. Descriptive statistics is often used by researchers to describe the basic features and the structure of the data. This helps to arrive at meaning inferences from the results and also provides a meaningful way to manage large quantities of data.

Unit Root Test

An economic time series which is characterised by time varying mean and variance is said to be non-stationary. With increasing order, the autocorrelation coefficients of such a series decay very slowly. Generally it has been observed that time series data are non-stationary in their level form. Estimation of ordinary least squares (OLS) regression on non-stationary time series data would provide inaccurate estimates, that is, the R^2 and t-values of the regression would be high but the results will not have any economic meaning. This kind of regression has been called as spurious or non-sense regression by Granger and Newbold (1974). Before estimating any time series regression model, problem of non-stationarity should be dealt with. To check whether our variables are stationary or not, we have used the Augmented Dickey Fuller (ADF) test.

Augmented Dickey Fuller (ADF) Test

The ADF test is residual autocorrelation corrected version of the Dickey Fuller test. We have used the ADF test under Akaike Information Criteria (AIC) which is a higher lag length criterion. The following variants of ADF test besides our own test, which is a modified version of ADF test (with intercept and trend).

y_t is a random walk: $$\Delta y_t = \delta y_{t-1} + \varepsilon_t \quad (2)$$

y_t is a random walk with drift: $$\Delta y_t = \beta_1 + \delta y_{t-1} + \varepsilon_t \quad (3)$$

y_t is a random walk with drift around a deterministic trend: $$\Delta y_t = \beta_1 + \beta_2 t + \delta y_{t-1} + \varepsilon_t \quad (4)$$

The null and alternative hypotheses of this test are:

Null Hypothesis: H_0: $\delta = 0$ **(**Variable has a unit root, i.e., time series is non-stationary).

Alternative Hypothesis: H1: $\delta < 0$ (Variable does not have a unit root, i.e., time series is stationary)

Our version of unit root test employs different intercepts and trends that are defined in terms of various breaks in the time series due to economic cycles. Since the standard unit root test like ADF test in our case does account for the variation in prices due to crisis, we introduce a model with a set of intercept and slope dummies to account for the effect of various economic phases. Our argument is that the conventional ADF test doesn't account for the variation in trends across different economic phases and tests the unit root properties of a particular time series with a common time trend while ignoring the possible shifts in the trend within the entire series. Our methodology of unit root testing is a modified version of the ADF test wherein we don't test the stationarity of a series with a common time trend only but also introduce separate intercept and slope dummies to account for variation in prices due to the effect of various economic phases.

$$\ln p_t = \alpha + \beta_1 t + D_2 + D_3 + \beta_2 D_2 * t + \beta_3 D_3 * t + \varepsilon_t \quad (5)$$

Where, α represents the initial value of the dependant variable ($\ln p_t$) in the crisis period, β_1 represents the trend in y_t in the crisis period, D_2 and β_2 are the differential intercept and trend coefficients respectively in the pre-crisis period, D_3 and β_3 represent the differential intercept and trend coefficient in the post crisis period and ε_t is the random error component. The residuals of the above regression model obtained after accounting for effects of different policy periods will be tested for unit root without trend and intercept to validate the claim that the series is trend stationary. This would establish that the non-stationary nature of the logarithmic price series is due to an underlying data generating process that is trend stationary and not purely non-stationary. The apparent non-stationary nature of the logarithmic price series is therefore explained in terms of the complex set of slope and intercept dummies that emulate the changing shifts and trends caused by crisis and other 'exogenous generic factors' which are systematic in nature. If crisis is not incorporated in this manner in the methodology for estimating idiosyncratic volatility, the resultant measure of the estimated random error would be biased. Hence, the basis of arriving at idiosyncratic volatility would also be biased. This analysis, therefore, lays down the link between the two parts of the study.

Growth Analysis

To analyse the behaviour of stock index prices and returns over time, we propose to use a semi-log model where the dependant variable in its log form is regressed against time. This model is also called as semi-log growth model in which the time variable captures the trend in the dependant variable in exponential terms. The slope coefficient associate with the time variable

provides information regarding the magnitude and direction of the growth of the Y variable. If the coefficient of the time variable is positive, it denotes an upward trend in the dependant variable. Likewise, if the coefficient of the time variable is negative, it signifies a downward trend in the dependant variable. The growth model is expressed as:

$$\ln y_t = \beta_1 + \beta_2 t + \varepsilon_t \quad (6)$$

Where, y_t is the log of the dependant variable, β_1 is intercept explaining the initial value of the dependant variable, t is the time variable and β_2 is the coefficient associated with time variable explaining the growth rate of the dependant variable. In our case, it is the price of the index.

Dummy Regression Model

In our study, we propose to introduce modelling of the effect of crisis on the stock prices/returns. This aspect of variation in the stock prices/returns can be captured by using dummy variable in the regression equation. A dummy is a categorical variable that takes the value of 1 or 0 to account for presence and absence of a certain attribute in given variable. We will be using a set of intercept and slope dummies to account for differences in the intercept as well as trend across different economic phases. The crisis period has been assigned the control or reference category and all the comparisons will be made in relation to this category. The dummy regression model can be expressed as:

$$\ln y_t = \alpha + \beta_1 t + D_2 + D_3 + \beta_2 D_2 * t + \beta_3 D_3 * t + \varepsilon_t \quad (7)$$

Where, α represents the initial value the dependant variable ($\ln y_t$) in the crisis period, β_1 represents the trend in y_t in the crisis period, D_2 and β_2 are the differential intercept and trend coefficients respectively in the pre-crisis period, D_3 and β_3 represent the differential intercept and trend coefficient in the post crisis period and ε_t is the random error component.

Efficiency Ratio

Efficiency Ratio is a measure of predictive efficiency of the regression model that has been used in our study. It is a ratio of the actual and predicted values of the dependant variable. The more this ratio is close to 1, the better is the predictive efficiency of a regression model. The Efficiency Ratio is measured in two steps. First, by measuring the ratio of the actual value of Y_t to the predicted value of Y_t at each point on X_t. For each observation in the sample, we estimate efficiency ratio and finally take its average value for evaluation of a given regression model. The efficiency ratio can be expressed as:

$$ER = \frac{\sum_{i=1}^{n} y_t / n}{\sum_{i=1}^{n} \hat{y}_t / n} \quad (8)$$

Where y_t is the actual value of the dependant variable, $\hat{y}_t$ is the predicted value of the dependant variable and n is number observations in the sample.

Residual Diagnostics

The error term "ε_t" or the residuals of equation (7) should be tested to confirm that they are pure white noise in order to validate the OLS regression model. The logic behind these tests is to check whether any information of the independent variables has not been captured by the model which eventually gets reflected in the residuals. If the model passes the residual diagnostic tests we can be assured of the fact that our model perfectly explains the variation in the dependent variable and the unexplained portion of our model reflected in the error term represents the inherent randomness. If the results of the test of residuals show that the error series in not purely 'white noise' then this would prove that there is some unexplained variation that contains some more information. This, therefore, is the source of idiosyncratic volatility which is not explained by crisis and other 'exogenous generic factors' which are systematic in nature.

We have used the following residual diagnostic tests;

Breusch-Godfray Serial Correlation Lagrange Multiplier (LM) Test

The Breusch-Godfray Serial Correlation Lagrange Multiplier (LM) test checks the presence of autocorrelation in the residuals of the regression. If we find that the residuals are auto-correlated, it implies that there is a problem of model specification. Given the regression model,

$$y_t = \beta_1 + \beta_2 x_t + \varepsilon_t \quad (9)$$

the BG test assumes the error term ε_t to follow p^{th} order autoregressive process

$$\varepsilon_t = \rho_1 \varepsilon_{t-1} + \rho_2 \varepsilon_{t-2} + \ldots + \rho_p \varepsilon_{t-p} + \nu_t \quad (10)$$

such that;

Null Hypothesis: H_0: $\rho_1 = \rho_2 = \ldots = \rho_p = 0$ (The time series has no autocorrelation)

Alternative Hypothesis: H_1: $\rho_1 = \rho_2 = \ldots = \rho_p \neq 0$ (The time series suffers from autocorrelation)

ARCH Test

If the model is having heteroscedasticity (not homoscedastic), it violates the basic assumptions of the Gauss-Markov theorem. Even though presence of heteroskedasticity does not estimate biased coefficients, but leads to biased standard errors which can cause a problem of inference. To check whether residuals are heteroskedastic, we have used Auto Regressive Conditional Heteroskedasticity (ARCH) test. For a given regression model,

$$y_t = \beta_1 + \beta_2 x_t + \varepsilon_t \tag{11}$$

the ARCH test assumes the squared residuals of the above regression model to follow p^{th} order autoregressive process

$$\varepsilon_t^2 = \lambda_1 \varepsilon_{t-1}^2 + \lambda_2 \varepsilon_{t-2}^2 + \ldots + \lambda_p \varepsilon_{t-p}^2 + \nu_t \tag{12}$$

such that,

Null Hypothesis: H_0: $\lambda_1 = \lambda_2 = \ldots = \lambda_p = 0$ (The residuals have no heteroscedasticity, or residuals are homoskedastic)

*Alternative Hypothesis***:** H_1: $\boldsymbol{\lambda_1 = \lambda_2 = \ldots} = \lambda_p \neq 0$ (The residuals suffer from Heteroscedasticity, or residuals are not homoskedastic)

Jarque-Berra Test

The Jarque-Berra test has been used to test whether the regression residuals are normally distributes or not. Even though the violation of normality assumption does not lead to biased estimates, yet it causes a problem of statistical inference. Thus, choosing a higher confidence interval and equivalently a conservative significance level can solve the problem of statistical inference. However in large samples, based on the central limit theorem, even in case of violation of the normality assumption the t-statistics is reliable. The Jarque-Berra test of normality tests the joint hypothesis that skewness and kurtosis are 0 and 3 respectively. Following is the Jarque-Berra test statistics:

$$JB = n\left[\frac{s^2}{6} + \frac{(k-3)^2}{24}\right] \tag{13}$$

such that,

Null Hypothesis: H_0: JB = 0 **(**Residuals follow a normal distribution)

Alternative Hypothesis: H_1**:** JB $\neq 0$ (Residuals do not follow a normal distribution)

For the residuals to be normally distributed, Jarque-Berra statistic value is expected to be 0. Jarque-Berra test statistic follows a χ^2 distribution with 2 degrees of freedom.

RESULTS & DISCUSSION

We begin with analysis of the historical daily closing price movement of the Bombay Stock Exchange's (BSE) main index, SENSEX from January of the 2003 to March 2017. As per its annual report for the year 2015-16, BSE as on March 2016 has been categorised as the 12th largest stock exchange in the world by market capitalisation. Similarly, SENSEX as its broader market index comprises of the stocks of 30 largest, most liquid and financially sound companies across key sectors of the Indian economy. The overall market capitalisation of BSE SENSEX as on May 25, 2017 stood at Rs. 5,16,242.28 crore which represented more than 50% of the total market capitalisation of listed universe at Bombay Stock Exchange. As reported by the BSE, SENSEX is the country's most widely tracked stock market benchmark index which has privilege of being traded internationally on the EUREX as well as leading exchanges of the BRCS nations (Brazil, Russia, China and South Africa).

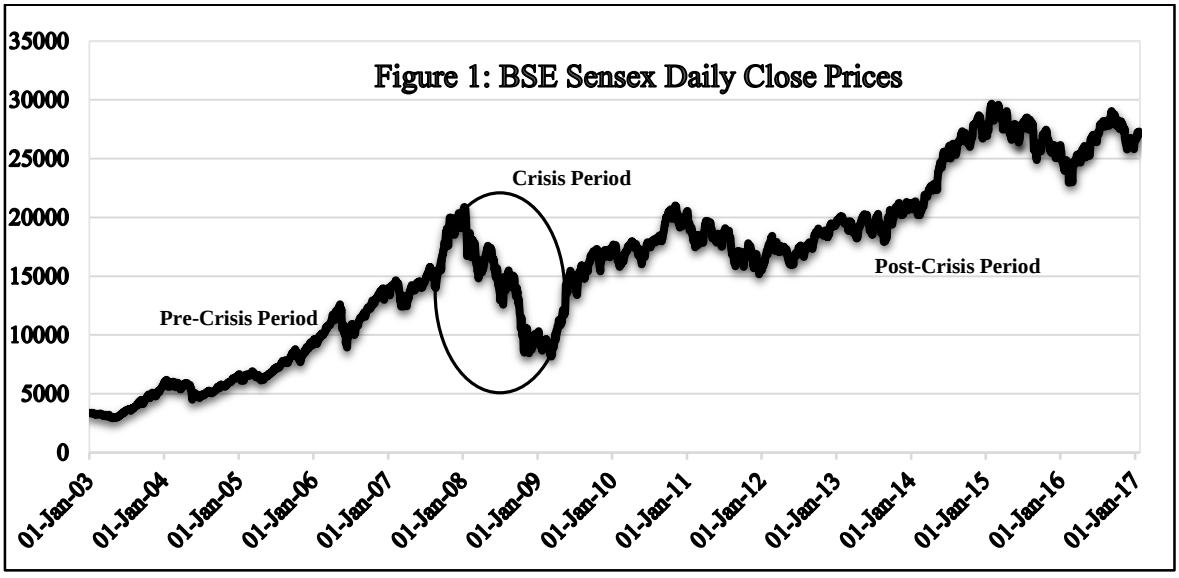

In our analysis, apart from examining the impact of common systematic factors on the movement of stock index prices, we have also taken into cognizance impact of the global financial crisis which we believe is addition of a new dimension to the analysis of stock price movements. Hence, the period of the study has been split into three segments covering, crisis period from January 1st 2008 to March 8th 2009, pre-crisis period from January 1st 2003 to December 31st 2007 and finally post crisis period ranging from March 9th 2008 to March 31st 2017. The graphical depiction of daily index closing prices in the Figure: 1 clearly reveals a

huge instability yet an upward rising trend in the daily close prices of one of the Indian major stock market index. Now, we proceed towards a formal analysis of the behaviour of stock price movements in the Indian stock market. Before analysing the behaviour of stock price movement of SENSEX, we present below the descriptive statistics of the log of its monthly closing prices:

Table 1: Summary of Descriptive Statistics of log monthly closing SENSEX prices

Mean	9.55796	Jarque-Bera	25.0893
Median	9.75477	Probability	4E-06
Maximum	10.2962		
Minimum	7.99287	Sum	1634.41
Std. Dev.	0.58328	Sum Sq. Dev.	57.8371
Skewness	-0.9383		
Kurtosis	2.99996	Observations	171

From the descriptive statistics shown in the Table 1, it can inferred that prices of the given index have increased over time. The prices does not seem to be normally distributed since the price series is negatively skewed. This is also supported by Jarque-Bera test statistics of 25.0893 being statistically insignificant at 5% level of significance. From this, it can be concluded that the log SENSEX is not normally distributed.

Table 2: Summary of Descriptive Statistics of log monthly closing SENSEX prices in different economic phases

Description	Pre-Crisis	Crisis	Post Crisis
Mean	8.962838	9.904616	9.947242
Median	8.910767	9.89143	9.878821
Maximum	9.917735	10.0162	10.29622
Minimum	7.992874	9.831977	9.341654
Std. Dev.	0.526812	0.053608	0.217188
Skewness	-0.026634	0.480115	0.036036
Kurtosis	1.987649	2.25376	2.037601
Jarque-Bera	2.56923	0.924321	3.725625
Probability	0.276757	0.629921	0.155235
Sum	537.7703	148.5692	954.9352
Sum Sq. Dev.	16.37433	0.040234	4.481213
Observations	60	15	96

In order to have a better understanding of the behaviour of SENSEX prices, we have analysed the descriptive statistics in various economic cycles. Table 2 presents the descriptive statistics for the pre-crisis, crisis and the post-crisis of the Indian stock market. Higher average stock prices in the post crisis period of indicative of a fast recovery of the Indian stock market.

Surprisingly, volatility of the stock prices has been observed very less in the crisis period than the pre and post crisis periods. However, volatility in the post crisis period has been comparatively lower than in the pre-crisis period. In the crisis period, prices are highly positively skewed which is obvious due the steep crash of the stock market during the crisis period. The Jarque-Bera test statistics of all the three sub-period price series is statistically significant at 5% level of significance which is indicative of normality of the underlying price series.

After initial descriptive analysis of SENSEX prices, we have used Augmented Dickey Fuller (ADF) test to verify the unit root property of the given time series. The results of the ADF test in the entire sample as well as different economic phases are shown in the Table: 3 below:

Table 3: Augmented Dickey Fuller test results of monthly closing log SENSEX prices (Based on Akaike Information Criterion)

Description	Pre-Crisis Period	Crisis Period	Post-Crisis Period	Entire Period
Trend	-4.545148*	0.731494	-12.79311*	-2.386437
Trend and intercept	-0.86309	-3.293206	-2.537858	-2.474365
None	1.225388	5.831249	0.419165	2.374749

(significance at 5% level)*

From these results, it can be inferred that SENSEX prices are trend stationary at level in the pre and post crisis period. This indicates that there a trend in SENSEX prices during these two periods. However, the results show absence of any trend during the crisis and entire period of study. These results also support the random walk hypothesis for all the periods, since past prices do not explain the behaviour of future prices and prices evolve randomly.

After having confirmed that SENSEX monthly closing log prices are trend stationary in the pre and post crisis periods, we will use a linear trend regression model to analyse the direction of the trend. We will conduct detailed trend analysis for the entire sample period as well three defined economic phases. The Table 4 below presents the regression results of the simple linear trend regression model:

Table 4: Regression results of linear time trend model $[\ln p_t = \alpha + \beta t + \varepsilon_t]$

Description	Pre-Crisis		Crisis		Post-Crisis		Entire-Period	
	Constant	Trend	Constant	Trend	Constant	Trend	Constant	Trend
Coefficient	10.5347	0.00079	2.35466	7.64E-05	10.5939	0.00074	8.63988	0.01068
t-statistic	437447	1150.87	2532503	746.898	274155	1064.4	227.25	27.843
p-value	0.0000	0.0000	0.0000	0.0000	0.0000	0.0000	0.0000	0.0000

From Table 4, it can be deduced that SENSEX prices have an upward trend during all the defined economic phases. The upward trend in the crisis period is surprising, however, within the crisis period SENSEX prices have witnessed alternative ups and downs which could be a possible and plausible explanation of this upward trend in the crisis period.

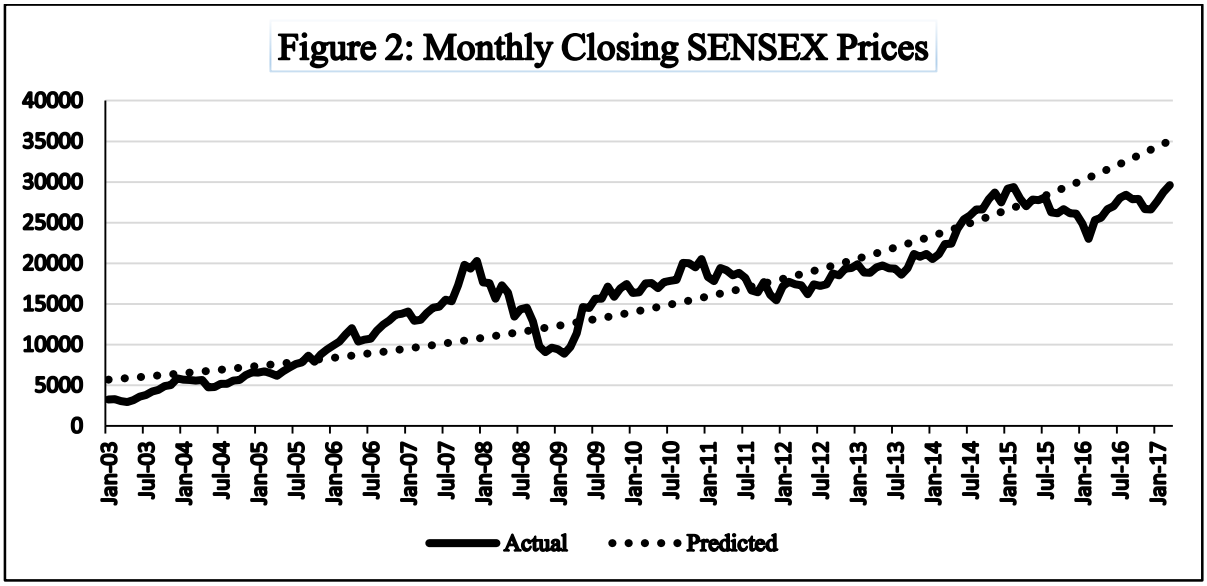

The positive trend in the SENSEX prices during the entire sample period is also revealed from Figure 2 shown by dotted line. In addition to this, efficiency ratio of the model which on an average is 0.999953 being close to 1 also explains the explanatory power of the linear trend model. While having a closer look on the fitted trend line in Figure 2, SENSEX prices have witnessed periods of swings and as such a model which captures these complex shifts due to different policy periods namely, pre-crisis, crisis and the post-crisis is estimated. The model incorporates shifts in the time trend during various defined economic phases. Table 5 presents the results of the dummy regression model (See).

Table 5: Regression results of dummy regression model:

$[\ln P_t = \alpha + \beta_1 t + D_2 + D_3 + \beta_2 D_2 * t + \beta_3 D_3 * t + \varepsilon_t]$

Description	Constant	Trend	$D_{pre\text{-}crisis}$	$D_{pre\text{-}crisis}$*T	$D_{post\text{-}crisis}$	$D_{post\text{-}crisis}$*T
Coefficient	13.2502	-0.0559	-5.1929	0.08562	-4.168	0.00074
t-statistic	34.1447	-9.8202	-13.354	14.9178	-10.671	11.0291
p-value	0.0000	0.0000	0.0000	0.0000	0.0000	0.0000

The average SENSEX prices and the corresponding trend during the crisis period has been taken as reference in the above dummy regression model and is represented by constant and trend respectively. As it can been noticed from the Table 5, the average SENSEX price in the crisis period is positive but with a negative time trend. However, during both pre and post

crisis period, average prices of SENSEX have come down with greater fall in prices during the pre-crisis period than the post-crisis period. During the pre-crisis period, the trend in SENSEX prices has been positive which is obvious since the Indian stock market had been growing during this particular period. In the post-crisis period, the results of the dummy regression model reveal that the Indian stock market has witnessed a stagnant phase with prices growing at a negligible rate. These results can be supplemented by the graphical demonstration of SENSEX prices during the entire period of study (See Figure 1). As it can be inferred from the Figure 1, during the pre-crisis period, Indian stock market is showing an upward trend while as during the post-crisis period, the prices have not grown significantly. Hence, the results presented in Table 5 support the trends and drifts in the Indian stock market during the period under consideration.

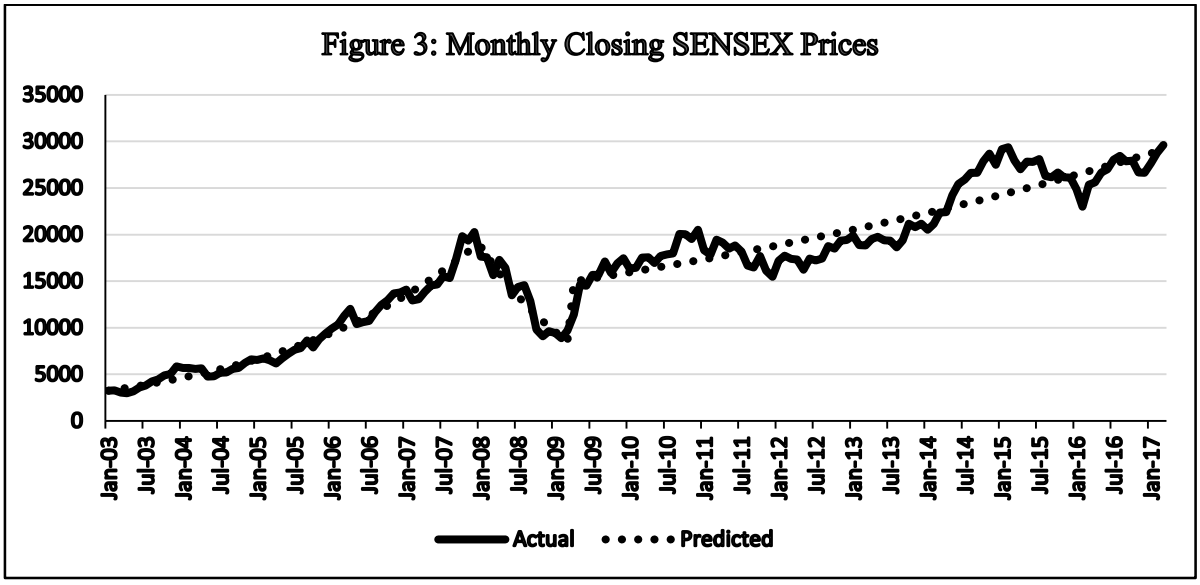

In contrast with Figure 2, where the predicted time trend in SENSEX prices has been estimated by using a simple linear time trend model, Figure 3 plots the trend in SENSEX prices after accounting for the effect of the crisis. It is clear that the trend predicted through the dummy regression model explains better the variation in SENSEX prices over time. The efficiency ratio of the dummy regression model equal to 1, which is a clear indication about the predictive efficiency of this model as compared to the previous linear time trend model. Finally, as per the argument, we have tested unit root properties of log SENSEX prices after incorporating intercept and slope dummies. For this purpose, the residuals of the dummy regression model which represent the de-trended log SENSEX price series after accounting for crisis effect have been put to ADF test. Here de-trending doesn't imply the removal of deterministic trend only, but also removal of the evident trend across the defined economic periods including the

variation in prices due to crisis effect. The results of the unit root test on the de-trended log SENSEX price series is given in Table 6 below:

Table 6: Augmented Dickey Fuller (ADF) test of de-trended log SENSEX prices without trend and intercept:

Description	t-statistics	C. V. at 5% level	p-value
ADF test statistic	-4.304905	-1.94272	0.0000

From Table 6, it can be found that the t-statistics of the ADF test on de-trended price series exceeds the critical value at 5% level of significance. Thus, it is concluded that de-trended series is stationary at its level. This modified version of the ADF test signifies that the log SENSEX prices are trend stationary which couldn't be captured by the classical ADF test.

The above analysis of SENSEX prices has no doubt led to the understanding of the behavioural properties of the stock prices, however, log of prices were found to be non-stationary at their level. Now, we shift our focus towards study of risk involved in stock market. Since risk is related to returns, we calculate monthly logarithmic returns of SENSEX by taking first difference of the log prices between two successive periods, i.e., months in our case.

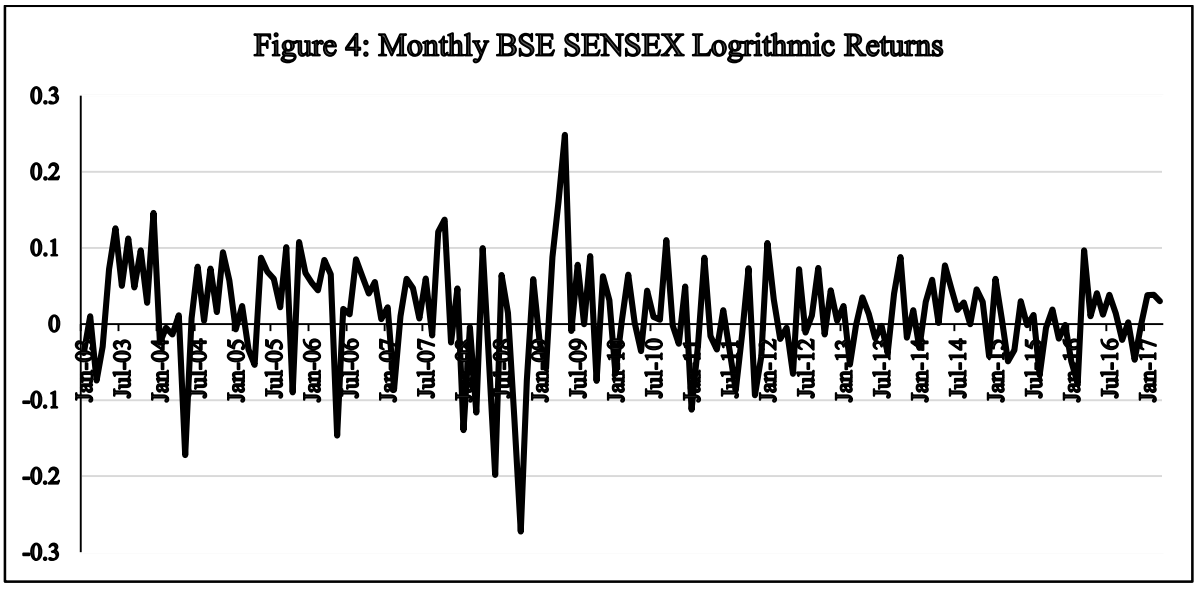

The graphical analysis of these returns is presented above in Figure 4. An initial look at this figure indicates about the mean-reverting nature of the returns which is one of the essential characteristics of stationary series. Figure 5 below plots the monthly excess logarithmic returns of SENSEX over monthly 91-days Treasury bill yield. We expect both of these return series to be stationary in nature at their level, however, such claim would be later verified by applying standard unit root test like ADF test to these time series of monthly returns.

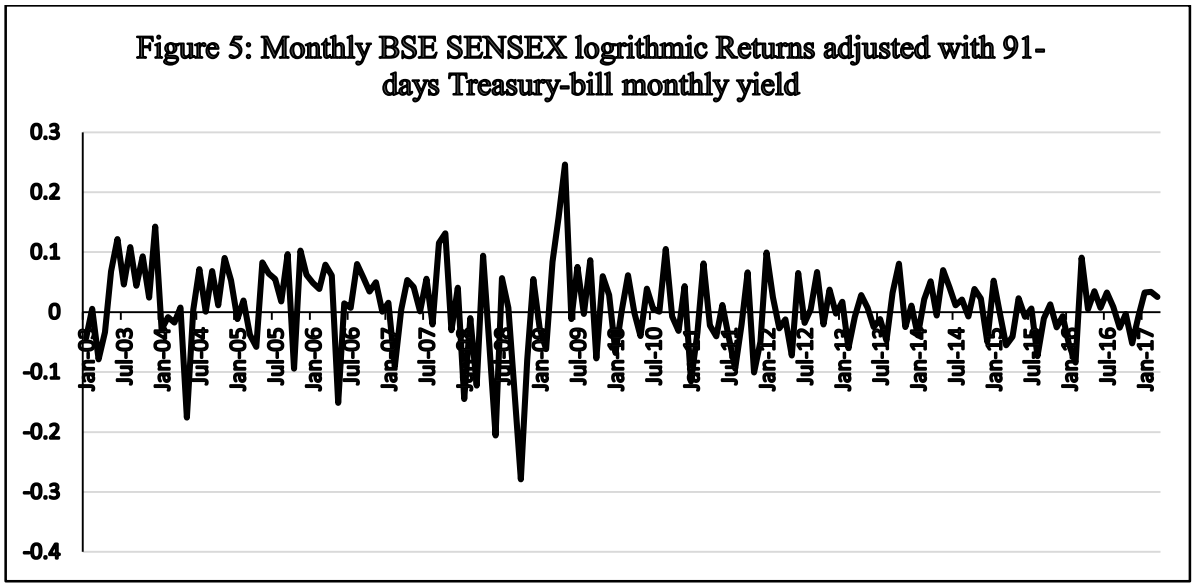

Next, we analyse descriptive statisics of both logrithmic monthly and logrithmic excess monthly returns of BSE SENSEX. The results shown in the Table 7 below indicate that both of these returns have increased over time. The return series during the sample period has ranged from a low of -2.73% to 24.88% incase of logrithmic returns and -2.78 to 24.61% in case of logrithmic excess monthly returns. Despite a fairly sufficeint number of observations in the sample, the results reveal about non-normal distributional property of these returns. Such a propery is inherent in stock returns which are generally found to follow leptokrytic fat tailed distributions with high kurtosis. In both the cases, we find a low negative skewnenss but high kurtosis with value of about 5.40. Hence, we can not argue that our sample of returns follows a normal distribution.

Table 7: Summary of Descriptive Statistics of monthly SENSEX Returns:

Description	Logarithmic	Excess Returns
Mean	0.0127	0.00724
Median	0.01236	0.00691
Maximum	0.24885	0.24616
Minimum	-0.273	-0.2788
Std. Dev.	0.06698	0.06725
Skewness	-0.5536	-0.5313
Kurtosis	5.40335	5.4019
Jarque-Bera	49.8876	49.1496
Probability	0.0000	0.0000
Sum	2.1714	1.23825
Sum Sq. Dev.	0.7626	0.76889
Observations	171	171

In the next step, we test both of these sample returns for their stationary properties using classical ADF test. However, in our further analysis, we may only use monthly excess returns of BSE SENSEX over 1 month 91-day Treasury bill yield. This adjustment in monthly returns has been made with the objective of hiving off riskless return, thereby arriving at that part of returns which are earned as risk premium for investing in stock market. Table 8 below presents the results of the ADF test of these monthly return series:

Table 8: Augmented Dickey Fuller test results of monthly logarithmic returns and excess monthly logarithmic returns of SENSEX ***(Based on Akaike Information Criterion)***

Description	Returns	Excess Returns
Trend	-11.67*	-11.581*
Trend and intercept	-11.771*	-11.709*
None	-11.321*	-11.485*

(significance at 5% level)*

From Table 8, it is evident that both logarithmic returns as well as excess logarithmic returns are stationary at level. Such a property in time series of stock returns enables to have reliable estimates from regression model. After satisfying the stationary condition, we proceed now with modelling of excess monthly SENSEX returns using linear time trend and dummy variable models which were used earlier for explaining the behaviour of underlying prices of the given return series. Now, our basic aim is to have a preliminary estimate of idiosyncratic volatility on SENSEX which we believe is volatility of the residual of its excess return series after having accounting for variations due to time and crisis effects. We argue that time in this case is a catch all variable that explains the effect of exogenous factors on the return series. Hence, trend and crisis effects are taken care of to arrive at a de-trended return series to get a preliminary estimate of idiosyncratic volatility.

Table 9: Regression results of linear time trend model $[\ln r_t = \alpha + \beta t + u_t]$

Description	Regression Results	
	Constant	Trend
Coefficient	0.020623	-0.000156
t-statistic	2.003498	-1.498945
p-value	0.0467	0.1358
R^2	0.01	
F-statistic (Prob.)	2.246837 (0.135754)	

Table 9 above presents the regression results of the linear time trend model. From these results, it is evident that excess monthly returns on SENSEX have a negative but statistically

insignificant time trend. Further, the model has a very low explanatory power which may be due to the reason that a simple linear trend model may not fit well when a time series is characterised by complex shifts in intercept and changes in slope caused due to different policy periods. We have observed earlier that during different economic phases, both average prices as well as their trend over time has not been similar. In order to verify the assumptions of the classical linear regression model we have conducted the residual diagnostics of the above reported linear trend model. Table 10 depicts the results of Breusch-Godfray and ARCH test which prove that there is no autocorrelation or heteroskedasticity problem in the model. The Jarque-Bera test of normality reveals that the residuals of the linear trend model are not normally distributed. However, due to the large size of the sample we can rely on the t-statistics of the regression model. Thus, we can conclude that the residuals of the linear time trend model are pure white noise and contain only unsystematic information.

Table 10: Residual diagnostics of linear time trend model $[\ln r_t = \alpha + \beta t + u_t]$

Description	Residual Diagnostics			
	Autocorrelation		Heteroskedasticity	
	Coefficient	Probability	Coefficient	Probability
F-statistic	0.8563	1.735819	2.848209	0.0933
Obs R-Squared	0.4266	0.4198	2.834069	0.0923

Figure 5: Histogram and Jarque-Bera test results

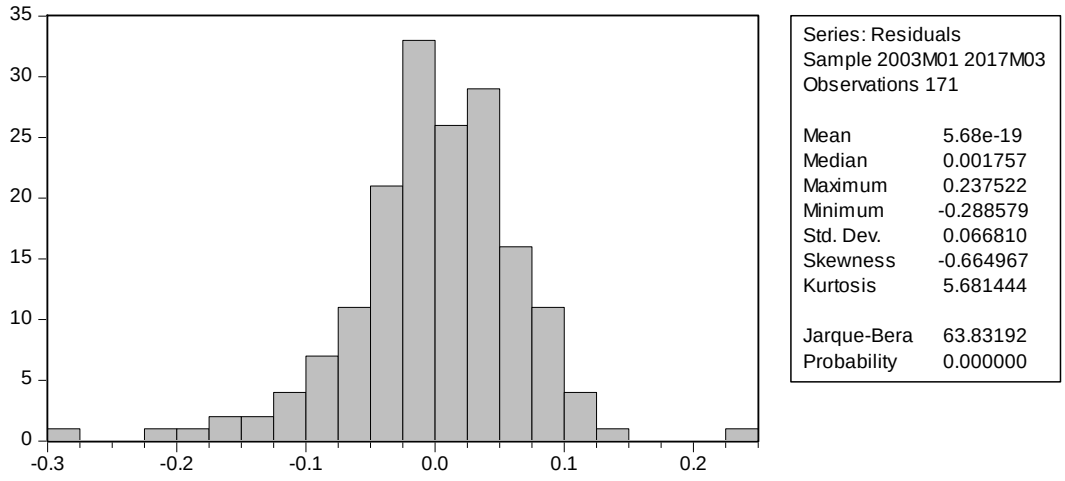

To capture the trend in excess returns after incorporation of the crisis effect, we have used a dummy regression model with the crisis period as the reference dummy, the impact of which is captured by the intercept and trend coefficient. The results of the dummy regression model presented in Table 11 reveal that the average excess returns in the crisis period are negative with a positive time trend, however, statistically insignificant at 5% level of significance. Apart

from this, the results show that average excess returns in the pre and post crisis periods are positive, but are not statistically different than the average excess returns in the crisis period. A positive trend with a coefficient (0.0002) has been found in the pre-crisis period which is not, however, statistically different than that in the crisis period. The post-crisis excess returns, by contrast, have a negative time trend with a coefficient (-0.0003) which is also not statistically different than the trend in excess returns in the crisis period.

Table 11: Regression results of dummy regression model:

$[\ln r_t = \beta_0 + \beta_1 T + D_2 + \beta_2 D_2 * t + D_3 + \beta_3 D_3 * t + u_t]$

Description	Constant	Trend	$D_{pre\text{-}crisis}$	$D_{pre\text{-}crisis}$*T	$D_{post\text{-}crisis}$	$D_{post\text{-}crisis}$*T
Coefficient	-0.34935	0.00433	0.368318	-0.004126	0.39056	-0.0046
t-statistic	-1.33713	1.129297	1.406826	-1.067639	1.48516	-1.202
p-value	0.183	0.2604	0.1614	0.2872	0.1394	0.2311
R^2	0.116532					
F-statistic (Prob.)	4.352811 (0.000953)					

The explanatory power of the regression model with intercept and slope dummies has significantly increased to 11% from 1% in the simple linear trend model. This is indicative of the dummy regression model capturing the variation in excess index returns due to shifts in intercept and changes in slope across different economic phases. The overall fit of the model measured from F-statistic has also improved and is now statistically significant. This implies that the model incorporating effect of various economic phases predicts the variations in excess returns due to systematic factors in a better way than the simple trend model. Further, to verify the reliability of the t-statistics of the regression coefficients, we have performed residual diagnostics of the dummy regression model which are shown in Table 12 and Figure 6 below.

Table 12: Residual diagnostics of dummy regression model

$[\ln r_t = \beta_0 + \beta_1 T + D_2 + \beta_2 D_2 * t + D_3 + \beta_3 D_3 * t + u_t]$

Description	Residual Diagnostics			
	Autocorrelation		Heteroskedasticity	
	Coefficient	Probability	Coefficient	Probability
F-statistic	0.36846	0.6924	0.41566	0.5200
Obs R-Squared	0.7696	0.6806	0.41957	0.5172

The results of Breusch-Godfray and ARCH test given in Table 11 above show that there is no autocorrelation or heteroskedasticity problem in the model as the probability of the test statistics for both the tests has been observed to be less than 5% level of significance. The Jarque-Bera test of normality reveals that the residuals of the dummy regression model are not

normally distributed. However, due to the large size of the sample we can rely on the t-statistics of the regression model. Thus, we can conclude that the residuals of the dummy regression model are pure white noise and contain only unsystematic information.

Figure 6: Histogram and Jarque-Bera test results

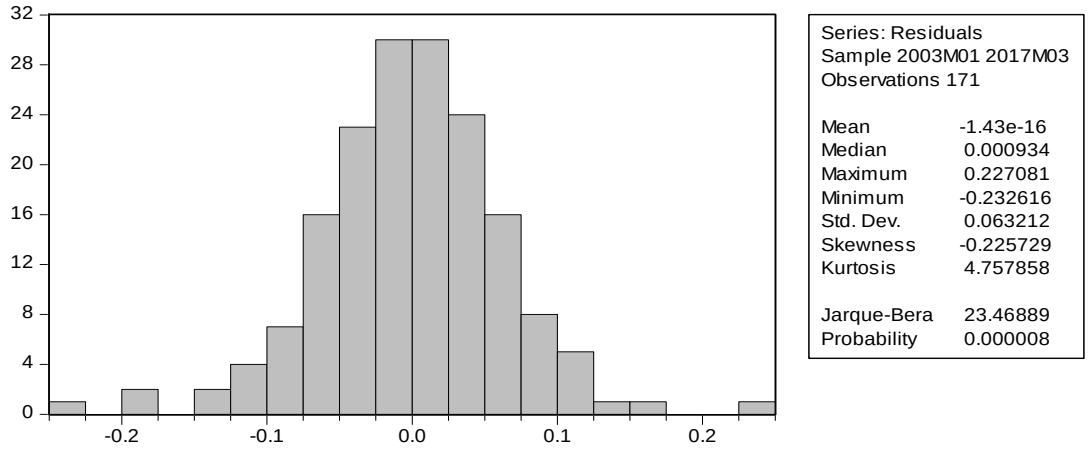

From the Figure 7, we observe that the trend in excess monthly index returns estimated using dummy regression model gives a better fit than that predicted by the simple linear trend model. It is evident from the graph that the dummy regression model takes into account the effect of crisis on the behaviour of stock returns.

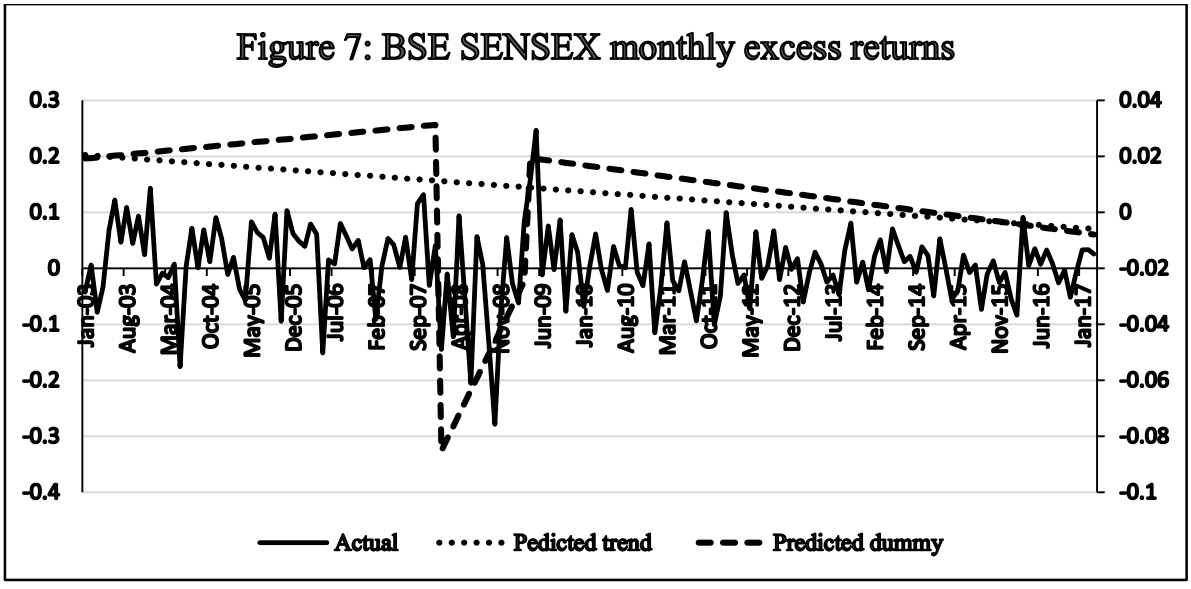

In addition to this, efficiency ratio of the simple linear trend and dummy regression model which are on an average equal to 1.00219 and 1.00198 respectively (See Appendix 2) is close to 1 in both the cases, however in cases of dummy regression model, this ratio is slightly better

than the trend model. In our dummy regression model, we argue that time is a 'catch all proxy' which captures variation in the stock returns due to systematic factors. Further, we have added crisis dimension to our model. We believe that crisis is a common external influence or systematic risk that effects all firms uniformly, as such, needs to be accounted for before attempting to estimate any preliminary measure of idiosyncratic volatility. Since, we have accounted for variation in index returns due to systematic risk factors by incorporating time and crisis, whatever remains unaccounted for can be argued to represent variation in the index returns due to unsystematic risk factors. These unsystematic risk factors are captured by the residuals of the regression model. Earlier, we tested residual series of dummy regression model which was found to have constant variance over time. Thus, we use a simple time invariant measure, i.e., square of regression residuals as a measure of our idiosyncratic volatility. However, explanatory power of the dummy regression model is very low, which indicates about other systematic factors that our model couldn't take into account. Therefore, we can't argue about the robustness of our estimate of idiosyncratic volatility unless missing systematic factors are identified and accounted for. However, as a preliminary estimate of idiosyncratic volatility, the squared residuals of dummy regression model represent a convenient proxy. Figure 8 below plots monthly idiosyncratic volatility of BSE SENSEX returns.

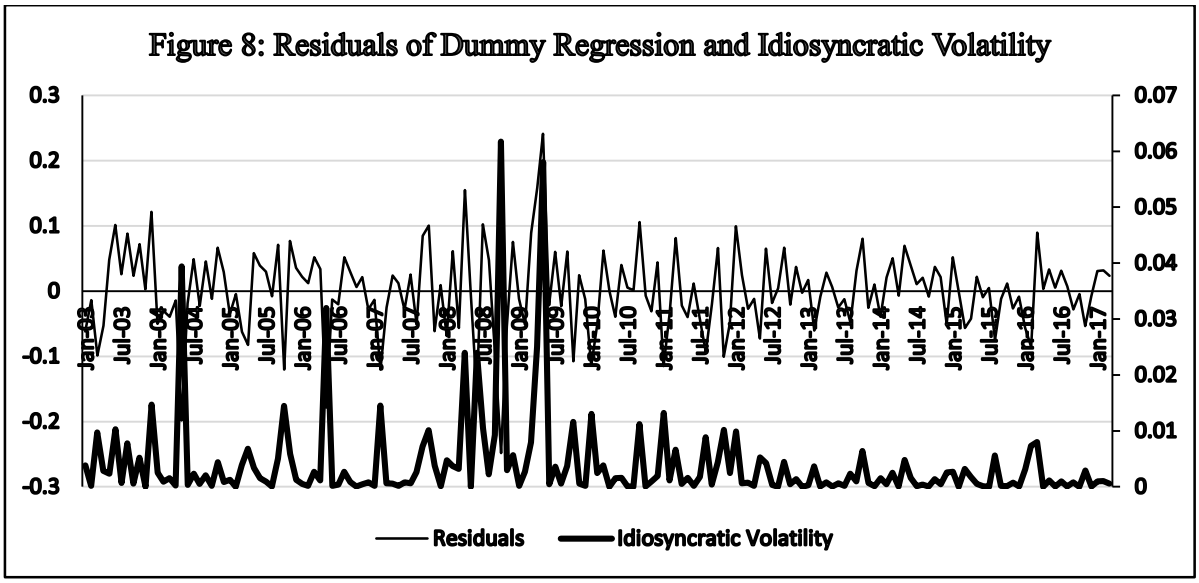

In the Figure 9 below, we compare our monthly estimate of idiosyncratic volatility of SENSEX index returns with its market volatility. Over time, it is found that idiosyncratic volatility doesn't exceed market volatility and is lesser than the market volatility. This is a plausible evidence, because an index being a collection of different stocks is believed to be like a well-diversified portfolio with no or negligible idiosyncratic risk.

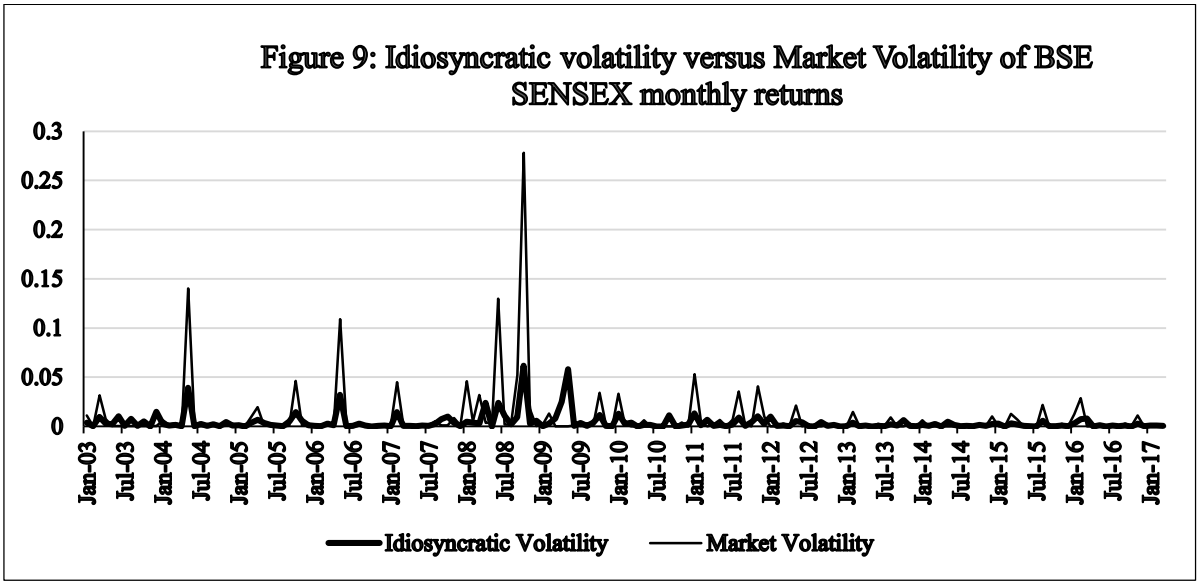

In the end, we examine the time trend in our idiosyncratic volatility estimate. We employ a simple linear time trend model to analyse the behaviour of idiosyncratic volatility. The below Table 13 present the results of the linear time trend model.

Table 13: Regression results of linear time trend model $ivol_t = \alpha + \beta t + \upsilon_t$

Description	Regression Results	
	Constant	Trend
Coefficient	0.006471	-2.78E-05
t-statistic	5.118734	-2.18435
p-value	0.00000	0.0303
R^2	0.03	
F-statistic (Prob.)	4.771386 (0.030314)	

The results of the linear time trend model reveal that idiosyncratic volatility of BSE SENSEX returns has witnessed a significant downward trend. The possible explanation of such a behaviour of idiosyncratic volatility could be that in the beginning of our sample, idiosyncratic volatility has been high particularly during the crisis period followed by low and stable idiosyncratic volatility in the post crisis period. A downward trend in idiosyncratic volatility leads to reduction in the number of stocks needed to achieve a well-diversified portfolio. Hence, in that sense, behaviour of idiosyncratic volatility which is trending downwards can be interpreted as investor favourable in the Indian stock market. Such a trend in idiosyncratic volatility in the Indian market is also in contract of result found in stock markets of many developed countries including USA.

CONCLUSION

In finance theory, EMH acts as the basic premise underlying behaviour of stock prices and returns. As per EMH, stock prices reflect all the available information, such that above average returns cannot be achieved without assuming above average risk. However, tests of EMH revolve around testing of an equilibrium model for the market. Over the period, CAPM has evolved as a standard asset pricing model which explains risk-return trade off of financial assets. Under CAPM framework, overall risk in a financial security comprises of two components which include systematic or market wide risk and unsystematic or firm specific risk. CAPM argues that only systematic risk being non-diversifiable should be priced, while as unsystematic risk or idiosyncratic risk being diversifiable should not be compensated. However, in many cases, it has been found that CAPM doesn't explain properly the relationship between risk and returns of assets. The contemporary asset pricing models, like multi-factor models criticise CAPM for its inability to fully capture risk factors effecting the returns of financial securities. At the same time, complete diversification by investors and consequently no reward for idiosyncratic risk has been in essence found to be impossible, hence some amount of idiosyncratic risk due to inadequate diversification is borne by the investors in general and therefore should command a premium.

Generally, asset pricing models including CAPM use market risk proxy to explain variation in stock returns due to systematic risk factors, however, effect of trend and crisis on the behaviour of stock prices and subsequently on returns is not taken care of. Our study intends to capture a preliminary measure of idiosyncratic volatility. Further, it doesn't claim to develop a full-fledged model nor to explain idiosyncratic volatility. We model the behaviour of stock prices and returns by including the effect of trend and crisis. In doing so, we have used semi-log growth model and dummy variable regression model to incorporate the effect of trend and crisis on stock prices/returns. Our argument is that time is a "catch all variable" that explains variation in stock prices/returns due to systematic risk factors. Besides, we have tested the stationarity of prices and returns by using Augmented Dickey Fuller (ADF) test. The ADF test accounts for single intercept and slope for testing of stationarity of a time series. However, in our sample, due to different economic phases around crisis, we notice multiple shifts in the drift (intercept) and changes in the trend (slope) across different economic phases. Since the standard unit root test like ADF test in our case doesn't account for variation in prices due to crisis, we introduce a model with a set of intercept and slope dummies to account for the effect

of various economic phases surrounding crisis. Our results show monthly closing prices of SENSEX are trend stationary after accounting for the impact of crisis. After analysing behaviour of trend in SENSEX prices, we examine the behaviour of SENSEX returns. After incorporating crisis effect into our model, we notice that there is an improvement in predictability of the model over a simple trend model that used only time as an explanatory variable. However, the coefficients of dummies are not significant, it implies that excess return are not being significantly affected by dummies which indicates that there are other factors which may be included- both systematic and unsystematic factors; other than crisis that are likely to affect return in the case of a full blown model. Moreover, we have noticed time dummies affect prices more crucially than returns because returns are very small and their standard error is large. If crisis is not incorporated in this manner for estimating idiosyncratic volatility, the resultant measure of the estimated random error would be biased. Hence, the basis of arriving at idiosyncratic volatilely would also be biased. The dummy regression is a parsimonious estimation of excess returns as explained by the systematic risk factors, the residuals of this model forms the basis of measurement of idiosyncratic volatility. Further, results of trend analysis of idiosyncratic volatility reveal a statistically significant downward trend. Such a trend in idiosyncratic volatility indicates a decrease in the number of stocks required for diversification of portfolio.

We measure efficiency ratio for comparing the predictive efficiency of different models. The results show that efficiency ratio of a model improves as we move from a simple time trend model to dummy variable regression model. The square of the residuals of the dummy regression model forms the preliminary estimate of the idiosyncratic volatility. We applied residual diagnostic tests to the residual of the dummy regression model to check whether or not the residual are pure white noise. The results of the residual diagnostic including LM and ARCH tests reveal that the residuals are free from autocorrelation and are homoscedastic. However, the Jarque-Bera test results reject the assumption of normally distributed residuals. Thus, we can say that residuals of regression which incorporate crisis effect are not pure 'white noise'. This implies that some portion of variance in returns which is left unexplained by crisis and other 'exogenous generic factors' which are systematic in nature is a source of idiosyncratic volatility. We believe that 'time' as a catch all variable is a proxy and a gross measure (systematic) which cannot capture all the information. It does not account for finer changes which could be associated with unsystematic risk. Even if time is a proxy, it only represents systematic factors (not unsystematic ones). The analysis of residuals obtained from

the dummy regression model reveals that there is a need to analyse further because the properties show that there is more information contained in the residuals. Apart from this, the R-Square of the model is quiet low which is a valid outcome since we deal with a univariate model. Thus, a fully specified model needs to be identified which can lead to better result in terms of explanatory power. Hence, there is a need to have separate approach to get a better measure of firm specific or idiosyncratic volatility.

The present study has important insights for investors, portfolio managers and academicians. For the academic community, our study tries to fill the research gap by incorporating crisis in modelling the behaviour of stock prices and returns. This is aimed to provide future direction for reassessing the behaviour of stock prices and returns by use of more advanced research tools and techniques. For investors and asset managers, this study indicates that with a downward trending idiosyncratic volatility, there may be a reduction in number of assets needed to create a well-diversified portfolio. Obviously, reduction in idiosyncratic volatility should bring a relief to investors in terms of requirement of less number of stocks in portfolio if they do not want to bear idiosyncratic volatility.

We have demonstrated that extant studies which have ignored the crisis effect may have wrongly found idiosyncratic volatility trending upwards. Our model may not be perfect, but we have attempted to minimise the problems that have been left out by others. However, our model needs to be supplemented with a more detailed study using multivariate structural equations. There is a need to specify more of control and cohort variables that could capture idiosyncratic shocks are required.

REFERENCES

Angelidis, T. (2010). Idiosyncratic risk in emerging markets. *Financial Review*, *45*(4), 1053-1078.

Bali, T. G., Cakici, N., & Levy, H. (2008). A model-independent measure of aggregate idiosyncratic risk. *Journal of Empirical Finance*, *15*(5), 878-896.

Bekaert, G., Hodrick, R. J., & Zhang, X. (2008). Is there a trend in idiosyncratic volatility? *Available at SSRN 1108170*.

Brandt, M. W., Brav, A., Graham, J. R., & Kumar, A. (2010). The idiosyncratic volatility puzzle: Time trend or speculative episodes? *Review of Financial Studies*, *23*(2), 863-899.

Brown, G., & Kapadia, N. (2007). Firm-specific risk and equity market development. *Journal of Financial Economics*, *84*(2), 358-388.

Campbell, J. Y., Lettau, M., Malkiel, B. G., & Xu, Y. (2001). Have individual stocks become more volatile? An empirical exploration of idiosyncratic risk. *The Journal of Finance*, *56*(1), 1-43.

Chaudhuri, K., & Wu, Y. (2003). Random walk versus breaking trend in stock prices: Evidence from emerging markets. *Journal of Banking & Finance*, *27*(4), 575-592.

Chen, Z., & Petkova, R. (2012). Does idiosyncratic volatility proxy for risk exposure? *Review of Financial Studies*, *25*(9), 2745-2787.

Fama, E. F. (2014). Two pillars of asset pricing. *The American Economic Review*, *104*(6), 1467-1485.

Fink, J., Fink, K. E., Grullon, G., & Weston, J. P. (2010). What drove the increase in idiosyncratic volatility during the internet boom? *Journal of Financial and Quantitative Analysis, (45)5,* 1253–1278

Garcia, R., Mantilla-Garcia, D., & Martellini, L. (2014). A model-free measure of aggregate idiosyncratic volatility and the prediction of market returns. *Journal of Financial and Quantitative Analysis*, *49*(5-6), 1133-1165.

Gerlach, R., Obaydin, I., & Zurbruegg, R. (2015). The impact of leverage on the idiosyncratic risk and return relationship of REITs around the financial crisis. *International Review of Economics & Finance*, *38*, 207-219.

Goyal, A., & Santa-Clara, P. (2003). Idiosyncratic risk matters! *The Journal of Finance*, *58*(3), 975-1007.

Gujarati, D. N., Porter, C. D. & Gunasekar, S. (2009). *Basic econometrics*. New Delhi, India: Tata McGraw-Hill Education.

Hamao, Y., Mei, J., & Xu, Y. (2003). *Idiosyncratic risk and the creative destruction in Japan* (No. w9642). National Bureau of Economic Research.

Huberman, G. (2001). Familiarity breeds investment. *Review of financial Studies*, *14*(3), 659-680.

Kearney, C., & Potì, V. (2008). Have European stocks become more volatile? An empirical investigation of idiosyncratic and market risk in the euro area. *European Financial Management*, *14*(3), 419-444.

Liu, Z., Nartea, G. V., & Wu, J. G. (2017). Patterns and pricing of idiosyncratic volatility in French stock market. *Available at SSRN 2973142*.

Malkiel, B. G., (2005). Reflections on the efficient market hypothesis: 30 years later. *Financial Review*, *40*(1), 1-9.

Malkiel, B. G., & Xu, Y. (2002). Idiosyncratic risk and security returns. *University of Texas at Dallas (November 2002)*.

Malkiel, B. G., *A Random Walk Down Wall Street*, 1st Edition, New York, W.W. Norton, 1973.

Miralles-Marcelo, J. L., del Mar Miralles-Quirós, M., & Miralles-Quirós, J. L. (2012). Asset pricing with idiosyncratic risk: The Spanish case. *International Review of Economics & Finance*, *21*(1), 261-271.

Nartea, G. V., Wu, J., & Liu, Z. (2013). Does idiosyncratic volatility matter in emerging markets? Evidence from China. *Journal of International Financial Markets, Institutions and Money*, *27*, 137-160.

Newbold, P., & Granger, C. W. (1974). Experience with forecasting univariate time series and the combination of forecasts. *Journal of the Royal Statistical Society.* Series A (General), 131-165.

Panait, I., & Constantinescu, A. (2012). Stylized facts of the daily and monthly returns for the European stock indices during 2007-2012. *Journal of Applied Quantitative Methods.* 8(1), 26-39

Perron, P. (1989). The great crash, the oil price shock, and the unit root hypothesis. *Econometrica: Journal of the Econometric Society*, 1361-1401.

Roll, R. (1977). A critique of the asset pricing theory's tests Part I: On past and potential testability of the theory. *Journal of financial economics*, *4*(2), 129-176.

Sousa, S. R., & Serra, A. P. (2008). What drives idiosyncratic volatility over time? *Portuguese Economic Journal*, *7*(3), 155-181.

Annual Report for the year 2015-16 and website disclosures of Bombay Stock Exchange accessed at: http://www.bseindia.com/downloads1/BSE_Annual_Report_2015_2016.pdf on 26-05-2017.

https://quantivity.wordpress.com/2011/02/21/why-log-returns/ accessed on 04-06-2017.

Further, the extant literature reveals that researches that have ignored the effect of financial crisis may have wrongly observed that idiosyncratic volatility is trending upwards.

Clean Energy, 2018, 1–14

doi: 10.1093/ce/zky011
Homepage: https://academic.oup.com/ce

Research Article

Energy- and exergy-based performance evaluation of solar powered combined cycle (recompression supercritical carbon dioxide cycle/organic Rankine cycle)

Harwinder Singh* and R.S. Mishra

Department of Mechanical, Production & Industrial, Automobile Engineering, Delhi Technological University, Bawana Road, New Delhi-110042, India

*Corresponding author. E-mail: harrymehrok14@gmail.com

Abstract

Nowadays, the recompression supercritical carbon dioxide (R-SCO_2) cycle has emerged as a promising option for power conversion systems because of its boundless potential to tackle energy and environmental issues. In this study, we examined the performance of the solar parabolic trough collector (SPTC) integrated combined cogeneration system for the purpose of power generation as well as recovery of waste exhaust heat from the R-SCO_2 cycle with the help of the organic Rankine cycle (ORC). An exergy and energy analysis was performed for a combined recompression cycle (R-SCO_2-ORC) by varying the input variables such as intensity of solar irradiation (G_b), pressure at the inlet of SCO_2 turbine (P_5), mass flow rate of SCO_2 ($\dot{m}_{SCO_2}$) inlet temperature of SCO_2 turbine (T_5), inlet temperature of main compressor (T_9) and effectiveness of the high- and low-temperature recuperator (ε_{HTR} and ε_{LTR}). Eight organic working fluids were considered for the ORC: R123, R290, isobutane, R1234yf, R1234ze, toluene, isopentane and cyclohexane. The study revealed that R123-based R-SCO_2-ORC demonstrates the highest thermal and exergy efficiency: ~73.4 and 40.89% at G_b = 0.5 kW/m^2; 78.8 and 43.9% at P_5 = 14 MPa; 63.86 and 35.57% at T_5 = 650 K; 74.84 and 41.69% at $\dot{m}_{SCO_2}$ = 7 kg/s; 85.83 and 47.82% at T_9 = 300 K; 84.57 and 47.11% at ε_{HTR} = 0.65; 85.06 and 47.38% at ε_{LTR} = 0.65, respectively. Alternatively, R290 showed the minimum value of exergy and thermal efficiency. As can be seen, the maximum amount of exergy destruction or exergy loss occurs in a solar collector field, ~58.25% of the total exergy destruction rate (i.e. 6703 kW) and 18.99% of the solar inlet exergy (i.e. 20 562 kJ). Moreover, R123 has the highest net work output, ~4594 kJ at T_5 = 650 K and 6176 kJ at T_9 = 300 K.

Key words: SPTC; recompression SCO_2 cycle; ORC; exergy and thermal efficiency; exergy destruction rate; organic fluids

Introduction

The well-known features of the supercritical carbon dioxide (SCO_2) Brayton cycle—simplicity, compactness, superior economy, sustainability, low capital cost due to the small size of equipment and plant footprint, enhanced safety, and high cycle efficiency—make it an attractive option for power generation plants [1, 2]. CO_2 is a promising and prominent option as a working fluid because of its low cost, abundance in nature, nonflammability, nonhazardous nature and ability to resist at higher temperature [3]. SCO_2 exhibits more reasonable values as compared to other working fluids such as water and available gases (i.e. ammonia and helium) at critical temperature (i.e.

Received 15 January, 2018; **Accepted** 24 April, 2018

© The Author(s) 2018. Published by Oxford University Press on behalf of National Institute of Clean-and-Low-Carbon Energy
This is an Open Access article distributed under the terms of the Creative Commons Attribution Non-Commercial License (http://creativecommons.org/licenses/by-nc/4.0/), which permits non-commercial re-use, distribution, and reproduction in any medium, provided the original work is properly cited. For commercial re-use, please contact journals.permissions@oup.com

Downloaded from https://academic.oup.com/ce/advance-article-abstract/doi/10.1093/ce/zky011/5059098
by Delhi Technological University user
on 15 July 2018

~31°C) and critical pressure (i.e. 7.38 MPa), respectively [4]. Feher [5] proposed a SCO_2-based power cycle for electricity generation and concluded that the thermal efficiency of the cycle is around 55% under ideal working conditions. Kulhánek and Dostál [6] compared different configurations of the SCO_2 Brayton cycle and found that both the R-SCO_2 cycle and SCO_2 cycle with partial cooling show higher thermal efficiency in contrast to a simple SCO_2 cycle. Sarkar and Bhattacharyya [7] conducted a study to optimize the thermal performance of the R-SCO_2 cycle with and without reheating through sensitivity analysis. They found an improvement in thermal efficiency results with a decrease in minimum temperature and with an increase in maximum temperature, and pressure of the cycle. Turchi et al. [8] concluded that the SCO_2 Brayton cycle possesses the highest thermal performance as compared to the steam Rankine cycle based on energy efficiency.

Furthermore, some studies are available in the literature regarding the application of the organic Rankine cycle (ORC) for proper utilization of waste exhaust heat of the SCO_2 Brayton cycle or in other configurations so that overall performance of the cycle can be maximized. Chacartegui et al. [9, 10] conducted a study to utilize the waste heat of ORC in power production and found that, on the basis of the turbine inlet temperature, the thermal efficiency of the combined-cycle layout can be enhanced by 7–12% as compared to the other selected layouts. Wang and Dai [11] examined the performance of two different combined cogeneration cycles, in which the ORC and transcritical CO_2 (tCO_2) cycle act as bottoming cycles to recover waste heat from the R-SCO_2 cycle. Based on parametric investigations and exergoeconomic analysis, their results revealed that the SCO_2/tCO_2 cycle has better performance than SCO_2/ORC at a lower compression pressure ratio. Finally, they found from the results of optimization that the SCO_2/tCO_2 cycle has an exergy efficiency comparable with the SCO_2/ORC.

Sánchez et al. [12] examined the utilization of waste heat of the SCO_2 cycle via the ORC with the use of hydrocarbon mixtures and found that the mixture composition directly affects the performance of combined cycle. Akbari and Mahmoudi [13] studied the exergy performance of a combined SCO_2/ORC cycle and found that the exergy efficiency increased up to 11.7%; their results also revealed that isobutane and RC318 working fluids were the best option in term of exergy efficiency. Besarati and Goswami [14] concluded that the maximum overall efficiency can be achieved by a recompression SCO_2/ORC cycle in contrast to a simple configuration. Apart from this, Tunc et al. [15] analyzed the thermal performance of a single-flash geothermal power-driven ORC by the application of different organic fluids such as isobutane, HCFC123, R134a and R12. Finally, their results revealed that isobutane gives the maximum thermal efficiency and power generation (i.e. 30% and 6626 kWe).

Furthermore, solar energy has been proven as an efficient heat source for deployment in cogeneration, trigeneration, or poly-generation plants to produce electricity [16, 17]. Concentrating solar collectors such as the parabolic trough collector, linear Fresnel reflector (LFR) and solar concentrating dish are the most customary high-temperature devices for the operation of a recompression combined cycle in contrast to simple configuration of an SCO_2 cycle [18–21]. Many researchers investigated the use of solar collectors for the operation of a simple and combined power cycle. For instance, Gao et al. [22] investigated the performance of solar based ORC under various working conditions such as the inlet temperature and turbine pressure. They found that the efficiency increases with an increase in inlet temperature as well as with the inlet pressure when the system is held above the critical temperature. Mokheimer et al. [23] observed the exercise of various solar collectors in the combined-cycle function and found that, for Saudi Arabian climate conditions, SPTC and LFR are the most sustainable solutions. Amelio et al. [24] examined the application of solar collectors in a combined cycle that reduces the amount of fuel consumption in the combustion chamber of the gas turbine. Their results revealed that fuel consumption diminishes up to 22% at nominal conditions and 15.5% on a yearly basis.

Al-Sulaiman [25] performed energy and sizing analysis of an SPTC integrated steam Rankine cycle (SRC) and a binary vapor cycle (SRC/ORC) with seven refrigerants and found that the R134a binary vapor cycle requires a smaller solar field size and also shows the best performance among the other cycles considered. He also carried out an exergy analysis of these cycles and evaluated the exergetic parameters and concluded that R134a gives the highest exergy efficiency, 26%, whereas R600a shows the least value for exergy efficiency of the combined cycle, ~20–21% [26]. Seidel [27] determined that, for a wide range of pressure ratios, a concentrated solar power (CSP) integrated R-SCO_2 cycle has the highest thermal efficiency among the other configurations. Turchi et al. [28] found that an R-SCO_2 cycle working at a temperature germane to CSP application provides higher cycle efficiency in contrast to supercritical steam cycles.

Najjar and Sadeq [29] carried out a performance study in Saudi Arabia of an SPTC integrated supercritical organic Rankine cycle (SORC) in the environment of several sites and found that the availability of solar radiation in Jeddah is higher than other places. Their results also revealed that ammonia possesses the highest thermal efficiency as compared to R141b, propane, R143a and R500. Singh and Mishra [30] have also analysed the performance of an SPTC integrated SORC system by using R600a, toluene, R152a, isobutene and cyclohexane. They found that R600a has the highest exergy efficiency and minimum exergy losses among the fluids analysed. Rashidi et al. [31] performed a parametric study of regenerative Clausius and ORC integrated with two feedwater heaters for R717 and water.

Downloaded from https://academic.oup.com/ce/advance-article-abstract/doi/10.1093/ce/zky011/5050906
by Delhi Technological University user
on 15 July 2018

They optimized their results with the help of an artificial neural network (ANN) and the artificial bee colony (ABC) algorithm. They concluded that R717 has the maximum value of specific network thermal and exergy efficiency when compared with water.

In addition, solar parabolic trough collector (SPTC) technology has greater potential to generate electric power due to its higher commercial performance and reliability, and its suitability in India's sunny climate. The available solar energy potential in India is 20 MW/km^2 and the solar intensity is 6 kwh/m^2 /day [32]. The concentrated solar power-driven SCO_2 cycle also has some important merits: at dry cooling conditions, the SCO_2 cycle possesses superior performance compared to a steam Rankine cycle, and can operate with a thermal storage system economically [33]. The simple configuration of the SCO_2 cycle is less efficient, but due to its design simplicity, it can potentially attract the commercial market. On the other hand, the recompression cycle also has a simple design and can be employed in those applications that require high thermal efficiencies [33]. One more advantage of the recompression cycle is that more heat can be recovered than with the simple configuration due to flow splitting after the low-temperature recuperator (LTR) that decreases the heat capacity of the high-pressure stream in the LTR, and consequently the problem of pitch point can be avoided in the recuperator [14].

In this direction, important research has been reported in recent years that concentrates specifically on the recompression SCO_2 (R-SCO_2) cycle. Cheng et al. [34] performed an optimization study based on sensitivity analysis of the R-SCO_2 cycle and found that, by adjusting the maximum pressure of 27.75 MPa and split flow ratio of 0.687, the efficiency of the cycle could be enhanced to 0.447. Ma et al. [35] developed a mathematical model for an R-SCO_2 cycle with the application of main compression intercooling (MCIC) and concluded that its 2.65% efficiency could be improved with the use of MCIC. Kim et al. [36] performed an effectiveness and pitch point temperature difference analysis to evaluate irreversibility in the recuperator of an R-SCO_2 cycle. Their results reveal that, at optimum conditions, the efficiency of the R-SCO_2 cycle is ~44.67%. Reyes-Belmonte et al. [37] optimized the performance of an R-SCO_2 cycle for a solar central receiver power plant based on the recuperators' effectiveness and found that the cycle efficiency could be between 43–49% for a turbine inlet temperature varying from 630–680°C. Wu et al. [38] carried out a parametric and optimization study of a combined R-SCO_2/absorption refrigeration cycle and concluded that the energy utilization factor and exergy efficiency of the combined cycle was enhanced by 38.80 and 1.95%, respectively, for the optimal design case.

Based on the aforementioned research, it has been observed that the parametric analysis of a SPTC integrated combined R-SCO_2 cycle/ORC system is crucial for power generation along with the minimum wastage of heat. Research on the theoretical simulation of the SPTC system, thermodynamic analysis and optimization of the R-SCO_2 cycle and some experimental tests have been put forward in recent years. However, few studies are available on parametric analysis of SCO_2-based combined cycles as understood from the above mentioned literature work. Previously, Singh and Mishra [39] conducted a performance analysis of a SPTC-driven combined SCO_2 cycle/ORC system but this current study replaces the simple configuration of an SCO_2 cycle by a recompression cycle, which makes it completely different from the previous work. The use of a parabolic trough collector as an energy source also brings much novelity in itself, as it has an ability to provide a limited and sufficient temperature range for the operation of a combined cycle.

Therefore, we conducted an energy- and exergy-based parametric analysis of a SPTC integrated combined R-SCO_2 cycle/ORC system to determine the exergy and thermal efficiency and the net work output. The main design and operating parameters are as follows: intensity of solar irradiation, pressure at the inlet of SCO_2 turbine, mass flow rate of SCO_2, inlet temperature of SCO_2 turbine, inlet temperature of main compressor, and effectiveness of high- and low-temperature recuperator under the best operating conditions used to analyse the performance.

1 Technology description

A combined recompression cycle is a combination of an R-SCO_2 cycle (i.e. topping cycle) and an ORC (i.e. bottoming cycle) as shown in Fig. 1. The geometrical data for the SPTC system and thermophysical properties of heat transfer fluid (HTF) flowing in the collector field have been adapted from Singh and Mishra [39]. Apart from this, CO_2 is used as a working fluid in the topping cycle and it becomes incompressible under critical pressure and critical temperature condition (about 7.38 MPa and 30.98°C, respectively) [40]. Also, recompression configuration reduces the heat losses from the R-SCO_2 cycle and enhances the thermal efficiency with the help of flow splitting in order to compensate the difference in specific heats in the LTR [40]. The stream from the LTR is split upstream of the heat exchanger (state 7′); the main stream with high mass flow rate after passing through the heat exchanger (state 7′–8) is cooled in the cooler unit (state 8–9) and then compressed up to high pressure in the main compressor (9–10); and finally, this heated stream enters the LTR again (state 10) and exchanges its heat with the incoming stream (state 7). On the other side, another fraction of the split stream with low mass flow rate goes directly to the recompressing compressor, where it is compressed to the higher pressure side (state 9′) and mixed with the main stream returned from the LTR (state 10′) prior to the high-temperature recuperator (HTR). Furthermore, flow splitting should be adjusted so that the outlets for the recompressor and exiting cold stream of the LTR always remain the same [1]. Moreover, other processes of the considered configuration are the

Downloaded from https://academic.oup.com/ce/advance-article-abstract/doi/10.1093/ce/zky011/5050906
by Delhi Technological University user
on 15 July 2018

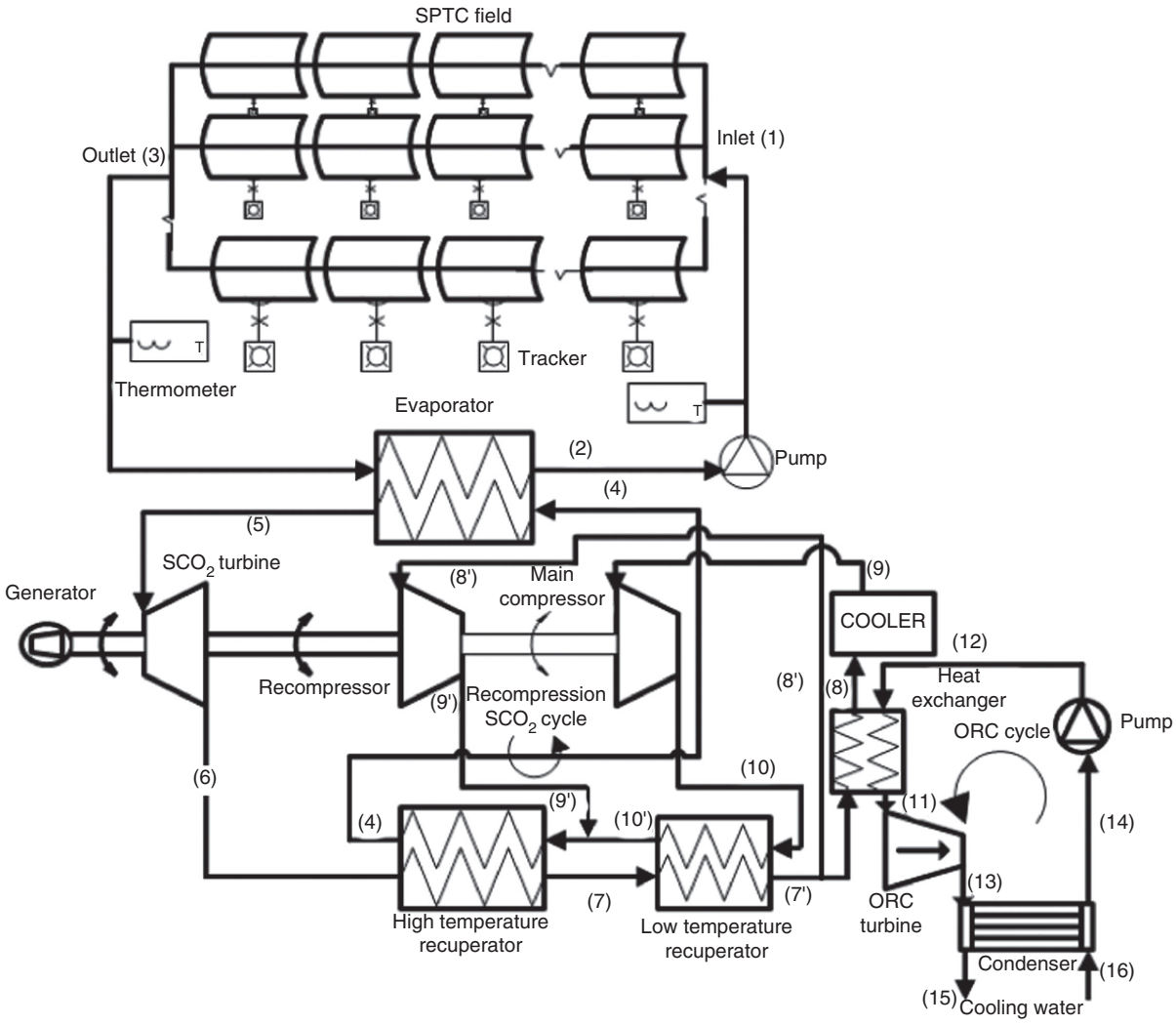

Fig. 1 Schematic of the SPTC-driven combined R-SCO_2 cycle/ORC system

same as in the simple configuration of the SCO_2 cycle. Figs 2 and 3 represent the temperature entropy diagrams of the R-SCO_2 cycle and ORC system.

Lastly, Table 1 represents the input data selected for the considered system and Table 2 denotes the physical and environmental properties along with safety data for all the selected organic fluids.

2 System modeling

This section deals with the modeling of a combined recompression cycle (i.e. R-SCO_2 cycle and ORC). Modeling of the solar parabolic trough collector (SPTC) system has been discussed already in the study conducted by Al-Sulaiman [26]. Therefore, the modeling of a combined recompression cycle has been conducted based on the exergy and energy balance of each component included in the system. However, the modeling of the recompression cycle follows the equations derived from previous research by Sarkar [1] and results have been computed with the help of

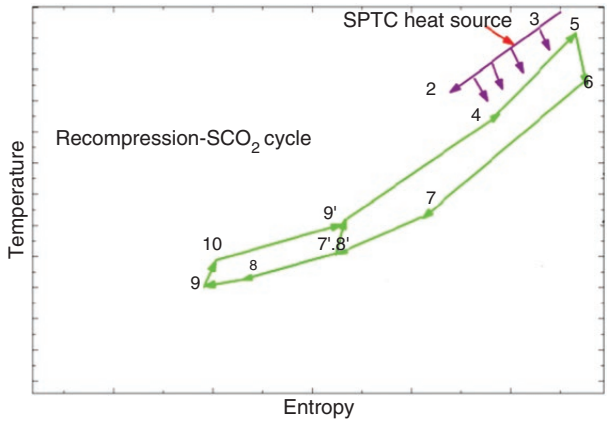

Fig. 2 Temperature entropy (*T*-*S*) diagram of recompression SCO_2 cycle

a computational numerical method (Engineering Equation Solver software, www.fChart.com). The following necessary assumptions have been made for the analysis:

Downloaded from https://academic.oup.com/ce/advance-article-abstract/doi/10.1093/ce/zky011/5050906
by Delhi Technological University user
on 15 July 2018

(1) All the processes in the combined cycle are in steady state.
(2) Drop in pressure in whole system is assumed to be neglected except in pump and turbine.
(3) Pump and turbine efficiency are considered to be constant.
(4) Negligible heat transfer with the surroundings except in the cooler unit.

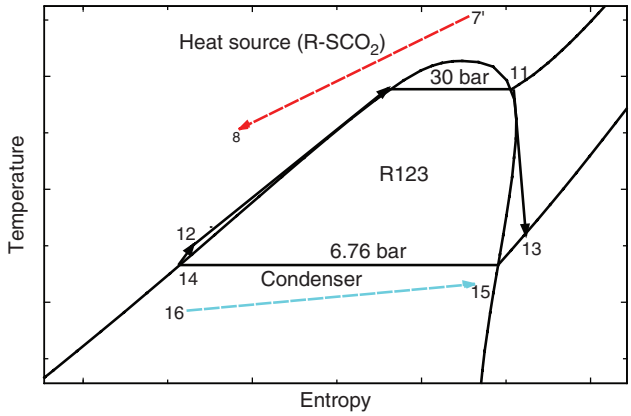

Fig. 3 Temperature entropy diagram of R123-based ORC system

Table 1 Input data taken for combined recompression (R-SCO_2-ORC) cycle

Isentropic efficiency of SCO_2 turbine	90% [35]
Isentropic efficiency of main compressor	89% [35]
Isentropic efficiency of recompressor	89% [35]
ORC pump efficiency	85% [14]
ORC turbine efficiency	87% [14]
Mass flow rate of SCO_2	10 kg/s
Split mass flow rate	4 kg/s
Mass flow rate of ORC	5 kg/s
Minimum pinch point temperature	5°C [44]
SCO_2 cycle high pressure	25 MPa [44]
Baseline ORC turbine inlet pressure	3 MPa
HTR effectiveness	95% [35, 37]
LTR effectiveness	95% [35, 37]
Heat exchanger effectiveness	95% [14]

(5) The process of expansion and compression is assumed to be adiabatic.

Thermodynamic relations for specific enthalpy balance in HTR and LTR are given by:

$$(h_4 - h_{9'}) = (h_6 - h_7) \quad (1)$$

$$(1-y)(h_{10'} - h_{10}) = (h_7 - h_{7'}) \quad (2)$$

Note that the hot side's heat capacity is comparatively lower than the cold side's; therefore the effectiveness of HTR is shown below:

$$\varepsilon_{\cdot H} = (T_6 - T_7)/(T_6 - T_{9'}) \quad (3)$$

Also effectiveness depends upon the heat capacity, which is the product of mass flow rate and specific heat capacity. Therefore the effectiveness of the LTR is as shown below:

$$\varepsilon_{\cdot L} = (T_7 - T_{7'})/(T_7 - T_{10}) \text{ if minimum in hot side} \quad (4)$$

or

$$\varepsilon_{\cdot L} = (T_{10'} - T_{10})/(T_7 - T_{10}) \text{ if minimum in the cold side} \quad (5)$$

Next, we consider important thermodynamic relations for the components of the recompression SCO_2 cycle used to operate the cycle. The total specific heat provided in the combined recompression cycle from the SPTC through the evaporator unit and the specific work output of each component involved in the combined recompression cycle are given by:

$$q_i = (h_5 - h_4) \quad (6)$$

$$W_{R-SCO_2,\text{turbine}} = (h_5 - h_6) \quad (7)$$

$$W_{ORC,\text{turbine}} = (h_{11} - h_{13}) \quad (8)$$

$$W_{\text{main compressor}} = (1-y) \times (h_{10} - h_9) \quad (9)$$

Table 2 Input data of selected working fluids for ORC adapted from[a] [47–52]

	Physical properties data					Security	Environmental properties		
Working substance	Type	Weight (kg/kmol)	T_b (°C)	T_c (°C)	P_c (MPa)	Group	Lifetime (years)	ODP	GWP
R123	D	152.93	27.8	183.7	3.668	B1	1.3	0.020	77
R290	W	44.10	-42.1	96.68	4.247	A3	0.041	0	~20
R1234yf	I	114.04	-29.5	94.7	3.38	A2L	0.029	0	<1
R1234ze(E)	I	114.04	-19.0	109.4	3.64	A2L	0.045	0	<1
Toluene	D	92.138	110.6	318.6	4.1263	n/a	n/a	n/a	n/a
Cyclohexane	D	84.16	80.7	280.5	4.075	A3	n/a	n/a	n/a
Isobutane	D	58.1	-11.7	134.7	3.63	A3	0.016	0	20
Isopentane	D	72.1	27.8	187.2	3.38	A3	0.009	0	20

[a]W = Wet, D = Dry, I = Isentropic, T_b = normal boiling temperature, T_c = critical temperature, P_c = critical pressure, ODP = potential of ozone depletion relative to R11; GWP = potential of global warming relative to CO_2.

Downloaded from https://academic.oup.com/ce/advance-article-abstract/doi/10.1093/ce/zky011/5050906
by Delhi Technological University user
on 15 July 2018

$$W_{recompressor} = y \times (h_{9'} - h_{8'}) \quad (10)$$

$$W_{pump} = (h_{12} - h_{14}) \quad (11)$$

$$W_{net,R\text{-}SCO_2} = W_{R\text{-}SCO_2\ turbine} - W_{main\ compressor} - W_{recompressor} \quad (12)$$

$$W_{net,ORC} = W_{ORC,\ turbine} - W_{pump} \quad (13)$$

$$\eta_{th,combined} = \frac{W_{net,R\text{-}sco_2} + W_{net,ORC}}{q_i} \quad (14)$$

Furthermore, exergy is defined as the maximum theoretical work obtained directly from the system as it interacts with the surroundings in equilibrium condition. Now, the steady-state exergy balance of the control volume of each component associated with the combined cycle is given by [26]:

$$\sum_U \left(1 - \frac{T_o}{T_U}\right) \dot{Q}_U - \dot{W}_{C.V.} - \sum_i \dot{m}_i eX_i - \dot{E}x_d = 0 \quad (15)$$

Physical exergy per unit total mass flow rate in each state can be calculated by:

$$ex_{ph} = (h - h_o) - T_o(s - s_o) \quad (16)$$

Now the total exergy input to the cycle can be calculated by assuming the constant outlet temperature of SPTC that is utilized as a heat source and is defined as:

$$ex_{input} = q_i \times (1 - T_o / T_3) \quad (17)$$

In other words, exergy at the inlet point to the system (exempt) is also considered as maximum useful work obtained from the solar radiations, calculated by Petela's formula as defined below [26, 41]:

$$ex_{input} = A_{ap} \cdot G_b \cdot \left[1 + \frac{1}{3}\left(\frac{T_o}{T_{su}}\right)^4 - \frac{4}{3}\left(\frac{T_o}{T_{su}}\right)\right] \quad (18)$$

The fraction of exergy destruction or irreversibilities in each component of the combined cycle is defined as the difference of input exergy and output exergy of the component, and it can be calculated by:

$$\dot{E}x_{d,R-SCO_2turbine} = [(ex_5 - ex_6) - W_{R-SCO_2turbine}] / ex_{input} \quad (19)$$

$$\dot{E}x_{d,main\,compressor} = [W_{main\ compressor} - (1-y)(ex_{10} - ex_9)] / ex_{input} \quad (20)$$

$$\dot{E}x_{d,recompressor} = [W_{recompressor} - y(ex_{9'} - ex_{8'})] / ex_{input} \quad (21)$$

$$\dot{E}x_{d,HTR} = [(ex_6 - ex_7) - (ex_4 - ex_{9'})] / ex_{input} \quad (22)$$

$$\dot{E}x_{d,LTR} = [(ex_7 - ex_{7'}) - (1-y)(ex_{10'} - ex_{10})] / ex_{input} \quad (23)$$

$$\dot{E}x_{d,evaporator} = [ex_{input} - (ex_5 - ex_4)] / ex_{input} \quad (24)$$

$$\dot{E}x_{d,heat\,exchanger} = [(1-y)(ex_{7'} - ex_8) - (ex_{11} - ex_{12})] / ex_{input} \quad (25)$$

$$\dot{E}x_{d,ORC\,turbine} = [(ex_{11} - ex_{13}) - W_{O,turbine}] / ex_{input} \quad (26)$$

$$\dot{E}x_{d,condenser} = [(ex_{13} - ex_{14}) - (ex_{15} - ex_{16})] / ex_{input} \quad (27)$$

$$\dot{E}x_{d,pump} = [(ex_{12} - ex_{14}) - W_{pp}] / ex_{input} \quad (28)$$

The exergy efficiency of the combined cycle can be expressed by the ratio of net output exergy to input exergy through the SPTC system.

$$\eta_{II} = \frac{W_{net,R-SCO_2} + W_{net,ORC}}{ex_{input}} = 1 - \sum \dot{E}x_{d,component} \quad (29)$$

The results of the study were validated with a modified LS-3 SPTC using the model of Dudley et al. [42] and the NREL model of Forristall [43]. The collector efficiency for both the vacuum and air cases in the current model has been evaluated with the help of the performance equations of Dudley et al. The results of collector efficiency for both cermet and black chrome coatings are calculated at the present baseline simulated conditions as described in Table 1; we found that the collector efficiency values closely match the results of previous models, as shown in Fig. 4.

This section also includes the validation of the combined recompression cycle (R-SCO_2-ORC) as well as the simple configuration of recompression SCO_2 cycle as shown in Tables 3 and 4. We found that results of the thermal efficiency in the current model agreed well with the predicted values from the literature [6, 8, 14, 44].

3 Results and discussion

In this study, we conducted exergy and energy analysis on the SPTC integrated combined R-SCO_2 cycle/ORC system under baseline conditions. The effect of intensity of solar irradiation, pressure at the inlet of R-SCO_2 turbine, inlet temperature at R-SCO_2 turbine, mass flow rate of SCO_2, inlet temperature of main compressor and effectiveness of HTR and LTR on both exergy and thermal efficiency have been examined under the fixed simulated conditions illustrated in Table 1.

3.1 Effect of intensity of solar irradiation and pressure at the R-SCO_2 turbine inlet

Fig. 5 shows the variation in exergy and thermal efficiency with the variation in intensity of solar irradiation (G_b); we observed that both thermal and exergy efficiency increase with an increase in G_b, which has been analyzed under fixed baseline conditions such as pressure at the inlet of R-SCO_2 turbine (P_5 = 25 MPa) and mass flow rate of SCO_2

Downloaded from https://academic.oup.com/ce/advance-article-abstract/doi/10.1093/ce/zky011/5050906
by Delhi Technological University user
on 15 July 2018

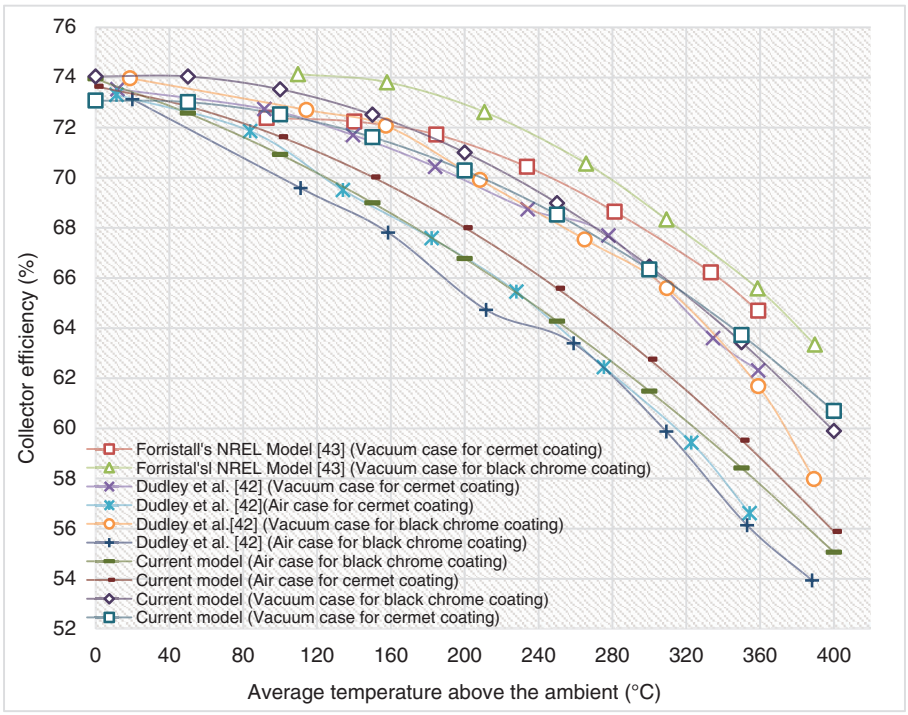

Fig. 4 Collector efficiency versus average temperature above ambient

Table 3 Validation of combined recompression cycle at the same simulated conditions

Working fluid	Reference	Thermal efficiency in reference	Thermal efficiency predicted	Error
Isobutane	Besarati and Goswami [14]	0.5357	0.517	-3.4%

Table 4 Validation of simple recompression SCO_2 cycle at T_5 = 500°C

Working fluid	Reference	Thermal efficiency predicted in references	Thermal efficiency in current study	Error
SCO_2	Besarati and Goswami [14]	0.4421	0.4377	-0.9%
SCO_2	Kulhánek and Dostál [6]	0.4419		-0.95%
SCO_2	Turchi et al. [8]	0.4441		-1.4%
SCO_2	Padilla et al. [44]	0.4424		-1.06%

($\dot{m}_{SCO2} = 10\,kg/s$), respectively. The optimum use of solar collector rows present in the overall SPTC field can be achieved through enhancing the intensity of solar irradiation that directly concentrates on the overall solar plant. From Fig. 5, we see that the R123-based combined recompression cycle (R-SCO_2-ORC) has the highest exergy and thermal efficiency followed by R1234ze, R1234yf, toluene, cyclohexane, isopentane and isobutene, with R290 having the minimum value. Notice that the exergy and thermal efficiency of the R123 combined recompression cycle varied from 73.4% at G_b = 0.5 kW/m² to 86.75% at G_b = 0.95 kW/m² and 40.89% at G_b = 0.5 kW/m² to 48.33% at G_b = 0.95 kW/m², respectively. On the other hand, exergy and thermal efficiency of the R290-based R-SCO_2-ORC increase from 72.22% at G_b = 0.5 kW/m² to 86.17% at G_b = 0.95 kW/m² and 40.23% at G_b = 0.5 kW/m² to 48% at G_b = 0.95 kW/m², respectively. Results also showed that R1234yf- and R1234ze-based combined recompression cycles have a marginal difference between their efficiency values. As can be seen, the efficiency value of R1234ze, R1234yf, toluene, cyclohexane, isopentane and isobutane lies between the R123 and R290 values, as shown in Fig. 5. In addition, Fig. 6 illustrates the variation in exergy and thermal efficiency of the SPTC integrated combined recompression cycle (SPTC-R-SCO_2-ORC). We found that the R123-based SPTC integrated combined cycle has the maximum value of exergy and thermal efficiency among the other selected refrigerants, increasing from 44.53% at G_b = 0.5 kW/m² to 70.83% at G_b = 0.95 kW/m² and 24.81% at G_b = 0.5 kW/m² to 39.46% at G_b = 0.95 kW/m². R290-based SPTC-R-SCO_2-ORC, however, has the lowest value of exergy and thermal efficiency, increasing from 43.47% at G_b = 0.5 kW/m² to 70.28%

Downloaded from https://academic.oup.com/ce/advance-article-abstract/doi/10.1093/ce/zky011/5050906
by Delhi Technological University user
on 15 July 2018

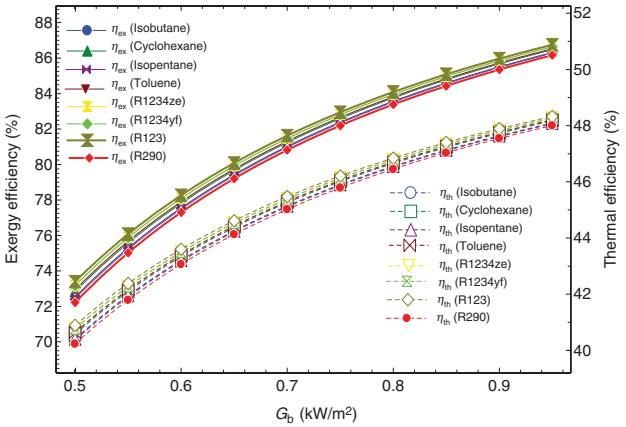

Fig. 5 Exergy and thermal efficiency of combined recompression cycle versus intensity of solar irradiation

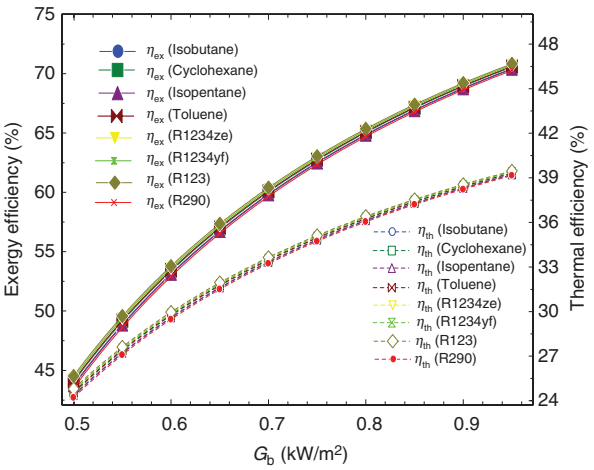

Fig. 6 Exergy and thermal efficiency of SPTC integrated combined recompression cycle versus intensity of solar irradiation

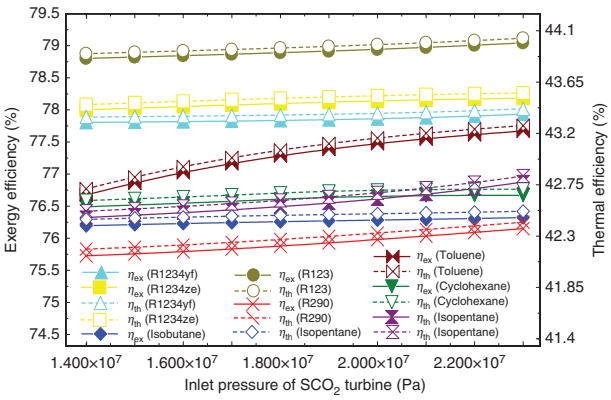

Fig. 7 Exergy and thermal efficiency of combined recompression cycle versus the pressure at the inlet of R-SCO_2 turbine

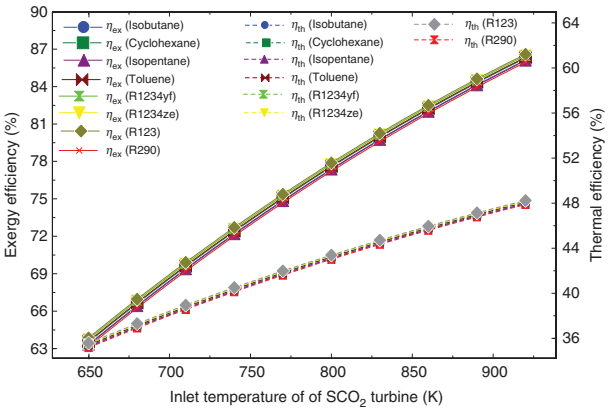

Fig. 8 Exergy and thermal efficiency of combined recompression cycle versus inlet temperature at R-SCO_2 turbine

at G_b = 0.95 kW/m² and 24.22% at G_b = 0.5 kW/m² to 39.15% at G_b = 0.95 kW/m². As observed, the SPTC integrated combined recompression cycle has a comparatively lower value of exergy and thermal efficiency than the simple configuration (i.e. without SPTC), due to the maximum amount of exergy destruction associated with the solar collector field. On the other hand, the effect of pressure at the inlet of the R-SCO_2 turbine on the exergy and thermal performance of a combined cycle under baseline conditions, for instance, T_5 = 652.8 K and $\dot{m}_{SCO_2}$ = 10 kg/s, has also been analyzed here. Fig. 7 demonstrates that R123-based R-SCO_2-ORC has the highest exergy and thermal efficiency among the other combined cycles: ~78.8% at 14 MPa increasing to 79.04% at 23 MPa and 43.9% at 14 MPa increasing to 44.03% at 23 MPa, respectively. Alternatively, R290-based R-SCO_2-ORC shows the least value of efficiency, probably due to the presence of high exergy losses in this cycle in contrast to the other considered cycles as shown in Fig. 7. The value of exergy and thermal efficiency for R290 is ~75.73% at 14 MPa increasing to 76.15% at 23 MPa, and 42.19% at 14 MPa increasing to 42.42% at 23 MPa, respectively. However, all other fluids have efficiency values between fluids such as R123 and R290.

3.2 Effect of inlet temperature at R-SCO_2 turbine and mass flow rate of SCO_2

The inlet or maximum cycle temperature is a crucial parameter that helps maintain the optimum temperature range for the combined recompression cycle (R-SCO_2-ORC). A survey of the literature indicated that the inlet or high temperature can be enhanced up to a certain limit of 750°C so that the layer of oxide formation on the metal alloys could be prevented [45, 46]. Fig. 8 shows the effect of variations in inlet temperature at a R-SCO_2 turbine on the exergy and thermal performance of the considered R-SCO_2-ORC. With an increase in inlet temperature, exergy and thermal efficiency of R-SCO_2-ORC also increase, as analysed under fixed baseline conditions such as $\dot{m}_{SCO_2}$ = 10 kg/s and P_5 = 25 MPa as shown in Fig. 8. The reason behind the increasing exergy and thermal efficiency is that, as the inlet or high temperature of the turbine increases, the enthalpy inflow to the turbine increases correspondingly, resulting in an increase in the work output of the turbine for certain heat input rate. However, work output of the

Downloaded from https://academic.oup.com/ce/advance-article-abstract/doi/10.1093/ce/zky011/5050906
by Delhi Technological University user
on 15 July 2018

recompressor and main compressor at the same time has the reasonable value because it is affected moderately with the increasing turbine inlet temperature. Therefore, the net work output increases in the recompression combined cycle. Consequently, exergy and thermal efficiency increase as the turbine inlet temperature increases. Another reason for increasing exergy and thermal efficiency is that, as the inlet temperature of the turbine increases, the temperature difference between heat addition and heat rejection also increases, and as a result the efficiency of the cycle increases [1]. We have observed that R123-based R-SCO_2-ORC has the maximum value of exergy and thermal efficiency, which increases continuously from 63.86% at 650 K to 86.59% at 920 K and 35.57% at 650 K to 48.24% at 920 K, respectively. Alternatively, R290-based R-SCO_2-ORC has the minimum value of exergy and thermal efficiency, increasing from 63.13% at 650 K to 85.94% at 920 K and 35.17% at 650 K to 47.87% at 920 K, respectively, as illustrated in Fig. 8. In addition, the effect of inlet or high temperature on the SPTC integrated combined recompression cycle (SPTC-R-SCO_2-ORC) has been analyzed in Fig. 9. The study reveals that R123 has the maximum exergy and thermal efficiency, increasing from 25.37% at 650 K to 70.68% at 920 K and 14.14% at 650 K to 39.37% at 920 K, respectively. On the other hand, R290 has the lowest value of exergy and thermal efficiency, increasing from 24.76% at 650 K to 70.06% at 920 K and 13.79% at 650 K to 39.03% at 920 K, respectively. As mentioned above, the exergy and thermal efficiency value of all other recompression combined cycles lies between these two cycles. Moreover, the effect of inlet or high temperature of SCO_2 turbine on the net work output of R-SCO_2-ORC also has been analyzed in Fig. 10. It has been observed that R123 has the highest net work output of 4594 kJ at 650 K, increasing to 6231 kJ at 920 K, followed by R1234ze, R1234yf, toluene, cyclohexane, isopentane and isobutane. R290 has the lowest value of net work output, increasing from 4542 kJ at 650 K to 6183 kJ at 920 K, as demonstrated in Fig. 10.

Apart from this, the mass flow rate of working fluid also has a significant effect on the combined recompression cycle's power generation and efficiency because, by enhancing the mass flow rate, the heat transfer coefficient increases and the pressure drop also increases and that can enhance the requirement of pumping power. Fig. 11 shows the effect of the mass flow rate of SCO_2 on exergy and thermal performance of the combined recompression cycle (R-SCO_2-ORC), which was analyzed under the baseline conditions P_5 = 25 MPa and T_5 = 652.8 K. We found that, with the increase in mass flow rate of SCO_2, thermal and exergy efficiency of the considered combined recompression cycle also increased. R123-based R-SCO_2-ORC illustrates the maximum value of exergy and thermal efficiency, increasing from 74.84% at 7 kg/s to 89.59% at 16 kg/s and 41.69% at 7 kg/s to 49.91% at 16 kg/s, respectively. On the other hand, R290-based R-SCO_2-ORC demonstrates the minimum value of exergy and thermal efficiency, increasing from 74.32% at 7 kg/s to 88.71% at 16 kg/s and 41.4% at 7 kg/s to 49.42% at 16 kg/s, respectively, as shown in Fig. 11. We also observed that exergy and thermal efficiency of the SPTC-R-SCO_2-ORC increase as the mass flow rate increases, as shown in Fig. 12. Results revealed that R123-based SPTC-R-SCO_2-ORC possesses the highest value of exergy and thermal efficiency, increasing from 58.77% at 7 kg/s to 71.41% at 16 kg/s and 32.74% at 7 kg/s to 39.78% at 16 kg/s, respectively. However, R290-based SPTC-R-SCO_2-ORC illustrates the lowest value of exergy and thermal efficiency, increasing from 58.3% at 7 kg/s to 70.57% at 16 kg/s and 32.48% at 7 kg/s to 39.31% at 16 kg/s, respectively, as shown in Fig. 12.

3.3 Effect of inlet temperature of main compressor

The effect of the inlet temperature of the main compressor on the exergy and thermal performance of the combined recompression cycle (R-SCO_2-ORC) is discussed under fixed simulated conditions in this section. As can

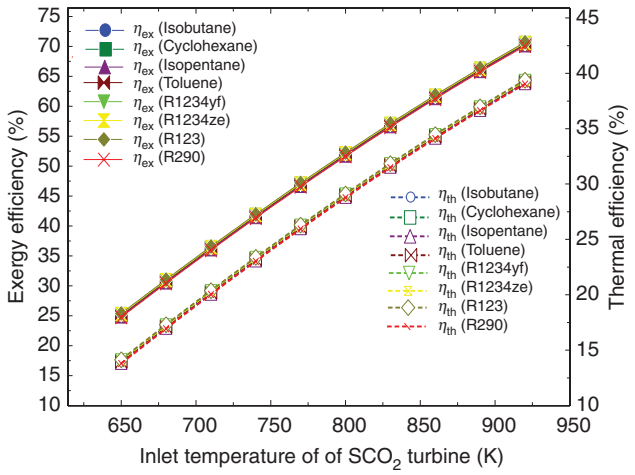

Fig. 9 Exergy and thermal efficiency of SPTC integrated combined recompression cycle versus inlet temperature at R-SCO_2 turbine

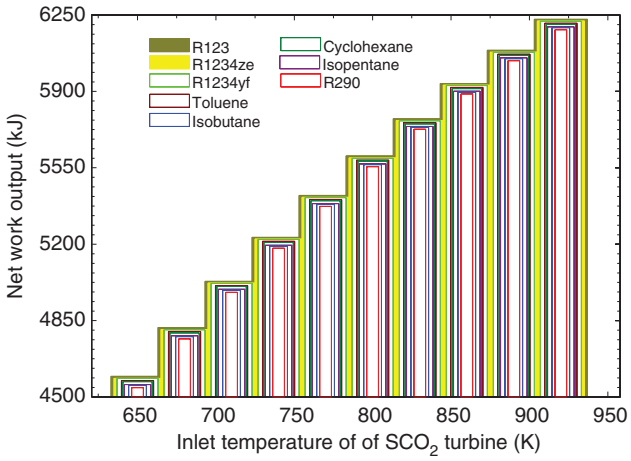

Fig. 10 Net work output of combined recompression cycle versus inlet temperature at R-SCO_2 turbine

Downloaded from https://academic.oup.com/ce/advance-article-abstract/doi/10.1093/ce/zky011/5050906
by Delhi Technological University user
on 15 July 2018

be observed from Fig. 13, the exergy and thermal efficiency of R-SCO_2-ORC decrease as the inlet temperature of the main compressor increases. The reason behind the decreasing efficiency is that the specific heat capacity of CO_2 decreases as the inlet temperature of the main compressor increases (i.e. away from the critical point). Therefore, specific enthalpy inflow decreases in the main compressor. As a result, work output of the main compressor increases notably but work output of the recompressor and SCO_2 turbine are not affected as much. Thus the net work output decreases and hence the exergy and thermal efficiency also decrease simultaneously. In other words, with the increase in inlet temperature of the main compressor, the difference between the maximum and minimum temperature of the cycle decreases correspondingly, resulting in a decrease in the efficiency of the cycle [1]. From Fig. 13, we can see that both exergy and thermal efficiency of R123-based R-SCO_2-ORC decrease from 85.83% at 300 K to 84.64% at 327 K and 47.82% at 300 K to 47.15% at 327 K, respectively; its value is highest among the other considered working fluids such as R1234ze, R1234yf, toluene, cyclohexane, isopentane and isobutane, and R290 possesses the lowest value of exergy and thermal efficiency, decreasing from 84.91% at 300 K to 84.12% at 327 K and 47.3% at 300 K to 46.86% at 327 K, respectively.

The effect of inlet temperature of the main compressor on the SPTC-R-SCO_2-ORC is also analyzed in this section. From Fig. 14, we found that R123-based SPTC-R-SCO_2-ORC has the highest value of exergy and thermal efficiency, decreasing from 68.1% at 300 K to 66.98% at 327 K and 37.94% at 300 K to 37.31% at 327 K, respectively. R290 has the lowest value of exergy and thermal efficiency, decreasing from 67.24% at 300 K to 66.49% at 327 K and 37.46% at 300 K to 37.04% at 327 K, respectively. Also the efficiency for all other fluids, i.e. R123 and R290, lies between the values of these two fluids, as demonstrated in Fig. 14.

Moreover, the effect of inlet temperature of the main compressor on the net work output of the R-SCO_2-ORC

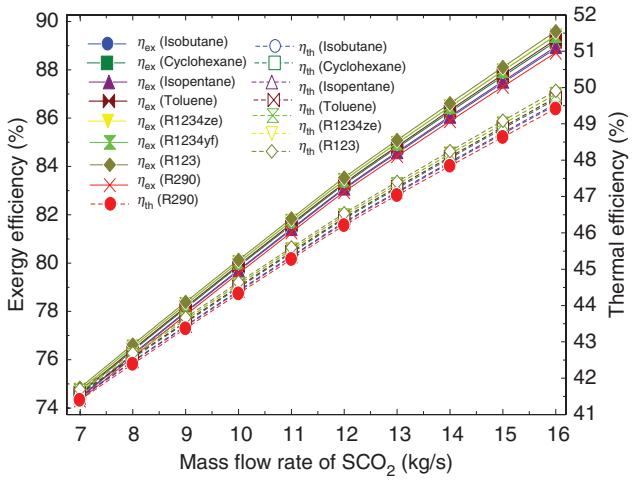

Fig. 11 Exergy and thermal efficiency of combined recompression cycle versus mass flow rate of SCO_2

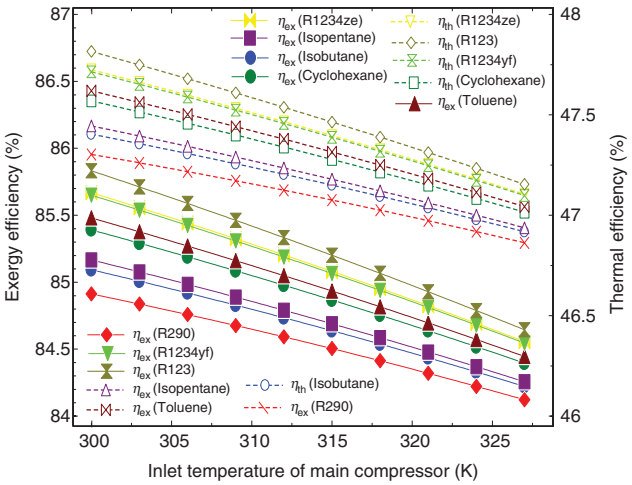

Fig. 13 Exergy and thermal efficiency of combined recompression cycle versus inlet temperature of main compressor

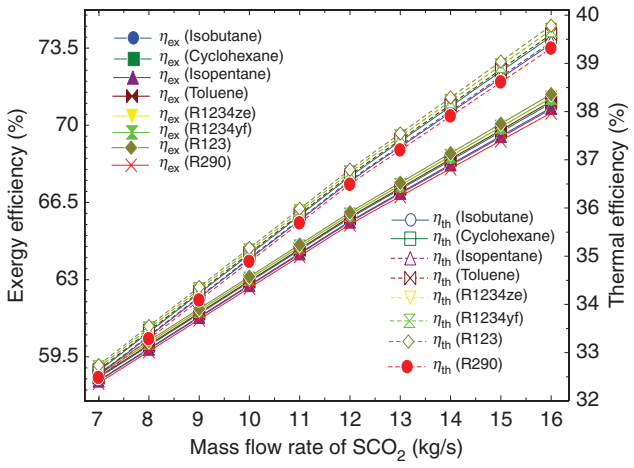

Fig. 12 Exergy and thermal efficiency of SPTC integrated combined recompression cycle versus mass flow rate of SCO_2

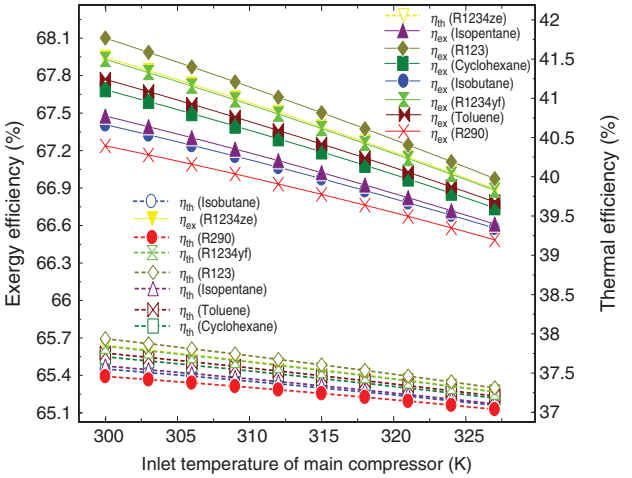

Fig. 14 Exergy and thermal efficiency of SPTC integrated combined recompression cycle versus inlet temperature of main compressor

Downloaded from https://academic.oup.com/ce/advance-article-abstract/doi/10.1093/ce/zky011/5050906
by Delhi Technological University user
on 15 July 2018

was studied in Fig. 15. As can be seen, the net work output decreases continuously as the inlet temperature of the main compressor increases, and R123 has the highest value of net work output, ~6176 kJ at 300 K and 6090 kJ at 327 K. Alternatively, R290 has the lowest value of net work output, ~6109 kJ at 300 K and 6052 kJ at 327 K, as shown in Fig. 15.

3.4 Effect of the effectiveness of the HTR and LTR

The effect of the effectiveness of a high-temperature recuperator (HTR) and low-temperature recuperator (LTR) on the exergy and thermal performance of combined recompression cycle (R-SCO_2-ORC) is discussed in this section. As can be seen, an increase in the effectiveness of the recuperator can increase the heat exchange and exergy gain, resulting in a decrease in the exergy destruction of the recompression cycle. Thus, exergy efficiency increases. On the other hand, with the increase in effectiveness of the recuperator, the input-specific exergy of the recompression cycle decreases, whereas the net output-specific exergy remains uniform due to the unaffected cycle pressure ratio, isentropic efficiencies and other operating conditions with the change in effectiveness and hence exergy efficiency increases [1]. From Fig. 16, we observe that as the effectiveness of the HTR increases, exergy and thermal efficiency increase, and R123-based R-SCO_2-ORC has the highest exergy and thermal efficiency, ~84.57% at ε_{HTR} = 0.65 increasing to 85.01% at ε_{HTR} = 0.92 and 47.11% at ε_{HTR} = 0.65 increasing to 47.35% at ε_{HTR} = 0.92, respectively. Alternatively, R290 has the lowest value of exergy and thermal efficiency, ~83.72% at ε_{HTR} = 0.65 increasing to 84.32% at ε_{HTR} = 0.92 and 46.64% at ε_{HTR} = 0.65 increasing to 46.97% at ε_{HTR} = 0.92, respectively.

Furthermore, the effect of the effectiveness of LTR on the exergy and thermal efficiency has been illustrated in Fig. 17. We found that the efficiency of R123-based R-SCO_2-ORC increases as the effectiveness of LTR increases, and it possesses the highest value of exergy and thermal efficiency among the other fluids, increasing from 85.06% at ε_{LTR} = 0.65 to 85.1% at ε_{LTR} = 0.92 and 47.38% at ε_{LTR} = 0.65 to 47.41% at ε_{LTR} = 0.92, respectively. Alternatively, R290 has the lowest value of exergy and thermal efficiency, increasing from 84.39% at ε_{LTR} = 0.65 to 84.44% at ε_{LTR} = 0.92 and 47.01% at ε_{LTR} = 0.65 to 47.04% at ε_{LTR} = 0.92, respectively. Also the efficiency value of all other fluids lies between these two fluids as mentioned above. Moreover, it is clear from Figs 16 and 17 that the HTR effectiveness has more predominant effects on efficiency as it exchanges more heat as well as exergy compared to LTR.

Moreover, the results of the study show that the R-SCO_2-ORC has higher exergy and thermal efficiency than a simple configuration of a combined cycle (SCO_2-ORC), mainly due to the split of SCO_2 flow in the recompression cycle

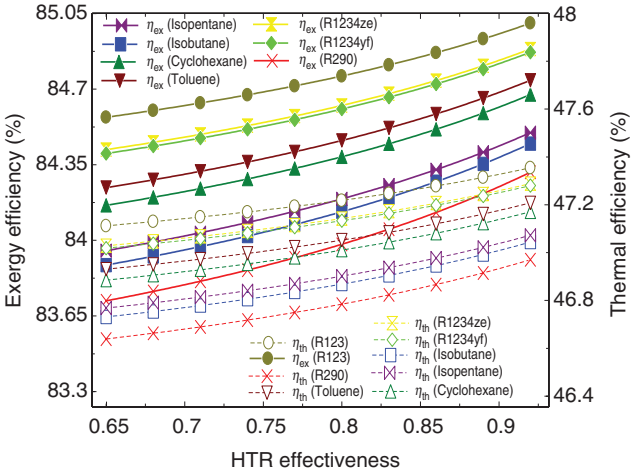

Fig. 16 Exergy and thermal efficiency of combined recompression cycle versus HTR effectiveness

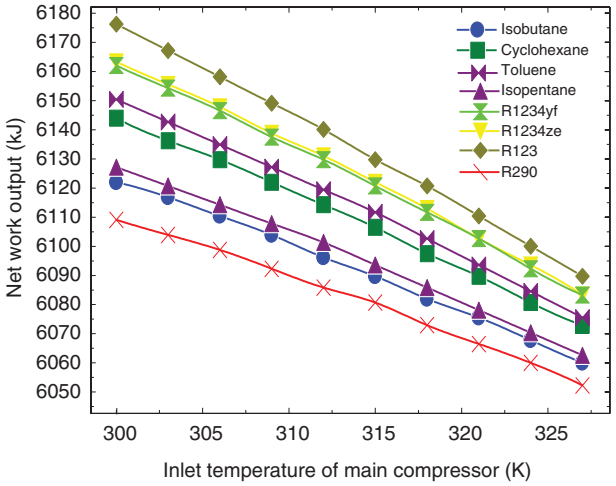

Fig. 15 Net work output of combined recompression cycle versus inlet temperature of main compressor

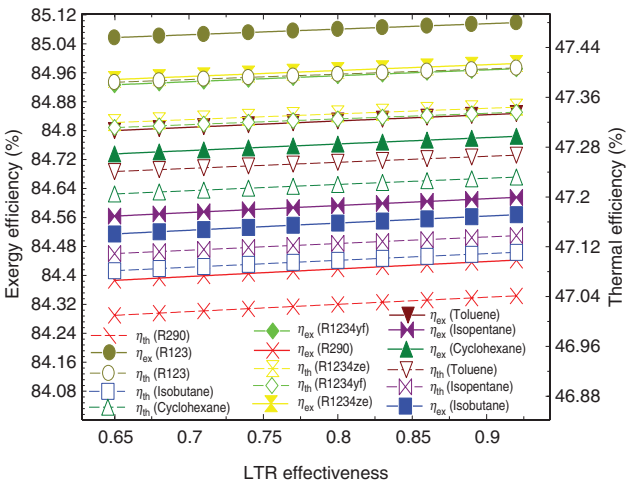

Fig. 17 Exergy and thermal efficiency of combined recompression cycle versus LTR effectiveness

Downloaded from https://academic.oup.com/ce/advance-article-abstract/doi/10.1093/ce/zky011/5050906
by Delhi Technological University user
on 15 July 2018

Table 5 Thermodynamic properties of SPTC-driven R123-based combined recompression cycle at the selected stations [53, 54]

Selected stations	Fluid type	$\dot{m}$ (kg/s)	P (MPa)	T (K)	h (kJ/kg)	s (kJ/kg-K)
SPTC receiver outlet (3)	Syltherm 800	0.575	10	673.15	832.36	2.383
SCO_2 turbine inlet (5)	SCO_2	10	25	652.8	819.08	2.4037
SCO_2 turbine outlet (6)	SCO_2	10	13.2	588.8	759.81	2.4273
HTR outlet (7)	SCO_2	10	13.2	462.4	607.39	2.1355
LTR outlet (7')	SCO_2	10	13.2	385.2	498.68	1.8772
Heat exchanger outlet (8)	SCO_2	6	13.2	327.8	342.60	1.4321
Main compressor outlet (10)	SCO_2	6	25	369.1	395.44	1.5272
Recompressor outlet (9')	SCO_2	4	25	438.4	529.14	1.8907
LTR outlet (10')	SCO_2	6	25	436.8	526.51	1.8847
HTR outlet (4)	SCO_2	10	25	532.3	665	2.1825
ORC turbine inlet (11)	R123	5	3	359.2	290.303	1.280
ORC turbine outlet(13)	R123	5	0.676	312.7	240.277	1.294
Condenser outlet (14)	R123	5	0.676	297.2	224.363	1.083
Heat exchanger inlet (12)	R123	5	3	306.9	235.067	1.117

that helps compensate the difference between specific heat in the LTR along with the maximum heat recuperation in the topping layout (i.e. R-SCO_2 cycle); in turn the quantity of waste heat declined and, finally, the thermal efficiency of the cycle will be improved [40]. The current study showed that the exergy and thermal efficiency of the R123-based combined recompression cycle is around 85.09% and 47.4%, respectively, significantly higher than the exergy and thermal efficiency of a simple combined cycle (SCO_2-ORC), i.e. 83.63% and 46.59%, which has been observed under the same baseline or simulated conditions such as G_b = 0.85 kW/m^2, T_5 = 652.8 K, P_5 = 25 MPa, and $\dot{m}_{(SCO_2)}$ 10 kg/s. Furthermore, the important thermodynamic properties such as temperature, pressure, mass flow rate, enthalpy and entropy at the selected stations for R123-based R-SCO_2-ORC are described in Table 5.

Lastly, the results of the study revealed that the maximum amount of exergy destruction occurs in a collector field, which is ~58.25% of the total exergy destruction rate, ~6703 kW, possibly due to temperature and material restrictions of SPTCs. Also, note that the total exergy destructed in R123-based SPTC-R-SCO_2-ORC is ~32.59% of the inlet exergy from the SPTC field (i.e. 20 562 kJ).

4 Conclusion

The current study reveals the exergy and energy performance of the combined recompression cycle (R-SCO_2-ORC) with the utilization of different organic fluids in the low temperature ORC. The following results are concluded from this research work:

(1) The exergy efficiency of R-SCO_2-ORC increases with the increase in intensity of solar irradiation (G_b), inlet or maximum pressure of R-SCO_2 turbine (P_5), inlet or high temperature at R-SCO_2 turbine (T_5), mass flow rate of SCO_2 ($\dot{m}_{SCO_2}$) and effectiveness of HTR and LTR (ε_{HTR} and ε_{LTR}). In contrast, the efficiency of R-SCO_2-ORC decreases as the inlet temperature of the main compressor (T_9) increases. The current study revealed that R123-based R-SCO_2-ORC has maximum exergy efficiency under the fixed baseline conditions: ~73.4% at G_b = 0.5 kW/m^2; 78.8% at P_5 = 14 MPa; 63.86% at T_5 = 650 K; 74.84% at $\dot{m}_{SCO_2}$ = 7 kg/s; 85.83% at T_9 = 300 K; 84.57% at ε_{HTR} = 0.65; and 85.06% at ε_{LTR} = 0.65. Alternatively, R290-based R-SCO_2-ORC possesses the least value of exergy efficiency due to the maximum amount of exergy losses present in this cycle.

(2) The thermal efficiency of the R-SCO_2-ORC also follows the same trend of exergy efficiency, and its value continuously increases with the increase in quantity of input or independent variables such as G_b, P_5, T_5, $\dot{m}_{SCO_2}$, ε_{HTR} and ε_{LTR} except T_9. Note that R123-based R-SCO_2-ORC has the maximum value of thermal efficiency among the other selected fluids: ~40.89% at G_b = 0.5 kW/m^2; 43.9% at P_5 = 14 MPa; 35.57% at T_5 = 650 K; 47.82% at T_9 = 300K; 47.11% at ε_{HTR} = 0.65; and 47.38% at ε_{LTR} = 0.65. Again, R290-based R-SCO_2-ORC has the lowest value of thermal efficiency. On the other hand, exergy and thermal performance of R1234ze, R1234yf, toluene, cyclohexane, isopentane and isobutane lie between the two above-mentioned fluids, with a marginal difference between their efficiency values and comparable performance under the specified range of each independent variable.

(3) In addition, the exergy and thermal efficiency of SPTC-R-SCO_2-ORC increase with the increase in G_b, T_5 and $\dot{m}_{SCO_2}$, except T_9 due to its inverse effect on the performance of recompression cycle in contrast to other independent variables. Results revealed that R123-based SPTC-R-SCO_2-ORC has the highest exergy and thermal efficiency: ~44.53 and 24.81% at G_b = 0.5 kW/m^2; 25.37 and 14.14% at T_5 = 650 K; 58.77 and 32.74% at $\dot{m}_{SCO_2}$ = 7 kg/s; 68.1 and 37.94% at T_9 = 300 K, respectively. The exergy and thermal efficiency of SPTC-R-SCO_2-ORC have comparatively less value than the simple configuration (i.e. R-SCO_2-ORC), possibly due to the large amount of exergy destruction or exergy loss present in the overall solar collector field followed by

Downloaded from https://academic.oup.com/ce/advance-article-abstract/doi/10.1093/ce/zky011/5050906
by Delhi Technological University user
on 15 July 2018

the SCO_2 turbine and evaporator: ~3905, 1278 and 1274 kW, respectively. Apart from this, the calculated value of the destructed exergy in SPTC is ~58.25% of the total exergy destruction rate (i.e. 6703 kW) and 18.99% of the inlet exergy coming from the SPTC field (i.e. 20 562 kJ).

(4) Last but not least, the R123-based R-SCO_2-ORC shows the highest value of net work output, ~4594 kJ at T_5 = 650 K and 6176 kJ at T_9 = 300 K, whereas the R290 has the least value of net work output in contrast to other fluids.

Nomenclature

h specific enthalpy (kJ/kg)
y recompression split mass fraction
T temperature (K)
P pressure (Pa)
q inlet specific heat (kJ/kg)
w specific work output (kJ/kg)
T_o surrounding temperature (K)
T_U particular state temperature (K)
s specific entropy (kJ/kg-K)
$\dot{E}x_d$ exergy destruction rate (kW)
ex exergy (kW)
R-SCO_2 recompression supercritical CO_2
ORC organic Rankine cycle
$\dot{m}$ mass flow rate (kg/s)
$\dot{Q}$ heat rate (kW)
G_b intensity of solar irradiation (W/m^2)
A_{ap} area of the aperture (m^2)
T_{su} temperature of outer surface of sun
HTR high-temperature recuperator
LTR low-temperature recuperator

Greek letters

ε effectiveness
η_{th} thermal efficiency
η_{ex} exergy efficiency

Subscripts

i inlet
e exit
o ambient conditions
U partcular state

Acknowledgements

The author (Harwinder Singh) acknowledges the support of Delhi Technological University, New Delhi, India.

Conflict of interest statement. None declared.

References

[1] Sarkar J. Second law analysis of supercritical CO_2 recompression Brayton cycle. *Energy* 2009; 34:1172–8.
[2] Zhu Q. Innovative power generation systems using supercritical CO_2 cycles. *Clean Energy* 2017; 1:68–79.
[3] Milani D, Luu MT, McNaughton R, et al. A comparative study of solar heliostat assisted supercritical CO_2 recompression Brayton cycles: Dynamic modelling and control strategies. *J Supercrit Fluids* 2017; 120:113–24.
[4] Niu X-D, Yamaguchi H, Iwamoto Y, et al. Optimal arrangement of the solar collectors of a supercritical CO_2-based solar Rankine cycle system. *Appl Therm Eng* 2013; 50:505–10.
[5] Feher EG. The supercritical thermodynamic power cycle. *Energy Convers* 1968; 8:85–90.
[6] Kulhánek M, Dostál V. Thermodynamic analysis and comparison of supercritical carbon dioxide cycles. In: *Proceedings of Supercritical CO_2 Power Cycle Symposium*, Boulder, Colorado, 24–25 May 2011. https://drive.google.com/file/d/1KcvMoLYNYXxxkbXjJWjSSixKQr4DVhmnHqAFQk-R3mybERAXd3TieAus5QmQ/view (2 June 2018, date last accessed).
[7] Sarkar J, Bhattacharyya S. Optimization of recompression S-CO_2 power cycle with reheating. *Energy Convers Manag* 2009; 50:1939–45.
[8] Turchi CS, Ma Z, Neises TW, et al. Thermodynamic study of advanced supercritical carbon dioxide power cycles for concentrating solar power systems. *J Sol Energy Eng* 2013; 135:041007.
[9] Chacartegui R, Sánchez D, Jiménez-Espadafor F, et al. Analysis of intermediate temperature combined cycles with a carbon dioxide topping cycle. In: *ASME Turbo Expo 2008: Power for Land, Sea, and Air, Vol. 2*, Berlin, Germany, 9–13 June 2008, 673–80.
[10] Chacartegui R, Munoz JM, Sánchez D, et al. Alternative cycles based on carbon dioxide for central receiver solar power plants. *Appl Therm Eng* 2011; 31:872–9.
[11] Wang X, Dai Y. Exergoeconomic analysis of utilizing the transcritical CO_2 cycle and the ORC for a recompression supercritical CO_2 cycle waste heat recovery: A comparative study. *Appl Energy* 2016; 170:193–207.
[12] Sánchez D, Brenes BM, Munoz JM, et al. Non-conventional combined cycle for intermediate temperature systems. *Int J Energy Res* 2013; 37:403–11.
[13] Akbari AD, Mahmoudi MS. Thermoeconomic analysis & optimization of the combined supercritical CO_2 (carbon dioxide) recompression Brayton/organic Rankine cycle. *Energy* 2014; 78:501–12.
[14] Besarati SM, Goswami DY. Analysis of advanced supercritical carbon dioxide power cycles with a bottoming cycle for concentrating solar power applications. *J Sol Energy Eng* 2014; 136:010904-1-7.
[15] Tunc M, Sisbot S, Camdalib U. Exergy analysis of electricity generation for the geothermal resources using organic Rankine cycle: Kızıldere-Denizli case. *Environ Prog Sustain Energy* 2012; 32:830–6.
[16] Baghernejad A, Yaghoubi M, Jafarpur K. Exergoeconomic optimization and environmental analysis of a novel solar-trigeneration system for heating, cooling and power production purpose. *Sol Energy* 2016; 134:165–79.
[17] Calise F, d'Accadia MD, Macaluso A, et al. Exergetic and exergoeconomic analysis of a novel hybrid solar–geothermal polygeneration system producing energy and water. *Energy Convers Manag* 2016; 115:200–20.
[18] Qiu Y, Li M-J, He Y-L, et al. Thermal performance analysis of a parabolic trough solar collector using supercritical CO_2 as heat transfer fluid under nonuniform solar flux. *Appl Therm Eng* 2017; 115:1255–65.
[19] Bellos E, Korres D, Tzivanidis C, et al. Design, simulation and optimization of a compound parabolic collector. *Sustain Energy Technol Assess* 2016; 16:53–63.

Downloaded from https://academic.oup.com/ce/advance-article-abstract/doi/10.1093/ce/zky011/5050906
by Delhi Technological University user
on 15 July 2018

[20] Cheng ZD, He YL, Qiu Y. A detailed non-uniform thermal model of a parabolic trough solar receiver with two halves and two inactive ends. *Renew Energy* 2015; 274:139–47.
[21] Guo J, Huai X. Multi-parameter optimization design of parabolic trough solar receiver. *Appl Therm Eng* 2016; 98:73–9.
[22] Gao W, Li H, Xu G, et al. Working fluid selection and preliminary design of a solar organic rankine cycle system. *Environ Prog Sustain Energy* 2014; 34:619–26.
[23] Mokheimer EMA, Dabwan YN, Habib MA. Optimal integration of solar energy with fossil fuel gas turbine cogeneration plants using three different CSP technologies in Saudi Arabia. *Appl Energy* 2017; 185:1268–80.
[24] Amelio M, Ferraro V, Marinelli V, et al. An evaluation of the performance of an integrated solar combined cycle plant provided with air linear parabolic collectors. *Energy* 2014; 69:742–8.
[25] Al-Sulaiman FA. Energy and sizing analyses of parabolic trough solar collector integrated with steam and binary vapor cycles. *Energy* 2013; 58:561–70.
[26] Al-Sulaiman FA. Exergy analysis of parabolic trough solar collectors integrated with combined steam and organic Rankine cycles. *Energy Convers Manag* 2014; 77:441–9.
[27] Seidel W. Model development and annual simulation of the supercritical carbon dioxide Brayton cycle for concentrating solar power applications. *Master's thesis*. The University of Wisconsin-Madison, 2010.
[28] Turchi CS, Ma Z, Dyreby J. Supercritical CO_2 for application in concentrating solar power systems. In: *Proceedings of SCCO$_2$ Power Cycle Symposium 2009*, RPI, Troy, New York, 2009.
[29] Najjar YSH, Sadeq J. Modeling and simulation of solar thermal power system using parabolic trough collector. *J Energy Eng* 2017; 143:04016056-1-9.
[30] Singh H, Mishra RS. Performance evaluation of the supercritical organic rankine cycle (SORC) integrated with large scale solar parabolic trough collector (SPTC) system: An exergy energy analysis. *Environ Prog Sustain Energy* 2018; 37:891–9.
[31] Rashidi MM, Galanis N, Nazari F, et al. Parametric analysis and optimization of regenerative Clausius and organic Rankine cycles with two feedwater heaters using artificial bees colony and artificial neural network. *Energy* 2011; 36:5728–40.
[32] Sarangi SK, Barpujari B, Dawar R. Emerging technology option for clean power generation - concentrated solar power (CSP). In: *Petrotech-2009*, New Delhi, India, 2009.
[33] Neises T, Turchi C. A comparison of supercritical carbon dioxide power cycle configurations with an emphasis on CSP applications. *Energy Procedia* 2014; 49:1187–96.
[34] Cheng WL, Huang WX, Nian YL. Global parameter optimization and criterion formula of supercritical carbon dioxide Brayton cycle with recompression. *Energy Convers Manag* 2017; 150:669–77.
[35] Ma Y, Liu M, Yan J, et al. Thermodynamic study of main compression intercooling effects on supercritical CO_2 recompression Brayton cycle. *Energy* 2017; 140:746–57.
[36] Kim S, Cho Y, Kim MS, et al. Characteristics and optimization of supercritical CO_2 recompression power cycle and the influence of pinch point temperature difference of recuperators. *Energy* 2018; 147:1216–26.
[37] Reyes-Belmonte MA, Sebastian A, Romero M, et al. Optimization of a recompression supercritical carbon dioxide cycle for an innovative central receiver solar power plant. *Energy* 2016; 112:17–27.
[38] Wu C, Wang SS, Feng XJ, et al. Energy, exergy and exergoeconomic analyses of a combined supercritical CO_2 recompression Brayton/absorption refrigeration cycle. *Energy Convers Manag* 2017; 148:360–77.
[39] Singh H, Mishra RS. Performance analysis of solar parabolic trough collectors driven combined supercritical CO_2 and organic Rankine cycle. *Eng Sci Technol J* 2018; 21:451–464.
[40] Ahn Y, Bae SJ, Kim M, et al. Review of supercritical CO_2 power cycle technology and current status of research and development. *Nucl Eng Technol* 2015; 47:647–61.
[41] Petela R. Exergy analysis of the solar cylindrical-parabolic cooker. *Sol Energy* 2005; 79:221–33.
[42] Dudley VE, Koib GJ, Mahoney AR, et al. Test results: *SEGS LS-2 solar collector*. *Technical Report SANDIA94-1884*. Albuequerque: Sandia National Laboratories, 1994.
[43] Forristall R. *Heat Transfer Analysis and Modeling of a Parabolic Trough Solar Receiver Implemented in Engineering Equation Solver*. Golden, CO: National Renewable Energy Laboratory (NREL), 2003.
[44] Padilla RV, Too YCS, Benito R, et al. Exergetic analysis of supercritical CO_2 Brayton cycles integrated with solar central receivers. *Appl Energy* 2015; 148:348–65.
[45] Gibbs JP. Corrosion of various engineering alloys in supercritical carbon dioxide. *Ph.D. thesis*. Massachusetts Institute of Technology, Cambridge, MA, 2010.
[46] Parks CJ. Corrosion of candidate high temperature alloys in supercritical carbon dioxide. *Master's thesis*. Carleton University, Ottawa, Ontario, Canada, 2013.
[47] Chys M, van den Broek M, Vanslambrouck B, et al. Potential of zeotropic mixtures as working fluids in organic Rankine cycles. *Energy* 2012; 44:623–32.
[48] Wang E, Yu Z, Zhang H, et al. A regenerative supercritical-subcritical dual-loop organic Rankine cycle system for energy recovery from the waste heat of internal combustion engines. *Appl Energy* 2017; 190:574–90.
[49] Saleh B. Parametric and working fluid analysis of a combined organic Rankine-vapor compression refrigeration system activated by low-grade thermal energy. *J Adv Res* 2016; 7:651–60.
[50] Tchanche BF, Papadakis G, Lambrinos G, et al. Fluid selection for a low-temperature solar organic Rankine cycle. *Appl Therm Eng* 2009; 29:2468–76.
[51] Nouman J. Comparative studies and analyses of working fluids for Organic Rankine Cycles – ORC. *Master's thesis*. KTH School of Industrial Engineering and Management, Stockholm, 2012.
[52] Vivian J, Manente G, Lazzaretto A. A general framework to select working fluid and configuration of ORCs for low-to-medium temperature heat sources. *Appl Energy* 2015; 156:727–46.
[53] Lemmon EW, McLinden MO, Huber ML. *NIST Reference Fluid Thermodynamic and Transport Properties—REFPROP*. Gaithersburg, MD: National Institute of Standards and Technology, NIST Standard Reference Database 23.
[54] Klein SA. Engineering Equation Solver (EES), Academic Commercial V7.714. F-Chart Software, 2006. www.fChart.com.

Downloaded from https://academic.oup.com/ce/advance-article-abstract/doi/10.1093/ce/zky011/5050906
by Delhi Technological University user
on 15 July 2018

ResearchGate

See discussions, stats, and author profiles for this publication at: https://www.researchgate.net/publication/326439886

Experimental comparative study of chrome steel pin with and without chrome plated cast iron disc in situ fully flooded interface lubrication

Article · July 2018

CITATIONS
0

READS
29

2 authors:

Roop lal Rana
Delhi Technological University
14 PUBLICATIONS **15** CITATIONS
SEE PROFILE

R. C. Singh
Delhi Technological University
40 PUBLICATIONS **53** CITATIONS
SEE PROFILE

Some of the authors of this publication are also working on these related projects:

Working in the area of Tribology (Engine tribology, bearing design, tribology by nano particles and tubes. View project

Thermoelectric Device, Thermoelectric Material & Property View project

All content following this page was uploaded by R. C. Singh on 17 July 2018.

The user has requested enhancement of the downloaded file.

PAPER

Experimental comparative study of chrome steel pin with and without chrome plated cast iron disc in situ fully flooded interface lubrication

To cite this article: Roop Lal and R C Singh 2018 *Surf. Topogr.: Metrol. Prop.* **6** 035001

View the article online for updates and enhancements.

Related content

- Tribological performance analysis of textured steel surfaces under lubricating conditions
R C Singh, R K Pandey, Rooplal et al.
- Mechanical and tribological behaviour of molten salt processed self-lubricated aluminium composite under different treatments
C Kannan and R Ramanujam
- Effect of load on the tribological properties of hypereutectic Al–Si alloy under boundary lubrication conditions
Parveen Kumar and M F Wani

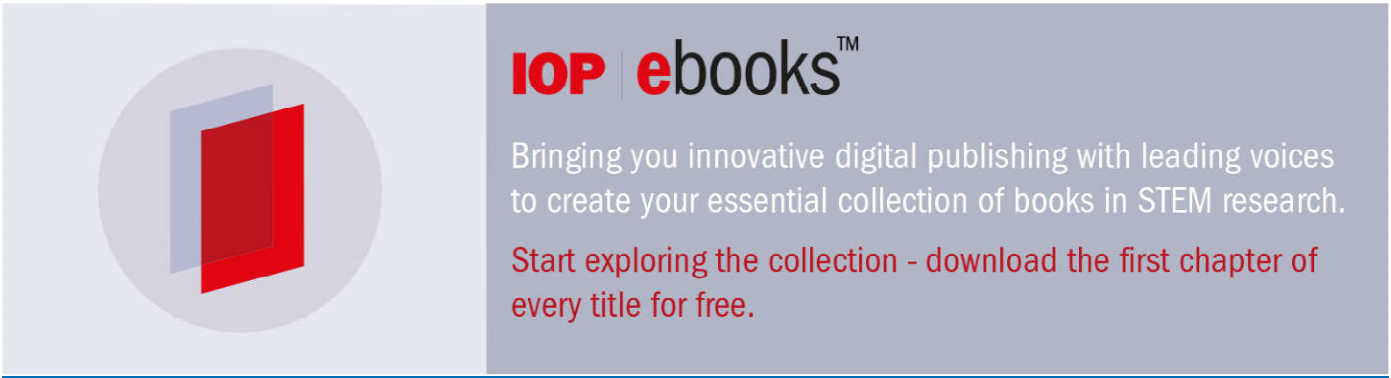

This content was downloaded from IP address 14.139.251.107 on 05/07/2018 at 03:41

Surface Topography: Metrology and Properties

PAPER

RECEIVED
6 November 2017

REVISED
10 May 2018

ACCEPTED FOR PUBLICATION
18 May 2018

PUBLISHED
7 June 2018

Experimental comparative study of chrome steel pin with and without chrome plated cast iron disc in situ fully flooded interface lubrication

Roop Lal and R C Singh

Department of Mechanical Engineering, Delhi Technological University, Delhi 110042, India

E-mail: rooplalrana@gmail.com **(R Lal)**

Keywords: friction, wear, pin-on-disc, wet friction, microstructure

Abstract

This paper reports the findings of an experimental study pertaining to the tribo dynamic investigations of contacts formed between chrome base pin and cast iron/chrome plated cast iron discs in situ conditions. Pin on disc geometrical configurations were employed for conducting the experiments at different operating parameters using SAE-15W40 lubricating oil. The fully flooded lubricating condition was insured by directed supply of lubricant at the interface. The friction coefficient, wear rate, vibration amplitude, temperature rise and sound intensity were measured at different loads (varying in the range of contact pressure 1.9–3.1 MPa) and sliding speeds (2–10 m s^{-1}) for the travelling distances between 1000–5000 m. Based on experimental investigations, reductions in the friction coefficient and wear rate were recorded for the chrome steel pin/chrome plated cast iron disc in comparison to chrome steel pin/cast iron disc contact. However, increases in the temperature rise, vibration, and noise were recorded with chrome steel pin/chrome plated cast iron disc contact.

1. Introduction

Fuel consumption, crude oil depletion, emission legislative, friction losses and wear are considered vital parameters in the automotive industry constituting the true motivators. In the modern era there is extensive use of Diesel Engine in the field of transportation, power generation, agriculture and manufacturing. The life of an engine depends on the losses and wear experienced by the engine in terms of piston rings and cylinder liner. The piston rings and cylinder liner combine to form the tribopair that plays a significant role in power transformation from the chemical energy of the fuel in the combustion chamber. The largest source of frictional losses in the internal combustion engine is cylinder and piston system which comprises nearly 50% of the total frictional losses. The piston rings contribute 70%–80% of friction in the cylinder and piston system. Thus, the cylinder and piston system being the paramount needs optimization to achieve high efficiency. In addition to frictional losses, this system also consumes a large volume of lubricating oil and releases a considerable amount of particulate emissions. In order to optimize the cylinder and piston system, an experimental investigation is of utmost importance to study its tribological behaviour.

Generally, the pin-on-disc method is considered to analyse the nature of materials in contact. The material of pin represents the cylinder liner while the disc material represents the piston rings. A comprehensive research has been done during the second half of the twentieth century for the development of more compact, fuel efficient and eco-friendly internal combustion engines for automobiles. Improvement in mechanical efficiency of internal combustion engines can be achieved by decreasing the frictional losses occurring in cylinder and piston assembly. Wear measurements had been carried out and analysed in cylinder and piston ring during their mating with each other when the automotive engine was operated under artificially created dusty environmental conditions [1–3]. Tests were conducted on pin-on-disc test apparatus with boundary-lubricated cast iron materials and the values of specific wear rates were observed to be between 10^{-13} and 10^{-10} $mm^3/mm/N$ [4]. Based on the Newton-Raphson-Murty algorithm, the non-linear finite-element method was used to analyse the piston rings problems based on the theories of elasto

© 2018 IOP Publishing Ltd

hydrodynamic and hydrodynamic lubrication [5]. The understanding of theoretical concepts and use of a methodology for estimating the service life of an I C engine, based on the law of adhesive wear and experimental evidence, were explained extensively [6]. The study and experimental research were conducted on materials, metallurgical aspects of piston ring scuffing, piston ring lubrication in a two-stroke diesel engine and the film thickness between the cylinder liner and piston rings [7, 8]. Experiments were also performed on a reciprocating test rig having the supply of lubricant into the contact patch and measuring the friction force between specimen and counter-specimen. Tribological behaviors of cylinder liner with and without oil pockets were examined and compared [9, 10]. A test method was developed for evaluation of the friction and wear of piston rings and cylinder liner used in heavy-duty diesel engines. These work focussed on the conditions of the lubricating oil and its effect [11, 12]. At Volvo, technology had been updated for better evaluation of the friction between different combinations of materials. The elements under considerations were the piston rings and the cylinder liner which were analysed for friction, wear, and change in surface morphology during the running conditions [13]. The author investigated the role of sulfur for the high performance of the current tribo system. The field worn samples were examined to conclude that no tribo film containing sulphur existed under the tribological conditions set up for the piston rings and cylinder liner in the reciprocating test rig [14]. A similar work was carried out using the mathematical model to solve the Reynolds equation [15]. A non-firing engine simulator was developed which operated at same linear speed, load and stroke as that of an actual engine. Except firing pressures, all engine operating conditions were simulated [16]. Experimental investigation was carried out to study the characteristics of the cylinder liner-piston ring tribopair. The process parameters selected for the experiment were sliding velocity, applied load and type of lubricating oil. A mathematical model was developed using L16 Taguchi orthogonal design to optimize the reciprocating wear for minimum weight loss and friction [17]. Author did an experimental study of single cylinder diesel engine operating at steady state to measure wear and surface roughness of cylinder liner by a WYKONT 1100 optical surface profile meter at various locations on the surface of cylinder liner before and after each test. It was observed that surface roughness decreased with time following which it experienced a steep decrease in rate during the run-in period. The results obtained in terms of volume of wear were reasonable and within the tolerance limits [18]. An investigation of temperature effect on wear and friction was carried out when steel to steel contacts was un—lubricated, in various aerobic gaseous atmospheres and at high temperature of about 200 °C. The inference was drawn considering the current results compared to previously published results [19]. A ring segment was tested in Laboratory to evaluate wear and friction behavior of piston ring on a flat specimen of grey cast iron representing cylinder liners in real engine. Various lubricants including mineral oil, Jet aviation fuel, fully formulated 15W40, category of heavy duty oil, were used to evaluate the condition of lubricant. During the test the temperatures were maintained from 25 to 100 °C. An incremental load procedure was used to evaluate friction behavior which showed boundary lubrication for all lubricants at 100 °C. Wear tests were performed at 240 N for 6 h at a constant temperature of 100 °C with new ring segments following which weight loss method was used to measure the wear. A geometric model was designed for wear volume and wear depth to take into account the compound curvatures before and after testing [23].

Carbon fabric was treated with gamma irradiation technique with varying doses (100–300 kGy) to develop composites with polyetherimide (PEI) matrix which was characterized for inter-laminar shear strength (ILSS) and adhesive wear studies. FTIR and SEM indicated presence of carbonyl functional group and roughening of surface inferred improved fiber–matrix interface [20]. Investigation was carried out to develop and analyse the material properties of a Polybenzimidazole (PBI)—Polyetherketone (PEK) blend based composite and composites containing solid lubricants (SLs), short fibers of glass and carbon. It was inferred from the experimental work that the SLs or fibers together showed excellent tribo-properties in accordance to the composite based on PBI–PEEK blend [21]. Experimentation was carried out for two diesel fuels i.e. EN590 and GDK650 as lubricants in the pin-on-disc model during the testing of wear behaviour of hydrogenated diamond like-carbon (DLC) coating in DLC/steel. It was concluded that anti-wear additives were harmful to DLC influencing its wear rate while steel remains unaffected by pressure, temperature, speed and type of lubricant used [22]. The investigation was conducted to analyse the tribological properties of ground, lapped and textured lapped discs against polished pins for reciprocating motions. Various output parameters were analysed among which coefficient of friction showed 30% reduction and vibrations between contact points of textured surface-balls interface showed a prominent dip at the resonance frequency in comparison to interface of polished surface-balls [24]. This work laid down the tribological analysis carried out for the dimpled piston rings. In order to curb the fuel consumption, research is being conducted to reduce the friction between cylinder liner and the piston rings. The experimental work yielded the result in favour of the dimpled piston rings as it helped saved considerable amount of fuel and lubricating medium. The tribological parameters, coefficient of friction and wear had been studied in this research work under full lubricating conditions for smooth/textured surfaces of steel

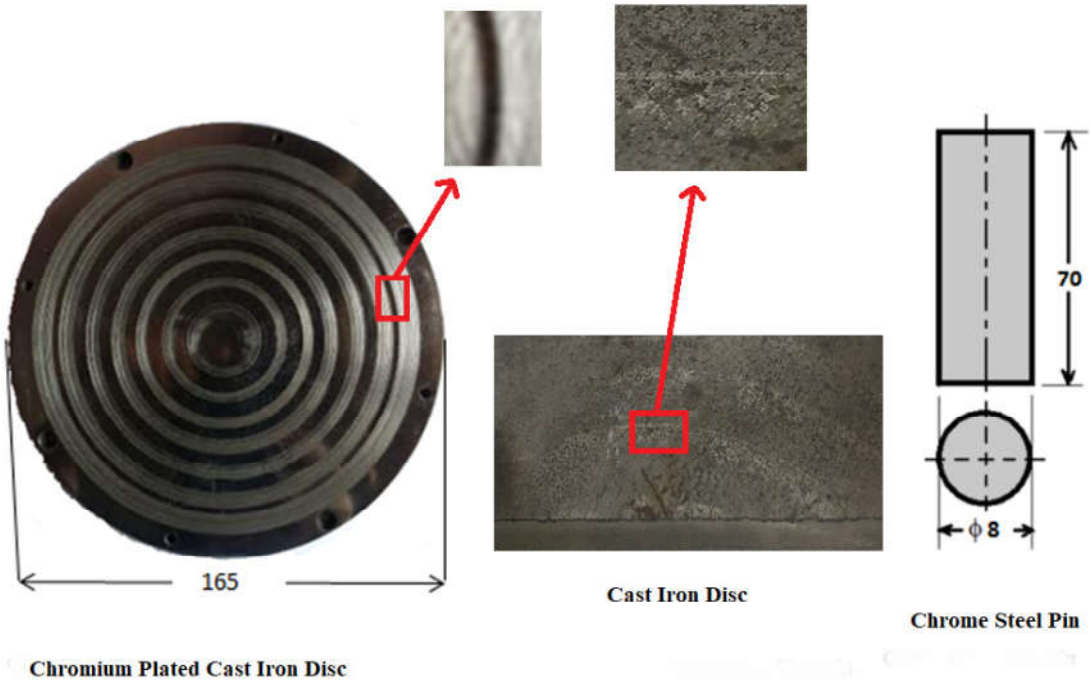

Figure 1. Schematic and dimensional details of disc and pin.

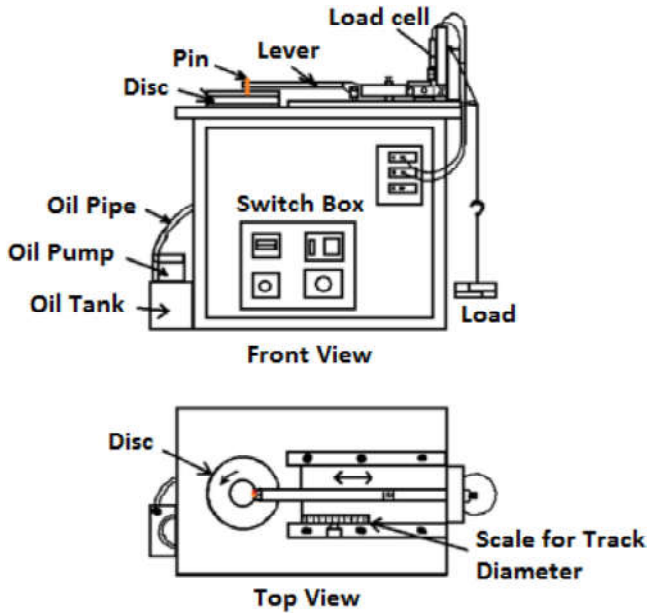

Figure 2. Schematic of friction and wear tester.

discs and smooth surface of steel pins. Reduction in considered tribological parameters had been recorded in textured steel disc for fully flooded and starved conditions [25]. Another work investigated the mechanical properties of synthesised Mg_2Si co-doped with Bi and Sb through in situ spark plasma reaction sintering. The synthesis process displayed enhanced mechanical properties such as hardness ~5.4 ± 0.2 GPa and an elastic modulus ~142.5 ± 6 GPa with a fracture toughness of ~1.71 ± 0.1 MPa $\sqrt{m}$, t as thermal shock resistance as ~300 W m^{-1}. It promised the sustainability of their thermoelectric modules under all circumstances [28]. Investigation was carried out on the stir casted aluminium based composite reinforced with 2–4–6% weight flyash. The pin-on-disc test rig was used to conduct the experiment for the smooth surfaces of cast iron disc and smooth MMC pin tribo-pair for the study of tribological parameters i.e. friction force and wear. The experimental work concluded that MMC with 6% flyash wears less while MMC with 4% flyash provides low coefficient of friction or friction force [27].

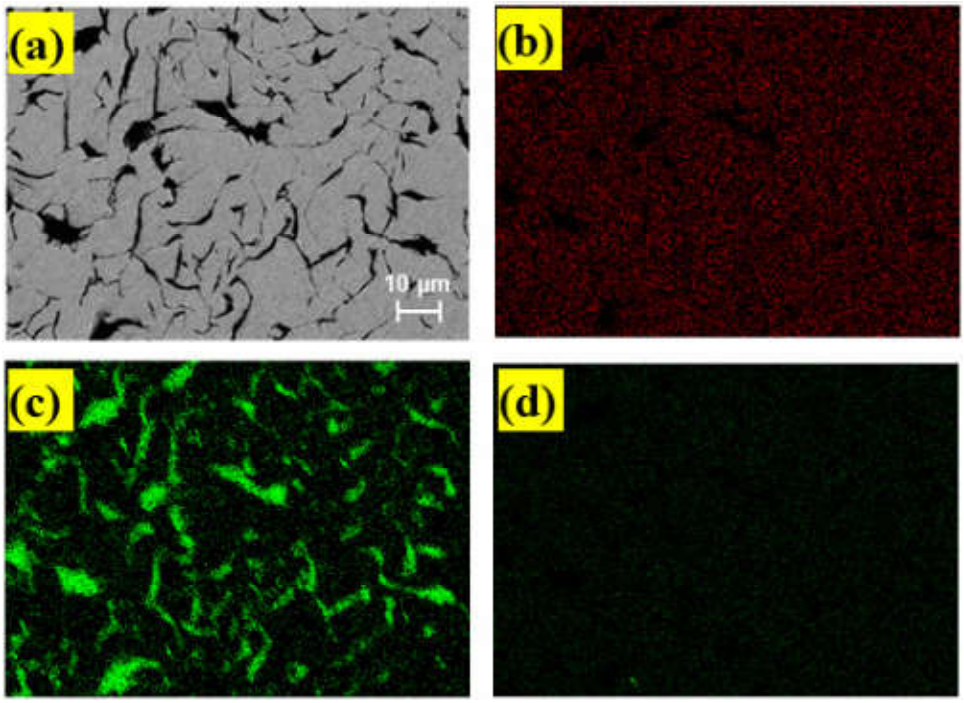

Figure 3. Scanning electron images of (a) cas iron disc and elemental mappings of (b) iron, (c) carbon and (d) silicon.

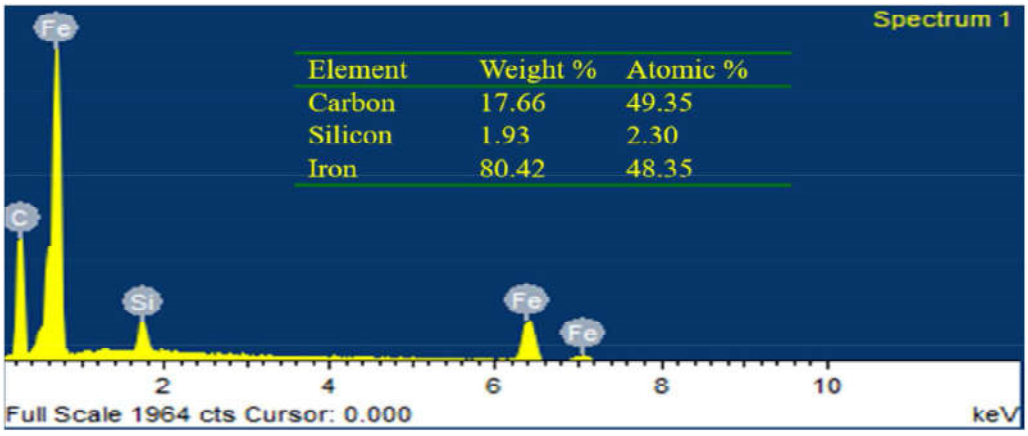

Figure 4. EDS spectrum showing the elements of Fe, C and Si presence in the disc (inset shows the chemical stoichiometric of the individual elements).

Based on the literature review, it is noticed that friction and wear reduction in piston and piston ring system are vital task. It has also been noticed that there is dearth of experimental studies towards exploring the tribo-dynamic behaviours of piston and piston ring system in situ condition under thin/mixed film lubrication. Hence, the objective of this paper is to present the experimental tribodynamic findings of fully flooded contacts of chrome steel pin and cast iron/chrome plated cast iron discs in situ condition for highlighting the possibility of manufacturing of chrome coated liners and piston rings.

2. Experiments details

The specimens of the Cast Iron disc and Chromium-coated Cast Iron disc of diameter 165 mm and thickness 8 mm were manufactured as depicted in the figure 1, for the conduction of experimental investigation. The surface finished discs attained the surface roughness level in the range 0.15 to 0.3 μm R.M.S. value. Surface roughness was measured by Telly Surf; 8 readings along the radial direction at interval of 45° and 8 readings perpendicular to it from middle of the stroke of Telly Surf. A cylindrical

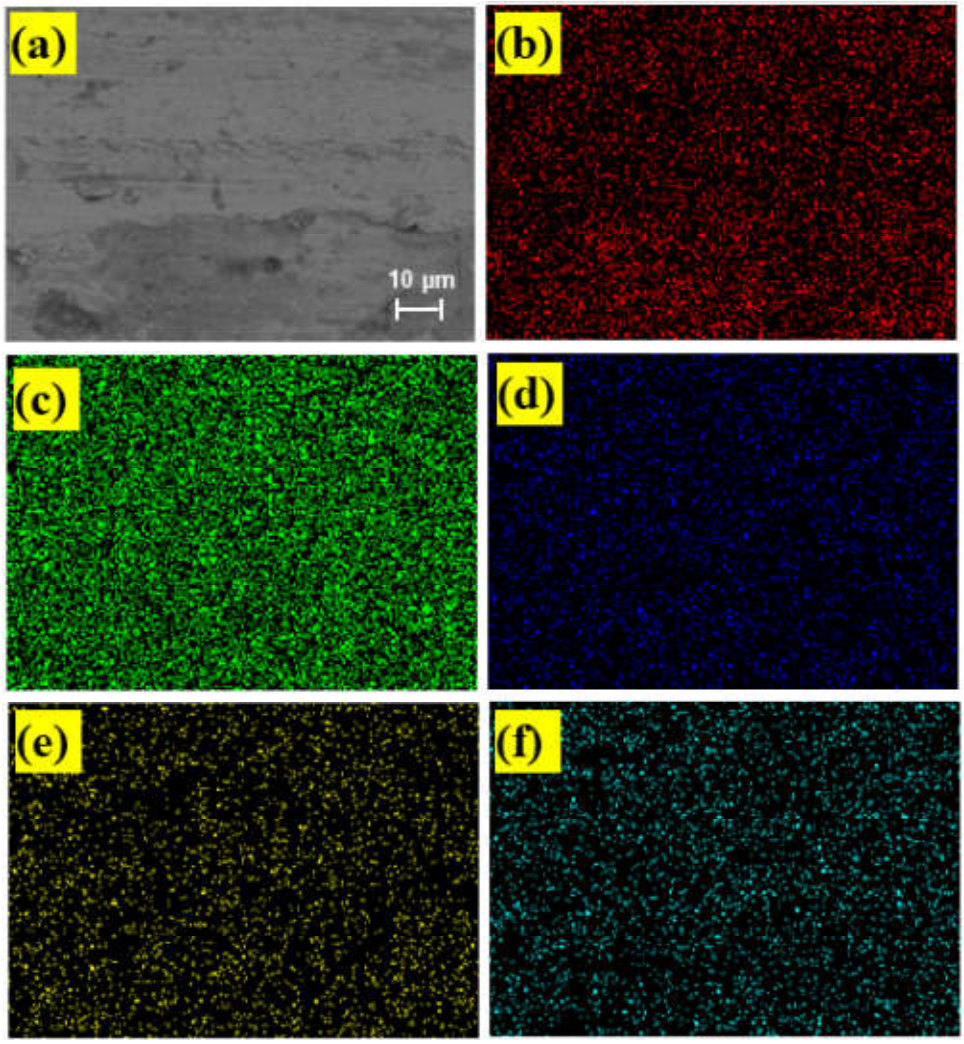

Figure 5. Scanning electron images of (a) pin material and elemental mappings of (b) oxygen, (c) iron, (d) silicon, (e) carbon, and (f) chromium.

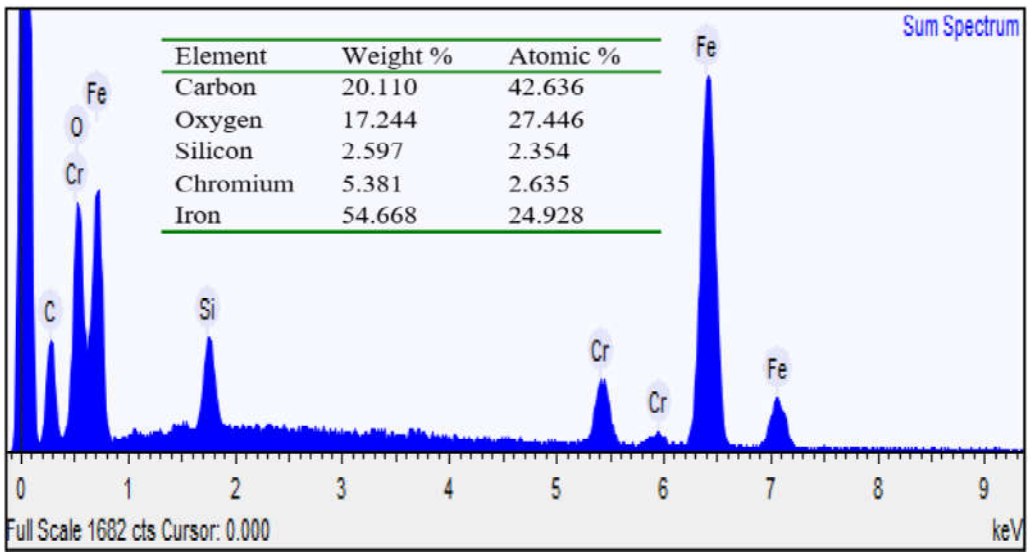

Figure 6. EDS spectrum showing the elements of Fe, C, O, Cr and Si presence in the pin (inset shows the chemical stoichiometric of the individual elements).

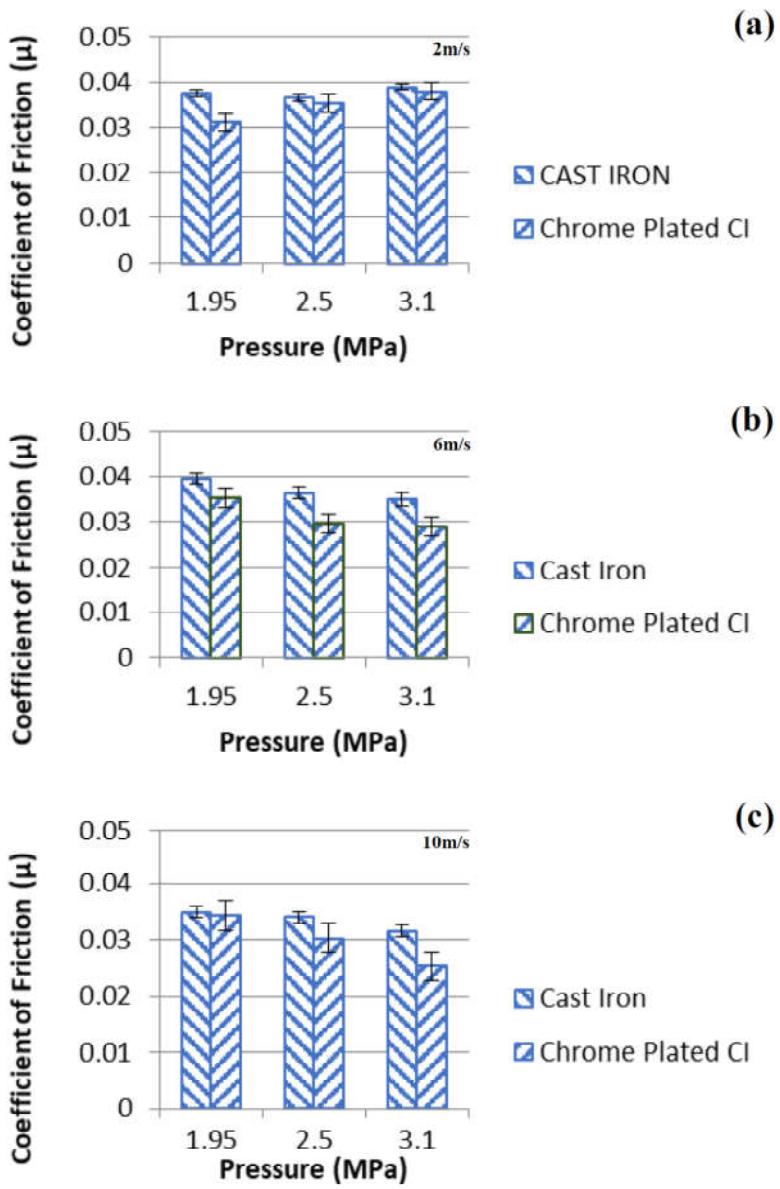

Figure 7. Coefficient of friction (μ) of cast iron/chromium plated cast iron against steel pin with three different pressure (1.95, 2.5, 3.1 MPa) and speed (a) 2 m s^{-1}, (b) 6 m s^{-1} and, (c) 10 m s^{-1} conditions.

Steel pin with diameter 8 mm and length 70 mm was considered for testing the circular discs made of Cast Iron and Chromium-Coated Cast Iron. The face of the circular pin was leveled and checked by rubbing it against a soft paper for removing the debris if any. Face flatness was checked with the help of ink impression on paper. Pin was held rigidly 4 mm below the clamp for the test purpose on the disc to minimize bending and this distance was ignored while evaluating the tribological properties. Generally the lubricating oil (15W40) used in tropical regions was considered for the experimentation. The characteristics determined in the laboratory at 40 °C and atmospheric pressure were (1) kinematic viscosity of 160.32 mm^2 s^{-1} as per ASTM D—445, (2) Density of 0.8744 g cm^{-3} as per ASTM D—4052 and (3) Specific gravity of 0.8752 as per ASTM D—287 [26].

The schematic diagram of friction and wear tester used in the present study is shown in figure 2. It has a motor which can rotate at varying speeds based on the rheostat position. The desired speed was selected between 200–2000 r.p.m. There is a horizontal fixture on which the specimen disc was bolted at 4 points along with the speed sensor and the probe for measurement of wear. Weights for loading were placed on the pan which has a horizontal platform to support it in the direction of gravity. Weight placed in the pan is transmitted through a bell-crank mechanism comprising uni-lever via wire and pulleys. A force detector probe attached to the side of the bell crank to measure the shear friction force. Specifications of Friction and Wear tester used in these experiments were: Pin diameter 8 mm of chrome steel; Disc (i) diameter 165 mm and thickness 8 mm made of cast iron and disc (ii) diameter 165 mm and thickness 8 mm made of the chrome plated cast iron disc. According to the specifications of Tribometer the range of speed varies between 200 to 2000 r.p.m and frictional force can be

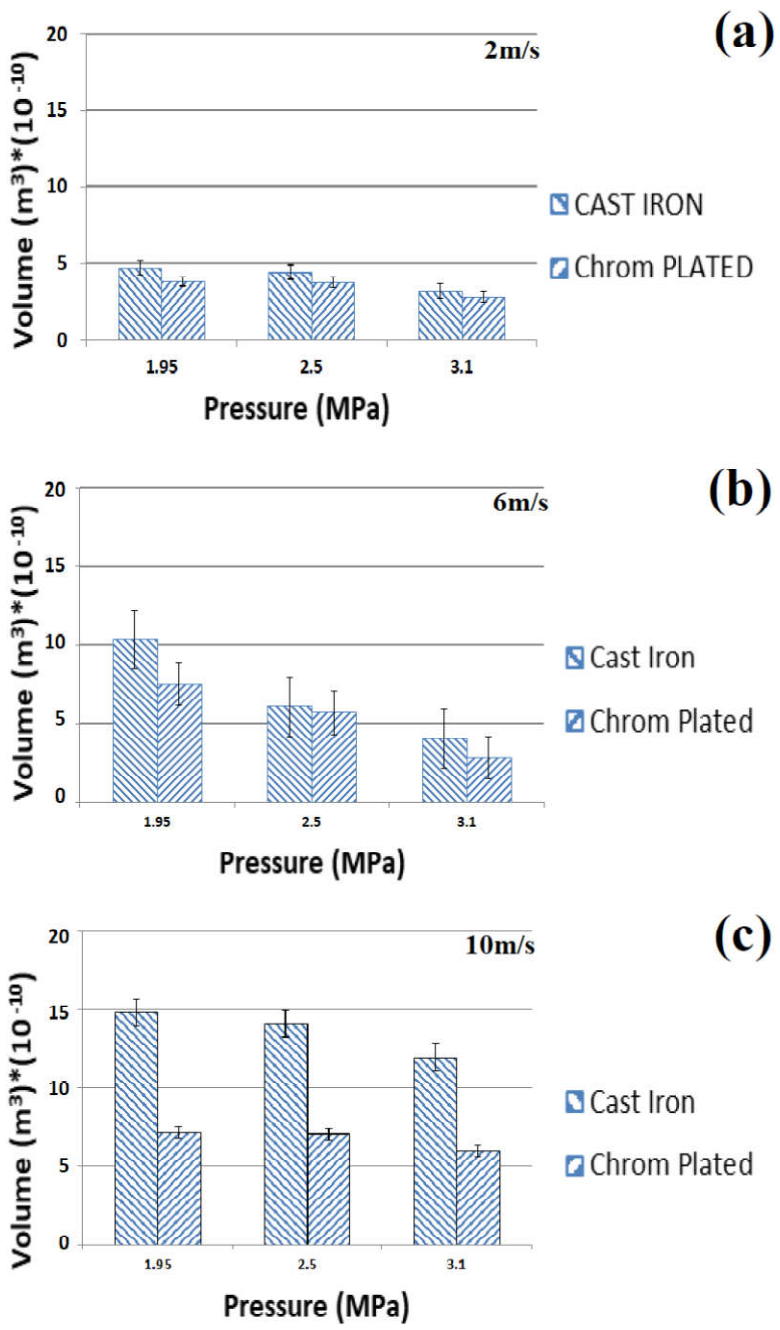

Figure 8. Wear loss of Steel pin against cast iron/chromium plated cast iron with three different pressure (1.95, 2.5, 3.1 MPa) and speed (a) 2 m s^{-1}, (b) 6 m s^{-1} and, (c) 10 m s^{-1} conditions.

measured upto 200 N with the least count of 0.1 N and Accuracy of 0.1% ± 2% measured frictional force in Newton (N).

In this experimental plan, the analysis has been designed in such a manner that each factor was analysed independently. Implementation of this plan showed significant reduction in the execution time needed for conducting the experiment. It was very efficient in investigating the effects of multiple performance factors and also to study the effect of individual factors. The experiment was performed in Tribological Lab, Delhi Technological University, Delhi. Pressure was varied between 1.95 MPa to 3.1 MPa and pin used for the same was 8 mm in diameter and 70 mm in length as shown in figures 1 and 2. Parameters were selected on the basis of preliminary investigations and 27 experiments were performed on each disc. Tribological study was carried out for the loads represented by pressure varying from 1.95 MPa to 1.4 MPa, at varying sliding speeds 2–10 m s^{-1} (equivalent to 200–2000 rpm) and distances traversed by the pin between 1000 m to 5000 m as per the experimental plan.

3. Results and discussions

Figure 3 shows a typical microstructural image of the cast iron disc and the corresponding elemental distribution maps, employing scanning electron

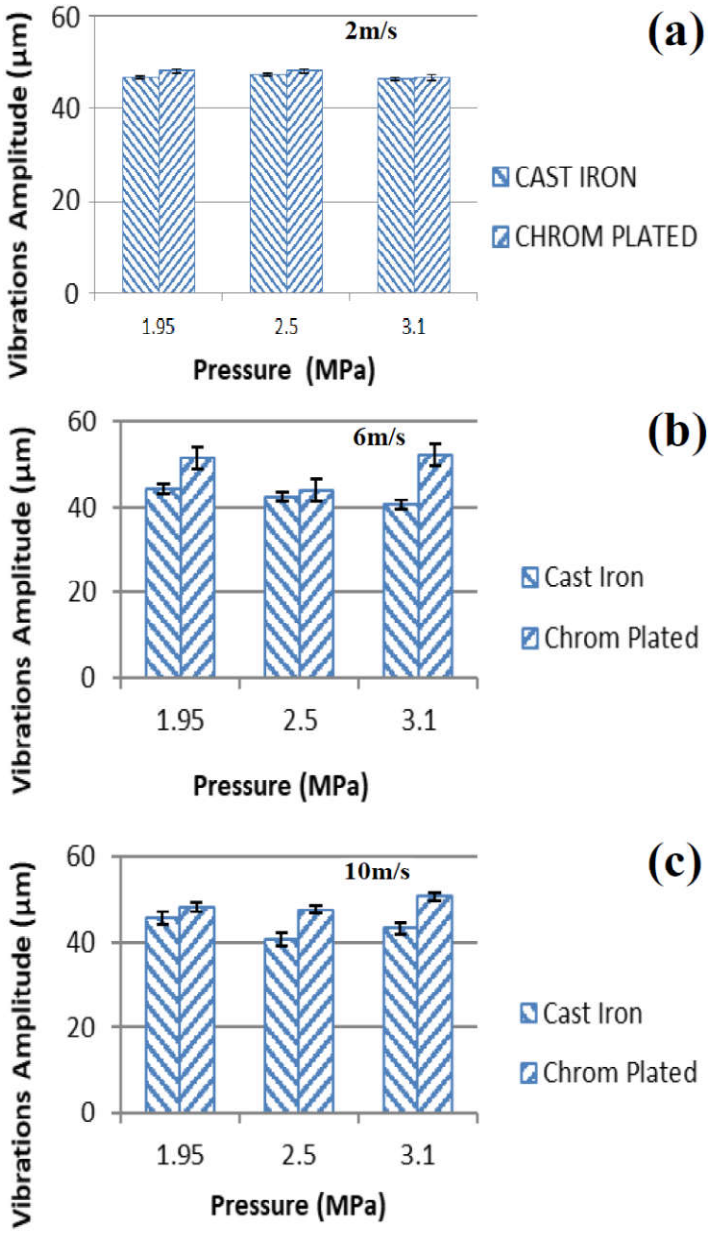

Figure 9. Vibration amplitude of cast iron/chromium plated cast iron against steel pin with three different pressure (1.95, 2.5, 3.1 MPa) and speed (a) 2 m s^{-1}, (b) 6 m s^{-1} and, (c) 10 m s^{-1} conditions.

microscope. Figure 4 shows the EDS spectrum, exhibiting the individual constituent elements in the cast iron disc, and the inset confirms the chemical composition of the individual elements. Figure 5 shows a microstructural image of the pin material and the corresponding elemental distribution maps, using scanning electron microscope. Figure 6 shows the EDS spectrum, depicting the individual constituent elements in the pin material, and the inset confirms the chemical composition of the individual elements. The morphology and composition were analyzed for the cast iron disc-steel pin tribopair which was then subjected to tribological performance employing Pin-on-Disc Tribometer (Make: Ducom, India). The results obtained have been discussed in the following paragraphs.

3.1. Coefficient of friction

The trend of the coefficient of friction (μ) versus pressure (MPa) considering sliding speed of 2 m s^{-1}–10 m s^{-1} has been plotted in figure 7 for the pressure ranging between 1.95 MPa–3.1 MPa for flooded lubrication. Chromium plated disc shows improvement in the tribological parameters immensely in comparison to the cast iron disc. Experiments were performed by varying the distance between 1000 m to 5000 m at the same pressure range and in the presence of same lubricating oil (SAE 15W40). The coefficient of friction as in figure 7 was observed 0.03–0.04 between the steel pin and the cast-iron disc, that the plain cast iron disc had the maximum value of coefficient of friction i.e. 0.04. Under the same corresponding conditions, Chromium Plated cast iron disc had a

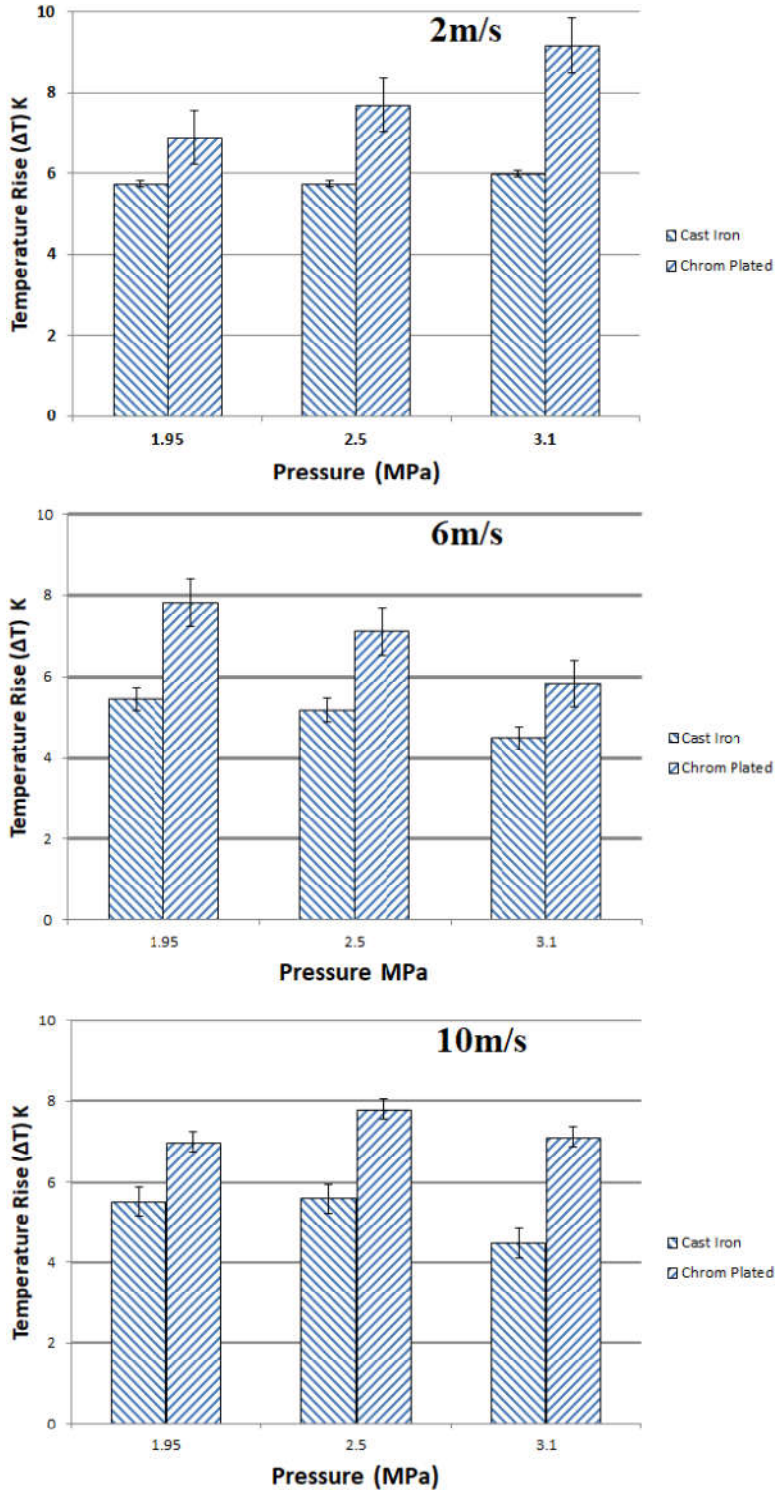

Figure 10. Temperature rise of cast iron/chromium plated cast iron against steel pin with three different pressure (1.95, 2.5, 3.1 MPa) and speed (a) 2 m s^{-1}, (b) 6 m s^{-1} and, (c) 10 m s^{-1} conditions.

coefficient of friction as 0.025–0.035. It was observed that coefficient of friction continuously decreased with an increase in pressure and attained the least value of coefficient of friction 0.025, at the pressure of 3.1 MPa. So the hard surface in relative motion had low coefficient of friction in fully flooded condition.

3.2. Wear

Wear characteristics were shown in figure 8, where initially fast growth in wear was observed at the start due to solid contact, interlocking of asperity and as tribopair had relative motion, breaking of the asperty took place as shown in figure 12. The variation of wear with different pressure values under the condition of fully flooded lubrication were displayed in figure 8. A decrease in wear rate was observed as the pressure increased. This phenomenon was governed by thin layer mixed and elasto hydrodynamic lubrication. Under contact stresses, a very thin film of lubricating oil formed that separate the contact surfaces. It resulted

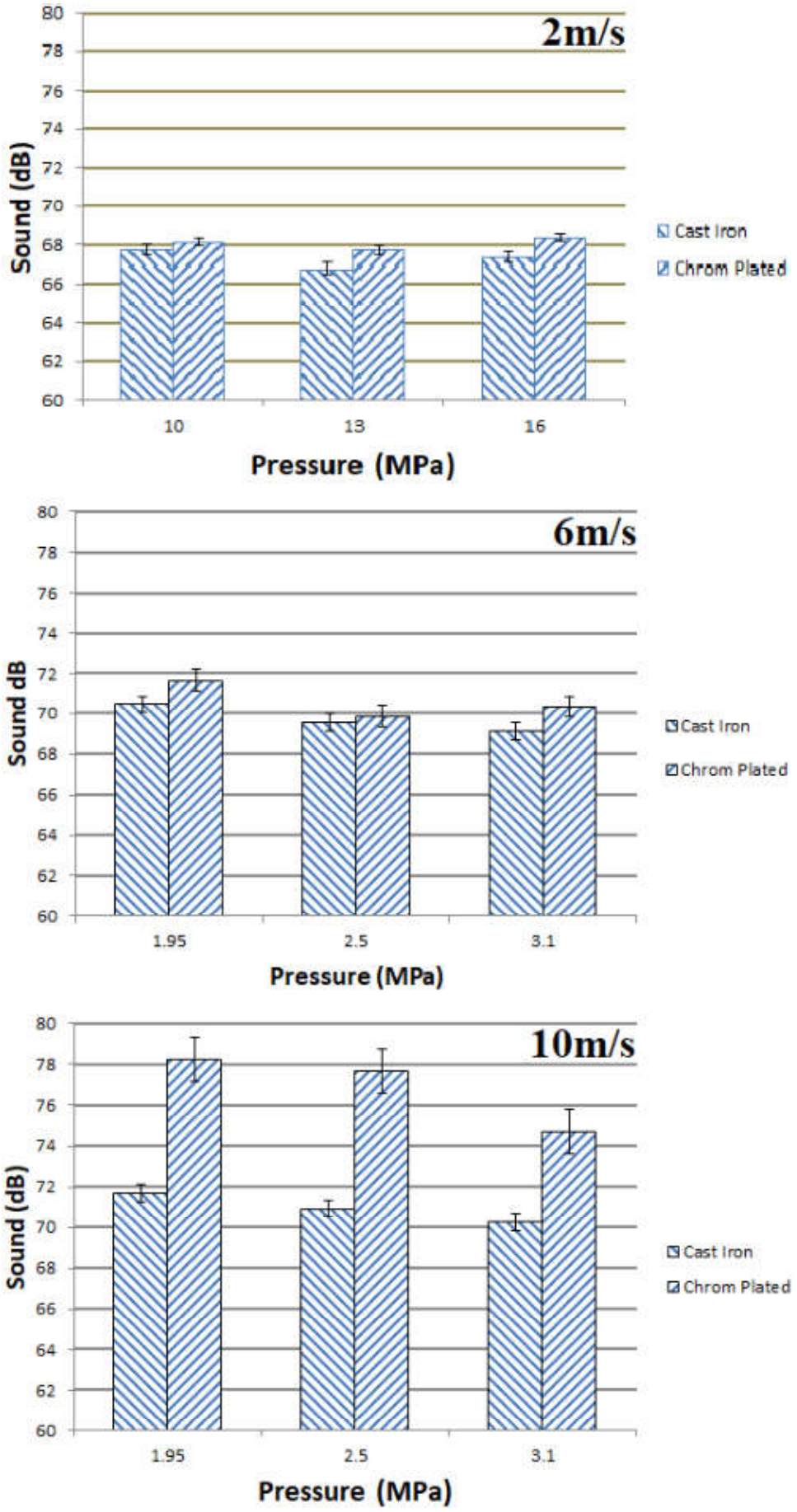

Figure 11. Frictional sound of cast iron/chromium plated cast iron against steel pin with three different pressure (1.95, 2.5, 3.1 MPa) and speed (a) 2 m s^{-1}, (b) 6 m s^{-1} and, (c) 10 m s^{-1} conditions.

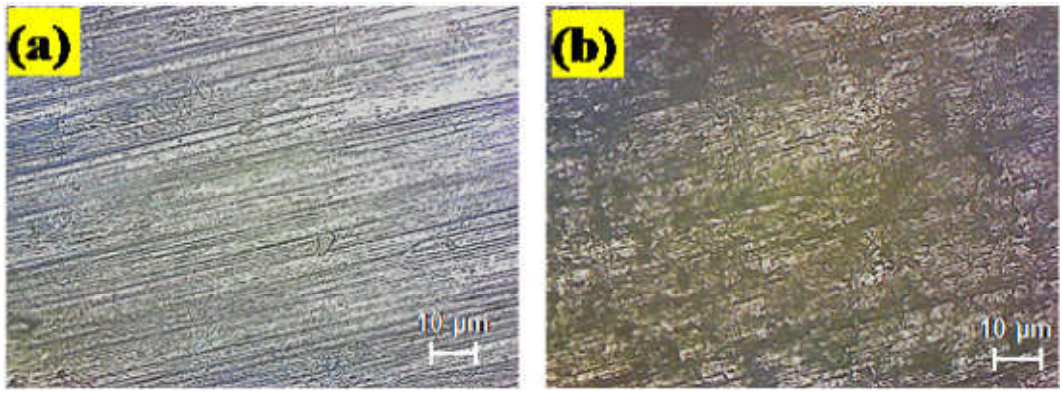

Figure 12. Microscopic view of worn surface of (a) and (b) cast iron disc.

in elasto hydrodynamic lubrication. This resulted in reduction of friction and wear. Wear pattern on the pin material was shown in figure 12(a). The initial increase in wear occurred due to the abrasion wear owing to the highly strained fragments in between the contact surfaces and later decrease was due to the diffusion of surface debris which was insignificant in comparison to the abrasion wear.

The decrease in wear was also due to the formation of thin layer of lubricant at the interface of the discs and pin. This resulted into thin layer mixed lubrication processes. In experiment, the various values of distances were taken from 1000–5000 m for the disc with predefined diameter against varying pressure values i.e. 1.95 MPa, 2.5 MPa, and 3.1 MPa. Under fully flooded lubrication, the wear increased from 1×10^{-10} m^3 to 15×10^{-10} m^3, was due to thin layer mixed and elasto hydrodynamic lubrication. Hence, it was inferred that the pin material wears more as the pressure is increased.

Microscopic views as in figure 12 and extended view as in figure 1 depict the abrasive wear and ploughing took place in thin layer lubrication.

3.3. Vibrations amplitude

Experiments were conducted taking various values of distances from 1000 m to 5000 m at different disc diameters and different pressure. It was observed that when lubrication was fully flooded, the vibration amplitude varied between 40 μm and 52 μm as shown in figure 9. It was due to the hydrodynamic lubrication. As per figure 9, the amplitude of vibrations increases with the pressure at the considered values i.e. 1.95 MPa, 2.5 MPa, and 3.1 MPa. This was caused by excessive pressure at the interface of the tribopair. The vibrational values showed the experiment carried out was stable.

3.4. Temperature rise

Continuous relative motion between two metals is the source of temperature and as the motion continues the temperature rises continuously. The rise in temperature was governed by the surface roughness of the materials in contact along with the mechanical properties of the materials of pin and disc. Experiments were conducted at varying distance travelled in the range of 1000–5000 m for different diameter of the disc with the pressure values as 1.95 MPa, 2.5 MPa and 3.1 MPa. Figure 10 depicts the temperature rise at the interface of the tribopair and it varies between 4 K and 9 K as measured by thermal image camera when lubricant was flowing continuously.

Observed temp rise value showed the experiment was conducted with the stable pace and energy loss was very less.

3.5. Sound

The rules of noise pollution, 2000, had set different acceptable limits depending upon the category i.e. day and night. For industries, it is 75 dB for the day and 70 dB for the night. Similarly, for residential areas, it is 55 dB for the day and 45 dB for the night. Figure 11 shows the trend of sound as observed during the experimentation procedure. It was noted in the figure 11 that sound varies from 66.8 dB to 78 dB. High noise observed in the Chromium plated disc as compared to the Cast Iron disc. This was due to the property of cast iron of absorbing the energy or vibration experienced during the running conditions. At low speeds and for longer distance traversed it was ascertained that cast iron disc absorbed more energy and hence made less noise. The continuous flow of lubricant also acted as the medium of sound for the base material in motion with respect to pin material. The measuring instrument was the sound meter which was kept 0.25 m away from the pin and disc.

4. Conclusion

1. It has been observed that Chromium plated cast iron disc significantly improved the coefficient of friction and the value 0.025 found to be at 3.1 MPa and 6 m s^{-1} relative velocity at the interface under the condition of fully flooded lubrication as compared with cast iron disc with chrome steel pin. In such condition, the

lubricating oil helped in reducing the shear force which further reduced the coefficient of friction with the increase in speed. The chrome plated cast iron disc had hard surface to reduce coefficient of friction at thin layer tribo lubrication.

2. Chrome plated cast iron disc experienced less wearing due to the formation of hard surface layer of chromium and the presence of thin layer mixed and elasto hydrodynamic lubrication in the contact area of the tribopair. The chrome plated cast iron disc had hard surface to reduce wear rate at thin layer tribo lubrication.
3. The amplitude of vibration was observed to be minimum at 40 μm and maximum at 52 μm. The Chromium Plated cast iron disc had more amplitude of vibration in comparison to cast iron disc due to less energy absorption in the chromium plated cast iron disc.
4. The rise in temperature at the interface of the tribo—pair formed between the cast Iron, Chromium plated cast Iron discs and the steel pin was observed from 4 K to 9 K. The combination of chromium plated cast iron disc with steel pin showed more temperature rise when compared with cast iron disc and steel pin. This rise in temperature was negligible due to the condition of fully flooded lubrication.
5. The experimental results show that sound varied between 66.8 dB to 78 dB. Chromium plated cast iron disc owing to hard surface generated more noise while the cast iron disc generated less noise due to its property of absorption of energy and also the continuous flow of lubrication acted as the sound absorber leading to a quiet movement between the two surfaces in contact.

Acknowledgment

Authors would like to thank Nanoscale Research Facility (NRF) of IIT Delhi, India and Tribology Lab of Delhi Technological University, Delhi, India for their kind help in characterization.

ORCID iDs

Roop Lal https://orcid.org/0000-0001-8638-9608

References

[1] Wakuri Y, Hamatake T, Soejima M and Kitahara T 1992 Piston ring friction in internal combustion engines *Tribol. Int.* **25** 299–308
[2] Nautiyal P C, Singhal S and Sharma J P 1983 Friction and wear processes in piston rings *Tribol. Int.* **16** 43–9
[3] Pawlus P 1993 Effects of honed cylinder surface topography on the wear of piston-piston ring-cylinder assemblies under artificially increased dustiness conditions *Tribol. Int.* **26** 49–55
[4] Childs T H C and Sabbagh F 1989 Boundary-lubricated wear of cast irons to simulate automotive piston ring wear rates *Wear* **134** 81–97
[5] Hwu C J and Weng C 1991 Elastohydrodynamic lubrication of piston rings *Wear* **150** 203–15
[6] Picken D J and Hassaan H A 1983 A method for estimating overhaul life of internal combustion engines including engines operating on biogas and methane *J. Agric. Eng. Res.* **28** 139–47
[7] Scott D, Smith A I, Tait J and Tremain G R 1975 Materials and metallurgical aspects of piston ring scuffing—a literature survey *Wear* **33** 293–315
[8] Moore S L 1981 Piston ring lubrication in a two-stroke diesel engine *Wear* **72** 353–69
[9] Grabon W, Pawlus P and Sep J 2010 Tribological characteristics of one-process and two-process cylinder liner honed surfaces under reciprocating sliding conditions *Tribol. Int.* **43** 1882–92
[10] Grabon W, Koszela W, Pawlus P and Ochwat S 2013 Improving tribological behaviour of piston ring–cylinder liner frictional pair by liner surface texturing *Tribol. Int.* **61** 102–08
[11] Truhan J J, Qu J and Blau P J 2005 The effect of lubricating oil condition on the friction and wear of piston ring and cylinder liner materials in a reciprocating bench test *Wear* **259** 1048–55
[12] Michalski J and Woś P 2011 The effect of cylinder liner surface topography on abrasive wear of piston–cylinder assembly in combustion engine *Wear* **271** 582–89
[13] Johansson S, Nilsson P H, Ohlsson R and Rosén B G 2011 Experimental friction evaluation of cylinder liner/piston ring contact *Wear* **271** 625–33
[14] Olander P, Hollman P and Jacobson S 2013 Piston ring and cylinder liner wear aggravation caused by transition to greener ship transports–comparison of samples from test rig and field *Wear* **302** 1345–50
[15] Mezghani S, Demircia I, Zahouani H and Mansori M El 2012 The effect of groove texture patterns on piston-ring pack friction *Precis. Eng.* **36** 210–7
[16] Srivastava D K, Agarwal A K and Kumar J 2007 Effect of liner surface properties on wear and friction in a non-firing engine simulator *Mater. Des.* **28** 1632–40
[17] Kapsiz M, Durat M and Ferit F 2011 Friction and wear studies between cylinder liner and piston ring pair using Taguchi design method *Adv. Eng. Soft.* **42** 595–603
[18] Gara L, Zou Q, Sangeorzan B P, Barber G C, McCormick H E and Mekari M H 2010 Wear measurement of the cylinder liner of a single cylinder diesel engine using a replication method *Wear* **268** 558–64
[19] Velkavrh I, Ausserer F, Klien S, Voyer J, Ristow A, Brenner J, Forêt P and Diem A 2016 The influence of temperature on friction and wear of un-lubricated steel/steel contacts in different gaseous atmospheres *Tribol. Int.* **98** 155–71
[20] Tiwari S, Bijwe J and Panier S 2011 Gamma radiation treatment of carbon fabric to improve the fiber–matrix adhesion and tribo-performance of composites *Wear* **271** 2184–92
[21] Bijwe J, Gupta M K, Parida T and Trivedi P 2015 Design and development of advanced polymer composites as high performance tribo-materials based on blends of PEK and ABPBI *Wear* **342–3** 65–76
[22] Djoufack M H, May U, Repphun G, Brögelmann T and Bobzin K 2015 Wear behaviour of hydrogenated DLC in a pin-on-disc model test under lubrication with different diesel fuel types *Tribol. Int.* **92** 12–20
[23] Truhan J J, Qu J and Blau P J 2005 A rig test to measure friction and wear of heavy duty diesel engine piston rings and cylinder liners using realistic lubricants *Tribol. Int.* **38** 211–8
[24] Sudeep U, Pandey R K and Tandon N 2013 Effects of surface texturing on friction and vibration behaviours of sliding lubricated concentrated point contacts under linear reciprocating motion *Tribol. Int.* **62** 198–207
[25] Pandey R K, Tandon N and Singh A K 2013 Fuel saving in IC engine by surface texturing of piston rings *Nat. Conf.*

on Recent Advancements in Mech. Engg. (NCRAME-2013) (8–9 November 2013) (Itanagar, Arunachal Pradesh, India: NERIST) pp 1–4

[26] Singh R C, Pandey R K, Lal Roop, Ranganath M S and Maji S 2016 Tribological performance analysis of textured steel surfaces under lubricating conditions *Surf. Topogr.: Metrol. Prop.* **4** 034005

[27] Sharma V K, Singh R C and Chaudhary R 2017 Effect of fly ash particles with aluminium melt on the wear of aluminium metal matrix composites *Int. J. Adv. Res.* **20** 1318–23

[28] Muthiah S, Singh R C, Pathak B D and Dhar A 2017 Mechanical properties of thermoelectric n-type magnesium silicide synthesized employing in situ spark plasma reaction sintering *Mater. Res. Express* **4** 075507

View publication stats

Macromolecular Research

Article

DOI 10.1007/s13233-018-6121-1

www.springer.com/13233 pISSN 1598-5032 eISSN 2092-7673

Fabrication of 3D Self-Assembled Nonmulberry *Antheraea Mylitta* (tasar) Fibroin Nonwoven Mats for Wound Dressing Applications

Chandra Mohan Srivastava[1,2]
Roli Purwar*[,2]

[1] Centre for Polymer Technology, Amity School of Applied Science, Amity University, Gurgaon, Haryana-122413, India
[2] Department of Applied Chemistry, Delhi Technological University, Shahbad Daulatpur, Bawana Road, Delhi-110042, India

Received November 9, 2017 / Revised March 21, 2018 / Accepted March 31, 2018

Abstract: This research was focused on the two-step regeneration of *Antheraea mylitta* (tasar) fibroin in the form of electrospun 3D self-assembled nanofibrous nonwoven mats using ionic liquid and formic acid/$CaCl_2$.The self-assembled structure of tasar nanofibrous nonwoven mats was dependent on the silk fibroin concentration and spinning voltage. The secondary conformation of tasar fibroin protein before and after electrospinning was analyzed by Fourier transformation infrared spectroscopy. The morphology of the nanofibrous mat was studied by scanning electron microscope. The self-assembled 3D tasar nonwoven nanofibrous construct was a highly porous and spongy structure with high water absorption and water vapor transmission. Highly porous 3D self-assembled tasar nonwoven nanofibrous construct favored good growth and proliferation of L929 skin fibroblast cells. Based on these properties, 3D self-assembled tasar nonwoven nanofibrous construct is a promising material for skin tissue engineering and wound dressing applications.

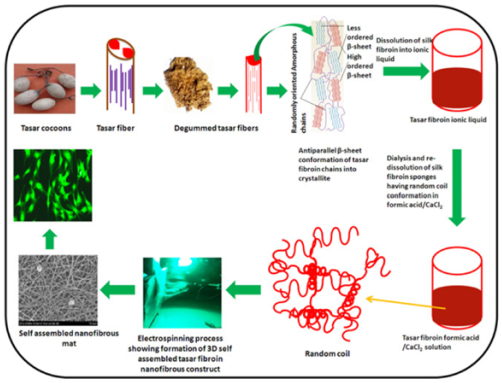

Keywords: tasar fibroin, self-assembled nanofibrous mat, electrospinning, skin tissue engineering.

1. Introduction

Wound healing is a very complex phenomenon involving several integrated biological and molecular events such as cell migration, proliferation, extracellular matrix (ECM) deposition and remodeling[1] that may get altered under certain pathophysiologic and metabolic conditions.[2] The ideal wound dressing should have following properties such as good exudates absorption ability, provide moist environment, biocompatible, biodegradable, porosity, non-adherent nature, water vapor and gas permeability, soft and comfort and adequate mechanical properties. There are different types of wound dressings available commercially, namely foam, hydrocolloids, alginate, hydrogel, iodine and silver impregnated dressings. The choice of particular wound dressing must be on the basic nature of wound. Nanofibrous mats have been successfully utilized in wound management. The highly porous architecture of nanofibrous mats allows the materials to absorb the large amount of exudates, promote higher adherence, growth, proliferation and migration of cells. This is achieved due to the high surface area, roughness, permeation of gases and water vapors as well as ease passage of metabolites & nutrients which is essential for the growth of neo-tissue and regeneration of damaged tissues. Due to high surface area, porosity and structural similarity of natural extracellular matrix, these cells seeded nanofibrous scaffolds may be good substitute of autografts, allografts and xenografts.[3,4]

Electrospinning is a straightforward and proficient technique to produce the polymeric nanofibers with size ranging from submicron to nano range. The nanofibrous mats produced by electrospinning have very high surface area and microporous architecture. This makes them an ideal matrix for cells growth and its proliferation.[5] Recently, electrospinning is used for producing self-assembled architectures for biomedical applications.[6,7] The concept of self-assembled nanofibers yarn by electrospinning was given by Okuzaki *et al.*[8] The presence of the low molecular weight salt in the spinning solution was considered as the main prerequisite for initiation of the self-organization process. The diameter of the yarns was also depended on the salt and polymer concentration. In general, the self-assembled nanofiber yarns are not stable and collapsed once the high electric field is removed. This generates a highly porous and spongy 3D nanofibrous matrix.[9]

Tasar fibroin protein has been explored as potential biomaterial due to its very good biocompatibility, controlled biodegradability and tuned mechanical properties.[10] The higher biocompatibility of nonmulberry tasar silk fibroin protein over mulberry silk fibroin protein is due to the presence of tripeptide sequences (Arg(R)-Gly(G)-Asp(D), which promotes proliferation of fibroblast and remodeling of epithelial tissues.[6] Nanofibrous 2D

Acknowledgments: Authors would like to thank the Council of Scientific and Industrial Research (CSIR-HRDG) for providing SRF grant (08/133(0009)/2014-EMR-I). Authors acknowledge Dr. Amit Misra and co-worker Mr. Deepak Sharma, CSIR-CDRI Lucknow for providing lab facilities to carry out cytocompatibility tests.

***Corresponding Author:** Roli Purwar (roli.purwar@dce.edu)

© The Polymer Society of Korea and Springer 2018

architectures from tasar gland fibroin and its blend have been prepared by various researchers.[11,12] The highly porous tasar nanofibrous mats have been prepared through electrospinning by dissolving the tasar gland protein into formic acid/chloroform (60:40 v/v). These mats showed higher adherence and proliferation of mesenchymal stem cells as compared to mulberry and gelatin nanofibrous mats.[11] Bhattacharjee *et al.*[12] fabricated tasar gland fibroin proteins and polyvinyl alcohol blends based 2D nanofibrous mats using electrospinning for bone tissue engineering applications. Eri/tasar blends based nanofibrous 2D mats showed higher mechanical integrity and very good adherence, proliferation and differentiation of human mesenchymal stem cells over mulberry and gelatin nanofibrous mats.[12] Zhao *et al.*[13] developed self-assembled electrospun mulberry silk nanofibers for biomedical applications. To the best of our knowledge based on literature search, electrospun self-assembled 3D architecture from nonmulberry silk especially from tasar fibroin obtained from cocoon has not been reported yet.

The present work was focused on the fabrication and characterization of self-assembled tasar silk fibroin nanofibrous nonwoven 3D constructs using electrospinning. The strong hydrophobic interaction in crystalline region of tasar fibroin protein makes it insoluble in most of solvents in which mulberry silk fibroin dissolve. Two steps dissolution process was adopted for preparation of electrospinning dope solution. The tasar fibroin was first dissolve in the 1-butyl-3-methylimidazolium acetate ionic liquid. By this process tasar fibroin polymer chains were converted into random coil conformation from β-sheet. The random coil tasar fibroin protein was extracted from the ionic liquid solution by dialysis and freeze drying. The obtained tasar fibroin protein was easily dissolved in formic acid/$CaCl_2$ to prepare dope solution for electrospinning. By varying the process parameters of electrospinning, self-assembled architecture of tasar fibroin was obtained and characterized. A schematic diagram for preparation of self-assembly tasar nanofibrous construct is shown in Figure 1.

2. Experimental

2.1. Materials

The tasar cocoons were procured by Central Silk Board, Sonbhadra, U.P, India. The ionic liquid 1-butyl-3-methylimidazolium acetate was procured from Sigma Aldrich. The L929 mouse skin fibroblast cells were purchased from National Centre of Cell Science, Pune. All other chemicals used in this study were purchased from Sigma-Aldrich till it is specified.

2.2. Preparation of tasar silk fibroin solution

Degumming and dissolution of tasar cocoon were performed as per protocol we have used in our previous research.[14] Briefly, tasar silk fibroin cocoons were cut in small pieces (4-8 mm), washed with distilled water and boiled in 0.02 M $NaHCO_3$ for

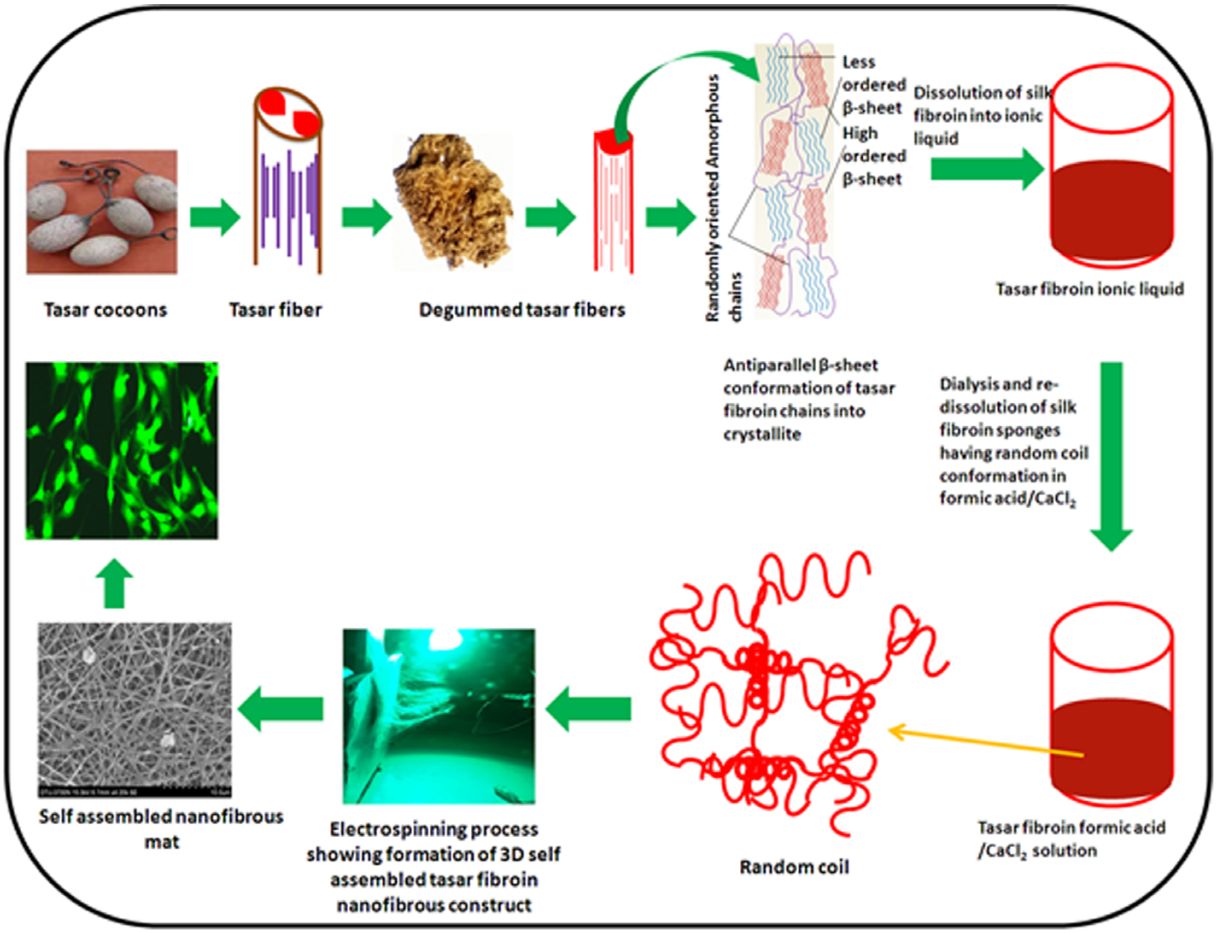

Figure 1. Schematic representation for the preparation of self-assembled tasar nanofibrous mat.

© The Polymer Society of Korea and Springer 2018

ISSN: 2350-0328

International Journal of AdvancedResearch in Science, Engineering and Technology

Vol. 5, Issue 6 , June 2018

Hydraulic Analysis and Modelling of Small Hydro Power: A Case Study of a Plant at Gogripur, Karnal

Satish Kumar Kadian, Dr. J.P. Kesari , Dr. R.S. Mishra

M.Tech. Student, Department of Mechanical Engineering, Delhi Technological University
Associate Professor, Department of Mechanical Engineering, Delhi Technological University
Professor, Department of Mechanical Engineering, Delhi Technological University

ABSTRACT: India's renewable energy sector has an estimated renewable energy potential of about 900 GW from sources like wind – 102 GW, Bio energy – 25 GW, Small hydro – 20 GW and Solar power – 750 GW. Renewable energy enjoys 20% shares of total installed capacity of 69022 W in India as on 31 March 2018. Small hydro is the development of hydro electric power on a scale suitable for local community and industry. Most hydro electric powers from the potential energy of dammed water driving a water turbines and generator. This paper discusses the potential of hydropower, renewable energy in India and case study of a small hydro plant at Gogripur, Karnal.

KEYWORDS: Head, Flow, Renewable energy, Potential, Kalpan, Turbine, Efficiency

I. INTRODUCTION

Renewable energy sources (RES) that use indigenous resources have the potential to provide energy with negligible emissions of air pollutants and greenhouse gases. Renewable energy technologies produce marketable energy by converting natural phenomena or resources into useful energies. The usage of renewable energy resources is a promising prospect for the future as an alternative to conventional energy. Therefore, an attempt has been made through to review the availability of renewable energy options in India, and provides information about the current status of renewable, future potentials of their uses, major achievements, and current government policies, delivery and outreach in Indian context. It paints a remarkable overall picture of renewable energy resources and position of India on global map in utilizing these resources.

Renewable energy supplies 18% of the world's final energy consumption counting traditional biomass, large hydropower, and "new" renewables (small hydro, modern biomass, wind, solar, geothermal, and biofuels). New renewables represents 2.4% and are growing very rapidly in developed countries and in some developing countries. Global renewable energy capacity grew at rates of 15-30% annually.

II. THE RENEWABLE ENERGY POTENTIAL AND HYDRO POWER POTENTIAL IN INDIA

The role of new and renewable energy has been assuming increasing significance in recent times with the growing concern for the country's energy security. The renewable energy industry has approximately USD 500 million as turnover, the investment being' about USD 3 billion. Of the estimated potential of approx. 10,00,000 MW from RE only about 69022 MW has been exploited to date. Current installed capacity hydro power is 45,403 MW which is more than 26% of the assessed potential. In the beginning of year 2018, the total installed capacity of electrical energy from all sources is 3,43,778 MW.

India has set a new target of achieving 175 GW from all renewable sources and out of which 100 GW is from solar power alone by 2022. Four of the top seven largest solar plants worldwide are in India including the second largest solar park in the world at Kurnool, Andhra Pradesh, with a capacity of 1000 MW[17] India at the centre of its "Sunshine Countries" International Solar Alliance project promoting the growth and development of solar power internationally to over 120 countries. India set a target of achieving 40% of its total electricity generation from non-fossil fuel sources by 2030, as stated in its Intended Nationally Determined Contributions statement in the Paris

ISSN: 2350-0328

International Journal of AdvancedResearch in Science, Engineering and Technology

Vol. 5, Issue 6 , June 2018

Agreement[16]. The estimated potential for power generation in the country from small hydro plants is about 20,000 MW. The mission aims is that at least 50% of the potential in the country is harnessed in the next 10 years[18]. The public sector accounts for 92.5% of India's hydroelectric power production. The National Hydroelectric Power Corporation (NHPC), Northeast Electric Power Company (NEEPCO), Satluj Jal Vidyut Nigam (SJVNL), THDC, and NTPC-Hydro are some of the public sector companies producing hydroelectric power in India. The private sector is also expected to grow with the development of hydroelectric energy in the Himalayan mountain ranges and in the northeast of India[14]. A map is given below to show major hydroelectric plants in India.

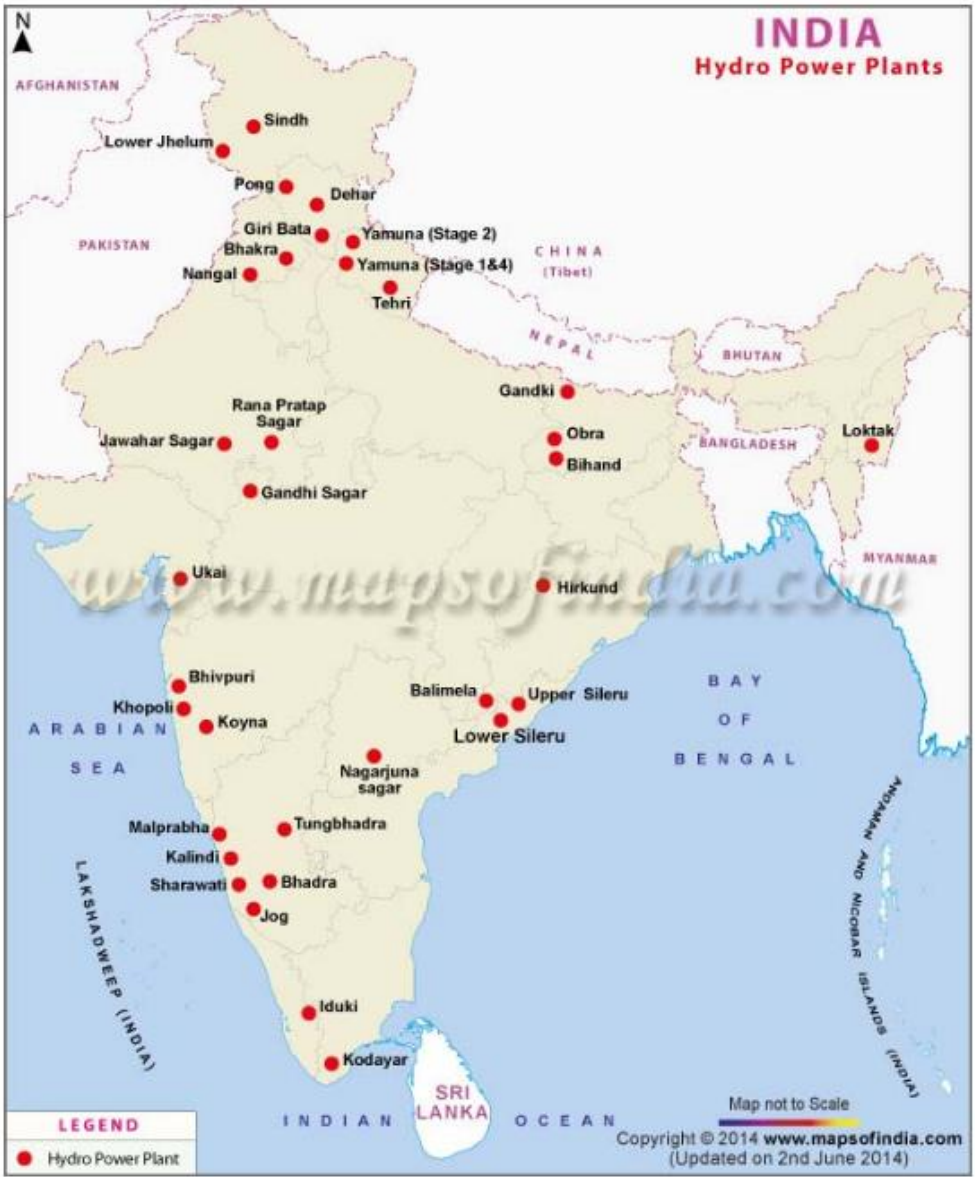

III. MODELLING OF HYDRO POWER PLANT

Cost effective and efficient project we need to study the optimal selection of hydro turbine.An analysis of cost of electro-mechanical equipment for small hydropower has been made and a co-relation is developed[8,9]. The power availability will change the livelihood of the villagers, resulting into creation of jobs such as small business enterprises. This will add some income to the village community[5].

ISSN: 2350-0328

International Journal of AdvancedResearch in Science, Engineering and Technology

Vol. 5, Issue 6 , June 2018

A. Flow analysis

Thus by using the Bernoulli's equation to analyze the fluid flow from point 1 to point 2 as used by Kelly. J.R for the Euler's equation to obtain Bernoulli's equation by integrating along a streamline for steady, incompressible, frictionless flow which gives to Eq. 3.1.

$$H = \frac{p}{pg} + \frac{v^2}{2g} + z \tag{3.1}$$

Where;$\frac{p}{pg}$= the head due to local static pressure, $\frac{v^2}{2g}$ = the head due to local dynamic pressure, Z = the elevation head, H = the head for the flow.

From Eq.3.1;

$$H = \frac{p}{pg} + \frac{vr^2}{2g} + z_1 = \frac{pn}{pg} + \frac{vn^2}{2g} + z_n \tag{3.2}$$

At the surface of the river bed, the fluid moves very slowly compared to the flow along the pipe. We say that $u_r = 0$, Also the pressure is atmospheric pressure, $p_r = p_n$ = Patomspheric. $Z_r - Z_n$ is the elevation of the river bed and the turbine.

$$Z_r = \frac{vn^2}{2g} + Z_n \tag{3.3}$$

$$Z_r - Z_n - H_f = \frac{vn^2}{2g} \tag{3.4}$$

The velocity is the velocity of the water jet at the nozzle. The pressure head at point 1 and 2 is equal to zero.

From Eq. 3.4, $Z_r - Z_n - H_f = \frac{vn^2}{2g}$; $v_n\left(\frac{M}{S}\right) = \sqrt{2xg\ (Z(m) - Z_m - H_f}$ (3.5)

Where; V_n is the same as $V_1 H_f$ is equal to f $L/d_{pipe} \times \frac{vn^2}{2g}$. therefore the flow rate entering the turbine from the nozzle is expressed as Q = AV.

$$Q = V \times A = V \times \frac{\pi d^2}{4} \tag{3.6}$$

Power at turbine wheel:

$$\text{Power}[P] = \rho g Q H \tag{3.7}$$

B. Terminology used

(i) tangential velocity[u] = $\frac{\pi \times D_M \times N}{60}$

(ii) flow rate [Q] = $\frac{\pi\left(D_2^2 - D_1^1\right)}{4} \times vf$

(iii) absolute velocity [v] = $\sqrt{2g\ H_{net}}$

(iv) Flow Ratio = $\frac{v(f)}{v}$

(v) Speed ratio = $\frac{u}{v}$

(vi) specific speed of time [Ns] = $\frac{N \times \sqrt{P}}{H^{5/4}}$

(vii) Overall efficiency [N0] = $\frac{H_{turbine}}{H_{net}}$

ISSN: 2350-0328

International Journal of AdvancedResearch in Science, Engineering and Technology

Vol. 5, Issue 6 , June 2018

(viii) Power = $\rho g Q H_{turbine}$

C. Analysis of axial flow turbine

Analysis procedure for axial flow turbine was done. Let for Kalpan turbine suffixes 1 and 2 denote inlet and outlet conditions respectively. Thus, for example D_1 represents the inlet location at the tip of the runner. (Since for a Kaplan turbine, $D_1 = D = D_2$, in the diameter of the runner of a Kaplan propeller turbine is consistently referred to as D_1). The flow in axial through the blades.

Area of flow $A = \frac{\pi}{4}(D_1^2 - D_h^2)K_1$ where $K_1$is the net area factor after deducting for the area occupied by the blades in the cross section. For preliminary studies, it is usual to take $K_1 = 1.0$.

$$\text{Area of flow } A = \frac{\pi}{4}(D_1^2 - D_h^2) \tag{3.8}$$

$$\text{Discharge } Q = \frac{\pi}{4}(D_1^2 - D_h^2)V_{f1} \tag{3.9}$$

$V_{f1} = V_{f2}$ = Velocity of flow which is taken as constant in the entire inlet-outlet space, i.e. all along the inlet radius as well as all along the outlet radius.

Let u_1 = Peripheral velocity an inlet at any radius r, and u_2 = Peripheral velocity at the outlet at the same radius r. Then

$$u_1 = u_2 = u = \frac{2\pi rN}{60} \tag{3.10}$$

The flow is assumed to leave the runner axially without any whirl component. Thus, at the outlet $\alpha_2 = 90°$ and $V_2 = V_{f2}$, as used in the case of a Francis turbine.

It is assumed that the flow entering the whirl chamber from the guide vanes creates a free vortex in the whirl and runner chambers where the velocity is inversely proportional to the radius. Thus, if $r_h = (D_h/2)$ is the radial distance of the hub from the axis, $r_t = (D_1/2)$ is the radial distance of the blade tip and $r_m$is the radial distance of the midpoint of the blade then

$$(V_{u1})_t r_t = (V_{u1})_m r_m = (V_{u1})_h r_h = \text{Constant} \tag{3.11}$$

In this $(V_{u1})_x$is the velocity of whirl at the given radius x on the inlet side of the blade.

The Euler equation is applicable given in Euler head $H_e$as

$$H_e \frac{V_{u1}u_1 - V_{u2}u_2}{g} = \frac{V_{u1}u_1}{g} = \quad (\because V_{u1} = 0) \tag{3.12}$$

Further, the hydraulic efficiency

$$\eta_h = \frac{H_e}{H} = \frac{V_{u1}u_1}{gH} \quad \text{[where H = Net head]} \tag{3.12a}$$

IV. CASE STUDY OF A SMALL HYDRO POWER PLANT AT GOGRIPUR, KARNAL

Gogripur is a village situated in Karnal district of Haryana. It is along the left bank of WYC canal about 3 km from Karnal town. The small Hydro power plant was set up in Gogripur by Haryana Renewable Energy Development Agency (HREDA) through P&RGogripur Hydro Power Private Ltd. The small hydro power plant has 2 turbines both are operational. The small hydro power plant has the capacity of 2000 KW (2 MW) where each unit have 1000 KW capacity. The main purpose of the plant is to generate electrical energy through sustainable means by exploiting the potential energy of the flowing water for power generation. It leads to a cleaner environment through lower greenhouse gas emissions and other pollutants and greater security of the nation through lower fuel consumption, fossil fuel conservation for other activities. As it generates electricity through sustainable means, it will not cause any negative impact on the environment and there by contribute to climate change mitigation efforts. The total gross generation potential is 11913.60MWhbased on 75% dependable year. The generated power is supplied to the grid by connecting it with HAREDA transmission lines.

ISSN: 2350-0328

International Journal of AdvancedResearch in Science, Engineering and Technology

Vol. 5, Issue 6 , June 2018

Generating Units

A. Turbine

- Type : **Semi kaplan**
- Shaft : **Vertical**
- Rated discharge : **68.3 m^3/s**
- Rated output : **1000 kW each unit**
- Rated speed : **110 rpm**
- Number of generating units : **2**

B. Generator

- Type (Synchronous / induction) : **Synchronous**
- Rated speed : **110 rpm**
- Overload : **10%**
- Frequency : **50 Hz**
- Generation Voltage : 66.5 kva
- Power factor : **0.8**

C. Power Evacuation:

- Transmission voltage (grid) : **33 kV**
- Transmission line : **11 kV**

By using EES software program using EES software and by using different mathematical equations to determine the overall efficiency of the Gogripur small hydro power plants. Hence input parameters such as tangential velocity, flow rate, absolute velocity flow ratio, speed ratio, specific speed of turbine, and head of turbine are calculated to obtain the overall efficiency.

The following curves were obtained by ESS software:

Figure 1.1,shows the flow rate against the net head as, the head increases from 2m to 4m. The volumetric flow rate was decreasing from 95 m3/sec to 47 m3/sec as the volume of water decreases the pressure is increased. This increase in pressure influences the power delivered to wheal by jet of water.

ISSN: 2350-0328
International Journal of AdvancedResearch in Science, Engineering and Technology
Vol. 5, Issue 6 , June 2018

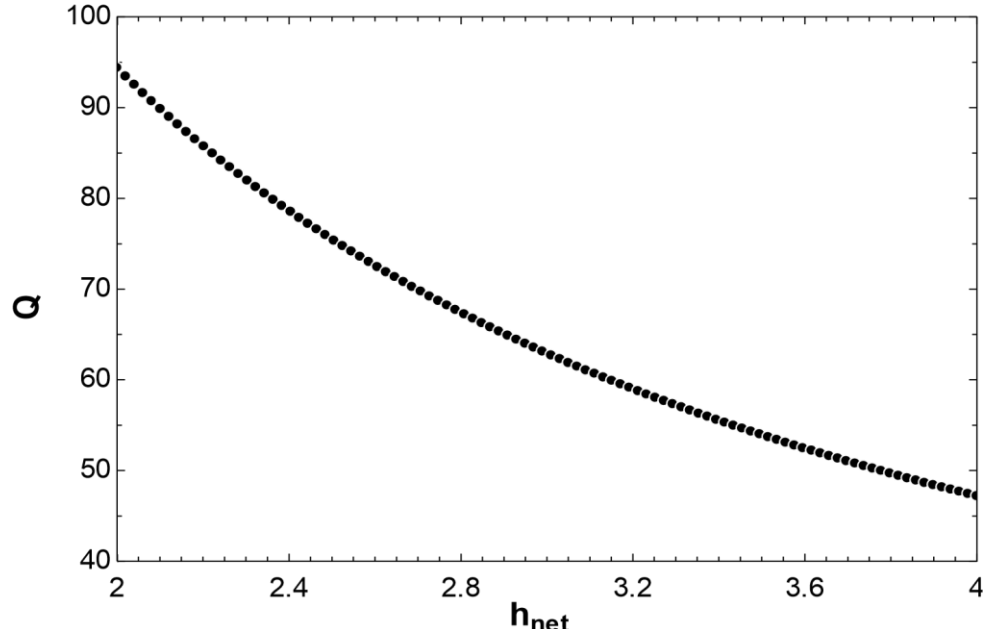

Figure 1.1: Flow rate (m^3/s) versus Net head (m)

Figure 1.2, shows the head of turbine is directly proportional to the net head. Thus head of the turbine was increased with the increase of net head from 2m to 4m and vice versa.

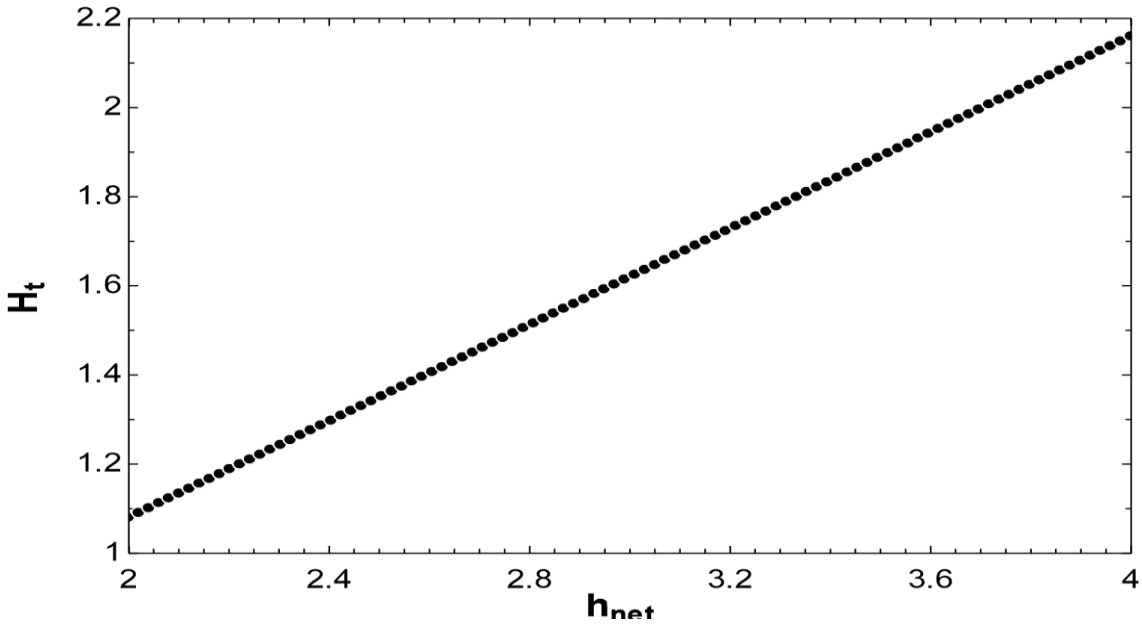

Figure 1.2: Turbine Head (m) versus Net head (m)

Figure 1.3, shows the overall efficiency of power plant decrease from 0.75% to 0.38% with increased net head from 2m to 4m respectively. Hence, the power load factor of power plant decreases.

ISSN: 2350-0328
International Journal of AdvancedResearch in Science, Engineering and Technology
Vol. 5, Issue 6 , June 2018

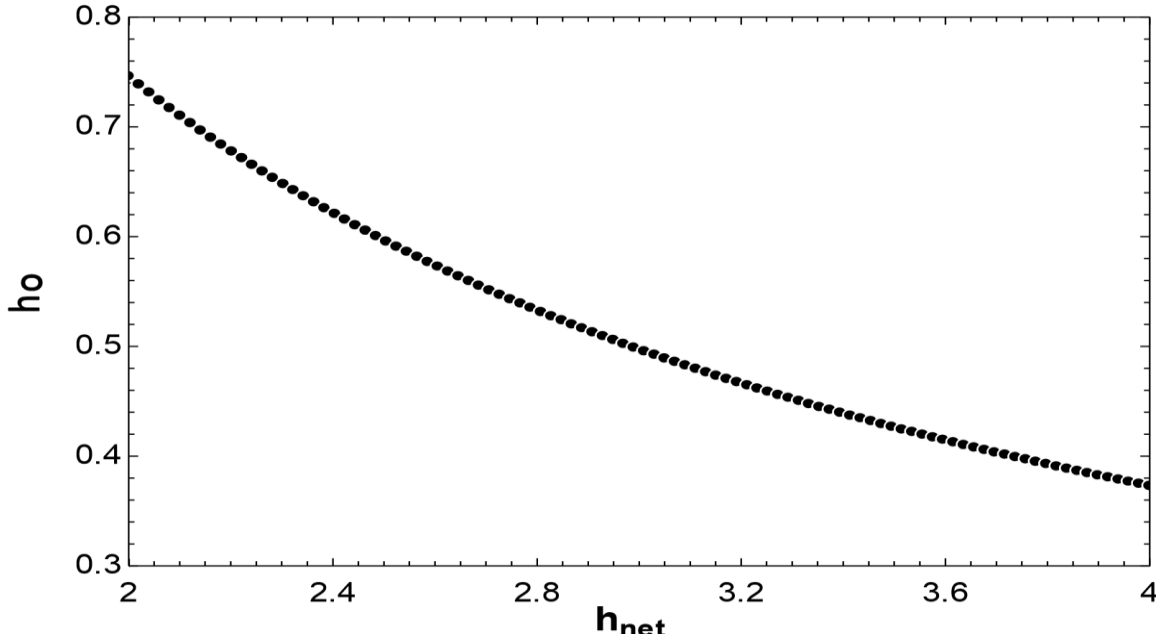

Figure 1.3: Overall efficiency (%) versus net head (m)

Figure 1.4, shows similarly the overall efficiency of the power plant decreases from 0.75% to 0.38% with the increased flow rate from 50m3/sec to 100 m3/sec. Thus here also the power load factor of the power plant decreases.

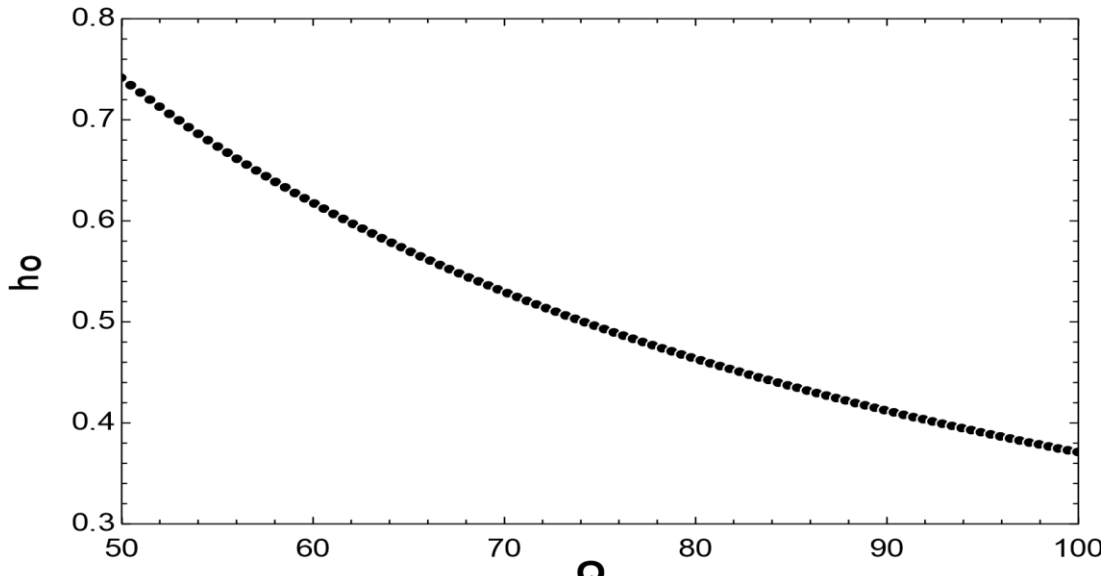

Figure 1.4: Overall efficiency (%) versus flow rate (m^3/s)

Figure 1.5, shows as the flow rate increases with decreased elevation, the power delivered to the wheal is decreased as the elevation decreased from 2m to 1.2m by increasing the flow rate from 50m3/sec to 100m3/sec.

ISSN: 2350-0328
International Journal of AdvancedResearch in Science, Engineering and Technology
Vol. 5, Issue 6 , June 2018

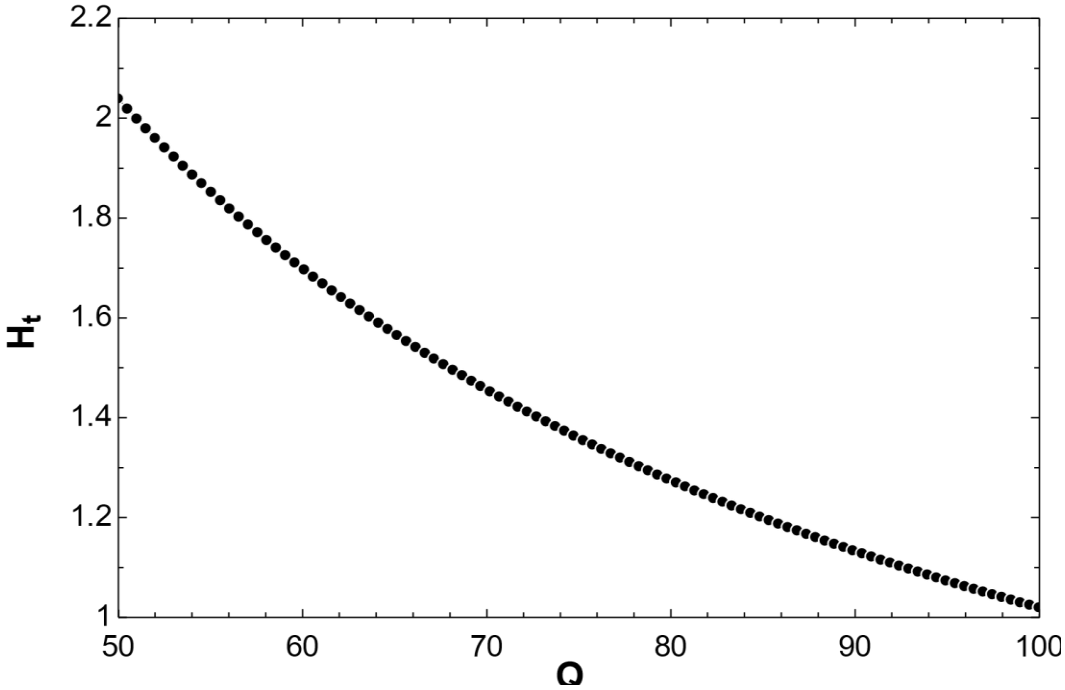

Figure 1.5: turbine head (m) versus flow rate (m^3/s)

Therefore, after the discussion of all the figures from 1.1 to 1.5 and consider their results outputs and there after carry out various calculation as shown above, we comes to the result that the overall efficiency of the power plant is 54.5% and hence the power load factor is also 54.5%.

V. CONCLUSION

The research work investigated by doing head and flow analysis on the 2 MW Gogripur, hydro power plant to calculate the overall efficiency hydro power plant. The analysis was presented by EES computer program. The Kaplan turbine operating on small head and high flow condition generated an overall efficiency higher while that of high head and high flow with decreased pressure will generate lesser overall efficiency and could be applied in sitting a small hydro power plant.

The operating condition for the Kaplan turbine is calculated by considering various input parameters i.e. head, flow rate, RPM, power, tangential velocity, absolute velocity are used to calculate and finally obtain the overall efficiency. The flow rate decrease from 100 m^3/s to 50 m^3/s with head and also the head is varied from 2m to 4 m with flow rate. Hence, small head and high flow are recommended for power generation of a small hydro power plant that could help to attain required level of overall efficiency of the plant instead of large head and low flow which is applicable for power generation of a large SHPP.

REFERENCES

[1] National Renewable Energy Laboratory (NREL). 2012. Renewable Electricity Futures Study.
[2] Ales Drab, JaromirRiha& Miroslav Spano (2015). Failures and durability analysis of a small hydro power plant. Institute of Water Structures, Brno University of Technology, Czech Republic.
[3] K.H. Motwani, S.V. Jain , R.N. Patel (2012). Cost analysis of pump as turbine for pico hydropower plants – a case study. Institute of Technology, Ahmedabad, India.
[4] Kelley J. B. (1950). The Extension Bernoulli's Equation. American J. Phys. 202– 204. India.
[5] Miguel M. Umausse, DinisJuizo, Kenneth M. Person (2015). Hydro Power Potential in Mozambique "Chua-Manica". DuardoMondlane University, Maputo, Mozambique.
[6] PimnapatIemsomboon, TrirathPati and KrischonmeBhumkittipich (2012). Performance Study of Micro Hydro Turbine and PV for Electricity Generator, Case Study :Bunnasopit School, Nan Province, Thailand.

ISSN: 2350-0328

International Journal of AdvancedResearch in Science, Engineering and Technology

Vol. 5, Issue 6 , June 2018

[7] S.U. Patel, Prashant N. Pakale (2015). Study on Power Generation by Using Cross Flow Water Turbine in Micro Hydro Power Plant. COE, Shahada, Maharashtra.
[8] Sachin Mishra, S.K. Singal, and D.K. Khatod (2012). Costing of a Small Hydropower Projects. Roorkee, India.
[9] SaurabhSangal, Arpit Garg, Dinesh Kumar (2013). Review of Optimal Selection of Turbines for Hydroelectric Projects. IITRoorkee, India.
[10] Staubli T. et al. (2009). Jet quality and Pelton efficiency. Proceeding of Hydro2009, Lyon, France.
[11] Suraj Y. (2011). Some aspects of performance improvement of Pelton wheel turbine with reengineered blade and auxiliary attachments. International journal of Scientific and Engineering Research. 2(9), 1-4.
[12] Vesely J. and Pochyly F. (2003). Stability of the flow through Pelton turbine nozzles. Hydro-2003, Dubrovnik, Croatia.
[13] "Harnessing gigantic hydro power potential of Indus, Jhelum and Chenab rivers by diverting water to Ravi and Beas rivers". Retrieved 30 November 2017.
[14] Gajic, A, Cam Characteristics of the Kaplan turbine determined by Efficiency and Bearing Vibrations, 6th International conference on Hyd. Mach. and Hydrodynamics, Romania, 2004.
[15] http://www.cea.nic.in of Central Electricity Authority (CEA), Ministry of Power, Government of India.
[16] "Here are India's INDC objectives and how much it cost". The Indian Express 2015-10-02. Retrieved 2017-12-27.
[17] "All India Installed Capacity of Utility Power Stations" (PDF). Retrieved 13 April 2016.
[18] Information related to SHP potential in India can be obtained from the website of the Ministry of New and Renewable Energy, Government of India. See: <⟨https://mnre.gov.in/small-hydro⟩> [accessed20 June 2018]; 2018.
[19] Ashish Kumar, Dr.Kesari, J.P. and Prof. Mishra, R.S (2017). Economic Feasibility, Profitability And Mathematical Analysis of 432 Kw Rooftop Solar Photovoltaic Power Plant, International Journal of Development Research Vol. 07, Issue, 09, pp.14951-14967, September, 2017, ISSN: 2230-9926
[20] Ashish Yadav , Dr. Rajesh Kumar , Dr. J P Kesari , Dr. R S Mishra (2017) Thermo-Economic Analysis of Concentrated Solar Heat Applications in Hospitality Industries, International Journal of Emerging Technology and Advanced Engineering Website: www.ijetae.com (ISSN 2250-2459, ISO 9001:2008 Certified Journal, Volume 7, Issue 9, September 2017), http://www.ijetae.com/files/Volume7Issue9/IJETAE_0917_ 49.pdf

Volume 6 Issue 2 (2018) 132-134 ISSN 2347 - 3258
International Journal of Advance Research and Innovation

Improving the Tractive Performance with Four-Wheel Drive (4WD) System

Neeraj Budhraja, Amit Pal
Department of Mechanical Engineering, Delhi Technological University, New Delhi-110042, India

Article Info
Article history:
Received 24 January 2018
Received in revised form
10 March 2018
Accepted 20 May 2018
Available online 15 June 2018

Keywords- Four-wheel drive; differential; propeller shaft; tractive effort; traction

Abstract
This paper gives a brief study of the components, operating modes, merits and demerits of a four-wheel drive system over two-wheel drive system, and a case study of Mahindra Scorpio S11 is done for tractive effort by 4WD and 2WD (front wheel drive). The results for Mahindra Scorpio S11 showed that the tractive effort by 4WD system increases as the gear ratio decreases, i.e., highest for reverse gear (14362.96 Nm) with gear ratio 3.28:1, 1st gear (13000.00 Nm) with gear ratio 2.97:1, 2nd gear (9066.67 Nm) with gear ratio 2.07:1 whereas lowest for 6th gear (2451.85 Nm) with gear ratio 0.56:1. Similar results for tractive efforts by 2WD (front wheel drive) system can be depicted, i.e., highest tractive effort for reverse gear (7674.07 Nm), 1st gear (6940.74 Nm), 2nd gear (4837.04 Nm) whereas lowest for 6th gear (1311.11 Nm). As observed, the tractive effort by a 4WD system is comparatively higher than a 2WD (front wheel drive) vehicle. Thus, this results into reduced wheel slippage tendency, better climbing capability in hilly areas and better driving control over the vehicle on the low frictional surfaces such as wet/snowy surfaces. Whereas additional components in 4-wheel drive system adds on weight; increases cost, maintenance, repair, noise and vibrations; and makes the construction comparatively more complex.

1. Introduction

In order to improve efficiency and to reduce pollution from vehicles various significant efforts have been carried out in research and development of new age vehicles [1]. A wide range of improvement is done in engine, i.e. engine cylinder; piston head; valve and spark plug mounting; and valve timing. Also, some auxiliary arrangements such as turbocharging and supercharging have been performed to improve efficiency and to control pollution emissions. All these practices have improved efficiency of the engine and reduced pollution emissions significantly. But still there is further loss of power from engine to wheels. As the research further extended, it was found that the transmission loss of power can be reduced upto a certain extent which will directly contribute to improved efficiency, thus resulting in reduced emissions [2].

Till 1980s, the engines were placed at front of the vehicle with the rare axle as the driving axle due to cost and better stability point of view. These vehicles have simple construction and no torque steer since the front axle is not connected with power transmission. This gives increased traction as during acceleration vehicle weight is transferred backwards whereas more components of the transmission increases the weight, cost and reduces interior space [3-4]. As the vehicle is pushed, thus low grip surface (wet road, ice, snow, etc) handling becomes difficult. This arrangement has also oversteering tendency.

Most of the modern vehicles come with front axle as driving axle and the engine is placed at front of the vehicle. In this way, driving axle is nearer to the engine which results in less components of the transmission reducing low chassis weight, increasing interior spacing and thus lighter construction and lesser mechanical inertia in the power train gives greater fuel economy. Pulling action of the engine proves to be safer as it reduces skidding tendency providing better road adhesion and understeering characteristics helps in better controlling of the vehicle [4]. On the other hand, the front axle is burdened with both steering and power transmission making the whole arrangement complicated. Ordinary universal joints will not work, thus two constant velocity joints have to be used which wear out much faster. Also, decreased tractive effort while going up and heavier steering on levelled roads makes this arrangement less suited for racing cars [5]. Torque steer and increased turning circle are other problems faced in this arrangement.

Another arrangement was also tried with rear axle as driving axle and the engine placed at the rear of the vehicle. This arrangement gives better traction through improved road adhesion on levelled roads as well as on slopes. Front axle is used only for steering thus resulting in simplified construction, reduced chassis weight, better visibility and better design from streamline point of view. Compact silencer system and exhaust pipe contribute in carrying away noise and heat from the passengers [5]. While increased weight at rear of the vehicle makes it unstable at high speeds and cause oversteering conditions. Positioning of the engine at the rear require complicated linkage to operate engine, clutch and transmission; and reduces cooling efficiency making relatively more difficult to access, servicing and repair. Lastly, fuel tank placed at the front results in fatal condition during a collision.

There is one more arrangement which is called four-wheel drive (4WD) system. In 4-wheel drive system, a two-speed transfer case (two driving axle) is designed mainly for low-speed, off-road driving. 4-wheel drive reduces wheel slippage tendency and provides better driving control over the vehicle [6-9]. 4-wheel drive system consists of a transfer box called auxiliary box which divides equal torque between the rear and front axles, normal universal joints on propeller shafts, special constant universal joints on the front axle to provide large angular movement during steering. The vehicle is capable of driving over the rough roads and snowy roads as well as over the roads with changing surface characteristics due to changing weather conditions [10].

2.Additional Components of 4-Wheel Drive system

Figure 1 depicts diagram of 4-wheel drive system showing various components required. The main components of 4-wheel drive system are discussed-

2.1 Differential

A 4-wheel drive vehicle has two differentials, one located on the front axle and one on the rear axle. The torque from the driveshaft or transmission is transmitted to the wheels using differentials. Also during taking a turn, the inside and the outside wheels of the vehicle rotate at varying speed and in similar fashion the front and the rear wheels of the vehicle rotate at the varying speed. Thus, differentials are used to enable this speed difference between the inside and outside wheels as well as front and rare wheels.

2.2 Transfer case

Splitting of the engine power between the front and rear axles on a 4-wheel drive vehicle is done by the transfer case. It interlocks the front axle drive shaft with the rear axle drive shaft in order to force the wheels to spin at the same speed. Transfer case enables the driver for better driving condition for cross-country operation and smoother drive in high or low gear as required.

2.3 Four-Wheel Drive System

A block diagram of 4-wheel drive system is shown in figure 3 with all essential components. The power of the engine is transmitted through the gearbox to the transfer case where the power splits between the front and rear axles on a 4-wheel drive vehicle. Then through the front and rear axle the power is transferred onto the differential. The torque (turning force) applied to the differential is transferred along two drive

***Corresponding Author,**
E-mail-address:neeraj_budhraja@yahoo.com; amitpal@dce.ac.in
All rights reserved: http://www.ijari.org

shafts, which are joined to each wheel, causing them to rotate in the direction of travel.

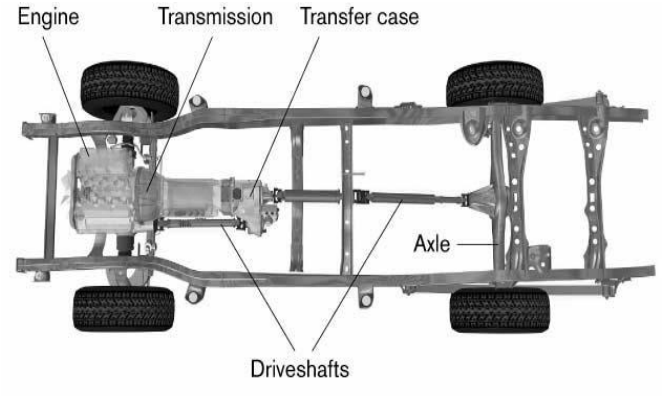

Fig. 1: Key Components of four-wheel drive [12]

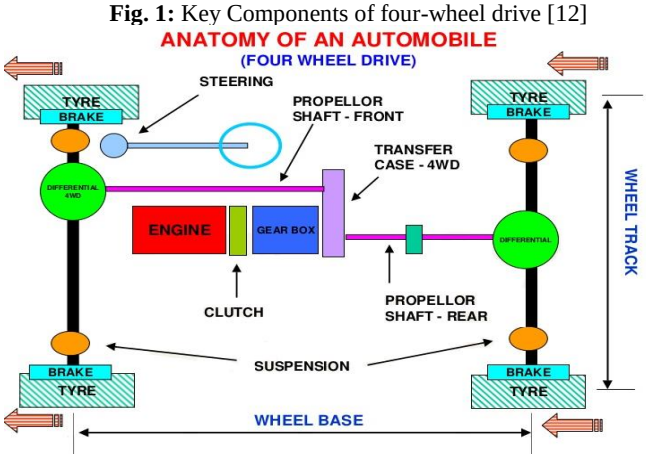

Fig. 1: Schematic of four-wheel drive system

3.Basic Considerations of Four-Wheel Drive [11]

3.1 Transmission wind-up

When a positive torque occurs in one of the axle and a negative torque in the other, such a condition is known as transmission wind-up. Transmission wind-up causes unusual torsional deflection or twisting resulting into permanent distortion.

3.2 Torque distribution

The tractive force to propel the vehicle is translated from the driving torque applied to the wheels depends upon the coefficient of friction between the road and tyres, and the vertical load. Thus, acceptable condition to achieve equal distribution of driving torque is only with equally distribution of weight between the rear and front axles.

3.3 Tractive Effort

The total force which is available at the contact between the road and the drive wheel tyres is termed as Tractive Effort. How tractive effort is related to engine power is as follows:-

Engine Torque, $T_e = \frac{60000\,P_e}{2\pi N}$ Nm .....(1)

Torque at Drive wheels $T_w = (g.r \times a.r \times t.r)\eta_t\, T_e = G\eta_t\, T_e$ .....(2)

Tractive effort, $F = \frac{T_w}{r} = \frac{G\eta_t\, T_e}{r}$ N .....(3)

Overall transmission efficiency, $\eta_t = \frac{P_{out}}{P_{in}} \times 100$ .....(4)

Overall gear ratio, $G = g.r \times a.r \times t.r$ .....(5)

where, P_e → engine power (kW)
T_e → mean engine torque (Nm)
P_{out} → output power (kW)
P_{in} → input power (kW)
g.r → gearbox ratio
a.r → axle ratio
t.r → transfer case ratio
G → overall gear ratio
r → radius of tyre (m)
N → r.p.m. of crankshaft

3.4 Merits of 4-Wheel Drive

3.4.1. Cornering stability

Load reduction on each tire of the vehicle due to equally transmission of power by all four tires instead of only two effectively utilizes the cornering force of the tire and thus provides excellent cornering stability.

3.4.2. Straight-line stability

Each tire is having additional grip with road which increases the road adhesion resulting with better stability from external turbulence (or cross-winds), thus giving better straight-line stability to the vehicle.

3.4.3 Starting performance and acceleration

4-wheel drive vehicles having nearly double the tire gripping as compared to two-wheel drive vehicles perform better during starting, sudden acceleration or braking and do not allow spinning of the tires of the vehicle even mounted with a high torque engine. Thus, improving the starting performance and acceleration of the vehicle.

3.4.4. Performance during Hill-climbing

The best advantage of 4-wheel drive is during climbing hill or climbing a slope. Four-wheel drive approximately doubles the climbing capability of the vehicle thus making the vehicle safer on hilly areas.

3.4.5. Driving on low friction snowy/rough roads

In 4-wheel drive, equal power transmissions by all four wheels will approximately double the power transmitted by two-wheel drive. Thus, 4-wheel drive vehicles perform extremely well on roads with low coefficients of friction like wet, snowy roads. This is achieved by greater power provided by all four wheels. Basically, the front and rear wheels help each other as a result the performance increases significantly.

3.4.6. Better turning stability

The driving becomes more secure with 4-wheel drive vehicle due to better steering precision and better steering response. The turning radius of the vehicle reduces allowing the vehicle for easier and quicker corner parking and also easier maneuvering.

3.5 Demerits of 4-Wheel Drive

3.5.1. Weight is increased

As the number of parts in the power transmission line increases, the weight of the vehicle increases and thus, reduces the loading capacity.

3.5.2. Cost is increased

Increase in number of parts in the power transmission system with complex construction of transmission line significantly increases the cost of the vehicle while the repair and maintenance cost also increases simultaneously.

3.5.3. Construction is complex

Additional components such as transfer case, propeller shaft, differential, etc., required for the transmission of power from the engine to the wheels make the construction more complex.

3.5.4. Enhanced vibrations and noise

Increase in number of moving parts (transfer, propeller shaft, etc.) in the transmission line impart more vibrations and noise; and this increased vibrations and noise results in more wear and tear of the vehicle.

4. Case Study

Specifications of Mahindra Scorpio [13]

Model	=	S11
Engine	=	mHawk
Number of cylinders	=	4
Displacement	=	2179cc
Maximum engine output	=	103 kW @ 3750rpm
Maximum torque	=	320 Nm @ 1500-2800rpm
Number of gears	=	6 (Manual)
Tyre	=	P235/65 R17 (Radial Tubeless)
Wheel Base	=	2.68m

Turning radius = 5.4m (2WD) & 5.65m (4WD)

Table 1: Table for Gear ratio

Gear	1st	2nd	3rd	4th	5th	6th	reverse
Ratio	2.97	2.07	1.43	1.00	0.84	0.56	3.28

Axle ratio, a.r =3.47 (FWD) & 3.55 (RWD)

Transfer ratio, t.r =1.83 (4WD) & 1.00 (2WD)

From equation (1) & (4):-

$$P_{out} = \frac{2\pi N}{60000} T_e = \frac{2\pi \times 2800}{60000} \times 320 = 93.8\ kW$$

$$\eta_t = \frac{P_{out}}{P_{in}} \times 100 = \frac{93.8}{103} \times 100 = 91\%$$

Table 2: Torque at drive wheels and tractive effort by 4WD vehicle

S. No.	Gear	Gear ratio, g.r	Overall gear ratio, G	Torque, T_w (in Nm)	Tractive Effort, F (in N)
1.	1st	2.97	19.29	5616.0	13000.00
2.	2nd	2.07	13.45	3916.8	9066.67
3.	3rd	1.43	9.29	2704.0	6259.26
4.	4th	1.00	6.50	1891.2	4377.78
5.	5th	0.84	5.46	1590.4	3681.48
6.	6th	0.56	3.64	1059.2	2451.85
7.	reverse	3.28	21.31	6204.8	14362.96

Table 3: Torque at drive wheels and tractive effort by 2WD (front wheel drive) vehicle

S. No.	Gear	Gear ratio, g.r	Overall gear ratio, G	Torque, T_w (in Nm)	Tractive Effort, F (in N)
1.	1st	2.97	10.30	2998.4	6940.74
2.	2nd	2.07	7.18	2089.6	4837.04
3.	3rd	1.43	4.96	1443.2	3340.74
4.	4th	1.00	3.47	1011.2	2340.74
5.	5th	0.84	2.91	848.0	1962.96
6.	6th	0.56	1.94	566.4	1311.11
7.	reverse	3.28	11.38	3315.2	7674.07

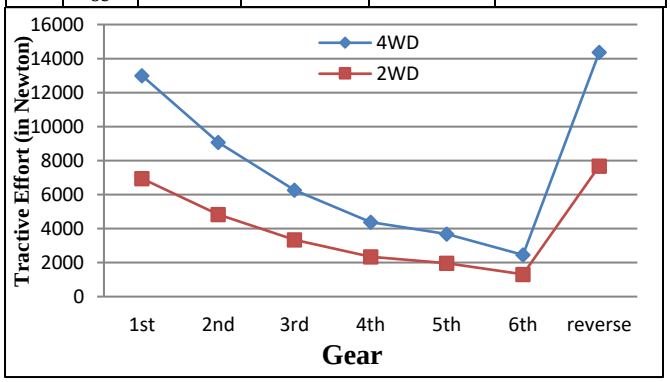

Fig. 1: Gear vs Tractive Effort (in Newton) of 4WD and 2WD

From the table 2, it is clear that the tractive effort by a four wheel drive vehicle increases as the gear ratio decreases, i.e., highest for reverse gear (14362.96 Nm), 1st gear (13000.00 Nm), 2nd gear (9066.67 Nm) whereas lowest for 6th gear (2451.85 Nm).

From Table 3, the similar results for tractive efforts by a two wheel drive (front wheel drive) vehicle can be observed, i.e., highest tractive effort for reverse gear (7674.07 Nm), 1st gear (6940.74 Nm), 2nd gear (4837.04 Nm) whereas lowest for 6th gear (1311.11 Nm).

But as observed from graph 1, the tractive effort by a 4-wheel drive is comparatively higher than a two wheel drive (front wheel drive) vehicle. This is due to the fact that a 4-wheel drive system requires transfer case (with transfer case ratio 1.83), which interlocks the front axle drive shaft with the rear axle drive shaft in order to split the power between front and rear axle wheels. In this way, better climbing capability on hilly areas and reduces slipping tendency of the vehicle.

5.Conclusions

This paper gives a brief study of 4-wheel drive system on various merits of 4-wheel drive system over two-wheel drive system. The results showed that the tractive effort by a 4-wheel drive vehicle increases as the gear ratio decreases, i.e., highest for reverse gear (14362.96 Nm) with gear ratio 3.28:1, 1st gear (13000.00 Nm) with gear ratio 2.97:1, 2nd gear (9066.67 Nm) with gear ratio 2.07:1 whereas lowest for 6th gear (2451.85 Nm) with gear ratio 0.56:1. Similar results for tractive efforts by a two wheel drive (front wheel drive) vehicle can be observed, i.e., highest tractive effort for reverse gear (7674.07 Nm), 1st gear (6940.74 Nm), 2nd gear (4837.04 Nm) whereas lowest for 6th gear (1311.11 Nm). But as observed, the tractive effort by a 4-wheel drive is comparatively higher than a two wheel drive (front wheel drive) vehicle.

Thus, it is concluded from the study that a 4-wheel drive system reduces wheel slippage tendency, gives better climbing capability on hilly areas and provides better driving control over the vehicle on the low frictional surfaces such as wet road, snowy road, mud and sand. Whereas additional components in four-wheel drive system adds on weight; increases cost, maintenance, repair and noise; and makes the construction more complex. But still the merits of 4-wheel drive system overcome the demerits upto a great extent.

References

[1]. CH Yu, CY Tseng, CM Chang. Study on Power Train of Two Axles Four Wheel Drive Electric Vehicle, Energy Procedia 14, 2012, 1528-1535.

[2]. HB Das, SA Evangelou, SJ Dhinagar. An objective analysis of drivability for two wheeler powertrain with control oriented dynamic model, IFAC-Papers OnLine 48-15,2015, 292-299.

[3]. K Matsun, R Nitta, K Inoue, K Ichikawa, Y Hiwatashi. Development of a New All-Wheel Drive Control System, Seoul 2000 FISITA World Automotive Congress, 6, 2000.

[4]. P Russell and Osborn Taehyun Shim, Independent control of all-wheel-drive torque distribution, Vehicle System Dynamics, 44 (7), 2006, 529-546.

[5]. Kirpal Singh, Automobile Engineering, 1, 12th edition 2011, 3-11.

[6]. Smyth T and King M, Driver-Vehicle Interactions in 4WDs: A Theoretical Review, Australasian Road Safety Research, Policing Education Conference,2006.

[7]. W Zhifua, ZYangb, LI Chaopenga, F Jun. Research on Straight Line Stability Control Strategy of Four Wheel Drive Vehicle Based on the Sliding Mode Variable Structure Control and Optimization Algorithm, Energy Procedia 104, 2016, 342-347.

[8]. G Li, W Hong, D Zhang, C Zong. Research on Control Strategy of Two Independent Rear Wheels Drive Electric Vehicle, International Conference on Applied Physics and Industrial Engineering, Physics Procedia 24, 2012, 87-93.

[9]. B Gasbaoui, A Nasri. A novel 4WD electric vehicle control strategy based on direct torque control space vector modulation technique, Journal of Intelligent Control and Automation, 3 (3), 2012, 236-242.

[10]. Abdelfatah Nasri, Brahim Gasbaoui and Ben Mohammed Fayssal, Sliding Mode Control for Four Wheels Electric Vehicle Drive, 9th International Conference Interdisciplinarity in Engineering, INTER-ENG 2015, 8-9 October 2015, Tirgu Mures, Romania, Procedia Technology 22, 2016, 518-526.

[11]. MJ Nunney. Light and Heavy Vehicle Technology, 4th edition 2007, 432-433.

[12]. https://www.google.co.in/search?q=four+wheel+drive&rlz=1C1CHBF_enIN747IN747&source=lnms&tbm=isch&sa=X&ved=0ahUKEwiq74zelq7XAhVM2hoKHQRFBkoQ_AUICigB&biw=1366&bih=588#imgrc=3S91rFUtn4xjIM:

[13]. http://www.mahindrascorpio.com/mahindra-scorpio-model.aspx

International Journal of Applied Engineering Research ISSN 0973-4562 Volume 13, Number 12 (2018) pp. 10733-10740
© Research India Publications. http://www.ripublication.com

Influence of geotextiles in enhancing shear strength of Yamuna sand

Ankur Mudgal[1], Raju Sarkar,[2] and Amit Kumar Shrivastava[3]

[1]Research Scholar, Department of Civil Engineering, Delhi Technological University, Delhi -110042, India.

[2]Associate Professor, Department of Civil Engineering, Delhi Technological University, Delhi -110042, India.

[3]Professor, Department of Civil Engineering, Delhi Technological University, Delhi -110042, India.

Abstract

The present study exhibits the characterization of Yamuna sand through various experiments like SEM, sieve analysis and triaxial tests. The literature study puts forth the numerous complications associated with Yamuna sand from construction point of view. The continual conduct of any construction project chiefly depends on the engineering quality of underlying soil. Hence, its highly imperative to check these complications, which can be mitigated with the help of soil reinforcements such as soil nailing, fiber reinforcement, geosynthetic reinforcement, and soil stabilizers like bitumen, cement etc. The current study delineates the impact of both woven and non-woven type geotextiles on the shear strength of Yamuna sand. In totality, thirty-seven consolidated drained triaxial tests were brought about, of which twenty-one were successful. The principal focus of the study was to determine the application of both woven and non-woven geotextiles with Yamuna sand.

Keywords: Yamuna Sand, Triaxial test, Scanning Electron Microscopic (SEM).

INTRODUCTION:

The present study investigated upon Yamuna sand found along the Yamuna River, India. The river originates from Yamunotri glacier and also flows through Delhi, National Capital Territory of India. The Yamuna sand found in Delhi possesses weak shear strength moreover, it is also susceptible to erosion. If the soil is weak in shear then shallow foundation cannot be constructed in the area and deep foundations are adopted. The cost of construction of deep foundation is considerably immense, thus it is more fitting to stabilize the weak soil. There are various methods by which shear strength of sandy-soil can be improved like vibrofloatation, fiber reinforcement and also through admixtures like bitumen, cement etc. Geotextile reinforcement is used in our present study for the soil reinforcement because it has been seen by literature study that it is very effective alternative for soil reinforcement. Geotextiles is derived from the words geo-soil and textile-fiber. The textile can either be conceived of synthetic material like polyester, polypropylene fiber or with the natural material like jute, coir etc. In essence there are two forms of geotextiles namely woven and non-woven geotextile. Woven geotextiles are fabricated from the synthetic or natural fibers by employing weaving techniques in which the fibers are arranged in a perpendicular direction to each other. The fiber, which runs along longitudinal direction, is called as warp whereas along transverse direction, it is called as weft (Sarsby, R. W.) [1]. Both monofilament and multifilament yarn can be used for woven geotextile. Non- woven geotextiles are composed by the random arrangement of filaments or fibers by bonding them together to form a planar structure. Bonding can be accomplished by in the form of Thermal, Chemical and Mechanical bonding.

Many researchers have instigated to elevate the strength of Yamuna Sand with distinct types of Geotextile to best of their results. M.D. Nguyen et al. [2] proffered the volumetric strain and shear stress variation in Geotextile reinforced sand by triaxial test. It was culminated that Geotextile comprisal increases compressive volumetric strain during initial shearing together with dilatancy after farther shearing. The mobilized shear stresses between the geotextile and sand are distributed non-uniformly in the geotextile layer. R. Ziaie Moayed et. al. [3] thought-through dynamic behavior of reinforced sand and premeditated that by augmenting space between geotextile and cap of sample reinforcement, the liquefaction resistance attenuates. Latha and Murthy [4] studied the parameter geotextile & geocell effect on reinforced sand and they observed that the Polyester geocells proved to be highly efficient in improving the strength of sand compared to geotextile cell because of indent formation. Ojha et. al [5] checked the shear strength behavior of Yamuna sand based on relative compaction and relative density, and they found that the sensitivity of shear strength parameter significantly contributes to evaluation of shear strength of Yamuna sand. Limited researches are available regarding the utilization of woven and non-woven geotextiles as a soil reinforcement to improve the shear strength of Yamuna sand.

MATERIALS:

Yamuna Sand

For the present study, Soil sample has been amassed Okhla, Delhi. The top layer of the soil has been withdrawn with the help of a shovel up to a depth of 0.5m before gathering the soil sample. The soil was cohesionless with fine-grained particles and is dark grey in colour. The Geotechnical properties of Yamuna sand is shown in table I

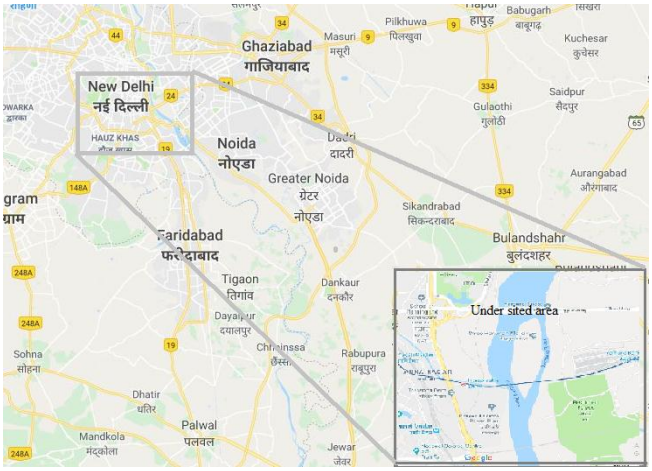

Figure 1. Location of the understudied site area

Table I. Geotechnical Properties of Yamuna Sand

Properties	Value
Specific gravity	2.60
Maximum dry unit weight (kN/m^3)	17.77
Optimum moisture content (%)	10
Coefficient of uniformity (C_u)	1.26
Coefficient of curvature (C_c)	1.57
Angle of friction (Φ)	24.3

Geotextiles

Two types of Geotextiles have been put to use in our study of which woven type of geotextile is made of polyester together with multifilament yarn, furthermore is bluish-off white in colour. While the non-woven geotextile is made of polypropylene fiber as well as black in colour. For the characterization of geotextile, Scanning Electron Microscope test (SEM) and tensile tests had been conducted. Table II shows the properties of Geotextiles.

Table II. Tensile Test Results of Woven and Non-woven types of Geotextile

Parameters	Woven type	Non-woven type
Load at maximum extension (N)	520.14	120.61
Maximum extension (mm)	105.2	170.48
Modulus (MPa)	33.24	4.11
Stress at yield point (MPa)	5.59	1.62
Stress at break point (MPa)	37.5	5.69
Percentage elongation (%)	0.31	0.85

Table III. Tensile properties of Geotextiles

Property	Woven Geotextile	Non-woven Geotextile
Breaking strength	Higher	Lower
Breaking elongation	Lower	Higher
Initial modulus	Higher	Lower

EXPERIMENTAL INVESTIGATIONS

The collected soil sample was characterized in Geotechnical laboratory of Delhi Technological University. Tests were conducted to determine the geotechnical properties of soil sample. The Triaxial tests were performed on Yamuna sand in Consolidated drained (CD) condition with the following conditions:-s

- Unreinforced Yamuna sand
- Yamuna sand reinforced with woven type geotextile in single, double and triple layers respectively.
- Yamuna sand reinforced with non-woven type geotextile in single, double and triple layers respectively.

The dimensions of mould were 100 mm in length and 50 mm in diameter. The cell pressures were applied at 50 kPa, 100 kPa and 150 kPa respectively.

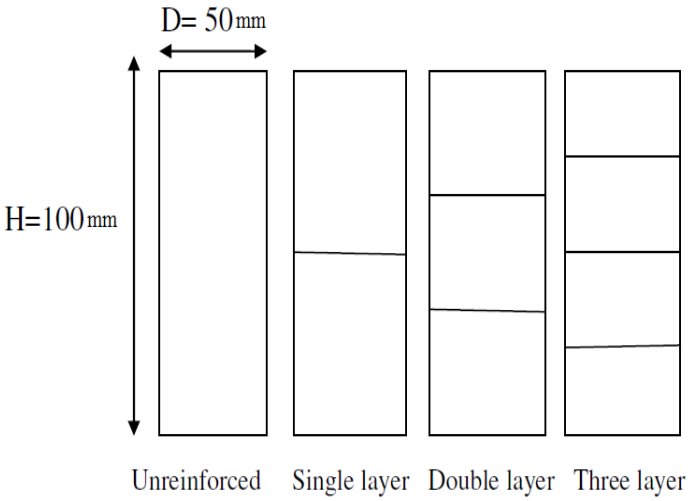

Figure 2. Geotextile arrangement in Triaxial Test

Sample Preparation

Triaxial tests were performed on soil sample having two Length-diameter ratios. Soil samples were prepared in split mould and the sample was compacted by means of static compaction at optimum moisture content. In case of reinforced soil sample, the diameter of geotextiles layer was kept less than the mould diameter and geotextile layers were placed horizontally in compacted soil.

DETAILS OF TESTS CONDUCTED

Specific gravity

The specific gravity of the soil was determined as per the Indian standard specifications [14].

Grain size distribution

The grain size distribution of soil was carried out as per the Indian standard specifications [15].

Compaction characteristics

Light (standard Proctor) test were carried out to determine the maximum dry density (MDD) and optimum moisture content (OMC) of virgin and reinforced soil as per Indian standard specifications [16].

TEST RESULTS AND DISCUSSION

Specific Gravity

The specific gravity of Yamuna Sand was found 2.6.

MORPHOLOGY

The morphology of Yamuna sand and Geotextile were analyzed by Scanning Electron Microscopic (SEM) Hitachi S 3700. From figure 3 (a), it can be concluded that the geotextile is woven type in which warp has double filament and weft along the transverse direction having a single strap. Both the layers are interlocked with each other. The fibre arrangement is orthogonal and the openings are regular. The aperture size is 0.2m. Whereas in fig 3 (b), it can be concluded that the geotextile is of non- woven in nature having strands interlocked with each other. Fibre arrangement is random and openings are irregular. The aperture size is 0.1mm. While fig 3 (c) shows that sand particles are angular, undergone non-uniform weathering and have greater silica dissolution.

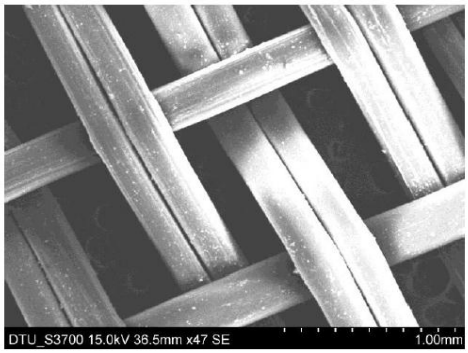

Figure 3 (a)

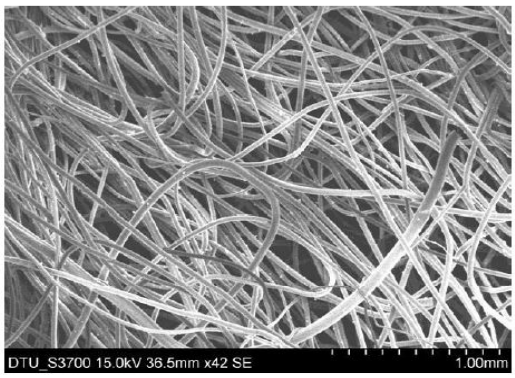

Figure 3 (b)

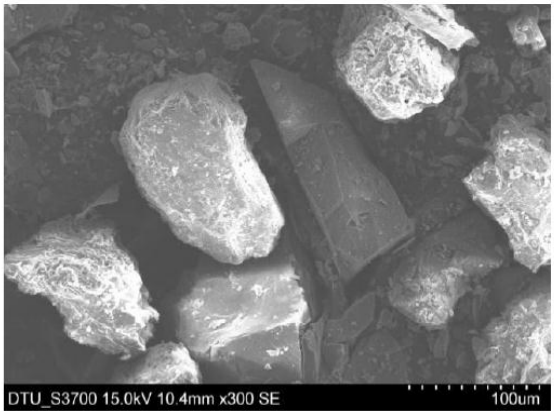

Figure 3 (c)

Tri-axial analysis:

A series of Triaxial tests were conducted in laboratory to check the effect of reinforcement on the properties of sand. The test condition was consolidated drained condition and the tests were performed on both unreinforced and reinforced soil. Figure 4 (a) shows the variations of stress-strain at different confining pressures i.e. 50,100 and 150 (kPa) respectively. Figure 4 (b-d) revels the maximum shearing strength of woven geotextile reinforced sand while Figure 4 (e-g) shows the maximum shearing strength in respect of nonwoven geotextile reinforced soil. Reinforced soil with woven geotextile gives better performance than the Nonwoven geotextile, it may be due to more stiffness and more proper bonding between the sand particles and woven geotextile apertures.

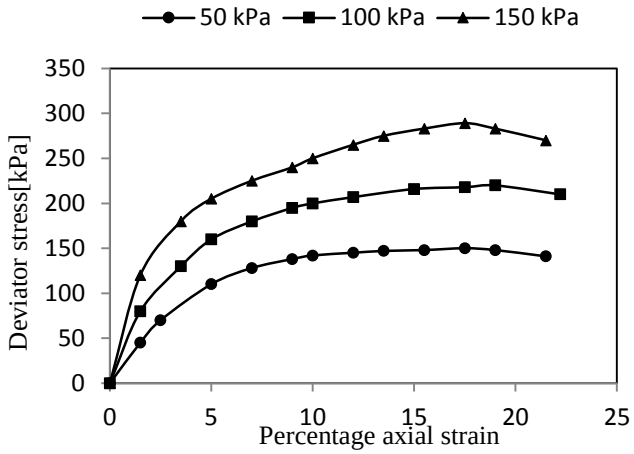

Figure 4 (a). Variation of stress vs. strain in unreinforced Yamuna Sand

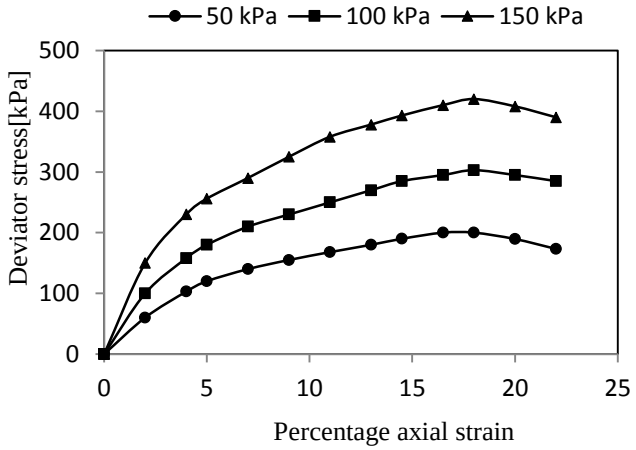

Figure 4 (b). Placement of two layers of woven geotextile in Yamuna sand

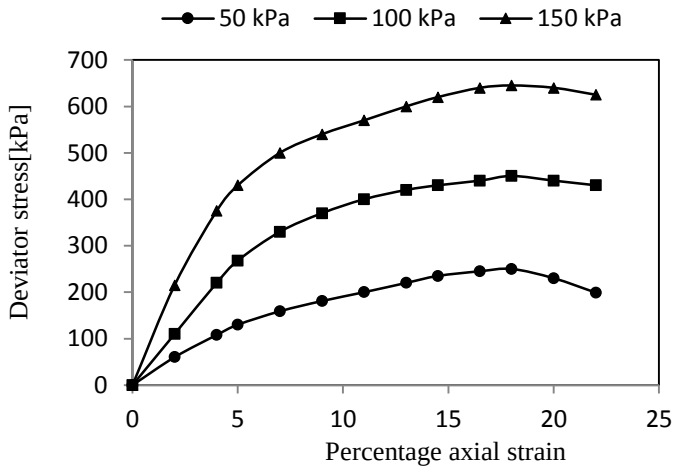

Figure 4. (c)placement of two layers of woven geotextile in Yamuna sand

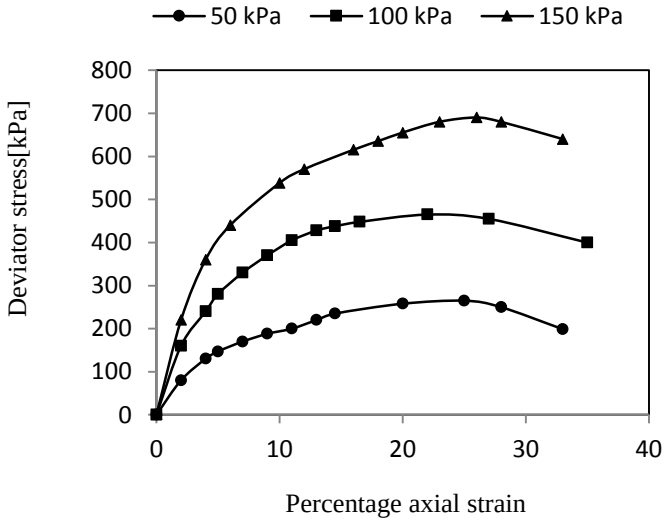

Figure 4. (d) placement of three layers of woven geotextile in Yamuna sand

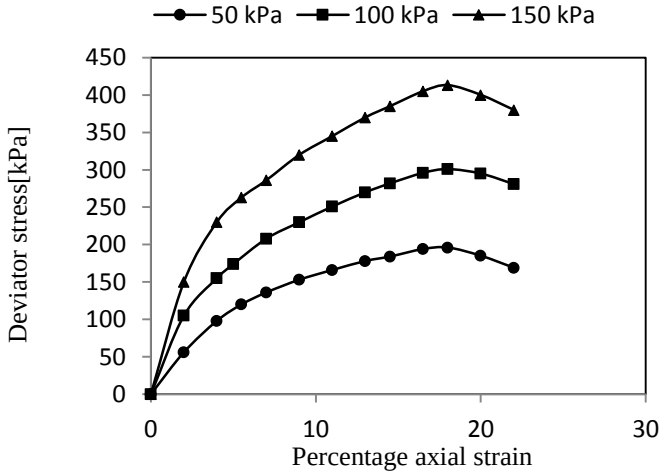

Figure 4. (e) Triaxial test on Yamuna sand reinforced with non-woven geotextile in single layer

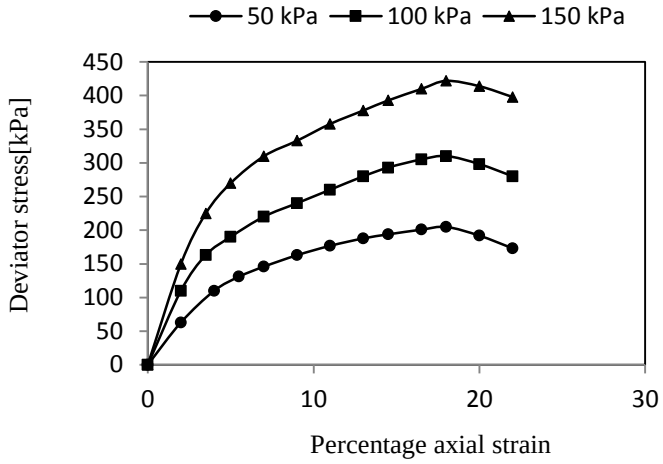

Figure 4. (f)Triaxial test on Yamuna sand reinforced with non-woven geotextile in double layer

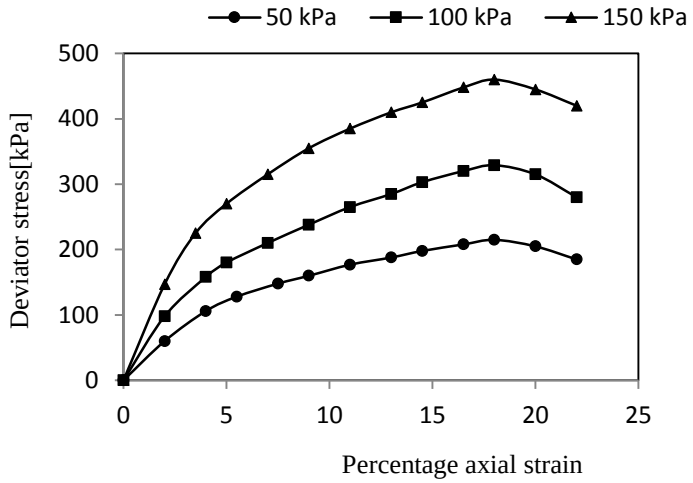

Figure 4. (g) Triaxial test on Yamuna sand reinforced with Non-Woven Geotextile in three layer

Strength ratio:

The strength ratio is defined as the peak deviator stress of reinforced specimen to the peak deviator stress of unreinforced specimen. From figure 5 (a-b) it is cleared that the strength ratio increases as reinforcement layers increases but at third layer all values of strength ratios become constant.

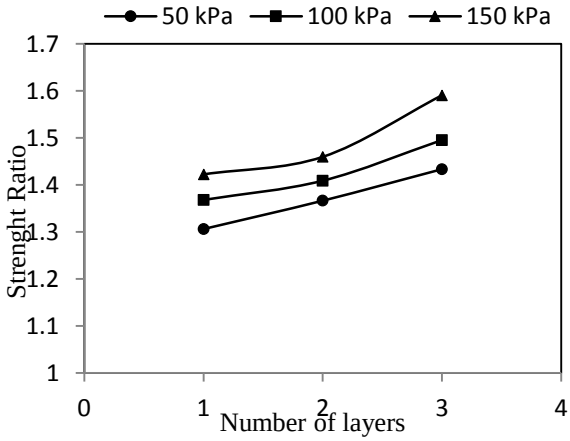

Figure 5 (a). Strength ratio of Non woven geotextile reinforced soil,

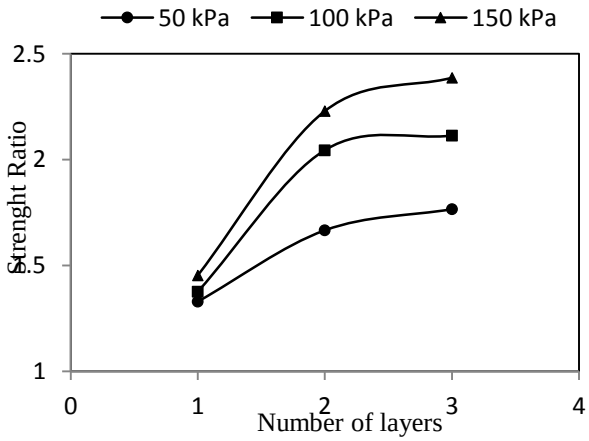

Figure 5 (b). Strength ratio of woven geotextile reinforced soil

Table V. Strength difference with respect to unreinforced Yamuna sand

Confining Pressure (kPa)	Strength difference					
	Woven Geotextile			Non woven Geotextile		
	1 layer	2 layers	3 layers	1 layer	2 Layers	3 Layers
50	51.33	100.8	115.7	48.22	55.8	65.7
100	85.54	230.8	245.6	80.43	90.1	95.72
150	131.01	356.8	401.2	121.2	136.	171.4

Strength difference:

The strength difference $\Delta\sigma 1$ is defined as the difference between shear strength of reinforced soil and that of unreinforced soil under the same confining pressure, which also indicates the net strength improvement by reinforcement. Table V shows the Strength difference with respect to unreinforced Yamuna sand

Interface frictional angle:

From the graph shown in figure 6, it can be seen that the non-woven has higher interface angle than woven geotextile and hence the interlocking of sand is better with non-woven geotextile.

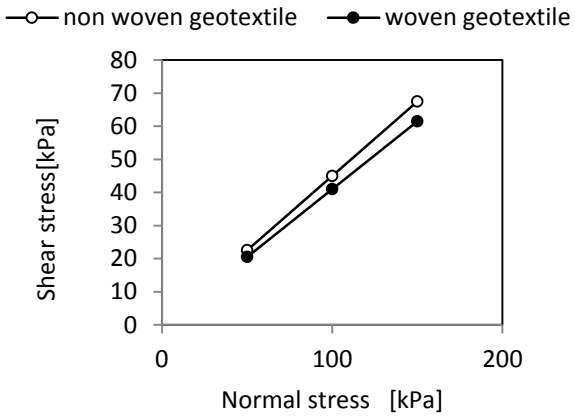

Figure 6. Comparison of interface friction angle

CONCLUSIONS

From the Triaxial analysis, it is clear that the geotextile improves the strength of Yamuna sand. In comparison with woven geotextile, the bonding of non-woven geotextile is more with Yamuna sand in comparison to woven geotextile, but the strength of Yamuna sand is enhanced more if reinforced with woven Geo textile. So it can be concluded that depending on the application of Geo textile, the suitable geotextile can be used. For the purpose of Reinforcement the woven Geo textile should be used as the shear strength is improved significantly.

REFERENCES

[1] Sarsby, R. W. (2007) "Geosynthetics in civil engineering" Text book, Woodhead Publishing Limited, ISBN-13: 978-1-85573-607-8.

[2] M.D. Nguyen K. H. Yang, S. H. Lee, C. S. Wu and M. H. Tsai (2013), "Behavior of nonwoven-geotextile-reinforced sand and mobilization of reinforcement strain under triaxial compression" Geosynthetics International, 20 (3), pp. 206-225.

[3] R. Ziaie Moayed and M. Alibolandi (2014), "Reinforcement Effect on Dynamic Properties of Saturated Sand" International Journal of Civil, Environmental, 8 (1), pp. 72-76.

[4] Latha, G.M., And Murthy, V.S. "Investigations On Sand Reinforced With Different Geosynthetics." Geotechnical Testing Journal, 2006, Vol.29, No.6, pp. 474-481.

[5] Ojha, S and Trivedi, A., "Shear Strength Parameters for SiltySand Using Relative Compaction" Electronic journal of geotechnical engineering,2013, vol 18, pp. 88-99.

[6] Al-Omari, R. R., Al-Dobaissi, H. H., Nazhat, Y. N. & Al-Wadood, B. A. (1980) "Shear strength of geomesh reinforced clay"Journal, Geotextiles and Geomembranes 8, pp.325–336.

[7] Athanasopoulos, G.A. (1993), "Effect of particle size on the mechanical behaviour of sand geotextile composites", Journal, Geotextiles and Geomembranes 12, pp.255-273

[8] Ashmawy, A.K., Bourrdeau, P.L., (1998)," Effect of geotextile reinforcement on the stress-strain and volumetric response of sand", Journal, Proceedings of the Sixth International Conference on Geosynthetics, Vol. 2, Atlanta, pp. 1079-1082.

[9] Broms, B.B. (1977), "Triaxial tests with fabric reinforced soil", Journal, Proceedings of the International Conference on the Use of Fabric in Geotechnics, Vol. 3, Ecole Nationale des Ponts et Chaussees, Paris, pp. 129-134

[10] Gray, D.H., Ohashi, H., (1983) , "Mechanics of fiber reinforcement in sand", Journal of Geotechnical Engineering 109 (3), pp.335–353

[11] Haeri, S.M., Noorzad, R., Oskoorouchi, A.M. (2000), "Effect of geotextile reinforcement on the mechanical

behavior of sand", Geotextiles and Geomembranes 18, pp.385–402

[12] Krishnaswamy, N.R., Issac, N.T. (1995), "Liquefaction analysis of saturated reinforced granular soils", Journal of Geotechnical Engineering ASCE 121 (9), pp.645-651.

[13] McGown, A., Andrawes, K.Z., Al-Hasani, M.M., (1978), "Effect of inclusion propertieson the behavior of sand", Journal, Geotechnique 28 (3), pp.327-347

[14] IS: 2720 (Part 3) (1980). Methods of Test for Soils: Determination of Specific Gravity, Bureau of Indian Standards, New Delhi, India.

[15] IS: 2720 (Part 4) (1985). Methods of Test for Soils: Determination of Grain Size Analysis, Bureau of Indian Standards, New Delhi, India.

[16] IS: 2720 (Part 7) (1980). Methods of Test for Soils: Determination of Water Content- Dry Density Relation Using Light Compaction, Bureau of Indian Standards, New Delhi, India.s

INTERNATIONAL JOURNAL OF ADVANCE RESEARCH, IDEAS AND INNOVATIONS IN TECHNOLOGY

ISSN: 2454-132X

Impact factor: 4.295

(Volume 4, Issue 2)

Available online at: www.ijariit.com

Influent of Overall Architectural Arrangement on Structural Elements Design

Gatbel Buony
nyeyianp@gmail.com
Delhi Technological University, Delhi,

Dr. A. K. Gupta
akgupta@dce.ac.in
Delhi Technological University, Delhi

ABSTRACT

In designing a civil structure, difference professionals are involved from the conceptual stages through the constructions up to the final project stages. Because of this, there are difference links which exist between difference professionals which need to be addressed properly to obtain the best environmentally friend structure with adequate cost as well as strength and durability.

In particular, when we look at the cooperation of architects and engineers, we may observed that they have some difficulty in working together harmony. This is due to the complexity of intangibility and tangibility as well as actual and abstract notion of the Architecture. Structural engineers focus more on tangible and actual notion on structures and detail aspects. On the other hand, Architects put great prominence on global and general aspects, such as spatial forms and atmosphere generated. This contradictory ways of thinking sometimes result in difficulty in communication [10].

Moreover, in the design processes the general arrangement or structural form chosen for a building at initial stage will normally determine the type of structure which will have to be adopted to support it and will perhaps also dictate the selection of structural material [4].

In fact the structural dimensioning of previously defined morphological system results in it being a less trustworthy system, leading to a structure that is greatly susceptible to seismic damage This is because of the delinquency of relating the already defined architectural form and that of the structural design [11].

Furthermore, "reference [7]"quoting different architects ideas and stating: "All professionals need to learn the art of Architecture because it concerned altogether - John Ruskin. Le Corbusier said that "Architecture is the accurate, proficient, and outstanding play of masses brought together in light". For these reason, Architects and structural engineers need to have a better understanding on the joint works and carry out the activities in close proximity to produce a sound architectures.

Keywords: *Structural form, Architecture, Architects, Structural Engineers.*

1. INTRODUCTION

Throughout the antiquity, buildings has usually been designed and built by only one person, hence called Master Builder. It was an architect, engineer as well as constructor, all professionals in one. During the time when the industrialization has begun, the complexity of the constructions became more and more, and the demands of the buildings by the society became greater than before. Material of the construction and tools developed with the technical development. This became the challenging factors for one person to know everything plus to think about every aspects in the constructing/ designing of a building or a bridge structures. These result in the division of works between Architects, builder and difference Engineers [5]. Besides, the separation of work lead to the cause of other problems. The utmost problem among these was probably the communication between the different professions in the processes. In a building project both good communication and efficient collaboration is required between different professionals. What was in the past as one man works became now a collaborations between different professions and at the same time they works apart from each other rather than closer. In the previous decade, this issue has got more and more attention, both out on the field as well as in the Institutions. It is clear that in the near future the advancement of both construction technologist and method of construction will be unrealistic. Because of these, it is necessary for architects and engineers to work together much closer, both in the school plus out on the field [3]. In addition to these, the chosen structural form has a great influence on optimization techniques in structural design which is the need to find the best way to gain the maximum output from the resources in hands. In these paper

© 2018, www.IJARIIT.com All Rights Reserved

we will look closely on the correlation of architect works with that of Structural engineers in particular throughout the Design processes and their influent.

A. Objective

1).To gain a knowledge on how structural forms influent structural element design and Vic versa

2).To create awareness on the connection between both structural engineers as well as Architects.

3).To elaborate how to design a safe, durable, aesthetic and economical structure by regarding the importance of the connection of overall architectural arrangement and structural elements throughout the design processes.

2. LITERATURE REVIEW

The process of structural design may be subdivided into two parts: the first one is preliminary design stage, when the form and general arrangement of the structure is developed, and the second is the analysis and the determination of various structural elements dimension. The general arrangement or structural form chosen for a building at initial stage will normally determine the type of structure which will have to be adopted to support it and will perhaps also dictate the selection of structural material [4].

In fact the outcome of dimensioning of already defined structural form can result in a less truth worthy structural system which is greatly susceptible to seismic damage. This is because of the delinquency of relating the already defined architectural form and that of the structural design [11]).Engineers use Optimization techniques in structural design as a tool. The purpose of these Technique is to select the best option by the Decision makers or Designers from the available resources in order to gain the maximum benefit [16]. However, structural optimization process and methodology adopted for a given problem is also influenced by Model of Structure, dimensionality, choice of design variable and the type of structure [12]. According to [15], based on the structural form classifications, four types of structure are distinguishable such as: Truss, Shell, Solids, and Composite materials. The Truss structural form can be perceived in all areas of engineering sciences that involve structural mechanics. The properties of In-plane and out-of-plane of Shell structures deformations are commonly used in optimization and aerospace structural analysis. In geo-technical and mechanical engineering, solids structures play an important role [13].In aerospace and other engineering discipline usually civil engineering the application of the composite structural types can be seen. All these factors affect the way by which the optimization technique is carried out. Furthermore, the model in which the structure is idealized for optimization also affect the processes. The engineers model the structure in such a way that it represent the real structural form. This approximate model for mathematical sense must accurately represent the original structures for optimizations prototypical [14].

The influence of structural form can be observed from the “Willis, Faber and Dumas building (Fig.2)”case. Where there was a requirement of external glass wall as well as large wall free interior spaces, there was no alternate to the adoption of a frame-type structure. The reinforced concrete was selected as a structural material rather than steel due to the need for a curvilinear plan-form as well as columns which were set back from the perimeter. The result in this case was a building in which both architectural and structural requirements were satisfied in equal measure. The building was in such a way that it is free from both technical as well as architectural criticism. Due to the complexity of roof top arrangement of The office in Viena by” Coop Himmelblau group” (Fig. 2.1),the selection of skeleton frame type of structure and steel as a construction material to ensure that the element are slender enough was a mandatory option rather other type[4].

Fig.2.0: Willis, Faber and Dumas office, Ipswich, England 197

Anthony Hunt, structural engineer and Foster Associates, architects. The architectural expression was provided by the translucent walls of this building, the curvilinear plan and cantilevered floor slabs on the structural properties of reinforced concrete (Photo: Alastair Hunter).

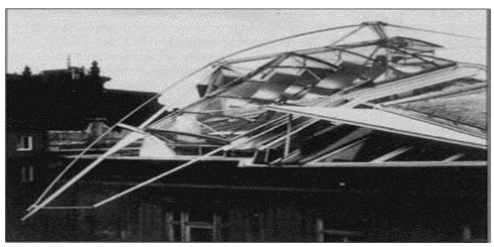

Fig.2.1: Rooftop Remodeling in Vienna, Austria, 1988

Coop Himmelblau, architects. [Photo: Gerald Zugmann).

© 2018, www.IJARIIT.com All Rights Reserved

A. Defining Architecture

Before we look at what the Architect and Structural Engineers ways of working is with corresponding definitions, we need to understand the basic concept behind the Architecture. Most architects and architectural critics have tried, at least once during their professional lives, to define architecture. Even in architecture schools, one popular exercise in theory classes has been to ask students to define architecture. A list of such definitions for architecture is compiled by Francis Ching (1996, p.S [7] quoting different architects ideas and stating: "All professionals need to learn the art of Architecture because it concerned altogether - John Ruskin. Le Corbusier said that "Architecture is the accurate, proficient, and outstanding play of masses brought together in light". The only way you can build, the only way you can get the building into being, is through the measurable. You must follow the laws of nature and use quantities of brick, methods of construction, and engineering. Architecture also exists without necessary assistance from an architect and architects sometimes create buildings which are not architecture. - Norval White." If architecture is seen solely as the province of architects, whether heroic or not, then it is likely that people may not only misunderstand their role in creating the built environment, but also become suspicious of their activities and blame them if they do not like the results [8]).Architecture is a course about interior and exterior arrangements of structure so as to achieve operational functions. The arrangement does not only have to meet the requirements of spatial combination but also have to provide an artistic configuration as well as a sense of harmony with the surrounding environment [10].

1) Elements Of Good Architecture:

Architecture can be evaluated based on different perspective, but for Good Architecture the following elements under the major two categories should be fulfilled [9].

Table I: Elements of Good Architecture

"**PRIMARY CATEGORIES**				
Greek categories	**Architectural elements**			
1 Quantity'	Form	Pattern	Structure	Geometry, etc
2 Activity'	Function	Needs	Effects	Exchange etc
3 Quality	Meaning	Association	Resemblance	Style, etc.
SECONDARYCATEGORIES				
1Substance	Construction	Materials	Design, etc	
2 Relation	Context	Community	Nature	Feeling, etc.
3 Will	Spirit	Power	Politics	Attitudes, etc.

B. Structural Engineer's Way of Working

"Engineers for many people, especially to the public, are mysterious figures. The most frequent remark is: 'What do they do? They just make things stand up,' as though this were not a noble thing to do [2]. What do engineers learn? Most engineers agree upon solving problems. Engineers are "problem solvers". Engineer select the best solution of the project in hand from the different alternative which has the least total cost and simple to be carryout. The projects are often a part of a bigger connection and often there are discussions about which solution is the best. For winning this argument, the engineer has to have proof in calculations of costs and productions. "Engineer: 'this is so, because Newton said so', 'we should take this course of action because calculations indicate it will be the cheapest'" [1]. In the design processes, the major responsibility of Structural engineers are as follow. First, the synthetization of the overall structural system that is select the geometry and the type of structural members that make up the structure. Second, the dimensioning of the structural element to support the apply loads comfortably. Creating a structural concept requires a deep knowledge of structural behavior. Sizing the members requires information about the internal forces resulting from the loading. The internal response of the structures can be acquired using mainly computer based approach for structural analysis [6]. Besides these, Engineers do often work in teams, in large project teams where they each have a small part in the whole project. Engineers' carryout the detailed analysis of the structure which have a great important to the overall system. Even though the details seem small for others, there are a lot of calculations that have to be done to know that it will hold for all the load cases that could be possible. However engineers can also dig themselves too deep into details and they are not always too keen on coming back up again [1].

C. Architect Areas of Work

Architect is more concerning about the spatial compositions, aesthetic values of the Structures, the schematization design process and management of the internal and external configuration, and decoration and coordination with surrounding environment [10]. Architects put more emphasis on general and global aspects, such as spatial forms and atmosphere created.

1) Inspirational Source Of Form Finding By Tyas And Popovic Larsen:

As explained at [5] the most important source of motivation for form finding processes was given by Tyas and Popovic Larsen for structures. Form finding's sources of motivations are divided into a few large sections as follow.

© 2018, www.IJARIIT.com All Rights Reserved

The first one is the nature. Many architects use the beauty in nature to find different forms for a particular structure, but what they might not think about is the knowledge of mechanics. As an example: trees can be very beautiful with their colors and their strange combination of their branches. Many architects find this as a very interesting and try to imitate them. Trees have aesthetic attribute and they also show a classical physical law. The size of the branches is in such a way that it goes decreasing from the intersection point of the support to the far ends. This can be compared to a normal cantilever case. The best way of forming a cantilever is to do it as trees branches.

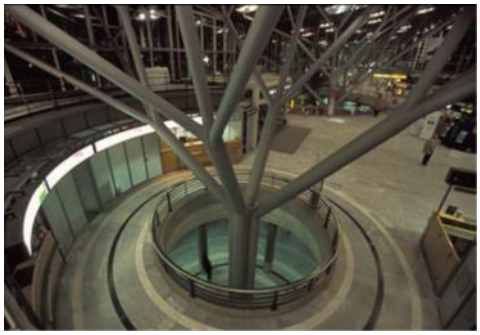

Fig 2.2: Stuttgart Airport

Fig2.3: The Millennium Dome

The second is intuition or common sense. This ability is what everybody has; even those who are not engineers know that you cannot use a cable as a column in a building because it can fall if it tries to stand on its own. These are the conditions on the grounds on how the tents where developed. Our ancestors quickly understood that in order for the fabric/skin to span over the distance, it needs to be tensioned and they do learn these by trial and error. They also observed that if it is not anchored in poles it will fall to the ground. This basic idea can be seen in many of the modern tensed membrane structures today; as an example: the Millennium Dome (fig2.3).

The third source would be inspiration from precedent engineers and architects, or Master Builders. Today we study how to construct a building by applying scientific principles. We learn how to calculate, analyze, and use computers to find the best solutions from difference options. It has not always been in this ways. Before the industrialization concepts, people learned by apprenticeship. You watched older, more experienced Master Builders, during construction processes and if you were a good apprentice you could take over after your teacher. This process is still used today, though not as specific. You acquire knowledge from others mistakes or successes and develop it. The example of this could be the Egyptian pyramids; they were the precedents of I.M. Pei's Louvre Pyramid.

Fig 2.4: The Egyptian Pyramid

© 2018, www.IJARIIT.com All Rights Reserved

Fig 2.5: The Louvre Pyramid

The fourth is the one people are using nowadays in institutions which are known as scientific knowledge. Due to the concept of industrialization, it leads to the needs for faster, adequate and low cost of constructions of, especially factories. And because of the fact that new materials for construction were being used, the knowledge of its properties, how it works and how it reacted on the application of difference loading became very important for the builders to know in order to use it efficiently than ever. The development of scientific knowledge had already begun, as an example: Galileo and Leonard Euler. The bending stresses in the beam were studied by Galileo and Later the buckling of Beam was studied by Leonard Euler respectively. This is the way how the new builders used and further developed to understand how different structural elements and materials worked. The development of theoretical analysis made it possible to understand the structural behavior of new Structural forms before building it. Due to this, the today's designers do not have to depend on only experience and intuition, to form new architecture. Furthermore, the development of science also made it difficult for one person to know everything being carryout during design processes. This lead to the subdivision of master builder into different professions, as the Architects and Engineers. However, to construct a building, both professions were still needed in the processes. What became the most Challenging problem now is the collaboration between the different people needed in the process. For a good collaboration to happen, there has to be a respect and understanding for each other, which is not always there.

3. STUDY AND DISCUSSIONS

When we think about structures, we usually consider bridge, tank, and towers. Even though these structures are appealing, the reality is the objects which surround us in our daily lives are a structure. As an example: A bread being made by mixing different ingredients is also a structure. If you pay attention carefully to a wide variety of structures, you will notice that many of them have resemblances. Different structures might serve the same function example: Bridge, no matter how complicated the form maybe, its function is to span the gap in a location where there is an obstruction safely. People most often, classify the structure based on the function it is made for. Some structures are made to contain something, some structures support something on top, and some span space. Structures which serves the same function may have difference structural form which may lead to complicated design. Based on the structural form classification we have a shell, solid and framed types of Structures, which have difference design characteristic [15].

Despite the fact that, from the conceptual stages through the constructions up to the final project stages, the involvement of difference professionals in the processes, the importance of the link between architect and structural engineer inspired the me to study it started from when I was in my region Gambella. This is due to the fact that the influence of structural form in the later stage of the design is indispensable. In consideration to these, to obtain the best environmentally friend structure with adequate cost as well as strength and durability, architect and Structural Engineer needs to works in close proximity.

A. The concept of Architectural Development.

Before the architecture development by the concerning professionals, people (owners) may grasp the idea of the functional characteristics of it. The activities that are going to be carryout creates difference types of functions for which experts develop them by creating difference architectural part. Architecture concentrates more on the spatial functionality and aesthetic attribute of the works in hand and is more concerning with the artistic views, feel and functionality of the design. In consideration of these, space will be turned into architecture. In harmony with the owner requirements, the schematic design of the architecture of the whole structural arrangement will be visualized prior to the preliminary and detailed design stage. Now if one begins with the analytical views of the space, the dimensions of architectural elements are at the ends of the chain's relationship, which will be influenced by the overall form of the structural arrangements.

Angus J Macdonald. (1997) state that Thus, although some aspects of the design of structures such as the precise geometry of the beams, column grid or the dimensions of the elements may remain undefined until the lateral stage in the design, many important structural choices will be closed once the overall form of a building has been determined. The early concept of a structure, which determine it over all arrangement of it forms and the proportioning of solid and void with in it, therefore, exerts a high influence on its subsequent structural make-up. These imply that the architect is thus, consciously or unconsciously, a structural designer.

B. Structural Engineers and Architects Ways of Working

Architectural products are totally differenced from each other based on their form together with their constituents at micro-level. Structures are supposed to be a creative product completed by architects and structural engineers together. The capability of architectural design of architects and that of the structural design of structural engineers should be tightly integrated and harmoniously complemented. The architect has a relatively limited role in infrastructure construction than in building projects.

© 2018, www.IJARIIT.com All Rights Reserved

Therefore, architects and structural engineers relay on each other in a corresponding way as for different projects, primary role shifts between them. Furthermore, due to the complexity of intangibility and tangibility as well as actual and abstract notion of the Architecture. Structural engineers focus more on tangible and actual on structures and detail aspects. On the other hand, Architects put great prominence on global and general aspects, such as spatial forms and atmosphere generated. This contradictory ways of thinking sometimes result in difficulty in communication.

This different ways of thinking sometimes result in difficulty in communication. Architects deal with issues in a global and top-to-bottom way. On the basis of experience, they take primal conditions, restraints, and available resources into consideration so as to conceive a spatial arrangement with more concentration on the overall structural form. This will allow for the expression of aesthetic as well as the operational functionality of the architectural system [10].

On the other hand, Structural engineers start their analysis from the bottom to top approach that is from the detailed analysis of difference structural elements as taught by traditional education. Those elements may include a specific beams and columns with certain neglect of an overall performance of structures and requirements of sustainable development. Due to these contradictory ways of working, the creative cooperation as well as effective communication of both structural engineers and architects will be greatly affected and this is one of the constraint in schematic and preliminary design processes [10].

C. Collaborations of Architects and Structural Engineers

As we have seen from the definitions given by difference scholars for an Architectures, we understood that it is the results of the collaboration works of structural engineers, architects, and others professionals. Prior to the detailed design stages which mainly focus on the design of substructures and all structural components including the selections of specific materials, determination of construction technology and detailed design for construction, architect and structural Engineer need to cooperate from the schematic stages. Shaopei, L, Huang, Z. (2016) state that designing from the perspective of the overall performance of the structural arrangement is very important for both structural engineers and architects. It does not mean that detail design is not important. Actually, inappropriate details analysis led to many structural failures. Generally, the first important thing in the design is the comprehensive understanding of the overall form of the structural arrangement as well as the operational functionality of the structure for both Structural engineers and architects which need to be established in advance. Then this will be followed by the focus on the detailed design of the specific overall system, substructures, and components to achieve an optimized design. It is possible and necessary to introduce concepts of mechanics in the early stage of design. The application of the concept of mechanic can be seen during the incorporation of important facility such as vertical and horizontal transportation services which are embodied on the structure as elevator shaft and others essential services for life such as water, electricity, gas, heating, ventilation, air conditioning, and acoustics, lighting and waste disposal. Since those are incorporated from the perspective of functions within the specific geometry, a coordinate arrangement is necessary.

4. CONCLUSIONS

From the definitions of architecture given by difference great scholars, it shows a multi-disciplinary characteristic of its existence. The three essentials elements of architectural design which need to be given proper concerns to evaluate an existing or to design a new structure are functions, Aesthetic and that of structural integrity of the components. Functional consideration means the structures should possess certain operational purposes to meet the need of human activities. Structural integrity means the economic feasibility, Structural liability, and constructability of the structure. Aesthetic experiences mean the harmony of the structure with its surrounding environment and it should also provide the symbol of social and aesthetic values for the user. From the above three essentials elements, architects are more concerned with the functional and aesthetic performance. Structural engineers on the other hands are more concerned with the structural integrity. The Author recommended that the best architectural product could be the work completed by both architect and structural engineers from the commencement of the project and up to the final stage.

5. ACKNOWLEDGEMENT

No work, however big or small, has ever been done without the contributions of the others. It would be a great pleasure for me to write a few words which would not suffice as acknowledgment, but in the absence of which these minor project would necessarily be incomplete. These words of appreciation are not enough for those people who help me a lot throughout the works of the project which I could not complete by myself.

I would like to express my deep gratefulness toward Dr. A K Gupta who gives me his valuable suggestion, motivation, and direction to proceed at every stage. They are like a beam of light to me, his kind guidance shows me the way of doing the project and is unforgettable. He extends toward his valuable guidance, indispensable help and inspiration at times in appreciation, I offer him my sincere gratitude.

I am very thankful also to all my friends who help me a lot throughout the project without which the realization of the completion of the project would be unrealistic.

Lastly but not the least; I would extend my gratitude toward Almighty Father for his blessings that keep me awake day and night working on the project.

I have tried my best to make these minor project error free, but I regret errors if any.

6. REFERENCES

[1] Holgate, Alan (1986). The Art in Structural Design. Clarendon Press, Oxford.

© 2018, www.IJARIIT.com All Rights Reserved

[2] Rice, Peter (1994). An Engineer Imagines. London.
[3] Louise Pedersen and Jonas Täljsten. (July 2007). The structure as Architecture. Kfs I Lund Ab, Lund, Sweden.
[4] Angus J Macdonald. (1997). Structural Design for Architecture, Reed Educational and Professional Publishing Ltd.
[5] Larsen, O.P. and Tyas, A. (2003). Conceptual Structural Design: Bridging the Gap between Architects and Engineers. T. Telford, London.
[6] Jerome J. Connor • Susan Faraji. (2013). Fundamentals of Structural Engineering. Springer New York Heidelberg Dordrecht London.
[7] Ching, Francis DK., (1996). A Visual Dictionary of Architecture. NY.: Van Nostrand Reinhold.
[8] Conway, Hazel, and Roenisch, Rowan, (1994). Understanding Architecture: An Introduction to Architecture and Architectural History. London: Routledge.
[9] Capon, David Smith, (1999a). Architectural Theory, Volume One: The Vitruvian Fallacy, A History of the Categories in Architecture and Philosophy. West Sussex: John Waley & Sons.
[10] Shaopei, L, Huang, Z. (2016).Comparative Design of Structures Concepts and methodologies.
[11] Parducci A. "Seismic Isolation and architectural configurations" Specialty Conference on The conceptual approach to structural design. Singapore. 2001.
[12] Edgar, T. F. And Lasdon, L. S. (2001). "Optimization of Chemical Process". McGraw Hill, Toronto.
[13] Suzuki, K, Terad, K, Ohtsubo, H. And Yonesato, N. (1997). "Analysis Method for Solid Structures Using Multiple Voxel Information" (in Japanese). Papers of the Japanese Society of Computational Mechanics, 2 (5), 234 – 246.
[14] Allaire, G., Gournay, F., Jouve, F. And Toader, A. (2004)." Structural Optimization Using Topological And Shape Sensitivity Via A Level Set Method". http://www.cmap.poly technique.fr/ (assessed on 31 – 01- 2014).
[15] Backlund, J. And Is by, R. (1988). "Shape Optimization of Holes in Composite Shear Panels". Structural Opti mization, 9 (16), 16 – 25.
[16] Iyengar, N. G. R. (2004) "Optimization in Structural Design". http://www.iitk.ac.in/kangal/pub.htm, as-sessed on 30 – 01 – 2014).

© 2018, www.IJARIIT.com All Rights Reserved

Investigations on the plasma enabled growth of vertical graphene sheets on CNT surface

Neha Gupta, and Suresh C. Sharma

Citation: Physics of Plasmas **25**, 073509 (2018); doi: 10.1063/1.5030559
View online: https://doi.org/10.1063/1.5030559
View Table of Contents: http://aip.scitation.org/toc/php/25/7
Published by the American Institute of Physics

Articles you may be interested in

Numerical study on helium-oxygen dielectric barrier discharges: From single-breakdown to multi-breakdowns per half-cycle
Physics of Plasmas **25**, 073508 (2018); 10.1063/1.5028289

Quadrupolar mode measurements for space charge dominated beams
Physics of Plasmas **25**, 073107 (2018); 10.1063/1.5026677

Computational simulation of atmospheric pressure discharges with the needle-array electrode
Physics of Plasmas **25**, 072101 (2018); 10.1063/1.5029266

H-mode access and the role of spectral shift with electrode biasing in the TCABR tokamak
Physics of Plasmas **25**, 072301 (2018); 10.1063/1.5029561

Optical and electrical investigation of DC micro-hollow cathode discharge in He/O_2 and He/H_2 mixture
Physics of Plasmas **25**, 073506 (2018); 10.1063/1.5037699

Electrical behavior of exploding copper wire in ambient air
Physics of Plasmas **25**, 072108 (2018); 10.1063/1.5020252

PHYSICS OF PLASMAS **25**, 073509 (2018)

Investigations on the plasma enabled growth of vertical graphene sheets on CNT surface

Neha Gupta and Suresh C. Sharma
Department of Applied Physics, Delhi Technological University, Shahbad Daulatpur, Bawana Road, Delhi 110042, India

(Received 22 March 2018; accepted 24 June 2018; published online 13 July 2018)

A theoretical model is developed to describe the plasma-assisted nucleation and growth kinetics of a vertical graphene (VG) sheet on a carbon nanotube (CNT) surface. The present model accounts the formalization of a charge separation region, i.e., plasma sheath between the bulk plasma and substrate surface in one-dimension along with the kinetics of all the plasma species (neutrals, positively charged species, and electrons), rate of charge accumulation on the graphene sheet surface, and growth of the VG sheet on the CNT surface owing to defect generation and various processes on the CNT surface. Using the model, we demonstrated that variations in the plasma enhanced chemical vapor deposition process control parameters such as the total gas pressure, input power, and substrate bias can be used for significant variation in the plasma composition and characteristics that in turn control the ion bombardment and generation of carbon species on the CNT surface and consequently tune the VG sheet growth characteristics such as height, thickness, and number density profiles of the VG sheet on the CNT surface. The results of the present study indicate that as the total gas pressure is lowered and the input power and substrate bias are enhanced, the number densities and height of the VG sheet on the CNT surface are increased; however, the thickness of the VG sheet is reduced. Some of our theoretical findings are in good agreement with the existing experimental results. *Published by AIP Publishing*. https://doi.org/10.1063/1.5030559

I. INTRODUCTION

Owing to their outstanding properties and unique structure, graphene nanostructures (GNs) have drawn the considerable interest of many materials scientists and engineers in their wide range of applications.[1] These properties and applications of GNs are strongly related to their structure, the number of graphene layers, their stacking orientation with respect to the substrate, and the type of substrate.[2,3] The vertically oriented (perpendicular to the substrate) GNs are known to outperform their horizontally oriented (parallel to the substrate) counterparts for various high-performance applications, e.g., electron field emitters, sensors, and fuel cells, due to the non-agglomerated morphology, exposed reactive edges, and high surface to volume ratios per substrate area of the vertical GNs.[3,4] Thus, it is of a critical need to control over the growth of GNs, dimensions, orientation, and properties of resulting GNs to enable their effective realization into the advanced graphene-based nanoscale devices.

The growth of vertical graphene (VG) has been realized on various substrates such as dielectrics,[5,6] semi-conductive Si,[7] metals,[8,9] carbon cloth,[10] silicon nanowires and nanocones,[11,12] diamond-like carbon films,[13] and carbon nanotubes (CNTs).[13–19] Recently, the growth of VG on the CNT surface (or graphenated CNT) has attracted substantial interest since this hybrid structure is reported to have potential applications in high-performance field emitters than individual CNT or VG. The graphene layer protrusions or foliates growing from the CNT surface enable significantly higher charge storage capacity and field emission stability than either of the two materials can achieve on their own. The exemplary field emission from this VG-CNT hybrid is expected owing to the adorable properties of CNT (incomparable high aspect ratio and excellent electrical conductivity) and increased surface area due to the exposed sharp edges of graphene protruded from the CNT surface.[13–17] This unique hybrid structure is also reported to be widely used for making photoconductors,[20] supercapacitors,[21] fuel cells,[22] gas sensors,[18] and transparent conductors.[23] For the first time, the graphene sheets growing radial to the tube axis of nitrogenated CNTs were synthesized by Kurt and Karimi[24] via a hot filament chemical vapor deposition (HF-CVD) technique in a nitrogen–methane–ammonia environment.

The plasma enhanced chemical vapor deposition (PECVD) method has been widely used for the production of graphene foliates on CNT.[13–18] According to previous reports,[13–16] the VG nucleation on CNT is defect guided, i.e., VG growth starts with the induced defects of CNT by intensive bombardment of ions in PECVD. Parker *et al.*[19] proposed a model of nucleation of graphitic foliates from external CNT walls resulting from the buckling of large diameter CNT walls due to the build-up of residual stress at the outer CNT walls. PECVD is a complex process, owing to the existence of energetic electrons, various ions, radicals, and other neutral species in the plasma and thus possible to attain the controllable structure and growth characteristics of as-grown VG by adequately altering the plasma parameters, input power, gas type and proportion, and gas pressure for specific applications.[4]

In our previous works,[25–27] we developed an analytical model to unveil the catalyst-aided growth mechanism of the VG sheet in the complex plasma environment and also studied the influence of growth time, plasma parameters, different gas mixtures, and doping on the growth characteristics of the VG sheet. However, in order to augment the relevance of

typical PECVD synthesis experiments of graphenated CNTs,[13–18] we endeavor to develop a phenomenological model to describe the major processes responsible for the VG sheet growth on a CNT template in a plasma environment, such as creation of defects on the CNT surface, formation of clusters, and growth of graphene nuclei and the VG sheet on CNT. This model considers the multi-fluid plasma sheath related effects linked to the surface deposition processes along with the kinetics of neutrals, positively charged species, and electrons and rate of charge accumulation on the VG sheet surface. In addition, we report the effects of controlling the total gas pressure, input power, growth time, and substrate bias on the amount and size of the VG sheet grown on the CNT surface. Specifically, we exhibit that variations in gas pressure, input power, and substrate bias affect the plasma characteristics (i.e., number density, temperature, and energy of plasma species), which subsequently alter the carbon generation on the CNT surface and defect sites and influence the density as well as dimensions of VG sheets grown over the CNT surface.

The rest of this paper is structured as follows: In Sec. II, the analytical model, which includes the plasma-sheath related effects, surface deposition processes, defect nucleation on the CNT surface, number density balance equations of charged and neutral species, rate of charge accumulation on the graphene sheet surface, and equation corresponding to the growth rate of the VG sheet grown on the CNT template, is introduced. In Sec. III, the repercussions of change in total gas pressure, input power, and substrate bias on the growth characteristics of VG are presented and discussed. Finally, the conclusion of the present work is given in Sec. IV.

II. ANALYTICAL MODEL

In this section, we present the basic assumptions and equations to describe the nucleation and growth dynamics of the VG sheet on the CNT surface via PECVD route. We consider the hemispherical tip CNT of diameter ($2a_C = 60\,\text{nm}$) and length ($l_C = 1.5\,\mu\text{m}$) as a template for the growth of the graphene sheet in the plasma constituting the ionized gas mixture of CH_4/H_2.[16] Figure 1(a) shows the sketch of CNT erected on a conductive silicon substrate (maintained at negative potential U_s) subjected to plasma of CH_4/H_2 gas mixture. The present model considers the plasma comprising electrons and various positively charged and neutral species of CH_4 and H_2. Table I details the neutral and positively charged species accounted in the model which is representative of experiments on plasma chemistry of the CH_4/H_2 gas mixture.[28] It is known that in a typical plasma-aided growth of the nanostructures, a region of charge separation, i.e., the plasma sheath, is formed between the plasma bulk and plasma-exposed surface, and the microscopic sheath electric force (due to space charge separation) directs the ion acceleration towards the surface.[29] We consider the induced sheath electric field to be in the vertically downward direction, i.e., along the z-axis. The density and speed of the charged species, neutral number density, and sheath structure are investigated using the following plasma sheath equations:[30,31]

$$\frac{d}{dz}(n_{ij}u_{ijz}) = f_{ij}n_e, \tag{1}$$

$$\frac{d}{dz}(n_e u_{ez}) = \sum_j f_{ij}n_e, \tag{2}$$

$$m_{ij}n_{ij}u_{ijz}\frac{du_{ijz}}{dz} = -en_{ij}\frac{d\phi}{dz} - T_{ij}\frac{dn_{ij}}{dz} - m_{ij}n_{ij}f_{ijn}u_{ijz}, \tag{3}$$

$$0 = en_e\frac{d\phi}{dz} - T_e\frac{dn_e}{dz} - m_e n_e f_{en}u_{ez}, \tag{4}$$

where m_{ij}, n_{ij}, T_{ij}, and u_{ijz} are the masses, number densities, temperature, and fluid velocities of the positively charged species, respectively [j corresponds to the 1 and 2 type of positively charged ions (see Table I)]. m_e, n_e, T_e, and u_{ez} are the masses, number densities, temperature, and fluid velocities of electrons, respectively.

Equations (1) and (2) are the continuity equations for ions and electrons, respectively, and account the electron-impact ionization of neutrals with ionization frequency $f_{ij} = \xi_{ij}\eta_{ij}N_n$, where ξ_{ij} is the ionization potential, $\eta_{ij} = \frac{n_{ij}}{n_e}$ or $\frac{p_j}{p_0}$ [here, p_j and $p_0 (= N_n T_i)$ are the pressure of the jth gas and total gas pressure, respectively), and $N_n = \sum_j \eta_j n_j$ corresponds to the total number density of neutral species, where n_j is the number density of the jth neutral. Thus, the ionization rate [i.e., $f_{ij} \propto n_j \exp(-E_{ij}/T_e)$, where E_{ij} is the first ionization potential energy of the jth neutral] rises with both the neutral density and temperatures of electrons. Furthermore, the collisions of ions and electrons with neutrals with collision frequency, $f_{\alpha n} = \sigma_\alpha N_n U_\alpha$ (where α refers to the electrons and j ions, σ_α is the collision cross section, and U_α is the mean speed of the charged species α), have been taken into account in momentum balance equations, i.e., Eqs. (3) and (4), respectively.[30]

Finally, the sheath equations to be solved are completed by Poisson's equation that correlates the number densities of ions and electrons to the electric sheath potential ϕ, as follows:

$$\frac{d^2\phi}{dz^2} = -4\pi e\left(n_e - \sum_j \eta_{ij}n_{ij}\right). \tag{5}$$

The ion energies and fluxes of the ionic and neutral species at the CNT surface are determined by solving the above set of Eqs. (1)–(5) with the following boundary conditions:[30]

$$\phi = 0, \frac{d\phi}{dz} = -\frac{T_e}{e\lambda_i},$$

where $\lambda_i (= T_n/\sigma p_0)$ is the ion mean free path and

$$u_{ez} = 0,\ u_{ijz} = v_{ij0}, \text{where } v_{ij0} = \sqrt{T_e/m_{ij}}.$$

The main processes accounted in the present model for the nucleation and growth of graphene sheets on CNT, using CNT as a starting material in the plasma environment, are shown in Fig. 1. Figure 1(b) shows the preliminary stage in which the defects sites are created on the CNT surface when exposed to the plasma. The applied plasma power dissociates the gases in the chamber, and a range of hydrocarbon and

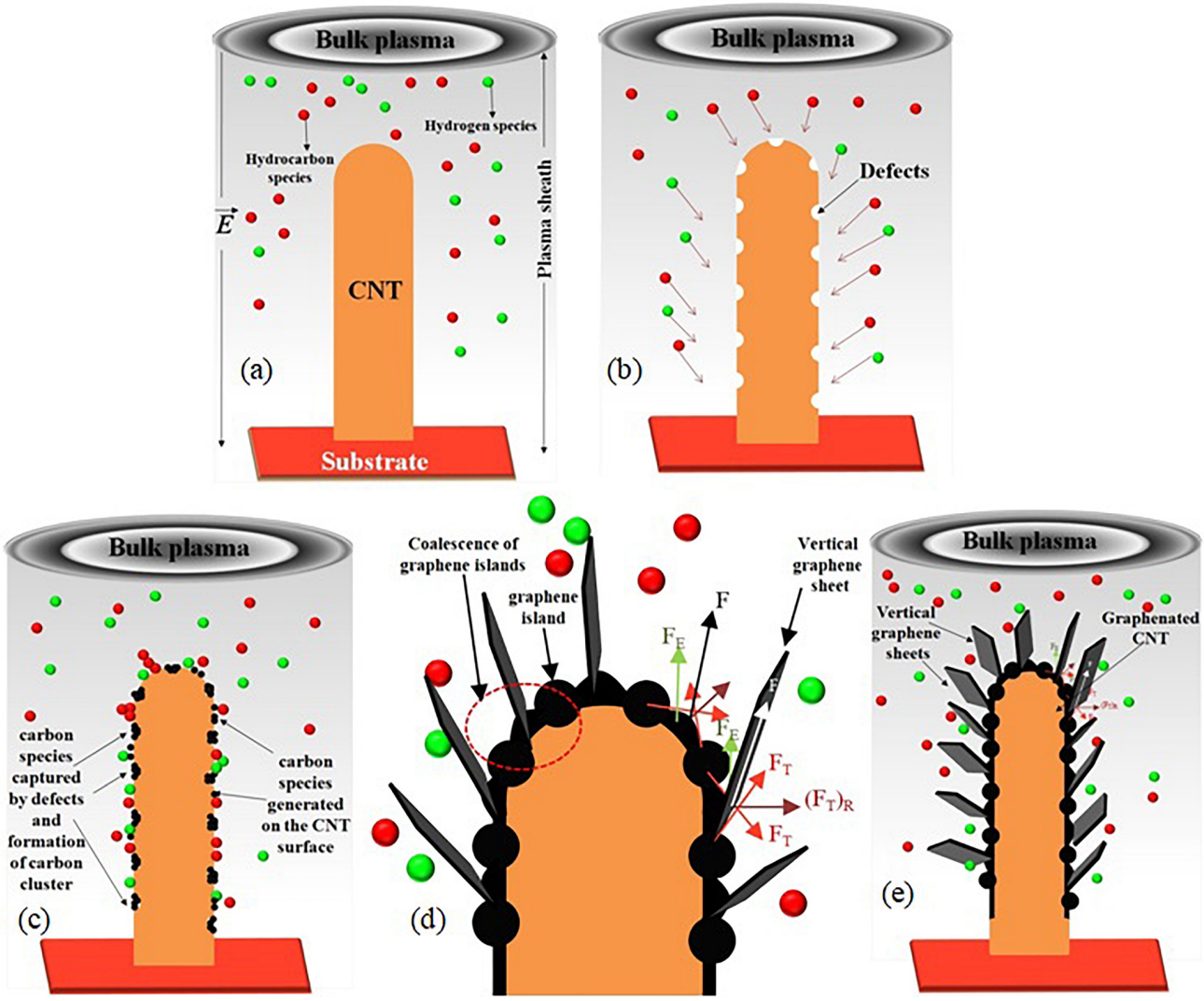

FIG. 1. Schematic showing the (a) charged and neutral species impinging on the CNT surface, (b) formation of defects on the CNT surface, (c) carbon species generation on the CNT surface and formation of C-clusters at the defective sites, (d) amalgamation of GIs and vertical growth of the graphene sheet, and (e) VG sheets growing like plant leaves on the CNT surface.

hydrogen ions are created, which subsequently results in the formation of an electric field near the CNT surface.[32] Under the electric field and applied substrate bias, ions with high enough energy keep bombarding the CNT surface to break some C-C bonds; some get replaced by C-H bonds and thereby create local defects that act as nucleation sites for the growth of two-dimensional graphene sheets on the CNT surface.[17,33] Further, we consider that the growth of graphene sheets on these defective sites proceeds in the same manner as discussed previously in many studies.[3,34,35] The carbon atoms generated on the CNT surface on account of several surface processes get captured by defects present on the CNT surface, which then diffuse and agglomerate to form C (carbon)-clusters [cf. Fig. 1(c)].[34,35] Furthermore, these C-clusters at the defective sites diffuse and collide with each other forming the graphene islands (GIs) and subsequently these GIs amalgamate or stitch with each other to form large GIs or flat graphene sheet with respect to the CNT surface [see Fig. 1(d)].[34,36] During the amalgamation of these GIs, internal tensile force F_T may build-up at the GIs boundaries, which may tend to align the upper edge of these graphitic layers in the direction normal to the CNT surface as shown in Fig. 1(d).[35] The ion bombardment, temperature gradients, and difference in structure and expansion coefficients of amorphous CNT and flat graphene nanosheet are the main sources of internal stress.[3,34] Furthermore, the in-built electric field induced by the plasma sheath also exerts a force (F_E) on these graphitic layers in the direction parallel to the CNT surface [see Fig. 1(d)].[35] Under the action of the resultant (F) of these two forces [i.e., $(F_T)_R$ and F_E] and continuous dissociation and diffusion of hydrocarbon and carbon species, respectively, graphene sheets grow like plant leaves erected on the stem (CNT) [cf. Fig. 1(e)].[18]

TABLE I. Ions and neutral species considered in the model.

Neutrals		Ions	
Type 1	Type 2	Type 1	Type 2
CH_3, CH_4, C_2H_2, C_2H_4	H, H_2	CH_3^+, CH_4^+, $C_2H_2^+$, $C_2H_4^+$	H^+, H_2^+

A. Formation of defects on the CNT surface

Equation (6) describes the rate of energy balance at the surface of CNT placed over the Si-substrate during its interaction with plasma of CH_4 gas diluted in H_2. The power transferred to the CNT surface (i.e., tip and curved surface of CNT) [R.H.S. of Eq. (6)] by incident plasma species, i.e., positively charged ions, neutrals, and electrons (first term), due to formation of neutrals at the CNT surface (second term), etching of the CNT surface by hydrogen (third term), and ion sputtering (fourth term) leads to the CNT surface modification and the formation of defects on the CNT surface. The LHS of Eq. (6) accounts the rate of formation of defects per micron length of the CNT surface. Hydrogen and ion irradiation induced defects on the CNT surface and the introduction of micro-defects on the Si-substrate in the presence of H_2/CH_4 plasma have been reported earlier[37–39]

$$\begin{aligned} P_{in} &= \frac{\partial}{\partial t}(m_C C_C T_s) = \rho_C A_C l_C C_C T_S \frac{1}{n_D}\dot{n_D} \\ &= \left[\sum_j^{1,2}\left[\left[\left(j_{ij}^{C_{tip}} + j_{ij}^{C_{cur}}\right)\varepsilon_{ij}^C\right] + \left[\left(j_j^{C_{tip}} + j_j^{C_{cur}}\right)\varepsilon_j^C\right]\right]\right. \\ &\quad \left. + \left(j_e^{C_{tip}} + j_e^{C_{cur}}\right)\varepsilon_e^C\right] + \left[\frac{3}{2}k_B T_S \sum_j^{1,2}(1-\gamma_{ij})\left(j_{ij}^{C_{tip}} + j_{ij}^{C_{cur}}\right)\right] \\ &\quad + [(\upsilon_0 \sigma_{ads} J_2 U_b) A_C] + \left[\left(\sum_j^{1,2} J_{ij} y_s(E_i)(1-\theta_t)\right) A_C\right], \end{aligned} \tag{6}$$

where m_C, $A_C(= 2\pi a_C^2 + 2\pi a_C l_C)$, C_C, and ρ_C are the mass, area, specific heat, and density of CNT, respectively. n_D is the number of defects produced per micron length of the CNT surface and T_S is the CNT surface temperature (T_s is assumed to be uniform along the CNT). During the plasma-surface interaction, the CNT surface gets heated up and attains a constant temperature T_s.[40] $J_j\left(= \frac{n_j v_{thj}}{4}\right)$ and $J_{ij}\left(= n_{ij}\left(\frac{k_B T_e}{m_{ij}}\right)^{\frac{1}{2}}\right)$ are the fluxes of impinging neutral and positively charged species of type j, respectively (subscript j refers to species of type 1or 2).[25,30] $\varepsilon_\alpha^C[= ((\frac{2-Z\xi_\alpha}{1-Z\xi_\alpha}) - Z\xi_\alpha)k_B T_\alpha]$ refers to the mean energies collected by the CNT surface due to α species (subscript α refers to electrons, ions, and neutrals of type j; j refers to species of type 1or 2), where $\xi_\alpha = \frac{E_b}{k_B T_\alpha}$ and E_b is the energy barrier at the CNT surface.[41] $J_{ij}^{C_{tip}}[= \pi a_C{}^2 \left(\frac{8k_B T_{ij}}{\pi m_{ij}}\right)^{\frac{1}{2}} n_{ij}(x)[1 - Z\gamma_i]\ (\exp[-\frac{eU_s}{k_B T_s}])]$ and $j_{ij}^{C_{cur}}[= n_{ij}(x) a_C l_C \left(\frac{2\pi k_B T_{ij}}{m_{ij}}\right)^{\frac{1}{2}}\left\{\frac{2}{\sqrt{\pi}}\left(\frac{eV_s}{k_B T_{ij}}\right)^{\frac{1}{2}} + \exp\left[\frac{eV_s}{k_B T_{ij}}\right] erfc\left[\left(\frac{eV_s}{k_B T_{ij}}\right)^{\frac{1}{2}}\right]\right\} \exp\left[-\frac{eU_s}{k_B T_s}\right]]$ are the collection currents at the CNT tip and curved surface, respectively, due to positively charged species of type j;[42] Z is the charge number over the CNT surface,[43] $n_{ij}(x) = n_{ij0}\left(1 - \frac{2e\phi(x)}{m_{ij} v_{ij0}^2}\right)^{\frac{-1}{2}}$ is the density of positively charged species as a function of spatial coordinate within the plasma sheath; v_{ij0} is the velocity of positively charged species, $\phi(x) = \phi_0 \exp\left(-\frac{|x|}{\lambda_d}\right)$ is the plasma sheath potential as a function of spatial coordinate; ϕ_0 is the negative bias applied at the substrate surface, $\lambda_d\left(= \sqrt{\frac{k_B T_e}{n_e e^2}}\right)$ is the Debye length, and $\gamma_i = eV_{tip}(z)$; $V_{tip}(z)\left(= \frac{e}{2\sqrt{2}\pi\varepsilon_0 a_C}\right)$ is the potential at the hemispherical tip of the CNT (evaluated using Ref. 42), T_{ij} and m_{ij} are the temperature and mass of the positively charged species of type j, respectively, and V_s is the potential at the CNT curved surface. $\gamma_{ij}(\simeq 1)$ is the sticking coefficient of positively charged species, $j_e^{C_{tip}}[= \pi a_C^2 \left(\frac{8k_B T_e}{\pi m_e}\right)^{\frac{1}{2}} n_e(x) \exp\left[\frac{Z\gamma_i}{k_B T_e} + \frac{eU_s}{k_B T_s}\right]]$ and $j_e^{C_{cur}}[= n_e(x) a_C l_C \left(\frac{2\pi k_B T_e}{m_e}\right)^{\frac{1}{2}} \exp\left[\frac{eV_s}{k_B T_e} + \frac{eU_s}{k_B T_s}\right]]$ are the electron collection current at the CNT tip and curved surface, respectively; $n_e(x) = n_{e0} \exp\left[\frac{|e|\phi(x)}{k_B T_e}\right]$ is the electron density as a function of spatial coordinate within the plasma sheath, $j_j^{C_{tip}} = n_j(x)\pi a_c^2 \left(\frac{8k_B T_j}{\pi m_j}\right)^{\frac{1}{2}}$ and $j_j^{C_{cur}} = n_j(x)\pi a_c l_c \left(\frac{2\pi k_B T_j}{m_j}\right)^{\frac{1}{2}}$ are the collection currents at the tip and curved surface of CNT, respectively, due to neutral species of type j,[43] $\upsilon_0(\approx 10^{15}\text{cm}^{-2})$ is the number of adsorption sites per unit area, $\sigma_{ads}(\approx 10^{-16}\text{cm}^2)$ is the cross-section of the reactions with atomic hydrogen,[29] y_s is the sputtering yield which is dependent on ion energy,[44] U_b is the surface binding energy of carbon in CNT, and θ_t is the total surface coverage.[29]

Using Eq. (6), we estimated the linear density of defects generated on the CNT surface upon interaction with CH_4/H_2 plasma, and using mass conservation, the size of the resulting defects is estimated to be $r_D = \frac{a_C\left(1 + \frac{a_C}{l_C}\right)}{2n_D}$.

B. Generation of hydrogen radicals and carbon species

The incoming fluxes of neutrals and ions of types 1 and 2 interact with the CNT surface and contribute to the generation of hydrogen radicals and carbon species on the CNT surface via various surface processes, which have been accounted in the underneath equations

$$\begin{aligned} \dot{N_H} &= \sum_2 J_2(1-\theta_t) + \sum_1 n_{S1}\upsilon \exp\left(\frac{-\delta E_{td}}{k_B T_S}\right) \\ &\quad + \sum_{i1}\left(\sum_1 \frac{n_{S1} y_d}{\upsilon_0}\right) J_{i1} + \sum_{i1} J_{i1} - \sum_2 n_{S2}\upsilon \exp\left(\frac{-\delta E_{aH}}{k_B T_S}\right) \\ &\quad - \sum_2 n_{S2}\sigma_{ads} J_2 - \sum_{i2}\left(\sum_2 n_{S2}\sigma_{ads}\right) J_{i2}, \end{aligned} \tag{7}$$

$$\begin{aligned} \dot{N_c} &= \sum_1 J_1(1-\theta_t) + \sum_1 n_{S1}\upsilon \exp\left(\frac{-\delta E_{td}}{k_B T_S}\right) \\ &\quad + \sum_{i1}\left(\sum_1 \frac{n_{S1} y_d}{\upsilon_0}\right) J_{i1} + \sum_{i1} J_{i1} \\ &\quad + \sum_{i2}\left(\sum_{i1} \frac{J_{i1}\sigma_{ads}}{\upsilon}\right) J_{i2} - \sum_1 n_{S1}\upsilon \exp\left(\frac{-E_{ads}}{k_B T_S}\right) \\ &\quad - \sum_2\left(\sum_1 n_{S1}\sigma_{ads}\right) J_2 - N_c\upsilon \exp\left(\frac{-E_{ev}}{k_B T_S}\right), \end{aligned} \tag{8}$$

where N_H and N_c are the surface concentrations of hydrogen radicals and carbon species generated on the CNT surface, respectively. The other symbols and terms used in Eqs. (7) and (8) are explained in Tables II and III, respectively.

TABLE II. Explanation for the symbols used in Eqs. (7) and (8).

Symbols	Explanation
$n_{Sj}(=\theta_j \upsilon_0)$	Surface concentration of neutral species of type j[29]
θ_j	Surface coverage by species of type j[29]
$\upsilon(\approx 10^{13}\,\text{Hz})$	Thermal vibration frequency[29]
$y_d(\approx 2.49\times10^{-2}+3.29\times10^{-2}\times E_i)$	Stitching probability[44]
E_i	Ion energy in eV
$\delta E_{td}(=2.1\,\text{eV})$	Thermal dissociation energy of hydrocarbons[31]
$E_{ads}(=1.8\,\text{eV})$	Adsorption energy of hydrocarbons[31]
$\delta E_{aH}(=1.8\,\text{eV})$	Adsorption energy of hydrogen species[31]
$E_{ev}(=1.8\,\text{eV})$	Carbon evaporation energy[31]

C. Growth rate equation of graphene nuclei/island

The carbon species generated on the CNT surface get captured by defects, which then diffuse and agglomerate to form C-clusters, and further these C-clusters diffuse and collide, forming the graphene nuclei/island. These GIs then grow in size due to diffusion and coalescence among them.[34,36] The growth rate of the graphene nuclei/island is expressed in velocity units (nm/s) in the following equation:

$$\dot{r_{gn}} = \left[N_c\left[D\exp\left(\frac{-(E_{sdc}+E_{inc})}{k_BT_s}\right) + D'\exp\left(\frac{-(E_{sdcl}+E_{incl})}{k_BT_s}\right) + D''\exp\left(\frac{-(E_{sdgn})}{k_BT_s}\right)\right]\right] \times\left[\left(\frac{A_d}{A_{gn}}\right)\times\left(\frac{2\pi r_d\times j_{i1}^{gn}}{\upsilon}\right)\right] + \gamma_1(2\pi r_{gn})j_1^{gn}, \tag{9}$$

TABLE III. Explanation for the functional terms used in Eqs. (7) and (8).

Functional terms	Explanation
$J_2(1-\theta_t)$	Adsorption of neutral hydrogen
$n_{S1}\upsilon\exp\left(\frac{-\delta E_{td}}{k_BT_S}\right)$	Thermal dissociation of adsorbed hydrocarbon species
$\frac{n_{S1}y_d}{\upsilon_0}J_{i1}$	Ion-induced dissociation of adsorbed hydrocarbon species
J_{i1}	Decomposition of hydrocarbon ions
$n_{S2}\upsilon\exp\left(\frac{-\delta E_{aH}}{k_BT_S}\right)$	Desorption of hydrogen radicals
$n_{S2}\sigma_{ads}J_2$	Loss of adsorbed hydrogen species due to the interaction with the hydrogen atom from the plasma
$n_{S2}\sigma_{ads}J_{i2}$	Loss of adsorbed hydrogen species due to the interaction with hydrogen ions from the plasma
$\frac{J_{i1}\sigma_{ads}}{\upsilon}J_{i2}$	Carbon generation due to reaction between hydrocarbon and hydrogen ion
$n_{S1}\upsilon\exp\left(\frac{-E_{ads}}{k_BT_S}\right)$	Desorption of hydrocarbon species
$n_{S1}\sigma_{ads}J_2$	Loss of adsorbed hydrocarbon species due to the interaction with hydrogen atom from the plasma
$N_c\upsilon\exp\left(\frac{-E_{ev}}{k_BT_S}\right)$	Evaporation of carbon

where r_{gn} and $A_{gn}(=\pi r_{gn}^2)$ are the radius and area of the graphene nuclei/island, respectively. A_d $(=\pi r_D^2)$ is the area of the defect at the CNT surface. j_{i1}^{gn} and j_1^{gn} are the collection currents due to ions and neutrals of type 1 at the growing GI, respectively.[25] $\gamma_1(\approx 1)$ is the sticking coefficient of neutral hydrocarbon species. $E_{sdC}\approx 0.1\,\text{eV}$, $E_{inc}\approx 0.85\,\text{eV}$, $E_{sdCl}\approx 0.82\,\text{eV}$, $E_{incl}\approx 0.85$, and $E_{sdIs}\approx 2.6\,\text{eV}$ are the energy barriers for surface diffusion and incorporation of carbon atoms, surface diffusion and incorporation of C-clusters, and diffusion of GIs, respectively.[36]

Equation (9) traces the growth of GI owing to the surface diffusion and incorporation of carbon monomers and C-clusters into the defective sites at the CNT surface (first and second terms) and due to diffusion or amalgamation of GIs (third term).[36] Furthermore, the factors j_1^{gn} and j_{i1}^{gn} account the accretion of neutral atoms and ion collection current of type 1 species at the surface of the growing GIs.

D. Growth of vertical graphene sheet over CNT

The amalgamation or stitching of GIs leads to the formation of planar graphitic layers or flat graphene on the CNT surface, and consequently, tensile force is build-up at the GIs boundaries due to the difference in the structure and expansion coefficients of amorphous CNT and flat graphene sheets, which then trigger the growth of the VG sheet[34]

$$l_g\frac{d}{d\tau}[(t_g\times h_g)] = \left[\left(\frac{N_c}{\upsilon}\times D\exp\left(-\frac{(E_{sdc}+E_{inc})}{k_BT_s}\right)\times(A_{gn}\times 2\pi r_d)\times j_{i1}^g + \left(\gamma_1 j_1^g\right)\right) + \left(\left(\gamma_{i2}j_{i2}^g+\gamma_2 j_2^g\right)N_H h_g(\tau)\right)\right]\times\left(\frac{m_g}{\rho_g}\right), \tag{10}$$

where l_g, h_g, t_g, $m_g(\approx 12g)$, and ρ_g are the length, height, thickness, mass, and density of the graphene sheet, respectively. $j_j^g = n_j(l_gt_g + h_gt_g + l_gh_g)\left(\frac{k_BT_n}{2\pi^2m_j}\right)^{\frac{1}{2}}$ and $j_{ij}^g = n_{ij}(x)(l_gt_g + h_gt_g + l_gh_g)\left(\frac{k_BT_{ij}}{2\pi^2m_{ij}}\right)^{\frac{1}{2}}\left\{\frac{2}{\sqrt{\pi}}\left(\frac{eV_{gs}}{k_BT_i}\right)^{\frac{1}{2}} + \exp\left[\frac{eV_{gs}}{k_BT_{ij}}\right]erfc\left[\left(\frac{eV_{gs}}{k_BT_{ij}}\right)^{\frac{1}{2}}\right]\right\}\times\exp\left[-\frac{eU_s}{k_BT_s}\right]$ are the collection currents at the surface of graphene sheet due to neutral and positively charged species, respectively,[25] and V_{gs} is the potential at the graphene sheet surface.[25]

Equation (10) accounts the processes responsible for the VG sheet growth over the CNT surface. The first term on the R.H.S. of Eq. (10) represents the increase in the area of the VG sheet due to diffusion and attachment of carbon atoms at the borders of the growing VG sheet. In addition, under the influence of the in-built electric field and substrate bias, the VG sheet grows due to ion collection current and sticking of neutrals at the GIs boundaries and VG sheet surface. Finally, the VG sheet growth terminates due to etching of terminal carbons present at the edges of the VG sheet by hydrogen. The last term on the R.H.S. of Eq. (10) represents the accumulation of positively charged and neutral species of type 2 on the VG sheet surface.

E. Charge developed over the graphene sheet surface

$$\dot{Q} = \sum_{1} j_{i1}^{g} + \sum_{2} j_{i2}^{g} - \gamma_e j_e^{g}, \tag{11}$$

where Q is the charge number over the graphene sheet surface, $j_e^g = \left(\frac{k_B T_e}{2\pi^2 m_e}\right)^{\frac{1}{2}} n_e(x)(l_g t_g + h_g t_g + l_g h_g)\exp\left[\frac{eV_{gs}}{k_B T_e} + \frac{eU_s}{k_B T_s}\right]$ is the collection current at the graphene sheet surface due to electrons,[25] and $\gamma_e(=1)$ is the electron sticking coefficient.

Equation (11) accounts the charge build-up over the graphene sheet surface due to accretion of positively charged species (first and second terms). The last term signifies the decay rate of charge because of accumulation of electrons at the graphene sheet surface.

F. Number density balance equations of plasma species

$$\dot{n_e} = \sum_{j=1}^{2} \beta_j n_j - \sum_{j=1}^{2} \alpha_j n_e n_{ij} - \frac{\gamma_e}{\lambda_d}\left(\eta_g j_e^g + \eta_C\left(j_e^{C_{tip}} + j_e^{C_{cur}}\right)\right), \tag{12}$$

$$\dot{n_{i1}} = \beta_1 n_1 - \alpha_1 n_e n_{i1} - \frac{1}{\lambda_d}\left(\eta_g j_{i1}^g + \eta_C\left(j_{i1}^{C_{tip}} + j_{i1}^{C_{cur}}\right)\right) + \sum_{l12} k_l n_1 n_{i2} + \frac{P_{in}}{E_{dis1} V}, \tag{13}$$

$$\dot{n_{i2}} = \beta_2 n_2 - \alpha_2 n_e n_{i2} - \frac{1}{\lambda_d}\left(\eta_g j_{i2}^g + \eta_C\left(j_{i2}^{C_{tip}} + j_{i2}^{C_{cur}}\right)\right) - \sum_{l12} k_l n_1 n_{i2} + \frac{P_{in}}{E_{dis2} V}, \tag{14}$$

$$\dot{n_1} = \alpha_1 n_e n_{i1} - \beta_1 n_1 + \frac{(1-\gamma_{i1})}{\lambda_d}\left(\eta_g j_{i1}^g + \eta_C\left(j_{i1}^{C_{tip}} + j_{i1}^{C_{cur}}\right)\right) - \frac{\gamma_1}{\lambda_d}\left(\eta_g j_1^g + \eta_C\left(j_1^{C_{tip}} + j_1^{C_{cur}}\right)\right) - J_{ad1} + J_{des1} - \sum_{l12} k_l n_1 n_{i2}, \tag{15}$$

$$\dot{n_2} = \alpha_2 n_e n_{i2} - \beta_2 n_2 + \frac{(1-\gamma_{i2})}{\lambda_d}\left(\eta_g j_{i2}^g + \eta_C\left(j_{i2}^{C_{tip}} + j_{i2}^{C_{cur}}\right)\right) - \frac{\gamma_2}{\lambda_d}\left(\eta_g j_2^g + \eta_C\left(j_2^{C_{tip}} + j_2^{C_{cur}}\right)\right) - J_{ad2} + J_{des2} + J_{th} - \sum_{l12} k_l n_1 n_{i2}, \tag{16}$$

where β_j is the ionization coefficient of the neutral species, $\alpha_j(T_e) = \alpha_{j0}\left(\frac{300}{T_e}\right)^k \text{cm}^3/\text{s}$ is the coefficient of recombination of electrons and positively charged species, $\alpha_{10} \approx \alpha_{20}(=1.12 \times 10^{-7}\ \text{cm}^3/\text{s})$, $k(=-1.2)$ is a constant,[41] J_{adj} and J_{desj} are the adsorption and desorption flux of type j species onto/from the CNT surface, J_{th} is the flux of etching species (i.e., hydrogen) due to thermal dehydrogenation,[25] E_{disj} is the dissociation energy of the jth neutral, V is the volume of the plasma chamber, and k_l is the rate coefficient of ion-neutral reaction, which have been accounted from Ref. 28.

Equation (12) indicates the growth of electron density per unit time in plasma. The first term on the R.H.S. of Eq. (12) signifies the rate of increase in electron density due to ionization of neutral species. The last two terms indicate the rate of decay in electron density on account of recombination of electrons and positively charged species and electron collection current at the graphenated CNT surface, respectively.

Equations (13) and (14) describe the balance of positively charged species of types 1 and 2, respectively, in the plasma because of the ionization of neutral species (first term), recombination of the electrons and positively charged species (second term), collection current at the graphenated CNT surface due to positively charged species (third term), ion-neutral reactions (fourth term), and due to the dissociation by applied input power.

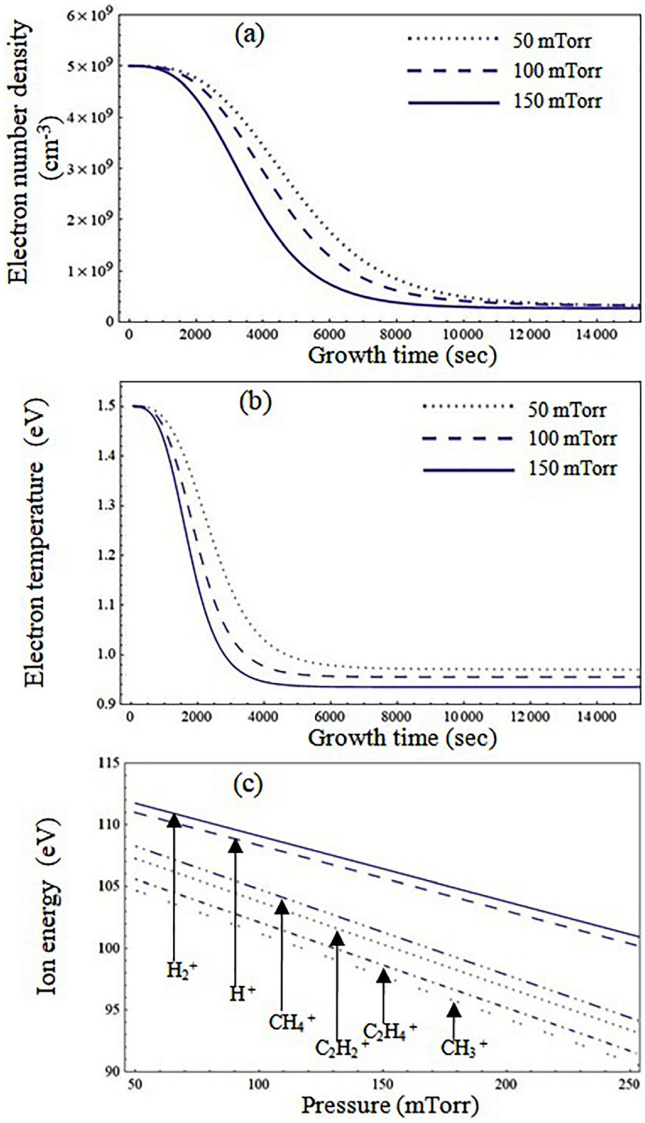

FIG. 2. Variations of (a) electron density as a function of time, (b) electron temperature as a function of time, and (c) ion energy for different values of the total gas pressure at fixed P_{in} = 300 W and U_s = −50 V. The other parameters are given in the text.

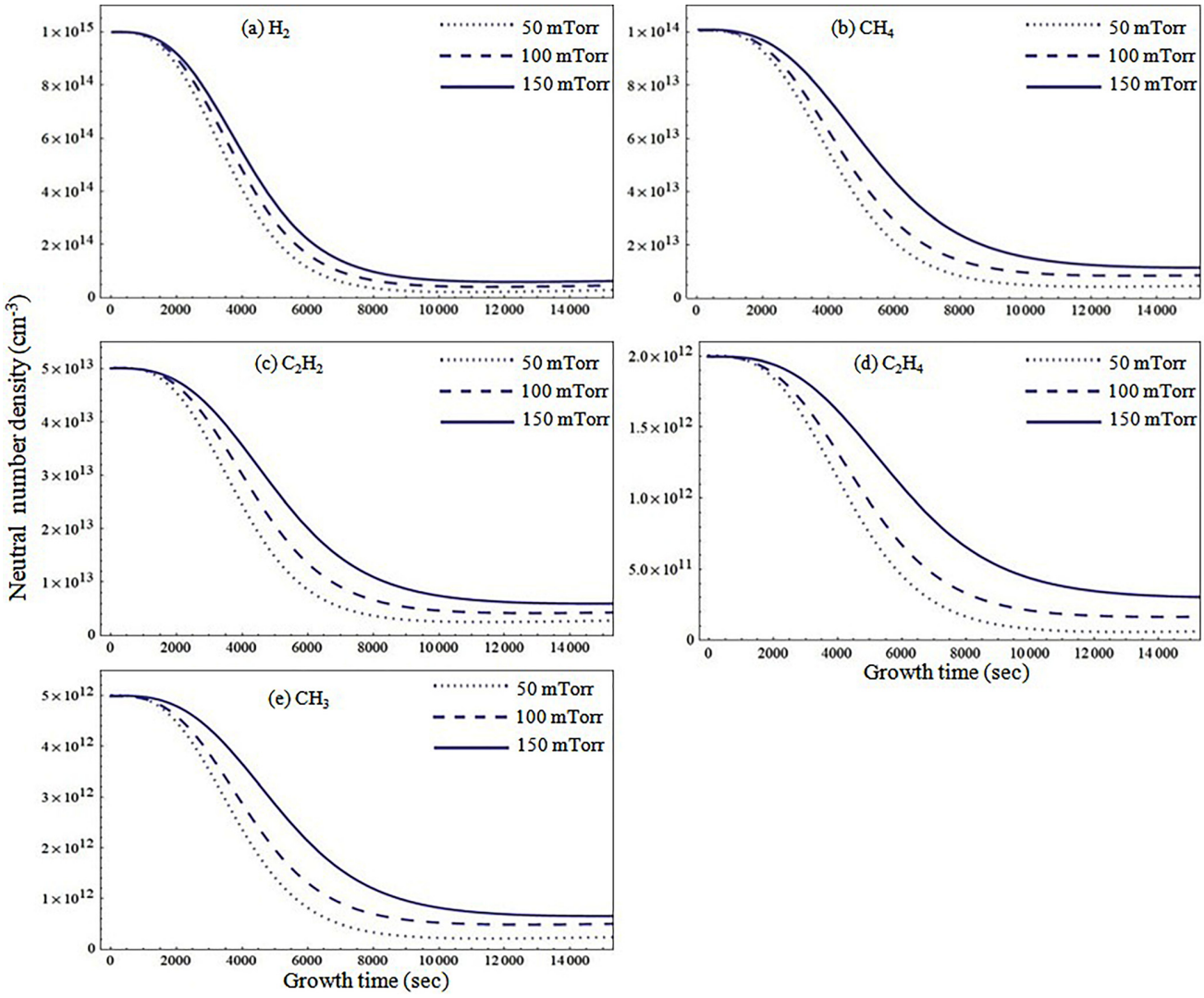

FIG. 3. Time variations of different neutral species in plasma for different gas pressures at fixed $P_{in} = 300$ W and $U_s = -50$ V. The other parameters are given in the text.

Equations (15) and (16) describe the balance of neutral atoms of types 1 and 2, respectively, in the plasma on account of the recombination of electrons and positively charged species (first term), ionization of neutral species (second term), neutralization of ions collected at the graphenated CNT surface (third term), accumulation and adsorption of neutral species at the graphenated CNT surface (fourth and fifth terms), desorption of neutrals from the graphenated CNT surface (sixth term), and reactions between neutral and positively charged species (last term).

III. RESULTS AND DISCUSSION

In the present work, a multiscale analytical model comprising the plasma sheath formalization linked with the kinetics of the plasma species and surface deposition processes has been invoked to elucidate the evolution of size and density of VG sheets on the CNT substrate during PECVD growth involving the rapid variation of plasma operational parameters. The analytical model Eqs. (1)–(16) presented in Sec. II are solved simultaneously using MATHEMATICA software, and their numerical solutions are used to investigate the effect of variation in total gas pressure, input power, and substrate bias on the plasma composition and characteristics that in turn control the amount and size of VG on the pre-grown CNT surface. The default set of parameters used for the calculation are electron number density $n_{e0}(=0.5 \times 10^{10}$ cm$^{-3})$, electron temperature $T_{e0}(= 1.5$ eV), ion temperature T_{i0} $(= 0.05$ eV), neutral temperature T_{n0} $(= 0.05$ eV), total gas pressure p_0 $(= 50$ mTorr), substrate temperature T_s $(= 630$ K), mass of the neutral atom of type 1 m_1 $[= (12 \times x) + (1 \times y)$ a.m.u. for $C_xH_y]$, mass of the neutral atom of type 2 m_2 $[= (1 \times x)$ a.m.u. for $H_x]$, mass of the ion of type 1 m_{i1} $[= (12 \times x) + (1 \times y)$ a.m.u. for $C_xH_y^+]$, mass of the ion of type 2 m_{i2} $[= (1 \times x)$ a.m.u. for $H_x^+]$, and chamber volume $V = 1.05 \times 10^4$ cm^{-3}. From the study by Mao and Bogaerts,[28] it can be found that for the CH_4/H_2 gas mixture, neutral atom number density $n_{10}(= 1 \times 10^{14}, 5 \times 10^{12}, 5 \times 10^{13}$, and 1.5×10^{12} for CH_4, CH_3, C_2H_2, and C_2H_4, respectively), $n_{20}(= 7 \times 10^{13}$ and 1×10^{15} for H and H_2, respectively), ion number density, $n_{i10}(= 5 \times 10^8, 4 \times 10^8, 4 \times 10^9$, and 6×10^8 for

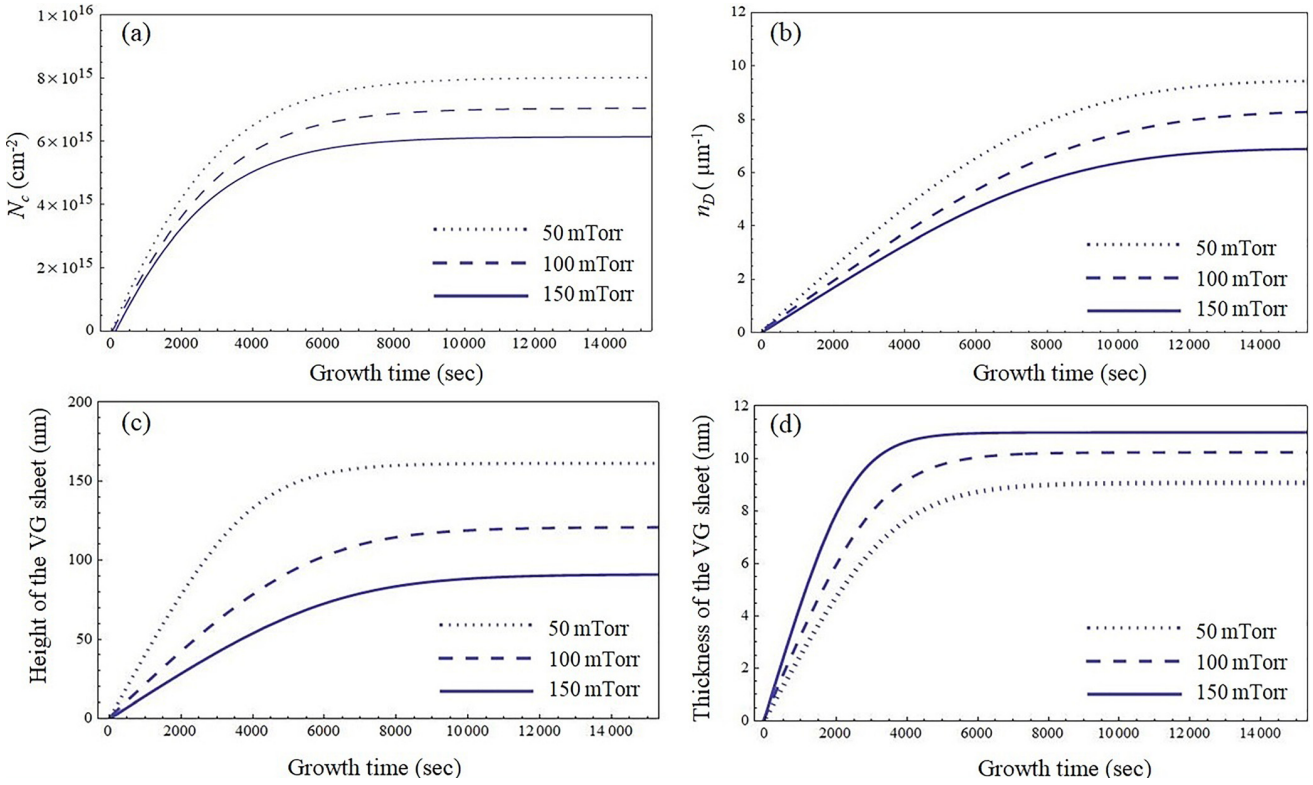

FIG. 4. Time variations of the (a) number of carbon species generated per unit area on the CNT surface, (b) number density of defects generated per unit micron length of the CNT surface, (c) height of the VG sheet, and (d) thickness of the VG sheet for different gas pressures at fixed $P_{in} = 300$ W and $U_s = -50$ V. The other parameters are given in the text.

$CH_4^+, CH_3^+, C_2H_2^+$, and $C_2H_4^+$, respectively), and $n_{i20}(=7 \times 10^7$ and 8×10^7 for H^+ and H_2^+, respectively).

In order to study the effects of variation of total gas pressure on the VG sheet growth characteristics (e.g., nucleation density of the VG sheet on the CNT surface, height, and thickness of VG sheet protruded from the CNT surface), we first explore the influence of variation of p_0 (at fixed input power and substrate bias) on plasma parameters and composition, such as electron density, electron temperature, number densities of neutrals, and energy of ions.

Figures 2(a) and 2(b) show the temporal variations of electron density and electron temperature for different total gas pressures (i.e., $p_0 = 50$ mTorr, 100 mTorr, and 150 mTorr). It can be seen from Figs. 2(a) and 2(b) that electron density and electron temperature decrease with time and get significantly reduced with increasing p_0 at a fixed input power of 300 W and a substrate bias of −50 V, respectively. These results can be explained on the fact that the pressure increase is accompanied by the decrease in the mean free path due to which there are more collisions between electrons and other neutral species in the chamber which subsequently makes the electrons to lose their energy faster and results in reduced electron temperature and electron density. The effect of variation of electron density and electron temperature with pressure is in agreement with the works of Mao and Bogaerts[28] and Shivkumar *et al.*[45] for CH_4/H_2 and H_2 plasma, respectively. The variations of electron density and electron temperature with time are in agreement with the observations of Harilal *et al.*[46] In addition, the reduction in electron temperature and sheath width with p_0 results in the decrease in velocity (i.e., Bohm velocity) and kinetic energy of ions (i.e., E_i) impinging on the CNT surface.[47] The effect of increasing p_0 on the energy of ions is shown in Fig. 2(c).

Since electrons lose their energy faster at high pressures, the dissociation rate of neutrals in plasma is low. However, with increasing pressure at fixed rf power and substrate bias, the decreasing plasma energy was sufficient to dissociate hydrogen molecules but unable to dissociate increasing hydrocarbon molecules.[4] The comparable effect can be seen from Fig. 3, which specifies that the decay rate of hydrogen species in plasma is higher than the hydrocarbon species accounted in the model. Therefore, on increasing pressure, the density ratio of hydrogen to carbon atoms in plasma increases, which in turn leads to augmentation in the hydrogen radical flux onto the CNT surface. This result is in accordance with the study conducted by Takeuchi *et al.*[48] to measure the influence of operating pressure on hydrogen and carbon atom densities in plasmas employing the C_2F_6/H_2 gas mixture. They reported that the hydrogen to carbon atom densities in plasma increases on increasing gas pressure.

Moreover, at low pressures, the plasma sheath becomes wider, as a result of which a very strong electric field is generated which quickly drives the energetic ions towards the substrate. These energetic ions enhance the ion-induced dissociation and ion decomposition processes on the CNT surface (at low substrate temperature, i.e., $T_s < 800$ K),[29] which results in the enhancement of N_c (i.e., number of carbon species generated per unit area on the CNT surface). This effect

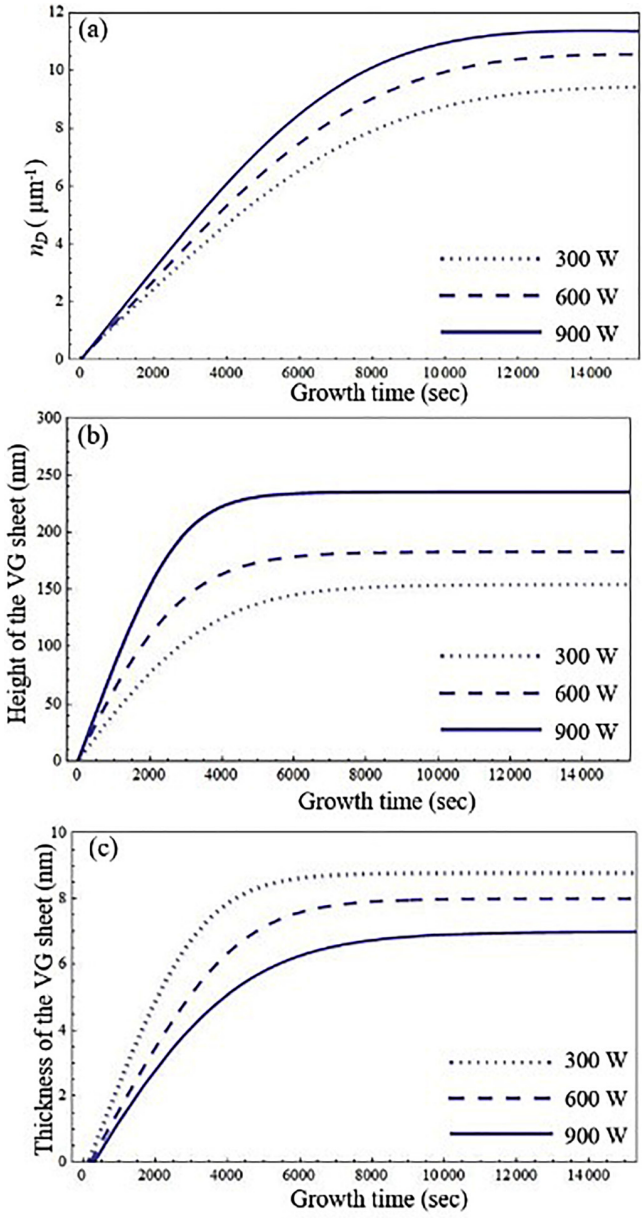

FIG. 5. Time variations of the (a) linear density of defects generated on the CNT surface, (b) height of the VG sheet, and (c) thickness of the VG sheet for different input powers at fixed $p_0 = 50$ mTorr and $U_s = -50$ V. The other parameters are given in the text.

can be seen from Fig. 4(a) which illustrates that the surface concentration of carbon species on the CNT surface increases upon reducing the total gas pressure. Also, the interaction of adsorbed hydrocarbon species with hydrogen atoms from the sheath is reduced at relatively low pressures because the hydrogen atom density in plasma is substantially low at reduced gas pressures (cf. Fig. 3). All these changes result in the excessive supply of carbon on the CNT surface. Thus, we estimate that increased ion energy at relatively low pressures results in amorphous carbon deposition on the CNT surface with increased defect density.

Figure 4(b) shows the time-evolution of the defect number density on the CNT surface for different total gas pressures (i.e., $p_0 = 50$ mTorr, 100 mTorr, and 150 mTorr). It can be seen from Fig. 2 that at relatively low pressure, i.e., at $p_0 = 50$ mTorr, the defect generation on the CNT surface is the highest. This is evidence of the fact that the energy of ions impinging on the CNT surface is high at low pressures [cf. Fig. 2(c)] and thus dislocates C-atoms from their original positions. As discussed previously in Sec. II, the graphene sheet nucleation on the CNT surface is defect guided; we conjecture that the availability of more carbon atoms on the CNT surface at relatively low pressures increases the cluster formation on the increased defect sites generated on the CNT surface. Subsequently, the diffusion and agglomeration of these clusters lead to the formation of large GIs with increased number density, and therefore, we depict that the number density of VG sheets increases on reducing the gas pressure. The increased densities of defects, as well as VG sheet density on the CNT surface on decreasing the total gas pressure, have also been reported by Qi *et al.*[16] [cf. Figs. 2(c)–2(f) of Qi *et al.*[16]]. In addition, Cho *et al.*[49] [cf. Fig. 2(a) of Cho *et al.*[49]] and Takeuchi *et al.*[48] have also observed that the number density of carbon nanowalls grown on the Si substrate decreases with increasing pressure.

Furthermore, on decreasing the gas pressure, the diffusion of high energy carbon radicals generated due to the interaction of high energy hydrocarbon ions and adsorbed hydrocarbon radicals occurs rapidly.[50] Due to the availability of high N_c and their faster diffusion and attachment at the growing VG sheet edges, the height of the VG sheet increases at reduced gas pressures. The effect of variation of pressure on the height (h_g) of the VG sheet grown on CNT is shown in Fig. 4(c). Moreover, Fig. 4(d) shows that the thickness (t_g) of the VG sheet is low at reduced gas pressures. This is because the etching effect due to high energy ion bombardment is prominent at low pressures. The similar effect of pressure on thickness of the VG sheet has also been reported by Wang *et al.*[50] The results illustrated in Fig. 4(c) are in compliance with the experimental works of Cho *et al.*[49] [cf. Fig. 2(a) of Cho *et al.*[49]] and Takeuchi *et al.*[48] [cf. Fig. 7(a) of Takeuchi *et al.*[48]].

Figure 5 shows temporal evolution of the linear defect density, height, and thickness of the VG sheet on the CNT surface for different input powers (i.e., P_{in}=300W, 600 W, and 900 W) at constant gas pressure, $p_0 = 50$ mTorr, and substrate bias, $U_s = -50$ V. It can be seen from Fig. 5 that n_D, i.e., the linear density of defects (number of defects produced per unit micron length of the CNT) on the CNT surface and height (h_g) of the VG sheet protruded from the CNT increases with P_{in}, while the thickness of the VG sheet is reduced with P_{in}.

When the input power is raised at constant pressure and substrate bias, the electric field as well as ionization of gases inside the chamber increases; as a result, the electron density, electron temperature, and energy of ions in the plasma sheath increase [cf. Figs. 6(a)–6(c)], and consequently, the ion decomposition and ion-induced decomposition processes on the CNT surface (at low substrate temperature) are expected to get enhanced, which in turn lead to plentiful generation of carbon on the CNT surface [cf. Fig. 6(d)]. Thus, at high input power, the high energy ion bombardment on the CNT surface results in amorphous carbon deposition with increased defect density. The high N_c on the CNT surface at high input

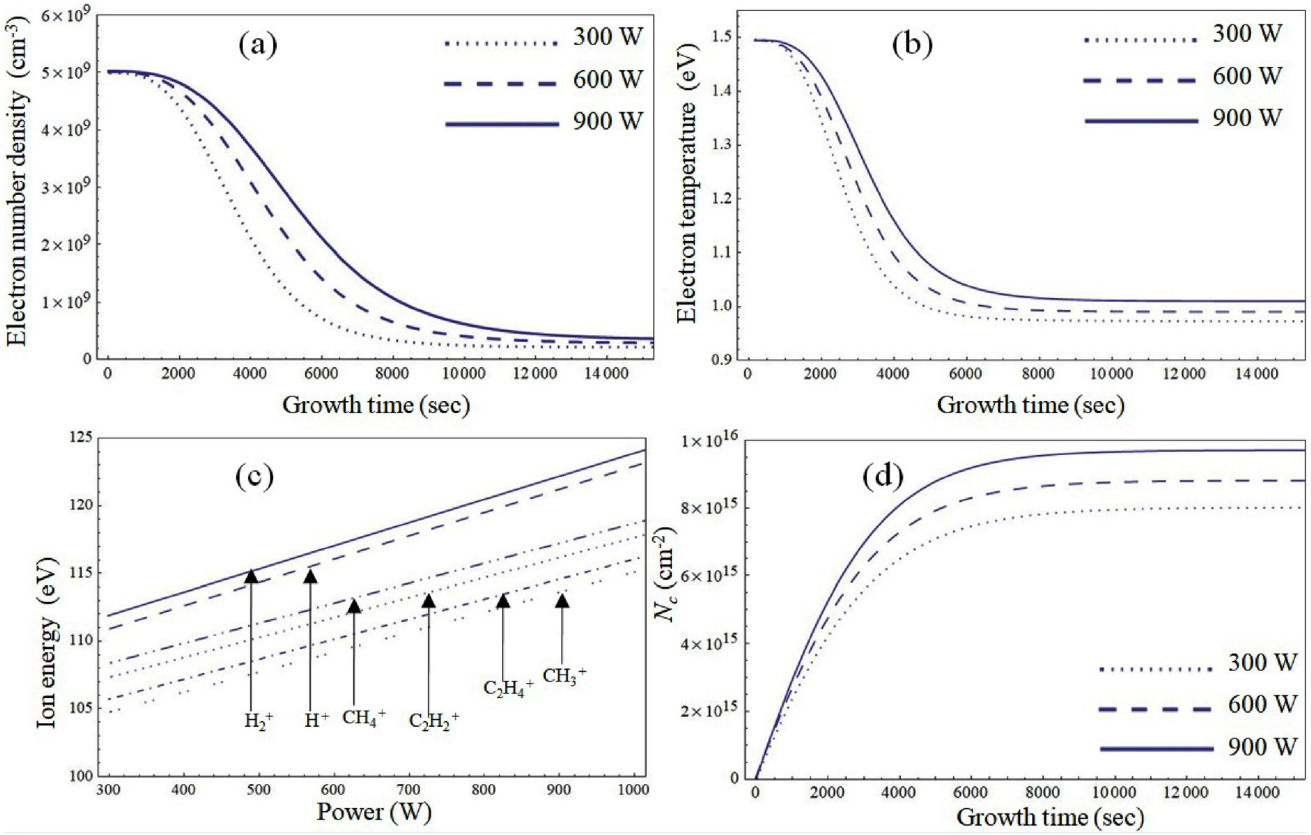

FIG. 6. Variations of (a) electron density as a function of time, (b) electron temperature as a function of time, (c) ion energy, and (d) number of carbon species generated per unit area on the CNT surface as a function of time for different values of input power at fixed $p_0 = 50$ mTorr and $U_s = -50$ V. The other parameters are given in the text.

power enables the faster generation of graphitic clusters at the defect sites, and consequently, the diffusion and amalgamation of GIs become more effective leading to the formation of large size GIs with increased number density, and therefore, we can infer that the number density of VG sheets increases on raising the input power. Moreover, the high energy hydrocarbon ions on colliding with hydrocarbon radicals on the CNT surface generate carbon radicals that effectively diffuse to the edges of the growing VG sheet on the CNT surface due to high energy owing to the collision reaction and thereby increase the height of the VG sheet at high input power [cf. Fig. 5(b)].[50] On the other hand, at high plasma power, the highly energetic hydrogen species etch the VG sheets at a higher rate, due to which the thickness of the VG sheet decreases [cf. Fig. 5(c)].

The similar effect of augmentation in the densities of defects and VG sheets on the CNT surface upon increasing the input power has been reported by Liu *et al.*[15] Moreover, the similar variations of height and thickness of VG sheets with input power have been observed by Cho *et al.*[49] and Nang and Kim[51] for VG sheets grown on the Si and Cu substrate, respectively.

Now, we investigate the effect of variation of applied substrate bias on the growth characteristics of the VG sheet protruded from the surface of pre-grown CNT. The applied substrate bias plays an important role in controlling the sheath width, electric field, direction, and kinetic energy of ions focusing on the CNT surface.[12,31] On increasing the applied bias at the conductive substrate, the sheath width increases, as a result of which the electric field and energy of ions in the plasma sheath get enhanced, which in turn augments the ion bombardment induced sputtering process leading to the increase in linear defect density on the CNT surface with U_s. The effects of variation of substrate bias on the energy of ions and defect density on the CNT surface are depicted in Figs. 7(a) and 7(b), respectively. Moreover, the high energy ions at high applied bias boost the ion-decomposition and ion-induced dissociation processes, which results in high carbon generation on the CNT surface [cf. Fig. 8(a)]. Therefore, the height and graphene sheet density on the CNT increase with applied bias due to the generation of high N_c and n_D, respectively. The time variation of the height of the VG sheet with substrate bias is shown in Fig. 8(b). The increase in height and density of the VG sheet on CNT due to high N_c and n_D has been discussed in the previous results. The behavior of the number density of VG sheets compares favorably with the experimental observations of Kumar and Ostrikov.[12] Moreover, the thickness of the VG sheet decreases due to enhanced etching of graphene sheet edges by high energy hydrogen species. The temporal evolution of the thickness of the VG sheet for different bias conditions is shown in Fig. 8(c).

IV. CONCLUSION

Using a theoretical model, which includes the plasma kinetics and plasma-surface interaction processes, the

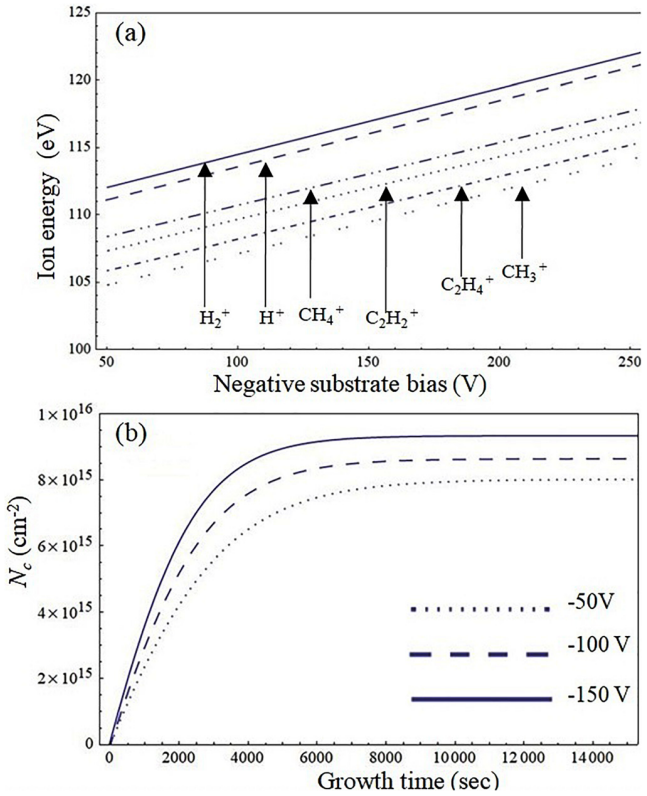

FIG. 7. Variations of (a) ion energy and (b) number of carbon species generated per unit area on the CNT surface as a function of time for different values of substrate bias at fixed $p_0 = 50$ mTorr and $P_{in} = 300$ W. The other parameters are given in the text.

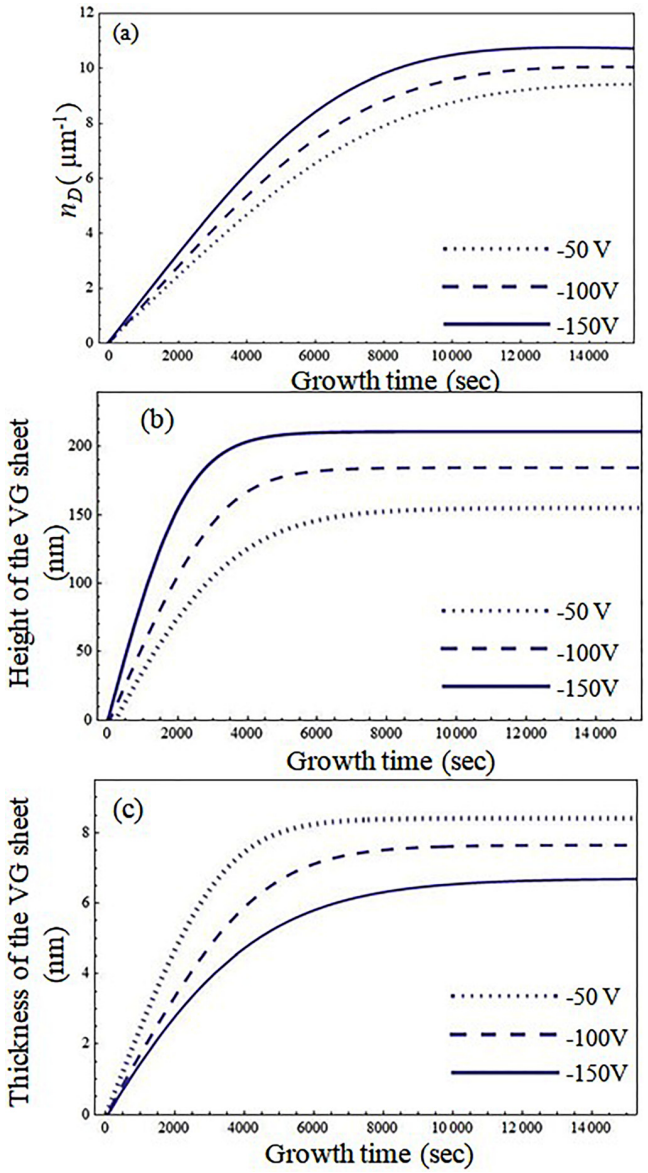

FIG. 8. Time variations of the (a) linear density of defects generated on the CNT surface, (b) height of the VG sheet, and (c) thickness of the VG sheet for different values of substrate bias at fixed $p_0 = 50$ mTorr and $P_{in} = 300$ W. The other parameters are given in the text.

kinetics and key processes of the VG sheet growth on the CNT substrate in a PECVD process are studied. The effects of process control parameters such as gas pressure, input power, and substrate bias on the number density and dimensions of the VG sheet grown over CNT are investigated. It is observed that the electron density, electron temperature, and ion energies in the plasma increase on reducing the total gas pressure and on increasing the input power and substrate bias, which subsequently enhances the ion bombardment and carbon generation on the CNT surface, and thereby, the height as well as the number density of VG sheets on CNT increases and the thickness of the VG sheet decreases.

These results would be beneficial for the fabrication of plasma-enabled graphene nanosheet-CNT hybrids with structural and electronic properties specifically tailored for various applications. For example, in any electron-field emission experiment, the area irradiated by the emitter is fixed, and if the active emission sites on the emitter are increased, the field emission would noticeably get enhanced. Moreover, the field enhancement factor, characteristic of FE current density, is dependent on the aspect ratio and the density of active emission sites of the emitter. Thus, by controlling over the size and density of the VG sheet on the CNT surface by tuning the process control parameters of the PECVD technique, graphenated CNT can be employed for the development of efficient field emission devices.

ACKNOWLEDGMENTS

This work was partially supported by the Science and Engineering Research Board (SERB)−Department of Science and Technology (DST), Government of India.

[1]W. Choi, I. Lahiri, R. Seelaboyina, and Y. S. Kang, Crit. Rev. Solid State Mater. Sci. **35**, 52 (2010).
[2]D. H. Seo, S. Kumar, and K. Ostrikov, Carbon **49**, 4331 (2011).
[3]Z. Bo, S. Mao, Z. J. Han, K. Cen, J. Chen, and K. Ostrikov, Chem. Soc. Rev. **44**, 2108 (2015).
[4]Z. Bo, Y. Yang, J. Chen, K. Yu, J. Yan, and K. Cen, Nanoscale **5**, 5180 (2013).
[5]M. Hiramatsu, K. Shiji, H. Amano, and M. Hori, Appl. Phys. Lett. **84**, 4708 (2004).
[6]J. J. Wang, M. Y. Zhu, R. A. Outlaw, X. Zhao, D. M. Manos, B. C. Holloway, and V. P. Mammana, Appl. Phys. Lett. **85**, 1265 (2004).

[7]S. Wang, J. Wang, P. Miraldo, M. Zhu, R. Outlaw, K. Hou, X. Zhao, B. C. Holloway, D. Manos, T. Tyler, O. Shenderova, M. Ray, J. Dalton, and G. McGuire, Appl. Phys. Lett **89**, 183103 (2006).
[8]K. H. Yu, P. X. Wang, G. H. Lu, K. H. Chen, Z. Bo, and J. H. Chen, J. Phys. Chem. Lett. **2**, 537 (2011).
[9]K. Yu, Z. Bo, G. Lu, S. Mao, S. Cui, Y. Zhu, X. Chen, R. S. Ruoff, and J. Chen, Nanoscale Res. Lett. **6**, 202 (2011).
[10]H.-C. Chang, H.-Y. Chang, W.-J. Su, K.-Y. Lee, and W.-C. Shih, Appl. Surf. Sci. **258**, 8599 (2012).
[11]R. R. Devarapalli, R. V. Kashid, A. B. Deshmukh, P. Sharma, M. R. Das, M. A. More, and M. V. Shelke, J. Mater. Chem. C **1**, 5040 (2013).
[12]S. Kumar and K. Ostrikov, Nanoscale **3**, 4296 (2011).
[13]J.-H. Deng, G.-A. Cheng, R.-T. Zheng, B. Yu, G.-Z. Li, X.-G. Hou, M.-L. Zhao, and D.-J. Li, Carbon **67**, 525 (2014).
[14]J.-H. Deng, R.-N. Liu, Y. Zhang, W.-X. Zhu, A.-L. Han, and G.-A. Cheng, J. Alloys Compd. **723**, 75 (2017).
[15]J. Liu, B. Zeng, X. Wang, W. Wang, and H. Shi, Appl. Phys. Lett. **103**, 053105 (2013).
[16]J. L. Qi, F. Zhang, L. X. Zhang, J. Cao, and J. C. Feng, Mater. Res. Express **1**, 025601 (2014).
[17]L.-A. Gautier, V. Le Borgne, and M. A. El Khakani, Carbon **98**, 259 (2016).
[18]K. Yu, G. Lu, Z. Bo, S. Mao, and J. Chen, J. Phys. Chem. Lett. **2**, 1556 (2011).
[19]C. B. Parker, A. S. Raut, and B. Brown, J. Mater. Res. **27**, 1046 (2012).
[20]Y. Liu, F. Wang, X. Wang, X. Wang, E. Flahaut, X. Liu, Y. Li, X. Wang, Y. Xu, Y. Shi, and R. Zhang, Nat. Commun. **6**, 8589 (2015).
[21]H.-C. Hsu, C.-H. Wang, S. K. Nataraj, H.-C. Huang, H.-Y. Du, S.-T. Chang, L.-C. Chen, and K.-H. Chen, Diamond Relat. Mater. **25**, 176 (2012).
[22]H.-Y. Du, C.-H. Wang, H.-C. Hsu, S.-T. Chang, H.-C. Huang, L.-C. Chen, and K.-H. Chen, Int. J. Hydrogen Energy **37**, 18989 (2012).
[23]C. Li, Z. Li, H. Zhu, K. Wang, J. Wei, X. Li, P. Sun, H. Zhang, and D. Wu, J. Phys. Chem. C **114**, 14008 (2010).
[24]R. Kurt and A. Karimi, Chem Phys Chem **2**, 388 (2001).
[25]S. C. Sharma and N. Gupta, Phys. Plasmas **22**, 123517 (2015).
[26]N. Gupta, S. C. Sharma, and R. Sharma, Phys. Plasmas **23**, 083509 (2016).
[27]N. Gupta and S. C. Sharma, Phys. Plasmas **24**, 073510 (2017).
[28]M. Mao and A. Bogaerts, J. Phys. D: Appl. Phys. **43**, 315203 (2010).
[29]H. Mehdipour, K. Ostrikov, and A. E. Rider, Nanotechnology **21**, 455605 (2010).
[30]H. Mehdipour, K. Ostrikov, A. E. Rider, and Z. Han, Plasma Processes Polym. **8**, 386 (2011).
[31]Z. Marvi, S. Xu, G. Foroutan, and K. Ostrikov, Phys. Plasmas **22**, 013504 (2015).
[32]Y. P. Raizer, *Gas Discharge Physics* (Springer-Verlag, Berlin, 1991).
[33]L. Zeng, D. Lei, W. Wang, J. Liang, Z. Wang, N. Yao, and B. Zhang, Appl. Surf. Sci. **254**, 1700 (2008).
[34]B. B. Wang, K. Zhu, K. Ostrikov, R. W. Shao, and K. Zheng, J. Appl. Phys. **119**, 024302 (2016).
[35]B. B. Wang, K. Zeng, Q. J. Cheng, and K. Ostrikov, Appl. Surf. Sci. **325**, 251 (2015).
[36]H. Mehdipour and K. Ostrikov, ACS Nano **6**, 10276 (2012).
[37]A. S. Barnard, M. L. Terranova, and M. Rossi, Chem. Mater. **17**, 527 (2005).
[38]A. V. Krasheninnikov, K. Nordlund, M. Sirvio, E. Salonen, and J. Keinonen, Phys. Rev. B **63**, 245405 (2001).
[39]B. B. Wang, W. L. Wang, and K. J. Liao, Thin Solid Films **401**, 77 (2001).
[40]S. K. Srivastava, A. K. Shukla, V. D. Vankar, and V. Kumar, Thin Solid Films **492**, 124 (2005).
[41]M. S. Sodha, S. Misra, S. K. Misra, and S. Srivastava, J. Appl. Phys. **107**, 103307 (2010).
[42]See http://www.its.caltech.edu/~teinav/Lectures/Ph%201b/Lecture%2010%20-%2002-09-2017.pdf for potential of a hemisphere.
[43]R. Gupta, S. C. Sharma, and R. Sharma, Plasma Sources Sci. Technol. **26**, 024006 (2017).
[44]N. V. Mantzaris, E. Gogolides, A. G. Boudouvis, A. Rhallabi, and G. Turban, J. Appl. Phys. **79**, 3718 (1996).
[45]G. Shivkumar, S. S. Tholeti, M. A. Alrefae, T. S. Fisher, and A. A. Alexeenko, J. Appl. Phys. **119**, 113301 (2016).
[46]S. S. Harilal, C. V. Bindhu, R. C. Issac, V. P. N. Nampoori, and C. P. G. Vallabhan, J. Appl. Phys. **82**, 2140 (1997).
[47]M. A. Lieberman and A. J. Lichtenberg, *Principles of Plasma Discharges and Materials Processing* (Wiley, NY, 1994).
[48]W. Takeuchi, H. Sasaki, S. Kato, S. Takashima, M. Hiramatsu, and M. Hori, J. Appl. Phys. **105**, 113305 (2009).
[49]H. J. Cho, H. Kondo, K. Ishikawa, M. Sekine, M. Hiramatsu, and M. Hori, Carbon **68**, 380 (2014).
[50]Y. Wang, L. Li, Q. Cheng, and C. He, J. Lumin. **161**, 7 (2015).
[51]L. V. Nang and E.-T. Kim, J. Electrochem. Soc. **159**, K93 (2012).

Available online at www.ijapie.org

INTERNATIONAL JOURNAL OF ADVANCED PRODUCTION AND INDUSTRIAL ENGINEERING

IJAPIE-2018-01-121, Vol 3 (1), 01-04

IJAPIE
Connecting
Science & Technology
with Management.

A Journal for all
Products & Processes.

Material Selection for a Fuel Tank and its FE Simulation in deep drawing

Vijay Gautam[1] , Subhajit Konar[2]

[1,2](Department of Mechanical Engineering, Delhi Technological University, Delhi, India)

Vijay.dce@gmail.com, subhokonar94@gmail.com,

Abstract : Deep drawing is a sheet metal forming process in which deformation forces are oriented in plane of the sheet, and the surface pressures in the tool are generally lower than the yield stress of the sheet material. The present work discusses the selection of sheet material suitable for a fuel tank by experimental evaluation of tensile properties of interstitial free steel and deep draw quality steel sheets of the same thickness 0.8mm. The tensile specimens are laser cut from a blank with known rolling direction and are tested for tensile properties and anisotropy. These tensile properties of the sheets are used in material model in FE simulation of the deep draw process using HYPERWORKS. It is observed that an optimum blank holder force is necessary to remove the wrinkling defects. It is concluded that higher ductility and normal anisotropy are the key factors for higher thinning resistance in deep drawing and hence, interstitial free steel sheet qualifies as the better material for the fuel tank.

Keywords: Deep drawing, yield stress, cold rolled draw quality, blank holding force, FE simulation, HYPERWORKS.

I. INTRODUCTION

Deep drawing is very common sheet metal operation used in automobiles, aviation, daily utilities industries etc [1]. Fuel tank is vital part of the automobile which is frequently deep drawn and requires practical testing which incurs cost and time. So it becomes important to develop computational simulation model for finite element analysis of the deep drawing. Jackson et al. [2] recognized the importance of the variation of r-value with orientation in the plane of sheet for low carbon steel. It was reported that the variation in r-values could be exploited for unsymmetrical stampings. The variation of the plastic behavior with direction is assessed by a quantity called Lankford parameter or anisotropy coefficient which is determined by uniaxial tensile tests on sheet specimens in the form of a strip. Zaky et al. [3] presented theoretical results of strain hardening and plastic strain ratio on the limiting draw ratio when drawing with a flat headed punch. It was concluded through experiments that n-value has little effect on limiting draw ratio and while increasing r-value increases the draw ratio. They have shown that at least two instability modes are possible. The first mode in the cup wall occurs under plane strain tension and is most likely to apply to annealed materials. The second mode is in the flange under uniaxial tension and this is most likely to apply to materials that have been previously cold-worked. The limiting drawing ratios for drawing with rough punch are somewhat greater than those for drawing with smooth punch. Darendeliler et al. [4] studied a variable friction model that relates the parameters of sheet metal drawing to the local lubrication conditions taking place during the deformation, integrated to a finite element simulation. Variable friction coefficients for the contacting surfaces were determined and used in the simulations. Faraji et al. [5] obtained an LDR of 9 for cylindrical components in FE analysis of the multi-stage deep drawing carried out by ABAQUS/explicit FE code. Furthermore, to predict the onset of necking, the forming limit diagram and the forming limit stress diagram were computed and implemented into FE analysis. The best LDRs for each stage were obtained from FE analysis. Gensamer [6] studied the impact of strength and ductility during forming. Improvement in deformation distribution by modification of the plastic properties of substances should be more profitable, when the intrinsic ductility is considerable. However, this should not be true at high strength levels, where intrinsic ductility is low enough to be a more important factor. It is still important for us to try to improve the limiting, local deformation prior to fracture in high strength materials, even though it be of less importance in our more ductile alloys.

The process of selection of a material for a fuel tank is quite cumbersome and it requires lot of trial and error methods. Thus it is highly imperative to analyze deep drawing using computational design and modeling techniques.

II. METHODOLOGY

Methodology adopted in the present work is discussed below:

A. Material selection

Two different sheet metals in the annealed state, Interstitial Free steel (IF) and Cold Rolled Deep Draw quality (DDQ) steel of same thickness of 0.8mm were selected in the present work. The chemical composition of the selected materials was determined by spark based spectrometer and the values

are given in Table 1. IF steel sheets are also known as the extra deep draw steel. These are steels from which carbon and nitrogen have been reduced to extremely low levels (less than 0.005%). After vacuum degassing, titanium is added to react with any carbon or nitrogen in solution. Titanium reacts preferentially with sulfur so the stochiometric amount of titanium that must be added to eliminate carbon and nitrogen is given by: %Ti = (48/14)(%N)+(48/32)(%S)+ (48/12)(%C). These steels have superior formability, ductility and anisotropy which are required for deep drawing operation.
Whereas, DDQ steel offers a wide variety of properties including ease of formability, a smooth and clean surface that's why there are mostly used in automobiles, aerospace and other appliances. Annealed coils are lightly rolled by a skinpass mill to prevent a defect called stretcher strain, improve strip shape, and adjust mechanical properties. Skinpass rolling is also used to produce dull finish and bright finish products.

Table 1. Chemical composition of the DDQ & IF steel used (by weight %)

Steel	C	Si	Mn	Ni	Cr	Cu	V	Al	Ti	S	P
DDQ	0.053	0.018	0.076	0.039	0.037	0.022	0.017	0.018	0.025	0.020	0.016
IF	0.004	0.002	0.112	0.012	0.012	0.009	0.036	.0048	0.045	0.009	0.017

B. Experimental determination of tensile properties

The specimens as per ASTM standard E8M as shown in Fig. 1 are used for uniaxial tensile testing. The specimens were prepared by CO2 laser in three directions such as parallel (0°), diagonal (45°) and perpendicular (90°) with respect to the rolling direction of the sheet.

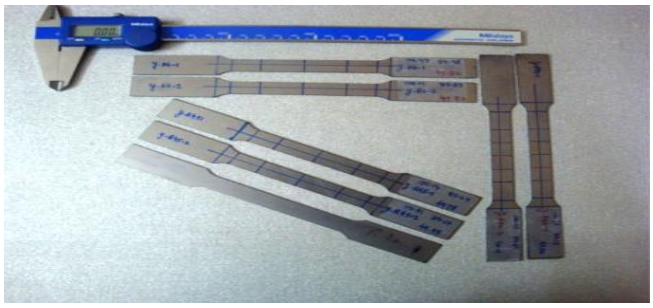

Fig. 1. Tensile test specimens in 0º, 45º and 90º w.r.t. the rolling direction

The tensile samples were tested in uniaxial tension in a UTM of 50kN. Load and elongation data were obtained for all the tests and was converted into engineering stress strain data. The standard tensile properties such as yield stress, ultimate tensile stress, uniform elongation and total elongation are determined from the stress- strain plot. The log true stress and log true strain values are calculated in the uniform plastic deformation range (between YS and UTS) and using linear regression (least square method) a best fit was plotted. The slope of this line gives n value and Y- intercept gives log K. Similarly, plastic strain ratio for both the steels were determined by giving a plastic strain of 20%.

C. Modeling & Simulation

Modeling of the die has been done using the HYPERFORM die module. Initially, the part was modeled in the SOLIDWORKS and split in half along the XY plane. Then the IGES file is created which is further imported to the HYPERFORM die module as shown in Fig. 2.

Fig. 2. Die Face Designed in Die Module

The IGES file of the split part is imported to the HYPERFORM Die Module and geometry clean up is performed to toggle the open edges. After the geometry clean up trim line is created by using create by part option. Then the flat binder is generated and by trimming the binder along the trim line die cavity is created. Similarly, a punch was designed and IGES file data was imported to the die module of HYPERFORM.
A blank of size 410mmX615mm was designed for the deep drawing operation using incremental forming. Two modules of HYPERFORM RADIOSS are used, namely RADIOSS One-Step and Incremental RADIOSS. One-Step is a designer friendly model setup for forming feasibility analysis. The solver is very fast and accurate in predicting the blank shape and forming feasibility early in the product development cycle, minimizing downstream formability challenges and associated costs. Its intuitive nesting interface proposes proper blank-sizing, minimizing material scrap in the early stages of the product development process.
Incremental is the module where actual forming simulation takes place. Here, we setup the deep drawing process, either manually through User Process or automatically through Auto Process. It also has function known as Tool Setup that auto generates punch/die and blank holder meshes form the die/punch mesh using input data such as clearance percentage and blank holding area. The results are viewed and processed in HYPERVIEW.
In this module we can generate binder and punch from the die face designed in the die module section with the suitable percentage clearance between the punch and die. There are two different solvers in this section named as, Incremental RADIOSS and LS-DYNA. Intuitive interface for designers and engineers for quick model setup. Multistage transfer die or progressive die forming modeling using multistage

manager. Supports modeling of single, TWB, Multilayer blanks as shell and solids. Options to create custom process and store it as templates for reuse and share to establish uniform model setup. Fast, Robust, Accurate and Scalable Incremental solver RADIOSS provides quick and best-in-class forming and spring back results. Efficient result interpretation in HYPERVIEW with special tools for forming relevant post processing. The die face as shown in Fig. 3(a) designed using die module is imported in the incremental RADIOSS. Along with this IGES blank file is also imported. Then we go to the mesh>organize>element>components and assign the elements to the die face and blank. Similarly, the punch face is designed as shown in Fig. 3(b).

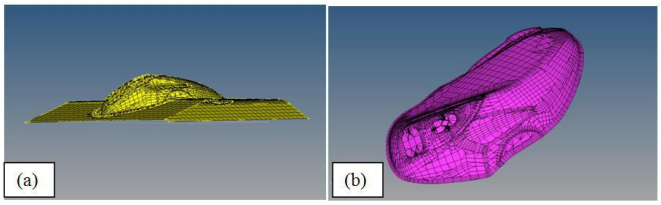

Fig. 3. (a) Die and (b) Punch after meshing

First, the die and blank are meshed and then Tool-Setup function is used to build and setup the punch and binder from die surface. The binder and the blank after meshing is 5

shown in Fig. 4. The Tool Setup function also automatically assigns meshes to punch and binder.

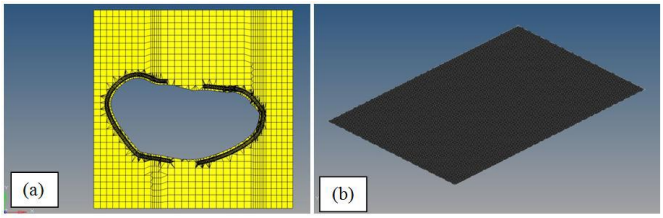

Fig. 4. (a) Binder and (b) Blank after meshing using HYPERMESH

The following figure shows the outcome of the Tool Setup function using die-punch clearance as 10% of sheet thickness. Die, punch and binder are placed such that they just touch the blank surface as shown in Fig. 5.

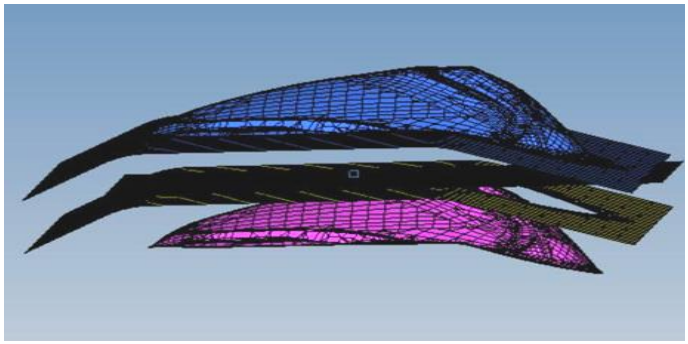

Fig. 5. Assembly of the (1) Die at the top, (2) Blank, (3) Binder and the (4)Punch at the bottom

Die, punch and binder have been assigned rigid meshes known as R-Mesh consisting of four-node shell elements as they are tools and do not need to be analyzed. Binder has been assigned fine B-Mesh or Belytschko-Tsay shells in order to capture the results with accuracy. After the Tool Setup, User Process is selected in order to finally setup the analysis. We set the material model to be used for sheet.

As this is a double action press, draw, travel and velocity details for punch or die are given in the module. When we click on calculate distance, then it will calculate the travel details. These calculated are automatically fed, with respect to the condition that all other tools just touch the blank. We can also change these values according to our requirements. The final part is drawn in by using 200 KN blank holding force and draw depth of 78mm. The frictional coefficients between various surfaces were taken as 0.125.

III. RESULT AND DISCUSSION

A. Tensile Properties of Materials.

The average tensile properties of the steels samples tested in uniaxial tension tests are given in Table 2. It is observed that the DDQ steel is much stronger than the IF steels with higher UTS and YS, whereas IF steel is softer with highest percentage elongation, strain hardening exponent and normal anisotropy. Therefore, IF steel sheets have higher 6

thinning resistance and deeper components can be drawn easily without necking. Engineering stress and engineering strain plots for the selected samples only are shown in Fig. 6.

Table 2. Tensile properties of steels

Steel	UTS (MPa)	Yield Stress (MPa)	%EL	Hardness (HRB)	Normal Anisotropy	Strain hardening exponent (n)
DDQ	342	186.89	44.20	69-70	1.5	0.22
IF	249	110.67	47.35	30-35	2.0	0.28

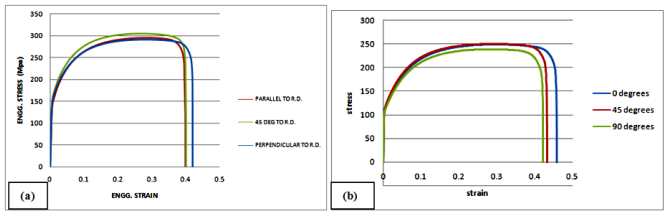

Fig. 6. Engineering Stress and strain plots for (a) DDQ and (b) IF steel sheets

B. Simulation Results.

The simulation results of deep drawing of fuel tank, for the case of IF and DDQ steel with thickness 0.8 mm are shown in Fig. 7(a) and (b) respectively. In the case of IF steel sheets, simulation exhibits the maximum percentage thinning of 26.12% and value of percentage thinnining of -18.83%. The equivalent plastic strain remains confined to the upper limit of 0.07633.

From the simulation results of deep drawing of fuel tank for the case of DDQ steel, maximum percentage thinning came out to be 34.89% and minimum value of percentage thinning is -13.10%. The equivalent plastic strain remains confined to the upper limit of the .07588. It is also evident from Forming Limit Diagram (FLD) results as depicted in Fig. 8(a) that in the case of IF steel sheets, there is no failure of material although some wrinkles are developed in the flange region due to circumferential hoop stress which would not be the

part of final component as they would be trimmed in finishing stages.

In the case of DDQ steel, the FLD results as depicted in Fig. 8(b) there is significant necking and failure of material and hence, poor drawability as compared to the IF steel.

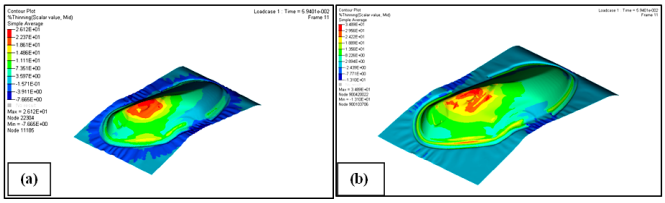

Fig. 7. Thinning contour plots for (a) IF and (b) DDQ steel sheets

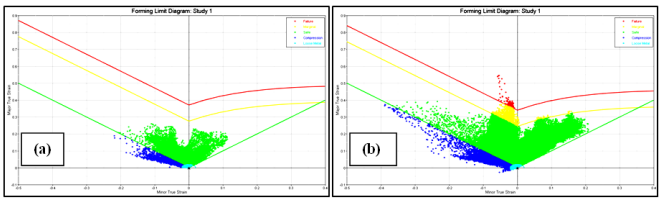

Fig. 8. Forming limit plots for (a) IF and (b) DDQ steel sheets

V. CONCLUSION

The following conclusions are drawn on the basis of the experimental studies and simulations:

I. DDQ steel is much stronger than the IF steels with higher UTS and YS, whereas IF steel is softer with highest percentage elongation, strain hardening exponent and normal anisotropy. Therefore, IF steel sheets have higher thinning resistance and deeper components can be drawn easily without necking.

II. In the case of IF steel sheets, simulation exhibits the maximum percentage thinning of 26.12% and value of percentage thinnining of -18.83%. The equivalent plastic strain remains confined to the upper limit of 0.07633.

III. In the case of DDQ steel, maximum percentage thinning is 34.89% and minimum value of percentage thinning is -13.10%. The equivalent plastic strain remains confined to the upper limit of the 0.07588.

REFERENCES

1. Banabic, D., et al., *Advances in anisotropy and formability.* International Journal of Material Forming, 2010. **3**(3): p. 165-189.
2. Jackson, L., K. Smith, and W. Lankford, *Plastic flow in anisotropic sheet steel.* Am. Inst. Mining. Metall. Eng, 1948. **2440**: p. 1-15. 8
3. Zaky, A., A. Nassr, and M. El-Sebaie, *Optimum blank shape of cylindrical cups in deep drawing of anisotropic sheet metals.* Journal of Materials Processing Technology, 1998. **76**(1): p. 203-211.
4. Darendeliler, H., M. Akkök, and C.A. Yücesoy, *Effect of variable friction coefficient on sheet metal drawing.* Tribology International, 2002. **35**(2): p. 97-104.
5. Faraji, G., M.M. Mashhadi, and R. Hashemi, *Using the finite element method for achieving an extra high limiting drawing ratio (LDR) of 9 for cylindrical components.* CIRP Journal of Manufacturing Science and Technology, 2010. **3**(4): p. 262-267.
6. Gensamer, M., *Strength and ductility.* Metallography, Microstructure, and Analysis, 2017. **6**(2): p. 171-185.

ACTA SCIENTIFIC MICROBIOLOGY (ISSN: 2581-3226)

Volume 1 Issue 8 August 2018

Research Article

Microbiomics in the Molecular Era: A Bird's Eye View into the Future of Personalized Medicine

Ritcha Saxena[1]*, Ritwik Saxena[2] and Ananya Raj[2]

[1]*Department of Pathology, Medical University of the Americas, Nevis, West Indies*

[2]*Department of Biomedical Engineering, Delhi Technological University, Delhi, India*

***Corresponding Author:** Ritcha Saxena, Ex-Professor, Department of Pathology, Medical University of the Americas, Nevis, West Indies.

Received: May 29, 2018 ; **Published:** July 12, 2018

Abstract

Humans, like all other complex living beings, nurture trillions of microbiological cells within, and on the surface of, their bodies which they acquire from their environment right from their time in the womb, to their entry into their tomb. These living cells are termed as our microbiota, and their totality, when seen in their genotypical and phenotypical entity, is called the microbiome. The current paradigm of personalized medicine is heavily reliant on the variation in human host genomics. Research has proven that human microbiome varies from individual to individual to a much higher degree compared to the host genome, rendering it more individualized. This has behooved engendering a new shift in the personalized medicine modality from its current focus to a multi-omics approach, which encompasses not just microbiomics as one of its principal reinforcers, but also metabolomics and proteomics. The ambitious projects to decode human microbiome and mapping it to various faucets human health and disease with completeness or near completeness, in spite of the mighty volume of their task, which aim for goals much more complicated than the Human Genome Project, throw a light of promise on an already optimistic future of personalized medicine.

Keywords: Microbiota; Microbiogenomics; Personalized Medicine; Human Genome; Bioinformatics; Pharmacogenomics

Introduction

Evolution has rendered humans, taxobiologically, as one of the most complex living entities on earth [1]. Like others of their kind, they survive as holobionts, which are systems of microbiological organisms within a eukaryote [1,2]. A human body, as a holobiont, is composed of different microbial symbionts, apart from itself, in order to subsist as a single ecological unit [1,3]. Microbiotic cells amounting up to 10 to 100 trillion within a single human, form a significant proportion of the total living cells in the body, with a share as high as fifty percent of total cellular count therein [4-6]. The population of our microbial occupants is known as our microbiome [5], Joshua Lederberg [7], the Nobel Prize winner who is credited with coining the term 'microbiome,' used the argot 'to signify the ecological community of commensal, symbiotic, and pathogenic microorganisms that literally share our body space and have been all but ignored as determinants of health and disease. Encouraged by the prospects that its study and application produces on humans, microbiome projects worldwide have been started in order to create capacity and resources for the characterization of the human microbiome, determine with exactness the functionalities that the microbiota exhibit and to gauge their impacts on our health [6,8-11].

One of these projects, the Meta-HIT consortium, has compiled an array of more than three million functional genes in the microbiome resident in the human alimentary canal [11,12] as compared to the about twenty-two thousand genes present in the entire human genome [13]. Additionally, individual humans' microbiome has an enormous diversity, when seen against their genomic variation. Each human is about 99.9% identical to another seen in light of the host genome [14] but individual microbiomic similarities are only up to ninety per cent seen in the light of the microbiome of the human gut [15,16]. These observations emphasize that in conjugation with human metabolomic differences [17-19] utilizing the human microbiome - which is much more specific compared to human host genome - can be very positively impactful in the arena of personalized medicine [20-25].

A number of human disorders and diseases have been directly and indirectly associated with the microbiome, that may include the pseudocommensals as well (which are those microbiota that do not replicate in the gut [26] but, from their presence in infected water, supplies and soil, through oro-fecal, dermal and other channels, have had continuously used human body as passage, over the centuries [27,28]. For example, Shukla., *et al.* [29] have enlarged

upon how the gut microbiota may play a role in myalgic encephalomyelitis/chronic fatigue syndrome. The greater uniqueness of individual microbiome (the individual microbiomic fingerprint) can help us tackle these health issues, pharmacogenomically, with greater ease now. The emergence of new genomic technologies and bioinformatics tools, enhancements in the definition of new and existing clinical phenotypes, development of new sequencing techniques, and the presence of advanced statistical tools to analyze a broad range of data associated with human microbiome, which has provided a commanding measure to recognize the influence of microbiome on human health [30-33].

Kilian., *et al.* [31] have suggested for the adoption of an ecological approach to the maintenance of oral health, along with a shift to personalized strategies to refurbish the health of the helpful oral microbiota subsequent to the dysbiosis after treatment of oral ailments like periodontitis. Their research draws attention to not only the immense utility of our microbiome, but also the essentiality of shifting to personalized medicine.

Microbiomics can consort personalized medicine to revolutionize patient treatment modalities [34], in an era when non-communicable disease is a burden compared to waning communicable disease [35-38]. Rapid environmental transformations, in conjugation with human interventions, combined with altered lifestyles may have been the agency of a shift in the biodiversity, metabolite production, and pathophysiological responses of the human gut microbiota, as an evolving and adaptation course [39-41]. This not only increases their individual specificity, giving a boost to personalized medical intercessions, but also their variation within a single individual, enabling us to understand microbiota-disease linkages more precisely [32-45]. In an effort to establish how disease can potentially be prevented through precise targeting of microbiome, Santilli., *et al.* [46] have, in their experiments with acarbose, discovered that small doses of the drug can negatively impact the starch utilization system in bacteroides, leaving the rest of the colon-inhabiting beneficial bacteria and other microbiota unaffected.

Sex specificity of human microbiome [47-52] can help us personalize medicine based on sex. Further, the sex specificity of pathophysiology of non-communicable diseases [53,54] which showcases their personalized characters, can help us target them much better with further research on host/microbiome interaction.

The microbiome has been found to have bearing on the psychological and mental aspects of the hosts. The advancements in the knowledge and research on the pathophysiology of cerebral illness coupled with psychoneuroimmunology [55-57] have kicked off an entirely novel discipline, the "psychobiotics" [55,59-61] which is the study of impact of the ingested microbiota on mental health by the way of their interaction with commensal gut bacteria [59]. The study of the effects of gut microbiota on mental health and psychobiotics, has been characterized as the microbiota-gut-brain axis [59,62-64]. With pharmacogenomics increasingly directing towards the incorporation of, apart from the physical, other personal faucets like psychosomatic [65-67] and emotional traits, borrowing eagerly and effectually from the Sansong's oriental systems of medicine [68,69], the in-depth study of microbiota-gut-brain axis shows immense promise in the maturation of personalized medicine [70-72].

The relation between microbiome and lifestyle choices, and thus pharmacogenomics [73], is a suggestive deliberation. Research has revealed that people who binge drink have fewer good bacteria like *Lactobacillus* and more bad bacteria like *Bacteroides, Actinomyces* and *Neisseria* species [74]. Binge drinking has been associated not only with higher risks of gum disease, but also certain cancers of head and neck, which can be attributed to the change in oral microbial flora in drinkers [75-78]. Alcoholism disrupts the gut microbiome activity which can be linked to liver disease [79], affecting the microbiota-gut-liver axis [80]. Thus, cirrhosis in chronic alcoholics can be from direct damage to liver cells, or from distressing of gut microbiota, influencing neutrophils leading to gut inflammation and liver scarring [81-83]. However, it is possible that these disorders may not be linked to alcohol intake but to a disrupted immune system due to a faltered microbiome [84-86]. Apart from genetic predisposition, alteration in gut microbiota and the resultant gut inflammation plays an important role in the development of colorectal cancer [87-96]. This knowledge not only helps in understanding the role of microbiome in liver disease, but also in personalizing medicine.

There are many more illustrations that show how microbiomics can be a panacea for personalized medicine. But there remain impediments in fully utilizing this approach. Shukla., *et al*. [34] and Qin J., *et al.* [10], have independently hinted towards the enormity of the task of completely decoding the role of microbiome in human pathophysiology.

For the attainment of an implementable worldwide personalized medicine regimen, with one of its major basis as microbiomics, age-, sex-, population-, environment- and diet preference-wise determination of microbial ingredients of humans through their orofecal and skin remnants needs to be carried out on a substantial and pertinent scale, and further research to associate metabolites and microbiomic specificities to disease susceptibility and causations, needs to be carried out. There have already been efforts for headways here. For example, it has been revealed how aspirin in-

take can inhibit the activity of the microbiological constituents of the gut that produce metabolite trimethylamine N-oxide (TMAO) by acting on dietary ingredients like phosphatidylcholine, resulting in the control of hyperactivity of platelets and thrombosis, and reduction of cardiovascular risk, which has been associated with TMAO activity [97-100]. ElRakaiby., *et al.* [101] believe that with a more extensive penetration of sequencing of humans from all over the world, along with more intensive and detailed sequencing from the same individuals over longer durations, biomarkers may be developed which can help diagnose microbiome-driven impacts on health and the necessary evolvement of therapeutics. The assessments of the effect of microbiome and metabolome, in concurrence with the genome and proteome of humans, on diseases like diabetes and cardiovascular events, may thus lead to novel medicinal strategies.

Conclusion

With our microbiome, the genome and the environment constantly interact to influence human pathophysiology. With newfangled biomedical research endeavors and their existential triumphant conclusions, as a future perspective, it is thought that the progno-diagnosis of simple and compound diseases will be personalized and so will be the treatment regime. This will be based on the microbiogenomics and other omics that render an individual, distinct from others. With the evolution of molecular diagnostics, there will be development in the field of microbiomics-based personalized and precision therapy. The resultant positivity in the prediction and medication of disease is to be witnessed in the years to come.

Bibliography

1. Richardson Lauren A. "Evolving as a Holobiont". *PLOS Biology* 15.2 (2017): e2002168.

2. Bordenstein Seth R and Kevin R Theis. "Host Biology in Light of the Microbiome: Ten Principles of Holobionts and Hologenomes". *PLOS Biology* 13.8 (2015): e1002226.

3. Theis, Kevin R., *et al*. "Getting the Hologenome Concept Right: an Eco-Evolutionary Framework for Hosts and Their Microbiomes". *MSystems* 1.2 (2016): e00028.

4. Sender Ron., *et al*. "Are We Really Vastly Outnumbered? Revisiting the Ratio of Bacterial to Host Cells in Humans". *Cell* 164.3 (2016): 337-340.

5. Ursell Luke K., *et al*. "Defining the Human Microbiome". *Nutrition Reviews* 70.1 (2013): S38-S44.

6. Turnbaugh Peter J., *et al*. "The Human Microbiome Project". *Nature* 449.7164 (2007): 804-810.

7. Lederberg Joshua. "'Ome Sweet 'Omics-- A Genealogical Treasury of Words". *The Scientist* (2001).

8. Peterson J., *et al*. "The NIH Human Microbiome Project". *Genome Research* 19.12 (2009): 2317-2323.

9. Rup Lal. "The Human Microbiome Project". *Indian Journal of Microbiology* 52.3 (2012): 315-315.

10. Qin Junjie., *et al*. "A Human Gut Microbial Gene Catalogue Established by Metagenomic Sequencing". *Nature* 464.7285 (2010): 59-65.

11. Web. "MetaHIT Consortium (Metagenomics of the Human Intestinal Tract Consortium)". Sanger Institute (2016).

12. Ehrlich S Dusko. "Metagenomics of the Intestinal Microbiota: Potential Applications". *Gastroenterologie Clinique Et Biologique* 34.1 (2010): S23-S28.

13. Consortium, International Human Genome Sequencing. "Finishing the Euchromatic Sequence of the Human Genome". *Nature* 431.7011 (2004): 931-945.

14. Wheeler David A., *et al*. "The Complete Genome of an Individual by Massively Parallel DNA Sequencing". *Nature* 452.7189 (2008): 872-876.

15. Turnbaugh Peter J., *et al*. "A Core Gut Microbiome in Obese and Lean Twins". *Nature* 457.7228 (2008): 480-484.

16. Fierer N., *et al*. "The Influence of Sex, Handedness, and Washing on the Diversity of Hand Surface Bacteria". *Proceedings of the National Academy of Sciences* 105.46 (2008): 17994-17999.

17. Nicholson Jeremy K and John C Lindon. "Systems Biology: Metabonomics". *Nature* 455.7216 (2008): 1054-1056.

18. Ryan Paul M., *et al*. "Microbiome and Metabolome Modifying Effects of Several Cardiovascular Disease Interventions in Apo-Eâˆ'/âˆ' Mice". *Microbiome* 5.1 (2017): 30.

19. Yan Shijuan., *et al*. "Metabolomics in Gut Microbiota: Applications and Challenges". *Science Bulletin* 61.15 (2016): 1151-1153.

20. Bashiardes Stavros., *et al*. "Towards Utilization of the Human Genome and Microbiome for Personalized Nutrition". *Current Opinion in Biotechnology* 51 (2018): 57-63.

21. Ejtahed HS., *et al*. "Human microbiome as an approach to personalized medicine". *Alternative Therapies in Health and Medicine* 23.6 (2017): 8-9.

22. Gurwitz David. "The Gut Microbiome: Insights for Personalized Medicine". *Drug Development Research* 74.6 (2013): 341-343.

23. Ercolini Danilo and Vincenzo Fogliano. "Food Design To Feed the Human Gut Microbiota". *Journal of Agricultural and Food Chemistry* 66.15 (2018): 3754-3758.

24. Wilkinson Ellen M., *et al*. "Microbiota-Drug Interactions: Impact on Metabolism and Efficacy of Therapeutics". *Maturitas* 112 (2018): 53-63.

25. Kashyap Purna C., *et al*. "Microbiome at the Frontier of Personalized Medicine". *Mayo Clinic Proceedings* 92.12 (2017): 1855-1864.

26. Rook Graham. "Genes Essential to the Immune System That Are 'Entrusted' to Microbial 'Old Friends'". *The Evolution and Medicine Review* (2008).

27. Rook Graham AW. "The Hygiene Hypothesis and Darwinian Medicine" (2009).

28. Rook Graham AW., *et al*. "Microbial 'Old Friends', Immunoregulation and Stress Resilience". *Evolution, Medicine, and Public Health* 1 (2013): 46-64.

29. Shukla Sanjay K., *et al*. "Changes in Gut and Plasma Microbiome Following Exercise Challenge in Myalgic Encephalomyelitis/Chronic Fatigue Syndrome (ME/CFS)". *Plos One* 10.12 (2015): e0145453.

30. Amare Azmeraw T., *et al*. "Pharmacogenomics in the Treatment of Mood Disorders: Strategies and Opportunities for Personalized Psychiatry". *EPMA Journal* 8.3 (2017): 211-227.

31. Kilian M., *et al*. "The Oral Microbiome - an Update for Oral Healthcare Professionals". *British Dental Journal* 221.10 (2016): 657-666.

32. Pareek Chandra Shekhar., *et al*. "Sequencing Technologies and Genome Sequencing". *Journal of Applied Genetics* 52.4 (2011): 413-435.

33. Fonseca Rute RDa., *et al*. "Next-Generation Biology: Sequencing and Data Analysis Approaches for Non-Model Organisms". *Marine Genomics* 30 (2016): 3-13.

34. Shukla Sanjay K., *et al*. "Personalized Medicine Going Precise: from Genomics to Microbiomics". *Trends in Molecular Medicine* 21.8 (2015): 461-462.

35. Ebrahim Shah and Liam Smeeth. "Non-Communicable Diseases in Low-Income and Middle-Income Countries: a Debate?" *International Journal of Epidemiology* 35.2 (2006): 494-495.

36. Prescott Susan L. "Disease Prevention in the Age of Convergence - the Need for a Wider, Long Ranging and Collaborative Vision". *Allergology International* 63.1 (2014): 11-20.

37. Barouki Robert., *et al*. "Developmental Origins of Non-Communicable Disease: Implications for Research and Public Health". *Environmental Health* 11 (2012): 42.

38. Rahim Hanan F Abdul., *et al*. "Non-Communicable Diseases in the Arab World". *The Lancet* 383.9914 (2014): 356-367.

39. Davenport Emily R., *et al*. "The Human Microbiome in Evolution". *BMC Biology* 15.1 (2017): 127.

40. Gillings Michael., *et al*. "Ecology and Evolution of the Human Microbiota: Fire, Farming and Antibiotics". *Genes* 6.3 (2015): 841-857.

41. Schnorr Stephanie L, *et al*. "Insights into Human Evolution from Ancient and Contemporary Microbiome Studies". *Current Opinion in Genetics and Development* 41 (2016): 14-26.

42. Renz Harald. "Faculty of 1000 Evaluation for Structure, Function and Diversity of the Healthy Human Microbiome". *F1000 - Post-Publication Peer Review of the Biomedical Literature* (2014).

43. Barroso-Batista Joao., *et al*. "The First Steps of Adaptation of Escherichia Coli to the Gut Are Dominated by Soft Sweeps". *PLoS Genetics* 10.3 (2014): 1004182.

44. Goodman Andrew L., *et al*. "Identifying Genetic Determinants Needed to Establish a Human Gut Symbiont in Its Habitat". *Cell Host and Microbe* 6.3 (2009): 279-289.

45. Foster Kevin R., *et al*. "The Evolution of the Host Microbiome as an Ecosystem on a Leash". *Nature* 548.7665 (2017): 43-51.

46. Santilli Anthony D., *et al*. "Nonmicrobicidal Small Molecule Inhibition of Polysaccharide Metabolism in Human Gut Microbes: A Potential Therapeutic Avenue". *ACS Chemical Biology* 13.5 (2018): 1165-1172.

47. Jašarević Eldin., *et al*. "Sex Differences in the Gut Microbiome-Brain Axis across the Lifespan". *Philosophical Transactions of the Royal Society B: Biological Sciences* 371.1688 (2016): 20150122.

48. Wallis Amy., *et al*. "Support for the Microgenderome: Associations in a Human Clinical Population". *Scientific Reports* 6.1 (2016).

49. Markle JGM., *et al*. "Sex Differences in the Gut Microbiome Drive Hormone-Dependent Regulation of Autoimmunity". *Science* 339.6123 (2013): 1084-1088.

50. Mueller S., *et al*. "Differences in Fecal Microbiota in Different European Study Populations in Relation to Age, Gender, and Country: a Cross-Sectional Study". *Applied and Environmental Microbiology* 72.2 (2006): 1027-1033.

51. Meleine Mathieu and Matricon Julien. "Gender-Related Differences in Irritable Bowel Syndrome: Potential Mechanisms of Sex Hormones". *World Journal of Gastroenterology* 20.22 (2014): 6725-6743.

52. Haro Carmen., *et al*. "Intestinal Microbiota Is Influenced by Gender and Body Mass Index". *Plos One* 11.5 (2016): e0154090.

53. Gabory Anne., *et al*. "Placental Contribution to the Origins of Sexual Dimorphism in Health and Diseases: Sex Chromosomes and Epigenetics". *Biology of Sex Differences* 4.1 (2013): 5.

54. Kautzky-Willer Alexandra., *et al*. "Sex and Gender Differences in Risk, Pathophysiology and Complications of Type 2 Diabetes Mellitus". *Endocrine Reviews* 37.3 (2016): 278-316.

55. Deans Emily. "Microbiome and Mental Health in the Modern Environment". *Journal of Physiological Anthropology* 36 (2016): 1.

56. Tanyi Ruth A., *et al*. "The Effects of a Psychoneuroimmunology (PNI) Based Lifestyle Intervention in Modifying the Progression of Depression in Clinically Depressed Adults". *The International Journal of Psychiatry in Medicine* 42.2 (2011): 151-166.

57. Robins Jo Lynne W., *et al*. "Psychoneuroimmunology-Based Stress Management during Adjuvant Chemotherapy for Early Breast Cancer". *Evidence-Based Complementary and Alternative Medicine* (2013): 372908.

58. Straub Rainer H and Maurizio Cutolo. "Psychoneuroimmunology-Developments in Stress Research". *Wiener Medizinische Wochenschrift* 168.3-4 (2017): 76-84.

59. Sarkar Amar., *et al*. "Psychobiotics and the manipulation of bacteria-gut-brain signals". *Trends in Neurosciences* 39.11 (2016): 763-781.

60. Kali Arunava. "Psychobiotics: An Emerging Probiotic in Psychiatric Practice". *Biomedical Journal* 39.3 (2016): 223-224.

61. Misra Snigdha and Debapriya Mohanty. "Psychobiotics: A New Approach for Treating Mental Illness?" *Critical Reviews in Food Science and Nutrition* 30 (2017): 1-7.

62. Stilling RM., *et al*. "Microbial Genes, Brain and Behaviour - Epigenetic Regulation of the Gut-Brain Axis". *Freshwater Biology* (2013).

63. Montiel-Castro., *et al*. "The Microbiota-Gut-Brain Axis: Neurobehavioral Correlates, Health and Sociality". *Frontiers in Integrative Neuroscience* 7 (2013): 70.

64. Mayer Emeran A., *et al*. "Gut/Brain Axis and the Microbiota". *The Journal of Clinical Investigation* 125.3 (2015): 926-938.

65. Rundell James R., *et al*. "Pharmacogenomic Testing in a Tertiary Care Outpatient Psychosomatic Medicine Practice". *Psychosomatics* 52.2 (2011): 141-146.

66. Hamilton Steven P. "The Promise of Psychiatric Pharmacogenomics". *Biological Psychiatry* 77.1 (2015): 29-35.

67. Leon Jose De. "Pharmacogenomics: The Promise of Personalized Medicine for CNS Disorders". *Neuropsychopharmacology* 34.1 (2008): 159-172.

68. Kim Bong-Soo., *et al*. "Comparison of Gut Microbiota between Sasang Constitutions". *Evidence-Based Complementary and Alternative Medicine* (2013): 171643.

69. Kim Jong Yeol and Denis Noble. "Recent Progress and Prospects in Sasang Constitutional Medicine: A Traditional Type of Physiome-Based Treatment". *Progress in Biophysics and Molecular Biology* 116.1 (2014): 76-80.

70. Malan-Muller Stefanie., *et al*. "The Gut Microbiome and Mental Health: Implications for Anxiety- and Trauma-Related Disorders". *OMICS: A Journal of Integrative Biology* 22.2 (2018): 90-107.

71. Caso Javier., *et al*. "The Microbiota and Gut-Brain Axis: Contributions to the Immunopathogenesis of Schizophrenia". *Current Pharmaceutical Design* 22.40 (2016): 6122-6133.

72. Nemani Katlyn., *et al*. "Schizophrenia and the Gut-Brain Axis". *Progress in Neuro-Psychopharmacology and Biological Psychiatry* 56 (2015): 155-160.

73. Ries Nola M and Timothy Caulfield. "First pharmacogenomics, next nutrigenomics: genohype or genohealthy?" *Jurimetrics* 46.3 (2006): 281-308.

74. Fan Xiaozhou., *et al*. "Drinking Alcohol Is Associated with Variation in the Human Oral Microbiome in a Large Study of American Adults". *Microbiome* 6.1 (2018): 69.

75. Galvao-Moreira., *et al*. "Oral Microbiome, Periodontitis and Risk of Head and Neck Cancer". *Oral Oncology* 53 (2016): 17-19.

76. Wang Hannah., *et al*. "Microbiomic Differences in Tumor and Paired-Normal Tissue in Head and Neck Squamous Cell Carcinomas". *Genome Medicine* 9.1 (2017): 14.

77. Gong Hongli., *et al*. "Microbiota in the Throat and Risk Factors for Laryngeal Carcinoma". *Applied and Environmental Microbiology* 80.23 (2014): 7356-7363.

78. Wolf Axel., *et al*. "The Salivary Microbiome as an Indicator of Carcinogenesis in Patients with Oropharyngeal Squamous Cell Carcinoma: A Pilot Study". *Scientific Reports* 7.1 (2017): 5867.

79. Llorente Cristina and Bernd Schnabl. "Advances in Pediatrics". U.S. National Library of Medicine (2015).

80. Vajro P., *et al*. "Microbiota and gut-liver axis: their influences on obesity and obesity-related liver disease". *Journal of Pediatrics Gastroenterology Nutrition* 56.5 (2013): 461-468.

81. Lowe Patrick P., *et al*. "Alcohol-Related Changes in the Intestinal Microbiome Influence Neutrophil Infiltration, Inflammation and Steatosis in Early Alcoholic Hepatitis in Mice". *Plos One* 12.3 (2017): e0174544.

82. Engen Phillip A., *et al*. "The Gastrointestinal Microbiome: Alcohol Effects on the Composition of Intestinal Microbiota". *Alcohol Research Current Reviews* 37.2 (2015): 223-236.

83. Bishehsari Faraz., *et al*. "Alcohol and Gut-Derived Inflammation". *Alcohol Research Current Reviews* 38.2 (2017): 161-171.

84. Shi Na., *et al*. "Interaction between the Gut Microbiome and Mucosal Immune System". *Military Medical Research* 4.1 (2017): 14.

85. Hooper LV., *et al*. "Interactions Between the Microbiota and the Immune System". *Science* 336.6086 (2012): 1268-1273.

86. Thaiss Christoph A., *et al*. "The Microbiome and Innate Immunity". *Nature* 535.7610 (2016): 65-74.

87. Konstantinov Sergey R. "Diet, Microbiome, and Colorectal Cancer". *Best Practice and Research Clinical Gastroenterology* 31.6 (2017): 675-681.

88. Chen Ju., *et al*. "Microbiome, Inflammation and Colorectal Cancer". *Seminars in Immunology* 32 (2017): 43-53.

89. Sun Jun and Ikuko Kato. "Gut Microbiota, Inflammation and Colorectal Cancer". *Genes and Diseases* 3.2 (2016): 130-143.

90. Purcell Rachel Violet., *et al*. "Distinct Gut Microbiome Patterns Associate with Consensus Molecular Subtypes of Colorectal Cancer". *Scientific Reports* 7 (2017): 11590.

91. Maisonneuve Charles., *et al*. "The Impact of the Gut Microbiome on Colorectal Cancer". *Annual Review of Cancer Biology* 2.1 (2018): 229-249.

92. Rajagopala Seesandra V., *et al*. "The Human Microbiome and Cancer". *Cancer Prevention Research* 10.4 (2017): 226-234.

93. Zackular JP., *et al*. "The Human Gut Microbiome as a Screening Tool for Colorectal Cancer". *Cancer Prevention Research* 7.11 (2014): 1112-1121.

94. Zou Shaomin., *et al*. "Dysbiosis of Gut Microbiota in Promoting the Development of Colorectal Cancer". *Gastroenterology Report* 6.1 (2018): 1-12.

95. Bhutia Yangzom D., *et al*. "Gut Microbiome and Colon Cancer: Role of Bacterial Metabolites and Their Molecular Targets in the Host". *Current Colorectal Cancer Reports* 13.2 (2017): 111-118.

96. Oke Sofia and Alberto Martin. "Insights into the Role of the Intestinal Microbiota in Colon Cancer". *Therapeutic Advances in Gastroenterology* 10.5 (2017): 417-428.

97. Velasquez Manuel., *et al*. "Trimethylamine N-Oxide: The Good, the Bad and the Unknown". *Toxins* 8.11 (2016): E326.

98. Senthong Vichai., *et al*. "Intestinal Microbiota-Generated Metabolite Trimethylamine-N-Oxide and 5-Year Mortality Risk in Stable Coronary Artery Disease: The Contributory Role of Intestinal Microbiota in a COURAGE-Like Patient Cohort". *Journal of the American Heart Association* 5.6 (2016): e002816.

99. Zhu Weifei., *et al*. "Gut Microbial Metabolite TMAO Enhances Platelet Hyperreactivity and Thrombosis Risk". *Cell* 165.1 (2016): 111-124.

100. Brown Sherry-Ann and Naveen Pereira. "Pharmacogenomic Impact of CYP2C19 Variation on Clopidogrel Therapy in Precision Cardiovascular Medicine". *Journal of Personalized Medicine* 8.1 (2018): 8.

101. Elrakaiby Marwa., *et al*. "Pharmacomicrobiomics: The Impact of Human Microbiome Variations on Systems Pharmacology and Personalized Therapeutics". *OMICS: A Journal of Integrative Biology* 18.7 (2014): 402-414.

Volume 1 Issue 8 August 2018

© All rights are reserved by Ritcha Saxena*., et al.*

3 Biotech (2018) 8:344
https://doi.org/10.1007/s13205-018-1343-7

ORIGINAL ARTICLE

Molecular characterization, modeling, and docking analysis of late phytic acid biosynthesis pathway gene, *inositol polyphosphate 6-/3-/5-kinase*, a potential candidate for developing low phytate crops

Mansi Punjabi[1,2] · Navneeta Bharadvaja[1] · Archana Sachdev[2] · Veda Krishnan[2]

Received: 8 February 2018 / Accepted: 6 July 2018
© Springer-Verlag GmbH Germany, part of Springer Nature 2018

Abstract

The coding sequence of *inositol polyphosphate 6-/3-/5-kinase* (*GmIPK2*) gene was identified and cloned from popular Indian soybean cultivar Pusa-16. The clone was predicted to encode 279 amino acids long, 30.97 kDa protein. Multiple sequence alignment revealed an inositol phosphate-binding motif, PxxxDxKxG throughout the IPK2 sequences along with other motifs unique to inositol phosphate kinase superfamily. Eight α-helices and eight β-strands in antiparallel β-sheets arrangement were predicted in the secondary structure of GmIPK2. The temporal analysis of *GmIPK2* revealed maximum expression in the seed tissues during later stages of development while spatially the transcript levels were lowest in leaf and stem tissues. Endosperm-specific cis-regulatory motifs (GCN4 and Skn_1) which support high levels of expression, as observed in the developing seeds, were detected in its promoter region. The protein structure of GmIPK2 was modeled based on the crystal structure of inositol polyphosphate multikinase from *Arabidopsis thaliana* (PDB:4FRF) and subsequently docked with inositol phosphate ligands (PDB: 5GUG-I3P and PDB: 4A69-I0P). Molecular dynamics (MD) simulation established the structural stability of both, modeled enzyme and ligand-bound complexes. Docking in combination with trajectory analysis for 50 ns MD run confirmed the participation of Lys105, Lys126 and Arg153 residues in the formation of a network of hydrogen bonds to stabilize the ligand-receptor interaction. Results of the present study thus provide valuable information on structural and functional aspects of *GmIPK2* which shall assist in strategizing our long-term goal of achieving phytic acid reduction in soybean by genetic modification of its biosynthetic pathway to develop a nutritionally enhanced crop in the future.

Keywords Glycine max · Phytic acid · Inositol polyphosphate 6-/3-/5-kinase (IPK2) · Low phytate crops, spatiotemporal expression · Homology modeling · Molecular docking · Molecular dynamics simulation

Introduction

Soybean is a phenomenal crop with a unique nutrient profile. It is the only plant source which provides a complete protein with quality equivalent to animal protein yet its human consumption is found to be very limited, even in the countries where its production is very high. Besides, majority of its uses in the food industry owe primarily to its functional properties rather than nutritional gain. The above stated can be attributed to the presence of a variety of bioactive components including phytic acid (PA), saponins, protease inhibitors, isoflavones, lectins, etc. Amongst these, PA is probably the most well-known antinutrient that is found in abundance in cereal grains and legumes. It is a saturated cyclic acid whose metabolism has been substantiated to regulate phosphorous and myo-inositol homeostasis. Due to its highly negative chemical structure, it forms phytate–mineral–protein complexes which result in reduced bioavailability of phosphorus, other associated minerals and proteins and thus contribute to the debatable health effects associated with its consumption. Therefore, in a need to reduce the level of this compound several approaches were undertaken which blocked its constitutive

Electronic supplementary material The online version of this article (https://doi.org/10.1007/s13205-018-1343-7) contains supplementary material, which is available to authorized users.

✉ Archana Sachdev
arcs_bio@yahoo.com

[1] Department of Biotechnology, Delhi Technological University (Formerly Delhi College of Engineering), New Delhi 110042, India

[2] Division of Biochemistry, Indian Agricultural Research Institute, New Delhi 110012, India

Published online: 28 July 2018

synthesis, but often resulted in crop with deplorable agronomic performance (Bilyeu et al. 2008; Cichy and Raboy 2009; Feng and Yoshida 2004; Kuwano et al. 2009; Nunes et al. 2006). Recently trending reverse genetic approaches that target tissue-specific knockdown provide a promising alternative to eliminate this negative impact (Ali et al. 2013a, b). Research is thus underway to characterize PA biosynthetic pathway enzymes (Josefsen et al. 2007; Krishnan et al. 2015; Stiles et al. 2008; Sun et al. 2007; Sweetman et al. 2006, 2007) and study their expression patterns (Bhati et al. 2014; Fileppi et al. 2010; Suzuki et al. 2007) to generate adequate information for developing *lpa* soybean through metabolic engineering.

PA biosynthesis follows a succession of phosphorylation steps (Brearley and Hanke 1996a, b). One of its late pathway enzyme inositol polyphosphate 6-/3-/5-kinase (IPK2, EC 2.7.1.151) is a multiple specificity enzyme which phosphorylates the D-6, D-3, and/or D-5 positions on a variety of inositol polyphosphate substrates (InsP3/InsP4/InsP5) (Frederick et. al. 2005) that makes it a key enzyme in regulating PA turnover and is thus a crucial target for perturbing PA dynamics (Stevenson-Paulik et al. 2005). The enzyme has previously been studied in *Arabidopsis* (Stevenson-Paulik et al. 2002), yeast (Saiardi et al. 2000; York et al. 1999), mouse (Frederick et al. 2005) and human (Majerus 1992, 1996). A study has also been reported in soybean (Stiles 2007), however, it discusses only the gene's expression and enzyme kinetics. Therefore, with the intention to extend the current knowledge on its transcript expression (both spatial and temporal) as well as to understand its structure, biochemical features and evolutionary history, we investigated this gene in soybean and compared it with those of another 19 homologs in plants through various bio-computational tools. Furthermore, to elucidate complete molecular and biochemical mechanisms regulating PA synthesis as well as inositol metabolism and signalling in plants, an insight into IPK2 protein's structural features is required. Very less information regarding the three-dimensional structure of plant IPK2 is available. To facilitate the same, we determined the three-dimensional (3D) model of soybean GmIPK2 protein through homology modeling and performed its docking simulation with the substrate [1D-*myo*-inositol 1,4,5-trisphosphate (PDB: 5GUG-I3P) and 1D-*myo*-inositol-1,4,5,6-tetra*kis*phosphate (PBD: 4A69-I0P)] molecules.

Through this work, we made an effort to study *IPK2* gene to lay a groundwork for achieving the main goal of our work which is, to develop low phytic acid soybean, a nutritionally and agriculturally important crop.

Materials and methods

Plant material

Field grown soybeans (Glycine max [L.] Merr. cv. Pusa-16) were procured from Division of Genetics, IARI, New Delhi for use in this study. For spatial and temporal expression profiling, root, stem, leaf, and flower tissues were collected from 30-day-old plants while developing seeds were collected regularly after flowering until maturation and sorted based on their sizes. After collection, the tissue samples were immediately frozen in liquid nitrogen and stored at − 80 °C until used.

PCR amplification, cloning and sequencing of partial *GmIPK2* sequence

Total RNA was isolated from soybean seeds 8 mm in size using TRIzol reagent method (Invitrogen, USA). Approximately, 1 µg of isolated total RNA was used for single stranded cDNA synthesis by reverse transcription with RevertAid™ H Minus First Strand cDNA synthesis kit (ThermoFisher Scientific, USA). Prior to cDNA synthesis, the RNA was treated with RNase-free DNase I (Thermo Scientific, USA) for removal of any residual genomic DNA. Polymerase chain reaction (PCR) amplification was performed using 0.2 µg of the initial RT reaction optimized at 94 °C for 4 min; 35 cycles of 94 °C for 30 s, 62.5 °C for 30 s, 72 °C for 30 s; 72 °C for 10 min, using the *GmIPK2* specific primers: *IPK2*F 5′-ATGCTCAAGATC CCGGAG-3′ and *IPK2*R 5′-CAGTTAGTCTGCGACACT AATTCAAGC-3′. On completion, 2 µl of amplified product was analyzed by electrophoresis on 1% agarose gel and purified using gel/PCR DNA Fragments Extraction Kit (DF100) by Geneaid. The purified amplicon was subsequently ligated in pGEM®-T Easy vector (Promega, USA) by TA cloning following protocol described in the manual and used directly for transformation of competent *Escherichia coli* DH5α cells. The recombinant plasmids were identified by blue-white screening and confirmed by restriction digestion with *EcoRI* to release the amplicon fragment. The nucleotide sequences of *GmIPK2* thus isolated was determined by DNA sequence analysis of overlapping plasmid clones using universal primers (SP6 and T7) on an automated sequencer (ABI 3730xl DNA Analyzer, USA). The nucleotide sequence data was submitted to INSDC database GenBank.

Gene expression analysis by semi-quantitative reverse transcription PCR and quantitative real-time PCR

To analyze *GmIPK2* gene expression in different soybean tissues, we first performed semi-quantitative reverse transcription PCR (RT-PCR) to obtain an expression pattern

and then further estimated the transcript levels by quantitative real-time PCR (qRT-PCR). For RT-PCR, first strand cDNA was synthesized from total RNA using RevertAid™ H Minus First strand cDNA Synthesis Kit (Thermo Scientific, USA) and PCR was subsequently performed using the same pair of *GmIPK2* specific primers and thermal cycling conditions which were described for its cloning. We further monitored the quantitative amplification of *GmIPK2* by performing qRT-PCR analysis on a PikoReal 96 Real-Time PCR platform (ThermoFisher Scientific, USA). The reactions were set up using DyNAmo Flash SYBR Green qPCR Kit (Thermo Scientific, USA) with cDNA first strands as the template DNA. The expression of *GmIPK2* was normalized to an endogenous control, the housekeeping gene phosphoenolpyruvate carboxylase (*PEPCo*) (Sugimoto et al. 1992; Tuteja et al. 2004). The primers for the gene (q*IPK2*F 5′-CGCGGATCCGCGTTGCAGAAGCTCAAG-3′ and q*IPK2*R 5′-TCCCCGCGGGGAGCGACACTAATT CAAG-3′) and the internal control (q*PEPCo*F 5′-CATGCA CCAAAGGGTGTTTT-3′ and q*PEPCo*R 5′-TTTTGCGGC AGCTATCTCTC-3′) were designed using PrimerQuest tool by IDT, USA. The reactions were setup following the standard protocol provided in DyNAmo ColorFlash SYBR Green qPCR Kit (Thermo Scientific). The thermal profile used for PCR amplification was: 95 °C for 4 min; 40 cycles of 95 °C for 15 s, 60 °C for 30 s and fluorescence data collection. To minimize variation in the output, three technical replicates were carried out for each of the three biological replicates. The baseline data was collected for first 15 cycles to generate a baseline-subtracted plot of the logarithmic increase in fluorescence signal (ΔRn) versus cycle number. A standard fluorescence threshold (Rn) was set to 0.5 on the log fluorescence scale to determine the fractional cycle number (Ct value). The relative abundance of *GmIPK2* was calculated using the 2-ΔΔCT method (Livak and Schmittgen 2001). Dissociation curve analysis from 60 to 95 °C was also performed at the end of the assay to check for any non-specific amplification and/or contamination.

Sequence analysis and phylogenetic tree construction

Homologous *IPK2* sequences from other plants were identified with National Center for Biotechnology Information (NCBI) Basic Local Alignment Search Tool (Protein BLAST, https://blast.ncbi.nlm.nih.gov/Blast.cgi) using the above deduced *GmIPK2* sequence as a query. The primary sequence composition of IPK2 sequences were computed using PEPSTATS (Rice et al. 2000). The physio-chemical parameters of proteins were predicted using the ProtParam tool of ExPASy web server (Gasteiger et al. 2005). TargetP 1.1 Server using the cutoffs of 95% specificity was implemented for subcellular location prediction of GmIPK2 protein (Emanuelsson et al. 2000) and the outcome was compared to predictions obtained from MemType-2L (Chou and Shen 2007), WoLF PSORT (Horton et al. 2007), SubLoc v1.0 (Hua and Sun 2001) and CELLO v2.5 (Yu et al. 2006). Its transmembrane topology was predicted with PSIpred (Buchan et al. 2013), TMpred (Hofmann and Stoffel 1993) and NPS@ web programs (Rost et al. 1996). A final consensus was drawn manually and the topology was generated and visualized using Protter version 1.0 (Omasits et al. 2014). Presence of potential secretory signal peptides or mitochondrial targeting peptides was analyzed with SignalP 4.1 web server (Petersen et al. 2011). M-Coffee multiple sequence alignment (MSA) of the selected amino acid sequences was carried out to produce quality alignments which served as the basis for phylogenetic analysis (Wallace et al. 2006) to detect its evolutionary placement and phylogenetic similarity with other similar genes. The evolutionary tree was constructed using neighbor joining (NJ) clustering method to compute distances and poisson model for amino acid substitution in MEGA Version 6.0 (Molecular Evolutionary Genetic Analysis, Tamura et al. 2013). Bootstrap replications were set at 1000 to assess the degree of confidence for each clade of the observed tree. The final image was rendered with the Interactive Tree of Life server (iTOL) (Letunic and Bork 2016).

Promoter isolation and prediction of regulatory motifs

A motif search was carried out to define putative cis-elements in the promoter sequences involved in the regulation of *IPK2* expression using PlantCARE (Lescot et al. 2002). To identify these cis-regulatory elements, around 2 kb upstream sequence of the *IPK2* homologs were retrieved by NCBI's nucleotide BLAST program and fed to PlantCARE web tool. The tool's database identified regulatory elements in the isolated upstream sequences and each of the elements observed were analyzed with previously reported properties of the particular element. Unlike CDS, the regulatory sequences indirectly influence their immediate phenotype.

Secondary structure analysis and domain prediction

M-Coffee multiple sequence alignment (MSA) of the selected amino acid sequences was carried out and the alignment file was imported to Jalview (Waterhouse et al. 2009) to identify and shade the conserved amino acid sequences. Ungapped motifs were also detected using MEME web tool available on MEME suite 4.11.1 (Bailey et al. 2009). The motifs present were further verified using My Hits motif scan tool (Pagni et al. 2007). The domain composition was analyzed using CDD tool (http://www.ncbi.nlm.nih.gov/cdd) on NCBI server. A secondary structure consensus from

amino acid sequences was built based on the joint prediction with SOPMA (nearest-neighbor method) and PHD (neural networks method) correctly predicting 82.2% of the residues for 74% of co-predicted amino acids (https://npsa-prabi.ibcp.fr/cgi-bin/npsa_automat.pl?page=/NPSA/npsa_seccons.html) (Geourjon and Deléage 1995; Rost and Sander 1993). Cysteine species and disulfide connectivity of protein sequences were determined using web tool DiANNA (Ferrè and Clote 2005). A secondary structure topology map of the 3D model was generated using ProMotif (http://www.ebi.ac.uk/thornton-srv/databases/pdbsum/Generate.html) and rendered using TopDraw (Bond 2003).

Homology modeling and quality assessment of predicted model

The 3D model of GmIPK2 was constructed by template-based homology modeling using automated comparative protein modeling servers, SWISS-MODEL (Biasini et al. 2014) and PHYRE2 (Kelley et al. 2015) as well as a standalone comparative modeling program MODELLER 9.16 (Webb and Sali 2016). Comparative modeling consists of five main steps: search for related protein structures, selection of one or more appropriate templates, target-template alignment, model building and model evaluation. The final step of comparative modeling was additionally performed with RAMPAGE (Lovell et al. 2003), VERIFY 3D (Eisenberg et al. 1997) and ProSA servers (Wiederstein and Sippl 2007) to evaluate the stereochemical and energetic properties of the obtained models. In addition to this, the quality of models can also be assessed by structural comparison to the template using the MatchMaker tool in UCSF Chimera (Pettersen et al. 2004), a molecular visualization software package and calculating the Cα root mean square deviation scores (RMSDs) for each of the comparative models. The secondary structures of the final and template proteins were also compared by pairwise 3D alignment using MATRAS 1.2 (Kawabata 2003). Agreement on the best model was made on the basis of the majority in best scores from these different quality analyses.

Refinement of the predicted homology model

Molecular dynamics (MD) simulation was performed to optimize the obtained GmIPK2 model. Simulation of the model was conducted in explicit solvent using the GROMACS (Groningen Machine for Chemical Simulations) 4.5.5 package (Pronk et al. 2013). The model was solvated with simple point charge (SPC216) water in a cubic box with edges that were 0.7 nm from the molecular boundary. Initially, energy minimization (maximum number of steps: 1000) was performed to remove steric conflicts between the protein and water molecules, using the steepest descent integrator. The system was then equilibrated by optimizing the solvent molecules surrounding the energy-minimized model with NVT (constant Number of particles, Volume, and Temperature) and NPT (constant Number of particles, Pressure, and Temperature) ensembles using Berendsen thermostat and Parrinello-Rahman barostat, respectively. Finally, the system was simulated for 50 ns thrice maintaining the same temperature (300 K) and pressure (1 bar) using the Particle Mesh Ewald (PME) electrostatics method. After completion of production run, we collected the data using a post-processing tool, trjconv (strips out coordinates and correct for periodicity) and used this corrected trajectory as the input for studying the conformational stability of our simulated protein via *g_rms* and *g_rmsf* tools. We subsequently generated and analyzed the output plots using a simple plotting program, xmgrace (Turner 2005).

Active site prediction, molecular docking and MD simulation of the docked complexes

The refined protein model thus generated was docked to characterize the 3D structure of the complex, to gain an insight into the crucial amino acid residues also referred to as active residues that are involved in the complex formation. Based on the available literature for IPK2, 1D-*myo*-inositol-1,4,5-trisphosphate (PDB: 5GUG-I3P) and 1D-*myo*-inositol-1,4,5,6-tetra*kis*phosphate (PDB: 4A69-I0P) ligands were selected for optimized GmIPK2 protein receptor. Docking of these ligands was performed using AutoDock Vina (version 1.1.2) (Trott and Olson 2010) following the semi-flexible approach of docking. AutoDock Vina reads all the molecules in a simplified PDB file representation, termed PDBQT and thus the coordinates of both GmIPK2 protein and its ligands (downloaded from the RCSB protein data bank) were prepared using MGL tools (version 1.5.4) AutoDock tools (Morris et al. 2009) prior to docking. All the water and solvent atoms of the protein were removed and the polar hydrogen atoms were added. The GmIPK2 molecule was kept rigid while the ligands were allowed to rotate and explore more flexible binding pockets. Vina used a customized rectangular 3D cartesian grid for specifying the binding site of the protein and for efficient geometric scoring. The dimensions of the grid were customized to make sure that the size of the search space is large enough for the ligand to rotate in. Once set, the docking run produced ligand poses each with a definite binding energy (kcal/mol) calculated based on the scoring function used in Vina. The conformations with the lowest binding affinity were chosen and the interaction diagrams were generated using Discovery Studio Visualizer 4.1 (Accelrys Software Inc., USA 2013). The amino acid residues present at a distance of 2 Å were considered as the binding partners of the ligands. The active amino acid residues were also predicted by combining results of

three different interface prediction web servers, CASTp (Dundas et al. 2006), FTSite (Kozakov et al. 2015) and FunFOLD2 (Roche et al. 2013) into a consensus. The final complexes were equilibrated by MD simulation by following the procedure described for protein model in explicit water in the previous section but by applying restraints on the ligands to prevent them from moving away from the binding site. Once equilibrated, we simulated the complexes for 50 ns and analyzed the resulting trajectories for their stability using *g_rms, g_rmsf, g_hbond* and *g_mmpbsa* tools.

Results and discussion

Cloning and sequencing of *GmIPK2*

We first performed a BLASTN analysis in the plant comparative genomics portal Phytozome v9.1 (Goodstein et al. 2012) with the soybean *IPK2* gene sequence available in NCBI (GenBank: NM_001250522) to retrieve a 1241 bp transcript sequence. Based on the sequence data thus derived, we designed primers specific to amplify complete *GmIPK2* coding sequence (CDS) as well as a fragment of its 3′ untranslated region (UTR) with the aim to design silencing construct in the future specific to this highly conserved region because of its substantial role in gene regulation. To accomplish this, we converted total RNA isolated from 8 to 10 mm developing seed stage to cDNA and performed PCR amplification from the synthesized cDNA template following the protocol described under sect. "PCR amplification, cloning, and sequencing of partial GmIPK2 sequence". The amplicon was then cloned into pGEM-T easy vector system and introduced into the bacterial host *E. coli* (DH5α). The putative cDNA clones were verified by restriction analysis with EcoRI and sequence characterized to ~ 910 bp residues in length (Fig. 1). It contains a single open reading frame ~ 840 bp long which potentially encode a single polypeptide of 279 amino acid residues and a ~ 70 bp 3′ UTR fragment. We submitted the obtained CDS data to NCBI (GenBank: KF297702) and used the information as query to conduct protein homology search using PSI-BLAST algorithm. Amongst the sequences producing significant alignment, we shortlisted 30 plant IPK2 sequences based on percentage sequence identity to carry out further in silico analysis.

Spatial and temporal expression profiling

As discussed above, tissue-specific modulation of *IPK2* gene to generate a *lpa* mutant is essential to evade any possible pleiotropic effects. Before this can be achieved it is vital to investigate its spatial expression profile in different tissues as well as its temporal expression profile in developing

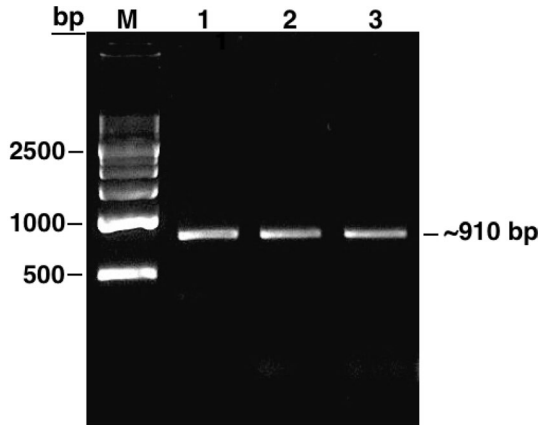

Fig. 1 Agarose gel showing PCR amplification product of *GmIPK2* gene isolated from developing seeds (8–10 mm) of *Glycine max cv*. Pusa-16. Lane M: 500 bp DNA ladder, lanes 1–3: ~ 910 bp *GmIPK2* fragment

seeds, to provide an initial point for strategic achievement of a desired level of silencing.

To study the expression of *GmIPK2* gene in different tissues of a soybean plant and during seed development, semi-quantitative as well as real-time PCR expression analysis was performed with total RNA isolated from root, stem, leaf and flower tissues of 30-day-old *G. max* plants and developing seeds ranging from 0 to 16 mm in size distributed in eight different progressive stages. Semi-quantitative PCR analysis revealed a differential pattern of *GmIPK2* transcript expression across the set of experimental tissues analyzed, with the highest level of transcripts observed in seeds (Fig. 2a). The same was confirmed by steady-state qRT-PCR analysis which also detected highest level of transcripts in seeds (Fig. 2b). This suggests that *GmIPK2* play a key role in PA biosynthesis in this tissue for use as a primary source of energy during germination. In both the analyses, same level of amplification was observed for *PEPCo* housekeeping gene. Since PA is also required for several other vital functions throughout the plant system, a basal level of it is observed in all the tissues as well. Thus, amongst the other tissues analyzed, expression of *GmIPK2* was also recorded in roots and flowers, but at a level lower than that observed in the cotyledons. The strong presence of *GmIPK2* transcripts in these tissues may be attributed to its role in regulating cytosolic calcium gradient which correlates with pollen germination, pollen tube growth (Franklin-Tong et al. 1996; Malho 1998; Pierson et al. 1994; Xu et al. 2005), root growth, and root hair development (Bibikova et al. 1997; Felle and Hepler 1997; Wymer et al. 1997). A low level of expression was also observed in stems and leaves as it is studied to be involved in regulating a vital function of axillary shoot branching by participating in auxin signaling (Zhang et al. 2007).

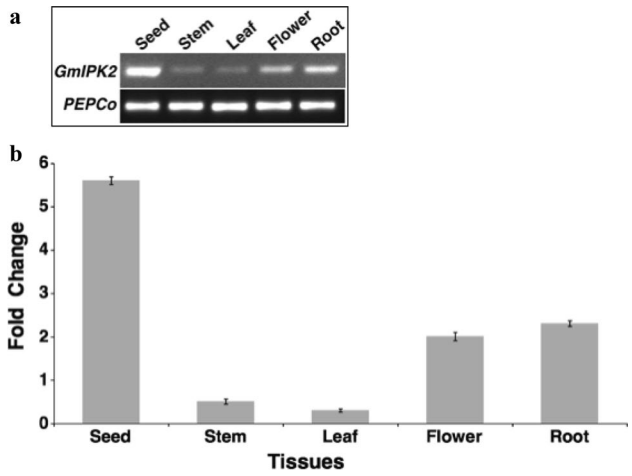

Fig. 2 **a** RT-PCR expression analysis of *GmIPK2* gene in different plant tissues of Pusa-16 cultivar using soybean housekeeping gene *PEPCo* as an internal control. **b** Relative quantification of *GmIPK2* transcript levels in the samples analyzed above by qRT-PCR, normalized to soybean housekeeping gene *PEPCo*. The leaf tissue was taken as calibrator. The data are mean of technical triplicates of each of the three biological replicates with error bars indicating standard deviation (SD)

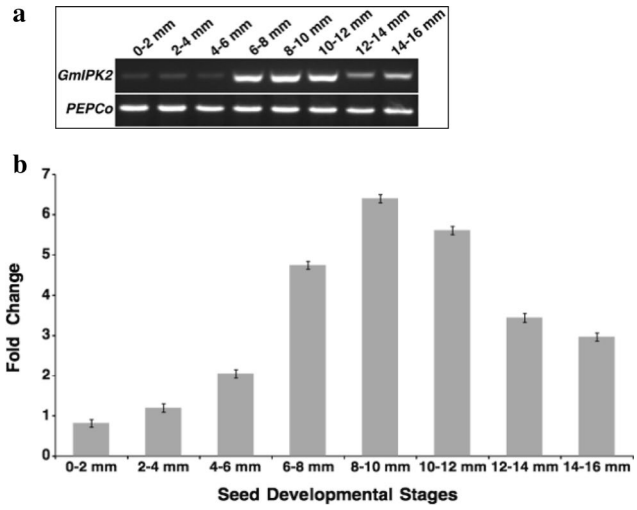

Fig. 3 **a** RT-PCR expression analysis of *GmIPK2* gene in developing seeds of Pusa-16 cultivar using soybean housekeeping gene *PEPCo* as an internal control. **b** Relative quantification of *GmIPK2* transcript levels in the samples analyzed above by qRT-PCR, normalized to soybean housekeeping gene *PEPCo*. The 0–2 mm seed stage was taken as calibrator. The data are mean of technical triplicates of each of the three biological replicates with error bars indicating SD

We then analyzed its temporal expression pattern during eight progressive seed development stages. In both semi-quantitative as well as real-time PCR expression analysis, we observed that its expression increased as the development progressed and reached a peak value at the later stages of seed development (Fig. 3). This pattern of expression coincides evenly with the pattern of accumulation of PA which is linear throughout most of seed development (Raboy and Dickinson 1987). Similar results were obtained in a microarray transcriptome study conducted in the past in our laboratory (GEO: GSE69821). This observation can be explained by the increase in production of phosphorous compounds required to support growth and development during initial stages of seed development when the synthesis of phosphorous reserve, PA is minimal (Raboy and Dickinson 1987).

The spatiotemporal analysis in summary identifies seed as the major tissue for its expression with maximum relative expression occurring during the later stages of its development. Thus, from the present study we can hypothesize that targeting the *GmIPK2* gene expression during late seed development stages may provide a potential strategy for generating *lpa* soybean with enhanced nutritional value.

Characterization of regulatory motifs in *IPK2* gene promoter

To understand the mechanism regulating the spatiotemporal expression pattern of *GmIPK2* gene thus observed, we analyzed the promoter region of all its homologs and identified different cis-regulatory elements located therein. A 2 kb sequence upstream to the open reading frame was identified and subjected to PlantCARE analysis. Database search revealed the presence of many motifs related to seed-specific promoters, hormone-responsive cis-elements (HRE) and cis-elements responsive to stresses (DSRE) that together contribute to the differential regulation of our gene (Table 1). Light responsive elements (Arguello-Astorga and Herrera-Estrella 1996; Feldbrugge et al. 1996; Lois et al. 1989; Lopez-Ochoa et al. 2007; Sessa et al. 1995) were observed most frequently which suggest a probable diurnal regulation of *IPK2* expression. The GCN4 and Skn_1 motifs highly conserved in the promoters of cereal seed storage protein genes were located within the *IPK2* promoter. These cis-acting elements play a central role in controlling endosperm-specific gene expression (Onodera et al. 2001; Takaiwa et al. 1996; Washida et al. 1999; Wu et al. 1998). Multiple HREs particularly those known to be involved in abscisic acid (ABA) and gibberellic acid (GA3) sensing were also identified. A ABA-responsive element (ABRE) with the core sequence PyACGTG/TC and three GA-responsive elements (GARE) AAACAGA, TCTGTTG and TATCCAC/T (Niu et al. 2016; Mongkolsiriwatana et al. 2009; Yamaguchi-Shinozaki et al. 1989) were identified which previously were reported to correlate with PA accumulation during grain filling (Abe et al. 2003; Matsuno and Fujimura 2014). Aggarwal et al. 2015 reported that *IPK2* is an ABA-induced gene which is antagonistically suppressed by GA3 underlining the crucial role played by these hormones in regulating PA pathway genes. Putative elements responsive

Table 1 Potential cis-acting elements identified in the 5′ regulatory sequences of plant *IPK2s*

Classification	Name	Sequence	Source organism	References
Endosperm	GCN_4 motif	GAAGCCA, TGAGTCA	*Oryza sativa*	Takaiwa et al. (1996), Onodera et al. (2001)
	Skn-1 motif	CAAGCCA, TGTGTCA, GTCAT	*Oryza sativa*	Washida et al. (1999)
ABA	ABRE	CACGTG, TACGTG	*Arabidopsis thaliana*	Yamaguchi-Shinozaki et al. (1989)
Gibberellin	GARE	AAACAGA, TCTGTTG, TATCCAC/T	*Brassica oleracea* *Oryza sativa*	Mongkolsiriwatana et al. (2009), Jun Niu et al. (2016)
Light	Box 4	ATTAAT	*Petroselinum crispum*	Lois et al. (1989)
	CATT-motif	GCATTC	*Zea mays*	Arguello-Astorga and Herrera-Estrella (1996)
	G-Box	CACGTG	*Pisum sativum, Arabidopsis thaliana, Zea mays*	Sessa et al. (1995), López-Ochoa et al. (2007)
	ATCC/T-motif	AATCTAATCC/T	*Pisum sativum, Arabidopsis thaliana*	Arguello-Astorga and Herrera-Estrella (1996)
	TCT-motif	TCTTAC	*Arabidopsis thaliana*	Arguello-Astorga and Herrera-Estrella (1996)
	Box-I	TTTCAAA	*Pisum sativum*	Arguello-Astorga and Herrera-Estrella (1996)
	ACE	AAAACGTTTA	*Petroselinum crispum*	Feldbrugge et al. (1996)
	GA-motif	AAGGAAGA	*Glycine max*	Arguello-Astorga and Herrera-Estrella 1996
MeJA	CGTCA-motif TGACG-motif	CGTCA TGACG	*Hordeum vulgare* *Hordeum vulgare*	Kim et al. (1993), Rouster et al. (1997)
Drought	MBS	T/CAACTG	*Arabidopsis thaliana*	Shinozaki and Yamaguchi-Shinozaki (2000), Abe et al. (2003)
Anaerobic	ARE	TGGTTT	*Zea mays*	Nguyen et al. (2003)

to methyl-jasmonate, drought inducibility and anaerobic induction were also observed which help combat assorted types of abiotic factors that plants are exposed to under natural environment (Abe et al. 2003; Kim et al. 1993; Nguyen et al. 2003; Rouster et al. 1997; Shinozaki and Yamaguchi-Shinozaki 2000).

Computation of physiochemical parameters and subcellular localization prediction

GmIPK2 sequence similarity search using PSI-BLAST revealed homology to IPK2 protein sequences from different plant sources showing maximum similarity with *Glycine soja* (98%) and *Vigna radiata* (74%) (Table 2). Primary sequence analysis of these homologs indicate that leucine is the most abundant amino acid which makes upto approximately 9–11 mol percent of its backbone residues whilst the percentage of tryptophan and methionine were found to be the least at approx. 1% across species. The isoelectric points (pI) of all IPK2 proteins were computed to be under 7 suggesting that they are most likely to precipitate in acidic buffers except *Glycine soja, Medicago truncatula, Zea mays and Sorghum bicolor* which has a pI of 7.1, 8.57, 10.48 and 8.26, respectively indicating their solubility in basic buffers. The calculated pI will be useful for empirical protein purification by isoelectric focusing and ion exchange chromatography. The extinction coefficient (EC) (Gill and Von Hippel 1989) of IPK2 proteins measured at 280 nm in water was found ranging from 25,440 to 34,380 M–1 cm–1 with respect to their concentration of aromatic amino acids (11–15%) and cystine (disulfide bonds). These EC values can be used to calculate protein concentration in a solution which in turn help in the quantitative study of biochemical interactions (protein–protein and protein–ligand). The instability indices (Ii) computed for selected IPK2 proteins are used to determine their in vivo half-lives (Guruprasad et al. 1990). Rogers et al., 1986 reported that proteins having Ii values greater than 40 have an in vivo half-life of less than 5 h while those proteins having Ii values less than 40 have a longer in vivo half-life of 16 h. Our study showed that Ii values of all the homologs are less than 40 and hence are thermally stable with a long half-life except for *Lotus japonicas* and *Zea mays* kinases that have a Ii above 40 which indicate their possible thermal instability. Thermostability of proteins result from a combination of several factors acting synergistically. Here we assess thermal stability of our proteins in direct proportionality with their aliphatic index (Ai) which is a measure of the relative volume occupied by aliphatic side chains (Ikai 1980). The Ai values determined for IPK2 kinases ranged from 68.79 to 96.70 with those from brassicaceae family showing lowest thermal stability. This in turn is indicative of their greater flexibility at a wide range of temperatures when compared to proteins of other families. Grand average of hydropathicity (GRAVY) number reflect

Table 2 Physiochemical parameters of shortlisted plant IPK2 sequences computed using the ProtParam tool

Organism	Accession no.	Sequence length	MW	pI	EC	Ii	Ai	GRAVY	−R	+R
Glycine max	AGW99177.1	279	30,979.2	6.29	29,910	29.72	89.07	−0.18	35	30
Glycine soja	KHN19419.1	178	19,898.87	7.10	23,950	29.73	95.73	−0.059	21	21
Vigna radiata	XP_022634636.1	286	31,482.10	6.59	28,420	38.17	93.67	0.045	29	27
Cajanus cajan	XP_020232596.1	267	29,463.71	6.86	28,420	33.70	91.31	−0.132	31	30
Phaseolus vulgaris	XP_007133857.1	264	28,951.0	6.59	26,930	38.90	90.38	−0.017	27	25
Lotus japonicus	AFK39224.1	283	31,348.76	5.66	32,430	42.36	87.74	−0.139	39	30
Cicer arietinum	XP_004510840.1	296	33,061.70	6.12	26,930	31.59	91.11	−0.250	38	33
Medicago truncatula	XP_003627882.1	426	47,961.8	8.57	29,910	31.89	85.02	−0.344	49	53
Arachis hypogaea	ALT56981.1	297	32,684.01	6.45	28,420	36.41	84.01	−0.227	34	32
Arachis duranensis	XP_015937330.1	297	32,883.25	6.45	28,420	37.35	84.01	−0.248	35	33
Corchorus capsularis	OMO94774.1	292	32,498.97	5.84	28,420	40.75	92.43	−0.159	38	33
Theobroma cacao	EOY22693.1	304	34,213.77	6.32	31,400	37.61	84.61	−0.292	39	36
Herrania umbratica	XP_021285810.1	305	34,392.01	6.56	36,900	40.38	83.38	−0.307	38	36
Durio zibethinus	XP_022738659.1	295	32,954.54	6.71	28,420	38.72	87.83	−0.237	36	35
Solanum lycopersicum	XP_004235863.1	294	32,476.9	5.93	28,420	34.32	83.23	−0.261	35	30
Solanum tuberosum	NP_001335929.1	408	44,295.0	5.96	28,420	20.21	93.19	−0.254	50	43
Brassica rapa	XP_009112000.1	274	30,640.7	6.25	34,380	30.25	80.66	−0.283	36	33
Capsicum baccatum	PHT32205.1	374	40,995.36	5.97	32,890	33.47	90.19	−0.297	50	44
Nicotiana attenuata	XP_019263239.1	368	40,865.55	5.51	31,400	30.30	93.51	−0.179	48	40
Capsicum annuum	PHT66064.1	374	41,015.41	5.91	32,890	32.27	92.01	−0.277	50	43
Capsicum chinense	PHU00941.1	374	40,986.37	5.81	32,890	32.27	92.27	−0.271	51	43
Brassica napus	XP_013749343.1	285	31,961.0	5.87	35,870	30.23	75.86	−0.387	40	34
Arabidopsis lyrata	XP_020870073.1	300	33,671.08	5.82	31,400	29.76	83.47	−0.324	42	35
Prunus avium	XP_021815221.1	281	31,100.28	6.20	31,400	26.98	86.41	−0.209	34	30
Trifolium pratense	PNY08557.1	273	30,275.83	5.50	23,950	29.99	96.70	−0.054	37	26
Arabidopsis thaliana	NP_200984.1	300	33,486.7	5.72	31,400	25.96	80.23	−0.329	40	31
Prunus persica	XP_007209445.1	282	31,303.57	6.50	31,400	28.39	85.39	−0.252	35	33
Lepidium latifolium	ACK86969.2	297	33,212.5	6.59	34,380	29.25	81.95	−0.285	31	29
Zea mays	XP_008649440.2	240	26,665.45	10.48	29,450	65.74	68.79	−0.517	22	37
Aegilops tauschii	XP_020147020.1	287	30,607.86	6.13	26,930	38.85	88.43	−0.052	33	29
Sorghum bicolor	XP_002452184.1	322	34,550.64	8.26	28,420	39.34	90.93	−0.013	32	34

MW molecular weight (g/mol), *pI* isoelectric point, *EC* extinction coefficient (M−1cm−1), *Ii* instability index, *Ai* aliphatic index, *GRAVY* grand average hydropathy, *(−R)* number of negative residues, *(+R)* number of positive residues

the average hydropathy of a protein, the positively rated being hydrophobic and negatively rated being hydrophilic in nature Kyte and Doolittle (1982). GRAVY index for IPK2 kinases was found ranging from −0.517 to −0.013 indicating that these proteins will interact favourably with water except for *Vigna radiata* with an index of 0.045 and hence is a potential hydrophobic protein.

Protein localization and target peptide predictions are significant studies as they aid in in silico protein function characterization as well as genome annotation. The acidic amino acid composition of IPK2 homologs determined by the physiochemical analysis conducted above suggest that they are cytoplasmic in nature as opposed to the basic amino acid composition of membrane proteins for their stability (Schwartz et al. 2001). Further sequence analysis based on TargetP scores (cTP: 0.163, mTP: 0.066, SP: 0.087, other: 0.906) also suggest that IPK2 kinases may be located anywhere in the cell besides chloroplast and mitochondria. The sequences were not predicted to have any signaling pre-sequence which was indicated by their low signal peptide (SP) score reinforced that they are soluble in nature. Besides, a consensus of predictions obtained from WoLF PSORT, CELLO v2.5, SubLoc v1.0 and MemType-2L servers (Table S1) also established the cytoplasmic character of IPK2 protein. However, TMpred, PSIPRED, NPS@ and DAS servers also identified a single consensus C-terminal transmembrane region positioned at 259–274. This could have been mistaken due to the presence of large regions

of hydrophobic residues in the C-terminal soluble region, as hydrophobicity alone is used as the criterion to predict membrane-spanning regions. The absence of any transmembrane helix is also well documented in the hydrophobicity plot generated using waveTM server (Fig S1) (Pashou et al. 2004) as majority of amino acids show negative for hydrophobicity.

Motif analysis and secondary structure characterization

Multiple sequence alignment (MSA) of the selected plant IPK2 homologs was performed using M-Coffee web server which is a meta-method for assembling MSA by combining the output of several individual methods into one to generate the best possible alignment. The consensus alignment thus generated revealed several significantly conserved motifs and sites unique to inositol phosphate kinases (Fig. 4). A signature inositol phosphate-binding motif, PxxxDxKxG was identified in all the aligned sequences (Odom et al. 2000; Saiardi et al. 1999) which confirms that they belong to inositol phosphate kinase (IPK) superfamily of IP kinases. Holmes and Jogl, 2006 state that the members of this superfamily share several strictly conserved signature motifs with each other and are predicted to assume the same overall fold, despite the low sequence conservation. The core catalytic tyrosine kinase motif, RxxxExxxY was also discovered in all the sequences which suggest that they are tyrosine-specific protein kinases (Cooper et al. 1984). IPK2 sequences from Solanaceae and Rosaceae families were found to contain a Glycine-rich consensus ATP-binding GxGxxG motif characteristic of protein kinase C (PKC) catalytic domain (Steinberg 2008). The classical PKC and plant CDPKs recognized phosphorylation S/TxK/R motif (Nishikawa et al. 1997; Neumann et al. 1996; Roberts and Harmon 1992) was also identified in some of the sequences speculating their role in lipid-dependent PA biosynthetic pathway. Such promiscuous kinase activity suggests that both lipid-dependent and independent pathways regulate PA biosynthesis as well as basic nuclear and cellular processes in plants (Josefsen et al. 2007; Stevenson-Paulik et al. 2002). A protein recognition LxxLL motif common to all of the aligned sequences indicate their participation in protein–protein interactions, regulating cell signalling, cell adhesion, and transcription (Plevin et al. 2005). Further analysis by MEME suite web server identified a total of 11 conserved ungapped motifs, with motif PxxxDxKxG being the most conserved amongst all IPK2 homologs as indicated by its lowest *E* value of 2.9e-487 (Fig S2). The obtained motifs were subjected to BLASTP analysis for conformation of their annotations which established that they all belong to IPK superfamily domain (CDD Acc: cl12283) and thus substantiate our previous results. We further explored GmIPK2 protein sequence by Motif Scan which recognized diverse protein kinase phosphorylation sites (Table S2). Since phosphorylation acts as a molecular switch in modulating protein function, structural rearrangement and cellular localization it can be suggested that GmIPK2 play a critical role in many biological regulatory events of signalling, proliferation, differentiation, and apoptosis. Its role in biological processes as diverse as mRNA export (York et al. 1999), DNA repair (Hanakahi et al. 2000), regulation of chromatin structure (Shen et al. 2003; Steger et al. 2003), maintenance of basal resistance to plant pathogens (Murphy et al. 2008) and apoptosis (Agarwal et al. 2009) have been studied in the past.

The secondary structure of a protein is more conserved than its nucleotide sequence and is, therefore, a prized source of information in understanding its classification, function, molecular evolution, and interaction with macromolecules (Reehana et al. 2013). In addition, secondary structure provides the first framework for homology based prediction of a protein 3D-model. Thus, in the current study, we inferred the secondary structure composition of IPK2 kinases from a three-state prediction done using NPS@ web server (Table 3). A high coil content was observed in most of the sequences including GmIPK2 while some showed them in nearly equal proportion with α-helix. This structural state can be justified based on the rich content of highly flexible glycine and kink inducing proline amino acid residues. The percentage of extended strands (% Ee) in all the kinases were found ranging from 13 to 29% except for the Poaceae family kinases which showed a low % Ee conformation (below 10%). PDBSum tool PROMOTIF analysis of GmIPK2 polypeptide identified total eight α-helices and eight β-strands arranged to form three antiparallel β-sheets, interspersed throughout by regions of coil or turn conformations (Fig. 5). We also recognized a varying number of bonded half-cystine pairs in all the IPK2 protein sequences using DIANNA server. It revealed the presence of 8 Cys residues in GmIPK2 and the most probable half-cystine pairs predicted by CYSREC were 94–121, 123–276 and 158–186. These potential long-term interactions participate in stabilizing the native conformations of our proteins and may as well contribute to differences in their tertiary structures.

Evolutionary analysis

Conserved motif analysis of IPK2 protein sequences point at a distinct evolutionary association between these kinases. Phylogenetic analysis would provide a further basis to determine their relatedness as well as to understand their collective evolution from a common ancestor. Previous research has reported that IPK superfamily of kinases to which *IPK2* belongs evolved from a common ancestor (Irvine and Schell 2001; Shears 2004). In our study, based on the alignment obtained in "Motif analysis and secondary structure

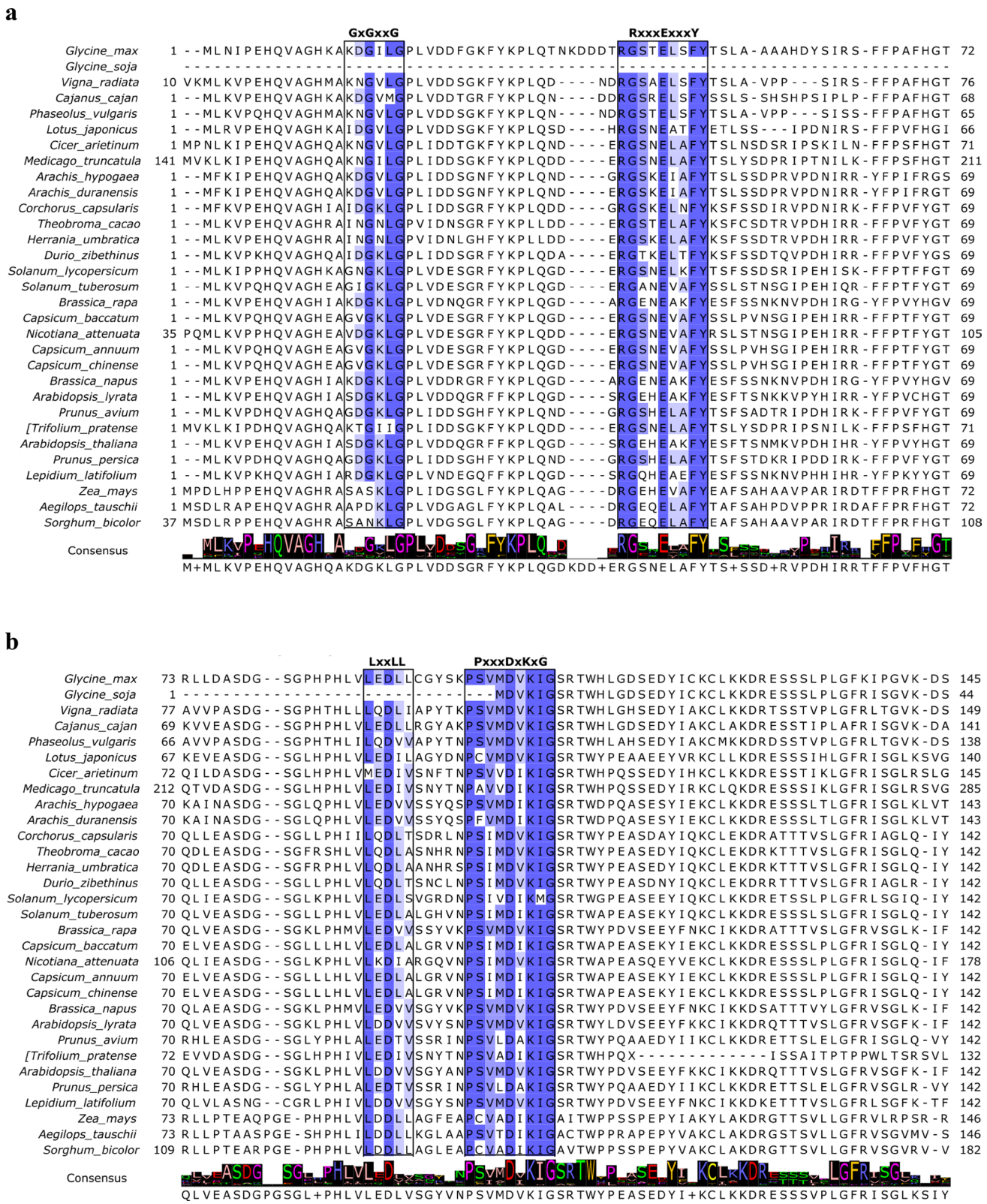

Fig. 4 M-Coffee *multiple* sequence alignment diagram of selected plant IPK2 protein sequences rendered with Jalview. The sequence motifs shared amongst all the representatives are coloured according to percentage identity. The consensus row at the bottom shows the most frequent residue at each column or a '+' if two or more residues are equally abundant

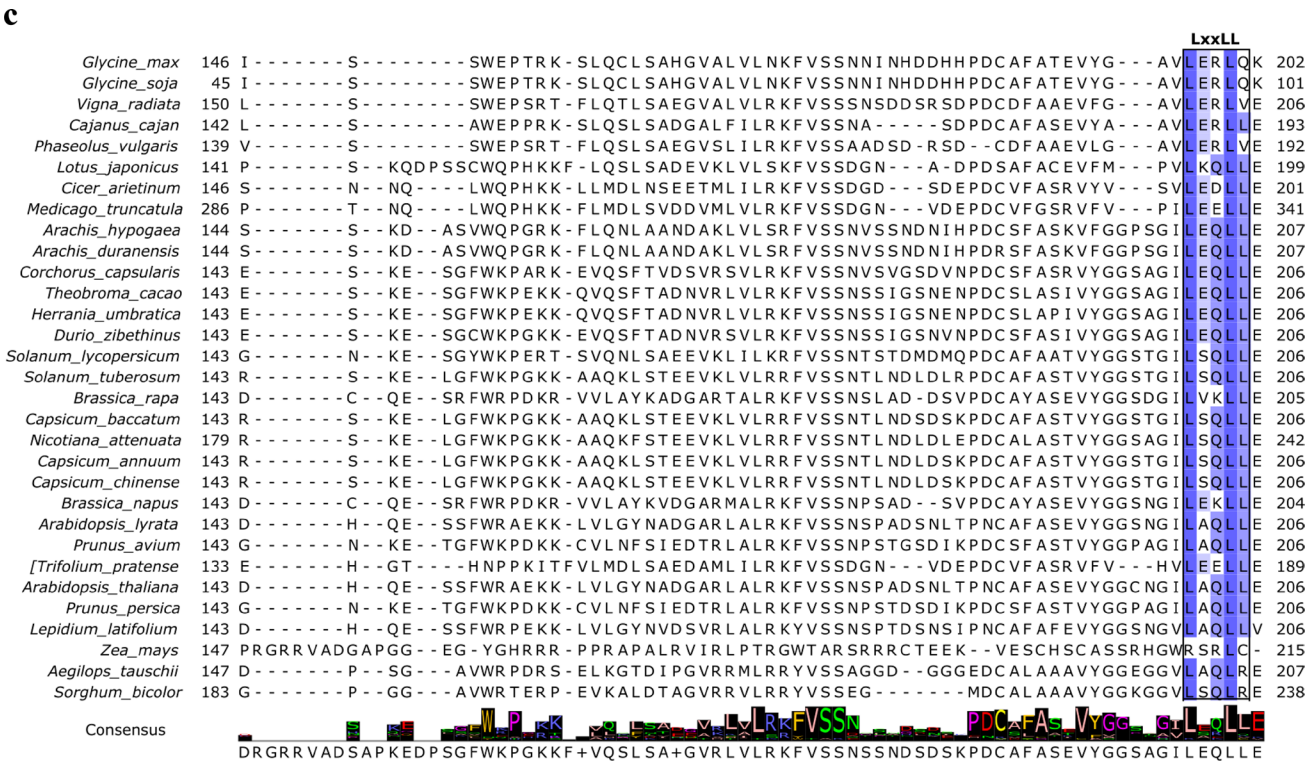

Fig. 4 (continued)

characterization" of GmIPK2 protein and its homologs, we constructed a neighbor-joining phylogenetic tree using MEGA 6.0 software (Fig. 6). The tree topology derived was supported by high bootstrap values. The IPK2s were clustered into six well delineated groups. The clusters consist of members of the Poaceae, Brassicaceae, Malvaceae, Rosaceae, Solanaceae and Fabaceae families. The Poaceae family of monocots (*Zea may, Sorghum bicolor and Aegilopus tauschii*) was found to be most distantly related to *G. max* in comparison to the fabaceae family of eudicots (*Glycine soja, Phaseolus vulgaris, Vigna radiata, Cajanus cajan, Trifolium pratense, Cicer arietinum, Medicago truncatula, Lotus japonicas, Arachis duranensis*, and *Arachis hypogaea*) which are most closely related.

Three-dimensional model construction

Model building

To derive structural information about GmIPK2 protein we built its theoretical model by following homology modeling approach since no X-ray crystal or NMR structure of it is available. The homology modeling technique takes advantage of structural conservation found in similar proteins that have evolved from a common ancestor. Yeast IPK2 protein was the first member of inositol multikinase family whose crystal structure was determined (Holmes and Jogl 2006), but it was found to show a very low sequence similarity with GmIPK2 protein. As we know, aligning two sequences can be a difficult process if the sequence similarity is low, we therefore, used the above derived GmIPK2 protein sequence as a query in PSI-BLAST to find more similar sequences amongst the PDB database proteins with resolved 3D structures to use as a potential template. The only closest homologous sequence available in PDB was that of chain A of *Arabidopsis thaliana* inositol phosphate multikinase (PDB:4FRF) which showed 55% sequence identity with an e value of 9e-99. The initial comparative models, i.e., GmIPK2-S and GmIPK2-P were built using fully automated SWISS-MODEL and PHYRE2 servers, respectively, which also identified 4FRF_A as the most reliable template using sensitive hidden markov model searches and used the same as the structural input. A global quality estimation score (GMQE) of 0.62 was provided by SWISS-MODEL which indicates a reasonably reliable structure. Homology model was additionally built using MODELLER 9.16 program from the X-ray crystal structure coordinates of the previously identified template structure (4FRF_A). The software generated five different models by optimizing the objective function of spatial restrains in a cartesian space. Three different energy scores viz. molpdf, DOPE and GA341 were computed for each of these models and compared to one

Table 3 Three-state description of secondary structure content and disulfide pattern prediction of IPK2 sequences

Organism	α-Helix (%Hh)	Extended strands (%Ee)	Random coil (%Cc)	Disulphide bridge prediction
Glycine max	26.88	13.26	31.54	94–121, 123–276, 158–186
Glycine soja	34.27	29.78	35.96	20–117, 22–85, 161–175
Vigna radiata	29.72	17.13	24.48	127–190, 263–281
Cajanus cajan	25.84	13.11	29.21	119–177
Phaseolus vulgaris	24.62	21.21	28.79	116–176, 208–249
Lotus japonicus	25.44	14.49	26.86	94–215, 149–187, 261–283
Cicer arietinum	21.96	14.53	28.72	122–185, 217–279, 260–274
Medicago truncatula	18.54	15.02	31.69	98–262, 325–357
Arachis hypogaea	24.58	14.48	33.67	120–188, 223–288, 269–292
Arachis duranensis	24.58	14.48	33.33	223–288, 269–292
Corchorus capsularis	19.52	20.21	25.34	120–187, 222–267
Theobroma cacao	19.74	16.78	39.14	50–120, 187–222, 267–298, 288–296
Herrania umbratica	18.69	14.75	42.95	120–296, 222–298, 267–288
Durio zibethinus	18.98	22.37	26.10	93–120, 149–222, 267–288
Solanum lycopersicum	18.03	18.37	30.27	120–187, 222–267
Solanum tuberosum	17.40	17.65	26.23	120–187, 222–283
Brassica rapa	13.50	21.17	22.63	144–186, 221–264
Capsicum baccatum	17.65	17.38	30.75	120–187, 222–283
Nicotiana attenuata	21.47	15.76	25.82	156–223, 258–303
Capsicum annuum	19.52	16.58	30.48	120–187, 222–267
Capsicum chinense	20.32	16.31	30.21	120–187, 222–267
Brassica napus	18.25	18.25	24.56	120–220, 144–185, 264–281
Arabidopsis lyrata	22.00	17.00	23.33	120–187, 222–272
Prunus avium	17.44	17.44	27.05	120–222, 156–187
Trifolium pratense	21.61	15.75	31.87	173–205, 203–250
Arabidopsis thaliana	22.00	16.67	24.67	120–187, 197–272
Prunus persica	17.02	17.02	29.79	120–222, 156–187
Lepidium latifolium	17.85	17.17	28.62	78–269, 120–187, 222–285
Zea mays	16.25	10.42	44.17	101–203, 192–200
Aegilops tauschii	28.57	7.67	31.36	110–188, 124–267
Sorghum bicolor	30.12	12.42	26.40	13–300, 137–160

The secondary structure data were generated by joint prediction with SOPMA and PHD while disulfide bonding pattern was determined using DiANNA (DiAminoacid Neural Network Application) 1.1 server

another to select the best 3D structure (Table S3). Model 4 (GmIPK2-M4), with the lowest molpdf and DOPE scores of 1734.48291 and − 27846.58203 respectively, was chosen as the principal conformational structure.

Structure validation

We then assessed the accuracy and reliability of all the three predicted models viz. GmIPK2-S, GmIPK2-P and GmIPK2-M4 using various online diagnostic tools (Table 4). RAMPAGE server which evaluates the 3D-structures based on Ramachandran plot calculations showed variable distribution of torsion angles in all the models. Fig S3a shows Ramachandran plot for GmIPK2-S model, showing 92.5% residues in favourable region and 4.9% in allowed region with just 2.7% residues in outlier region of the plot, which reflects its superior backbone geometry. We then utilized ProSA-web computational engine to analyze overall quality of the models based on their *z* scores and local quality based on their residue energies. GmIPK2-S model showed a better *z* score of − 6.56 which is displayed in the energy distribution plot derived from a group of experimentally determined protein structures of similar size. The *Z* score thus observed was very much within the range of scores typically found for native conformations of this group which indicates a good overall quality of the modelled protein (Fig S3b). Moreover, its residue energy was computed to be largely negative which further reflects that the local regions in the protein are modelled well (Fig S3c). The accuracy of 3D-models was further analyzed from energy profiles obtained by

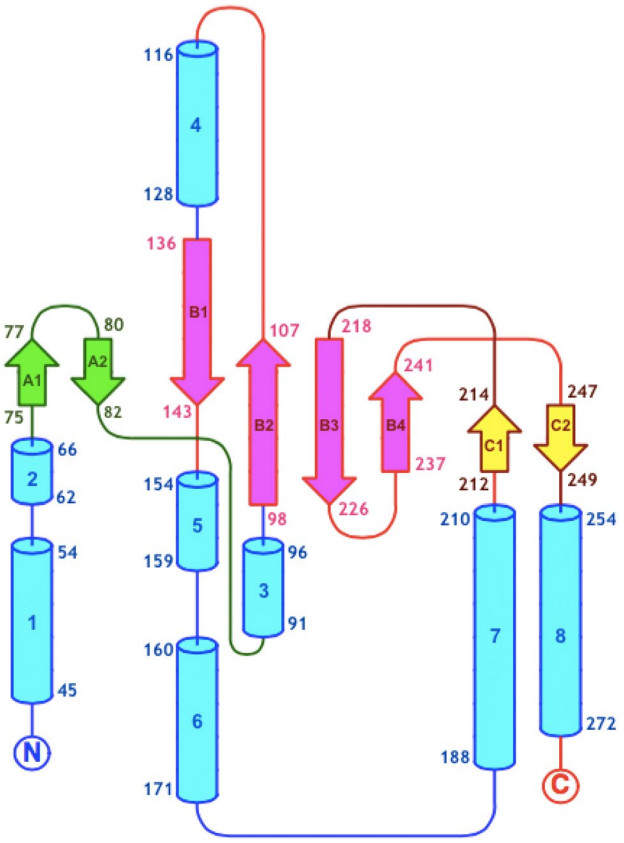

Fig. 5 Topology map of GmIPK2 generated using ProMotif. There are a total of eight α-helices (1–8) and three β-sheets (β-sheet 1: strands A1 and A2; β-sheet 2: strands B1, B2, B3 and B4; β-sheet 3: strands C1 and C2)

Verify3D program. Figure S3(d) shows 3D-1D profile for GmIPK2-S model with 97.82% of the model residues showing an average 3D-1D profile score >= 0.2 and hence validate that majority of its amino acid sequence reconcile to its environment in the 3D structure. Additionally, the pairwise 3D structural alignment of GmIPK2-S model with template protein, 4FRF_A using MATRAS 2.1 program revealed that both the structures shared 91.3% secondary structure identity (Fig S4a) and the average distance between the Cα backbone atoms of their 3D structures, i.e., root mean square deviation (RMSD) measured through superimposition was 0.44 Å (between 196 atom pairs) (Fig S4b). Based on the majority of winning scores, GmIPK2-S (Fig. 7) was chosen as the best comparative model for energy minimization and further analyses.

Molecular dynamics simulation

We subsequently performed MD simulation on our predicted GmIPK2-S model using GROMOS96 53A6 force field to compute its stability and dynamics. Initial potential energy minimization of solvated model showed that the maximum force dropped below the defined value of 1000 kJ mol^{-1} nm^{-1} in nearly 500 steps. The protein structure was then subjected to 50 ns of equilibration run at a constant temperature and pressure to obtain its molecular trajectory. The trajectory thus obtained was used to determine RMSD of Cα backbone atoms of the model using its starting structure as the reference, to determine its convergence towards an equilibrium state. Figure 8a shows RMSD as a function of simulation time. We observed that the protein stabilized around 10 ns of production run and converged to ~0.55 nm at 50 ns. The initial increase of RMSD could be attributed to the restraints in the system applied in the equilibration phase and their release later at the beginning of production phase. Besides RMSD, we also calculated root mean square fluctuations (RMSFs) to study mobility of the protein structure to draw an idea of its flexibility regions. From the RMSF plot (Fig. 8b), we identified Leu (75, 135, 272), Asp (76, 79, 127), Ala (77), Ser (78, 130–132), Gly (80, 136), His (84),

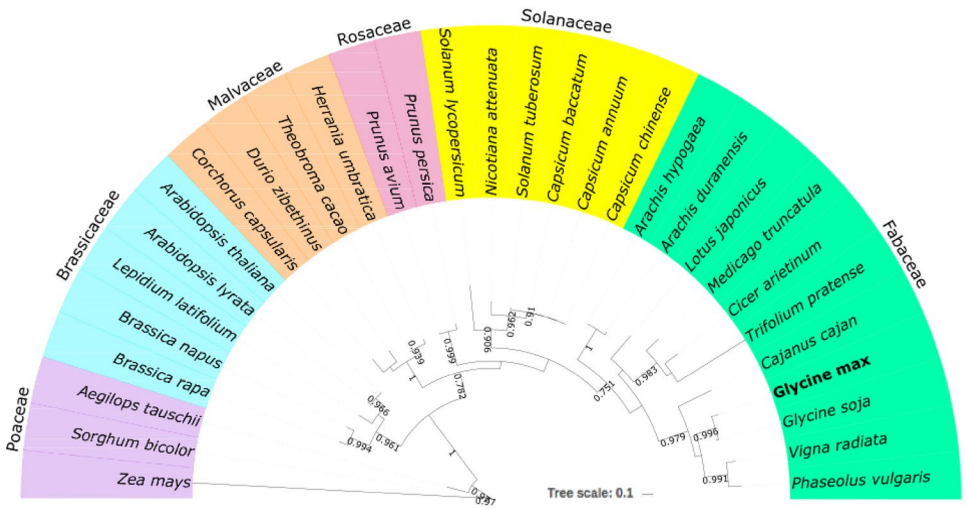

Fig. 6 Phylogenetic tree showing evolutionary relationship of 31 plant IPK2 sequences divided into different clades, colour coded to indicate the plant family to which they belong. The posterior probability values are indicated corresponding to every node

Table 4 Validation parameters computed for the energy-minimized 3D models of GmIPK2 protein built using different programs

Model	RAMPAGE Percentage of residues in favoured region	ProSA *Z* score	Verify3D Percentage of residues with 3D-1D score ≥ 0.2
GmIPK2-S	92.5	−6.56	97.82
GmIPK2-P	82.2	−6.28	84.95
GmIPK2-M4	87.7	−5.84	79.93

Fig. 7 Homology model of GmIPK2_S protein rendered using PyMOL

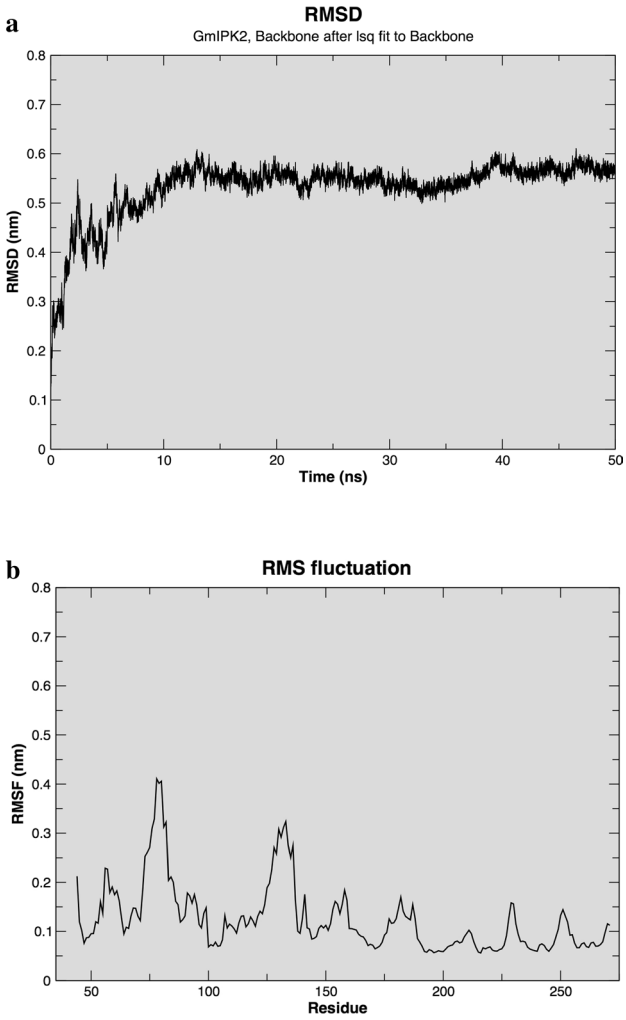

Fig. 8 **a** Root mean square deviations and **b** Root mean square fluctuations of the Cα backbone atoms in GmIPK2_S model over 50 ns MD simulation

Lys (126, 154), Glu (129, 230), Arg (128, 153) residues to be more flexible. This implies that the mentioned residues show greater movement from their native position, i.e., are dynamic in nature and thus are functionally more relevant. Thus, overall, the simulation results highlight the stable and reliable nature of our protein model and find it fit to be used for further active site predictions.

Molecular docking with inositol phosphates

Active site predictions

Once the protein model was refined, a comparative study was performed to detect possible binding pocket residues using CASTp, FTSite and FunFOLD2 binding site prediction servers (Fig S5). Lys105, Thr110, Lys122, Lys126, Ser130, Lys138, Ile139, Pro140, Arg153, Lys154, Gln157, and Ser219 were determined as possible active site residues in GmIPK2-S model. Similar predictions were also made in template protein (4FRF_A) which identified Arg104, Thr105, Pro108, Phe137, Lys149, Arg152, His216, Asn218, Ser219, Gln242, and Val246 as the probable binding site residues. From these studies, we could decipher that residues Lys, Arg, Pro, Thr, Gln and Ser are highly conserved in active sites of functionally identical model and template proteins.

Docking and residue interaction analysis

Molecular recognitions are vital to many biological processes. However, experimental determination of structures of molecular interactions is cost intensive, demand time, and expertise. We therefore, chose computational molecular docking to model our protein–ligand binding and characterize the interactions between its binding pocket residues and

known active ligands. Multiple substrate specificities have been described previously for IPK2 gene product, catalyzing primarily 5GUG-I3P and 4A69-I0P (Stevenson-Paulik et al. 2002). We thus docked these centroid ligands into the binding cavity of GmIPK2 protein using molecular docking program Autodock Vina based on a semi-flexible docking approach with the scaling factor defined within 0.1 nm to predict their bound geometry. VINA uses its iterated local search global optimizer algorithm to produce 9 different poses of which pose 1 corresponding to each ligand was identified as the best binding mode based on their lowest binding affinity score of − 6.2 kcal/mol for 5GUG-I3P and − 5.8 kcal/mol for 4A69-I0P computed by VINA's default statistical scoring function. We further inspected the molecular interactions between these protein substrate poses using Discovery Studio to predict functionally important amino acid residues and found that both the ligands were stabilized in their active site area by strong hydrogen-bonding interactions (Fig. 9a, b). Lys105 and Lys126 were identified as H-donors to the phosphate group oxygen of both 5GUG-I3P and 4A69-I0P while Arg153 a H-acceptor for hydrogen bonds formation suggesting that these binding pocket residues may play a pivotal role in enzymes function and protein structure stability. Based on the previous work conducted by Holmes and Jogl, we hypothesize that side chains of these amino acid residues may assist in inducing conformational changes on inositol phosphate binding, enabling the enzyme to interact with differently phosphorylated inositol polyphosphates in different orientations, thus endorsing its substrate versatility. Besides Ser217 was also found to form stabilizing hydrogen bond with I0P ligand. Gln157 and Pro140 were observed to form an unconventional carbon–oxygen hydrogen bond with 5GUG-I3P and 4A69-I0P respectively indicating their possible contribution to ligand binding affinity and ligand recognition (Klaholz and Moras 2002). Lengths and angles of hydrogen bonds stabilizing the GmIPK2-I3P and GmIPK2-I0P complexes are enlisted in Table 5a, b respectively. Moreover, our analysis indicates that Thr110, Lys138 and Lys154 show non-bonding interactions with the ligands. 2D protein GmIPK2-I3P/I0P ligand

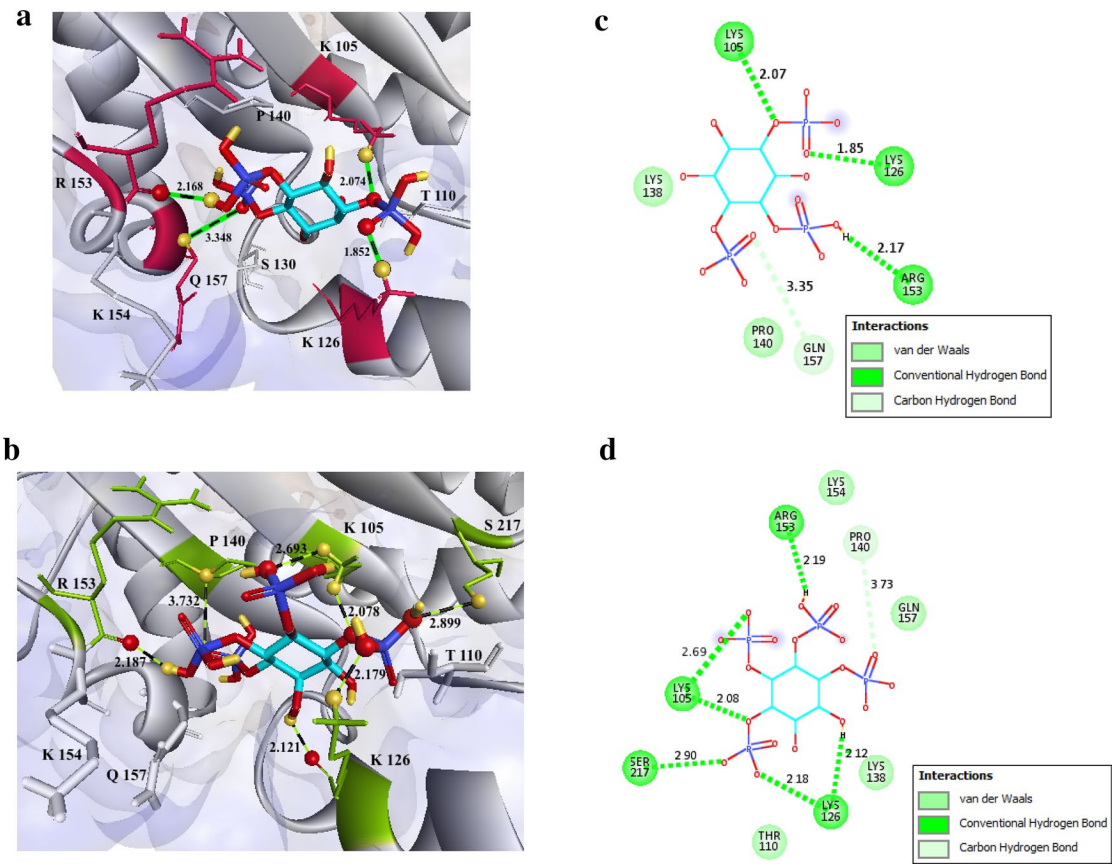

Fig. 9 Molecular docking of substrates to the GmIPK2_S homology model. Hydrogen-bonding interactions of **a** 5GUG-I3P and **b** 4A69-I0P substrates with residues in the active site of GmIPK2_S protein. The substrate is depicted in stick representation with carbon atoms coloured turquoise, oxygen atoms red, hydrogen atoms yellow and phosphorus atoms blue. The interacting protein side chains are represented as maroon sticks in **a** and green sticks in **b. c, d** 2D-schematic representation of the interactions shown in **a, b** respectively drawn using Discovery Studio Visualizer

interaction diagrams (Fig. 9c, d) were also generated using Discovery Studio.

Molecular dynamics simulation of GmIPK2-I3P and GmIPK2-I0P complexes

We subsequently subjected our docked protein–ligand complexes to MD simulation using GROMOS96 43A1 force field to understand their stability and dynamics. The trajectories obtained were utilized to construct their respective RMSDs, RMSFs and H-bond interactions. The GmIPK2-I3P and GmIPK2-I0P complexes exhibited a deviation between ~0.45–0.65 nm (Fig S6) and ~0.45–0.58 nm (Fig S7a), respectively, that converged to ~0.6 and ~0.55 nm, respectively, at 50 ns. This suggests that the structures were stabilized following simulation. From their RMSF plots, we observed fluctuations up to ~0.38 nm in the GmIPK2-I3P complex (Fig S6b) and ~0.29 nm in the GmIPK2-I0P complex (Fig S7(b)) which reveal the characteristic regional flexibilities of functional significance in each complex. We also analyzed the hydrogen bonds which participate in the maintenance of these complexes. Three main hydrogen bonds help to stabilize the ligands, 5GUG-I3P and 4A69-I0P, within the enzyme's active site, two of them acting as acceptors and only one as a donor. In particular, the hydrogen bonds formed with Lys105 and Lys126 and the oxygen atom of each ligand's phosphate group, were constantly held. Figure 10 shows the time evolution of these main H-bonds. Other less significant hydrogen bonds were formed sporadically between the ligands and the protein molecule. Lastly, we calculated the binding free energies ($\Delta G_{binding}$) of both the complexes using *g_mmpbsa* for their respective trajectories. $\Delta G_{binding}$ values of − 12.4 and − 11.9 kcal/mol were estimated for GmIPK2-I3P and GmIPK2-I0P complexes respectively. This indicates that the binding of ligand molecules is thermodynamically favourable and thus validates the reliability of our simulation.

Conclusion

The present work describes expression analysis and molecular characterization of *IPK2* multifunctional kinase involved in the late phase of PA biosynthesis. To initiate the study, we identified and cloned the partial gene sequence of *IPK2* from *G. max* cv. Pusa-16. *IPK2* transcripts, when assessed during seed development showed a predominant expression in the later stages of its development which consequently suggests that perturbing *IPK2* gene at this stage can be a viable strategy for manipulating PA levels in soybean seeds to achieve a *lpa* trait. Computational analysis of the gene further highlighted its molecular features including cis-acting promoter elements potentially regulating its observed expression; primary and secondary structural features shedding light on its physicochemical features, conserved functional motifs and major structural elements; and its evolutionary relationship, which can be used to design several experimental studies.

Table 5 Hydrogen bonds between the active site residues of GmIPK2 and its substrates (a) 5GUG-I3P and (b) 4A69-I0P along with their distances and angles measured using Accelrys Discovery Studio Visualizer 4.1

(a)						
GmIPK2			5GUG-I3P		Distance (A°)	Angle (Degree°)
Residue	Atom	Chemistry	Atom	Chemistry		
Lys105	HZ3	H-Donor	O7	H-Acceptor	2.074	49.9029
Lys126	HZ3	H-Donor	O14	H-Acceptor	1.852	44.2482
Arg153	O	H-Acceptor	H39	H-Donor	2.168	45.6080
Gln157	CA	H-Donor	O18	H-Acceptor	3.348	52.1869
(b)						
GmIPK2			4A69-I0P		Distance (A°)	Angle (Degree°)
Residue	Atom	Chemistry	Atom	Chemistry		
Lys105	HZ2	H-Donor	O18	H-Acceptor	2.693	47.8602
Lys105	HZ3	H-Donor	O24	H-Acceptor	2.078	28.0171
Lys126	HZ3	H-Donor	O28	H-Acceptor	2.179	35.7367
Lys126	O	H-Acceptor	H40	H-Donor	2.121	39.3959
Pro140	CA	H-Donor	O4	H-Acceptor	3.732	60.3277
Arg153	O	H-Acceptor	H36	H-Donor	2.187	16.0359
Ser217	HG	H-Donor	O27	H-Acceptor	2.899	22.5987

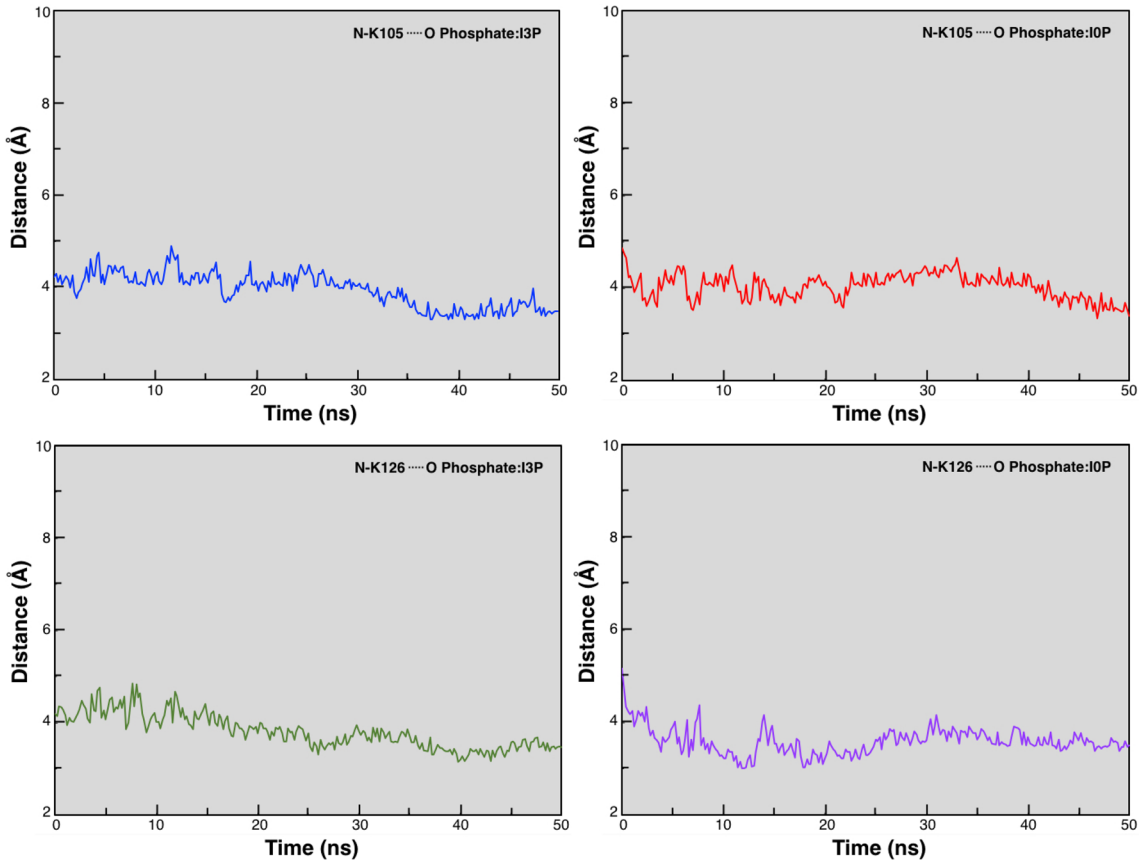

Fig. 10 Time evolution of main hydrogen bonds formed between the GmIPK2_S protein and the 5GUG-I3P and 4A69-I0P ligands over 50 ns MD simulation

The 3D model of IPK2 protein developed can assist in the experimental determination of its 3D model as well as can be considered as a working model for generating hypothesis to make more accurate predictions of protein function and catalytic mechanism in the future. The docking studies performed subsequently can be used for structure-based designing of potent IPK2 inhibitors, useful in studying IPK2 active site and substrate selectivity and for studying PA biosynthesis pathway in detail. In conclusion, the obtained results provide very important preliminary data needed to manipulate PA content in soybean seeds as well as other crops for improving their nutritional quality by biotechnological intervention in the future.

Acknowledgements Financial support for the work was provided by funding from the National Funds for Basic, Strategic and Frontier Application Research in Agriculture [Grant No. NFBSFARA/RNAi-2011/2011-12], ICAR, Government of India. The authors would also like to thankfully acknowledge the Supercomputing Facility for Bioinformatics and Computational Biology at IIT Delhi for the use of its facilities.

Compliance with ethical standards

Conflict of interest The authors declare that there is no conflict of interest regarding the publication of this article.

References

Abe H, Urao T, Ito T, Seki M, Shinozaki K, Yamaguchi-Shinozaki K (2003) Arabidopsis AtMYC2 (bHLH) and AtMYB2 (MYB) function as transcriptional activators in abscisic acid signalling. Plant Cell 15:63–78

Accelrys Software Inc (2013) Discovery studio modeling environment, release 4.0. Accelrys Software Inc., San Diego

Agarwal R, Mumtaz H, Ali N (2009) Role of inositol polyphosphates in programmed cell death. Mol Cell Biochem 328:155–165

Aggarwal S, Shukla V, Bhati KK, Kaur M, Sharma S, Singh A, Mantri S, Pandey AK (2015) Hormonal regulation and expression profiles of wheat genes involved during phytic acid biosynthesis pathway. Plants (Basel) 4:298–319

Ali N, Paul S, Gayen D, Sarkar SN, Datta SK, Datta K (2013a) Development of low phytate rice by RNAi mediated seed-specific

silencing of inositol 1,3,4,5,6-pentakisphosphate 2-kinase gene (IPK1). PLoS One 8:e68161

Ali N, Paul S, Gayen D, Sarkar SN, Datta SK, Datta K (2013b) RNAi mediated down regulation of myo-inositol-3-phosphate synthase to generate low phytate rice. PLoS One 6:12

Arguello-Astorga GR, Herrera-Estrella LR (1996) Ancestral multipartite units in light-responsive plant promoters have structural features correlating with specific phototransduction pathways. Plant Physiol 112:1151–1166

Bailey TL, Boden M, Buske FA, Frith M, Grant CE, Clementi L, Ren J, Li WW, Noble WS (2009) MEME SUITE: tools for motif discovery and searching. Nucleic Acids Res 37:W202–W208

Bhati KK, Aggarwal S, Sharma S, Mantri S, Singh S, Bhalla S, Kaur J, Tiwari S, Roy J, Tuli R, Pandey AK (2014) Differential expression of structural genes for the late phase of phytic acid biosynthesis in developing seeds of wheat (*Triticum aestivum* L.). Plant Sci 224:74–85

Biasini M, Bienert S, Waterhouse A, Arnold K, Studer G, Schmidt T, Kiefer F, Cassarino TG, Bertoni M, Bordoli L, Schwede T (2014) SWISS-MODEL: modeling protein tertiary and quaternary structure using evolutionary information. Nucleic Acids Res 42:W252–W258

Bibikova TN, Zhigiler A, Gilroy S (1997) Root hair growth in Arabidopsis thaliana is directed by calcium and an endogenous polarity. Planta 203:495–505

Bilyeu Kristin D, Zeng P, Coello P, Zhang Zhanyuan J, Krishnan Hari B, Bailey A, Beuselinck Paul R, Polacco Joe C (2008) Quantitative conversion of phytate to inorganic phosphorus in soybean seeds expressing a bacterial phytase. Plant Physiol 146:468–477

Bond CS (2003) TopDraw: a sketchpad for protein structure topology cartoons. Bioinformatics 19:311–312

Brearley CA, Hanke DE (1996a) Inositol phosphates in barley (*Hordeum vulgare* L.) aleurone tissue are stereochemical similar to the products of breakdown of Ins P6 in vitro by wheat bran phytase. Biochem J 318:279–286

Brearley CA, Hanke DE (1996b) Metabolic evidence for the order of addition of individual phosphate esters to the myo-inositol moiety of inositol hexakisphosphate in the duckweed Spirodela polyrhiza L. Biochem J 314:227–233

Buchan DWA, Minneci F, Nugent TCO, Bryson K, Jones DT (2013) Scalable web services for the PSIPRED protein analysis workbench. Nucleic Acids Res 41:W340–W348

Chou KC, Shen HB (2007) MemType-2L: a Web server for predicting membrane proteins and their types by incorporating evolution information through Pse-PSSM. Biochem Biophys Res Commun 360:339–345

Cichy K, Raboy V (2009) Evaluation and development of low-phytate crops. In: Hari Krishnan B (eds) Crop Science Society of America, Soil Science Society of America. American Society of Agronomy, Madison, pp 177–200

Cooper JA, Esch FS, Taylor SS, Hunter T (1984) Phosphorylation sites in enolase and lactate dehydrogenase utilized by tyrosine protein kinases in vivo and in vitro. Biol Chem 259:7835–7841

Dundas J, Ouyang Z, Tseng J, Binkowski A, Turpaz Y, Liang J (2006) CASTp: computed atas of surface topography of proteins with structural and topographical mapping of functionally annotated residues. Nucleic Acids Res 34:W116–W118

Eisenberg D, Lüthy R, Bowie JU (1997) VERIFY3D: assessment of protein models with three-dimensional profiles. Methods Enzymol 277:396–404

Emanuelsson O, Nielsen H, Brunak S, Heijne G (2000) Predicting subcellular localization of proteins based on their N-terminal amino acid sequence. Mol Biol 300:1005–1016

Feldbrugge M, Hahlbrock K, Weisshaar B (1996) The transcriptional regulator CPRF1: expression analysis and gene structure. Mol Gen Genet 251:619–627

Felle HH, Hepler PK (1997) The cytosolic Ca^{2+} concentration gradient of Sinapis alba root hairs as revealed by Ca^{2+} selective microelectrode tests and fura-dextran ratio imaging. Plant Physiol 114:39–45

Feng X, Yoshida KT (2004) Molecular approaches for producing low-phytic-acid grains in rice. Plant Biotechnol 21:183–189

Ferrè F, Clote P (2005) DiANNA: a web server for disulfide connectivity prediction. Nucleic Acids Res 33:W230–W232

Fileppi M, Galasso I, Tagliabue G, Daminati M, Campion B, Doria E, Sparvoli F (2010) Characterisation of structural genes involved in phytic acid biosynthesis in common bean (*Phaseolus vulgaris* L.). Mol Breed 25:453–470

Franklin-Tong VE, Drobak BK, Allan AC, Trewavas AJ (1996) Growth of pollen tubes of Papaver rhoeas is regulated by a slow moving calcium wave propagated by inositol 1,4,5-trisphosphate. Plant Cell 8:1305–1321

Frederick JP, Mattiske D, Wofford JA, Megosh LC, Drake LY, Chiou ST, Hogan BLM, York JD (2005) An essential role for an inositol polyphosphate multikinase, Ipk2, in mouse embryogenesis and second messenger production. Proc Natl Acad Sci 102:8454–8459

Gasteiger E, Hoogland C, Gattiker A, Duvaud S, Wilkins MR, Appel RD, Bairoch A (2005) Protein identification and analysis tools on the ExPASy server. In: Walker JM (ed) The proteomics protocols handbook. Humana Press, pp 571–607

Geourjon C, Deléage G (1995) SOPMA: significant improvements in protein secondary structure prediction by consensus prediction from multiple alignments. Comput Appl Biosci 11:681–684

Gill SC, Von Hippel PH (1989) Calculation of protein extinction coefficients from amino acid sequence data. Anal Biochem 182:319–326

Goodstein DM, Shu S, Howson R, Neupane R, Hayes RD, Fazo J, Mitros T, Dirks W, Hellsten U, Putnam N, Rokhsar DS (2012) Phytozome: a comparative platform for green plant genomics. Nucleic Acids Res 40:D1178–D1186

Guruprasad K, Reddy BVB, Pandit MW (1990) Correlation between stability of a protein and its dipeptide composition: a novel approach for predicting in vivo stability of a protein from its primary sequence. Protein Eng 4:155–161

Hanakahi LA, Bartlet-Jones M, Chappell C, Pappin D, West SC (2000) Binding of inositol phosphate to DNA-PK and stimulation of double-strand break repair. Cell 102:721–729

Hofmann K, Stoffel W (1993) TMbase—a database of membrane spanning proteins segments. Biol Chem 374:166

Holmes W, Jogl G (2006) Crystal structure of inositol phosphate multikinase 2 and implications for substrate specificity. Biol Chem 281:38109–38116

Horton P, Park KJ, Obayashi T, Fujita N, Harada H, Adams-Collier CJ, Nakai K (2007) WoLF PSORT: protein localization predictor. Nucl Acids Res 35:W585–W587

Hua S, Sun Z (2001) Support vector machine approach for protein subcellular localization prediction. Bioinformatics 17:721–728

Ikai AJ (1980) Thermostability and aliphatic index of globular proteins. J Biochem 88:1895–1898

Irvine RF, Schell MJ (2001) Back in the water: the return of the inositol phosphates. Nat Rev Mol Cell Biol 2:327–338

Josefsen L, Bohn L, Sorensen M, Rasmussen S (2007) Characterization of a multifunctional inositol phosphate kinase from rice and barley belonging to the ATP-grasp superfamily. Gene 397:114–125

Kawabata T (2003) MATRAS: a program for protein 3D structure comparison. Nucleic Acids Res 31:3367–3369

Kelley LA, Mezulis S, Yates CM, Wass MN, Sternberg MJE (2015) The Phyre2 web portal for protein modeling, prediction and analysis. Nat Protoc 10:845–858

Kim SR, Kim Y, An G (1993) Identification of methyl jasmonate and salicylic acid response elements from the nopaline synthase (nos) promoter. Plant Physiol 103:97–103

Klaholz B, Moras D (2002) C–H … O hydrogen bonds in the nuclear receptor RARgamma—a potential tool for drug selectivity. Structure 10:1197–1204

Kozakov D, Grove LE, Hall DR, Bohnuud T, Mottarella SE, Luo L, Xia B, Beglov D, Vajda S (2015) The FTMap family of web servers for determining and characterizing ligand-binding hot spots of proteins. Nat Protoc 10:733–755

Krishnan V, Jain P, Tripathi V, Hada A, Manickavasagam M, Ganapathi A, Rai RD, Sachdev A (2015) Molecular modeling and in-silico characterization of Glycine max inositol (1,3,4) tris 5/6 kinase-1 (Gmitpk1)—a potential candidate gene for developing low phytate transgenics. Plant Omics 8:381–391

Kuwano M, Mimura T, Takaiwa F, Yoshida KT (2009) Generation of stable 'low phytic acid' transgenic rice through antisense repression of the 1D-myo-inositol 3-phosphate synthase gene using the 18-kDa oleosin promoter. Plant Biotechnol 7:96–105

Kyte J, Doolittle RF (1982) A simple method for displaying the hydropathic character of a protein. J Mol Biol 157:105–132

Lescot M, Dehais P, Thijs G, Marchal K, Moreau Y, Van de Peer Y, Rouze P, Rombauts S (2002) PlantCARE, a database of plant cis-acting regulatory elements and a portal to tools for in silico analysis of promoter sequences. Nucleic Acids Res 30:325–327

Letunic I, Bork P (2016) Interactive tree of life (iTOL) v3: an online tool for the display and annotation of phylogenetic and other trees. Nucl Acids Res 44:W242–W245

Livak KJ, Schmittgen TD (2001) Analysis of relative gene expression data using realtime quantitative PCR and the $2\Delta\Delta C(T)$ method. Methods 25(4):402–408

Lois R, Dietrich A, Hahlbrock K, Schulz W (1989) A phenylalanine ammonia-lyase gene from parsley: structure, regulation and identification of elicitor and light responsive cis-acting elements. EMBO J 8:1641–1648

Lopez-Ochoa L, Acevedo-Hernández G, Martínez-Hernández A, Argüello-Astorga G, Herrera-Estrella L (2007) Structural relationships between diverse cis-acting elements are critical for the functional properties of a rbcS minimal light regulatory unit. J Exp Bot 58:4397–4406

Lovell SC, Davis IW, Arendall WB III, Bakker PIW, Word JM, Prisant MG, Richardson JS, Richardson DC (2003) Structure validation by C_α geometry: Φ,Ψ and C_β deviation. Proteins 50:437–450

Majerus PW (1992) Inositol phosphate biochemistry. Annu Rev Biochem 61:225–250

Majerus PW (1996) Inositols do it all. Genes Dev 10:1051–1053

Malho R (1998) Role of 1,4,5-inositol trisphosphate-induced Ca^{2+} release in pollen tube orientation. Sex Plant Reprod 11:231–235

Matsuno K, Fujimura T (2014) Induction of phytic acid synthesis by abscisic acid in suspension-cultured cells of rice. Plant Sci 217–218:152–157

Mongkolsiriwatana C, Pongtongkam P, Peyachoknagul S (2009) In silico promoter analysis of photoperiod-responsive genes identified by DNA microarray in rice (*Oryza sativa* L.). Kasetsart J (Nat Sci) 43:164–177

Morris GM, Huey R, Lindstrom W, Sanner MF, Belew RK, Goodsell DS, Olson AJ (2009) Autodock4 and AutoDockTools4: automated docking with selective receptor flexibility. J Comput Chem 16:2785–2791

Murphy AM, Otto B, Brearley CA, Carr JP, Hanke DE (2008) A role for inositol hexakisphosphate in the maintenance of basal resistance to plant pathogens. Plant J 56:638–652

Neumann GM, Thomas I, Polya GM (1996) Identification of the site on potato carboxypeptidase inhibitor that is phosphorylated by plant calcium-dependent protein kinase. Plant Sci 114:45–51

Nguyen T, Sherratt PJ, Cecil B, Pickett CB (2003) Regulatory mechanisms controlling gene expression mediated by the antioxidant response element. Annu Rev Pharmacol Toxicol 43:233–260

Nishikawa K, Toker A, Johannes FJ, Songyang Z, Cantley LC (1997) Determination of the specific substrate sequence motifs of protein kinase C isozymes. Biol Chem 272:952–960

Niu J, Wang J, Hu H, Chen Y, An J, Cai J, Sun R, Sheng A, Liu X, Lin S (2016) Cross-talk between freezing response and signalling for regulatory transcriptions of MIR475b and its targets by miR475b promoter in Populous suaveolens. Sci Rep 6:20648

Nunes ACS, Vianna GR, Cuneo F, Amaya-Farfan J, de Capdeville G, Rech EL, Aragao FJL (2006) RNAi mediated silencing of the myo-inositol-1-phosphate synthase gene (GmMIPS1) in transgenic soybean inhibited seed development and reduced phytate content. Planta 224:125–132

Odom AR, Stahlberg A, Wente SR, York JD (2000) A role for nuclear inositol 1,4,5-trisphosphate kinase in transcriptional control. Science 287:2026–2029

Omasits U, Ahrens CH, Müller S, Wollscheid B (2014) Protter: interactive protein feature visualization and integration with experimental proteomic data. Bioinformatics 30:884–886

Onodera Y, Suzuki A, Wu CY, Washida H, Takaiwa F (2001) A rice functional transcriptional activator, RISBZ1, responsible for endosperm-specific expression of storage protein genes through GCN4 motif. J Biol Chem 276:14139–14152

Pagni M, Ioannidis V, Cerutti L, Zahn-Zabal M, Jongeneel CV, Hau J, Martin O, Kuznetsov D, Falquet L (2007) MyHits: improvements to an interactive resource for analyzing protein sequences. Nucleic Acids Res 35:W433–W437

Pashou EE, Litou ZI, Liakopoulos TD, Hamodrakas SJ (2004) WaveTM: wavelet-based transmembrane segment prediction. In Silico Biol 4:127–131

Petersen TN, Brunak S, Heijne G, Nielsen H (2011) SignalP 4.0: discriminating signal peptides from transmembrane regions. Nat Methods 8:785–786

Pettersen EF, Goddard TD, Huang CC, Couch GS, Greenblatt DM, Meng EC, Ferrin TE (2004) UCSF chimera—a visualization system for exploratory research and analysis. J Comput Chem 25(13):1605–1612

Pierson ES, Miller DD, Callaham DA, Shipley MA, Rivers BA, Cresti M, Hepler PK (1994) Pollen tube growth is coupled to the extracellular calcium ion flux and the intracellular calcium gradient: effect of BAPTA-type buffers and hypertonic media. Plant Cell 6:1815–1828

Plevin MJ, Mills MM, Ikura M (2005) The LxxLL motif: a multifunctional binding sequence in transcriptional regulation. Trends Biochem Sci 30:66–69

Pronk S, Páll S, Schulz R, Larsson P, Bjelkmar P, Apostolov R, Shirts MR, Smith JC, Kasson PM, Spoel D, Hess B, Lindahl E (2013) GROMACS 4.5: a high-throughput and highly parallel open source molecular simulation toolkit. Bioinformatics 29:845–854

Raboy V, Dickinson DB (1987) The timing and rate of phytic acid accumulation in developing soybean seeds. Plant Physiol 85:841–844

Reehana N, Ahamed AP, Ali DM, Suresh A, Kumar RA, Thajuddin N (2013) Structure based computational analysis and molecular phylogeny of C-Phycocyanin gene from the selected cynobacteria. Int J Biol Vet Agric Food Eng 7:47–51

Rice P, Longden I, Bleasby A (2000) Emboss: the European molecular biology open software suite. Trends Genet 16:276–277

Roberts DM, Harmon AC (1992) Calcium modulated proteins: targets of intracellular calcium signals in higher plants. Annu Rev Plant Physiol Plant Mol Biol 43:375–414

Roche DB, Buenavista MT, McGuffin LJ (2013) The FunFOLD2 server for the prediction of protein-ligand interactions. Nucleic Acids Res 41:W303–W307

Rogers S, Wells R, Rechsteiner M (1986) Amino acid sequences common to rapidly degraded proteins: the PEST hypothesis. Science 234:364–368

Rost B, Sander C (1993) Prediction of protein secondary structure at better than 70% accuracy. Mol Biol 232:584–599

Rost B, Casadio R, Fariselli P (1996) Refining neural network predictions for helical transmembrane proteins by dynamic programming. Proc Int Conf Intell Syst Mol Biol 4:192–200

Rouster J, Leah R, Mundy J, Cameron-Mills V (1997) Identification of a methyl jasmonate-responsive region in the promoter of a lipoxygenase 1 gene expressed in barley grain. Plant J 11:513–523

Saiardi A, Erdjument-Bromage H, Snowman A, Tempst P, Snyder SH (1999) Synthesis of diphosphoinositol pentakisphosphate by a newly identified family of higher inositol polyphosphate kinases. Curr Biol 9:1323–1326

Saiardi A, Caffrey JJ, Snyder SH, Shears SB (2000) Inositol polyphosphate multikinase (ArgRIII) determines nuclear mRNA export in *Saccharomyces cerevisiae*. Biol Chem J 275:24686–24692

Schwartz R, Ting CS, King J (2001) Whole proteome pI values correlate with subcellular localizations of proteins for organisms within the three domains of life. Genome Res 11(5):703–709

Sessa G, Meller Y, Fluhr R (1995) A GCC element and a G-box motif participate in ethylene-induced expression of the PRB-1b gene. Plant Mol Biol 28:145–153

Shears SB (2004) How versatile are inositol phosphate kinases? Biochem J 377:265–280

Shen X, Xiao H, Ranallo R, Wu WH, Wu C (2003) Modulation of ATP-dependent chromatin-remodeling complexes by inositol polyphosphates. Science 299:112–114

Shinozaki K, Yamaguchi-Shinozaki K (2000) Molecular responses to dehydration and low temperature: differences and cross-talk between two stress signaling pathways. Curr Opin Plant Biol 3:217–223

Steger DJ, Haswell ES, Miller AL, Wente SR, O'Shea EK (2003) Regulation of chromatin remodeling by inositol polyphosphates. Science 299:114–116

Steinberg SF (2008) Structural basis of protein kinase C isoform function. Physiol Rev 88:1341–1378

Stevenson-Paulik J, Odom AR, York JD (2002) Molecular and biochemical characterization of two plant inositol polyphosphate 6-/3-/5-kinases. Biol Chem J 277:42711–42718

Stevenson-Paulik J, Bastidas GJ, Chiou ST, Frye RA, York JD (2005) Generation of phytate-free seeds in Arabidopsis through disruption of inositol polyphosphate kinases. Proc Natl Acad Sci 102:12612–12617

Stiles AR (2007) Identification and characterization of late pathway enzymes in phytic acid biosynthesis in Glycine max, Dissertation, Virginia Polytechnic Institute and State University

Stiles A, Qian X, Shears S, Grabau E (2008) Metabolic and signaling properties of an ITPK gene family in Glycine max. FEBS Lett 582:1853–1858

Sugimoto T, Kawasaki T, Kato T, Whittier RF, Shibata D, Kawamura Y (1992) cDNA sequence and expression of a phosphoenolpyruvate carboxylase gene from soybean. Plant Mol Biol 20:743–747

Sun Y, Thompson M, Lin G, Butler H, Gao Z, Thornburgh S, Yau K, Smith D, Shukla V (2007) Inositol 1,3,4,5,6-pentakisphosphate 2-kinase from maize: Molecular and biochemical characterization. Plant Physiol 144:1278–1291

Suzuki M, Tanaka K, Kuwano M, Yoshida K (2007) Expression pattern of inositol phosphate-related enzymes in rice (*Oryza sativa* L.): Implications for the phytic acid biosynthetic pathway. Gene 405:55–64

Sweetman D, Johnson S, Caddick S, Hanke D, Brearley C (2006) Characterization of an Arabidopsis inositol 1,3,4,5,6-pentakisphosphate 2-kinase (AtIPK1). Biochem J 394:95–103

Sweetman D, Stavridou I, Johnson S, Green P, Caddick S, Brearley C (2007) Arabidopsis thaliana inositol 1,3,4-trisphosphate 5/6-kinase 4 (AtITPK4) is an outlier to a family of ATP-grasp fold proteins from Arabidopsis. FEBS Lett 581:4165–4171

Takaiwa F, Yamanouchi U, Yoshihara T, Washida H, Tanabe F, Kato A, Yamada K (1996) Characterization of common cis-regulatory elements responsible for the endosperm-specific expression of members of the rice glutelin multigene family. Plant Mol Biol 30:1207–1221

Tamura K, Stecher G, Peterson D, Filipski A, Kumar S (2013) MEGA6: Molecular evolutionary genetics analysis version 6.0. Mol Biol Evol 30:2725–2729

Trott O, Olson AJ (2010) AutoDock Vina: improving the speed and accuracy of docking with a new scoring function, efficient optimization and multithreading. Comput Chem 31:455–461

Turner PJ (2005) XMGRACE, version 5.1.19. center for coastal and land-margin research. Oregon Graduate Institute of Science and Technology, Beaverton

Tuteja JH, Clough SJ, Chan WC, Vodkin LO (2004) Tissue-specific gene silencing mediated by a naturally occurring chalcone synthase gene cluster in glycine max. Plant Cell 16:819–835

Wallace IM, Sullivan O, Higgins DG, Notredame C (2006) M-Coffee: combining multiple sequence alignment methods with T-Coffee. Nucleic Acids Res 34:1692–1699

Washida H, Wu CY, Suzuki A, Yamanouchi U, Akihama T, Harada K, Takaiwa F (1999) Identification of cis-regulatory elements required for endosperm expression of the rice storage protein glutelin gene GluB-1. Plant Mol Biol 40:1–12

Waterhouse AM, Procter JB, Martin DMA, Clamp M, Barton GJ (2009) Jalview Version 2—a multiple sequence alignment editor and analysis workbench. Bioinformatics 25(9):1189–1191

Webb B, Sali A (2016) Comparative protein structure modeling using modeller. Curr Protoc Bioinform 54:5.6.1–5.6.37

Wiederstein M, Sippl MJ (2007) ProSA-web: interactive web service for the recognition of errors in three-dimensional structures of proteins. Nucleic Acids Res 35:W407–W410

Wu CY, Adach T, Hatano T, Washida H, Suzuki A, Takaiwa F (1998) Promoters of rice seed storage protein genes direct endosperm-specific gene expression in transgenic rice. Plant Cell Physiol 39:885–889

Wymer CL, Bibikova TN, Gilroy S (1997) Cytoplasmic free calcium distribution during the development of root hairs of *Arabidopsis thaliana*. Plant J 12:427–439

Xu J, Brearley CA, Lin WH, Wang Y, Ye R, Mueller-Roeber B, Xu ZH, Xue HW (2005) A role of Arabidopsis inositol polyphosphate kinase, AtIPK2α, in pollen germination and root growth. Plant Physiol 137:94–103

Yamaguchi-Shinozaki K, Mundy J, Chua NH (1989) Four tightly linked rab genes are differentially expressed in rice. Plant Mol Biol 14:29–39

York JD, Odom AR, Murphy R, Ives EB, Wente SR (1999) A phospholipase C-dependent inositol polyphosphate kinase pathway required for efficient messenger RNA export. Science 285:96–100

Yu CS, Chen YC, Lu CH, Hwang JK (2006) Prediction of protein subcellular localization. Proteins 64:643–651

Zhang ZB, Yang G, Arana F, Chen Z, Li Y, Xia HJ (2007) Arabidopsis inositol polyphosphate 6-/3-Kinase (AtIpk2β) is involved in axillary shoot branching via auxin signaling. Plant Physiol 144:942–951

Annals of **F**uzzy **M**athematics and **I**nformatics
Volume x, No. x, (Month 201y), pp. 1–xx
ISSN: 2093–9310 (print version)
ISSN: 2287–6235 (electronic version)
http://www.afmi.or.kr

@FMI
© Research Institute for Basic Science, Wonkwang University
http://ribs.wonkwang.ac.kr

New transitivity property of intuitionistic multiplicative preference relation and its application in missing value estimation

Mamata Sahu, Anjana Gupta

Received 24 April 2018; Revised 13 May 2018; Accepted 20 June 2018

Abstract. In the decision-making process, consistency is a crucial issue which causes wide public concern of exports. The lack of consistency in preference relations results in an inconsistent solution. In this paper, we propose a characterization of the consistency property using newly defined transitivity property for intuitionistic multiplicative preference relations (IMPR) together with complementing missing elements for incomplete IMPR. In 2015 Jiang et al. worked on incomplete intuitionistic multiplicative preference relations (incomplete IMPRs) in which the IMPRs split into two multiplicative preference relation (MPRs), and the missing elements were calculated by using the consistency of MPRs. Using new transitivity property of IMPR, and we have developed two different methods to find the missing element of IMPRs. The first method is two-step procedure method containing estimating step followed by adjusting step. In estimating step, the missing elements of incomplete IMPRs are calculated by using a new transitive property instead of splitting IMPRs into two multiplicative preference relations(MPRs). Sometimes the initial value may not satisfy the conditions of IMPRs. An optimization model is developed in the second step to adjust the initial values that are solved by MATLAB optimization tool. The second proposed method is goal programming model based on new transitivity property to calculate the missing elements directly. Acceptably Consistent with complete IMPRs is also checked. Two numerical examples are carried out to illustrate the above-said methods.

2010 AMS Classification: 03E72, 90C70

Keywords: Multiplicative preference relation(MPR), Intuitionistic multiplicative preference relation (IMPR), Consistent, Acceptably consistent, Transitivity, Goal programming.

Corresponding Author: Anjana Gupta (anjanagupta@dce.ac.in)

1. Introduction

Decision making is one of the most important tasks for individuals and organizations and is an interdisciplinary research area attracting researchers from almost all fields from psychologists, economists, to computer scientists. Among all the fields from psychologists, economists, to computer scientists, the fuzzy decision is an important branch of fuzzy theory. Liu and Liao [11] gave a bibliometric analysis of fuzzy decision-related research to find out some underlying patterns and dynamics in the direction of the fuzzy decision. Yu and Liao [28] make a scientometric review on IFS studies to reveal the most cited papers based on the 1318 references retrieved from SCIE and SSCI databases via Web of science. Liao, Zhang, and Luo [10] present some new distance measures between intuitionistic multiplicative sets, which incorporate the projection-based distance measure and the psychological distance measures. In 1980 Saaty[16] introduced the Analytic hierarchy process, is the most important working Multi-criteria decision making (MCDM) method. Mathematically to describe the decision making problem, different type of preference relation have been proposed (see [13, 15, 16, 20, 21, 22, 23]). In different decision-making problems, there are different types of preference relations indicate different forms of preference information in matrices and exert their power. The preference relations are classified into two forms: fuzzy preference relations (FPR) and multiplicative preference relations (MPRs). In FPRs, [13] the decision maker express the information by using 0-1 ratio scale whereas the MPR [15] the intensity of the pairwise comparison of objects by using $1/9 - 9$ ratio scale (also called 1-9 ratio scale). Due to the time pressure and lack of information or knowledge, sometimes it is complicated for the decision makers to provide their preferences. To express their preference information, interval-valued preference relations [17, 23] allow the decision makers to use the interval numbers.

All the elements of both FPRs and MPRs are single values, which only involves the intensities of preferences relation. But it is possible that, in the decision-making process, the decision maker not sure about the preference information namely, uncertainty degrees (hesitation degrees). Intuitionistic fuzzy preference relations (IFPRs) [22] and intuitionistic multiplicative preference relations (IMPRs) [20] are defined to indicate the positive information x_i is preferred to x_j, the degree of negative details x_i is not preferred to x_j and simultaneously the degree that cannot determine by the decision maker. Recently, Zhang et al.[33] created intuitionistic multiplicative ORESTE strategy and further featured by a contextual analysis concerning the patients' prioritization.

Consistency plays a significant role in decision-making process. Consistency measures the level of agreement among the preference data given by the individual DMs [19]. A good amount of researchers have paid their attention to the use of consistency of preference relations in decision making under uncertain environments. For good understanding one may refer to [4, 8, 26, 27].

In 2015 Jiang et al. [9] discussed the consistency property of an IMPR especially the acceptable consistency. Based on it, two approaches have developed to complement all missing elements of incomplete IMPRs. Ren[14] verified that the IMWGA operator is of excellent characteristics in remaining the consistency of the IMPRs.

To adjust the inconsistent IMPRs into an acceptably consistent one, they proposed an iterative process and also, they Provide an adjustment process to restore and improves the consistency of inconsistent IMPR. Zhang et al. [32] suggested several goal programming models to manage unity and consensus of IMPRs and develop consistency and consensus-based approach for dealing with group decision-making (GDM) with IMPRs. Zhang and Guo [29] has developed a linear programming-based algorithm to check and improve the consistency of an IMPR. Also, Zhang and Guo [29] discuss the relationships between an IMPR and a normalized intuitionistic multiplicative weight vector and develop two approaches to group decision making based on complete and incomplete IMPRs, respectively. In this paper, our work focuses on only IMPRs.

Sometimes decision maker may not yet have a good understanding of a particular question, and this he/she is unable to make a direct comparison between every two objects; therefore it is sometimes necessary to allow the decision maker to skip some dubious comparisons flexibly. In this case, incomplete preference relations are obtained, and the whole process may slow down. In the decision-making process, to present a complete preference relation, a decision maker should make $\frac{n(n-1)}{2}$ judgments at each level, and when n is large, it becomes an onerous task. Therefore sometimes, due to lack of time and busy schedule of the decision maker, incomplete preference relations are obtained. Our work focus on incomplete IMPR.

In this paper, the new consistency property of IMPR is defined. Based on which two novel method is provided for estimating the missing element of incomplete IMPRs, where one traditional "two-step procedure methods" is divided into two sub-steps such as: (i) "Estimating step": Initial values are evaluated for the missing elements of the incomplete IMPRs without splitting into two MPRs; (ii)"Adjusting step": An optimization model is developed to adjust the initial values derived from the estimating step which is solved by MATLAB optimization tool. We have also developed a goal programming model to estimate the missing element without splitting into two MPRs. Both novel methods give the equivalent result. Then the acceptably consistent of IMPR has been checked. Techniques are illustrated with suitable examples.

Paper is organised as follows. In section 2, some basic concepts are defined briefly, and new transitivity property of IMPR is defined. In section 3, we have developed an algorithm to find the missing elements by using newly defined transitivity property of IMPR and proposed an optimization model for adjusting the initial values. In section 4 a goal programming model is intended to complete the incomplete IMPRs. Two numerical examples illustrate the developed procedures. In the section 5, we have given a comparative analysis of our work with the work of [9] and [12]. Concluding remarks are provided in the last part.

2. Preliminaries

Let $X = \{x_1, \cdots, x_n\}$ be a discrete set of alternatives/criteria in a decision making problem and set $N = \{1, \cdots, n\}$ be the set of indices. A decision maker needs to provide his/her preferences over the alternatives/criteria using the pairwise comparison method. The preferences values are provided by the decision maker from the ratio scale $[1/9, 9]$ introduced by Satty [16] to estimate and differentiate the intensity

of preferences. Based on the above ratio scale, some basic concepts of IMPRs are defined.

2.1. **Intuitionistic multiplicative preference relation.**

Definition 2.1 ([20]). An intuitionistic multiplicative preference relation (IMPR) is $\tilde{R} = [\tilde{r}_{ij}(x_i, x_j)]_{n\times n}$, where $\tilde{r}_{ij}(x_i, x_j) = (\mu(x_i, x_j), \nu(x_i, x_j))$, $i, j \in N$, is an intuitionistic multiplicative number (IMN), and $\mu(x_i, x_j)$ indicates certainty degree to which x_i is preferred to x_j and $\nu(x_i, x_j)$ is the certainty degree to which x_i is not preferred to x_j, and they satisfy the following characteristics:

$$1/9 \leq \mu(x_i, x_j)\,, \quad \nu(x_i, x_j) \leq 9,\ \mu(x_i, x_j) = \nu(x_j, x_i)\,, \nu(x_i, x_j) = \mu(x_j, x_i)$$
$$\mu(x_i, x_i) = \nu(x_i, x_i) = 1\,, 0 < \mu(x_i, x_j)\,\nu(x_i, x_j) \leq 1\,, \quad \forall\, i, j \in N.$$

For the sake of convenience $\mu(x_i, x_j)$ and $\nu(x_i, x_j)$ are denoted by μ_{ij} and ν_{ij} respectively.

In 2013 Xu [24] gave the concept of the consistent property of IMPR $\tilde{R} = (\tilde{r}_{ij})_{n\times n} = (\mu_{ij}, \nu_{ij})_{n\times n}$ based on the transitivity

$$(\mu_{ij}, \nu_{ij}) = (\mu_{ik}\mu_{kj}, \nu_{ik}\nu_{kj}),\ \text{for all } i, j, k \in N \text{ and } i \leq k \leq j. \tag{2.1}$$

It is to note that the equation (2.1) is restricted for the condition $i \leq k \leq j$, while the transitive property of a MPR is unconstrained which satisfies for all $i, j, k \in N$. If the equation (2.1) is utilized to check the consistency of an IMPR for all $i, j, k \in N$, the transitivity and consistency properties some times do not hold. This is because that when 'k' comes from the row of lower triangular matrix, the equation does not hold. For example:

$$\begin{pmatrix} (1,1) & (1/2,1) & (1,1/2) \\ (1,1/2) & (1,1) & (2,1/2) \\ (1/2,1) & (1/2,2) & (1,1) \end{pmatrix}_{3\times 3}$$

is a consistent IMPR given in [24]. Jiang et al. [9] relax the condition $i \leq k \leq j$, it is follow that $a_{23} = (\mu_{21}\mu_{13}, \nu_{21}\nu_{13}) = (1, 1/4)$. But $a_{23} = (2, 1/2) \neq (1, 1/4)$. To over come this type of transitivity limitation, Jiang et al. [9] proposed a more general consistency property of an IMPR split into two MPRs by using the formula

$$a_{ij} = \begin{cases} \mu_{ij} & i < j \\ 1 & i = j \\ 1/\nu_{ij} & i > j \end{cases} \text{ and } b_{ij} = \begin{cases} \nu_{ij} & i < j \\ 1 & i = j \\ 1/\mu_{ij} & i > j\,. \end{cases} \tag{2.2}$$

where the MPR $A = (a_{ij})_{n\times n}$ is preferred information matrix given by the decision maker with respect to the alternative x_i over x_j and $B = (b_{ij})_{n\times n}$ is the non-preferred information matrix given by the decision maker with respect to the alternative x_i over x_j. Based on the above concept, Jiang et al. [9] defined the consistent IMPR.

Definition 2.2 ([9]). A IMPR $\tilde{R} = (\tilde{r}_{ij})_{n\times n}$ is said to be consistent, if both MPRs A and B given by the equation (2.2) are consistent such that

$$a_{ij} = a_{ik}a_{kj},\ b_{ij} = b_{ik}b_{kj}\ \ \forall i, j, k \in N$$

In this work, instead of splitting IMPRs into MPRs we have defined an new consistency property of IMPR.

Definition 2.3. An IMPRs $\tilde{R} = (\tilde{r}_{ij})_{n\times n}$ is called consistent, if it satisfy the transitivity property, where $\tilde{r}_{ij}$ is

$$(\mu_{ij}, \nu_{ij}) = \begin{cases} (\mu_{ik}, \nu_{ik}) \otimes (\mu_{kj}, \nu_{kj}) & \text{if } i \le k, k \le j \\ (\frac{1}{\mu_{ki}}, \frac{1}{\nu_{ki}}) \otimes (\mu_{kj}, \nu_{kj}) & \text{if } i \ge k, k \le j \\ (\mu_{ik}, \nu_{ik}) \otimes (\frac{1}{\mu_{jk}}, \frac{1}{\nu_{jk}}) & \text{if } i < k, k > j. \end{cases} \tag{2.3}$$

In this work for convenience, we have used the multiplication of two IMNs as the multiplication of two order pairs. Let $a = (\mu, \nu)$, $a_1 = (\mu_1, \nu_1)$ and $a_2 = (\mu_2, \nu_2)$ be intuitionistic multiplicative numbers (IMNs) and $\lambda > 0$. Then

$$a_1 \otimes a_2 = (\mu_1, \nu_1) \otimes (\mu_2, \nu_2) = (\mu_1\mu_2, \nu_1\nu_2)\,,$$
$$a^\lambda = \left(\frac{2\mu^\lambda}{(2+\mu)^\lambda - \mu^\lambda}, \frac{(1+2\nu)^\lambda - 1}{2}\right)$$

is given by Xia[20], for $\lambda > 0$.

In decision-making problem, it may be the case that decision maker may not have a good understanding on a particular question, and therefore he/she is unable to make a direct comparison between two alternatives or criteria. Consequently, it is more appropriate and flexible to skip some similarities, and in that cases, the decision maker may prefer to express their judgments with incomplete preference relation. According to previously discussed, the decision makers may provide less than $\frac{n(n-1)}{2}$ judgments in practical decision making and the incomplete IMPR will be presented. So, it is essential to investigate the incomplete preference relations as a useful tool in decision-making problem, and many research results have been developed. Herrera-Viedma et al. [7] proposed the definition of incomplete preference relation. The concept of IMPRs is extended to the situations where the preference information given by decision maker is incomplete. Jiang et al. [9] propose to extend the above situation to incomplete IMPR where some elements are missing in the preference relation matrix.

Definition 2.4 ([9])**.** An IMPR $\tilde{r}_{ij} = (\mu_{ij}, \nu_{ij})_{n\times n}$ is called an incomplete IMPR, if some elements in it are missing and all available elements satisfy the characteristics of IMPR stated in Definition 2.1.

3. Complement of an incomplete IMPRs

In this section, we define the consistent property of incomplete IMPR.

Definition 3.1. An incomplete IMPR is said to be consistent, if all the known element satisfy the equation (2.3).

In an incomplete MPR $P = (p_{ij})_{n\times n}$, the element p_{ij} and p_{kl} are called adjoining if $(i, j) \cap (k, l)$ is non empty set, e.g if $p_{i_0j_0} = p_{i_0k} \times p_{kj_0}$, where p_{i_0k} and p_{kj_0} are adjoining known elements and $p_{i_0j_0}$ be an unknown elements, then $p_{i_0j_0}$ can be found directly and the corresponding incomplete MPR is called acceptable. MPR P are called an unacceptable incomplete multiplicative preference relation, if there does not exist adjoining known element such that unknown factor can be calculated [21]. In that cases, therefore, it is necessary to return the unacceptable incomplete multiplicative preference relation to the decision maker for revaluation until an acceptable incomplete multiplicative preference relation can be obtained. Wang and

Xu [18] showed that if an incomplete MPRs are acceptable, then there exists at least one known element(except diagonal elements) in each line/column of MPR matrix P, i.e., their exit at least $n-1$ judgment provided by the decision maker. Later according to Cai and Deng[2], Xu[21] and Alonso et al.[1] prove that an incomplete multiplicative preference relation which is acceptable. Then there exists at least a set of an $n-1$ number of non-leading diagonal known elements, where each of the criteria is compared at least once, which includes the case when a complete row or column of preference values is known. In this work, we have applied the same above-said applications in the incomplete IMPRs scenario.

Taking inspiration from the work of Jiang et al. [9], we propose a two-step procedure method to estimate the missing values in an incomplete IMPR without splitting IMPRs into two MPRs. The idea is first to evaluate their value using the simple connecting path approach and subsequently improve upon them using an optimization problem.

3.1. **Estimating step.** To complement the missing elements in an incomplete MPR, Harker [5, 6] designed a geometric mean method based on the connective paths. The general structure of a connecting path of length $\theta+1$, denoted by $cp_{(\theta+1)}$, has the following form: $cp_{(\theta+1)}$: $*_{ij} = p_{i\,k_1} p_{k_1\,k_2} \dots p_{k_\theta\,j}$, where $*_{ij}$ denotes the missing element to be estimated and the elements on the right hand side are known entities in the path connecting i with j, where $i, j, k_1, \dots, k_\theta \in N,\ 0 \le \ell \le n-2$. The connecting path of length two is an elementary connecting path $cp_{(2)} : *_{ij} = p_{i\,k_1} p_{k_1\,j}$ for $k_1 \in N$, and $k_1 \neq i,\ j$. Harker [5, 6] argued that the value of the missing element $*_{ij}$ is the geometric mean of all elementary connecting paths related to it with no vertex repeats more than once in the path. Consequently, $*_{ij} = \left(\prod_{r=1}^{n_\theta} cp_{(r)}\right)^{1/n_\theta}$, where n_θ is the number of all possible connecting fully known paths (that is, no missing entries along the path) from i to j. A major limitation of this method is that the number of connecting paths of different lengths between i and j may be extremely large and computationally intractable for many real problems. For instance, Deschrijver and Kerre [3] presented an example of a matrix of size 10 only with the number of connecting paths exceeding 109,000. Jiang et al. [9] improved this method for incomplete IMPR by taking elementary connecting path instead of all connecting paths of all sizes. In that case the matrix of size 10, the number of all elementary connecting path would not surpass 8, which is much less than 109,000. Based on the new consistency property of IMPRs, the initial value of the missing element of incomplete IMPRs can be calculated by using a geometric mean method which is denoted by $\tilde{r}'_{ij}$, where $\tilde{r}'_{ij} =$

$$(\mu^*_{ij}, \nu^*_{ij}) = \begin{cases} \left(\prod_{k\in T_{ij}} \{(\mu_{ik}, \nu_{ik}) \otimes (\mu_{kj}, \nu_{kj})\}\right)^{1/t_{ij}} & \text{if } i \le k, k \le j; \\ \left(\prod_{k\in T_{ij}} \{(\frac{1}{\mu_{ki}}, \frac{1}{\nu_{ki}}) \otimes (\mu_{kj}, \nu_{kj})\}\right)^{1/t_{ij}} & \text{if } i \ge k, k \le j; \\ \left(\prod_{k\in T_{ij}} \{(\mu_{ik}, \nu_{ik}) \otimes (\frac{1}{\mu_{jk}}, \frac{1}{\nu_{jk}})\}\right)^{1/t_{ij}} & \text{if } i < k, k > j, \end{cases} \tag{3.1}$$

where $T_{ij} = \{k|(\mu_{ik}, \nu_{ik}), (\mu_{kj}, \nu_{kj}) \in \Omega\}$, Ω is the set of known element and t_{ij} is the number of element present in the set T_{ij} which indicates that there may exist different pairs of adjoining known elements to find out the unknown elements. The initial values are denoted by $\left(\mu^{*(0)}_{ij}, \nu^{*(0)}_{ij}\right)$.

Remark 3.2. It is to note that in equation 3.1, $\mu_{kj} \times \frac{1}{\mu_{ki}} \neq \mu_{kj} \times \mu_{ik}$, and it should follow in other expression also.

3.2. **Adjusting step.** The IMPR is consistent if equation 2.3 is satisfied. Sometimes initial values of the missing element may not satisfy the conditions of IMPRs. To overcome this difficulty we have developed a local optimization model(Model(M)) by minimizing the error.

$$
\begin{aligned}
&\text{Model(M)}\\
&\text{Min} \sum_{i,k=1}^{n} \sum_{j=i+1}^{n} \left(\varepsilon^{k}_{ij_{i\leq k,k\leq j}} + \varepsilon^{k}_{ij_{i\geq k,k\leq j}} + \varepsilon^{k}_{ij_{i<k,k>j}} \right)\\
&s.t.\\
&\varepsilon^{k}_{ij_{i\leq k,k\leq j}} = \mid (\mu_{ij},\nu_{ij}) - (\mu_{ik}\mu_{kj},\nu_{ik}\nu_{kj}) \mid;\\
&\varepsilon^{k}_{ij_{i\geq k,k\leq j}} = \left| (\mu_{ij},\nu_{ij}) - \left(\frac{\mu_{kj}}{\mu_{ki}}, \frac{\nu_{kj}}{\nu_{ki}} \right) \right|;\\
&\varepsilon^{k}_{ij_{i<k,k>j}} = \left| (\mu_{ij},\nu_{ij}) - \left(\frac{\mu_{ik}}{\mu_{jk}}, \frac{\nu_{ik}}{\nu_{jk}} \right) \right|;\\
&\mu_{ij}\nu_{ij} \leq 1;\ 1/9 \leq \mu_{ij};\ \nu_{ij} \leq 9;\\
&\mu^{(0)}_{ij} = \mu^{*^{(0)}}_{ij};\ \nu^{(0)}_{ij} = \nu^{*^{(0)}}_{ij};\ i \neq j \neq k;\ i,j,k \in N,
\end{aligned}
$$

where $\mu^{*^{(0)}}_{ij}$ and $\nu^{*^{(0)}}_{ij}$ are the initial value obtain from estimating step. For proper understanding, we have represented an algorithm that illustrates the above methods.

Algorithm 1

Step 1: Consider an incomplete IMPRs of $\tilde{R} = (\tilde{r}_{ij})_{n\times n}$ in which some elements are missing and the known elements satisfy the transitivity property of the equation (2.3).

Step 2: The initial value $r^{'}_{ij}$ of the missing element of incomplete IMPRs is calculated using the equation (3.1).

Step 3: Initial values obtained in step 2 are adjusted by the Model(M), and the adjusting values are denoted by $\tilde{r}^{''}_{ij}$.

Step 4: The complete IMPRs $\tilde{R}_c = (\tilde{r}_{c,_{ij}})_{n\times n}$, is obtained where

$$
\tilde{r}_{c,_{ij}} = \begin{cases} \tilde{r}^{''}_{ij} & \tilde{r}_{ij} \notin \Omega \\ \tilde{r}_{ij} & \tilde{r}_{ij} \in \Omega. \end{cases} \tag{3.2}
$$

In the next section, we have developed a goal programming model to estimate the missing values.

4. Goal programming model to estimate the missing values

In 2015 Meng and Chen [12] construct a linear programming model to evaluate the missing value with incomplete MPRs, which is based on consistency index. To cope with incomplete intuitionistic multiplicative preference relation (incomplete IMPR), this section developed a deviation model to evaluate the missing value which is based on new transitivity property which was discussed in Section 2. Let $\tilde{R} = (\mu_{ij},\nu_{ij})$ be an incomplete IMPR. We

know that $\tilde{R}$ is consistent if and only if the equation (2.3) holds for the strictly upper triangular elements. To minimize the errors, Approximate the equation (2.3). Define

$$
\begin{aligned}
(\varepsilon_{ij})_{i\leq k,k\leq j} &= \delta_{ij}\,|(\mu_{ij},\nu_{ij}) - (\mu_{ik}\mu_{kj},\nu_{ik}\nu_{kj})| \\
(\varepsilon_{ij})_{i\geq k,k\leq j} &= \delta_{ij}\left|(\mu_{ij},\nu_{ij}) - \left(\frac{\mu_{kj}}{\mu_{ki}},\frac{\nu_{kj}}{\nu_{ki}}\right)\right| \\
(\varepsilon_{ij})_{i<k,k>j} &= \delta_{ij}\left|(\mu_{ij},\nu_{ij}) - \left(\frac{\mu_{ik}}{\mu_{jk}},\frac{\nu_{ik}}{\nu_{jk}}\right)\right| \\
&\text{for } i,j=1,2,\cdots n,\ i<j \\
&\text{where, } \delta_{ij} = \begin{cases} 1 & k\in T_{ij} \\ 0 & \text{otherwise,} \end{cases}
\end{aligned} \tag{4.1}
$$

where $T_{ij}=\{k|(\mu_{ik},\nu_{ik}),(\mu_{kj},\nu_{kj})\in\Omega\}$, T_{ij} is the set of known element. Using the above equation (4.1), we construct the following goal programming model to estimate the missing value

$$
\begin{aligned}
&\text{Min}(\varepsilon_{ij})_{i\leq k,k\leq j} = \delta_{ij}|(\mu_{ij},\nu_{ij}) - (\mu_{ik}\mu_{kj},\nu_{ik}\nu_{kj})| \\
&\text{Min}(\varepsilon_{ij})_{i\geq k,k\leq j} = \delta_{ij}\left|(\mu_{ij},\nu_{ij}) - \left(\frac{\mu_{kj}}{\mu_{ki}},\frac{\nu_{kj}}{\nu_{ki}}\right)\right| \\
&\text{Min}(\varepsilon_{ij})_{i<k,k>j} = \delta_{ij}\left|(\mu_{ij},\nu_{ij}) - \left(\frac{\mu_{ik}}{\mu_{jk}},\frac{\nu_{ik}}{\nu_{jk}}\right)\right| \\
&\text{subject to,} \\
&\frac{1}{9}\leq\mu_{ij};\ \nu_{ij}\leq 9;\ (\mu_{ij},\nu_{ij})\in U; \\
&\text{where } U=\{(\mu_{ij},\nu_{ij})|(\mu_{ij},\nu_{ij}) \text{ is a missing value} \\
&\text{for } i,j=1,2,\cdots n,\ i<j\}.
\end{aligned}
$$

The solution of the minimization problem can be obtained by solving the goal programming Model(P).

Model(P)

$$
\begin{aligned}
\text{Min } D = &\sum_{i,k=1}^{n}\sum_{j=i+1}^{n}\left(d_{ij,k}^{(+)}\right)_{i\leq k,k\leq j} + \left(d_{ij,k}^{(-)}\right)_{i\leq k,k\leq j} + \left(d_{ij,k}^{(+)}\right)_{i\geq k,k\leq j} \\
&+ \left(d_{ij,k}^{(-)}\right)_{i\geq k,k\leq j} + \left(d_{ij,k}^{(+)}\right)_{i<k,k>j} + \left(d_{ij,k}^{(-)}\right)_{i<k,k>j} \\
&\text{subject to,} \\
&\delta_{ij}\{(\mu_{ij},\nu_{ij}) - (\mu_{ik}\mu_{kj},\nu_{ik}\nu_{kj})\} - \left(d_{ij,k}^{(+)}\right)_{i\leq k,k\leq j} + \left(d_{ij,k}^{(-)}\right)_{i\leq k,k\leq j} = 0;
\end{aligned}
$$

$$
\begin{aligned}
&\delta_{ij}\left\{(\mu_{ij},\nu_{ij}) - \left(\frac{\mu_{kj}}{\mu_{ki}},\frac{\nu_{kj}}{\nu_{ki}}\right)\right\} - \left(d_{ij,k}^{(+)}\right)_{i\geq k,k\leq j} + \left(d_{ij,k}^{(-)}\right)_{i\geq k,k\leq j} = 0; \\
&\delta_{ij}\left\{(\mu_{ij},\nu_{ij}) - \left(\frac{\mu_{ik}}{\mu_{jk}},\frac{\nu_{ik}}{\nu_{jk}}\right)\right\} - \left(d_{ij,k}^{(+)}\right)_{i<k,k>j} + \left(d_{ij,k}^{(-)}\right)_{i<k,k>j} = 0; \\
&\mu_{ij}\nu_{ij}\leq 1;\ 1/9\leq\mu_{ij};\ \nu_{ij}\leq 9; \\
&\left(d_{ij,k}^{(+)}\right)_{i\leq k,k\leq j},\ \left(d_{ij,k}^{(-)}\right)_{i\leq k,k\leq j},\ \left(d_{ij,k}^{(+)}\right)_{i\geq k,k\leq j},\ \left(d_{ij,k}^{(-)}\right)_{i\geq k,k\leq j},\ \left(d_{ij,k}^{(+)}\right)_{i<k,k>j},\ \left(d_{ij,k}^{(-)}\right)_{i<k,k>j}\geq 0;
\end{aligned}
$$

where,

$$\left(d^{(+)}_{ij,k}\right)_{i\leq k,k\leq j} = [(\mu_{ij},\nu_{ij}) - (\mu_{ik}\mu_{kj},\nu_{ik}\nu_{kj})] \vee 0;\ \left(d^{(-)}_{ij,k}\right)_{i\leq k,k\leq j} = [(\mu_{ik}\mu_{kj},\nu_{ik}\nu_{kj}) - (\mu_{ij},\nu_{ij})] \vee 0;$$
$$\left(d^{(+)}_{ij,k}\right)_{i\geq k,k\leq j} = \left[(\mu_{ij},\nu_{ij}) - (\frac{\mu_{kj}}{\mu_{ki}},\frac{\nu_{kj}}{\nu_{ki}})\right] \vee 0;\ \left(d^{(-)}_{ij,k}\right)_{i\geq k,k\leq j} = \left[(\frac{\mu_{kj}}{\mu_{ki}},\frac{\nu_{kj}}{\nu_{ki}}) - (\mu_{ij},\nu_{ij})\right] \vee 0;$$
$$\left(d^{(+)}_{ij,k}\right)_{i<k,k>j} = \left[(\mu_{ij},\nu_{ij}) - (\frac{\mu_{ik}}{\mu_{jk}},\frac{\nu_{ik}}{\nu_{jk}})\right] \vee 0;\ \left(d^{(-)}_{ij,k}\right)_{i<k,k>j} = \left[(\frac{\mu_{ik}}{\mu_{jk}},\frac{\nu_{ik}}{\nu_{jk}}) - (\mu_{ij},\nu_{ij})\right] \vee 0;$$

For the sake of convenience, here we use,

$$\left(d^{(+)}_{ij,k}\right)_{i\leq k,k\leq j} = \left(d^{(+)}_{\mu_{ij,k}},d^{(+)}_{\nu_{ij,k}}\right)_{i\leq k,k\leq j},\ \left(d^{(-)}_{ij,k}\right)_{i\leq k,k\leq j} = \left(d^{(-)}_{\mu_{ij,k}},d^{(-)}_{\nu_{ij,k}}\right)_{i\leq k,k\leq j},$$
$$\left(d^{(+)}_{ij,k}\right)_{i\geq k,k\leq j} = \left(d^{(+)}_{\mu_{ij,k}},d^{(+)}_{\nu_{ij,k}}\right)_{i\geq k,k\leq j},\ \left(d^{(-)}_{ij,k}\right)_{i\geq k,k\leq j} = \left(d^{(-)}_{\mu_{ij,k}},d^{(-)}_{\nu_{ij,k}}\right)_{i\geq k,k\leq j},$$
$$\left(d^{(+)}_{ij,k}\right)_{i<k,k>j} = \left(d^{(+)}_{\mu_{ij,k}},d^{(+)}_{\nu_{ij,k}}\right)_{i<k,k>j},\ \left(d^{(-)}_{ij,k}\right)_{i<k,k>j} = \left(d^{(-)}_{\mu_{ij,k}},d^{(-)}_{\nu_{ij,k}}\right)_{i<k,k>j},$$

where

$$\left(d^{(+)}_{\mu_{ij,k}}\right)_{i\leq k,k\leq j} = [\log\mu_{ij} - (\log\mu_{ik} + \log\mu_{kj})] \vee 0;$$
$$\left(d^{(-)}_{\mu_{ij,k}}\right)_{i\leq k,k\leq j} = [(\log\mu_{ik} + \log\mu_{kj}) - \log\mu_{ij}] \vee 0;$$
$$\left(d^{(+)}_{\nu_{ij,k}}\right)_{i\leq k,k\leq j} = [\log\nu_{ij} - (\log\nu_{ik} + \log\nu_{kj})] \vee 0;$$
$$\left(d^{(-)}_{\nu_{ij,k}}\right)_{i\leq k,k\leq j} = [(\log\nu_{ik} + \log\nu_{kj}) - \log\nu_{ij}] \vee 0;$$
$$\left(d^{(+)}_{\mu_{ij,k}}\right)_{i\geq k,k\leq j} = [\log\mu_{ij} - (\log\mu_{kj} - \log\mu_{ki})] \vee 0;$$
$$\left(d^{(-)}_{\mu_{ij,k}}\right)_{i\geq k,k\leq j} = [(\log\mu_{kj} - \log\mu_{ki}) - \log\mu_{ij}] \vee 0;$$
$$\left(d^{(+)}_{\nu_{ij,k}}\right)_{i\geq k,k\leq j} = [\log\nu_{ij} - (\log\nu_{kj} - \log\nu_{ki})] \vee 0;$$
$$\left(d^{(-)}_{\nu_{ij,k}}\right)_{i\geq k,k\leq j} = [(\log\nu_{kj} - \log\nu_{ki}) - \log\nu_{ij}] \vee 0;$$
$$\left(d^{(+)}_{\mu_{ij,k}}\right)_{i<k,k>j} = [\log\mu_{ij} - (\log\mu_{ik} - \log\mu_{jk})] \vee 0;$$
$$\left(d^{(-)}_{\mu_{ij,k}}\right)_{i<k,k>j} = [(\log\mu_{ik} - \log\mu_{jk}) - \log\mu_{ij}] \vee 0;$$
$$\left(d^{(+)}_{\nu_{ij,k}}\right)_{i<k,k>j} = [\log\nu_{ij} - (\log\nu_{ik} - \log\nu_{jk})] \vee 0;$$
$$\left(d^{(-)}_{\nu_{ij,k}}\right)_{i<k,k>j} = [(\log\nu_{ik} - \log\nu_{jk}) - \log\nu_{ij}] \vee 0.$$

To illustrate the above procedure we have presented two examples.

Example 4.1. Let us consider a decision making problem with five sets of alternatives $x_i (i = 1, 2, \cdots, 5)$. The decision maker judges these five alternatives by pairwise comparison and provides his/her judgement as $\tilde{r}_{12} = (\mu_{12},\nu_{12}) = (5, 1/7)$, $\tilde{r}_{14} = (\mu_{14},\nu_{14}) = (3, 1/7)$, $\tilde{r}_{23} = (\mu_{23},\nu_{23}) = (9/5, 3/7)$, $\tilde{r}_{25} = (\mu_{25},\nu_{25}) = (1/5, 3)$, $\tilde{r}_{35} = (\mu_{35},\nu_{35}) = (1/9, 7)$, $\tilde{r}_{45} = (\mu_{45},\nu_{45}) = (1/7, 3)$. The matrix representation of the above information is given by

$$\tilde{R} = \begin{bmatrix} (1,1) & (5,1/7) & (*,*) & (3,1/7) & (*,*) \\ (1/7,5) & (1,1) & (9/5,3/7) & (*,*) & (1/5,3) \\ (*,*) & (3/7,9/5) & (1,1) & (*,*) & (1/9,7) \\ (1/7,3) & (*,*) & (*,*) & (1,1) & (1/7,3) \\ (*,*) & (3,1/5) & (7,1/9) & (3,1/7) & (1,1) \end{bmatrix}_{5\times 5}$$

The initial value of missing element are calculated using the equation (3.1), are given in Table 1.

TABLE 1. Calculation of Missing element(initial value)

Missing element	Adjoining element	Calculated value
$\left(\mu_{13}^{*(0)}, \nu_{13}^{*(0)}\right)$	(μ_{12}, ν_{12}), (μ_{23}, ν_{23})	$(9, 3/49)$
$\left(\mu_{15}^{*(0)}, \nu_{15}^{*(0)}\right)$	(μ_{12}, ν_{12}), (μ_{25}, ν_{25}) (μ_{14}, ν_{14}), (μ_{45}, ν_{45})	$(1.44877, 0.0297)$
$\left(\mu_{24}^{*(0)}, \nu_{24}^{*(0)}\right)$	(μ_{21}, ν_{21}), (μ_{14}, ν_{14}) (μ_{25}, ν_{25}), (μ_{54}, ν_{54})	$(2.38454, 0.366025)$
$\left(\mu_{34}^{*(0)}, \nu_{34}^{*(0)}\right)$	(μ_{35}, ν_{35}), (μ_{54}, ν_{54})	$(0.777, 2.333)$

Some initial values does not satisfies the property of IMPRs e.g $\mu_{\mathbf{34}} \times \nu_{\mathbf{34}} \nleq \mathbf{1}$. To adjust these values solve this problem using an optimization Model(M) that minimize the error.

Model(M)

$$\text{Min } \{|\{(9-\mu_{13})^2 + (3/49-\nu_{13})^2\}^{0.5}| + |\{(1-\mu_{15})^2 + (3/7-\nu_{15})^2\}^{0.5}|$$
$$+|\{(3/7-\mu_{15})^2 + (3/7-\nu_{15})^2\}^{0.5}| + |\{(3/5-\mu_{24})^2 + (1-\nu_{24})^2\}^{0.5}|$$
$$+|\{(7/5-\mu_{24})^2 + (1-\nu_{24})^2\}^{0.5}| + |\{(0.777-\mu_{34})^2 + (2.333-\nu_{34})^2\}^{0.5}|\};$$

s.t.

$$\mu_{13} \times \nu_{13} \leq 1; \mu_{15} \times \nu_{15} \leq 1; \mu_{24} \times \nu_{24} \leq 1;$$
$$\mu_{34} \times \nu_{34} \leq 1; 1/9 \leq \mu_{13}; \nu_{13} \leq 9;$$
$$1/9 \leq \mu_{15}; \nu_{15} \leq 9; 1/9 \leq \mu_{24}; \nu_{24} \leq 9;$$
$$1/9 \leq \mu_{34}; \nu_{34} \leq 9; {\mu_{13}}^{*(0)} = 9, {\nu_{13}}^{*(0)} = 3/49;$$
$${\mu_{15}}^{*(0)} = 1.44877, {\nu_{15}}^{*(0)} = 0.0297;$$
$${\mu_{24}}^{*(0)} = 2.3845, {\nu_{24}}^{*(0)} = 0.366;$$
$${\mu_{34}}^{*(0)} = 0.777, {\nu_{13}}^{*(0)} = 2.333.$$

After solving the above optimization model, the adjusting values are given $\mu_{13} = 9, \nu_{13} = 0.111, \mu_{15} = 0.74, \nu_{15} = 0.429, \mu_{24} = 0.912, \nu_{24} = 1, \mu_{34} = 0.441, \nu_{34} = 2.268$. This model is solved by MATLAB optimization tool box. The complete IMPR $\tilde{R}_c$ is given below

$$\begin{bmatrix} (1,1) & (5,1/7) & (9,0.111) & (3,1/7) & (0.74,0.429) \\ (1/7,5) & (1,1) & (9/5,3/7) & (0.912,1) & (1/5,3) \\ (0.111,9) & (3/7,9/5) & (1,1) & (0.441,2.268) & (1/9,7) \\ (1/7,3) & (1,0.912) & (2.268,0.441) & (1,1) & (1/7,3) \\ (0.429,0.74) & (3,1/5) & (7,1/9) & (3,1/7) & (1,1) \end{bmatrix}_{5\times 5}$$

To check the consistency degree, the complete IMPR is split into two MPRs and their corresponding CR values are given in row-1 of table 2.

$$C = \begin{pmatrix} 1 & 5 & 9 & 3 & 0.74 \\ \frac{1}{5} & 1 & \frac{9}{5} & 0.912 & \frac{1}{5} \\ \frac{1}{9} & \frac{5}{9} & 1 & 0.441 & \frac{5}{9} \\ \frac{1}{3} & \frac{1}{0.912} & \frac{1}{0.441} & 1 & \frac{1}{7} \\ \frac{1}{0.74} & 5 & 9 & 7 & 1 \end{pmatrix}_{5\times5} \quad D = \begin{pmatrix} 1 & \frac{1}{7} & 0.111 & \frac{1}{7} & 0.429 \\ 7 & 1 & \frac{3}{7} & 1 & 3 \\ \frac{1}{0.111} & \frac{7}{3} & 1 & 2.268 & 7 \\ 7 & 1 & \frac{1}{2.268} & 1 & 3 \\ \frac{1}{0.429} & \frac{1}{3} & \frac{1}{7} & \frac{1}{3} & 1 \end{pmatrix}_{5\times5}$$

The Example 4.1 is also solved by the goal programming problem and the missing elements are $\mu_{13} = 9, \nu_{13} = 0.111, \mu_{15} = 1, \nu_{15} = 0.429, \mu_{24} = 1, \nu_{24} = 1, \mu_{34} = 0.428, \nu_{34} = 2.333$. This model(P) is solved using Lingo software. The consistency ratio of both MPRs obtain from two different methods such as two-step procedure method, and goal programming model method are given in Table 2. Therefore, the complete IMPR $\tilde{R_c}$ is acceptably consistent.

TABLE 2. Consistency ratio

Two-step procedure Method	CR(C)	0.0114
	CR(D)	0.0094
Goal programming model (Model(P))	CR(C')	0.0144
	CR(D')	0.0094

In Table 2 C',D' are two multiplicative preference relations are obtained by splitting the complete IMPRs where missing element are found from the model(P).

Example 4.2. Let us consider a decision making problem with seven sets of alternatives $x_i (i = 1, 2, \cdots, 7)$. The decision maker judge these seven alternatives by pairwise comparison and provides his/her judgement as follows: $\tilde{r}_{12} = (\mu_{12}, \nu_{12}) = (3/5, 1/4)$, $\tilde{r}_{16} = (\mu_{16}, \nu_{16}) = (1/5, 1/2)$, $\tilde{r}_{23} = (\mu_{23}, \nu_{23}) = (1/2, 8/5)$, $\tilde{r}_{26} = (\mu_{26}, \nu_{26}) = (1/3, 2)$, $\tilde{r}_{34} = (\mu_{34}, \nu_{34}) = (2/9, 15/4)$, $\tilde{r}_{36} = (\mu_{36}, \nu_{36}) = (2/3, 5/4)$, $\tilde{r}_{45} = (\mu_{45}, \nu_{45}) = (7, 1/7)$, $\tilde{r}_{46} = (\mu_{46}, \nu_{46}) = (3, 1/3)$, $\tilde{r}_{56} = (\mu_{56}, \nu_{56}) = (3/7, 7/3)$, $\tilde{r}_{67} = (\mu_{67}, \nu_{67}) = (1/7, 3)$. The matrix representation of the above information is given by $\tilde{R}_1$.

$$\tilde{R}_1 = \begin{bmatrix} (1,1) & (3/5,1/4) & (*,*) & (*,*) & (*,*) & (1/5,1/2) & (*,*) \\ (1/4,3/5) & (1,1) & (1/2,8/5) & (*,*) & (*,*) & (1/3,2) & (*,*) \\ (*,*) & (8/5,1/2) & (1,1) & (2/9,15/4) & (*,*) & (2/3,5/4) & (*,*) \\ (*,*) & (*,*) & (15/4,2/9) & (1,1) & (7,1/7) & (3,1/3) & (*,*) \\ (*,*) & (*,*) & (*,*) & (1/7,7) & (1,1) & (3/7,7/3) & (*,*) \\ (1/2,1/5) & (2,1/3) & (5/4,2/3) & (1/3,3) & (7/3,3/7) & (1,1) & (1/7,3) \\ (*,*) & (*,*) & (*,*) & (*,*) & (*,*) & (3,1/7) & (1,1) \end{bmatrix}_{7\times7}$$

The initial value of missing element is calculated by using the equation (3.1) which is given in Table 3.

TABLE 3. Calculation of Missing element(initial value)

Missing element	Adjoining element	Calculated value
$\left(\mu_{13}^{*(0)}, \nu_{13}^{*(0)}\right)$	(μ_{12}, ν_{12}), (μ_{23}, ν_{23})	$(3/10, 2/5)$
$\left(\mu_{14}^{*(0)}, \nu_{14}^{*(0)}\right)$	(μ_{16}, ν_{16}), (μ_{64}, ν_{64})	$(1/15, 3/2)$
$\left(\mu_{15}^{*(0)}, \nu_{15}^{*(0)}\right)$	(μ_{16}, ν_{16}), (μ_{65}, ν_{65})	$(7/15, 3/14)$
$\left(\mu_{17}^{*(0)}, \nu_{17}^{*(0)}\right)$	(μ_{16}, ν_{16}), (μ_{67}, ν_{67})	$(1/35, 3/2)$
$\left(\mu_{24}^{*(0)}, \nu_{24}^{*(0)}\right)$	(μ_{23}, ν_{23}), (μ_{34}, ν_{34}) (μ_{26}, ν_{26}), (μ_{46}, ν_{46})	$(0.17, 3.77)$
$\left(\mu_{25}^{*(0)}, \nu_{25}^{*(0)}\right)$	(μ_{26}, ν_{26}), (μ_{56}, ν_{56})	$(7/9, 6/7)$
$\left(\mu_{27}^{*(0)}, \nu_{27}^{*(0)}\right)$	(μ_{26}, ν_{26}), (μ_{67}, ν_{67})	$(1/21, 6)$
$\left(\mu_{35}^{*(0)}, \nu_{35}^{*(0)}\right)$	(μ_{34}, ν_{34}), (μ_{45}, ν_{45}) (μ_{36}, ν_{36}), (μ_{56}, ν_{56})	$(5.69, 0.13)$
$\left(\mu_{37}^{*(0)}, \nu_{37}^{*(0)}\right)$	(μ_{36}, ν_{36}), (μ_{67}, ν_{67})	$(2/21, 15/4)$
$\left(\mu_{47}^{*(0)}, \nu_{47}^{*(0)}\right)$	(μ_{46}, ν_{46}), (μ_{67}, ν_{67})	$(3/7, 1)$
$\left(\mu_{57}^{*(0)}, \nu_{57}^{*(0)}\right)$	(μ_{56}, ν_{56}), (μ_{67}, ν_{67})	$(3/49, 7)$

Some initial values does not satisfies the property of IMPRs e.g $\mu_{\mathbf{14}}, \mu_{\mathbf{17}}, \mu_{\mathbf{27}}, \mu_{\mathbf{37}}, \mu_{\mathbf{57}} \not\geq \frac{\mathbf{1}}{\mathbf{9}}$. To adjust these value we have solved optimization Model(M), that minimize the error.

$$\begin{aligned}
\text{Min } & \{2|\{(3/10-\mu_{13})^2+(2/5-\nu_{13})^2\}^{0.5}|+|\{(1/15-\mu_{14})^2+(3/2-\nu_{14})^2\}^{0.5}| \\
&+|\{(7/15-\mu_{15})^2+(3/14-\nu_{15})^2\}^{0.5}|+|\{(1/35-\mu_{17})^2+(3/2-\nu_{17})^2\}^{0.5}| \\
&+2|\{(1/9-\mu_{24})^2+(6-\nu_{24})^2\}^{0.5}|+|\{(7/9-\mu_{25})^2+(6/7-\nu_{25})^2\}^{0.5}| \\
&+|\{(1/21-\mu_{27})^2+(6-\nu_{27})^2\}^{0.5}|+2|\{(14/9-\mu_{35})^2+(15/28-\nu_{35})^2\}^{0.5}| \\
&+|\{(2/21-\mu_{37})^2+(15/4-\nu_{37})^2\}^{0.5}|+|\{(3/7-\mu_{47})^2+(1-\nu_{47})^2\}^{0.5}| \\
&+|\{(3/49-\mu_{57})^2+(7-\nu_{57})^2\}^{0.5}|\};
\end{aligned}$$

subject to

$\mu_{13}\times\nu_{13}\leq 1;\mu_{14}\times\nu_{14}\leq 1;\mu_{15}\times\nu_{15}\leq 1;\mu_{17}\times\nu_{17}\leq 1;\mu_{24}\times\nu_{24}\leq 1;\mu_{25}\times\nu_{25}\leq 1;$
$\mu_{27}\times\nu_{27}\leq 1;\mu_{35}\times\nu_{35}\leq 1;\mu_{37}\times\nu_{37}\leq 1;\mu_{47}\times\nu_{47}\leq 1;\mu_{57}\times\nu_{57}\leq 1;$
$1/9\leq\mu_{13};\nu_{13}\leq 9;1/9\leq\mu_{14};\nu_{14}\leq 9;1/9\leq\mu_{15};\nu_{15}\leq 9;1/9\leq\mu_{17};\nu_{17}\leq 9;$
$1/9\leq\mu_{24};\nu_{24}\leq 9;1/9\leq\mu_{25};\nu_{25}\leq 9;1/9\leq\mu_{27};\nu_{27}\leq 9;1/9\leq\mu_{35};\nu_{35}\leq 9;$
$1/9\leq\mu_{37};\nu_{37}\leq 9;1/9\leq\mu_{47};\nu_{47}\leq 9;1/9\leq\mu_{57};\nu_{57}\leq 9;$
$\mu_{13}{}^{*(0)}=0.5237;\nu_{13}{}^{*(0)}=0.0745;\mu_{14}{}^{*(0)}=1/15,\nu_{14}{}^{*(0)}=3/2;$
$\mu_{15}{}^{*(0)}=7/15,\nu_{15}{}^{*(0)}=3/14;\mu_{17}{}^{*(0)}=1/35,\nu_{17}{}^{*(0)}=3/2;$
$\mu_{24}{}^{*(0)}=0.17,\nu_{24}{}^{*(0)}=3.77;\mu_{25}{}^{*(0)}=7/9,\nu_{25}{}^{*(0)}=6/7;$
$\mu_{27}{}^{*(0)}=1/21,\nu_{27}{}^{*(0)}=6;\mu_{35}{}^{*(0)}=5.69,\nu_{35}{}^{*(0)}=0.127;$
$\mu_{37}{}^{*(0)}=2/21,\nu_{37}{}^{*(0)}=15/4;\mu_{47}{}^{*(0)}=3/7,\nu_{47}{}^{*(0)}=1;$
$\mu_{57}{}^{*(0)}=3/49,\nu_{57}{}^{*(0)}=7.$

The adjusting value are given by
$(\mu_{13},\nu_{13})=(0.3,0.4)$, $(\mu_{14},\nu_{14})=(0.111,1.5)$, $(\mu_{15},\nu_{15})=(0.467,0.214)$,
$(\mu_{17},\nu_{17})=(0.111,1.5)$, $(\mu_{24},\nu_{24})=(0.111,6)$, $(\mu_{25},\nu_{25})=(0.778,0.857)$,
$(\mu_{27},\nu_{27})=(0.111,6)$, $(\mu_{35},\nu_{35})=(1.556,0.536)$, $(\mu_{37},\nu_{37})=(0.111,3.748)$,
$(\mu_{47},\nu_{47})=(0.429,1)$, $(\mu_{57},\nu_{57})=(0.111,7)$.
Example 4.2 solved by Model(P) also and we obtained the same result. The complete IMPR is given in the matrix $\tilde{R}_{c_1}$.

$$\tilde{R}_{c_1} = \begin{bmatrix} (1,1) & (3/5,1/4) & (0.3,0.4) & (0.111,1.5) & (0.467,0.214) & (1/5,1/2) & (0.111,1.5) \\ (1/4,3/5) & (1,1) & (1/2,8/5) & (0.111,6) & (0.778,0.857) & (1/3,2) & (0.111,6) \\ (0.4,0.3) & (8/5,1/2) & (1,1) & (2/9,15/4) & (1.556,0.536) & (2/3,5/4) & (0.111,3.748) \\ (1.5,0.111) & (6,0.111) & (15/4,2/9) & (1,1) & (7,1/7) & (3,1/3) & (0.429,1) \\ (0.214,0.467) & (0.857,0.778) & (0.536,1.556) & (1/7,7) & (1,1) & (3/7,7/3) & (0.111,7) \\ (1/2,1/5) & (2,1/3) & (5/4,2/3) & (1/3,3) & (7/3,3/7) & (1,1) & (1/7,3) \\ (1.5,0.111) & (6,0.111) & (3.748,0.111) & (1,0.429) & (7,0.111) & (3,1/7) & (1,1) \end{bmatrix}_{7\times 7}$$

To check the consistency degree of IMPR, $\tilde{R}_{c_1}$ split into two MPRs C and D.

$$C = \begin{pmatrix} 1 & \frac{3}{5} & 0.3 & 0.111 & 0.47 & \frac{1}{5} & 0.111 \\ \frac{5}{3} & 1 & \frac{1}{2} & 0.111 & 0.778 & \frac{1}{3} & 0.111 \\ \frac{1}{0.3} & 2 & 1 & \frac{2}{9} & 1.556 & \frac{2}{3} & 0.111 \\ \frac{1}{0.111} & \frac{1}{0.111} & \frac{9}{2} & 1 & 7 & 3 & 0.429 \\ \frac{1}{0.467} & \frac{1}{0.778} & \frac{1}{1.556} & \frac{1}{7} & 1 & \frac{3}{7} & 0.111 \\ 5 & 3 & \frac{3}{2} & \frac{1}{3} & \frac{7}{3} & 1 & \frac{1}{7} \\ \frac{1}{0.111} & \frac{1}{0.111} & \frac{1}{0.111} & \frac{1}{0.429} & \frac{1}{0.111} & 7 & 1 \end{pmatrix}_{7\times 7}$$

$$D = \begin{pmatrix} 1 & \frac{1}{4} & 0.4 & 1.5 & 0.214 & \frac{1}{2} & 1.5 \\ 4 & 1 & \frac{8}{5} & 6 & 0.857 & 2 & 6 \\ \frac{1}{0.4} & \frac{5}{8} & 1 & \frac{15}{4} & 0.536 & \frac{5}{4} & 3.748 \\ \frac{1}{1.5} & \frac{1}{6} & \frac{4}{15} & 1 & \frac{1}{7} & \frac{1}{3} & 1 \\ \frac{1}{0.214} & \frac{1}{0.857} & \frac{1}{0.536} & 7 & 1 & \frac{7}{3} & 7 \\ 2 & 1/2 & \frac{5}{4} & 3 & \frac{3}{7} & 1 & 3 \\ \frac{1}{1.5} & \frac{1}{6} & \frac{1}{3.748} & 1 & \frac{1}{7} & \frac{1}{3} & 1 \end{pmatrix}_{7\times 7}$$

$CR(C)=0.0230$ and $CR(D)=0$ both are acceptable threshold value. According to Satty[16] both C and D are acceptably consistent. Therefore $\tilde{R}_{c_1}$ is also acceptably consistent.

5. A Comparative analysis with existing methods

In this section, we compare our proposed method with Jiang et al. [9] for IMPR and Meng and Chen [12] for MPRs.

(1) In 2015, Jiang et al. [9] discussed the consistency property, especially the acceptable consistency of an IMPR by splitting into two MPRs. Based on it, Jiang et al. developed two approaches to complement all missing elements of incomplete IMPRs. according to Jiang et al. [9], the incomplete IMPR split into two MPRs, and the calculation of missing factor involves two steps, i.e. "estimating step" and " adjusting step." A geometric mean method is used in the estimating step to calculate the initial values of missing element. Two different approaches are developed for improving the initial values: one is local optimization models, which is time-saving and other is an iterative method that can operate the whole optimization process suitably.

Using Jiang et al. [9] methods, Example 4.1 is solved where incomplete IMPRs is split into two MPRs as C and D. Using geometric mean method missing element is calculated and adjusting values are computed by using local optimization model (LOP1)[9]. Since the consistency ratio (CR) of C and D are 0.0197 and 0.0112. Hence the complete IMPR is acceptably consistent. Consistency ratio of C and D obtained from our methods (both two-step procedure method and Goal programming model) are less than(see Table 2) from Jiang et al. [9] methods. Similarly, in Example 4.2, the complete IMPR is also acceptably consistent. Both the model gives the equivalent result.

(2)To measure the multiplicative consistency of an MPR, Meng and Chen [12] proposed the notion of multiplicative geometric consistent index (MGCI). The consistency of an MPR is considered to be unacceptable if the MGCI of an MPR is less than the average value tabulated in Table 1 in their paper. The authors continued their study to include the case of incomplete MPR. They formulated multi-objective programming model to estimate the missing values. Using the goal programming approach and a suitable transformation, the proposed model was converted into an equivalent linear program. The missing values in an MPR were then obtained using the inverse transformation at the optimal solution of the linear program.

In Example 4.1, the incomplete IMPR is split into two incomplete MPRs using the equation (2.2). The missing elements of two incomplete MPRs are obtained using Meng and Chen's linear programming model (LP)(see [12]). Consistency ratio of two MPRs obtained from Meng and Chen's model are 0.0199 and 0.0097 respectively which are less than from both two-step procedure method and Goal programming model (Model(P)).

6. Conclusion

In this paper, we have introduced a new transitivity property of IMPR. Based on this, we have presented two approaches for completing incomplete IMPRs. In the first approach, missing element can be calculated by using the new transitivity property, and an optimization model has been developed to adjust the initials values. In the second approach, the missing elements are evaluated by goal programming model based on new transitivity property. Two numerical examples are presented that illustrate the above method. Acceptably consistent with complete IMPRs has been checked. Also, we have compared our method with Jiang et al. [9] and Meng and Chen [12] method.

The hesitant fuzzy preference relation (HFPR) is a useful tool for decision-makers to elicit their preference information over a set of alternatives. Recently lots of researchers have done in hesitant fuzzy preference relation (HFPR), that allow the decision makers (DMs) to provide several possible preference values over two alternatives. One may refer to [25, 30, 31]. Our work can extend to deal with HFPR and incomplete HFPRs. Also, the missing element of incomplete HFPR can find by using goal programming.

References

[1] S. Alonso, F. Chiclana, F. Herrera, E. Herrera-Viedma, J. Alcala-Fdez and C. Porcel, A consistency-based procedure to estimate missing pairwise preference values, International Journal of Intelligent Systems 23 (2008) 155–175.

[2] L.C. Cai and X.J. Deng, An approach to constructing judgment matrix with desirable consistency in AHP, In: H.C. Sun, ed. Decision science and its application, Beijing: Haiyang Press (1996) 88–91.

[3] G. Deschrijver and E. E. Kerre, On the composition of intuitionistic fuzzy relations, Fuzzy Sets and Systems 136 (2003) 333–361.

[4] D. Ergu, G. Kou, Y. Peng and Y. Shi, A simple method to improve the consistency ratio of the pair-wise comparison matrix in ANP, Eur. J. Oper. Res. 213 (2011) 246–259.

[5] P. T. Harker, Alternative modes of questioning in the analytic hierarchy process, Mathematical Modelling 9 (1987a) 353–360.
[6] P. T. Harker, Incomplete pairwise comparisons in the analytic hierarchy process, Mathematical Modelling 9 (1987b) 837–848.
[7] E. Herrera-Viedma F. Chiclana, F. Herrera and S., Alonso, Group decision-making model with incomplete fuzzy preference relations based on additive consistency, IEEE Trans. Syst. Man Cybern. - Part B 37 (2007) 176–189.
[8] E. Herrera-Viedma, F. Herrera, F. Chiclana and M. Luque, Some issues on consistency of fuzzy preference relations, Eur. J. Oper. Res. 154 (2004) 98–109.
[9] Y. Jiang, Z. Xu and X. Yu, Group decision making based on incomplete intuitionistic multiplicative preference relations, Inform. Sci. 295 (2015) 33–52.
[10] H. Liao, C. Zhang and L. Luo, A multiple attribute group decision making method based on two novel intuitionistic multiplicative distance measures, Inform. Sci. 000 (2018) 1–18.
[11] W. Liu and H. Liao, A Bibliometric Analysis of Fuzzy Decision Research During 1970–2015, Int. J. Fuzzy Syst., DOI 10.1007/s40815-016-0272-z.
[12] F. Meng and X. Chen, An approach to incomplete multiplicative preference relations and its application in group decision making, Inform. Sci. 309 (2015) 119–137.
[13] S. A. Orlovsky, Decision making with a fuzzy preference relation, Fuzzy Sets and Systems 1 (1978) 155–167.
[14] P. Ren, Z. Xu and H. Liao, Intuitionistic multiplicative analytic hierarchy process in group decision making. Computers & Industrial Engineering 101 (2016) 513–524.
[15] T. L. Satty, A scalling method for priorities in hierarchy structures, J. Math. Psychol. 15 (1977) 234–281.
[16] T. L. Satty, The Analytic Hierarchy process. McGraw-Hill, New York (1980).
[17] T. L Satty and L. G, Vargas, Uncertainty and rank order in the analytic hierarchy process, Eur. J. Oper. Res. 32 (1987) 107–117.
[18] L. F. Wang, and S. B. Xu, Introduction to the Analytic Hierarchy Process (Beijing: China Renmin University Press)(1990).
[19] M. M. Xia, Z. S. Xu and J. Chen, Algorithms for improving consistency or consensus of reciprocal [0, 1]-valued preference relations, Fuzzy Sets and Systems 216 (2013) 108–133.
[20] M. M. Xia, Z. S. Xu and H. C. Liao, Preference relations based on intuitionistic multiplicative information, IEEE Transactions on Fuzzy Systems 21 (2013) 113–133.
[21] Z. S. Xu, A survey of preference relations, International Journal of General Systems 36 (2007a) 179–203.
[22] Z. S. Xu, Intuitionistic preference relations and their application in group decision making, Inform. Sci. 177 (11) (2007b) 2363–2379.
[23] Z. S. Xu, On compability of interval fuzzy preference relations, Fuzzy Optim. Decis. Making 3 (2004) 217–225.
[24] Z. S. Xu, Priority weight intervals derived from intuitionistic multiplicative preference relations, Transactions on Fuzzy Systems 21 (2013) 642–654.
[25] Y. Xu, L. Chen, R. M. Rodriguez, F. Herrera and H. Wang, Deriving the priority weights from incomplete hesitant fuzzy preference relations in group decision making, Knowledge-Based Systems 99 (2016) 71–78.
[26] Z. Xu and H. Liao, Intuitionistic fuzzy analytic hierarchy process, IEEE Transactions on Fuzzy Systems 22 (2014) 749–761.
[27] Z. S. Xu and C. P. Wei, A consistency improving method in the analytic hierarchy process, Eur. J. Oper. Res. 116 (1999) 443–449.
[28] D. Yu and H. Liao, Visualization and quantitative research on intuitionistic fuzzy studies, Journal of Intelligent & Fuzzy Systems 30 (2016) 3653–3663.
[29] Z. Zhang and C. Guo, Deriving priority weights from intuitionistic multiplicative preference relations under group decision-making settings, Journal of the Operational Research Society 68 (12) (2017) 1582–1599.
[30] Z. Zhang, X. Kou and Q. Dong, Additive consistency analysis and improvement for hesitant fuzzy preference relations, Expert Systems with Applications 98 (2018) 118–128.

[31] Z. Zhang, X. Kou, W. Yu and C. Guo, On priority weights and consistency for incomplete hesitant fuzzy preference relations, Knowledge-Based Systems 143 (2018) 115–126.
[32] Z. Zhang and W. Pedrycz, Goal Programming Approaches to Managing Consistency and Consensus for Intuitionistic Multiplicative Preference Relations in Group Decision-Making, IEEE Transactions on Fuzzy Systems, DOI 10.1109/TFUZZ.2018.2818074.
[33] C. Zhang, X. Wu, D. Wu, H. Liao, L. Luo and E. Herrera-Viedma, An Intuitionistic Multiplicative ORESTE Method for Patients' Prioritization of Hospitalization, Int. J. Environ. Res. Public Health 2018 15 (4), 777: doi: org/10.3390/ijerph15040777.

MAMATA SAHU (mamata_phd2k13@dtu.ac.in) – Scholar, Department of Applied Mathematics, Delhi Technological University, Delhi 110042, India,

ANJANA GUPTA, (anjanagupta@dce.ac.in) – Professor, Department of Applied Mathematics, Delhi Technological University, Delhi 110042, India

International Journal of Technical Innovation in Modern Engineering & Science (IJTIMES)
Impact Factor: 5.22 (SJIF-2017), e-ISSN: 2455-2585
Volume 4, Issue 7, July-2018

PRESENT SCENARIO AND SUGGESTION FOR WATERSHED MANAGEMENT PROGRAMME: A REVIEW

Dr. Munendra Kumar[1*], Ruchika Dabas[2]

[1]Associate Professor Department of Civil Engineering
Delhi Technological University,New Delhi-110042, India
[2]Research Scholar Department of Civil Engineering
Delhi Technological University, New Delhi-110042, India

INTRODUCTION

In the water crisis area, crop production is the most difficult task due to low resource of water; rainwater is the only source and its effective use for successful crop production. In addition, the uncertainty in rain conditions resulting water shortages. The proper management of rain water, conservation and development of water resources is necessary to meet the needs for domestic use, drinking water, industrial use, irrigation etc. Since watershed is a hydrological entity, water resources planning and its utilization are best attempted by taking watershed as a unit of planning. Rain water management often involves interventions for runoff control and retention such as bunds and vegetative barriers and also water harvesting structures (e.g. farm ponds, check dams) and ground water recharge structures (e.g. Nala bunds and percolation tanks). All this is designed according to the intervention runoff, which resulted in the level of water above it. The basic natural resources, such as water, soil and water quantity and quality, decide to produce biomass in a basin and therefore maintain the human and livestock population. Therefore, while planning the use of resources, this aspect of the basin must be. A higher population will increase the pressure on the basin resources, resulting in a result of earthquake and resources resulting in a decrease in the result. The geographical area that drains to a common exit point in a drainage line is called a basin. The area of the river basin is always defined with reference to an exit point in a drainage line. The area of the watershed increases as we move downstream along a drainage line and decreases as we move upstream. A very large river basin is called a macro basin and a very small basin is called a micro basin. The micro basin generally has a single order flow as its drainage line where a macro basin has multiple higher order drainage lines.

Apparently, the nation's capital, New Delhi, has reached a situation in which it is perpetually trapped by the water crisis, especially during the dry season, when the situation deteriorates in particular. As the gap between supply and demand widens, more groundwater is exploited. Of the water supplied by the municipality, approximately 11 percent comes from the reserves of groundwater and remaining from the Yamuna River. However, it is difficult to establish the total amount of groundwater extracted because a large number of tube wells (owned by individuals, industries and bottled water companies) remain unregistered. In Delhi, approximately 13% of households do not receive water every day (Zerah and Helene, 2000).

LITERATURE REVIEW

S. P. Suryawanshi and Abhijeet Kamble: India occupies approximately 2.4% of the total geographical area of the world, while it supports over 15% of the world population. Unprecedented population pressure and demand of society on scarce land, water and biological resources and the increasing degradation of these resources is affecting the stability and resilience of our ecosystems and the environment as a whole. Therefore, the productive agriculture lands in the country are in constant process of varying degrees of degradation and are fast turning into wastelands.Sustainable water management is thus crucial for economic development and livelihood of the people. In a country like India, where a lot of running water goes waste, it becomes very important to apply the technology of watershed management to solve its annual problems of droughts and floods.

V. Ratna Reddy Irrigated agriculture in India has probably reached its limit and further sustainable increases in food production must come from dry land farming, especially watershed development and management. This calls for an analysis of situations under which watershed technology becomes economically viable, socially acceptable ceande ecologically sustainable. This paper attempts to lay the theoretical ground for a detailed and rigorous empirical work through collective action theories.

B.S. Chaudhary The conventional methods of surveying and mapping for water resources are not only time consuming but also labour intensive and tedious. More recent techniques of Remote Sensing (RS) and GIS can however be effectively and efficiently used for database generation in water resources. The mapping and monitoring of dynamic phenomenon such as floods, water logging, and deforestation can also be done very effectively with the aid of RS and GIS.

Budumuru Yoganand and Tesfa G. Gebremedhin: International development goals moved beyond increasing food production to include poverty reduction and protecting the environment in a sustainable way. Degradation of natural resources due to exploitation coupled with population pressure in developing countries causing food insecurity and environmental degradation further. Participatory watershed management approach is proposed to address this problem effectively.

Preety M. Bhandari, Suruchi Bhadwal &Ulka Kelkar India occupies 2.4% of the world's geographical area with a large percentage of its land under agriculture. About 228 Million hectares (Mha) of its geographical area (nearly 69%) fall within the dryland (arid, semi-arid and dry sub-humid) region. Of the total cultivated area of 142 Mha, major part of agriculture in the country is rainfed, extending to over 97 Mha and constituting nearly 68% of the net cultivated area, therefore making the agricultural sector vulnerable and exposed to the vagaries of weather conditions. Climate change adds to this dimension of stress. A strong need is felt for targeting programmes in these areas that address issues related to employing suitable soil and water conservation measures. In this context this paper seeks to examine the case for watershed development as an adaptive strategy. An examination of the possibility of fortifying the existing programme with a view to adapting to expected changes in climate in future is undertaken. Also, the possibility of watershed development integrating into a suitable mitigation strategy for the country is assessed.

Wani S.P. et al, Farmer-Participatory Integrated Watershed Management: Adarsha Watershed,Kothapally India – An Innovative and Upscalable Approach towards Integrated Natural Resources Management: Examples of Research Problems [6]

A.K. Goel, R. Kumar water management is an essential feature of any project related with overall development of agriculture. The Soan river catchment in the northwest Himalayas, is fed only by rainwater. Hence, a strategy of rainfed agriculture needs to be developed through water conservation and storage techniques. The Soan is an important river from a soil erosion and water management point of view and detailed economic analysis is needed for any proposal to be implemented in the field.[7]

Deepa Nathalia et al, Environmental change detection is very mandatory to understand the relationship of human activities with the environment and its importance to manage the change that has been take place due to their activities. Due to the Human activities in the Aravalli hills of Faridabad district lots of ecological imbalances has been occurred from last 10 years. In the present paper an attempt has been made to understand the changes occurred due to Mining and urbanization activities in Aravalli hills of Faridabad district of Haryana through the Geo spatial techniques. [8]

Nancy Johnson Many watershed development projects around the world have performed poorly because they failed to take into account the needs, constraints, and practices of local people. Participatory watershed managementFin which users help to define problems,set priorities, select technologies and policies,and monitor and evaluate impactsFis expected to improve performance. User participation in watershedmanagement raises new questions for watershed research, including how to design appropriate mechanisms for organizing stakeholders and facilitating collective action. Management of a complex system such as a watershed may also require user participation in the research process itself. [9]

K. H. V. Durga Rao1 and D. Satish Kumar presentprototype spatial decision support system (SDSS) is presented for watershed management. The SDSS integrates landuse/landcover derived from the remote sensing data, real-time hydrological data, geographic information system, and a model-based subsystem for computingsoil loss, land capability classification and engineering measures. A graphical user interface has been developed to allow effective use by decision makers.

THE OBJECTIVES OF WATERSHED MANAGEMENT PROGRAMME

Developing wastelands/degraded lands, drought-prone and desert areas on watershed basis, keeping in view the capability of land, site-conditions and local needs.Promoting the overall economic development and improving the socio-economic condition of the resource poor and disadvantaged sections inhabiting the programme areas.Mitigating the adverse effects of extreme climatic conditions such as drought and desertification on crops, human and livestock population for their overall improvement.Restoring ecological balance by harnessing, conserving and developing natural resources i.e. land, water, vegetative cover.

WATERSHED MANAGEMENT AND INDIA:

The management concept of Vajedee is old as the concept of cultivation under irrigation conditions and this concept has led to the growth of tanks / reserves to increase production to meet the demand of growing population. . In different areas, several governments must meet the needs of people and their needs according to the needs of the population to meet the needs of the population and meet the needs of food, according to the availability of funds, the available areas of the area, etc. The beneficiaries were taxed and their income was collected. In 18th Arthur and 1845, Sir Arthur Cotton submitted two reports in the British government after surveying the entire area of the Sigagam area of the Ganges River area of Strip Hills and used river water for agricultural development. To build a storage type survival in the desert Dwarwerm district. In the area The need to maintain a better environment and conserve natural resources, such as soil, water and plants, was discovered by the first rulers and by various types of village institutions (for example, officers of the valery level). , gram panchayas, Governors / village administrators). If the natural resources were damaged, then the efforts were punished.

Due to the liberation of the policies in the democratic configuration and the liberalization of the spirit of independence, the administrative authorities have slowly decreased significantly after the independence of India. It did more damage to plants in rural areas due to erosion caused by soil erosion. Therefore, the government of India and several provincial governments, such as measures of demolition measures, soil protection measures, and run-off water use programs, etc. However, the expected results are not consistent and consistent. . Therefore, government made a great way to promote water development programs (WWD) in 1983-84 and to save and utilize natural resources for mass and productivity and high social and economic status. Vajpayee's development program was spent on scanning. Since then, 100,000 lakhs per year. Although, it has been since 1983-84, reviewing the impact of resource programs to improve the growing population so far to develop strategies / policies, save natural resources and use to be taken.

India has about 16 percent of the world's population, but only 4 percent of its freshwater resources (Planning Commission, 2001). In India, the estimated rate of groundwater abstraction in the 1990s exceeded the replacement rate by 104 billion m3yr-1 compared to 30 billion m3yr-1 in China and 10 billion m^3yr-1 in northern China. Africa (Postel, 2000). Currently, more than 10 percent of the core blocks of groundwater boards (the smallest administrative units for water resource management in India) are overexploited. The World Bank (1999) has calculated that blocks where exploitation is beyond the critical level have been increasing at a rate of 5.5 percent each year. Since 1995, the government of India has moved towards the creation of common guidelines as a framework for the development of watersheds. However, concerns remain that legislative measures to protect and manage India's water resources will be hampered by the lack of an integrated framework for watershed management, the lack of effective departmental coordination and a focus on mechanisms of offer instead of demand. Another important problem is that disparities between scientific and public perceptions about the role of forests are included in the water and watershed policy.

WATERSHED DESIGN/DEVELOPMENT AND MANAGEMENT

In a broader sense, watershed management implies rural development with watershed as unit of planning. Apart from development of agriculture, it may encompass areas of infrastructure development such as transport and communication, and even health, energy and education for the overall well-being of watershed community. However, agricultural development and certain issues and challenges of watershed management should be emphasized.

The major objectives of a watershed programme are:

1. Increased crop production
2. Protection of environment
3. Drought mitigation and improved water availability/Flood control
4. Achieving social equity
5. Soil and Water Management
6. Alternate Land Use Systems
7. Livestock Management
8. Pisciculture
9. Apiculture
10. Other agri-based enterprises
11. Livelihood based farm and off farm activities

Various activities taken up in a watershed programme include:

SOIL AND WATER MANAGEMENT: Soil conservation works such as bunding and terracing, vegetative barriers etc in arable lands and contour trenching in non-arable area, loose rock and pucca check dams in water courses for soil conservation and grade stabilization and water harvesting and ground water recharge structures (nala bunds and percolation tanks) are taken up under this component. A number of specialised practices developed by research institutions such as conservation furrow, ridge and furrow, broad bed and furrow etc. have been found to be helpful for in-situ moisture conservation. Mulching is also recommended for soil moisture conservation. Of late, mulch-cum-manuring with organic mulches are being promoted with the twin objectives of moisture conservation and organic matter build-up.

IMPROVED CROP PRODUCTION: Improved crop management, practices include improved/high yielding varieties, integrated nutrient management, weed management, integrated pest and disease management and use of improved agricultural implements and machinery.

LAND USE SYSTEMS: In watershed management, it is often desirable to go for alternate land use systems for better resource utilization as well as for improving the income of farmers. Various options are afforestation, agro-forestry, agri-horticulture, horti-pastoral, Sivi-pastoral systems and bio fuel plantations. Of late medicinal and aromatic plants are being recommended for increased returns.

POST-HARVEST TECHNOLOGIES: Post-harvest technologies assume great importance for reducing post-harvest losses, value addition of agricultural products and marketing.

LIVE STOCK MANAGEMENT: Diversified farming systems are often the best way to insure against variation of weather and market. Animal husbandry (Dairy, Poultry, Sheep and Goats, Piggery, emu farming etc,) provides the best alternative source of income to the farmers. Some of the other programmes that can be taken up under watershed programmes are Sericulture (silk worm rearing), Pisci-culture (fish rearing), Apiculture (bee keeping) etc.

ACTION PLAN PREPARATION: Action plans are prepared based upon the need assessment made through Rapid Rural Appraisal (RRA) and Participatory Rural Appraisal (PRA) surveys.Detailed programme planning is done under the various components of watershed development such as soil and water management, improved crop management, alternate land use system etc. It may be necessary to carry out further detailed surveys in order to arrive at the exact locations and dimensions of interventions and to estimate cost and benefit/cost ratios of watershed development.Integrated Watershed Management (IWM) aims at holistic development of an area through optimal resource utilization by adopting watershed as a unit. Conservation of natural resources such as soil water and vegetation is of paramount importance in watershed programme for maintaining productivity and achieving sustainability. Following is a list of thrust areas needing attention of those involved in watershed research and development:

1. Low cost technologies for soil and water conservation

2. Monitoring of ground water status and ground water recharge mechanisms.

3. Crops and cropping systems which promote resource conservation and fetch higher returns such as medicinal and aromatic plants, floriculture, horticulture.

4. Farming systems development and increasing role of animal husbandry to provide stable income and returns to farmers.

5. Post-harvest technologies for preventing losses, processing and value addition.

6. Institutional mechanisms for market intelligence and marketing.

7. Water and air quality assessment and amelioration measures for pollution control.

8. Institutional mechanisms for meeting situations arising out of uncertain rainfall conditions.

PROBLEMS AND PROSPECTS IN WATERSHED MANAGEMENT

India's guidelines for watersheddevelopment programmes have been revised three times since their introduction in 1986. They aim to make investments in watershed management have a long-lasting impact on crop production and rural livelihoods in rain-fed cropping areas. They are reviewed periodically, but only to accommodate cost escalations and revise targets. The current guidelines were introduced in November 2000, renamed as the National Watershed Development Programme for Rain-fed Areas (NWDPRA) of the Ministry of Agriculture. In addition to setting a framework for watersheddevelopment in the country, the guidelines proclaim a blanket investment per unit area for diverse land–water interventions and make special provisions for promoting income generation for landless people. Watershed management needs to take a multipurpose approach to improving land and increasing water availability for crop growing, livestock and human use through soil and moisture conservation measures. An effective watershed project should aim to drought-proof areas by capturing every falling raindrop. This is technically possible. An assessment by the Centre for Science and Environment (Agarwal, 2000) estimates that if half of India's average annual rainfall of 1170 mm were captured over 1.12 ha of land in each of the country's 587 226 villages, then the 6.57 million litres of rainwater thus collected would meet the annual cooking and drinking needs for an average village of 1200 people. Doing this would help both to sustain surface water supplies and to recharge aquifers. However, the National Sample Survey (NSS, 1994) reported that despite the extensive programmes carried out to provide drinking-water to rural areas, 140975 villages (24 percent of India's total) still had a drinking-water problem. Even the watershed development programmes set up to complement the drinking-water programmes in villages did not improve the situation. As a result, much of the 420 hectare metres of average annual available precipitation flowed uninterrupted to the sea without fulfilling its ecological functions of enhancing surface water supplies and recharging groundwater to any appreciable extent. The experiences of watersheddevelopment projects have been quite varied. The few successful projects are outnumbered by the many unsuccessful ones. There are situations where some successful watershed projects have not even provided for the minimum amounts of drinking-water and fodder. Many watershed projects, designed to conserve rainwater to improve irrigation, have tended to ignore communities' primary need of access to drinking-water. On similar lines, some projects have neglected to develop pastureland and propagate soil-moisture conservation practices. A few community groups have taken the initiative themselves with some external assistance. For example, the villages of Sukhomajri in Haryana and the Chakriya Vikas Pranali scheme in Jharkhand have improved their socio-economic conditions in a relatively short time by linking improved *in situ* moisture conservation with economic activities that build up social capital. These examples show that watershed development is a viable model for the economic development of poverty-stricken rural areas. The two main problems of watershed development programmes have been the lack of any consistent criteria for selecting villages and the process of implementation. This raises several management-related questions. The poor performance of many development projects has not reduced the number of new projects. Andhra Pradesh has taken up an additional 2090 projects to treat 1 million ha since the November 2000. Typically, each development project is restricted to an area of 500 ha. Bilateral- and multilateral-funded projects usually cover many such sub-projects. For instance, the World Bank's Kandi development Area development Project in Haryana covers 619 separate watershed projects. One of the most intractable problems in development has been the lack of project sustainability. Many projects have failed to build in strategies to maintain their assets once project support ends.

Feedback from several projects indicates (Joy, 2003) that many farmers only benefit from watershed projects by getting short-term paid labouring work. Because communities see few long-term benefits emanating from these projects, they have little interest in operating and maintaining project assets. This issue is being confronted by some donors in their projects. Many watershed projects have failed in their primary objective of arresting land degradation. One study indicates that the rate of land degradation in rainfed areas in the 1990s is likely to have been more than twice the rate in the 1980s, largely because of increased soil erosion (Reddy, 2000). At the other extreme, many projects have failed because the guidelines provided a pattern of uniform treatments across diverse agro-ecological conditions, leading to a less than desired impact. The continued lack of drinking- and irrigation water in several Indian states shows that drought-proofing interventions have failed to stop land degradation in rural areas and have failed to improve rainfed agriculture and the availability of drinking-water. Why IWMP**:**Around 60% of cultivated area across India is rain-fed. Besides, these areas are also blighted by poverty, water scarcity, low productivity, and malnutrition and prone to severe land degradation. The watershed development programme has been adopted as a tool to address problems of the rain-fed or degraded areas in the country.

KEY POINTS OF IWMP: Launched in 2009-10 by the integration of various area development programmes of the Department of Land Resources, including the Drought Prone Areas Programme (DPAP), the Desert Development Programme (DDP) and the Integrated Wastelands Development Programme (IWDP).The 12th Plan allocates the programme an additional Rs. 29,296 crore.Cost sharing ratio of Central Government : State Government = 90 : 109% of the project cost is earmarked for development of livelihoods for asset-less people10% of the project cost is for productivity enhancement and development of micro-enterprises for small & marginal farmers.An average size of project under the IWMP is about 5,000 ha which is cluster of micro-watersheds.A portion of institution &capacity building (5% of the total project cost) has been provided to set up institutional mechanism at State, District, Project and Village levels and to build capacities of stakeholders.It also entails involvement of primary stakeholders in the form of grassroots community organizations.

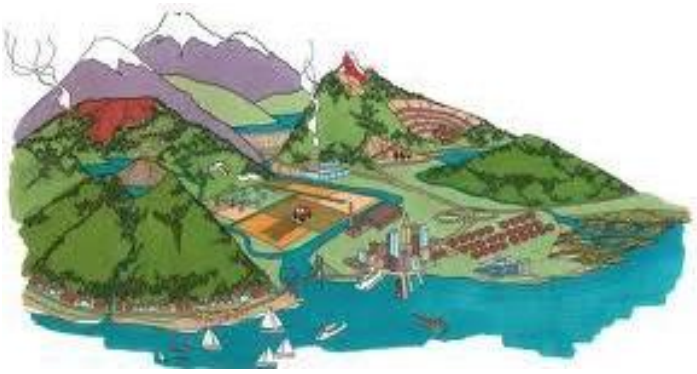

EXPECTED BENEFITS OF IWMP:

The benefits include increase in availability of surface water & groundwater, changes in cropping pattern from one to two crops annually, increase in fodder availability and increase in milk yield, increase in agriculture.

FUNDING PATTERN

Depending upon the ecosystem and major problems faced by different districts/blocks, each Watershed Development Project shall be eligible for funds as per the funding pattern for the whole project period. Department of Land Resources, Government of India may extend the project period in deserving cases without enhancement of cost and reduction of work components. This amount shall be divided amongst the following project components subject to the percentage ceiling mentioned against each:

I.	Watershed Treatment/Development Works/Activities	80%
II.	Watershed Community Organization including entry point activities	5%
III.	Training	5%
IV.	Administrative Overheads	10%
V.	TOTAL	100%

EMERGING ISSUES

The inclusion of livelihood security, poverty reduction, employment generation, social equity and the integration of the gender perspective in rural areas are key concerns in any development program. Climate change and its mitigation and adaptation strategies are receiving global attention and, therefore, interventions that promote such efforts should be incorporated into watershed management programs. We need to promote interventions of Clean Development Mechanisms, Organic Agriculture, Conservation Agriculture, non-pesticide methods of pest control, etc. to stop the degradation of resources and to make our environment a safe place to live. Greater use of modern technologies such as Geographic Information Systems and Remote Sensing is necessary to improve our efficiency in the planning, implementation and monitoring of watershed development programs

CONCLUSION

The problems of dry drought in India indicate that the drought tolerance approaches in the country have not worked for drought tolerance efforts. Central and state governments are still allocating a large budget to restore and develop water micro-layers. You need to think cool about the drought-proof water point. Many cascade projects have basic problem solving problems of design and implementation. Regardless of the revision of the government instructions, Vajpayee projects could not be reached yet. Many steps have only benefited a limited number of households and depend on technical reforms that often give rise to the lack of community property. The best performing projects are based on the promotion of traditional water collection and protection methods in the community. They have good community participation and low cost expenses. It has benefited people in a massive way and is generally based on promoting equality and environmental principles. On the contrary, most of the cascade is a clear qualification of the benefits and beneficiaries of the development programs. Farms also benefit from better irrigation, then farmers who form forms such as field packages. Unhealthy and those who do not own livestock take advantage of the minimum. These cases are treated more or less inevitably and are not kept at the centre of participation. Need to start negotiating between beneficiaries and acquisitions. An overview of Washington's plans in Karnataka and Maharashtra concluded that the importance of water development in India is of importance. Globalization and predictions of progress mean that local natural resources are compatible with the resources of the native system; these are often the last generation resources that have access to the rural poor.

REFERENCE

[1] S. P. Suryawanshi and Abhijeet Kamble, "Watershed management in India,"P.P:14-16

[2] V. Ratna Reddy,"Sustainable Watershed Management Institutional Approach",Economic and Political Weekly, Vol. 35, No. 38 (Sep. 16-22, 2000), pp. 3435-3444

[3] B.S. Chaudhary,"Operationalization of Remote Sensing And Gis For Ground Water Exploration And Management: Few Examples From Haryana State, India,"

[4] Budumuru Yoganand and Tesfa G. Gebremedhin," Participatory Watershed Management For Sustainable Rural Livelihoods In India",

[5] Preety M. Bhandari . Suruchi Bhadwal . Ulka Kelkar ,"Examining adaptation and mitigation opportunities in the context of the integrated watershed management programme of the Government of India," Mitig Adapt Strat Glob Change (2007),PP:919–933

[6] Wani S.P. et al, "Farmer-Participatory Integrated Watershed Management: Adarsha Watershed, Kothapally India An Innovative and Upscalable Approach,"August 2006 | Volume 2 | Issue 1,pp:1-26

[7] A.K. Goel*, R. Kumar ,"Economic analysis of water harvesting in a mountainous watershed in India,"Agricultural Water Management 71 (2005) , pp: 257–266

[8] Deepa Nathalia et al ," Environmental Change Detection using Geo - Spatial Techniques in Aravalli hills and Environs (Faridabad District, Haryana ," International Journal of Applied Environmental Sciences ISSN 0973-6077 Volume 12, Number 5 (2017), pp. 865-875

[9] Nancy Johnson ,"User participation in watershed management and research,"N. Johnson et al. / Water Policy 3 2001 , pp : 507–520

[10] K. H. V. Durga Rao1 And D. Satish Kumar ," Spatial Decision Support System for Watershed Management," Water Resources Management, pp: 423, 2004.

[11] Ch. Srinivasarao ," Zinc, boron and sulphur deficiencies are holding back thepotential of rainfed crops in semi-arid India: Experiences from participatory watershed management,"Ch. Srinivasarao et al. / International Journal of Plant Production (2008) 2: 89-99.

[12] Agarwal, A. 2000 Drought: Try capturing the rain. New Delhi, Centre for Science and Environment.

[13] Amezaga, J., Gosain, A., Gupta, A., Saigal, S. & Wilson, V. Forthcoming. Internal Policy Report I: Areview of water management, watersheddevelopment and forestry policy inIndia. Forthcoming at: www.cluwrr.ncl.ac.uk/.

[14] Gallart, F. & Llorens, P. 2003. Catchment management under environmental change: Impact of land cover change on water resources. Water International, 28(3): 334–340.

[15] Gosain, A.K., Rao, S. & Calder, I.R. 2003. New technologies for effective watershed management. Paper submitted for FAO/ICIMOD Workshop on Preparing the Next Generation of WatershedManagement Programmes (September 2003). Kathmandu, ICIMOD/FAO.

Journal of Remanufacturing
https://doi.org/10.1007/s13243-018-0049-7

RESEARCH

Reverse supply chain issues in Indian electronics industry: a case study

Saurabh Agrawal [1] · Rajesh K. Singh [2] · Qasim Murtaza [1]

Received: 13 November 2017 / Accepted: 18 July 2018/Published online: 26 July 2018
© Springer Nature B.V. 2018

Abstract

The electronics industry is growing fast with the advent of new technologies and product innovation across the globe. Short product life cycle coupled with the huge demand for electronics products, generating a pile of discarded products results in e-waste generation. The industry is also facing the higher product returns due to the increase in online business and liberal policies offered to the consumers. Effective and efficient reverse supply chain implementation may help in managing these returns along with the end of life product returns. Despite a growing body of research in the area of reverse supply chain, industries are reluctant to adopt best practices of the reverse supply chain. The proposed study aims at exploring the key strategic issues and challenges faced by the electronics industry by using case study method. A case of Indian Electronics Organization is analyzed to identify key strategic issues and challenges in the managing reverse supply chain. The study will help the managers in understanding the complexities of reverse supply chain management in the electronics industry such as critical success factors, outsourcing decisions, disposition decisions, performance evaluation, and forecasting product returns.

Keywords Reverse supply chain · Reverse logistics · Indian electronics industry · Strategic issues · Critical success factors

✉ Saurabh Agrawal
agrawals.iit@gmail.com

Rajesh K. Singh
rksdce@yahoo.com

Qasim Murtaza
qasimmurtaza@gmail.com

[1] Mechanical, Production & Industrial Engineering Department, Delhi Technological University, Delhi 110042, India

[2] Operations Management, Management Development Institute, Gurgaon 122 007, India

Introduction

The electronics industry is the fastest growing industry in the world. The demand for electronics products particularly consumer electronics is increasing rapidly due to computerization and mobile phone technology innovations worldwide. The Indian electronics industry is also growing with the worldwide growth and the electronics industry is among one of the fastest growing industries in the country. According to the annual report of the ministry of information technology, India, the market for the electronics industry is expected to be $400b by the year 2020. At present, the contribution of domestic production is approximate $31b and is expected to be $100b by the year 2020. Digital India, e-governance and other initiatives by the government of India offers a lot of future potential for growth of electronics industry in India. "Make in India" initiative by the government of India has turned the attention of global Organizations towards India and they are looking for building up manufacturing facilities in India to serve the domestic as well as global markets. Product life cycles are becoming shorter and shorter with the advent of new technologies and consumers quest for new products. The products are being discarded very fast by the consumers which result in electronics-waste, popularly known as e-waste. According to United Nations report (Global E-Waste Monitor [11]), India is the 5th biggest producer of e-waste in the world generating 1.7 million tons' e-waste in 2014 and its volume is expected to grow by 21% in next 3 years. One of the ways to manage this e-waste efficiently is the adaptation of reverse supply chain practices by the industry. The reverse supply chain may help in extending the products useful life cycle through reuse, repairing, remanufacturing, and minimizing the e-waste through recycling of discarded products. The reverse supply chain also plays an important role in managing the product returns because of the increased flow of product returns due to the liberalized return policy and allowances offered by the Organizations to the consumers. Prakash and Barua [25] identified barriers to the reverse logistics implementation in Indian electronics industry and suggested solutions to overcome these barriers. Heggde and Kumar [14] explored the strategies for collaboration among telecom Organizations in India. Agrawal et al. [1] developed a forecasting model for product returns in Indian mobile manufacturing Organization. In another study, the opportunities and challenges for mobile business activities were discussed through the case study of Indian Organizations [6]. Noman and Amin [22] studies the reverse logistics framework of cellphones exploring the practices and policies in Canada. In a study in Germany, Gurita et al. [12] examined the potential of reuse, remanufacturing, and recycling of mobile phones. Vogtlander et al. [39] analyzed the circular business models for consumer electronics products including mobile phones. Rathore et al. [26] proposed a framework for achieving sustainability through remanufacturing and illustrated the case of an Indian mobile manufacturing Organization. Authors have reviewed the waste management and recycling status of mobile phones and also explored the waste management of Indian mobile industry [30, 33, 34, 38]. The Organizations can manage product returns and end of life products through effective implementation of the reverse logistics system. Many Organizations are reluctant to the adoption of reverse logistics system because of several issues faced by the Organizations. It is evident from the previous research that issues like implementation of reverse logistics, prediction of reverse flow of products, outsourcing decisions, disposition decisions, performance measurement system for reverse logistics and so on have not explored much in the past [2, 3]. The proposed study aims at exploring the current practices of the reverse supply chain, and analyzing the key strategic issues and challenges faced by the electronics industry through a real-life case study. The case study is developed based on the research processes discussed in past literature [10, 37, 42].

The remainder of the paper is organized as follows. The second section discussed about the literature review related to reverse supply chain and various issues in reverse supply chain. The case method is explained step by step in the third section. The fourth section consists of details of the case study including organization profile, reverse supply chain process of the organization, SOWT analysis, and various issues in the organization. Last section, the fourth section concludes the findings of the case study.

Literature review

Reverse supply chain has gained importance since last decade because of legislation, environmental concerns, and corporate social responsibility. It has been found to be beneficial to various organizations in terms of the improvement in the profits. Some of the organizations like HP, Dell have implemented it for competitive advantage. Jayaraman and Luo [16] mentioned that Kodak has successfully implemented recycling facilities and is able to reuse up to 86% of a camera's parts. Similarly, other leading manufacturers such as Canon and Xerox have also attained remanufacturing rates of nearly 90 %. Recently, Paterson et al. [24] worked on incorporating remanufacturing into end-of-life vehicles in Europe. In India, the experience of the reverse supply chain is relatively new and there is lack of interest in the adaptation of reverse supply chain practices. This may be because of the absence of strong legislation or may be because of the lack of interest of top management and business partners to spend money for reverse supply chain system [27]. There is the number of factors affecting reverse supply chain practices and presence or absence of these factors can become drivers or barriers to reverse supply chain implementation in an industry [29]. Dowlatshahi [9] enumerated strategic factors such as government rules and regulations, environmental issues, consumer concerns, and costs; along with operational factors such as cost-benefit analysis, logistics, warehousing, supply chain management, recycling, and packaging. In a survey of consumer electronics, Janes et al. [15] identified main enablers of reverse logistics as top management awareness, strategic alliances with associates, understanding of cost and performance, recapturing value from used products, and ability to send products back into the market. Jindal and Sangwan [17] investigated economic factors, environmental issues, and social drivers for the Indian industry. Agrawal et al. [4] identified major critical success factors for Indian electronics industry as top management awareness, resource management, economic factors, and contracts terms & conditions. These factors help the Organizations to take appropriate action for adaptation and implementation of the reverse logistics system.

Another important issue is the outsourcing of reverse logistics activities. Manufacturers adopting reverse logistics, have to decide whether outsourcing those activities to the third party or performing themselves [21]. Outsourcing may reduce the cost because of economies of scale and also, manufacturers can reduce their asset base, and deploy the capital released for other productive usages by outsourcing reverse logistics. Other advantages include less uncertainty in operations, more concentration on core competency, more flexible, improved consumer receptiveness, and improved access to new technology [18, 19]. Product flows in reverse logistics are uncertain in terms of quantity, quality, and timing of returns. Forecasting product returns are important both for the strategic and operational decision-making in reverse supply chain. Long-term forecasting may not only help in determining the future capacity required and expected business from the reverse logistics but also in its outsourcing decisions. Short-term forecasting is important for the day to day planning and control of recovery processes [41].

Once the products are collected, inspected, and sorted into different categories, they are disposition either for reuse, or repairing, or remanufacturing, or recycling depending on the number of factors. Disposition of returned products may be industry or product specific and depends upon the number of factors including price/value / shelf life of the product, transportation cost, and the demand outlook [35]. The consumer expects the credit or replacement of returned product as quickly as possible while the manufacturer wants to disposition these products for recapturing the maximum value [13]. Strategic disposition of the returned product is important for the better performance of reverse logistics system of an organization [7].

Another key issue is the performance measurement system of the reverse supply chain. According to Song and Hong [36], 'the performance measurement systems can provide organizations with relevant, appropriate, complete, and accurate information. The organizations have opportunities to monitor, and reposition their management and operations to obtain highly competitive environment'. Ravi et al. [28] used balanced card approach and analytic network process technique for the selection of alternatives for the end of life computers. Shaik and Kader [32] developed a reverse logistics performance evaluation framework by using balanced scorecard approach and analytic hierarchy process. Paksoy et al. [23] developed a mathematical model for investigating a number of operational and environmental performance measures consisting of total transportation costs, total environmental costs, emission rates, consumer demand. Bai and Sarkis [8] introduced a performance evaluation framework by using AHP for evaluating the economic, environmental, and the operational performance. Agrawal et al. [4] developed fuzzy AHP approach for economic, environmental, and social performance measurement of reverse logistics.

Case method

The reverse supply chain has become essential for the organizations because of the increased flow of products return, growing concerns for the environment, and corporate social responsibility. The Organizations are adopting the practices of the reverse supply chain in order to comply with government rules and regulations and to remain competitive while using green as a marketing tool. These Organizations come across several issues while performing reverse logistics activities. Case research is one of the effective tools for in-depth understanding and analysis of these issues. According to [42] "A case study is an empirical inquiry that (i) Investigates a contemporary phenomenon within its real-life context, especially when, and (ii) The boundaries between phenomenon and context are not clearly evident".

Case studies are used as a research method if contextual factors are taken into account but at the same time limit the extent of the analysis [10, 40]. Applying a flexible, sometimes even opportunistic research strategy is one of its major strengths, but might also be a major weakness of case study research, in particular, if the process is not well documented. A single case has been considered as a representative case of a wider group of cases for the proposed study. The research methodology adopted for the study is based on literature review and discussion with executives of the Organization. The literature review enabled the identification of various reverse supply issues [5]. Discussions with executives provided a real-life scenario of the reverse supply chain in Indian electronics industry including the select reverse supply chain issues. A step by step approach to the proposed case study is developed based on the research processes discussed in past literature [10, 37, 42]. These steps are as followed.

Step 1: **Definition of research question**

The first step of case research methodology involves defining the research question. The research question is defined as "Study of select issues in reverse supply chain of Indian electronics industry". The case study will seek the answer to the following questions in context to a case from an electronics organization i.e. ABC Limited.

- What are the major reverse supply chain activities performed by the Organization?
- What are the critical success factors for reverse supply chain implementation?
- What are the major reverse supply chain activities outsourced by the Organization?
- How are the decisions for outsourcing taken?
- How is the future planning for reverse supply chain done in the Organization?
- How are the returned products disposition for further processing?
- How the Organization measures the performance of the reverse supply chain?

Step 2: **Instrument Development**

The second step of case research methodology is the development of a research instrument and selection of the field site. A single case with embedded issues has been considered as a representative case of a wider group of cases for the proposed study. The Organization for the study has been selected based on its size in terms of revenue and its office in NCR Delhi, India which is local for the researchers.

Step 3: **Data Collection**

The next step is data collection for the case study. The data may be collected through open interview, semi-structured interview, structured interview, questionnaire, documents/websites/publications, direct observation, participant observations [31]. The data for the proposed case study was collected both from primary and secondary sources through the web page and published material, and questionnaire followed by the semi-structured interviews with concerned people in the Organization. Total eleven number of people from various levels participated in the study and they were interviewed during the visit.

Step 4: **Data Analysis**

Information and data collected from the field visits to the Organization and other secondary sources were used to analyze the issues in reverse supply chain.

Step 5: **Dissemination**

Case-based approaches to research are often subject to criticism, some valid, some invalid. Yin [42] made an effort by providing logical validity tests for judging the reliability and validity of the case research. Data for the proposed study were also collected from the other sources like regulatory documents, web pages of the Organization to ensure the construct validity and internal validity of the collected data. The Organization executives from each stage were asked to answer questions according to the same interview guidelines. It helped in reaching the internal validity among different interviews.

Case study

A case of Indian electronics organization, ABC Limited was considered for the proposed study. The case study of the organization is explained in the following section.

Profile of the organization, ABC Limited

ABC Limited is one of the growing consumer's electronics organization having a corporate office in Gurgaon, near Delhi, India. The Organization has approximately 1000 employees and reported approximately 2.0 billion USD annual revenue in the financial year (2015–16). The revenue of this organization in last four financial years is shown in Fig. 1. It is evident from the figure that this organization is growing very fast in the Indian mobile manufacturing market.

The Organization offers a range of products including mobile phones, PC tablets, LED TV and data cards. The major business comes from the sale of mobile phones. The Organization is the largest domestic mobile phone Organization in low-cost market segmentation. The Organization is currently the 2nd largest mobile phone Organization in India having 16% market share in smartphone market and 13% market share in the overall mobile phone segment. The Organization is 2nd largest in Indian tablet PC segment also with 11% market share. The Organization initially started its business with mobile phones model based sourcing from the Organizations in Korea, China, and Taiwan to take full advantage of zero import duty on mobile phones. Later on Organization set up a manufacturing plant in Rudraprayag, Uttrakhand, India where it manufactures PC tablets and LED TV. Recently, the Organization has started manufacturing mobile phone devices at this plant. The Organization procures some of the components and parts from China and Taiwan and assembles them at this facility. The Organization has widespread supply chain network in India particularly in rural areas and sells approximately 2.3 million handsets every month. Recently, the Organization has started selling mobile phones in Russia also. Recently, Ministry of the environment, forest, & climate change; Government of India has notified the drafts of waste management rules 2016 (Amended in 2018) which includes e-waste management. These rules are based on the concept of extended producer responsibility. Also, online sale through e-retailers like Amazon India, snap deal, flip kart has increased considerably in last few years. The product returns have also increased due to the liberal return policies offered by these Organizations. The Organization is looking for long-term solutions for handling these returns along with the end of life products.

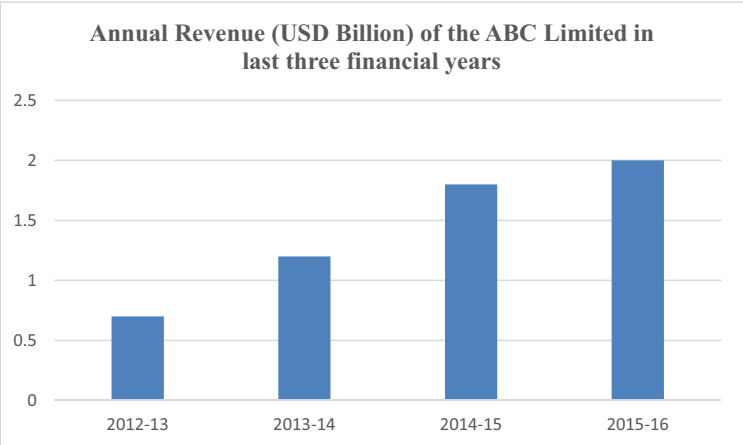

Fig. 1 Revenue of the ABC Limited in last four financial years

Reverse supply chain of the ABC Limited

ABC Limited has vast network of super-distributors, distributors, and retailers throughout the country in 560 towns in India. As shown in Fig. 2, it has 70 super-distributors, also known as super-stockist, more than 1500 distributors, and 125,000 retailers along with more than 500 customer service centers across the country. The Organization has given a lot of attention to the supply chain and has developed innovative way of supply chain distribution. It introduced cash-only model unlike other Organizations offering 60 days credit line to the distributors. They offered higher margin (Approx. 15%, higher than the industry average of 6%) to the distributors in lieu of cash payment to the ABC Limited before delivery of products. Its strategy is to offer more margin and no credit to the distributors with advance payment to the Organization. There are of the view that "If the distributor does not buy your handsets, there is no pressure on him to sell them," and at the same time it will offer more profit to the distributors. This strategy worked well for them. They not only managed to increase its sales but also managed cash flow very efficiently. The Organization tracked the sales of products on daily basis to monitor the success of the cash-only model. The products are supplied to the distributors on regular basis so that they do not locked in money in excess inventory. The products are sold through the online retailers and also by its retailers (Called merchants). The products returns have increased considerably due to online selling and their liberal policies like cash on delivery, 30 days replacement warranty, 1 year warranty etc. on products. The product returns comprised of new products, products for repair, non-repairable products, and end of life products. The product acquisition from consumers is carried out through retailers or service centers or products are collected by the third party and dispatched to the service centers. New products, returned are resold by retailer after repackaging by the service center, if required. Repair work is also performed at the service center and products after repair are given back to the consumers through respective retailers. The LED TV, and PC tablets, which are non-repairable are returned to the manufacturing facility. The refurbishment or

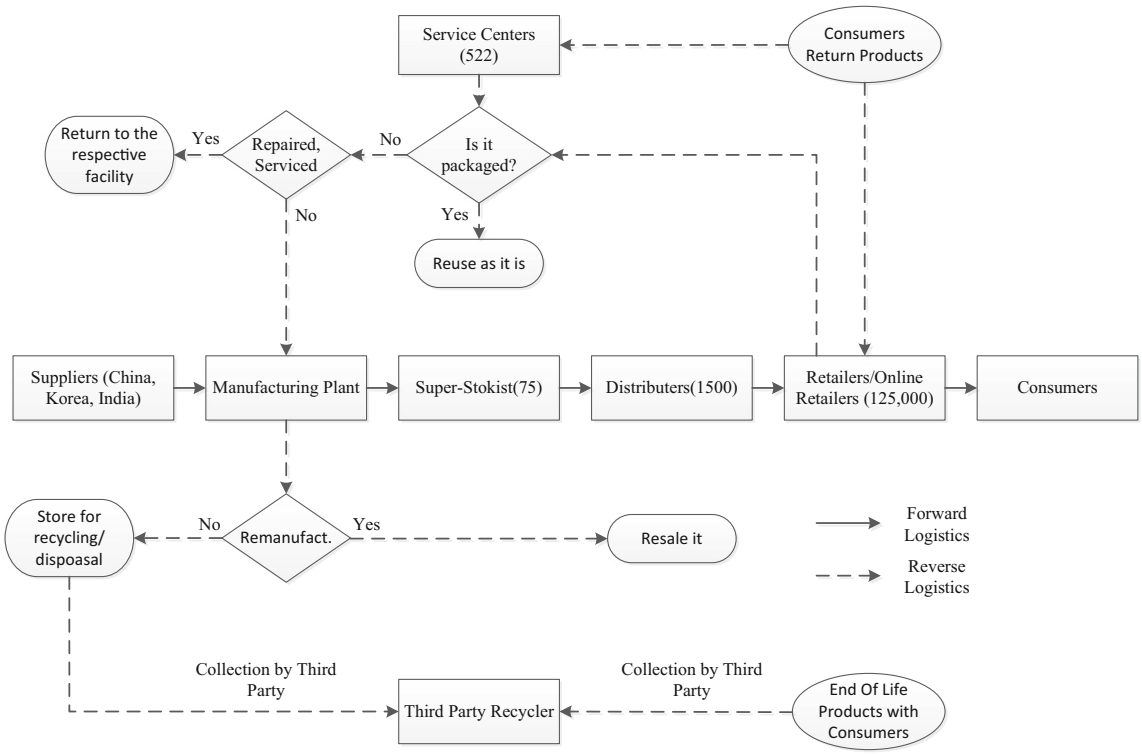

Fig. 2 Reverse supply chain of the ABC Limited

remanufacturing of these products is carried out at the manufacturing facility and products are resold through secondary markets. However, mobile phones are repaired or refurbished at the service center only. No remanufacturing of these products is considered because of higher logistics cost and non-availability of established remanufacturing. ABC Limited has authorized the third party recycler for collecting and recycling of the end of life mobile phones from the consumers, service centers, and also from the manufacturing facility. Although this is not outsourced where the Organization may have better control of the recycling operations. The Organization has not given much attention to the reverse activities of the supply chain. Pursuant to e-waste management rules-2016 (amended in 2018) in India, increased flow of product returns, and recently established manufacturing facility, the Organization has decided to explore the various recycling, remanufacturing options. Reverse supply chain of the ABC Limited is shown in Fig. 2 and processes are explained in the following sub-sections.

Product acquisition/gate keeping

The products are sold through retailers, e-retailers, and through own online portal of the ABC limited. The acquisition of returned products, sold online takes place at the site of the consumer by the e-retailers through an outsourced service provider. The products (sold through retailers) are returned by the consumer either at the store or at the consumer service center.

Collection

The returned products are collected by the e-retailers and sent it back to the point from where they were purchased during the monthly return policy. These products are mostly new and returned by the consumers due to price or change of mind for the products. After this one-month time, products are returned by the consumers to the service centers if they have an issue with the functioning of products. The product acquisition takes place at the service center. In case of sell through the retailers, the products are returned to the retailers during the one-month period. Otherwise, consumers return those products to the service center.

Inspection and sorting

The products returned during the 1 month are mostly new and need little or no inspection. The products at the service centers are inspected by the engineers. The products are repaired and returned to the consumer. In case of LED TV, the products are inspected at the site of consumer and shipped to the service center if not repaired at the site. If the products are not repaired at the service center, the products are transported to the manufacturing facility of the ABC Limited. If products are dead and there is no scope of any remanufacturing or further improvements, they are collected by the third party for the recycling.

Disposition

In recent years, the online sale of products through e-retailers and Organization's own portal has increased considerably. At the same time, the Organizations are experiencing the returns even up to 30–40% due liberal policies like cash on delivery and competition in the market. Many products are returned as new by the consumers. These products after repackaging, if required are directly reused by the retailers and distributors of the Organization, ABC. Repairing takes

place at the consumer service centers, and products are returned to the consumers. In case of LED TV, the repairing may be carried out at the consumer site or shipped to the service center. If products cannot be repaired at the service center, they are shipped to the manufacturing facility.

ABC Limited performs the Refurbishing or remanufacturing operations at the manufacturing facility. The LED TV is refurbished or remanufactured completely and after remanufacturing, they are either returned to the consumer or they are sold in the secondary market through the online website like greendust.com and other local dealers. The mobiles are only refurbished and resold or returned to the consumer. ABC Limited has only assembly facility for mobiles and remanufacturing is not the viable option. It has recently started manufacturing of mobiles in India and planning to go for 100% manufacturing of mobiles in India through local sourcing of components and parts. In case the products are not refurbished or remanufactured, they are the disposition for recycling. ABC Limited has authorized a third-party recycler to collect its product from consumer, service center and from the manufacturing facility, and recycle them. Although this authentication is formal in nature and ABC Limited may need to look into this pursuant to upcoming e-waste management rules and regulations in India. The products are collected by the recycler and thereafter Organization has no audit of these types of products. Disposal of products is carried out by the recycler Organization.

Redistribution

Products after refurbishment/remanufacturing are sold in the secondary market through online web portals and through local dealers. The new products returned by the consumers at service centers are resold in the market after repackaging if required.

SWOT analysis of the ABC Limited

Any organization needs to analyze its Strength, Weaknesses, Opportunities, and Threats (SWOT) for strategy formation to sustain and compete in the market. Therefore, SWOT analysis of the ABC Limited was carried to get in-depth insight of the business model of the organization. SWOT findings are summarized in the Table 1. Low-cost products, Innovative products entering the market at right time are the major strengths of the ABC Limited. The Organization has the strong widespread network across the country has deep penetration into the rural market segment of the country. ABC Limited has developed its own manufacturing facility in India. The Organization has bundled its products with some of the key telecom service providers and has better coordination with service providers. Consumer service centers with skilled capacities help in performing repairing work efficiently and reduce the remanufacturing need of the products. However, the low-cost brand image of the ABC Limited makes it less competitive in the urban markets. This organization takes the advantages of global research of other organizations for introducing the new products in the market. This may prove to be disadvantageous in future because of entry of many Chinese organizations with similar low-cost products. The profit margins on the products are reducing due to competition, online retailing and higher margins to the distributors. The rapid change in technology is also a big challenge for the Organization. For example, Demand for a 4G phone is growing very fast and 35% smartphone sold in India are 4G. According to International Data Corporation report, the ABC Limited is able to maintain second position with approximately 16.5% market share. As discussed above, it has limited remanufacturing facility which forces them for recycling of products. The recycling facility is authenticated to the third party which

Table 1 SWOT analysis of ABC Limited

Strengths	Weaknesses
Innovative Products and Features	Low-cost brand image in urban markets
Low-cost products	Image of low-quality Chinese products
Introducing new product at right time in the market	New products similar to products available in global market
Strong supply chain of distribution	Reduced profit margins due to low price and higher margins to distributors
Strong supply network in rural markets	No control over recycling and disposal of EOL products
Effective cash flow management	Limited remanufacturing facility
Co-Ordination with telecom service providers	Products are not designed for easy to disassemble
State of art manufacturing facility	Do not have robust reverse supply chain
Repairing facilities at Consumer Service centers	No, Take back type initiative for promoting sustainability
Opportunities	**Threats**
Huge demand for mobile phones	Growing competition in domestic and International market
Penetration in urban market	Replication of business model by other Organizations
Profits from precious metal extracted through recycling	Strict e-waste management rules and regulations-2016, further amended in 2018
Exports to international markets	Entry of Chinese Organizations through online retailers
New Market Segment for remanufactured products	If Organization cannot take responsibility for e-waste management adequately, it may be forced to go out of business in future
Green Products can improve brand image and can be a competitive image	Price reduction due to online business offerings
Digital India Initiative	Reach of e-retailers to rural markets
Make in India Initiative	Establishment of other mobile manufacturing facilities in India

recycles the products. There is an opportunity to extract precious metals from the recycling of products. This organization has not given much attention to reverse supply chain and sustainability which may become a threat in future with strict rules and regulations by the government of India. There is opportunity of new emerging market for remanufactured products and also, better brand image by taking green initiative which may be a competitive advantage to the Organization. Digital India, and Make in India initiative provide an opportunity for future market potential and other benefits offered by the government for extension of manufacturing in India.

Key strategic issues and challenges: findings and discussion

After studying and going through the profile of ABC Ltd. and business practices of its reverse supply chain, the case was analyzed based on case methodology to illustrate the various reverse supply chain issues in the Organization. Different strategic issues were identified and are explained as follows.

Returned products acquisition and collection issues

ABC Limited sells products to the consumers through multiple channels of distribution. As discussed above, the product acquisition takes places at multiple points in the channel. The collection of products through service centers provides an edge to the organization because of a vast network of distributors and retailers. In case of the end of life, there is an issue of collecting the products from the consumers. This organization has no visibility and control of

products. In future, there may be problems of compliance with the e-waste management regulations. There is a lot of uncertainty in terms of quality, quantity, and timing of product returns particularly the end of life products. These uncertainties may result in inefficiency in planning and control of reverse supply chain [20]. The short-term forecasting is managed by the organization through tracking of sales from the distributors. The Organization has authorized the third party for the end of life products from consumers directly but there is no audit of the recycling of these products. This is more a formal type arrangement for providing business to the recycler and cannot be considered as equivalent to outsourcing where the Organization has better control and shares the business. Long-term forecasting is important for the strategic decisions related to setting up of own facilities for recycling or outsourcing these activities. The future predictions may help in future economic benefits of owning reverse logistics by the Organization.

Disposition related issues

Inspection and sorting are carried out at the service centers of the organization. These centers are equipped with modern facilities and trained engineers providing best service to the customers. In case of LED TV and tablets, the products after inspection are the disposition for recycling or remanufacturing depending on their quality if they cannot be repaired. Mobile phones are repaired and returned to the customers. In most of the cases, the PCB is replaced with the new one if it cannot be repaired. However, it was noticed that charges for the repairing phones, not covered under warranty or after warranty period are very high and consumers mostly prefer to get repair them in the local market. The organization may provide better service to the consumers by resolving this issue. The organization is used to disposition the mobile for recycling if they cannot be repaired. The reason was that the mobiles were sourced from the foreign country and they had no remanufacturing facilities in India. Since low cost is the key for this organization, it perceived no potential to disposition them for remanufacturing. ABC Limited has established the manufacturing facilities within the country and also, the remanufacturing is recently being offered by some of the third-party service providers. The Organization is considering the remanufacturing operations of the mobile phones.

Critical success factors for reverse supply chain implementation

ABC Limited has established a vast chain of the network for the forward logistics and also committed to managing reverse supply chain to provide better service to the consumer. However, it is under pressure to manage the e-waste generated because of government rules and regulations. Since this organization has started manufacturing in India, it is looking for economic benefits by incorporating reverse supply chain practices into their business. In order to implement reverse supply chain practices, it is important to understand the critical success factors for the ABC Limited. After discussion with the management of the organization, it was observed that top management awareness is most important for complying with regulatory requirements and at the same time to invest money in the required resources. Another important factor observed was resource management including human resource, development of the remanufacturing facility, and establishing recycling facility. The economic factor is also among one of the critical success factors for the reverse supply chain of the organization. ABC Ltd. offers the low-cost products to the consumers and this is their unique selling point. So, it is important to keep the economic benefits in consideration while implementing reverse supply

chain practices. In order to comply with the government regulations and to achieve sustainable developments, it is important to have contract terms and conditions incorporating the government regulations regarding components/parts supplied by them. Management information system is already in place in this organization and they are able to track their sales and stock status very well. Although information system does not track the end of life products. Since products are sold and distribution through multiple channels, the integration of forward and reverse supply chain is not easy and economical for the organization. The joint consortium is important vertically but not significant horizontally because of competition in the market. Process capability will be important when the organization will start full-fledged manufacturing in-house. The legislation, taxes, and environmental concerns are the part of a discussion in this organization and will gain importance with the effective implementation by the concerned regulatory bodies. In summary, the major top four critical success factors for the ABC Ltd. have been identified as top management awareness, resource management, economic factors, and contract terms and conditions. Agrawal et al. [3] also identified the critical success factors for the Indian electronics industry as shown in Fig. 3. Observations made by Agrawal et al. [3] further validates the findings of this study.

Outsourcing decisions

Outsourcing is one of the important decisions in reverse supply chain [4]. ABC Limited has a vast distribution network for the forward supply chain. The reverse supply chain is mainly confined to the warranty period returns and new products return through online retailers. It has established the consumer service centers and logistics facilities for collection, reuse, and repair. However, remanufacturing is not explored due to model-based sourcing from the foreign countries like Korea, China, and Taiwan. Since now the manufacturing facilities have been established in India, ABC Limited can explore the option of remanufacturing. Also, third-party service providers are offering the remanufacturing of mobile phones. The organization can outsource the remanufacturing to these third-party service providers. The organization has authorized the third-party recycler for the collection and recycling of end of life products because it wants to focus on core activities. This organization is of the view that the third-party service providers have specialized infrastructure, IT capabilities, and logistics facilities which may be more beneficial for the Organization. Pursuant to the recent e-waste management rules and pressure from stakeholders, the organization needs to explore the option of recycling as per regulatory requirements.

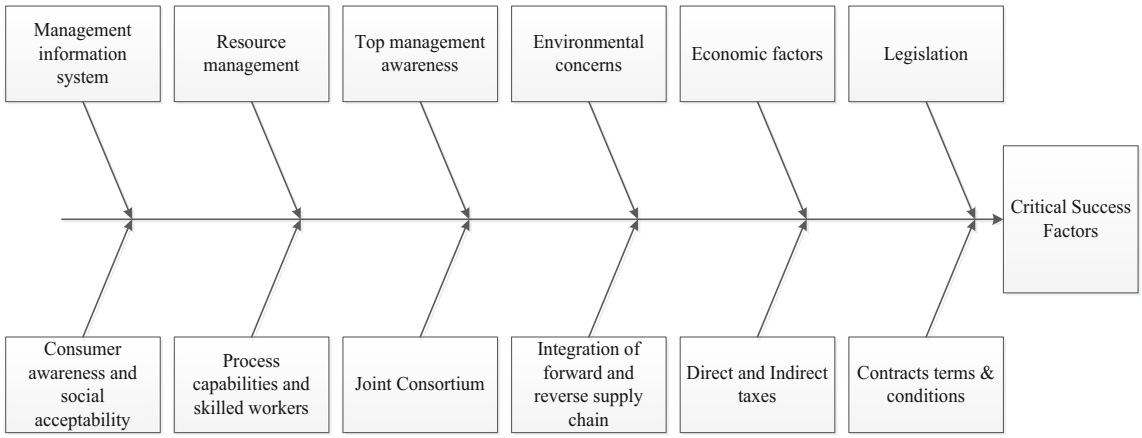

Fig. 3 Critical success factors for the ABC Limited

Performance measurement system

ABC Limited has no established performance measurement system for the reverse supply chain. The key performance measures include the number of products returned, reasons for product returns, quality of product returns, and cost of product returns. The performance measures are mainly focused on the economic performance, internal process capabilities, learning, and growth. This organization has not given much attention to the environmental and social factors. Agrawal et al. [5] have observed that for sustainable performance improvement and effective reverse supply chains, environmental and social factors should be part of the performance framework. Now ABC Ltd. sees the opportunity of utilizing corporate social responsibility funds for the management of reverse supply chain operations. The inclusion of some of the environmental and social factors and their measurements may provide an opportunity to spend money on them for the improvements.

Conclusion

In last few years, the reverse supply chain has gained a lot of attention due to environmental concerns, government regulations, and corporate social responsibility. It has also become important in the emerging economies like India because of huge product returns in online retailing business. Several strategic issues and challenges have been explored by the researchers in the past. Although, there are many studies on reverse supply chains they have not explored strategic issues and challenges in context to developing countries such as India or other South Asian countries. The present case study has provided an in-depth understanding of key strategic issues and challenges in the electronics industry by using a framework consisting of theoretical and real-life practical approach. The strategic issues which were found to be crucial in reserve supply chain are critical success factors, outsourcing decisions, disposition decisions, forecasting product returns, and performance evaluation system. Some of the major findings are summarized as follows.

(i) The electronics industry is coming across a new challenge of managing product returns because of the changed business environment, and complying e-waste management rules and regulations.
(ii) Top management awareness, Resource management, Economic factors, and Contracts terms & conditions with the supplier are the critical success factors for the industry.
(iii) The Organization has authorized third party recycler for collection and recycling of end of products. They need to differentiate between outsourcing, and authorizing the third party for recycling. The organization has no control over the third party to whom they have authorized for the collection and recycling of end of life products. Pursuant to new e-waste management rules and regulations by the government of India, the audit of the e-waste is not easy with this type of arrangement.
(iv) This organization is able to manage inventory through tracking of products with the distributors online. However, long-term forecasting product returns are important for the future planning and decision-making in the reverse supply chain activities.
(v) Another important issue is the disposition of products efficiently. This organization is yet to explore the remanufacturing options within the manufacturing facility. Since, the industry is more dependent on the import of products, components, and parts, the

remanufacturing has not been explored much. The initiative like Make in India may encourage the remanufacturing option while establishing new manufacturing facilities in the country.

(vi) Another key observation is that the Organization has not set up any formal evaluation of performance in reference to reverse supply chain activities. It may be important in the long run to establish comprehensive performance measurement system for reverse supply chain so that it could be monitored and improved.

These observations and findings may help other organizations to improve their reverse supply chain activities. These observations and findings may also be useful for decision-making. Despite providing in-depth analysis, the study is not without limitations. While study covered key strategic issues, the study does not consider all parts of the reverse supply chain due to lack of accessibility of all information. Furthermore, interviews may be biased and may not represent the realistic picture. The Organization may not be comfortable in talking about various issues openly because of regulatory requirements, and legal bindings. Therefore, to generalize the findings, more case studies and empirical study may be carried out as the future scope of the study.

References

1. Agrawal S, Singh RK, Murtaza Q (2014) Forecasting product returns for recycling in Indian electronics industry. J Adv Manage Res 11(1):102–114
2. Agrawal S, Singh RK, Murtaza Q (2015a) A literature review and perspectives in reverse logistics. Resour Conserv Recycl 97:76–92
3. Agrawal S, Singh RK, Murtaza Q (2015b) Prioritizing critical success factors for reverse logistics implementation using fuzzy-TOPSIS methodology. J Industrial Eng Int 1–3
4. Agrawal S, Singh RK, Murtaza Q (2016a) Outsourcing decisions in reverse logistics: sustainable balanced scorecard and graph theoretic approach. Resour Conserv Recycl 108:41–53
5. Agrawal S, Singh RK, Murtaza Q (2016b) Triple bottom line performance evaluation of reverse logistics. Compet Rev 26(3):289–310
6. Aithal PS (2016) A review on opportunities and challenges for mobile business activities in India. Int J Manage IT Eng 6(1):124–148
7. Attia A (2015) The impact of returned product disposition strategies on organizational performance applied to the Egyptian household appliance industry. Int J Business Manag 10(9):143
8. Bai C, Sarkis J (2013) Flexibility in reverse logistics: a framework and evaluation approach. J Clean Prod 47:306–318
9. Dowlatshahi S (2000) Developing a theory of reverse logistics. Interfaces 30(3):143–155
10. Eisenhardt KM (1989) Building theory from case study research. Acad Manag Rev 14(4):532–550
11. Global E-waste Monitor (2014) United Nations University, IAS–SCYCLE, 2015
12. Gurita N, Fröhling M, Bongaerts J (2018) Assessing potentials for mobile/smartphone reuse/remanufacture and recycling in Germany for a closed loop of secondary precious and critical metals. J Remanufacturing 1–12
13. Hall DJ, Huscroft JR, Hazen BT, Hanna JB (2013) Reverse logistics goals, metrics, and challenges: perspectives from industry. Int J Phys Distrib Logist Manag 43(9):768–785
14. Heggde G, Kumar S (2011) Strategies for Sustainable Channel relations in mobile telecom sector. J Economics Behavioral Studies 2(1):7–18
15. Janes B, Schuur P, Brito De MP (2010) A reverse logistics diagnostic tool: the case of the consumer electronics industry. Int J Adv Manuf Technol 47:495–513
16. Jayaraman V, Luo Y (2007) Creating competitive advantages through new value creation: a reverse logistics perspective. Acad Manag Perspect 21(2):56–73
17. Jindal A, Sangwan KS (2013) An integrated fuzzy multi-criteria evaluation of sustainable reverse logistics network models. IEEE Int Conf Fuzzy Sys 1-7 July, Hyderabad

18. Kannan G, Palaniappan M, Zhu Q, Kannan D (2012) Analysis of third party reverse logistics provider using interpretive structural modeling. Int J Prod Econ 140(1):204–211
19. Kumari S, Singh A, Mishra N, Garza-Reyes JA (2015) A multi-agent architecture for outsourcing SMEs manufacturing supply chain. Robot Comput Integr Manuf 36:36–45
20. Liang X, Jin X, Ni J (2014) Forecasting product returns for remanufacturing systems. J Remanufacturing 4:8
21. Martin P, VDR G Jr, Craighead CW (2010) Supply chain sourcing in remanufacturing operations: an empirical investigation to remake versus buy. Decis Sci 41(2):301–321
22. Noman R, Amin SH (2017) Characteristics of cellphones reverse logistics in Canada. J Remanufacturing 7(2–3):181–198
23. Paksoy T, Bektas T, Ozceylan E (2011) Operational and environmental performance measures in a multi-product closed-loop supply chain. Transp Res E 47(4):532–546
24. Paterson DAP, Kao CC, Ijomah WL, Windmill JFC (2018) Incorporating remanufacturing into the end-of-life vehicles directive: current presence and the waste problem. J Remanufacturing 8:23–37. https://doi.org/10.1007/s13243-018-0043-0
25. Prakash C, Barua MK (2015) Integration of AHP-TOPSIS method for prioritizing the solutions of reverse logistics adoption to overcome its barriers under fuzzy environment. J Manuf Syst 37(3):599–615
26. Rathore P, Kota S, Chakrabarti A (2011) Sustainability through remanufacturing in India: a case study on mobile handsets. J Clean Prod 19(15):1709–1722
27. Ravi V, Shankar R (2004) Analysis of interactions among the barriers of reverse logistics. Technol Forecast Soc Chang 72(8):1011–1029
28. Ravi V, Shankar R, Tiwari MK (2005) Analyzing alternatives in reverse logistics for end-of-life computers: ANP and balanced scorecard approach. Comput Ind Eng 48:327–356
29. Rogers DS, Tibben-Lembke R (1999) Going backwards: reverse logistics trends and practices. Reverse Logistics Executive Council, Reno
30. Sarath P, Bonda S, Mohanty S, Nayak SK (2015) Mobile phone waste management and recycling: views and trends. Waste Manag 46:536–545
31. Seuring SA (2008) Assessing the rigor of case study research in supply chain management. Supply Chain Manag Int J 13(2):128–137
32. Shaik M, Kader WA (2012) Performance measurement of reverse logistics enterprise: a comprehensive and integrated approach. Meas Bus Excell 16(2):23–34
33. Sharma SK, Panda BN, Mahapatra SS, Sahu S (2011) Analysis of barriers for reverse logistics: an Indian perspective. Int J Modeling Optimization 1(2):101–106
34. Singh RP (2013) India: a matter of electronic waste; the government initiatives. J Business Manag Social Sci 2(4):15–20
35. Skinner LR, Bryant PT, Richey RG (2008) Examining the impact of reverse logistics disposition strategies. Int J Phys Distrib Logist Manag 38(7):518–539
36. Song C, Hong Z (2008) Time scorecard: an integrative performance measurement framework for time-based organizations, Dalian, IEEE xplore. pp. 1–5
37. Stuart I, McCutcheon D, Handfield R, McLachlin R, Samson D (2002) Effective case research in operations management: a process perspective. J Oper Manag 20(5):419–433
38. Vats MC, Singh SK (2014) Status of E-Waste in India-A review. Transp 3(10)
39. Vogtlander JG, Scheepens AE, Bocken NMP, Peck D (2017) Combined analyses of costs, market value and eco-costs in circular business models: eco-efficient value creation in remanufacturing. J Remanufacturing 7(1):1–17
40. Voss C, Tsikriktsis N, Frohlich M (2002) Case research in operations management. Int J Oper Prod Manag 22(2):195–219
41. Xiaofeng X, Tijun F (2009) Forecast for the amount of returned products based on wave function. Int Conf Information Manag, Innovation Manag Industrial Eng 2:324–327
42. Yin RK (2003) Case study research: design and methods, 3rd edn. Sage Publications, Thousand Oaks

ResearchGate

See discussions, stats, and author profiles for this publication at: https://www.researchgate.net/publication/326543675

Thickness Computation for Byrd Glacier, East Antarctica

Conference Paper · January 2018

CITATIONS
0

READS
4

2 authors, including:

Anubha Aggarwal
Delhi Technological University
16 PUBLICATIONS **55** CITATIONS

SEE PROFILE

Some of the authors of this publication are also working on these related projects:

DST-SERB NPDF View project

All content following this page was uploaded by Anubha Aggarwal on 22 July 2018.

The user has requested enhancement of the downloaded file.

1st International Conference on New Frontiers in Engineering, Science & Technology,
New Delhi, India, January 8-12, 2018

NFEST/2018/R–059

Thickness Computation for Byrd Glacier, East Antarctica

Anubha Agrawal[1], Anubha Mandal[2]

[1,2]*Environemtnal Engineering Department, Delhi Technological University, India*
[1]*agrawal.anubha@gmail.com*

Abstract: *Byrd Glacier is an outlet glacier draining ice from the East Antarctica Ice sheet to the Ross Ice Shelf. Using surface based velocity measurements made in 1978-79; thickness is estimated for Byrd glacier using an algorithm based on surface velocity. Earlier, ice thickness has been reported using surface elevation from ground surveys and bed topography from air borne radar sounding.*

Keywords: *Antarctica; Thickness; velocity*

1. INTRODUCTION

Byrd glacier (Fig. 1) is one of the largest outlet glaciers of Antarctica with its catchment basin having an area of 1070400 km^2 and the ice being funneled into a ~20 km wide and ~100 km long fjord through the Transantarctic Mountains and after that diverging into the Ross ice Shelf [1]. There have been many quantitative glaciological investigations for Byrd glacier [2, 3, 4]. Brecher [4] measured 1003 elevations and 471 velocities for points on the main ice stream of Byrd glacier using photogrammetric triangulation from two sets of aerial photography in Dec 1978 and Jan 1979. These data were used by Whillans et al. [5] and Van der Veen et al. [1] to conduct a force-balance measurement. The same data are used in this study also.

Bed topography of Byrd glacier was studied by the Centre for Remote Sensing of ice sheets at the University of Kansas during the 2011-12 austral summer using airborne radar sounding. Ice thickness varied from 2300 m to 500 m as seen from plots in Van der Veen et al. [1], from 3200 m to 700 m as seen from plots in Whillans et al. [5]. Maximum deformation velocity of 57 m a^{-1} was calculated by Van der Veen et al. [1] with almost all discharge being due to basal sliding with the average basal drag of 130 kPa.

Viscosity parameter B = 600 kPa a$^{1/3}$, corresponding to an ice temperature of -20°C was used by Van der Veen et al. [1] for calculations. The same value of viscosity parameter is used in the present study.

Agrawal [6] reported a new algorithm for calculation of ice thickness using slope and surface velocity data. The same algorithm is used in this work. This algorithm is based on the work by Adhikari and Marshall [7]. They estimated the effect of longitudinal stress gradient on effective gravitational load. In addition to the slope and surface velocity data, this algorithm requires three more parameters, i.e., average basal drag, creep coefficient and sliding length to thickness ratio.

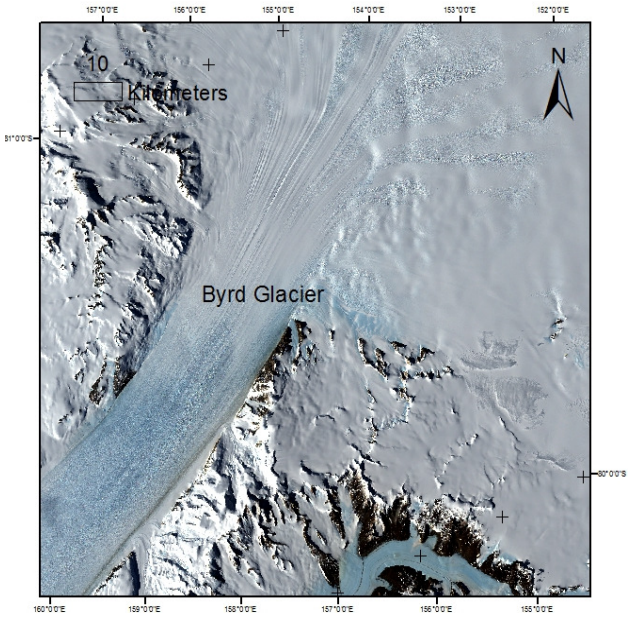

Fig. 1. Map showing the location of Byrd glacier in East Antarctica. This TIFF image of Byrd glacier is downloaded from [8]

In the present paper, a method is proposed to estimate the sliding length to thickness ratio. This ratio is important for estimating longitudinal sliding factor which is a function of slip ratio and sliding length to thickness ratio, as tabulated by Adhikari and Marshall [7]. Based on this algorithm, ice thickness is calculated corresponding to various velocity points for Byrd glacier in this work. The slope of the ice surface of Byrd glacier is less than 1 degree as seen from Brecher [4], so a constant slope of 1 degree is assumed in this work for the entire Byrd glacier. There is a requirement of a minimum threshold slope in the algorithm to reduce

errors in computation of thickness. Thickness is calculated in this work using above methodology for Byrd glacier.

2. METHODOLOGY

As discussed by Agrawal [6], the thickness at a point is estimated using data of surface velocity and slope. By an iterative method, ice thickness and basal surface velocity are estimated for that point. The iterative method depends on equating thicknesses found using two approaches. The first approach calculates thickness by assuming a linear shear stress distribution with maximum shear stress at bedrock equal to limiting basal shear stress value and zero value at glacier surface; and calculating surface velocity due to resultant shear flow.

The second approach finds thickness by considering shear stress at a layer at a distance 'z' from the surface as given by effective gravitational driving stress, i.e. , and calculating surface velocity due to resultant shear flow. The basal velocity is revised until thicknesses calculated from both approaches become equal. This approach is repeated for all pixels of the glacier. At every point, thickness and basal surface velocity are computed.

The methodology also incorporates the effect of longitudinal stress gradient (LSG) based on the work of Adhikari and Marshall [7]. The methodology computes ice thickness using the principle of local force balance and effect of driving stress on deformational velocity. Local equilibrium involves resistance due to basal, lateral, and LSG balancing the gravitational force. But according to Van der Veen et al. [1], there are some sticky points where linking basal shear stress is much higher and such locations help to stabilize the glacier, and lead to LSG which redistribute the basal shear stress and make it more uniform.

In the paper by Agrawal [6], a parameter, i.e. a sliding length to thickness ratio, plays an important role. In that paper, there is some arbitrariness about the choice of this ratio; the ratio was linked to length of the glacier. In the present work, this ratio is estimated by selecting a sticky point. The sticky point has been defined by Van der Veen et al. [1] as a point where basal shear stress is high enough to prevent basal sliding and these locations help in stabilizing the glacier. From surface velocity data the point of minimum surface velocity and a point nearest to this point are used to estimate this ratio. Zero slip is assumed at the minimum velocity point, and ice thickness and corresponding basal shear stress are calculated. This basal shear stress value is used for finding the thickness of the nearby point assuming zero slip again. Also, thickness is calculated using limiting average shear stress and different values of sliding length to thickness ratio. The ratio that gives thickness value closer to the thickness value corresponding to zero slip is taken as an estimate of sliding length to thickness ratio for the particular glacier. In this study sliding length to thickness ratio is seen to be one.

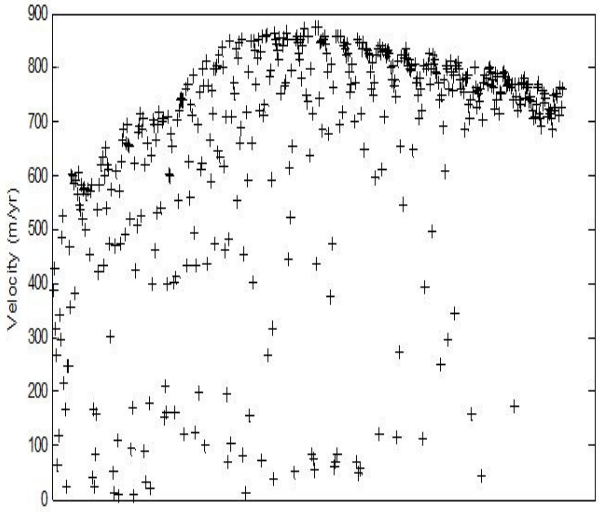

Fig. 2. Velocity data for Byrd glacier

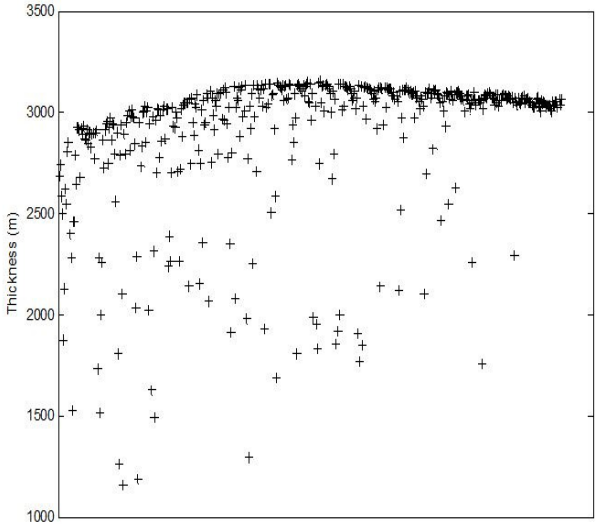

Fig. 3. Thickness values estimated for Byrd glacier

3. RESULTS

From the velocity data, the surface velocity is observed to be varying from 7.4 to 874.6 m/yr at different points on Byrd Glacier. Surface velocity and ice thickness for the 470 points are shown in Figs. 2 and 3 respectively. Average ice thickness is estimated to be 2890 m, with the maximum thickness being 3150 m and minimum thickness being 1160 m. The average basal velocity is 96% of surface velocity with maximum deformational velocity being 16 m/yr.

4. CONCLUSION

The average thickness of Byrd glacier is estimated to be ~2.9 km. The average basal velocity is 96% of surface velocity.

ACKNOWLEDGEMENTS

This work is done under the National Post-doctoral Fellowship funded by DST-SERB.

REFERENCES

[1] C.J. Van der Veen, L.A. Stearns, J.B. Castho, Flow dynamics of Byrd glacier, East Antarctica, Journal of Glaciology 60 (2014) 1053-1064.

[2] C.W. Swithinbank, Ice movement of valley glaciers flowing into Ross Ice Shelf, Antarctica.Science 141 (1963) 523-524.

[3] T.J. Hughes, J.L. Fastook, Byrd glacier: 1978-1979 field results, Antarctic Journal of the United States 16 (1981) 86-89.

[4] H.H. Brecher, Photogrametric determination of surface velocities and elevations on Byrd glacier, Antarctic Journal (1982) 79-81.

[5] I.M. Whillans, Y.H. Chen, C.J. Van der Veen, Force budget: III Application of three dimensional flow of Byrd glacier, Antarctica, Journal of Glaciology 35 (1989) 68-80.

[6] A. Agrawal, Estimation of volume of an eastern Himalayan glacier using a novel method based on the ice surface velocity data and basal sliding velocity, International Journal of Scientific Progress and Research 23 (2016) 170-180.

[7] S. Adhikari, S.J. Marshall, Improvements to shear deformational models of glacier dynamics through a longitudinal stress factor, Journal of Glaciology 57 (2011) 1003–1016.

[8] The National Aeronautics and Space Administration, Visible Earth: A catalog of NASA images and animations of our home planet: https://visibleearth.nasa.gov/view.php?id=7544, viewed on 29th July, 2017.

View publication stats

PAPER • OPEN ACCESS

UWB and miniaturized meandered stripline fed metamaterial loaded antenna for satellite applications

To cite this article: P. Dawar *et al* 2018 *IOP Conf. Ser.: Mater. Sci. Eng.* **377** 012080

View the article online for updates and enhancements.

Related content

- Transparent solar antenna of 28 GHz using transparent conductive oxides (TCO) thin film
  N I Mohd Ali, N Misran, M F Mansor et al.
- Compact Ultra-wideband Microstrip Antenna with Metamaterials
  Xiong Han, Hong Jin-Song, Zhu Qing-Yi et al.
- A compact ultra wideband antenna with WiMax band rejection for energy scavenging
  Y E Jalil, B Kasi and C K Chakrabarty

IOP ebooks™

Bringing you innovative digital publishing with leading voices to create your essential collection of books in STEM research.

Start exploring the collection - download the first chapter of every title for free.

This content was downloaded from IP address 14.139.251.107 on 19/07/2018 at 05:02

IOP Conf. Series: Materials Science and Engineering **377** (2018) 012080 doi:10.1088/1757-899X/377/1/012080

UWB and miniaturized meandered stripline fed metamaterial loaded antenna for satellite applications

P.Dawar[1], N.S. Raghava[2] and A. De[3]

[1]Department of Electronics and Communication Engineering, Guru Tegh Bahadur Institute of technology, Delhi, India

[2,3]Department of Electronics and Communication Engineering, Delhi College of Engineering, Delhi, India

Corresponding author: paru.dawar@gmail.com

Abstract. A novel metamaterial surface-inspired patch antenna is proposed, wherein different parameters, e.g. dimension of ground plane, no. of slots on radiating patch, shape of the feed and distance between the patch and metamaterial surface, have been optimized for maximum gain, bandwidth and miniaturization .It is observed that the pair of slots on radiating patch generate multiple resonances giving 400% miniaturization while varying ground plane and feed results in wide bandwidth of nearly 600%..

1. Introduction

Nowadays, the trend is developing devices for wireless communication systems which have inherent high bandwidth, gain and multi-resonance. Rectangular Microstrip Patch Antenna i.e. RMPA is not a good candidate as it has narrow bandwidth, in sufficient gain and directive properties. Thus, various optimization techniques have been introduced to make patch antenna as successful candidate in wireless communication applications.

With the development of metamaterials, came the concept of attaining altered behaviour of electromagnetic radiations, i.e. μ, ε, η. Thus, providing better solution for attaining enhanced antenna‟s performance

In this paper, a novel antenna structure is proposed with enhanced performance parameters and miniaturization. By using different dimensions of ground plane and by changing the dimension of feed line wider bandwidth is obtained. Also, by inserting slots on the radiating patch different resonant frequencies are observed. Further the performance is improved by introduction of metamaterial surface at an optimum spacing from the radiating patch.

2.Antenna Design

Transmission line representation of RMPA is by two slots of width, w, and height, h, separated by transmission line of length, l. It resonates at 38.5GHz frequency with dielectric constant (εr) = 2.2, substrate thickness h = 3.2mm, L = 24.3mm, W = 30.8 mm on a ground plane [1-4]. Nearly, ground plane is finite with size greater than the patch by six times the substrate thickness, with length, Lg=108mm and width, Wg=140mm. Figure 1 gives the constructional details.

Content from this work may be used under the terms of the Creative Commons Attribution 3.0 licence. Any further distribution of this work must maintain attribution to the author(s) and the title of the work, journal citation and DOI.
Published under licence by IOP Publishing Ltd

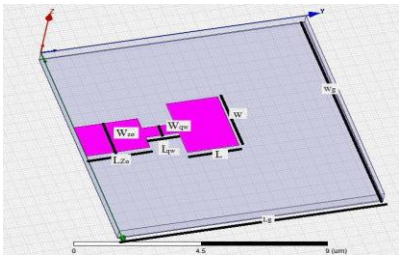

Figure 1. Rectangular microstrip patch antenna: constructional details

The input impedance at the base of microstrip feed line is 50Ω i.e. Zo. „Wqw" and „Lqw" represent the width (=16.3mm) and length (13.8mm) of the quarter wave transformer.

3.Paramateric Analysis of Patch

The antenna parameters e.g. size, feed position, gain and radiation characteristics are not considered in parametric study. The different design parameters of the antenna (number of slots, feed shape, size of ground plane and spacing between the patch antenna and metamaterial surface) are optimized using Ansoft HFSS software.

3.1. Analysis of size of ground plane

The size of the ground plane [5] is varied as 1/2, 1/4, 3/4 and full as shown in figure 2.

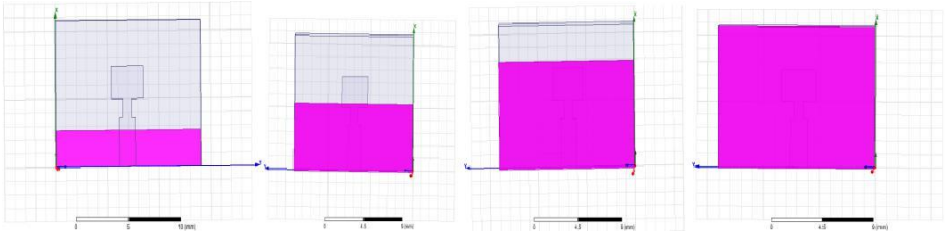

(a) (b) (c) (d)

Figure 2. Size of ground plane a) 1/2 ground b) 1/4 ground c)3/4 ground d)full ground

The size of ground plane affects the excitation modes and thus, the operational bandwidth. The curve in figure 3 depicts the effect of dimension of ground plane on S_{11} of radiating patch.

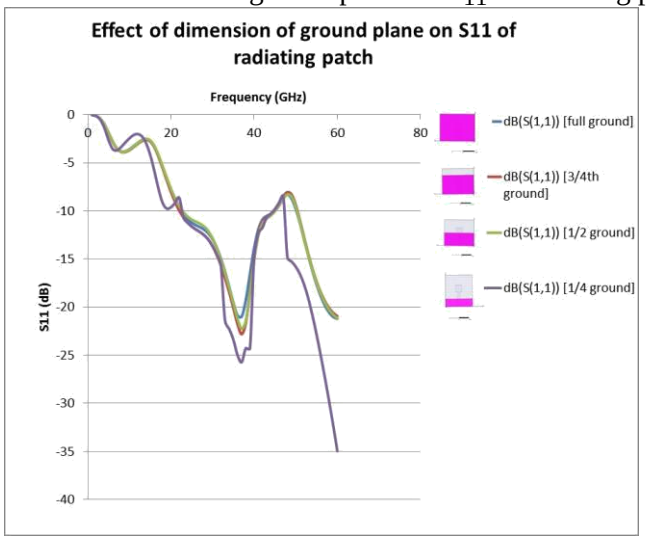

Figure 3. Effect of dimension of ground plane on S11 on radiating patch

It can be observed that using partial ground plane (1/4th) better reflection and bandwidth is obtained.

3.2. Analysis of different feed shape

The different feed shapes effect the input impedance mismatch of patch antenna [6]. Micro strip, L-strip and meander stripline has been used as feed in figure 4. .

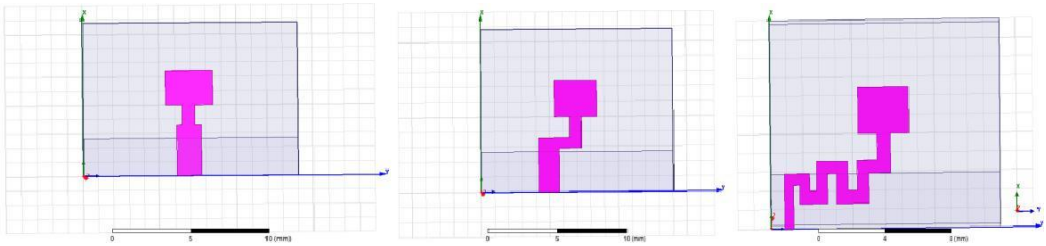

(a) (b) (c)

Figure 4. Different feeding techniques: a) microstrip b) L-strip c) Meander stripline feed

The curve in figure 5 depicts the response of different feeding techniques on S_{11}.

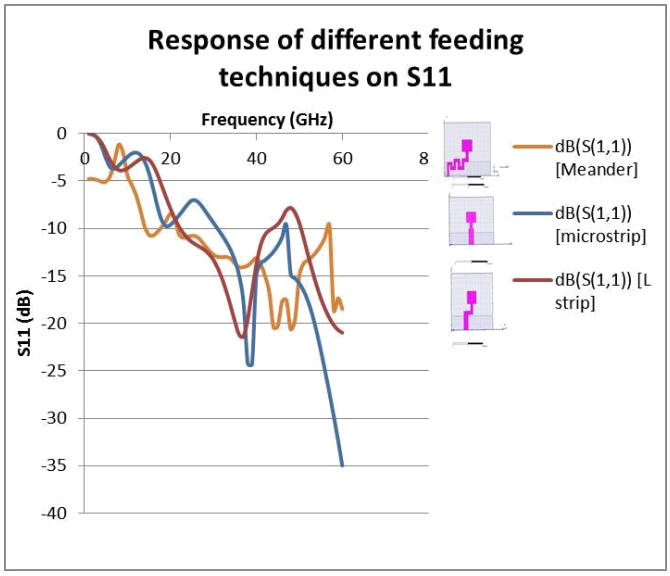

Figure 5. Response of different feeding techniques on S11 of patch

It can be seen that the meander strip-line feed structure has helps in attaining better impedance matching and thus wider bandwidth of 40GHz which is 400% enhancement over the conventional microstrip feed line.

3.3 Analysis of number of slots

The cutting of slots (in symmetrical pairs) [7] on the radiating patch has been done as shown in figure 6. Three pairs of equal size and spacing have been cut which leads to altered flow and direction of current. Thus, reducing the impedance of patch and introducing lower resonant frequencies.

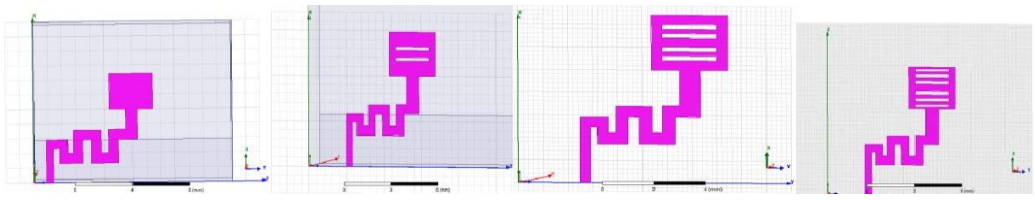

(a) (b) (c) (d)

Figure 6. Inserting different no. of slot pairs: a) No slot b) one slot pair c) two slot pair d) three slot pairs

The curve in figure 7 depicts the effect of inserting different no. of slots on radiating patch on the resonant frequencies.

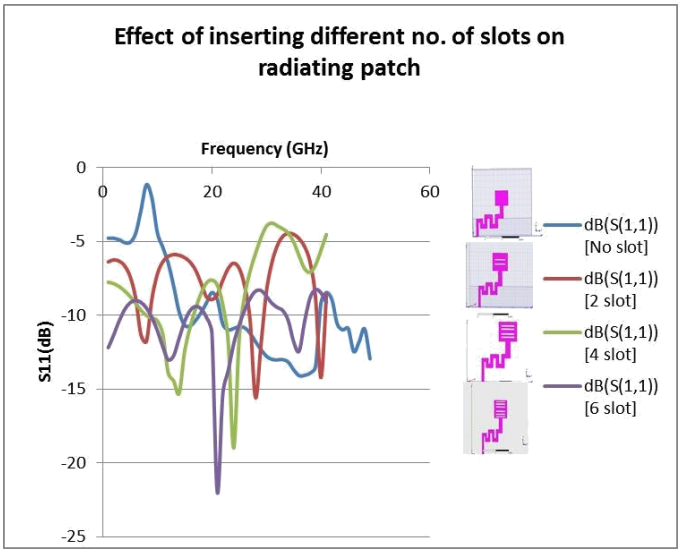

Figure 7. Effect of Inserting different no. of slot pairs on S_{11}

It can be observed that 50% miniaturization occurs with 6 slots on the patch.

3.4 Analysis of spacing between patch antenna and metamaterial surface

The metamaterial array of 2X2 swastika is used as reflector surface [8-9] by placing it at „ds‟ spacing below the patch antenna as shown in figure 8.

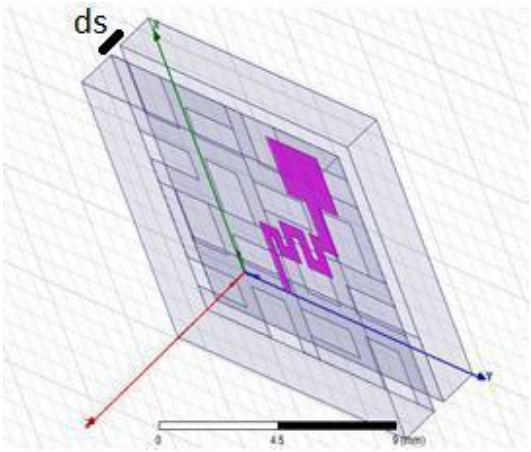

Figure 8. The metamaterial array as surface reflector

The ‘ds’ is varied as 0mm, 0.5mm, 0.75mm, 1mm, 1.5mm.The curve in figure 9 depicts the effect of spacing on the antenna‟s performance parameters.

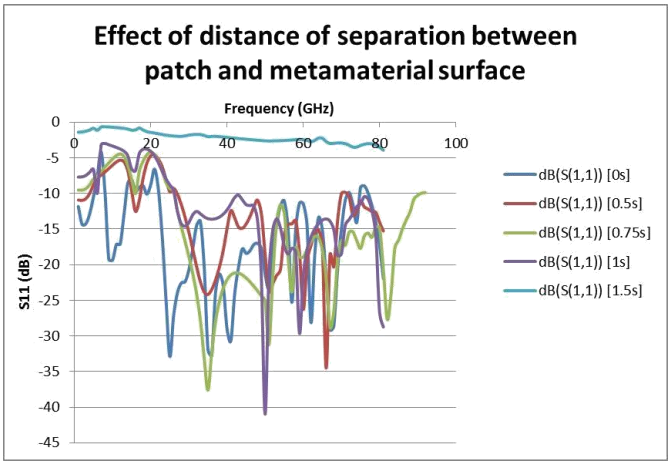

Figure 9. Effect of distance of separation between patch and metamaterial surface

It can be seen that the optimized value of ds is 0.75mm for maximum bandwidth improvement of nearly 600% over the conventional microstrip patch antenna [10].
The curve in figure 10 combines the effect of slots for obtaining both miniaturization and maximization of bandwidth.

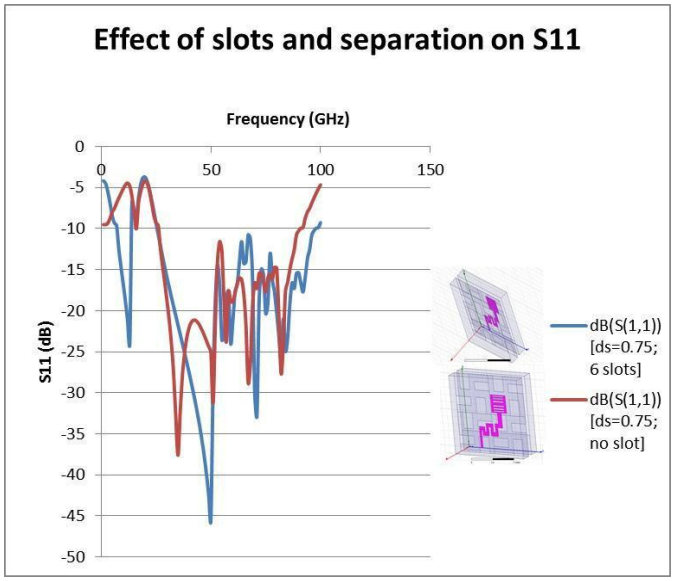

Figure 10. Effect of slots and separation distance on S11

It can be seen that the miniaturization of nearly ($1/4^{th}$) of the conventional patch is obtained.

4.Experimental validation of simulation results

In order to validate the above results, the patch antenna is fabricated by scaling the dimensions by a factor of 10 and frequency is scaled by (1/10). Thus, the new resonant frequency is 3.85GHz.
The fabricated antenna with meandered strip line and six slots is shown in Figure 11. The fabricated antenna is then embedded with metamaterial array in the middle of the substrate and is shown in Figure 12.

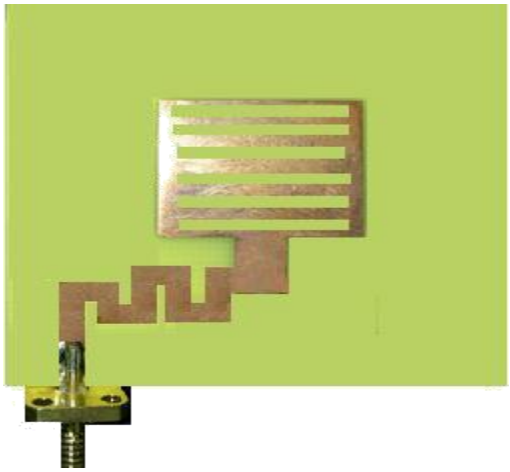

Figure 11. Fabricated Meandered patch antenna

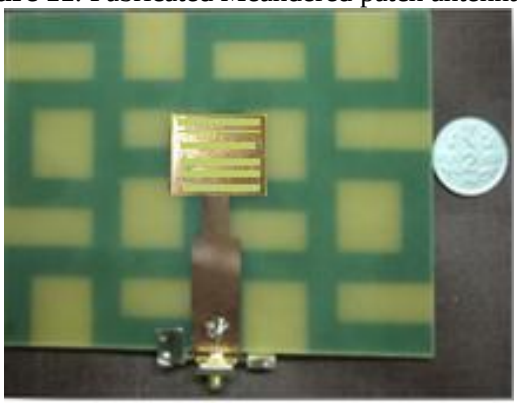

Figure 12.Fabricated metamaterial patch antenna

The simulation results are shown in figures 13 a, b, c and figure 14 a, b, c. below.

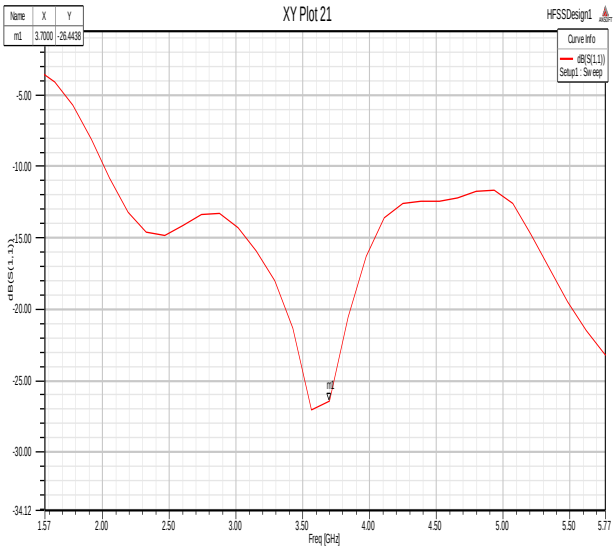

(a)

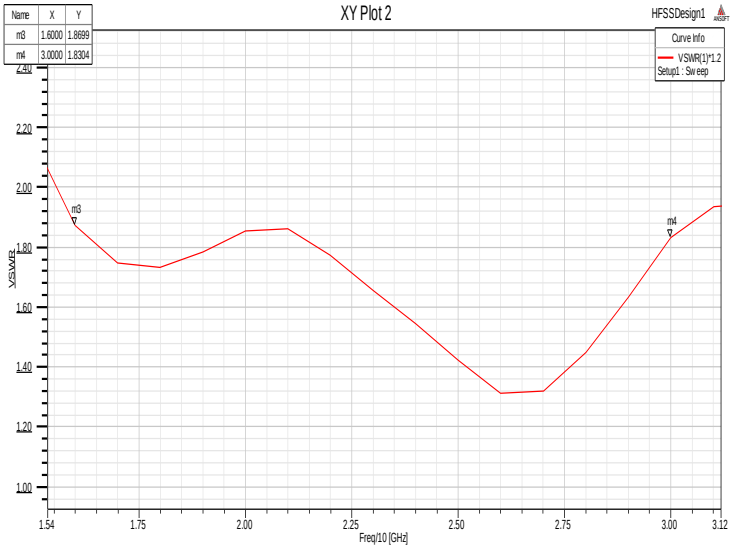

(b)

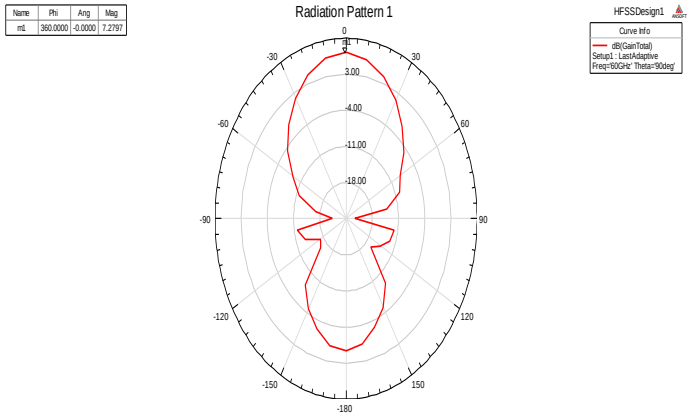

(c)

(c)

Figure 13 . Meandered stripline Patch Antenna :a)Return Loss b)VSWR c)Gain

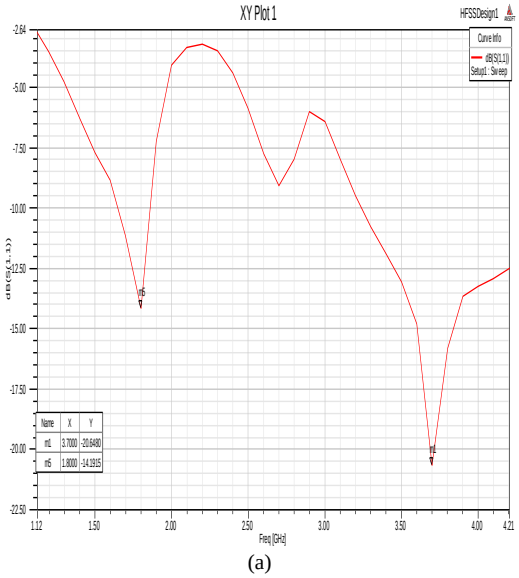

(a)

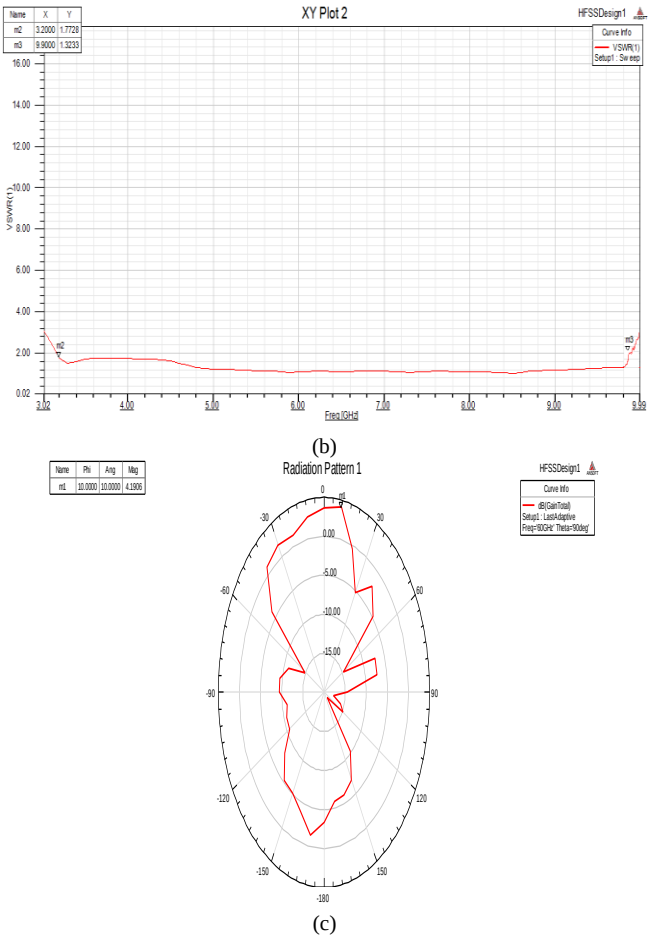

Figure 14. Meandered stripline Metamaterial Patch Antenna: a) Return Loss b) VSWR c) Gain

Using Keysight RF Fieldfox Network Analyser as shown in Figure 15, we compared the fabrication results in figure 16.

Figure 15. Keysight Fieldfox RF Network Analyser

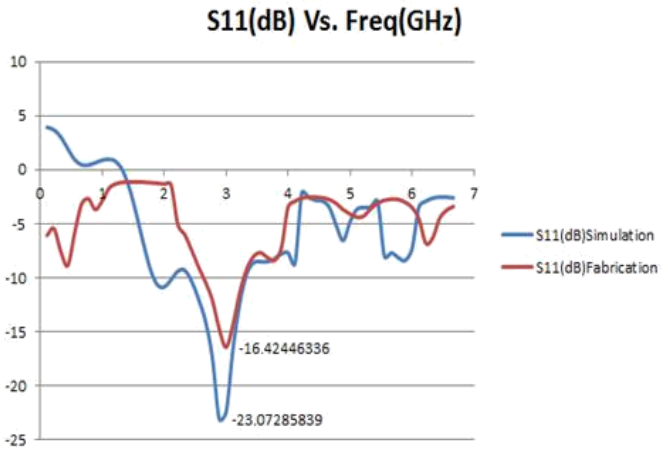

(a)

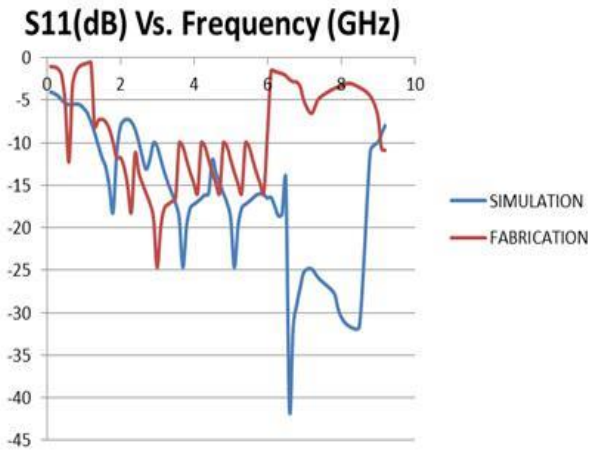

(b)

Figure 16. Comparison of simulation and fabrication results: a) Meandered Stripline Patch Antenna b) Meandered stripline metamaterial Patch Antenna

Using AMITECH gain measurement set-up as shown in figure 17, gain and radiation pattern have been obtained in figure 18.

Figure 17. AMITECH Gain measurement set-up

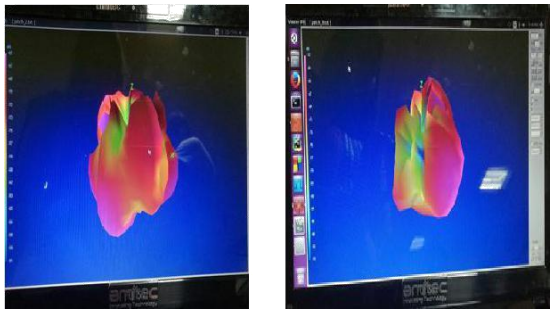

(a) (b)

Figure 18. Gain and Radiation Pattern measurement: a) Meandered Stripline Patch Antenna b) Meandered Stripline metamaterial patch Antenna

The above results have been tabulated in Table 1.

Table 1. Fabrication results of RMPA

Configurations	Gain(dB)	Directivity(dB)	Miniaturozation (%)	Return Loss(dB)
Meandered stripline Patch Antenna	3	5	51	20
Meandered stripline metamaterial Patch Antenna	3	4	84	25

Thus, "fabricated and simulated antennas" helps in achieving miniaturization and bandwidth enhancement which is in coherence with the proposed antenna configurations

5.Conclusion

In this paper, a proposed novel microstrip antenna attains miniaturization by nearly 400% and maximization in bandwidth of nearly 600% with ds=0.75mm between the metamaterial surface as reflector and patch , quarter ground plane, meander stripline feed and three slot pairs on the radiating patch. The simulation results are in coherence with the fabrication results.

6.References

[1] Schantz, H., "The Art and Science of Ultra Wide Band Antennas", Artech House, 2005.
[2] Balanis, C. A., "Antenna Theory," John Wiley & Sons, Inc., 1997.
[3] Pozar, D. M., "Microstrip antenna," Proc. IEEE, Vol. 80, 79–81, 1992.
[4] Volakis, "Antenna Engineering Handbook", McGraw Hills, Chapter-7, pp: 147574-5.
[5] Wang S, Feresidis AP, Goussetis G, Vardaxoglou JC, " Low-profile resonant cavity antenna with artificial magnetic conductor ground plane", Electronics Letters ,2004,40: 405–406.
[6] Ahsan MR, Islam MT, Ullah MH, Misran N , "Bandwidth Enhancement of a Dual Band Planar Monopole Antenna Using Meandered Microstrip Feeding.",The Scientific World Journal 2014.
[7] Lee KF, Luk KM, Mak KM, Yang SLS , " On the Use of U-Slots in the Design of Dual-and Triple-Band Patch Antennas",IEEE Antennas and Propagation Magazine,2011, 53: 60–74.